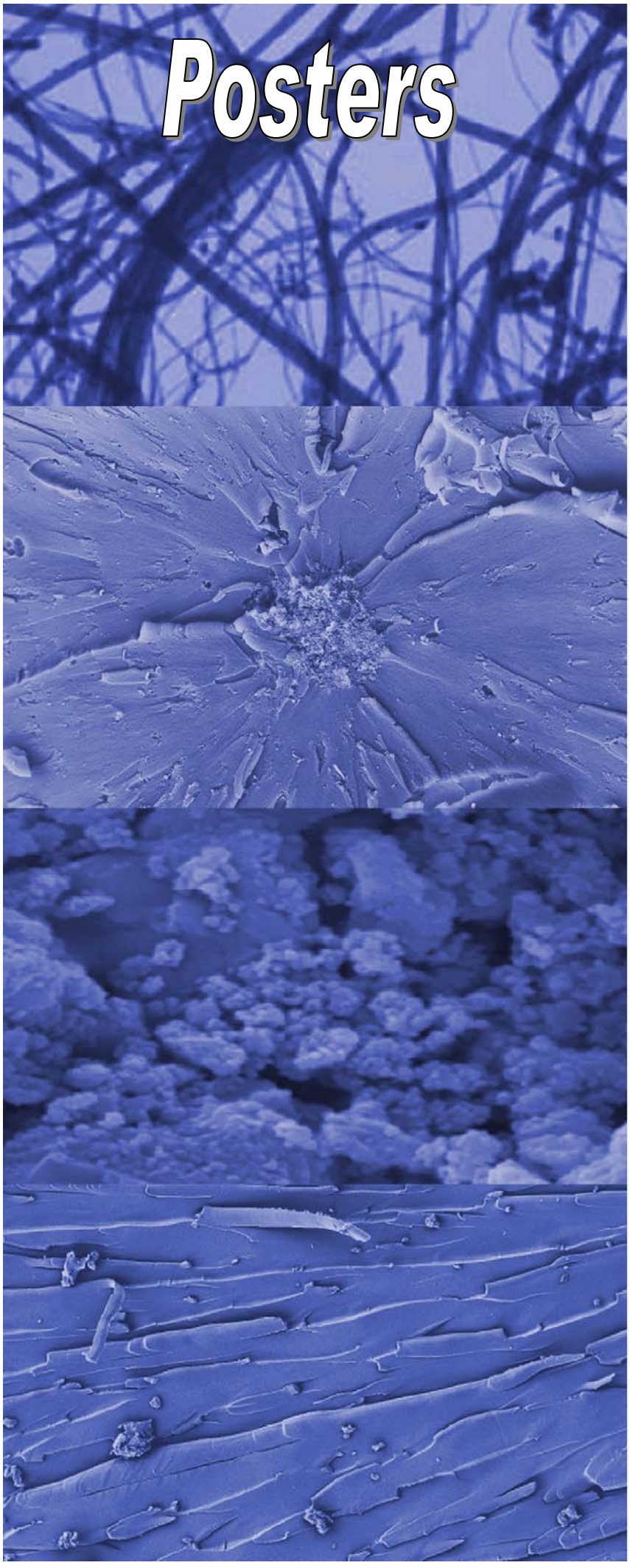

TNT2008
Trends in NanoTechnology
Oviedo (Spain)
September 01-05, 2008

PHANTOMS foundation

400 cuarto centenario

Universidad de Oviedo 1608-2008

Georgia Tech

Purdue University

DONOSTIA INTERNATIONAL PHYSICS CENTER

CIC nanoGUNE nanoscience cooperative research center

D.I.P.C.

UAM 4ñOs

NIMS

CSIC

UNIVERSITAS FRIBURGENSIS

Leti

cea

TNT2008
Trends in NanoTechnology
Oviedo (Spain)
September 01-05, 2008

INDEX

POSTERS

ALPHABETICAL ORDER
&
SESSION PA / SESSION PB

Session A (PA) is dedicated to students and **Session B (PB)** to seniors (Doctors)

Name	Last Name	Institution	Country	Topic	Title	Page
Alfonso	**Alarcón Pardo**	Universitat Autònoma de Barcelona	Spain	Theory and modelling at the nanoscale	*Time-dependent Electron Driven Tunneling Phenomena for multipurpose Terahertz applications: self-consistent computation of conduction and displacement current in mesoscopic systems*	**3**
Alejandro	**Alija**	Universidad de Oviedo	Spain	Nanomagnetism and Spintronics	*Ratchet effects on domain wall motion in Co-Si amorphous films with arrays of asymmetric holes: experiments and theoretical simulations*	**5**
Amanda	**Alonso**	Universidad Autónoma de Barcelona	Spain	NanoChemistry	*Intermatrix synthesis of metal nanoparticles with core-shell or core-sandwich structure for antibacterial aplications*	**7**
Lucia	**Alvarez**	ICMM-CSIC	Spain	Nanostructured and nanoparticle based materials	*Metalorganic nanostructures: 2d- extended structures*	**9**
Pablo	**Alvarez**	Universidad de Oviedo	Spain	Nanostructured and nanoparticle based materials	*Magneto-volume anomalies and Magnetocaloric effect on ball-milling nanostructured Pr2Fe17 compounds*	**11**
Jesus	**Alvarez**	Universidad Politécnica de Valencia	Spain	NanoOptics & NanoPhotonics	*A theoretical comparison of strip and vertical slot-waveguide resonators in silicon nitride for sensing purposes*	**13**
Carolina	**Aubéry Torres**	IIQAB-CSIC	Spain	Nanostructured and nanoparticle based materials	*Synthesis and Characterization of Mn-Zn Ferrite Magnetic Nanoparticles by the Microemulsion Reaction Method*	**15**
Claire	**Barrett**	Tyndall National Institute	Ireland	Low dimensional materials (nanowires, clusters, quantum dots, etc.)	*Formation and Electrical Interfacing of Nanocrystal-Molecule Nanostructures*	**17**
Stéphane	**Bedwani**	Ecole Polytechnique de Montreal	Canada	Theory and modelling at the nanoscale	*Electronic Properties of Strongly Reshaped Organic-Metal Interfaces*	**19**
Birgit	**Bittmann**	Institut fuer Verbundwerkstoffe	Germany	Nanostructured and nanoparticle based materials	*A Model for the Ultrasonic Dispersion of Nanoparticles in Epoxy Resin*	**21**
Barbara	**Blasiak**	University of Calgary	Canada	Nanobiotechnologies	*A magnetic resonance study of iron and cobalt based nanoparticles as potential contrast agents for molecular imaging of cancer*	**23**
Jordi	**Bonastre**	Girona University	Spain	Nanostructured and nanoparticle based materials	*Development of nanostructured materials by mechanical alloying and/or rapid solidification*	**25**
Pablo	**Carballeira**	Institute für Verbundwerkstoffe GmbH (IVW)	Germany	Nanostructured and nanoparticle based materials	*Upgrading thermosets with carbon nanofibers*	**27**
Laura	**Castro**	Universidad Complutense de Madrid	Spain	NanoChemistry	*Characterization of metallic nanoparticles obtained by biomass reduction*	**29**
Oleksandr V.	**Chayka**	Institute of Physics ASCR	Czech Republic	Nanomagnetism and Spintronics	*Influence of field annealing on AC magnetic properties of nanogranular FeCo-AlN films.*	**31**
Kuek	**Chian Shiun**	University Tunku Abdul Rahman	Malaysia	Theory and modelling at the nanoscale	*Temperature dependence of electrical conduction through1, 4-dithiolbenzene molecular assembly (part II)*	**32**

Name	Last Name	Institution	Country	Topic	Title	Page
Louis	**Chonco**	Hospital General Universitario Gregorio Marañon	Spain	Nanobiotechnologies	*Prevention of HIV-mucosal barrier interaction by new synthesised carbosilane polyanionic dendrimers*	**34**
Vincent	**Cunningham**	Universidad Carlos III de Madrid	Spain	Nanostructured and nanoparticle based materials	*Optoacoustic Spectroscopy of Spherical Gold Nanoparticle Contrast Agents in a Scattering Media*	**36**
Ramón	**Cuadrado**	ICMM-CSIC	Spain	Theory and modelling at the nanoscale	*A first principles study of Thiol-Capped Au Nanoparticles*	**38**
Afshin	**Dadvand**	INRS	Canada	Other	*Heterocirculenes as a new class of organic semiconductors*	**40**
Maria Adelaide	**de Carvalho Miranda**	Universidade do Porto	Portugal	NanoChemistry	*Gold Nanocubes: novel photo-synthetic method and morphological characterization*	**42**
Kadiatou Thérèse	**Dembélé**	Institut National de la Recherche Scientifique, centre EMT	Canada	Other	*Simulation of an absorption chiller dual effect operating with the couple H2O/LiBr*	**44**
Vincent	**Demers-Carpentier**	Université Laval	Canada	NanoChemistry	*Isolated Nanoscale Prochiral Reaction Assemblies on Pt(111)*	**45**
Riccardo	**Di Corato**	CNR-INFM-NNL	Italy	Nanobiotechnologies	*Development of a novel magnetic-fluorescent colloidal nano-cluster*	**46**
Girjesh	**Dubey**	NRC, Steacie Institute for Molecular Science	Canada	Low dimensional materials (nanowires, clusters, quantum dots, etc.)	*Use of Conductivity on Silicon-on-Insulator as a Probe of Molecule-Surface Interactions*	**48**
Kerry	**Dunn**	INRS-EMT, Université du Québec	Canada	Low dimensional materials (nanowires, clusters, quantum dots, etc.)	*The effect of single nanocrystal blinking on the luminescence decay of ensembles*	**49**
Ivan	**Fernandez**	IMM-CNM-CSIC	Spain	SPM	*Magnetostrictive drive of AFM cantilevers for liquid operation*	
María Teresa	**Fernández Argüelles**	Universidad de Oviedo	Spain	Low dimensional materials (nanowires, clusters, quantum dots, etc.)	*Quantum Dots-Based Fluorescent Inmunoassay for the Determination of Aflatoxins*	**51**
Mª Paz	**Fernández García**	Universidad de Oviedo	Spain	Nanostructured and nanoparticle based materials	*Competing Superparamagnetism and exchange bias in Fe nanoparticles embedded in an amorphous carbon matrix*	**52**
Lucas	**Fernández Seivane**	Universidad de Oviedo	Spain	Theory and modelling at the nanoscale	*On-site approximation for spin-orbit coupling in LCAO density functional methods: Application to clusters and chains*	**54**
Jorge	**Fernandez Torrado**	IMM-CSIC	Spain	Nanobiotechnologies	*Hybrid noble metal-ferromagnet nanoparticles for biosensing applications: a preliminary study*	**56**
Angela	**Fiore**	National Nanotechnology Laboratory of CNR-INFM	Italy	Nanostructured and nanoparticle based materials	*Seeded growth approach for synthesis of semiconductor nanotetrapods*	**57**

Name	Last Name	Institution	Country	Topic	Title	Page
Shawn	**Fostner**	McGill University	Canada	Nanofabrication tools & nanoscale integration	*Contacts at the nanoscale: Using silicon nanostencils to make wires and contacts on ultra high vacuum cleaved insulators*	**59**
Isabella Raffaella	**Franchini**	National Nanotechnology Laboratory of CNR-INFM	Italy	Nanostructured and nanoparticle based materials	*End-to-End Assembly of Shape-Controlled Nanocrystals via a Nano-welding Approach.*	**61**
Jorge	**Garcia**	Universidad de La Rioja	Spain	NanoChemistry	*Organometallic silver compoundsas precursors for nanomaterials. Use of thiols and polymers as nanoparticle stabilizers.*	**63**
Alberto	**Gomez-Casado**	University of Twente, MESA+/MNF	Netherlands	SPM	*Probing multivalent host-guest complexes using AFM*	**65**
Francois	**Goyer**	University of Montreal	Canada	Theory and modelling at the nanoscale	*Using complex potentials to describe electron transmission through molecules*	**67**
Till	**Hagedorn**	McGill University	Canada	SPM	*Characterizing contact formation at the atomic scale: A combined Scanning Tunneling Microscopy (STM) and Atomic Force Microscopy (AFM) study*	**68**
Solmaz	**Hajizadeh**	Noshirvani university of technology	Iran	Carbon nanotubes based nanoelectronics and field emission	*Catalysts effects on the production of carbon nanotubes by an automatic arc discharge set up*	**70**
Solmaz	**Hajizadeh**	Babol university of technology	Iran	Nanobiotechnologies	*Evaluation of hydrodynamic parameters of fluidized bed adsorption on purification of nanobioproducts*	**73**
Jesús	**Herranz Zamorano**	IMM-CNM-CSIC	Spain	Low dimensional materials (nanowires, clusters, quantum dots, etc.)	*Growth of site-controlled InAs quantum dots on prepatterned GaAs (001) substrates by AFM local oxidation*	**75**
Aurelio	**Hierro Rodríguez**	Universidad de Oviedo	Spain	Nanofabrication tools & nanoscale integration	*Growing up of magnetic nanostructures by EBL using double layer resist system and characterization by AFM and magneto optical SNOM.*	**77**
Pejman	**Hojati Talemi**	Monash University	Australia	Other	*Effect of Different Microwave-Based Treatments on multiwalled carbon nanotubes*	**79**
Radim	**Hrdý**	Brno University of Technology	Czech Republic	Nanobiotechnologies	*Detection of Ureasa Enzyme Analysis Using Electrode Modified with Vertically Aligned Ni Nanopillars*	**81**
Chien-Wen	**Hsieh**	University of Cambridge	United Kingdom	Low dimensional materials (nanowires, clusters, quantum dots, etc.)	*ZnO nanowires for nanocomposite organic thin film transistors*	**83**
Jongmo	**Im**	University of Hanyang	Korea	Nanostructured and nanoparticle based materials	*Comparison of electro and air-blast spray deposition for preparing lanthanum strontium manganite films*	**85**
Norbert	**Jahr**	Institute of Photonic Technology (IPHT)	Germany	NanoOptics & NanoPhotonics	*Single nanoholes with gold nanoparticles a novel tool in nanooptics*	**87**

Name	Last Name	Institution	Country	Topic	Title	Page
Sungeun	**Jang**	University of Hanyang	Korea	Nanostructured and nanoparticle based materials	*Fabrication of Ni-YSZ anode for SOFC by ESD*	**88**
Vicente	**Jimenez**	Universidad de Castilla La Mancha	Spain	Other	*Chemical activation of fish-bone type carbon nanofibers*	**90**
Prem Kumar	**Kandaswamy**	CEA-Grenoble	France	Low dimensional materials (nanowires, clusters, quantum dots, etc.)	*Polarization effects in GaN/AlN Short-Period Superlattices for Intersubband Optoelectronics*	**92**
Mykola	**Kondratenko**	McGill University	Canada	NanoChemistry	*Design and rectification study of different Aviram-Ratner model molecules*	**94**
Aleksander	**Labuda**	McGill University	Canada	SPM	*Atomic-Scale Friction of Gold and Copper in Perchloric Acid*	**96**
Tobias	**Lockwood**	McGill University	Canada	Nanostructured and nanoparticle based materials	*Electrochemically grown PEDOT on nanotube films for transparent electrodes*	**97**
Pierre	**Lovera**	Tyndall National Institute	Ireland	Low dimensional materials (nanowires, clusters, quantum dots, etc.)	*Determination of Molecular Orientations in Single Polyfluorene Nanowires Using Polarisation Dependent Nonlinear Microscopy*	**98**
Arnaud	**Maillard**	Ecole Polytechnique de Montreal	Canada	Theory and modelling at the nanoscale	*Band-Alignment Engineering of Organic Photovoltaic Materials*	**100**
Emma	**Martín Rodríguez**	Universidad Autónoma de Madrid	Spain	NanoOptics & NanoPhotonics	*Second Harmonic Generation by ferroelectric nanoparticles of Strontium Barium Niobate*	**102**
Florian	**Massuyeau**	Institut des matériaux Jean Rouxel de Nantes (IMN)	France	NanoOptics & NanoPhotonics	*Conjugated polymer nanofibers: effects of nanostructuration on photoemission properties*	**104**
Marcel	**Mohr**	Inst of solid state physics, TU Berlin	Germany	Low dimensional materials (nanowires, clusters, quantum dots, etc.)	*Ab-initio calculations of core-shell CdSe/ZnS nanowires*	**106**
Lana	**Norman**	Unversity of Montreal	Canada	NanoChemistry	*Towards the Controlled Nanomechanical Actuation of Microcantilevers Using Redox Reactions in Electroactive Self-Assembled Monolayers*	**107**
Inyu	**Park**	Hanyang University	Korea	Nanostructured and nanoparticle based materials	*Fabrication of Sm0.5Sr0.5CoO3 cathode thin films for IT-SOFCs by Electrostatic Spray Deposition*	**109**
Samuel	**Peláez Machado**	ICMM-CSIC	Spain	Theory and modelling at the nanoscale	*Mechanical properties at the nanoscale: the dependence of Young\'s modulus of nanowires on the shape and axial orientation*	**111**
Beatriz	**Pérez García**	Universidad de Murcia	Spain	SPM	*P3OT surface characteritation as a function of temperature by Variable Temperature Scanning Force Microscopy.*	**113**

Name	Last Name	Institution	Country	Topic	Title	Page
Miquel	**Pons**	Universitat de les Illes Balears	Spain	Low dimensional materials (nanowires, clusters, quantum dots, etc.)	*Spin contamination in quantum dot RHF states: a phase diagram*	**115**
Elisabetta	**Primiceri**	National Nanotechnology Lab of CNR-INFM	Italy	Nanobiotechnologies	*On-Line Monitoring of Cytotoxic Effects Using EIS based Cell-Chips*	**116**
Marie-Ève	**Provencher**	Université Laval	Canada	Nanobiotechnologies	*Design of peptides nanostructures having antimicrobial activity*	**118**
Alan	**Reguer**	CINAM	France	Nanofabrication tools & nanoscale integration	*Growth study of silicon nanowires using gold and gallium as catalyst by In Situ scanning electron microscopy*	**120**
Ken	**Reynolds**	Tyndall National Institute	Ireland	Nanofabrication tools & nanoscale integration	*Manipulation, Assembly and Characterization of Optically Functional 1-D Organic Nanostructures*	**122**
Gaël	**Robert**	CEA Saclay / SPEC	France	Carbon nanotubes based nanoelectronics and field emission	*Carbon Nanotubes as Electrodes for Molecular Electronics: from SAMs to Single-Molecule Connection*	**124**
Philippe	**Rocheleau**	Université de Montréal	Canada	Theory and modelling at the nanoscale	*Molecular conductance in terms of orbital densities and polarizabilities*	**126**
Gabriel	**Rodríguez-Rodríguez**	Universidad de Oviedo - CINN / CSIC	Spain	SPM	*Micromagnetic simulation of MFM tip hysteresis and stray field*	**127**
María J.	**Rodríguez-Vázquez**	University of Santiago de Compostela	Spain	Low dimensional materials (nanowires, clusters, quantum dots, etc.)	*Synthesis of metallic atom clusters by soft methods. Characterization and properties.*	**129**
Loránd	**Románszki**	Chalmers University of Technology	Sweden	Other	*Hydrogen Storage in Thin Metallic Films*	**131**
Patricia	**Ruiz**	Universidad Autónoma de Barcelona	Spain	NanoChemistry	*Intermatrix synthesis of polymer-copper nanocomposites with predetermined parameters by using coproportionation reaction.*	**132**
Francisco Javier	**Salgado-Remacha**	Universidad Complutense de Madrid	Spain	Other	*Diffraction gratings embedded in bulk fused silica by laser ablation*	**134**
Tomas	**Samuely**	University of Basel	Switzerland	NanoChemistry	*Phthtalocyanine derivatives on (111) noble metal surfaces – multiphase behavior and capability of hosting other molecules*	**136**
Hernán	**Santos Expósito**	Universidad de Castilla la Mancha	Spain	Low dimensional materials (nanowires, clusters, quantum dots, etc.)	*Friedel Oscillations in Carbon Nanotube Quantum Dots*	**138**
Sirilak	**Sattayasamitsathit**	Prince of Songkla University	Thailand	Low dimensional materials (nanowires, clusters, quantum dots, etc.)	*Electrochemical Synthesis and Characterizations of Versatile Nanowires*	**140**

Name	Last Name	Institution	Country	Topic	Title	Page
Franziska	**Schäffel**	IFW_Dresden	Germany	Carbon nanotubes based nanoelectronics and field emission	*CVD routes to carbon nanotube systems with highly anisotropic nanomagnets*	**142**
Hugo	**Silva**	University of Oporto	Portugal	Theory and modelling at the nanoscale	*Temperature and Voltage TMR Dependencies for High Performance Magnetic Junctions*	**144**
Andrea	**Steinbrueck**	Institute of Photonic Technology	Germany	Nanostructured and nanoparticle based materials	*Nanoparticle constructs of metallic and core-shell nanoparticles based on DNA-hybridization*	**146**
Cristiana Sonia	**Steplecaru**	IMM-CNM-CSIC	Spain	Other	*Epitaxial p & n ZnO thin films grown by pulsed laser deposition*	**147**
Lev	**Tal Or**	Hebrew University	Israel	Low dimensional materials (nanowires, clusters, quantum dots, etc.)	*Controlled Charge Transport Measurements Through short dsDNA using Conductive AFM*	**149**
Nathalie Y-Wa	**Tang**	Université de Montréal	Canada	Nanostructured and nanoparticle based materials	*Enzyme-Assisted Attachment of Gold Nanoparticles onto Patterned Organic Surfaces*	**151**
José	**Teixeira**	University of Oporto	Portugal	Nanomagnetism and Spintronics	*Temperature dependent transport properties of MgO-based ultra-thin magnetic tunnel junctions: experiment and modeling.*	**153**
Israel	**Temprano**	Université Laval	Canada	Low dimensional materials (nanowires, clusters, quantum dots, etc.)	*Molecular contacts through inducing surface initiated polymerization of nanowires on molybdenum carbide*	**155**
Lidija	**Trandafilovic**	Institute "Vinca"	Yugoslavia	Low dimensional materials (nanowires, clusters, quantum dots, etc.)	*Properties of CdS and CdSe nanopoarticles in poly(2-(dimethylamino)ethyl methacrylate-co-acrylic acid) co-polymer matrix*	**157**
Igor	**Valtsifer**	Institute of Technical Chemistry	Russia	Nanostructured and nanoparticle based materials	*The influence of surface modification of nanoparticles on their structuring in a liquid medium*	**159**
Victor	**Vega**	University of Oviedo	Spain	Nanomagnetism and Spintronics	*Synthesis and magnetic properties of FePd hexagonally ordered nanohole arrays*	**160**
José Joaquín	**Velázquez García**	Universidad de La Laguna	Spain	Nanostructured and nanoparticle based materials	*Structure and up-conversion luminescence in transparent Er3+-Yb3+ co-doped SiO2-PbF2 sol-gel derived nano-glass-ceramics*	**162**
José Joaquín	**Velázquez García**	Universidad de La Laguna	Spain	Nanostructured and nanoparticle based materials	*Color tuneability and white light generation in Yb3+-Ho3+-Tm3+ doped SiO2-LaF3 nano-glass-ceramics prepared by sol-gel method*	**164**
JinJin	**Wang**	University of Cambridge	United Kingdom	Theory and modelling at the nanoscale	*Atomistic Simulations of Catalytic Carbon Nanotubes Growth*	**166**

Name	Last Name	Institution	Country	Topic	Title	Page
Masato	**Watanabe**	Tohoku University / CRESS	Japan	Nanostructured and nanoparticle based materials	*Fabrication of Fe-Pt and Au Monodispersed Nanoparticle Colloids by KrF Excimer Laser Irradiation*	**168**
Chien-Ching	**Wu**	Twente University/MESA+/BPE	Netherlands	Nanobiotechnologies	*Fabrication of Metal-Ion Patterns by uCP and DPN for Protein Immobilization*	**170**
Susana	**Yáñez Vilar**	Universidad de la Coruña	Spain	Nanostructured and nanoparticle based materials	*Magnetocapacitance in Fe3O4@SiO2 nanocomposite*	**172**

Name	Last Name	Institution	Country	Topic	Title	Page
Holger	**Lange**	Institut fuer Festkoerperphysik, TU Berlin	Germany	Low dimensional materials (nanowires, clusters, quantum dots, etc.)	*Experimental observation of the radial breathing mode in nanorods*	**226**
Alan	**Le Goff**	CEA / IRAMIS	France	Nanostructured and nanoparticle based materials	*Modified electrodes based on ferrocene attached to multi-walled carbon nanotubes: Application to glucose biosensing*	**227**
Soo-Keun	**Lee**	DGIST	Korea	Other	*Nitridation of Pt-TiO2 nanoparticle and their characteristics as a visible light photocatsyst*	**228**
Sang Kyoo	**Lim**	DGIST	Korea	Low dimensional materials (nanowires, clusters, quantum dots, etc.)	*ZnO nanorods fabricated by a wet chemical method*	**230**
Rosa	**Lopez**	Universidad de las Islas Baleares	Spain	Low dimensional materials (nanowires, clusters, quantum dots, etc.)	*Transport through hybrid double kondo dots*	**232**
Aitor	**Luque**	CEIT	Spain	Theory and modelling at the nanoscale	*Mode II loading behaviour of intergranular nanocracks lying on a S17(530) symmetrical tilt boundary in copper*	**233**
Eduardo	**Martinez**	Universitaet Osnabrueck	Germany	Other	*Response of Mn overlayers on Fe substrate to external magnetic fields*	**236**
Jorge	**Méndez Ramos**	Universidad de La Laguna	Spain	Nanostructured and nanoparticle based materials	*Sol-gel derived nano-glass-ceramics containing Eu3+-doped NaYF4 nanocrystals*	**237**
Jorge	**Méndez Ramos**	Universidad de La Laguna	Spain	Nanostructured and nanoparticle based materials	*Tuneable up-conversion phosphor based in sol-gel derived nano-glass-ceramics containing Yb3+-Er3+ co-doped NaYF4 nanocrystals*	**239**
Adina	**Morozan**	University of Bucharest	Romania	Other	*Plasma processing of polypyrrole-heparin thin films on titanium substrates for biomedical applications*	**241**
Claudia	**Nastase**	University of Bucharest	Romania	Other	*Plasma processing of PMMA films for biomedical applications*	**243**
Jim	**Partridge**	RMIT University	Australia	Nanostructured and nanoparticle based materials	*Films consisting of graphite-like sheets suitable for interconnects with high electrical and thermal conductivity*	**245**

Name	Last Name	Institution	Country	Topic	Title	Page
Luis	**Pastor-Abia**	Instituto Universitario de Materiales de Alicante	Spain	Low dimensional materials (nanowires, clusters, quantum dots, etc.)	*Stress-strain curves of aluminum nanowires: fluctuations in the plastic regime and absence of hardening*	**247**
David	**Perez de Lara**	Universidad Complutense	Spain	Low dimensional materials (nanowires, clusters, quantum dots, etc.)	*Nanorectifiers Based on Superconducting/magnetic Hybrids*	**249**
Henry	**Pinto**	Helsinki University of Technology	Finland	SPM	*Composition and structure of Si(001)/CaF2 interfaces*	**250**
Ondrej	**Podrazky**	Institute of Photonics and Electronics AS CR, v.v.i.	Czech Republic	Nanostructured and nanoparticle based materials	*Use of Nanoparticles for Preparation of Rare-Earth Doped Silica Fibers*	**252**
Jan	**Prášek**	Brno University of Technology	Czech Republic	Nanobiotechnologies	*Using of Carbon Nanotubes for Fabrication of Printed Electrodes and Their Employing in DNA Analysis*	**254**
Antonio	**Puente**	Universitat de les Illes Balears	Spain	Low dimensional materials (nanowires, clusters, quantum dots, etc.)	*Spin projection energies in RHF: application to quantum dots*	**256**
Susagna	**Ricart**	ICMA (CSIC)	Spain	Nanostructured and nanoparticle based materials	*Nanoparticles in YBa2Cu3O7 superconducting thin films*	**257**
Jesús	**Ricote**	ICMM-CSIC	Spain	Low dimensional materials (nanowires, clusters, quantum dots, etc.)	*Ferroelectric behavior of polycrystalline ultrathin lead titanate films*	**258**
Klemens	**Rumpf**	Karl Franzens University	Austria	Nanomagnetism and Spintronics	*Temperature dependence of a twofold magnetic behaviour of a nanoscopic metal/silicon hybrid system – a comparison between Ni/Si and Co/Si*	**260**
Adam	**Rycerz**	Institut fur Theoretische Physik	Germany	Low dimensional materials (nanowires, clusters, quantum dots, etc.)	*Graphene nanoconstriction as a single-level quantum dot*	**262**
Humberto	**Sanchez**	Erasmus University Medical Center	Netherlands	Nanobiotechnologies	*Nanometer localization and identification of DNA repair proteins by combined AFM-fluorescence analysis*	**264**
David	**Sánchez**	Universitat de les Illes Balears	Spain	Nanomagnetism and Spintronics	*Strong current modulation in quantum wires with localized Rashba interaction*	**265**

Name	Last Name	Institution	Country	Topic	Title	Page
Emilio	**Sanfabián**	Instituto Universitario de Materiales de Alicante	Spain	NanoChemistry	*Magnetic molecules derived from hydrogenation of polycyclic aromatic hydrocarbons*	**266**
Silvia	**Santalla**	Universidad Carlos III de Madrid	Spain	Low dimensional materials (nanowires, clusters, quantum dots, etc.)	*Substrate orientation effects on the lattice parameter profiles in the stranski-krastanov growth mode*	**268**
Pedro A.	**Serena**	ICMM-CSIC	Spain	Theory and modelling at the nanoscale	*MC simulation of water meniscus in nanocontainers: explaining the collapse of viral particles due to capillar forces*	**270**
Tsutomu	**Sonoda**	AIST	Japan	Other	*Coating of Pure Titanium with TiN/Ti Multi-Layered FIlms by Sputter-Deposition for Improving Blood Compatibility*	**272**
Rodica	**Stancu**	Mechanical Research and Enginnering Institute	Romania	Nanostructured and nanoparticle based materials	*Zn-Al2O3 electrodeposited nanocomposites*	**274**
Nery	**Suarez**	Universidad Simon Bolivar	Venezuela	Nanostructured and nanoparticle based materials	*Dynamics in Polymer-Clay Nanocomposites As Studied by FTIR, XRD, TEM, TSDC and DSC Techniques*	**276**
Judita	**Sukyte**	University of Technology	Lithuania	NanoChemistry	*The different species of telluropentathionates as precursors for formation of copper chalcogenides layers on the surface of polyamide*	**278**
Filipa	**Vale**	Universidade Católica Portuguesa	Portugal	Nanobiotechnologies	*A DNA Chip for Simultaneous Detection of Microorganims in Water Samples: Coliform Bacteria, non-mandatory bacteria, hepatitis A virus and noroviruses*	**280**
Mikhail	**Vantsyan**	Mendeleyev University of Chemical Technology of Russia	Russia	Low dimensional materials (nanowires, clusters, quantum dots, etc.)	*Low-dimensional Metallized Biodegradable Polymers Preparation, Study and Application*	**282**
Andrés	**Vega**	Universidad de Valladolid	Spain	Nanomagnetism and Spintronics	*Magnetization reversal process in spin spring magnets. Electronic structure calculations*	**283**
Giulio Paolo	**Veronese**	Istituto Nazionale Fisica Nucleare	Italy	Carbon nanotubes based nanoelectronics and field emission	*Field emission properties of carbon nanotube arrays grown in porous anodic alumina*	**285**

INDEX

POSTERS

ALPHABETICAL ORDER SESSION PA

Session A (PA) is dedicated to students

TIME-DEPENDENT ELECTRON DRIVEN TUNNELING PHENOMENA FOR MULTIPURPOSE TERAHERTZ APPLICATIONS: SELF-CONSISTENT COMPUTATION OF CONDUCTION AND DISPLACEMENT CURRENT IN MESOSCOPIC SYSTEMS

A.Alarcón and X. Oriols

Departament d´Enginyeria Electrònica, Universitat Autònoma de Barcelona
08193 Bellaterra, Barcelona, SPAIN *E-mail:alfonso.alarcon@uab.es*

Nowadays, systems for reaching the Terahertz (THz) electromagnetic gap are based on down-conversion of optical frequencies [1]. As alternative to these dominant strategies we propose a transistor-like tunneling electron device, that we named driven tunneling device (DTD), working at frequencies comparable to the inverse of the electron transit time (see Fig. 1). Our (single-device and room temperature) proposal provides future THz systems with reduced costs, sizes, and complexities. In this conference, we present several applications of the DTD for generating/manipulating signals at the THz gap (see Figs. 2, 3 and 4). For an accurate computation of tunneling transport through these DTDs at THz frequencies, a novel algorithm for the self-consistent computation of the time-dependent total (conduction plus displacement) current, $I(t)$, is presented.

The time-dependent evolution of a quantum system of N (coulomb and exchange) interacting electrons can be described by a many-particle Schrödinger equation [2]:

$$i\hbar\frac{\partial\Phi(\vec{r}_1,...,\vec{r}_N,t)}{\partial t}=\left\{\sum_{a=1}^{N}-\frac{\hbar^2}{2\cdot m}\nabla_a^2+U(\vec{r}_1,...,\vec{r}_N,t)\right\}\Phi(\vec{r}_1,...,\vec{r}_N,t) \quad (1)$$

However, from a computational point of view, the direct solution of equation (1) is inaccessible because (for a real space with N_L points) it implies manipulating matrixes of N_L^{3N} elements. We have recently shown [2] that many-particle Bohm trajectories associated to (1) can be computed from a (coupled) system of single-particle time-dependent Schrödinger equations whose numerical complexity is just $N\cdot N_L^3$:

$$i\hbar\frac{\partial\Psi_a(\vec{r}_a,t)}{\partial t}=\left\{-\frac{\hbar^2}{2\cdot m}\nabla_a^2+U(\vec{r}_1[t],.,\vec{r}_a,.,\vec{r}_N[t],t)+G_a(\vec{r}_a,t)+i\cdot J_a(\vec{r}_a,t)\right\}\Psi_a(\vec{r}_a,t) \quad (2)$$

The self-consistent coupling between the electron dynamics obtained from equation (2) and the electrostatic potential (obtained from the 3D Poisson solver) is achieved by using Bohm trajectories [2]. From a numerical point of view, we compute the total current, *I (t),* using a quantum version of Ramo-Shockley theorem [3], without numerical approximations, through a volume Ω limited by a surface S (See Fig. 1):

$$I(t)=-\int_{\Omega}\vec{F}(\vec{r})\cdot\vec{J}_p(\vec{r},t)\cdot d^3\vec{r}+\int_{S}\vec{F}(\vec{r})\cdot\varepsilon(\vec{r})\cdot\frac{\partial}{\partial t}A_o(\vec{r},t)\cdot d\vec{s} \quad (3)$$

In order to show the numerical viability of our approach and the great interest of the DTD at the THz gap, we develop three different THz applications: a rectifier, a harmonic generator, and an amplitude modulator [4]. In Fig. 2, we show a THz rectifier for a primary set of DTD parameters (i.e. the geometries of the barriers, quantum well, dielectric and contact shown in Fig. 1) with a input gate voltage $V_G(t)$ [see dashed line in Fig. 2]. The output voltage rectifies the signal [see solid line in Fig. 2] because negative gate voltages produce a very opaque barrier. In Fig. 3(a), we show a THz harmonic generator for a second set of DTD parameters and an input gate voltage $V_G(t)$ [see dashed line in Fig. 3(a)]. In this case, we accommodate three resonant energies inside the quantum well. The output voltage

[solid line in Fig. 3(a)] oscillates several times during a period of the input signal. The frequency multiplication is due to the fact that the DTD current acquires a maximum each time that a resonant energy of the quantum well crosses the Fermi energy. The power spectral density for output voltage is plotted in the solid line of Fig. 3(b) to show the harmonic generation. In Fig. 4(a), we show an amplitude modulator for THz frequencies for a third set of DTD parameters with a input gate voltage $V_G(t)$ and the input voltage $V_{in}(t)$ [see dashed and dotted lines, respectively, in Fig. 4(a)]. The output voltage [solid line in Fig. 4(a)] and its power spectral density [Fig. 4(b)] clearly show an amplitude modulator.

In conclusion, in this conference, we present a novel approach for the self-consistent simulation of the time-dependent total (conduction plus displacement) current in mesoscopic tunneling devices at THz frequencies [2]. This numerical approach is applied for the computation of tunneling currents in three different DTD configurations for developing (single-device and room temperature) THz applications [4].

References:

[1] C. Gmachl et al., Rep.Prog.Phys., 64, p. 1533, Nov. 2001.

[2] X.Oriols, Physical Review Letters, 98, 066803 (2007).

[3] X.Oriols A. Alarcón and E. Fernandez-Díaz, Physical Review B, 71, 245322 (2005).

[4] X.Oriols, F.Boano and A. Alarcón Appl. Phys. Lett. 92, 222107 (2008).

Figures

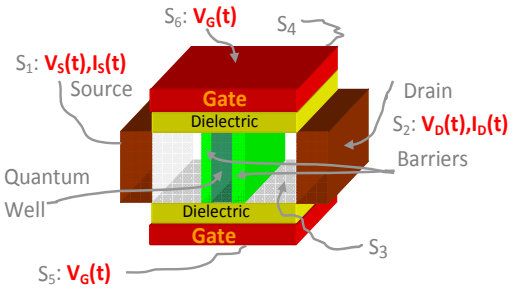

Fig. 1. 3D representation of the active region of the D. It consists in a double barrier structure inside a double-gate transistor-like tunneling electron device.

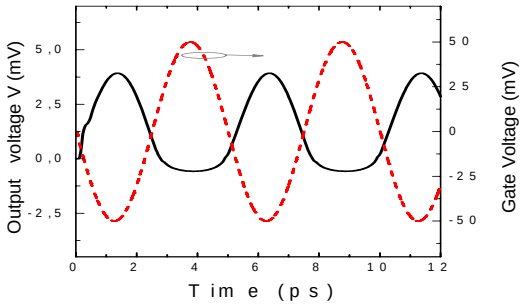

Fig. 2. (Solid line) Calculated output current for a THz rectifier. (Dashed line) input gate voltage $V_G(t)$.

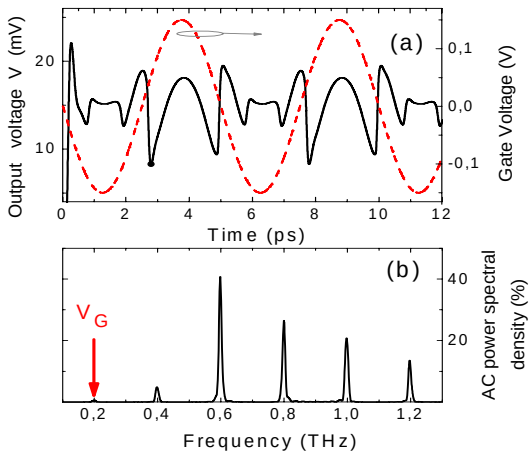

Fig. 3. *(a)* (Solid line) Calculated output current for a THz harmonic generation. *(b)* Calculated power spectral density.

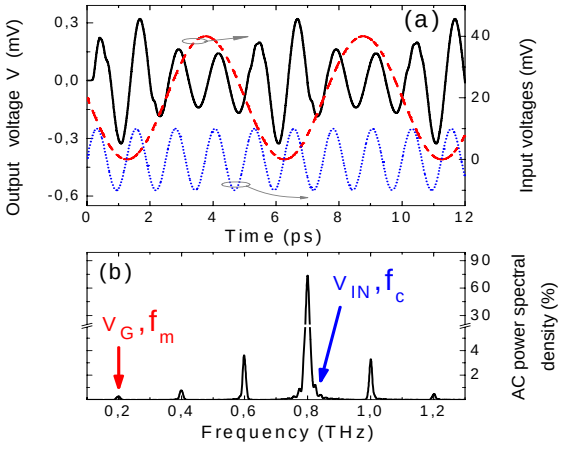

Fig. 4. *(a)* Amplitude modulated current (solid line), carrier input voltage (dotted line), and modulating gate voltage (dashed line) as a function of time. (*b*) Calculated power spectral density.

Ratchet effects on domain wall motion in Co-Si amorphous films with arrays of asymmetric holes: experiments and theoretical simulations

Alejandro Alija,[1] A. Pérez-Junquera,[1] G. Rodríguez-Rodríguez,[1] M. Vélez,[1] L.M. Álvarez-Prado,[1] J.M. Alameda,[1] J.I. Martín[1], J.V. Anguita,[2] Y. Souche,[3] V.I. Marconi,[4] A.B. Kolton,[4] and J.M.R.Parrondo.[4]

1. Depto. Física, Universidad de Oviedo - CINN, Oviedo, Asturias, Spain.
2. Depto. Dispositivos, Sensores y Biosensores, Instituto de Microlectrónica de Madrid (CNM-CSIC), Madrid, Comunidad de Madrid, Spain.
3. NANO, Institut Néel, CNRS and Universite Joseph Fourier, Grenoble, France.
4. Depto. Física Atómica, Molecular y Nuclear, and GISC, Universidad Complutense de Madrid, Madrid, Comunidad de Madrid, Spain.

alija@condmat.uniovi.es

The study of domain wall (DW) movement in magnetic films has long attracted a great interest since it provides both the basis for a wide number of magnetic devices [1] and a good experimental system to analyze the basic physics of an elastic interface in the presence of either ordered or random pinning defects [2,3]. When the pinning potential is asymmetric it can behave as a ratchet, so that DW propagation is favored in one direction. One of the first ratchet potentials used in the field magnetism were “angelfish” patterns that control the sense of propagation of bubble domains in shift registers [4]. Also, asymmetric motion of domain walls (DWs) in nanowires with triangular [5] or notched [6] shapes has been reported recently. However, up to now, in order to ensure a good control of the DW nucleation/propagation process, in all these cases DW motion has been confined to an essentially 1D path, so that its transverse wandering can be neglected. On the other hand, in a thin extended film with a 2D array of asymmetric pinning centers, novel ratchet phenomena can appear since a DW behaves as an elastic line that can distort all along its length in response to the 2D pinning potential.

In this work, the propagation of DWs in extended uniaxial Co-Si amorphous films patterned with a periodic array of asymmetric holes (see Fig.1) has been studied. For the first time, we have experimentally observed and theoretically simulated the existence of two crossed ratchet effects of opposite sign that change the preferred sense for DW motion depending on whether a flat or a kinked wall is moving.

When a magnetic field is applied to push a flat DW across the asymmetric holes, the DW moves more easily (i.e. with lower coercivity) in the direction in which the length of the pinned wall between two antidots increases smoothly. This asymmetric pinning has been experimentally observed [7] and confirmed by both numerical [7] and micromagnetic simulations with the OOMMF code [8]. In addition, micromagnetic simulations have been carried out on films with square arrays of triangular holes in order to optimize the flat domain wall ratchet effect as a function of the triangle base size (see Fig 2).

The novel ratchet behavior appears as the pinned wall inside the array develops kinks. This provides an extra mechanism for DW motion only possible in a 2D geometry through upward/downward kink propagation. This novel ratchet mechanism has an opposite sign in comparison to the flat DW ratchet and dominates the low field behavior. The interplay between both ratchets implies that the system keeps memory of the sign of the magnetization before a DW enters the array of asymmetric holes.

Work supported by Spanish CICYT (grants NAN2004-09087, MOSAICO and FIS2005-07392) and FICYT PhD grant ref BP06-109.

References:

[1] C.D. Mee and E.D. Daniel, Magnetic Storage Hand-book(1996) (New York: McGraw-Hill); G. Prinz, J.Magn. Magn. Mater. 200, 57 (1999).
[2] S. Lemerle et al., Phys. Rev. Lett. 80 849 (1998).
[3] E. Martínez et al., Phys. Rev. Lett. 98, 267202 (2007).
[4] N. Hayashi et al., IEEE Trans. on Magn. 8 370 (1972).
[5] D.A. Allwood et al., Appl. Phys. Lett. 85, 2849 (2004).
[6] A. Himeno et al., J. Appl. Phys. 97, 066101 (2005); M.Hayashi et al., Phys. Rev. Lett. 97, 207205, (2006); S.Savel'ev et al., New J. Phys. 7, 82(2005).
[7] A. Pérez-Junquera et al Phys. Rev. Lett. 100, 037203 (2008)
[8] OOMMF available at http://math.nist.gov/oommf

Figures:

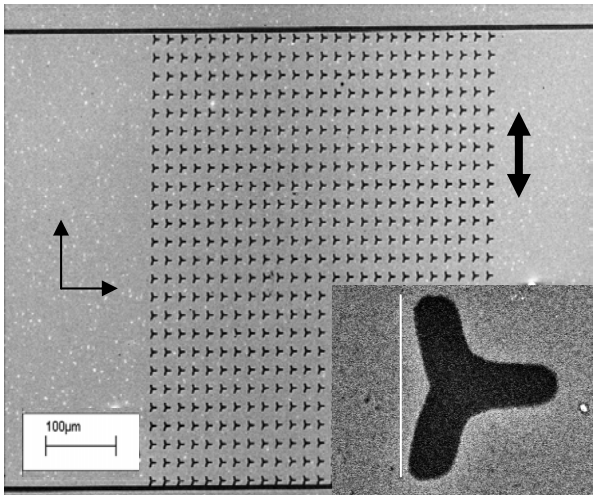

Fig.1 *Scanning electron microscopy image of an array of asymmetric holes on an uniaxial Co-Si film. Easy axis direction is indicated.*

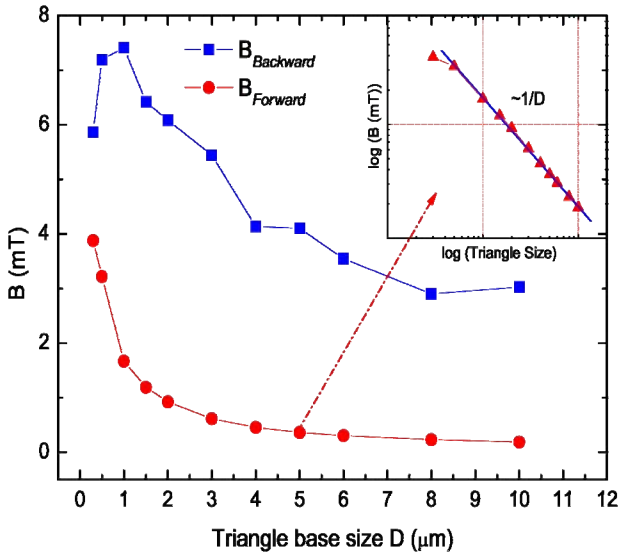

Fig.2 *Forward and Backward magnetic field related to the pinning and the de-pinning field. Inset shows 1/D law dependence of the depinning field versus triangle base size.*

INTERMATRIX SYNTHESIS OF METAL NANOPARTICLES WITH CORE-SHELL OR CORE-SANDWICH STRUCTURE FOR ANTIBACTERIAL APLICATIONS

A. Alonso[1,2], M. Muñoz[2] and D.N. Muraviev[1].*

[1] *Grup de Sensors i Biosensors (GSB), Unitat de Química Analítica, Departament de Química, Universitat Autònoma de Barcelona, 08193 Bellaterra, Barcelona, Spain*
[2] *Grup de Tècniques de Separació (GTS), Unitat de Química Analítica, Departament de Química, Universitat Autònoma de Barcelona, 08193 Bellaterra, Barcelona, Spain*
*Corresponding author: Dmitri N. Muraviev, Phone: +34 93 5814860, Fax: +34 93 5814860, e-mail: Dimitri.Muraviev@uab.es

Metal nanoparticles (MNPs) have some unusual physical and chemical properties in comparison with bulk metals, what opens in certain instances new routs for their practical applications. The main drawback of MNPs is a great tendency for aggregation that results in their uncontrollable growth and the loss of their unique characteristics. A possible solution of this problem can be immobilization of MNPs in stabilizing polymers by using the Intermatrix Synthesis (IMS) technique. In this case the polymer matrix serves both to synthesise MNPs and to protect them against undesirable aggregation and coalescence.

In this presentation we report the synthesis and characterization of MNPs with core-shell and core-double-shell (or core-sandwich) structures of the following compositions: Ag@Cu (Ag-shell at Cu-core) and Ag@Co-Ni@Cu with various thicknesses of Ag and Co-Ni shells. The use of copper as the core-forming metal has been shown to allow for easily increasing the population density of core MNPs in the polymer matrix. The coating of Co-MNPs with Ag-shell permits to produce polymer-metal nanocomposite with bactericide properties, however the escape of Ag@Cu-MNPs from the immobilizing polymeric matrix can result in undesired post-contamination of the treated liquid (e.g., water). The proposed solution of this problem is to use ferromagnetic core-MNPs coated with Ag-shell. In this case the escape of MNPs can be easily prevented by using electromagnetic traps. The first coating of Cu-MNPs with Co-Ni-shell allows for converting the diamagnetic core into the ferromagnetic one followed by the final coating with silver-shell. The characterization of MNP sizes and compositions was done by using TEM and ICP-OES techniques, respectively. The structural parameters of core-shell and core-sandwich MNPs were calculated by using a simple model, recently proposed by the authors [1]. Optimization of IMS conditions for the synthesis of MNPs with desired structural and stability parameters was carried out in the sulfonated polyetherether keton (SPEEK) membranes. The final synthesis of MNPs with optimal parameters has been carried out in the FIBAN-K4 matrix (fibrous analogue of SPEEK), which is better applicable for the water treatment purposes. The results of water disinfection tests by using FIBAN-MNP nanocomposite filter are also presented and discussed.

Figures

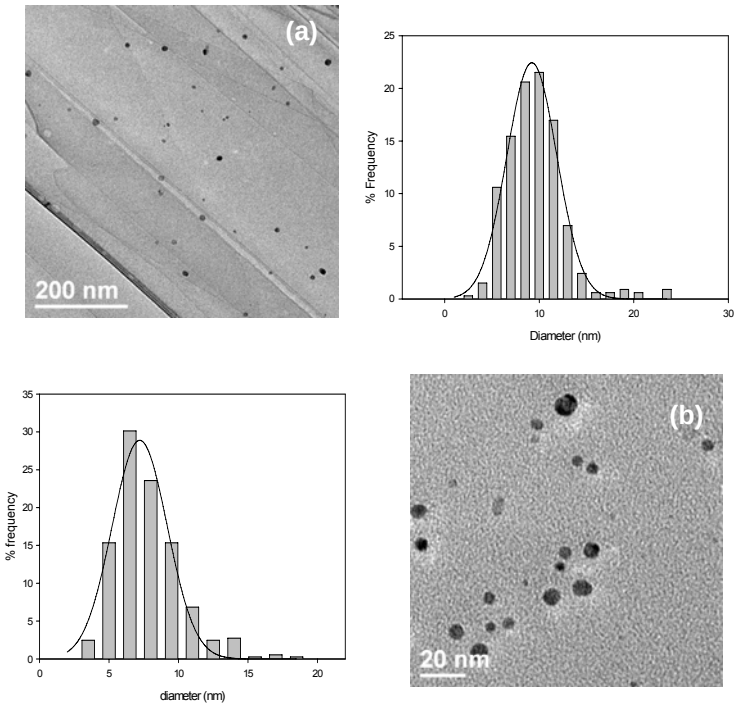

Figure 1. Typical TEM images and corresponding size-distribution histograms of Ag@CoNi@Cu MNPs obtained after loading with 16.0 mmols Ag/g membrane (a) and 1.5 mmols Ag/g membrane (b), respectively.

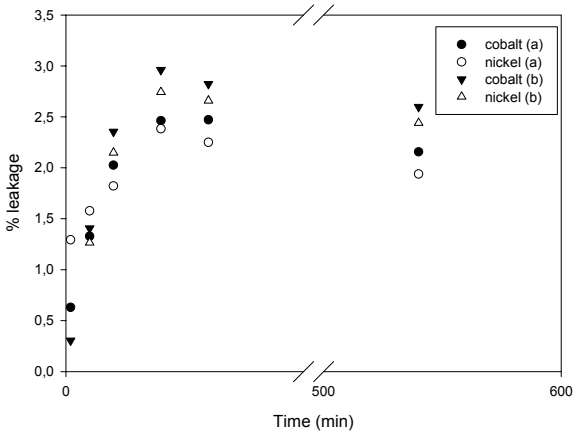

Figure 2. Percentage of Co^{2+} and Ni^{2+} leakage relative after treatment with HCl of Ag@CoNi@Cu MNPs (a) and with three times more quantity of CoNi alloy (b).

References

1. D.N. Muraviev, Contrib. Sci. 3(1), 19 (2005).
2. J. Macanas, J. Parrondo, M. Muñoz, S. Alegret, F. Mijangos, D.N. Muraviev, Phys. Stat. Sol. (a) 204, 1699 (2007).

METALORGANIC NANOSTRUCTURES: 2D- EXTENDED STRUCTURES

L. Álvarez, R. Caillard, J.A. Martín-Gago and J. Méndez
Instituto de Ciencia de Materiales de Madrid (CSIC), Cantoblanco 28049 Madrid.
lualpima@icmm.csic.es

ABSTRACT:

Nanotechnology is being developed as a new and very promising field of science. Very different kinds of nanomaterials are studied nowadays all around the world, looking for new materials which combine properties and applications. For example, hybrid materials obtained by a combination of inorganic and organic units, present properties and applications derived from their mixed nature [1] resulting metalorganic nanostructures, with different electronic properties than the original organic molecules.

In this work, we present a summary of nanostructuring phenomena using self-organizing strategies for structuring materials in the nanoscale range. We have studied by STM the structures resulting from the combination of iron atoms and organic molecules of PTCDA on a gold substrate. These metalorganic compounds presumably combine the properties of its components,. By choosing the growth conditions (substrate temperature and adsorbates quantities) we can control the structural order and form different stable nanostructures. Previously reported nanostructures [2], organic nanodots and molecular chains, result from linking PTCDA molecules with iron atoms, and present a modified electronic structure different than the one observed for the organic material. Next structure is the "ladder-like", resulting from two chains connected by perpendicular PTCDA molecules like the rungs of a ladder. These ladder structures can be extended over the entire surface. Figure 1 shows a STM image corresponding to a 0.9ML growth of this metalorganic 2D- structure. The image shows several domains of this "extended-ladder" structure, where the PTCDA molecules are clearly distinguished. This structure is stabilized by the iron, as it is never observed without the iron. The model for this structure suggests one iron atom per PTCDA molecule.

We have checked the stability of this structure by exposing it to oxygen atmosphere and annealing it at 420K, and no substantial changes have been observed. Finally, we have extended the growth for more than the monolayer, 1.4ML, where order at the second layer has been observed.

References:

[1] For a review on hybrid materials see for example the special issue: *Journal of Materials. Chemistry* **15** (2005).
[2] J. Méndez, R. Caillard, R. Otero, N. Nicoara, and J.A. Martín-Gago, *Advanced Materials* **18** (2005) 2048-2052.

Figures:

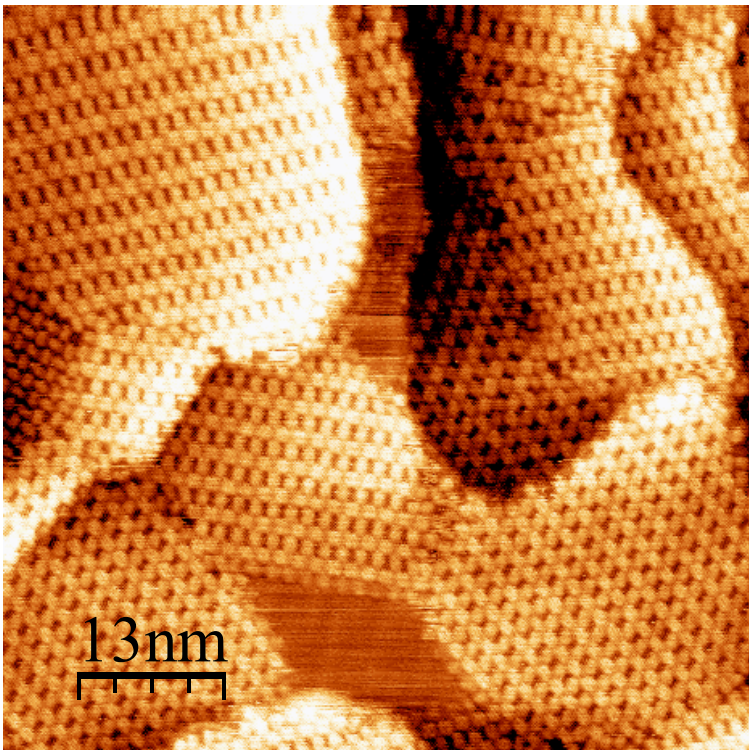

Figure 1. STM image of a gold substrate covered with 2D- metalorganic structures combining PTCDA organic molecules and iron atoms. It is remarkable that this structure is not observed in pure PTCDA growth.

MAGNETO-VOLUME ANOMALIES AND MAGNETOCALORIC EFFECT ON BALL-MILLING NANOSTRUCTURED Pr_2Fe_{17} COMPOUNDS

P. Álvarez[1], *J. L. Sánchez Llamazares*[1], *P. Gorría*[1], *J. A. Blanco*[1], *J. Sánchez Marcos*[2]
[1]*Departamento de Física, Universidad de Oviedo, Calvo Sotelo, s/n, 33007 Oviedo, Spain.*
[2]*Institut Laue Langevin, 38100, Grenoble, France.*
alvarezpablo.uo@uniovi.es

Intermetallic Pr_2Fe_{17} alloy crystallizes in the rhombohedral Th_2Zn_{17}–type crystal structure (space group $R\bar{3}m$), showing a ferromagnetic behaviour with a high spontaneous magnetization below its Curie Temperature (T_C = 285 K) [1]. The interest on this compound has been recently renewed due to its relatively high magnetocaloric effect in a broad temperature interval around room temperature, and a relative cooling power even higher than the reported value for $Gd_5(Si_{1-x}Ge_x)_4$. Strong magneto-volumic anomalies are also present, such as anomalous thermal expansion. As the magnetic behaviour of this alloy is determinated by exchange interactions between nearest-neighbours Fe atoms [2], changes in the structure can alter its magnetic properties. For this reason, we use high-energy ball milling in order to nanostructurate it with the aim of study the crystalline structure and the magnetic behaviour before and after milling. From the analysis of both X-Ray (K radiation Cu, = 1.5418 Å) and neutron at D2B (ILL) high resolution powder diffraction patterns, we conclude that after 10 hours milling (BM-10h) the almost single rombohedrical 2:17 phase persist with a slightly increase of cell parameters (less than 0.05%) and no evidence of microstrain due to the severe mechanical treatment, as it appears in other Fe-based compounds [3]. In addition, there is an important decrease of peak intensity and a huge broadening of the peak width after milling, which come from the formation of nanonoparticles with average crystalline grain size ≈ 20 nm. TEM images confirm that milled sample is nanostructurated with a grain size in the range 7 - 50 nm. An analysis of SEM images shows that these nanoparticles are forming micronic agglomerates with sizes of about 0.5 - 5.0 m.

Magnetization as a function of temperature, measured under an applied magnetic field $\mu_0 H$ = 20 mT, shows a well-defined T_C at 286 ± 1K in the case of bulk sample, whereas for the milled one is not possible to determine accurately a T_C, due to the fact that ferromagnetic to paramagnetic transition becomes broad. Moreover, this transition temperature shifts toward larger temperatures (305 ± 15 K). Magnetocaloric effect, i.e. the variation of magnetic entropy with magnetic field and temperature, is evaluated from the M(H,T) curves. A decrease of the peak of $|S_M|$ from 6.3 to 4.5 J kg^{-1} K^{-1} under an applied magnetic field $\mu_0 H$ = 5 T for both bulk and ball milled samples respectively is observed. Nevertheless, a broadening on the $|S_M(T)|$ curve entails an increase of the RCP value, defined as the product of $|S_M|$ peak value and the full width at half maximum.

Temperature dependence of cell volume is obtained from neutron thermo-diffraction experiments at D1B (ILL) in the temperature range 10 - 450 K. In Both samples the volume has a minimum near T_C, which is deeper and sharper in the case of bulk sample. Cell volume at 300 K (where milling process takes place) and 6c-6c Fe-Fe interatomic distances are greater in the milled one, which favours ferromagnetism and therefore increase the Curie temperature in the BM-10h sample.

References:

[1] D. Givord et al., IEEE Trans. Mag., **MAG-7** (1971) 657.
[2] M.S. Ben Kraiema et al., J. Magn. Magn. Mater. **256** (2003), 262.
[3] P. Gorria et al., J. Magn. Magn. Mater. **294** (2005), 159.

Figures:

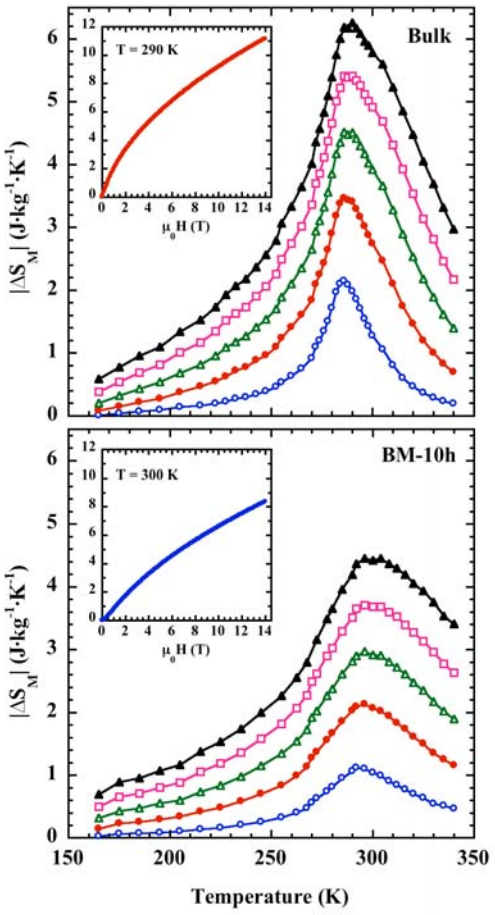

Fig. 1: Magnetic entropy change $|\Delta S_M|$ of Bulk (upper panel) and BM-10h (lower panel) samples under applied magnetic fields of 1 T (open circles), 2 T (solid circles), 3 T (open triangles), 4 T (open squares) and 5 T (solid triangles). The insets show $|\Delta S_M|$ vs. $\mu_0 H$ up to 14 T for each material

A THEORETICAL COMPARISON OF STRIP AND VERTICAL SLOT-WAVEGUIDE RESONATORS IN SILICON NITRIDE FOR SENSING PURPOSES

Jesús Álvarez[1], Laurent Vivien[2], Delphine Marris-Morini[2] Carlos Angulo Barrios [3], Daniel Hill[1]*

[1] Nanophotonics Technology Center, Universidad Politécnica de Valencia, Camino de Vera s/n, Valencia, Spain

[2] Institut d'Electronique Fondamentale, CNRS UMR 8622, Bât. 220, Université Paris-Sud 11, F-91405 ORSAY cedex – France

[3] Instituto de Sistemas Optoelectrónicos y Microtecnología, Universidad Politécnica de Madrid, ETSI Telecomunicación, Ciudad Universitaria s/n, 28040 Madrid, Spain

[*]Corresponding author: jealal@ntc.upv.es

For biosensing applications where small refractive index variations of the surrounding medium are monitored, light needs to have a strong interaction with such a surrounding biological medium. This is not the case for classical rib [1] and strip [2] waveguides where light is predominantly guided in the high index material. However, in slot waveguides, light is confined in a low index slot region sandwiched between two high index rails and due to the discontinuity of the electric field at the interface between the rails and slot, a significant fraction of the electromagnetic field is localized in the slot. As such slot waveguides present an interesting alternative [3] for biosensing applications especially when made using silicon nitride [4] which permits slot widths of up to 200nm and as such reachable fabrication tolerances, and reduced propagation losses [5] compared to silicon slot waveguides with its higher refractive index contrast. Furthermore, for biosensing, the wider slot facilitates sample transport [6] and using a multiple-slot structure, further enhancement of the optical confinement in low index slot regions is possible [7-8]. In this paper we present work in progress of theoretical modeling for strip, slot and multiple-slot waveguides and compare their characteristics for sensing purposes.

The electrical field of the quasi-TE mode at the wavelength of 1.3 um for the three structures is reported in fig. 1. For the strip and slot waveguides their heights are set to 300nm for good optical confinement, the strip waveguide width is of 900nm to reach single mode propagation. The width of rails for the slot waveguide is 400nm while the the slot's width is fixed at 200 nm. For the multiple-slot waveguide, its thickness is set to 400 nm to obtain a good confinement and the width of the central rail to 200 nm and that of the outer rail 250nm.The Beam Propagation Method was then used to determine the variation of effective index as a function of the add-layer refractive index changes for the three structures. For TE polarization, the effective index variation of the guided mode for the multiple-slot structure is twice that of a typical slot waveguide, and four times as much as that for strip waveguides (Figure 2) for a given variation of add-layer refractive index. The limit of detection (LOD) of the index variation is inversely proportional to these values. Thus, this clearly demonstrates the suitability of the multiple-slot structure for sensing purposes.

This work was done within the European Commission funded FP6-IST-SABIO project (026554).

References:

[1] S. Lardenois, D. Pascal, L. Vivien, E. Cassan, S. Laval, R. Orobtchouk, M. Heitzmann, N. Bouaida, L. Mollard, Opt. Lett. 28, 1150-1152, (2003).

[2] P. Dumon, W. Bogaerts, V. Wiaux, J. Wouters, S. Beckx, J. Van Campenhout, D. Taillaert, B. Luyssaert, P. Bienstman, D. Van Thourhout and R. Baets, IEEE Photon. Technol. Lett **16**, 1328-1330, 2004.
[3] V. Almeida, Q. Xu, C.A. Barrios and M. Lipson, Opt. Lett. 29, 1209-1211 (2004)
[4] C. A. Barrios, B. Sànchez, K.B. Gylfason, A. Griol, H. Sohlström, M. Holgado and R. Casquet, Opt. Express 15, 6846-6857 (2007)
[5] T. Baehr-Jones, M. Hochberg, C. Walker, A. Scherer, Appl. Phys. Lett. 86, 081101 (2005)
[6] C.A. Barrios, M. J. Bañuls, V. Gonzàlez-Pedro, K.B. Gylfason, B. Sànchez,A. Griol, A. Maquieira, H. Sohlström, M. Holgado and R. Casquet, Opt. Lett. 33, 708-710 (2008)
[7] R. Sun, P. Dong, N-N. Feng, C-Y Hong, J. Michel, M. Lipson, L. Kimerling, Opt. Express 15, 17967-17972 (2007)
[8] L. Vivien, D. Marris-Morini, A. Griol, K. B. Gylfason, D. Hill, J. Álvarez, J.Hurtado, H. Sohlström, D. Bouville and E. Cassan, [Submitted to Optics Express]

Figures:

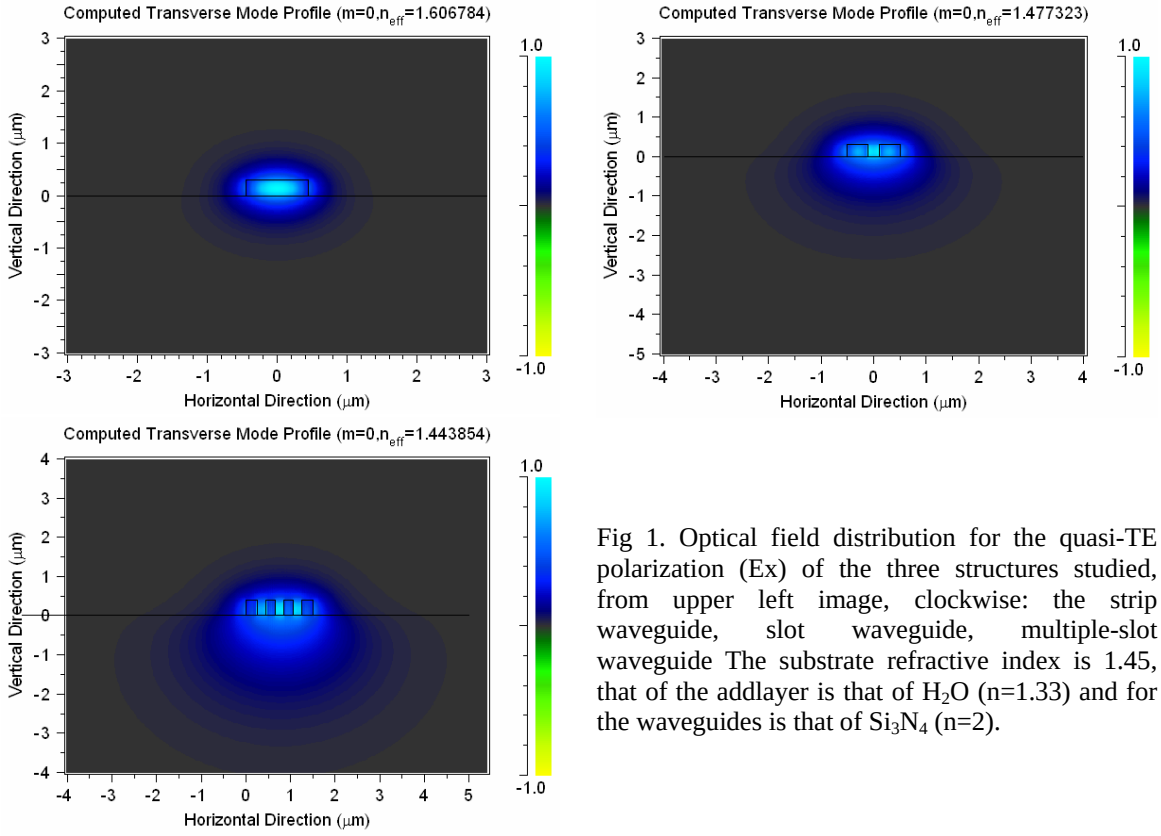

Fig 1. Optical field distribution for the quasi-TE polarization (Ex) of the three structures studied, from upper left image, clockwise: the strip waveguide, slot waveguide, multiple-slot waveguide The substrate refractive index is 1.45, that of the addlayer is that of H_2O (n=1.33) and for the waveguides is that of Si_3N_4 (n=2).

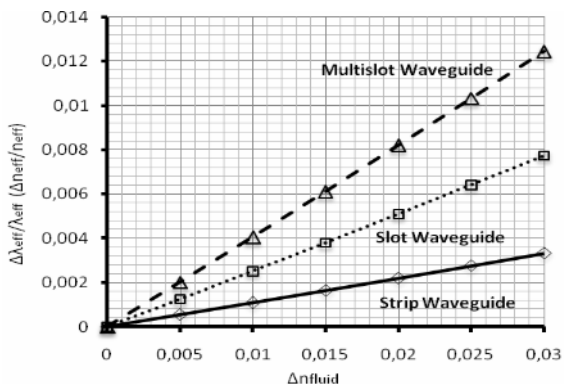

Fig 2. Simulation results for the three different waveguides. (Δn_{fluid} = change in addlayers refractive index, $\Delta n_{eff}/n_{eff}$ = change of effective refractive index normalized to the effective index for n_{fluid} = 1.33)

SYNTHESIS AND CHARACTERIZATION OF Mn-Zn FERRITE MAGNETIC NANOPARTICLES BY THE MICROEMULSION REACTION METHOD

Carolina D. Aubéry, Margarita Sánchez-Domínguez and Conxita Solans
Consejo Superior de Investigaciones Científicas (CSIC)
Instituto de Investigaciones Químicas y Ambientales de Barcelona (IIQAB)
CIBER en Biotecnología, Biomateriales y Nanomedicina (CIBER BBN)
Jordi Girona 18-26, 08034 Barcelona, Spain.
Fax: +34 93 2045904
e-mail: catqci@iiqab.csic.es, msdqci@iiqab.csic.es, csmqci@iiqab.csic.es

The development of novel and more efficient methods of nanoparticle preparation generates a great interest in areas such as chemistry, biology, physics and medicine. Conventional methods for the synthesis of nanoparticles, such as co-precipitation, sol-gel and impregnation processes, are often not capable of resulting in the very small and controlled size required in catalysis and other applications, in spite of modern refining which is present in such methods [1]. Other methods, such laser evaporation, sputtering, ionized beam deposition, laser or flame spray pyrolysis, chemical vapour deposition, sonochemical processing, etc. involve the use of complicated and expensive equipment. Hence, in recent years there has been a growing interest in the synthesis of nanoparticles by the microemulsion reaction method (MRM), which consists in promoting reactions of formation of species in small droplets of nanometric size, each of which could be considered as an individual nano-reactor [2]. Such technique has been used recently in the synthesis of nanoparticles (5-7 nm) formed by mixtures of oxides of Zr-Ce [3], as well as in the fabrication of oxide nanocatalysts active in reforming reactions [4]. It has also been used for the synthesis of spinels and perovskites [5, 6], and in some cases pure spinel phases have been obtained directly in the microemulsion [7].

Recently, Kosăk et al have shown that it is possible to synthesize nanostructured spinels [7] at relatively low temperature (50ºC), obtaining the pure crystalline phase directly in the microemulsion, without the need of calcination. In those studies, as well as in most of the investigations cited above, the surfactants used for microemulsion formation have been of the ionic type, such as single chain surfactants, alkyl sulphates or quaternary ammonium salts (which require a cosurfactant, a medium chain alcohol), as well as double-chain alkyl sulfosuccinate or Aerosol OT. Nonionic surfactants of the nonylphenol ethoxylated type have been used as well. The use of ionic surfactants has some drawbacks, as complex functional species could be absorbed at the particle surface and interfere with its growth as well as with the reaction itself. If ceramic materials whose properties are highly dependant on metallic dopant species are to be synthesized, the use of ionic surfactants (especially of the anionic type) should be avoided in order to prevent contamination with surfactant counterions. The possibility of using commercial linear nonionic surfactants with the appropriate HLB could help to overcome these drawbacks.

The aim of the present study is to explore the potential of nonionic microemulsion systems for the synthesis of mixed ceramic oxides, namely Mn-Zn ferrites. The mixed oxide chosen, Mn-Zn ferrite, is of interest in the biomedical field due to potential super paramagnetic properties and hence possible applications as a Magnetic Resonance Imaging (MRI) contrast agent. In addition, it could be useful as a starting point or model for the future synthesis of a variety of nanostructured spinels and perovskites, which could have potential applications in the catalytic production of hydrogen from alcohol and hydrocarbon fuels, thereby promoting a fundamental advance in the preparation of active and economical catalysts for the reforming processes.

The phase behavior of a ternary aqueous solution/nonionic surfactant/hydrocarbon system was investigated in order to identify w/o microemulsions, in the presence of the metallic precursors, or precipitant agent. Addition of cosurfactant was also investigated, in order to optimize the formulations in terms of surfactant content. The microemulsions were characterized by diverse techniques (conductimetry, Pulse-Field Gradient NMR, Dynamic Light Scattering, Small Angle Neutron Scattering), in order to determine their structure and size. Selected microemulsions with different compositions were used in order to determine its influence on the characteristics of the nanoparticles. Characterization of the obtained materials was performed by transmission electron microscopy, X-Ray Diffraction, and magnetic properties. Nanoparticles in the same size range of the microemulsions (3-10 nm), and with spinel-type crystalline structure were obtained (Figure 1), demonstrating the microemulsion template effect. The results suggest that these environmentally friendly microemulsion systems could be useful for the preparation of nanostructured mixed oxides and other materials, which could have potential applications in the catalytic production of hydrogen from alcohols and hydrocarbon fuels, as well as for the preparation of superparamagnetic nanoparticles with potential application as MRI agents.

Acknowledgements

Financial support from MEC (grant CTQ2005-09063-CO3-O2) and Generalitat de Catalunya (grant 2005-SGR-00812) is acknowledged. M.S.D. is grateful to CSIC for a JAE-Doc contract.

References:

[1] Cushing, B. L.; Kolesnichenko, V. L.; O'Connor, C. J. *Chem. Rev.*, **104** (2004) 3893.
[2] Lopez-Quintela, M. A.; Tojo, C.; Blanco, M. C.; Garcia Rio, L.; Leis, J. R. *Curr. Opin. Colloid Interface Sci.*, **9** (2004) 264.
[3] Martinez-Arias, A.; Fernandez-Garcia, M.; Hungría, A. B.; Conesa, J. C.; Munuera, G. *J. Phys. Chem. B*, **107** (2003), 2667.
[4] Agrell, J.; Boutonnet, M.; Melian-Cabrera, I.; Fierro, J. L. G. *Appl. Catalysis A-General*, **253** (2003), 201.
[5] Giannakas, A.E.; Vaimakis, T.C.; Ladavos, A. K.; Trikalitis, P. N.; Pomonis, P.J. *J. Colloid Interface Sci*., **259** (2003) 244.
[6] Giannakas, A. E.; Ladavos, A. K.; Armatas, G. S.; Petrakis, D. E.; Pomonis, P. J. *Appl. Surf. Sci*., **252** (2006), 2159.
[7] Makovec, D.; Košak, A.; Drofenik, M. *Nanotechnology*, **15** (2004) S160.

Figures:

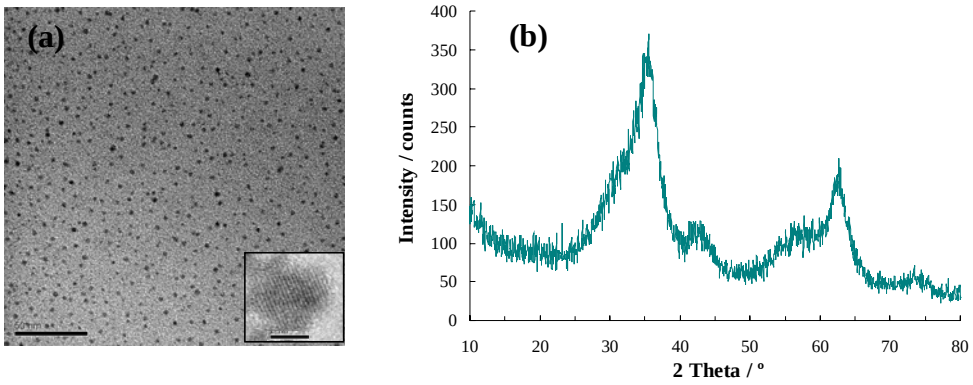

Figure 1. (a) High Resolution Transmission Electron Microscopy (HRTEM) of Mn-Zn ferrite nanoparticles obtained by MRM. Scale bar 50 nm (scale bar in inset 20 nm). (b) X-Ray Difraction (XRD) pattern for Mn-Zn ferrite nanoparticles obtained by MRM.

FORMATION AND ELECTRICAL INTERFACING OF NANOCRYSTAL-MOLECULE NANOSTRUCTURES

Claire Barrett, Aidan J. Quinn
Nanotechnology Group, Tyndall National Institute,
University College Cork, Lee Maltings, Cork, Ireland
claire.barrett@tyndall.ie

Investigation of the opto-electronic properties of single molecules remains a significant challenge, driven both by the scientific vision of wavefunction engineering at the nanometre scale and by the technological vision of molecules as functional building blocks in future nanoelectronic devices, circuits and architectures. However, interfacing individual molecules (~ 1 nm long) using top-down lithography remains a significant challenge. Ligand-stabilised inorganic nanocrystals (~2-30 nm core diameter) represent attractive candidates to bridge the gap between feature sizes routinely available using top-down lithograpy (30-50 nm) and the molecular length scale; see Figure 1. Nanocrystal-molecule assemblies also offer the potential for formation of nanostructures and architectures with novel (opto-) electronic properties arising from the individual characteristics of the nanocrystal and molecular building blocks and also the collective properties of the assembly.

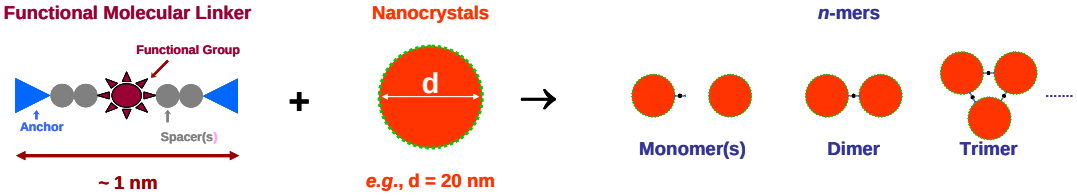

Figure 1. Schematic of solution-based formation of nanocrystal-molecule-nanocrystal *n*-mer nanostructures.

We have recently developed a robust process for formation in solution of nanocrystal-molecule *n*-mer nanostructures using ligand-stabilised size-similar metal nanocrystals with core diameters in the range 10-40 nm and bifunctional organic linkers. UV-Visible spectroscopy of these solutions reveals the evolution of a peak close to 630 nm, see Figure 2a, likely due to formation of dimer nanostructures. Scanning electron microscopy (SEM) measurements of the solution following drop-deposition onto Si substrates indicate formation of dimer and higher-order *n*-mer nanostructures (as well as individual "monomer" nanocrystals); see Figure 2b. Statistical analysis of >400 structures counted in SEM images acquired at random locations yields an *n*-mer distribution with ~ 15% dimers; see Figure 2c. Similar distributions can be reproducibly obtained by monitoring the evolution of the UV-Vis response in real-time. Simulations are currently underway to determine the influence of the dimer and higher order *n*-mer populations on the optical properties of the *n*-mer distribution.

We have also developed dielectrophoretic trapping processes for assembly of nanostructures between top-down fabricated contact electrodes (source-drain separations ~ 30 nm). Initial data for d = 20 nm nanocrystals indicate localised trapping of nanocrystal assemblies. Investigations of potential electronic functionality in nanocrystal-molecule *n*-mer structures are in progress.

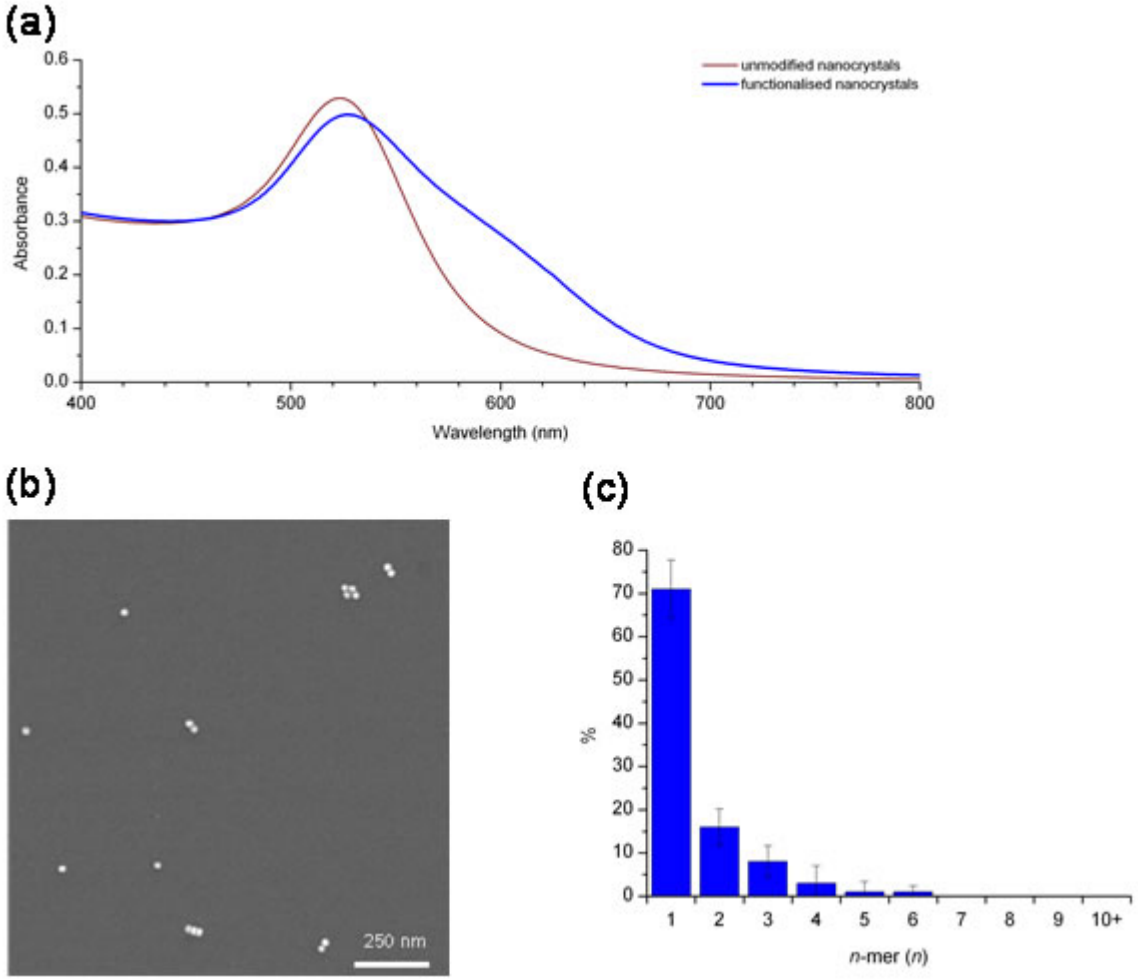

Fig. 2 (a) UV-Visible absorbance spectrum of unmodified d = 20 nm Au nanocrystals (wine) and nanocrystal-molecule nanostructures formed in solution (blue). **(b)** Typical high-resolution Scanning Electron Microscopy image showing a range of *n*-mer nanostructures**. (c)** Histogram showing the distribution of nanostructures corresponding to the UV-Visible absorbance data (blue) acquired in (a).

ELECTRONIC PROPERTIES OF STRONGLY RESHAPED ORGANIC-METAL INTERFACES

Stéphane Bedwani and Alain Rochefort
Département de génie physique, École Polytechnique de Montréal,
et Regroupement québécois sur les matériaux de pointes (RQMP)
Montréal, Canada
Stephane.Bedwani@polymtl.ca

The formation of self-assembled nanostructure on a surface results from a subtle equilibrium between the attractive intermolecular forces and the forces that drive molecules to the substrate. In the case of strong molecule-substrate interactions, molecules can even induce nanoscale surface reshaping, which is now a promising field in materials engineering [1]. In this work, we study the electronic properties of strongly reconstructed organic-metal interfaces using *ab initio* calculations and scanning tunneling microscopy (STM) simulations.

For the electronic structure calculations, we have used the density functional theory (DFT) within a local density approximation (LDA) included in the SIESTA package [2]. DFT-LDA calculations provided fully optimized geometries for each system under study along with their deformation and adsorption energy, density of states (DOS), Mulliken population analysis, and charge density. We also performed STM simulations with our SPAGS-STM (Strongly Parallel Adaptive Grid Solvers – STM) software. The software includes several algorithmic strategies such as parallel computation of the tunnel currents [3] and adaptive grids that minimize the probing sites needed to obtain a high resolution image [4]. In the simulations, the tunnel currents were computed within a scattering approach based on the Landauer-Büttiker formalism along with an extended Hückel theory Hamiltonian originally developed by Cerdá *et al* [5]. The good accuracy of our theoretical method will be shown by comparing a series STM images and dI/dV spectra with experimental data of Lu *et al* [6] on the adsorption of isolated C_{60} on the Ag(100) surface.

With these computational tools, we will address a recent and captivating STM investigation in which the adsorption of tetracyanoethylene (TCNE) molecule leads to striking behaviors on various noble metals [7]. More precisely, TCNE molecules on a Cu(100) surface are self-assembled into monolayer chains and islands where specific Cu atoms near these nanostructures appear strongly buckled. As shown in Fig. 1(a), DFT-LDA calculations predict a strong reconstruction of the Cu(100) surface, where high buckled Cu atoms rise more than 1 Å over the topmost plane. The surface buckling can be associated to a deformation energy of 3.55 eV. Also, a strong molecular bonding to the Cu surface is observed, where at least an energy of 1.65 eV is needed to break a single Cu-N bond. The generated STM image in Fig. 1(b) displays a good concordance with the experimental one and confirms the strong buckling of the Cu(100) surface around TCNE nanostructures. Mulliken population analysis clearly indicates a charge transfer of 0.4 *e* to the TCNE molecule. Other evidences of charge transfer from the high buckled Cu atoms to the TCNE molecule that are based on the shape and on the displacement of peaks observed in DOS will be also presented. These results suggest that TCNE self-assemblies could be used to design charge transfer compounds for molecule-based magnetic devices.

References:

[1] F. Rosei, M. Schunack, Y. Naitoh, P. Jiang, A. Gourdon, E. Laegsgaard, I. Stensgaard, C. Joachim and F. Besenbacher, Progress in Surface Science, **71** (2003) 95–146.

[2] J.M. Soler, E. Artacho, J.D. Gale, A. Garcia, J. Junquera, P. Ordejon, and D. Sanchez-Portal, Journal of Physics Condensed Matter, **14** (2002) 2745–2779.

[3] B.A. Janta-Polczynski, J.I. Cerdá, G. Éthier-Majcher, K. Piyakis and A. Rochefort, Journal of Applied Physics, (2008) in press.

[4] S. Bedwani, F. Guibault and A. Rochefort, Journal of Computational Physics, **227** (2008) 6720–6726.

[5] J. Cerdá. M.A. Van Hove, P. Sautet, and M. Salmeron, Physical Review B, **31** (1997) 15885.

[6] X. Lu, M. Grobis, K.H. Khoo, S.G. Louie, and M.F. Crommie, Physical Review Letter, **90** (2003) 096802.

[7] D. Wegner, R. Yamachika, Y. Wang, V.W. Brar, B.M. Bartlett, J.R. Long, and M.F. Crommie, Nano Letter, **8** (2008) 131–135.

Figures:

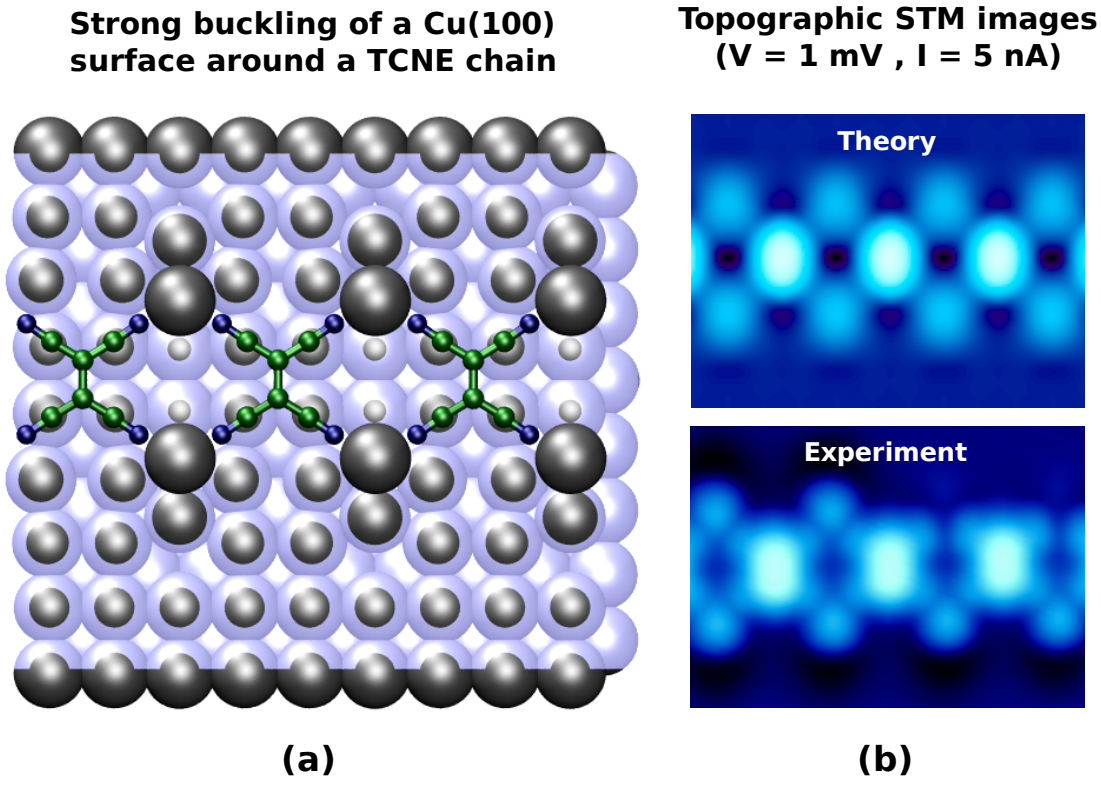

FIG. 1 – (a) DFT-LDA optimized structural geometry for a highly buckled Cu(100) surface around a TCNE chain. A transparent plane is used to guide the eye on the strong reconstruction of the topmost Cu layer. (b) Comparison between topographic STM images of (top) the theoretical model using the SPAGS-STM software and (bottom) experimental data from Ref. [7].

A MODEL FOR THE ULTRASONIC DISPERSION OF NANOPARTICLES IN EPOXY RESIN

Birgit Bittmann, Frank Haupert, Alois K. Schlarb
Institut fuer Verbundwerkstoffe, Erwin-Schroedinger-Str. Geb. 58, 67663 Kaiserslautern, Germany
birgit.bittmann@ivw.uni-kl.de

Nanoparticles in polymer matrices might lead to completely new material properties compared to conventional composites, e.g. an improved mechanical, electrical or optical behavior [1]. Several properties of the material can be enhanced simultaneously, i.e. the fracture toughness and the stiffness [2]. However, therefore a separation and homogeneous distribution of the particles in the matrix material is required in order to profit from the high specific surface of the nanoparticles, that hence can interact as an interphase with the polymer matrix.
In the present project the dispersion of nanoscale titanium dioxide (TiO_2) and barium sulfate ($BaSO_4$) particles in a high viscos epoxy resin by means of ultrasonic waves was studied systematically. The dispersion parameters, e.g. the ultrasonic amplitude and the dispersion time, were optimized to achieve a best possible dispersion. To be able to describe the development of the particle sizes in dependence on the dispersion parameters the dispersion model from Winkler for bead mills [3] was advanced and applied to the ultrasonic process. Thus, the particle size X in dependence on the sonication time t can be calculated by the following expression:

$$X(t) = \left(X_A - e^{-\frac{a^* \cdot P}{\sigma \cdot V_T}} - X_P \right) \cdot e^{-k \cdot \frac{V_{eff}}{V_T} \cdot t} + e^{-\frac{a^* \cdot P}{\sigma \cdot V_T}} + X_P$$

X_A ist he initial and X_P the primary particle size provided by the manufacturer. P describes the power input into the mixture, a* is a coupling constant, that describes the transference of the power to the agglomerates, and σ is the agglomerat's strength. V_{eff} describes the effective volume, where dispersion occurs and V_T is the total volume of the mixtura. The constant k describes te mixing in the prepolymer during sonication.
With the help of the developed model the developement of the particle size during sonication can be described in dependence on different parameters, as can be seen from Figure 1 for the dispersion of TiO_2 in epoxy resin. The transferability of the model to other particle systems was tested and approved by sonication of $BaSO_4$ nanoparticles in the liquid polymer.

References:

[1] Thostenson, Erik T.; Li, Chunyu; Chou, Tsu-Wei, Composites Science and Technology, **65** (2005) 491.
[2] Wetzel, Bernd; Haupert, Frank; Zhang, Ming Qui, Composites Science and Technology, **63** (2003) 2055
[3] Winkler, Jochen, Farbe und Lack, **2** (2006) 35

Figures:

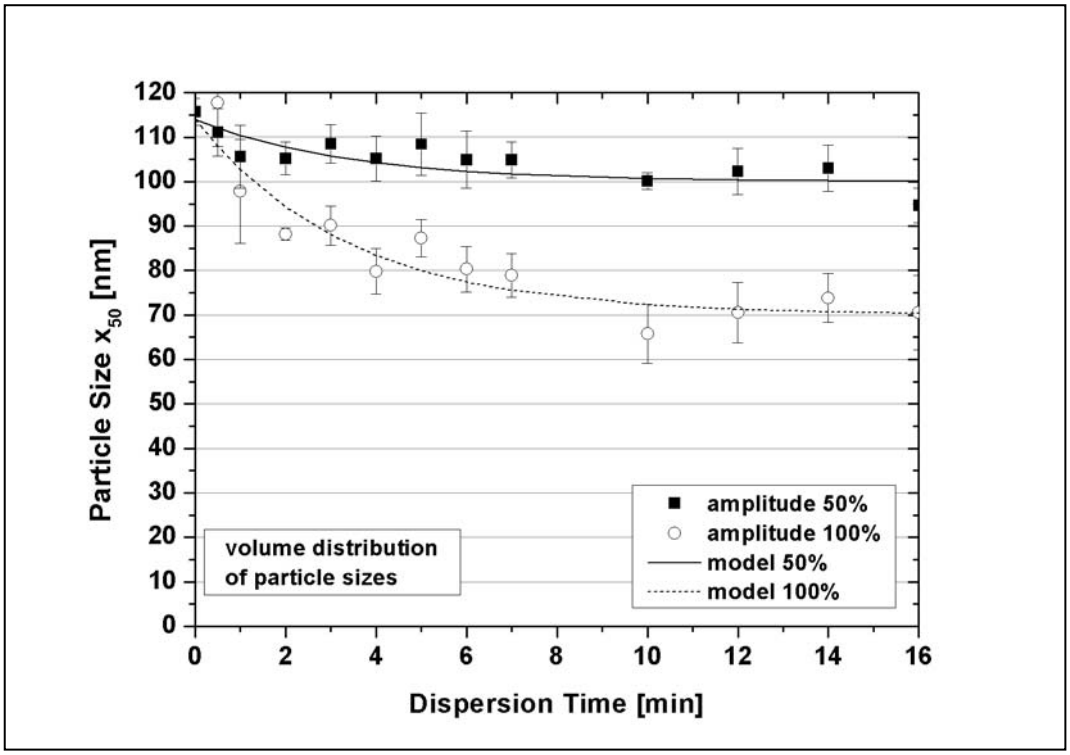

Figure 1: Experimental values and model curve for the ultrasonic dispersion of TiO_2 in epoxy resin at sonication amplitudes of 50 and 100%

A MAGNETIC RESONANCE STUDY OF IRON AND COBALT BASED NANOPARTICLES AS POTENTIAL CONTRAST AGENTS FOR MOLECULAR IMAGING OF CANCER

Barbara Blasiak[1,6], Boguslaw Tomanek[1,6,7], Ulrike Trojahn[2,3], Abedelnasser Abulrob[8,9], Zhijun Zhang[4], Teodor Veres[4,5], Celine Desvaux[4], Umar Iqbal[9], Maureen O'Connor[2,3], Garnette Sutherland[1]

[1]Department of Clinical Neurosciences, University of Calgary, 3330 Hospital Drive NW, Calgary AB T2N 4N1, Canada, [2]Biotechnology Research Institute, National Research Council of Canada, Montreal, QC, Canada, [3]McGill University, Montreal, Canada, [4]Functional Nanomaterials Group, Industrial Materials Institute, National Research Council of Canada, Boucherville, QC, Canada, [5]INRS - Énergie et matériaux Institut national de recherche scientifique, Montreal, QC, Canada, [6]Institute of Nuclear Physics, Polish Academy of Sciences, Krakow, Poland, [7]Institute for Biodiagnostics (West), National Research Council Canada, Calgary, Alberta, Canada, [8]Institute of Biological Sciences, National Research Council Canada, Ottawa, Ontario, Canada, [9]Faculty of Medicine, University of Ottawa, Ottawa, Canada

barbara.blasiak@nrc.ca

Molecular magnetic resonance imaging (MMRI) is an emerging area of research. It integrates several recently developed nano-technologies such as nanostructure, nanosynthesis, molecular biology and molecular magnetic resonance. While standard human MR imaging (MRI) provides resolution of about 1 mm, MMRI allows detection of much smaller biological objects. This technique uses paramagnetic nanoparticles (NP) conjugated with biological probes that target specific cancer cells. Delivery of the NPs to the cancer cell enable much higher sensitivity of MRI thus much earlier and precise diagnosis than with the application of standard non-targeted contrast agents. Because the NPs must be delivered to the cancer cell, antibodies or other binding proteins are used as probes to deliver the contrast to the specific site.

Because MR images are sensitive to changes of the magnetic field, the development of non-toxic NPs with high paramagnetic moments is necessary. Such NPs disturb local magnetic field produced by magnets used in MRI. The field distortion reduces the T_2 relaxation time of surrounding water, making NPs detectable with T_2-weighted MRI technique.

The magnetic properties of the NPs can be measured with different techniques, for example low temperature first order reversal and zero-field cooled magnetization methods. However to measure their MRI efficacy a direct, MR-based, method is needed. Therefore we used 9.4T MRI system to measure directly MR parameter, called T_2 relaxation time.

We have studied the influence of the composition of the NPs, including the core and the shell on their magnetic efficiency thus suitability for contrast enhanced MRI. The NPs were tested with MRI first *ex-vivo* and then *in-vivo*. The experiments *ex-vivo* were carried out using 1% agarose to ensure homogenous distribution of the contrast agents across the imaged glass tube. For the study we selected iron oxide (Fe_3O_4) and iron cobalt (FeCo) core NPs with SiO_2 and Au shell, with the core sizes 5 to 15 nm and the shell of 1 to 40 nm. We found the correlation between the structure of the NP and T_2 of the surrounding water molecules. The larger the core the stronger influence on T_2 and the larger the shell the weaker influence on T_2 was observed in *ex-vivo* studies. Furthermore Au coating had a stronger influence on T_2 than SiO_2. We have also compared the T_2 measurements of the NPs with commercially available iron based NP, Feridex® (Bayer Health Care Pharmaceuticals).

The NPs to become targeted contrast agents used *in-vivo* must have high affinity to specific cells or processes. Therefore antibodies (Ab) or other binding proteins can be used to deliver the NPs to the specific site. To test molecular imaging agents for glioblastoma tumors, we have

selected a glioma specific antibody and conjugated them with the previously tested *ex-vivo* NPs (Fe_3O_4/SiO_2 and FeCo/Au). The NPs were synthesized with poly(ethylene glycol) (PEG) to conjugate the antibody to the NP.

In-vivo experiments with mouse model of glioblastoma were carried out using a 9.4T/21 cm MRI system. T_2-weighted images were collected before and after the injection of the contrast agent. The effects on contrast enhanced MR images depended on the composition of the used agents and corresponded to *ex-vivo* measurements of the T_2 relaxation times.

Based on *ex-vivo* and *in-vivo* experiments we concluded that both the core and the shell and sizes of NPs have to be considered in the design of contrast agents for MRI. The tested NPs provided comparable (for Fe_3O_4) or stronger (for FeCo/Au) influence on T_2 as commercially available contrast agents.

Our final goal is to apply these NPs for enhanced MR imaging of central nervous system neoplasm in human to improve diagnosis and follow-up of cancer patients.

This project was supported by a CIHR team grant in nanomedicine and regenerative medicine.

References:

[1] Pankhurst, Q.A., J. Connolly, S.K. Jones, and J. Dobson, *J. Phys. D: Appl. Phys.*, **36** (2003): 167-181.
[2] Grancharov, S.G., H. Zeng, S. Sun, S.X. Wang, S. O'Brien, C.B. Murray, J.R. Kirtley, and G.A. Held (2005), *J. Phys. Chem. B*,**109** (2005): 13030-13035.
[3] Huang, P.L., R.S. Liu, H.T. Chan, Y.Y. Do, P.L. Chien, T.S. Chan, C.Y. Huang, S.Y. Yang, and H.E. Horng, *J. Magn. Magn. Mater.*, **304** (2006): 415-17.
[4] Desvaux, C., C. Amiens, P. Fejes, P. Renaud, M. Respaud, P. Lecante, E. Snoeck, and B. Chaudret, *Nature*, **4** (2005): 750-753.
[5] Weissleder R, Elizondo G, Wittenberg J, Rabito C, Bengele HH, Josephson L. Radiology, **175** (1990): 489-493.

DEVELOPMENT OF NANOSTRUCTURED MATERIALS BY MECHANICAL ALLOYING AND/OR RAPID SOLIDIFICATION

J. Bonastre, E. Chognon, L. Escoda, J.M. Güell, B. Hernando, J.J. Suñol*
P II, EPS, Campus Montilivi s/n, Girona University 17071 Girona, Spain
** Dept. Física, Univ. Oviedo, Calvo Sotelo s/n 33007 Oviedo, Spain.*
joanjosep.sunyol@udg.edu

Soft magnetic based alloys may be produced by both rapid solidification [1] and mechanical alloying [2] processes. This kind of alloys in nanocrystalline form was investigated for applications in magnetic devices as generators, motors, power transformers and sensors [3-4]. However, the magnetic properties of the mechanically attrited materials are inferior to rapidly quenched materials [5-6]. Nevertheless, the use of these materials in power transformers and other energy-conversion devices has been limited by their small thickness [4]. It has also, over the years, proved that MA to be superior to rapid solidification processing as a non-equilibrium processing tool [7]. In the last decades, mechanical alloying of previously melt-spun ribbons is applied as an alternative route to obtain powdered materials [8-9]. The MA of bulk amorphous metallic glasses is a two-step procedure prior to the consolidation or compacting of complicated shape materials in the powder metallurgy industry. Nevertheless, it is known that thermal and structural stability of mechanically alloyed samples is lower than that of the analogous material prepared by rapid solidification [10]. In this work, several Co and Fe rich melt-spun alloys were obtained and mechanically alloyed in low energy milling conditions, and their structure and thermal behavior was analyzed. A detailed knowledge of the temperature dependence of nucleation and crystalline growth is essential for nanomaterials design and to control their microstructure. Furthermore, in technical applications, the thermal stability of nanocrystalline alloys is a problem of fundamental interest to determine the useful working temperature ranges. The kinetics of transformation gives information relative to the stability and applicability of these materials.

An isoconversional method is applied to perform the kinetic analysis. The method was an adaptation to analyze both cold crystallization as well as solidification from the melt. This approach is applied to the study of the crystallization behavior. Once the value of the apparent activation energy is known, the function *f(x)* can be evaluated from the continuous heating and from isothermal experiments. If the kinetic behavior is the same in both kind of experiments, the experimentally measured $ln(k_o f(x))$ versus $ln(1-x)$ has to be independent of heating rate and identical to that obtained in an isothermal regime. That expression can be evaluated from *dx/dt* by taking

$$\ln(k_o f(x)) = \ln(\frac{dx}{dt}) - \frac{E}{RT} \quad (1)$$

In order to perform the kinetic analysis and to decide which kinetic model agrees better with our experimental crystallization data as the crystallized fraction *x*. We compare the experimental dependence of $ln(k_0 f(x))$ against $ln\ (1-x)$ and that predicted, assuming different model equations for *f(x).* Although there is a certain degree of dispersion, the kinetic model that gives the best fit of the experimental data is the Jhonson-Mehl-Avrami-Erofe'ev (JMAE) equation.

Financial support from MCYT (MAT2006-13925-C02-02 and 01) and DURSI (2005SGR00201) is acknowledged. J.B. agrees a FPI MICYT Spanish grant.

References:

[1] M. Xu, M. X. Quan, Z. Q. Hu, L. Z. Cheng and K. Y. He, *J. Alloys Compd.* **334** (2002) 238-242.
[2] A.F. Cabrera, C.E. Rodríguez Torres, P. Mendoza Zélis, M. Fernández Van Raap, L.M. Socolovsky, G. Pasquevich, F.H. Sánchez, *Physica B: Condensed Matter* **354** (2004) 129-132
[3] M.E. McHenry, M.A. Willard and D.E. Laughlin, *Progress in Materials Science* **44** (1999) 291.
[4] R.B. Schwarz, T.D. Shen, U. Harms and T. Lillo, *J. Magnetism and Magnetic Mater*. **283** (2004) 223-230.
[5] M.M. Raja, K. Chattopadhvav, B. Majumdar and A. Naravanasamy, *J. Alloys Compd*. **297** (2000) 199-205.
[6] K. Suzuki and J.M. Cadogan, *J. Appl. Phys.* **87** (2000) 7097.
[7] B.S. Murty and S. Ranganathan, *Intern. Mater. Reviews* **43** (1998) 101-141.
[8] E. Fechova, P. Kollar, J. Fuzer, J. Kovac, P. Petrovic, V. Kavecansky, *Mater. Sci. Eng. B* **107** (2004) 155-160.
[9] J.D. Sordelet, E. Roshkova, M.F. Besser, M.J. Kramer, *Intermetallics* **10** (2002) 1233-1240.
[10] J. Bonastre, L. Escoda, J. Saurina, J.J. Suñol, J.D. Santos, M.L. Sánchez, B. Hernando, *J. Non-Cryst. Solids* (2008). Accepted.

Figures:

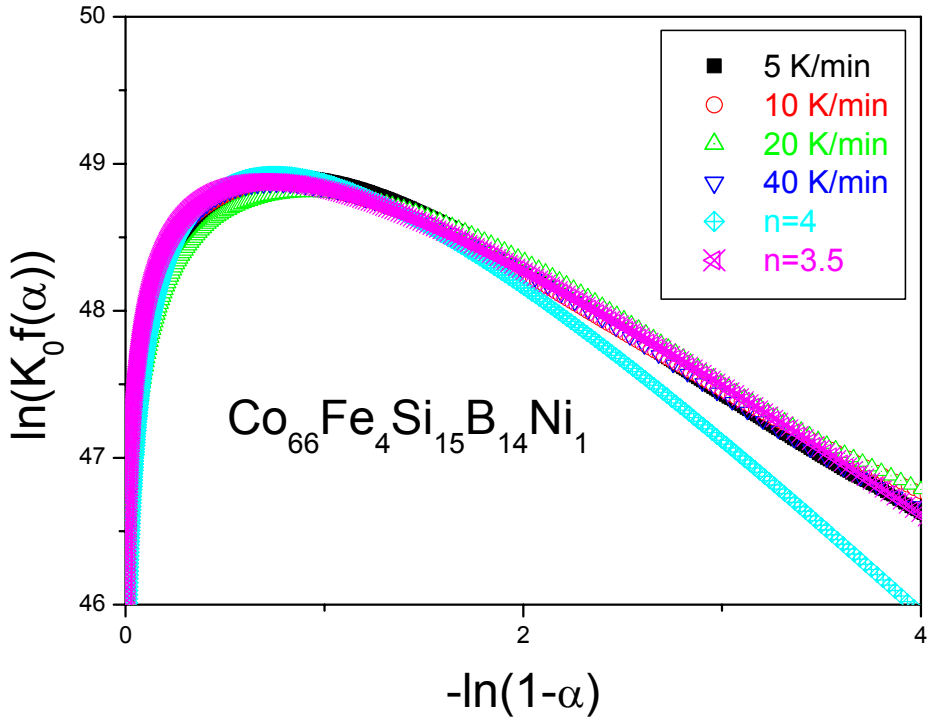

UPGRADING THERMOSETS WITH CARBON NANOFIBERS

P. Carballeira, F. Haupert, A.K. Schlarb
Institut fürVerbundwerkstoffe GmbH,
Erwin-Schrödinger-Straße, 67663 Kaiserslautern, Deutschland
pablo.carballeira@ivw.uni-kl.de

Carbon nanofibers (CNFs) have been used in recent times to increase the mechanical properties of polymer matrices [1-3], the use of CNFs provide several advantages compared with the use of micro-sized fillers; they allow the production of micromechanical components and thin coatings and they do not cause embrittlement and deterioration of tensile strength as microscopic fillers often do. These nanofillers also exhibit excellent thermal and electrical properties which make them excellent candidates for the production of conductive polymer composites, capable of dissipating electrostatic charges or even act as shielding devices from electromagnetic radiation. To benefit from the good reinforcing properties of the CNFs a good dispersion of the fibers in the polymer matrix is crucial since a well dispersed filler network results in a more uniform stress distribution within the composite. A good dispersion also minimizes the presence of agglomerates that can act as centres for stress-concentration which decrease the general strength and modulus of the composite.

In our research nanofibers were dispersed in the polymer matrix with the aid of a three roll calender (**Fig. 1**). The use of this device for the dispersion of carbon nanotubes in an epoxy matrix was first reported by F.H. Gojny et al. [4] .This technology achieved excellent dispersion results without reducing the aspect ratio of the fillers which is important to enable a good load transfer from the polymer matrix to the nanofillers. One further advantage of the calendering method is the possibility of up-scaling the manufacturing process to meet technical demands. The manufactured composites, containing different volume concentrations of carbon nanofibers, were characterized by mechanical and electrical analysis in order to study the effects that the nanofibers had on the epoxy resin. To gain knowledge of the impact energy of the nanocomposites standardised Charpy tests were performed on notched specimens. Flexural tests were carried out in three-point bending configuration from which the flexural strength, modulus and the strain at break of the samples were obtained. The complex modulus E* and damping tanδ were examined by dynamic mechanical thermal analysis (DMTA) using a tensile testing configuration. Lastly electrical measurements were conducted at room temperature on an Ohmmeter system with a measurement range of 10^4 to 10^{14} Ω. (**Fig.2** left) shows that the impact fracture toughness of epoxy resin increased with increasing volume of carbon nanofibers. (**Fig. 2** right) shows the evolution of the electrical conductivity of the nanocomposites with increasing filler content. A steep conductivity increase was evident in with a very low volume addition of fillers. This behaviour is indicative of a percolation transition; percolation theory predicts that there is a critical concentration of conductive fillers at which a conductive path is formed in the composite causing the material to change from capacitor to conductor. This critical concentration or percolation threshold was determined at about 0.15 vol. % vol. in our CNF nanocomposites. I

Scanning electron microscopy examinations was used to study the morphology of fracture surfaces (**Fig.3**). The aim was to obtain further information of the cause and location of failure and also to study the role of the added carbon nanofibers in terms of crack propagation and reinforcing mechanisms within the samples. Compared to the very brittle and smooth occurrence of the neat epoxy fracture surface (**Fig.3 left**) the nanocomposites reveal a micro-rough surface (**Fig.3 right**), which indicates additional fracture mechanisms responsible for higher energy dissipation during fracture. The latter leads to the observed higher toughness and improved mechanical properties of the nanocomposites.

References:

[1] B. Bai, A. Allaoui, Composites Part A **34(8)** (2003), 689–694.
[2] T. Prasse, J.-Y. Cavaille, W. Bauhofer, Composites Science and Technology. **63(13)** (2003), 1835–1841
[3] P. Richard, T. Prasse, J-Y. Cavaille, L. Chazeau, C. Gauthier, J. Duchet, Materials Science and Engineering. A **352(1–2)** (2003), 344–348..
[4] F.H. Gojny, M.H.G. Wichmann, U. Köpke, B. Fiedler, K. Schulte, Composites Science and Technology **64** (2004) 2363–2371.

Figures:

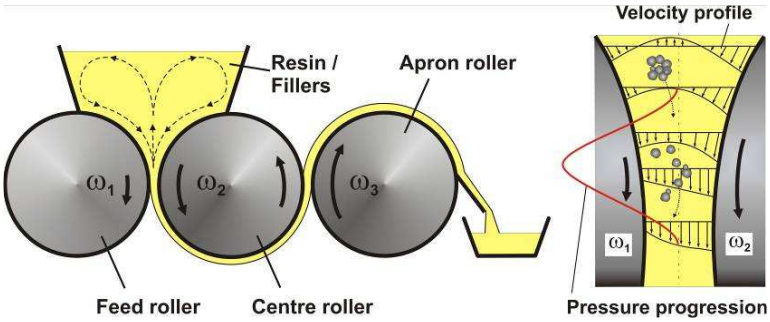

Fig. 1. Schematic view of the three roll calender and its working principle.

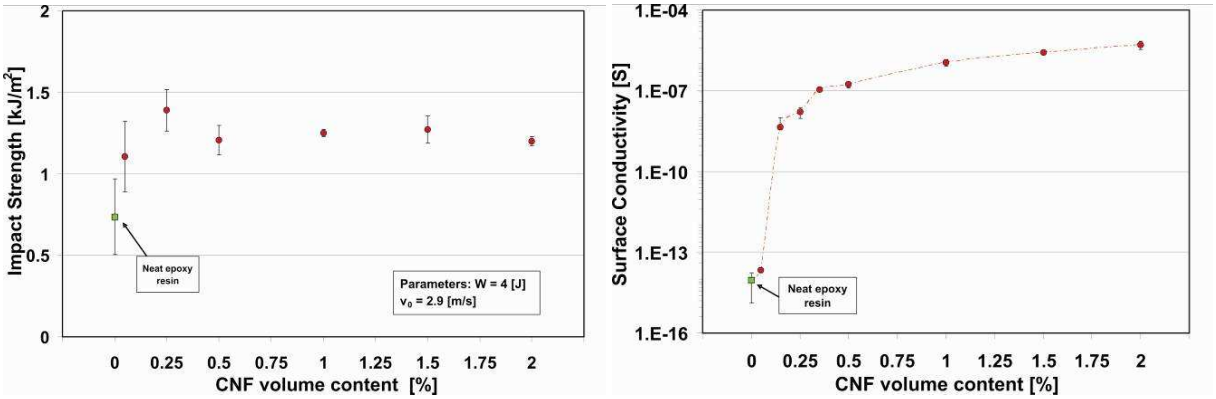

Fig.2 Impact fracture toughness (left) and surface conductivity (right) of the epoxy/CNF nanocomposites as a function of nanofiber volume content

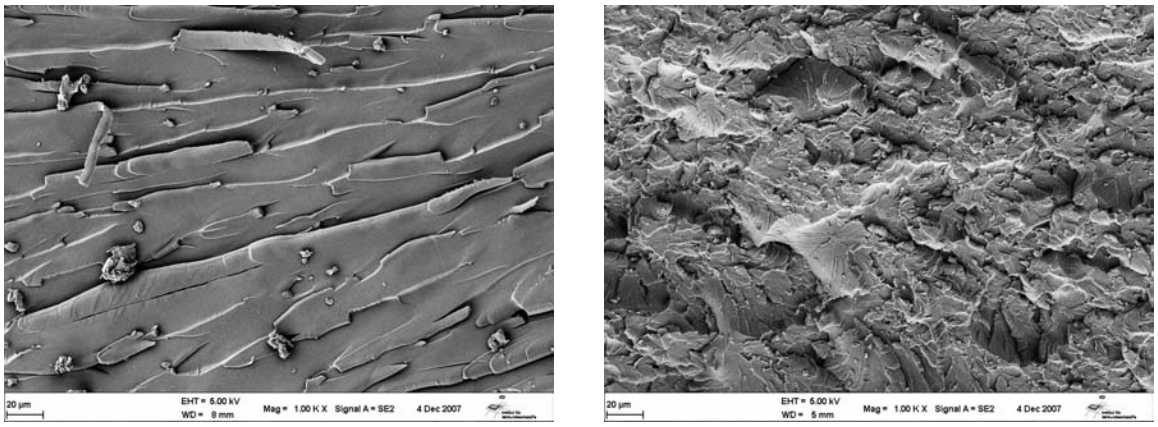

Fig.3 (Left) Neat epoxy fracture surface from flexural testing. Brittle fracture leads to a smooth surface appearance. (Right) Nanocomposite (2% vol. of CNF) fracture surface, rugged surface suggests bigger energy dissipation due to the presence of nanofibers within the resin.

CHARACTERIZATION OF METALLIC NANOPARTICLES OBTAINED BY BIOMASS REDUCTION

Laura Castro
Department of Material Science and Metallurgic Engineering, Complutense University of Madrid, Avda. Complutense s/n 28040 Madrid, Spain.
mailto:lauracr84@hotmail.com
mlblazquez@quim.ucm.es

Nowadays precious metal recovery technologies use harmful chemicals that may represent a risk to the environment and public health. This is the reason why it is necessary to develop clean, non-toxic and environmentally friendly procedures to recover precious metals. The use of biological organisms in synthesis and assembly of nanoparticles has received an increasing interest. In these experiments, dead brown and red seaweeds (*Ascophyllum nodosum* and *Chondrus crispus*) have shown to be efficient for gold (III) reduction. Seaweeds reduce gold (III) to gold (0) and produce nanoparticles. The reduction process was found to be dependant on pH, time, temperature and concentration of biomass. UV-vis spectrums and transmission electron micrographs showed nanoparticles of several shapes and sizes. In order to resolve the mechanism of reduction of gold (III), the evolution of pH and potential was measured.

References:

Bhattacharya, D., y Grupta, R. K.: Nanotechnology and potential of microorganisms. Critical reviews in biotechnology, **25** (2005), pp. 199-204.

Gadea-Torresday, J. L., Parsons, J.G., Gomez, E., Peralta-Videa, J., Troiani, H. E., Santiago, P., Yacaman, M. J.: Formation and growth of Au nanoparticles incide live alfalfa plants. Nano Letters, **2** (4) (2003) pp. 397-401.

Mukherjee, P., Senapati, S., Mandal, D., Ahmad, A., Khan, M. I., Kumar,R, Sastry, M.: Extracellular synthesis of gold nanoparticles by the fungus *Fusarium oxysporum*. Chem. Biol. Chem. 3 (2002), pp. 461-463.

Figures:

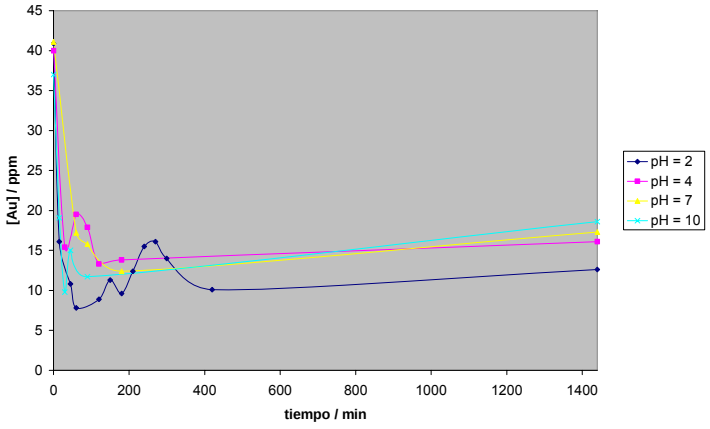

Fig. 1. Influence of initial pH in reduction of $AuCl_4^-$ with 2 g/L *Ascophyllum nodosum*.

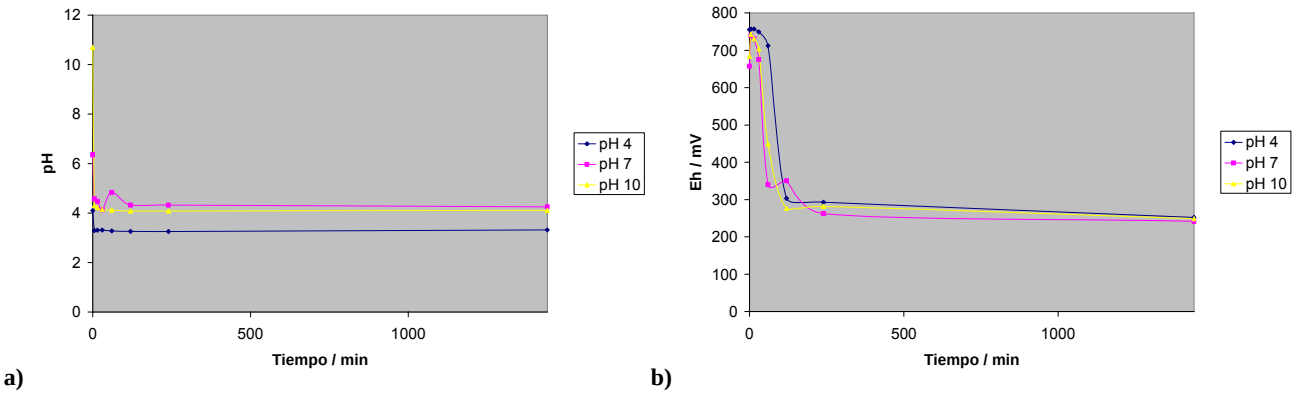

a) b)

Fig. 2. Evolution of pH (a) and potential (b) in reduction of $AuCl_4^-$ with 5 g/L *Ascophyllum nodosum* for different values of initial pH..

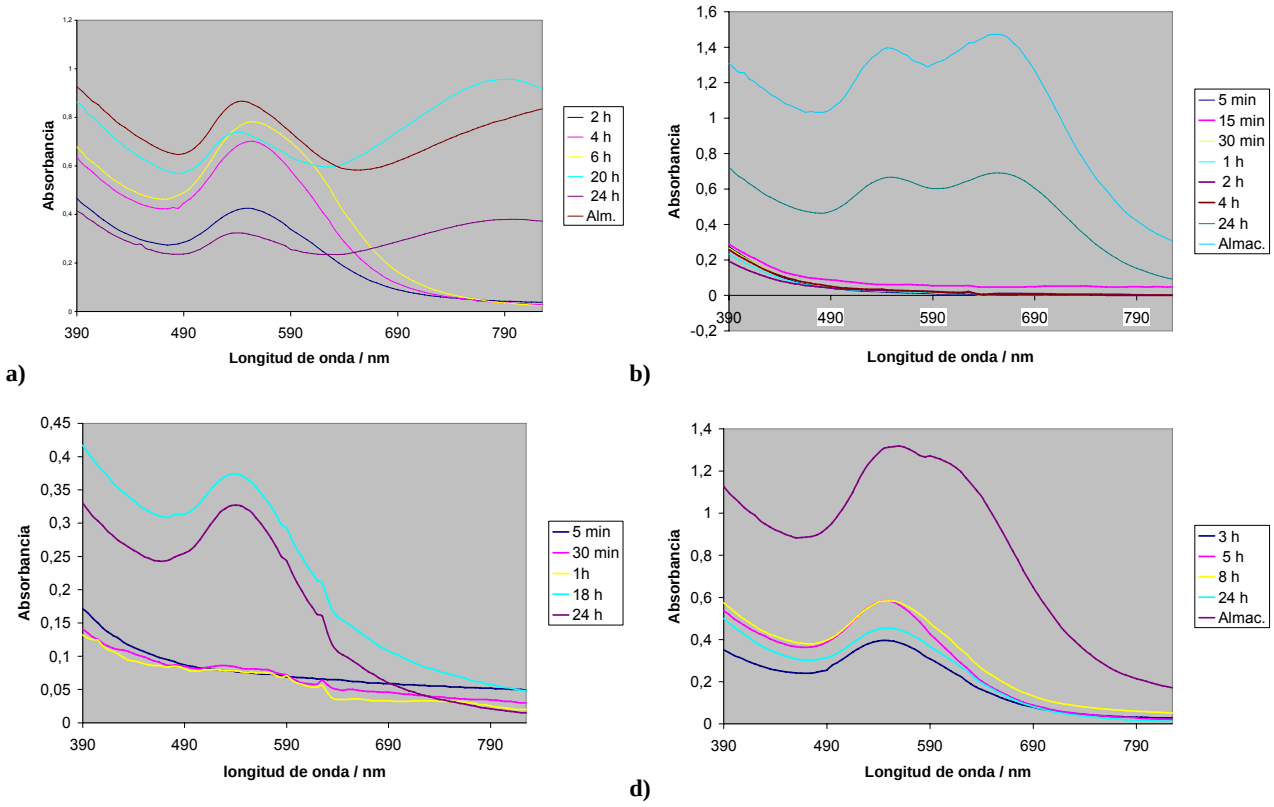

a) b) c) d)

Fig. 3. UV-vis spectrums of Au nanioparticles dissolutions produced with 5 g/L *Chondrus Crispus* with different values of initial pH: a) pH = 2, b) pH = 4, c) pH = 7, d) pH = 10.

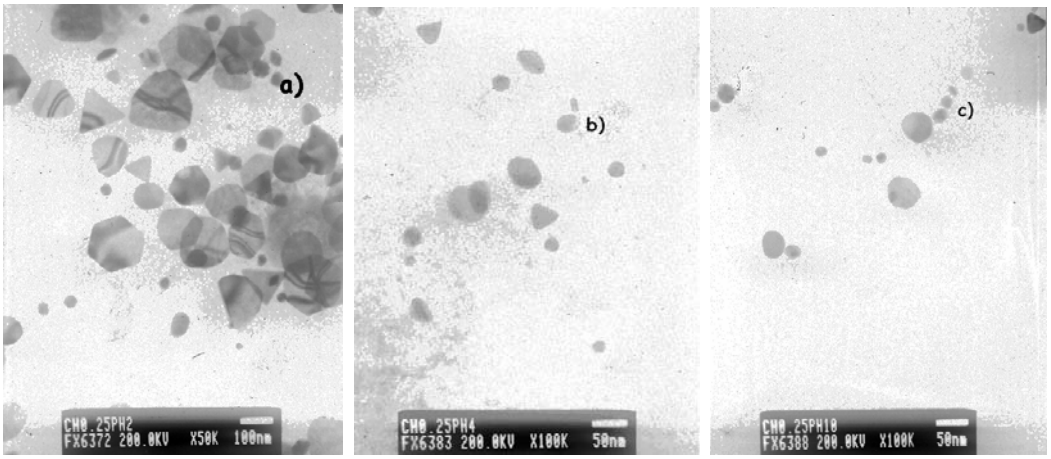

Fig. 4. Photographs of Au nanoparticles obtained with 5 g/L *Chondrus crispus* observed by TEM: a) pH 2, b) pH 4, c) pH 10.

INFLUENCE OF FIELD ANNEALING ON AC MAGNETIC PROPERTIES OF NANOGRANULAR FeCo-ALN FILMS.

Oleksandr Chayka, Luděk Kraus
Institute of Physics ASCR, Na Slovance 2, CZ-18221 Prague 8, Czech Republic
chayka@fzu.czl

The permanent increase of operational frequency of modern electronic devices implies an increasing demand of highly efficient soft magnetic films. Nanogranular Fe–Co based films with an insulating (oxide or nitride) intergranular phase, prepared by magnetron sputtering, well satisfy these requirements. In this work we present the investigation of FeCo-AlN films prepared by an alternative method with emphasize on modification of their AC magnetic properties under field annealing.

A series of nanogranular magnetic FeCo-AlN films was fabricated by plasma jet technique. X-ray diffraction and chemical analysis revealed that the films consist of crystalline FeCo grains with the size of about 10 nm and amorphous AlN matrix. Hysteresis loops were measured by an AC hysteresis loop tracer at 101 Hz. The frequency dependence of permeability was investigated in the range of 0.1 – 2 GHz by a strip line permeameter.

Magnetization curves of as-deposited samples show the presence of weak in-plane anisotropy and the easy axis distribution in the film plane. The last is confirmed by magnetooptical measurements. In order to improve magnetic properties (to induce strong uniaxial anisotropy and decrease the coercive field H_c, which is important for high frequency applications of these materials) annealing in Ar atmosphere under applied magnetic field was done. The influence of field annealing on magnetic, electrical and high frequency permeability is analysed.

Measurements of magnetic and electrical properties were done after each field annealing treatment of the films at 250, 300, 350 and 400°C. It was found that the critical annealing temperature T_c is around 300°C from the magnetic point of view. After field annealing at T_c the natural ferromagnetic resonance frequency f_r is 1.2GHz and the permeability μ has the highest value. Annealign at highest temperatures results in degradation of magentic properties, the coercive field is increases and permeability decreases, although ferromagnetic resonance frequency slightly increases.

TEMPERATURE DEPENDENCE OF ELECTRICAL CONDUCTION THROUGH 1, 4-DITHIOLBENZENE MOLECULAR ASSEMBLY (PART II)

Kuek Chian Shiun and Aissa Boudjella
Faculty of Science, Engineering and Technology, University Tunku Abdul Rahman, Jalan University, Bandar Barat, 31900 Kampar, Perak, Malaysia

e-mail: kuekcs@mail.utar.edu.my e-mail:aissab@mail.utar.edu.my

Abstract

Numerical simulations have been performed to investigate the effect of the temperature on the electronic transport through molecular assembly system (MAS). The model involves 1,4-dithiolbenzene (DTB) molecules stacked in (1D) ordered structure. The MAS can contain up to two DTB molecules packed in the parallel geometrical arrangement.[1)] With the Fermi level E_f located in the middle of the HOMO-LUMO gap (HLG), [2, 3)] the electronic transport through a single or two DTB molecular units connected in parallel between two metallic contact is presented. The calculations were performed into two steps. First, the energy levels HOMO (the highest occupied molecular orbital) and LUMO (the lowest unoccupied molecular orbital) were obtained using an approach based on Landauer formalism with the density functional theory Kohn-Sham.[4, 5)] Then, the current-voltage (*I-V*) as well as the conductance-voltage (*G-V*) characteristics were calculated using the molecular conduction toy (MolCtoy).[2, 6)] These calculations were carried out for various temperature T=50~325K and intermolecular distances d=3.3~6.9 $\mathring{A}$. The charging energy $U=1$ eV, and the molecule–metal coupling strength $\sigma_1=\sigma_2=\sigma_i=0.1$ eV are kept constant. The influences of the electrical and physical parameters such as HOMO-LUMO gap (HLG), π-orbital and the intermolecular distance between two adjacent molecular units on the electron transport of MAS are analyzed.

Figure 1 represents a molecular assembly of DTB molecules in the parallel geometrical arrangement connected between two metallic electrodes. The temperature related current-voltage *I(V,T)* and conductance-voltage *G(V, T)* characteristics of MAS containing two DTB molecular units with $d=6.9$ and 3.3 $\mathring{A}$ are illustrated in figures 2 and 3, respectively. For the *I-V* curves, there are three distinct regions of operation of molecular assembly: 1) the conductance gap region, in this region the current is zero. The molecular system behaves as open circuit with an absence of temperature dependence; 2) above a certain threshold voltage, the current starts to increase linearly. This region exhibits a little temperature dependence; 3) finally; a point will be reached on the *I-V* curve at which the current becomes saturated. In this saturation region, the current is not affected by the variation of the temperature. For the *G-V* characteristics, while the conductance increases as the temperature increases, the magnitude of the maximum peaks decreases. In this molecular configuration, we can expect a significant π-coupling for sufficient a small distance *d* between two DTB adjacent molecular units. When *d* changes from 6.9 to 3.3 Å, the HLG decreases by 34.32%. The author[1)] reported the variation of the HOMO, LUMO, and HLG as a function of the intermolecular distances *d* of molecular structure containing two DTB molecular units. Therefore, it is important to associate the temperature related *I-V* characteristics with HLG. The shorter HLG, the smaller threshold voltage is observed for the variation of *I (V, T)* characteristics.

To conclude, the electron conduction in our molecular system model may be explained by two distinct mechanisms: 1) the direct tunneling, the main transport mechanism with the absence of temperature dependence and 2) the thermionic conduction with little temperature effect which can not be ignored. The prediction by Moore's law, the number of transistor integrated on a chip would grow exponential with time. Therefore, the heat dissipation is a critical issue in circuit design, because the huge device density in modern VLSI circuits. To predict the functionality of this a new generation molecular electronic assembly devices that can be implemented on a chip, the temperature rise effect caused by the power consumption devices on I-V characteristics may need to be considered.

References:

1) A. Boudjella et al.. Will be published in Japanese journal of applied physics Vol. 47, No 6, 2008.
2) F. Zahid, M. Paulsson, and S. Datta: in Semiconductors and Organic Nano-tecniques, ed. H. Morkov (Academic Press, New York, 2003).
3) S. N. Yaliraki, M. Kemp, and M. A. Ratner: J. Am. Chem. Soc. 121 (1999) 3428.
4) M. Buttiker, Y. Imry, R. Landauer, and S. Pinhas: Phys. Rev. B 31(1985) 6207.
5) S. Datta: Electronic Transport in Mesoscopic (Cambridge University Press, Cambridge, U.K., 1995), p. 57.
6) www.nanohub.org

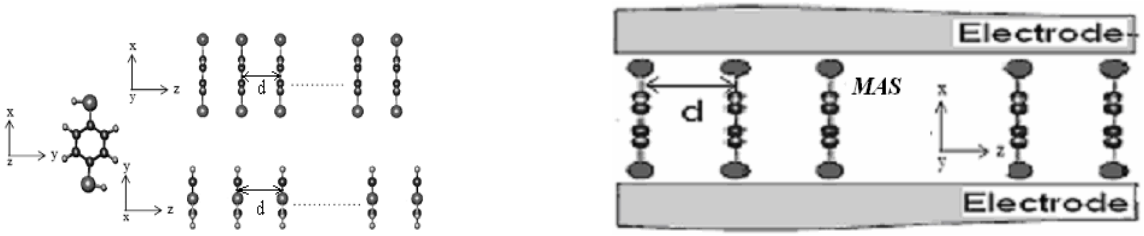

Fig. 1. Structure of MAS connected between two metallic electrodes.

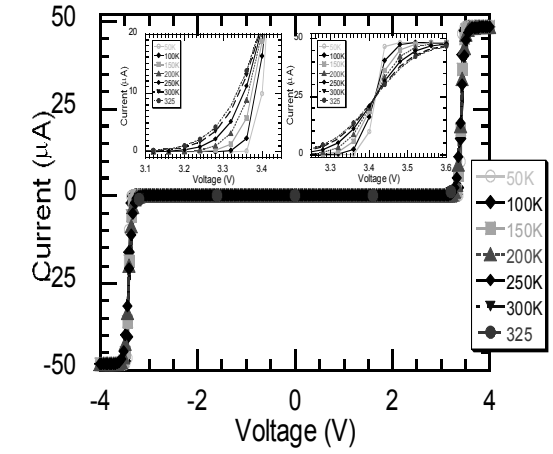

(a)

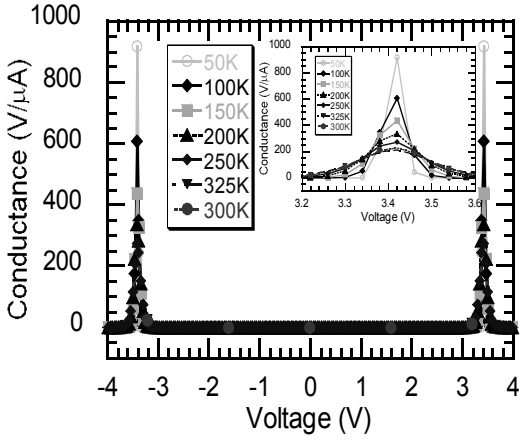

(b)

Fig. 2.The *I-V* (a) and *G-V* (b) characteristics For *N=2, HLG=3.411 eV*, *d =6.9 Å*, *U=1* eV, and $\sigma_1=\sigma_2=\sigma_i=0.1$ *eV*.

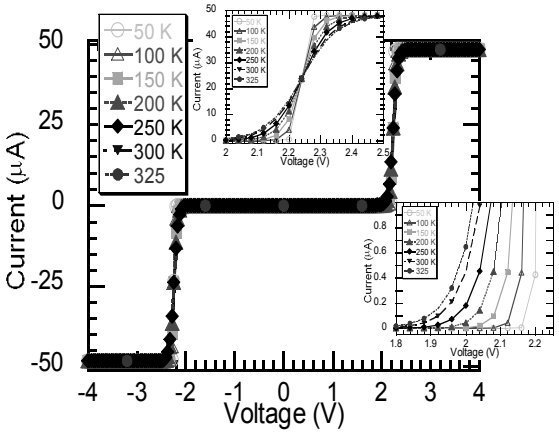

(a)

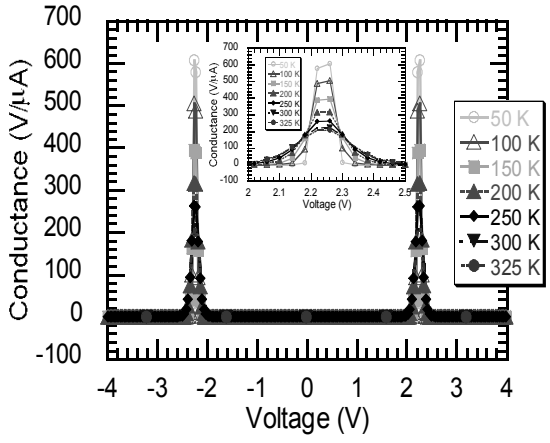

(b)

Fig. 3. The *I-V* (a) and *G-V* (b) characteristics For *N=2*, *HLG= 2.240 eV, d =3.3 Å*, *U=1 eV*, and $\sigma_1=\sigma_2=\sigma_i=0.1$ *eV*.

PREVENTION OF HIV-MUCOSAL BARRIER INTERACTION BY NEW SYNTHESISED CARBOSILANE POLYANIONIC DENDRIMERS

Louis Chonco, Paula Ortega, Rafael Gómez, F.Javier de la Mata and MªAngeles Muñoz-Fernandez

Hospital General Universitario Gregorio Marañon, Dr. Esquerdo 46, Madrid, Spain
mmunoz.hgugm@salud.madrid.org

The female genital tract is the primary route for heterosexual transmission of HIV and the mechanism of virus-epithelial vaginal cells interaction is poorly understood. In this context the development of nanosystems for its use as microbicides could be a point of inflexion in the prevention of HIV infection. We are designing three new generations of carbosilane polyanionic dendrimers (CPDs) with broad-spectrum antiviral activities and minimal toxicities (data not shown, under patent). We have been tested these CPMs using the endometrial epithelium-derived cell line HEC-1A and two different HIV isolates NL4.3 (X4 isolate) and BaL (R5 isolate). We found that cells are capable of sequestering large numbers of HIV-1 particles but are refractory to cell-free viral infection. The preincubation of cells with Suramin and Dextran Sulfate decrease HIV-1 strain adherent to the plasma membrane. We found an increase of anti-adherent effect using G2-CPM, without toxicity at 10µM. Our results show until 90% of inhibition treating cells 2h pre-infection. Evaluation of chemokines attracting monocytes/macrophages and proinflammatory cytokines release that could enhance HIV-1 spread, are under analysis. Our preliminary data indicate that G2-CPM is a promising candidate for development as a vaginal microbicide and a therapeutic agent.

References:

1. McCarthy et al, Molecular pharmaceutics, 2005,vol. 2, no. 4, 312-318
2. Fletcher et al, Retrovirology, **2006**, 3:46

Figures:

%Inhibition of antigen p24. Pretreatement of CPMs

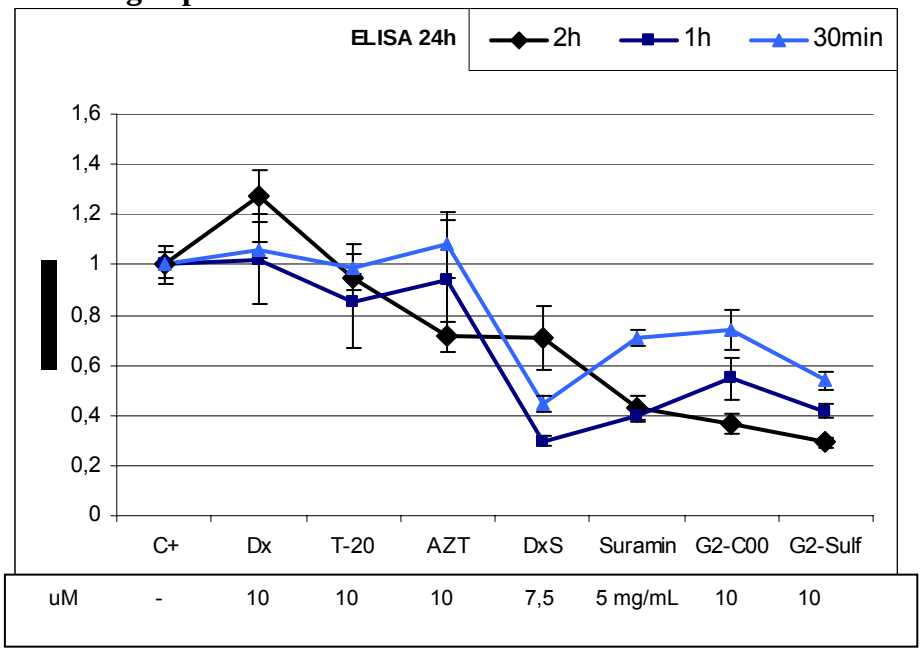

%Inhibition of antigen p24. and viability by Lactato DesHidrogenase assay

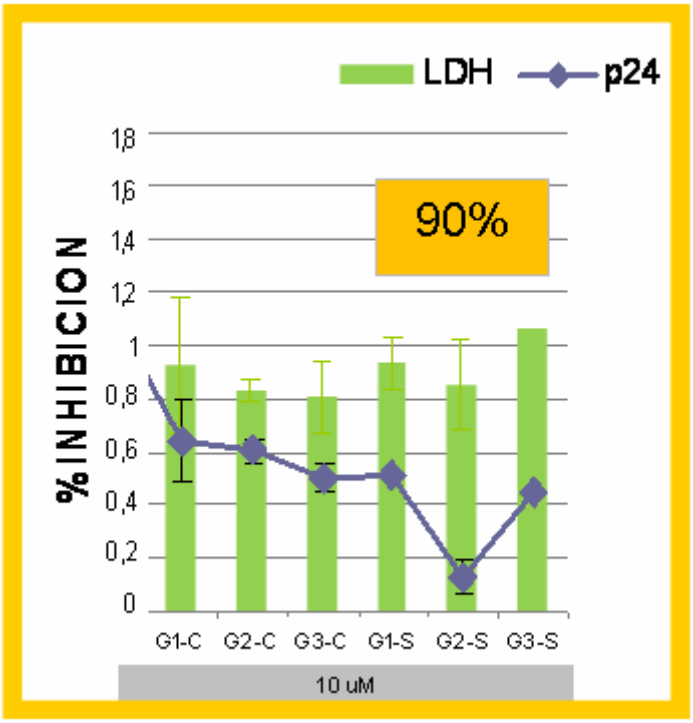

A FIRST PRINCIPLES STUDY OF THIOL-CAPPED Au NANOPARTICLES

R. Cuadrado[1], J. I. Cerdá[1]
(1)Instituto de Ciencia de Materiales de Madrid, CSIC, Cantoblanco 28049 Madrid, Spain
rcuadrado@icmm.csic.es

I. Introduction

Nanoparticles (NPs) have become a subject of major research due to their new optical, electronic and/or magnetic properties which may be controlled by varying the NP size or shape. Functionalizing these NPs with adequate organic capping layers further provides chemical specificity to the clusters, thus becoming highly interesting for biological applications (e.g. drug delivery within the body). In particular, gold NPs have received great attention because bulk gold is inert and, most surprisingly, several experiments recently reported on the ferromagnetic nature of these Au Nps [1,2]. There exist, however, conflicting results regarding the conditions required for achieving such magnetic clusters; whereas the first experiments required sulfur based capping ligands (alkane-thiols), subsequent theoretical and experimental works point to the existence of a permanent magnetism in bare gold clusters [3]. In this work, we address precisely the role that an alkane-thiol capping layer plays on the structural, electronic and magnetic properties of Au NPs by means of *ab initio* Density Functional Theory (DFT) based calculations.

II. Theoretical

We have modeled Au clusters of different sizes ranging from just 1 up to 38 gold atoms. The largest cluster considered, Au_{38}, has an octahedral shape preserving the bulk fcc arrangement. We considered short alkane-thiols of just two C atoms ($S\text{-}C_2H_5$) and systematically varied the thiol coverage for each of the Au clusters. The highest coverage considered here were 24 thiols, which amounts to a 3:4 ratio between the number of gold surface atoms (32 in the bare cluster) and the number of thiols. Starting from different initial trial configurations comprising adsorption at bridge sites, "staple" motifs [4], and ...-S-Au-S-Au... chain like structures, we explored their stability via Molecular Dynamics (MD) runs.

All calculations have been performed with the DFT based SIESTA code [5] under the Local Density Approximation (LDA). The electronic and magnetic properties of the clusters were studied by inspection of the Mulliken charges, the atom projected Density of States (PDOS) together with any net magnetic moments after Local Spin Density (LSD) calculations.

III. Results

Atomic Structure

Our calculations confirmed the ability of the Au NPs to adsorb a large number of thiols. Figure 1 shows several relaxed structures for the Au_{38} cluster and for different thiol coverages. In general, the relaxed geometries contain mixtures of the three adsorption models considered, making it difficult to extract a unique and simple picture for the structure of thiol capped NPs. As the coverage is increased, the reconstruction of the gold NP becomes more prominent. Indeed, we have often found that the stability of the cluster may strongly depend on the level of restructuring that takes place for the Au core atoms.

Electronic Structure

Figure 2 shows the evolution of the DOS for the Au_{38} cluster and for different thiol coverages. We include the projections on the gold and sulfur atoms as well as on the organic ligands (C_3H_5). As the coverage increases, the peaks are smeared and bands are formed implying that electrons become delocalized. The evolution of the Mulliken charges reveals that in the absence of thiols, there is a charge transfer from the core region to the surface atoms, thus leaving the inner (outer) regions in the NP positively (negatively) charged. The addition of thiols, however, cancels this charge transfer so that the core region becomes progressively neutral while the surface atoms reverse their net charge (see figure 3).

Magnetic properties

We have not found any evidence for ferromagnetism in any of the large clusters studied; the spin polarization vanished in all cases. Even for clusters with an odd number of electrons, the exchange split was of just a few meV and hence, the spin polarization became negligible after using a finite temperature in the Fermi occupation function. Whereas the Au_{38} cluster showed a slight paramagnetic behavior [6], thiol adsorption tends to remove any peaks close to the Fermi level thus reducing the number of d-holes. From

these results, it is clear that thiol capping does not help the development of any spin polarization in the cluster.

References:

[1] P. Crespo, R. Litrán, T. C. Rojas, M. Multigner, J. M. de la Fuente, J.C. Sánchez-López, M. A. García, A. Hernando, S. Penadés, and A. Fernández, Phys. Rev. Lett. **93**, 087204(2004).
[2] José S. Garitaonandia, *et al* Nano Lett. **8** nº 2 661-667 (2008)
[3] Y. Yamamoto, T. Miura, M. Suzuki, et al., Phys. Rev. Lett. **93-11**, 116801(2004)
[4] De-en Jiang, Murilo L. Tiago, Weidong Luo, and Sheng Dai J. Am. Chem. Soc. **130**, 2777-2779 (2008)
[5] José M. Soler, Emilio Artacho, Julian D. Gale, Alberto García, Javier Junquera, Pablo Ordejón and Daniel Sánchez-Portal J. Phys.: Condens. Matter **14**, 2745-2779 (2002).
[6] R. J. Magyar *et al* Phys. Rev. B **75** 144421 (2007)

Figures:

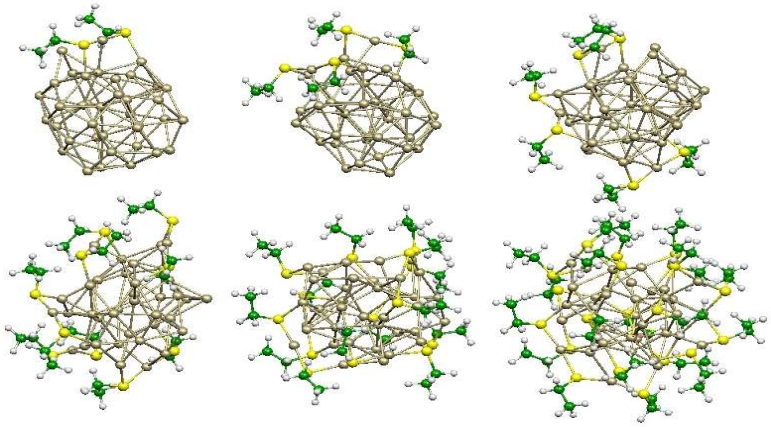

Fig. 1. Sketch of the relaxed Au_{38} clusters for different thiol coverages: 2, 4, 6, 10, 14 and 20.

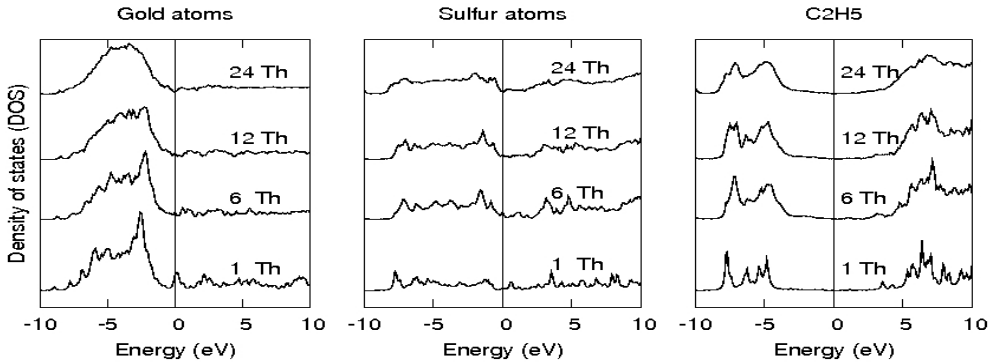

Fig. 2 PDOS corresponding to the Au_{38} cluster covered by 1, 6, 12 and 24 thiols. Left, middle and right panels correspond to the projections on the gold atoms, sulfur atoms and thiols, respectively.

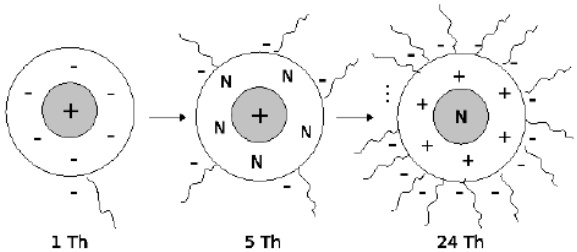

Fig. 3 Sketch of the charge distribution for NPs with 1, 5 and 24 thiols. Each NPs is split into three regions: core, surface and alkane-thiols. At nth = 1 (left) core atoms are positively charge and the surface is negatively charged. For nth = 5 (middle), the surface becomes neutral while core atoms still hold some positive charge. Finally, for nth = 24 (right), all the charge transfer occurs from the surface to the thiols.

OPTOACOUSTIC SPECTROSCOPY OF SPHERICAL GOLD NANOPARTICLE CONTRAST AGENTS IN A SCATTERING MEDIA

Vincent Cunningham[1], *Horacio Lamela*[1], *Daniel C Gallego*[1], *W. Fritzsche*[2], *A. Csaki*[2], *A. Steinbrük*[2]

[1]*Universidad Carlos III de Madrid, Avda. Universidad 30, Leganes, Madrid, Spain*

[2]*Istitute of Photonic Technology, e.V., Jena, Germany*

vcunning@ing.uc3m.es

The optoacoustics technique is proving to be a formidable player in research for the detection and monitoring of abnormalities in the human body. This method is based on the thermal excitation of acoustic waves from absorbed short pulsed laser energy. The temporal and amplitude characteristics of the acoustic signals produced indicate the amount of laser energy absorbed by the media [1]. Using these characteristics the optoacoustic technique can be employed for non-invasive real time biomedical imaging of soft tissue [2][3]. To enhance the contrast levels between healthy and un-healthy tissue, non-toxic contrast agents composed of spherical gold nanoparticles are used to increase the absorption efficiency. Recent work using the optoacoustic technique is based on optoacoustic spectroscopy (OAS). Using this approach important physiological information as regards the constitution of the biological matter is given by the light absorption properties.

OAS is carried out by irradiating the area of interest with a short pulsed tunable laser source, a study of the resulting acoustic signal characteristics for different emission wavelengths defines the amount of optical radiation absorbed for each wavelength. R.O. Esenaliev *et al* have studied the feasibility of using this technique to investigate cerebral venous oxygenation levels [4]. J. Sundararajan *et al* have implemented a similar system to quantify the blood glucose levels for diabetic patients [5]. There are many inherent advantages when using OAS, these are increased spatial resolution and spectroscopic information of deeply embedded media. Standard spectroscopic techniques are limited by the penetration depth, where detection of the attenuated light is hampered by the scattering of healthy soft tissue. In OAS the attenuation of the acoustic signals after absorption is minimal. Another advantage to this technique is that the acoustic signals produced are independent of the scattering and provide information on the absorbed light only.

In this paper we present the OAS characterization of spherical gold nanoparticles using a tunable optical parametric oscillator (OPO) laser pumped with a Nd:YAG laser. We will investigate the relation between the amplitude of the acoustic signal generated from optoacoustic excitation and the absorption for different wavelengths of the spherical gold particles in a scattering media. These results will be compared to spectroscopic results obtained using classical light transmission techniques.

References:

[1] H. Lamela, V. Cunningham, P. Pedreira, D.C. Gallego, P. Acedo, W. Fritzsche, A. Csaki, G. Festag, A. Steinbrük, Proc. SPIE, Vol. 6856 (2008).

[1] A.A. Oraevsky, E.V. Savateeva, S.V. Solomatin, A.A. Karabutov, Z. Gatalica, T. Khamapirad, Proceedings of the second joint EMBS/BMES conference, Vol. 3, (2002) page(s). 2329 – 2330.

[2] A.A. Karabutov, E.V. Savateeva, A.A. Oraevsky, Laser Methods in Medicine and Biology, Laser Physics, Vol. 13, No. 5, (2003), page(s). 711 – 723.

[4] R.O. Esenaliev, I.V. Larina, K.V. Larin, D.J. Deyo, M. Motamedi, D.S. Prough, Applied Optics, Vol. 41, No. 22, (2002), page(s). 4722 – 4731.

[5] J. Sundararajan, V. Palanisamy, K. Ganesan, K. Chatterjee, M. Sandeep, Proc. of the fifth LASTED International conference, Biomedical Engineering, (2007), page(s) 308 – 314.

Figures:

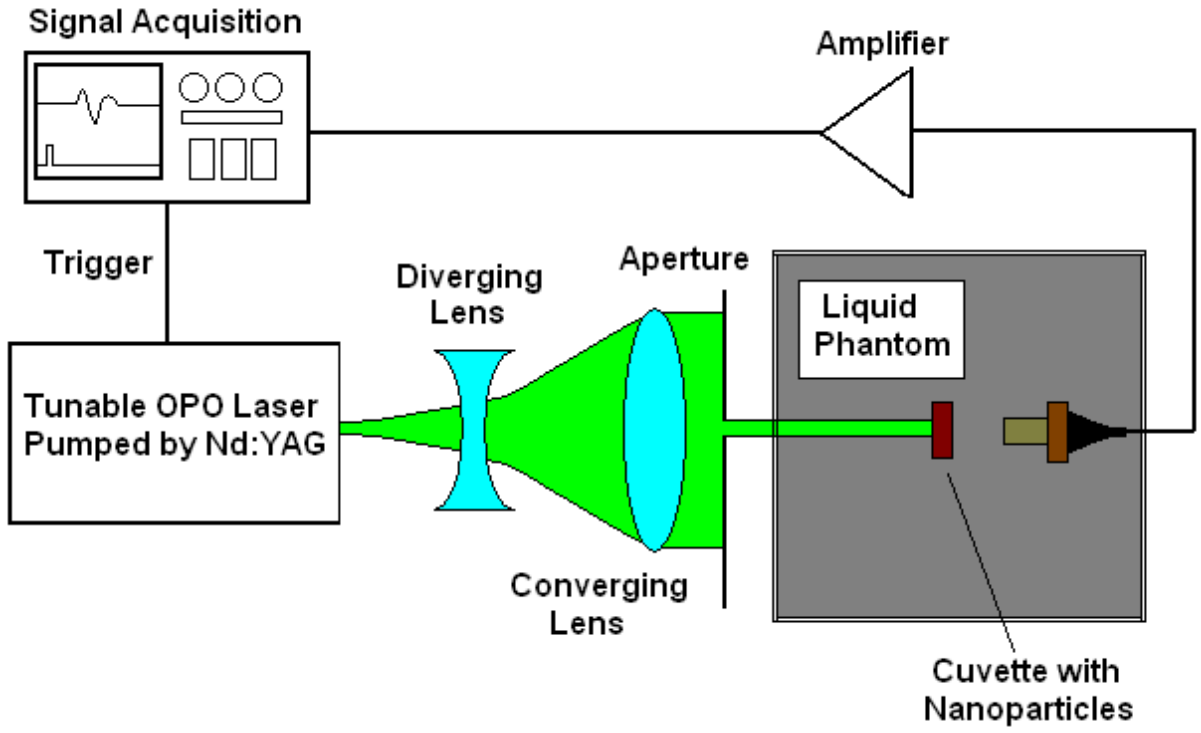

Optoacoustic Spectroscopy measurement scheme composed using tunable Nd:YAG laser for gold nanoparticle characterization in a liquid phantom representing human soft tissue

HETEROCIRCULENES AS A NEW CLASS OF ORGANIC SEMICONDUCTORS

Afshin Dadvand [a,b], *Fabio Cicoira,* [a] *Konstantin Yu. Chernichenko ,* [c] *Elizabeth S. Balenkova ,* [c] *Reyes M. Osuna,* [d] *Federico Rosei,* [a] *Valentine G. Nenajdenko,* [c] *Dmitrii F. Perepichka* [b]

[a] *INRS-EMT, University of Quebec, 1650, boul. Lionel-Boulet, Varennes, Québec, Canada, J3X 1S,*
[b] *Department of Ch30emistry, McGill University 801 Sherbrooke Street West, Montreal,H3A 2K6, Quebec, Canada, Fax: (514) 398 3797; Tel: (514) 398 6233; E-mail: dmitrii.perepichka@mcgill.ca*
[c] *Department of Chemistry, Moscow State University, 119992 Moscow, Russia*
[d] *Department of Chemistry, University of Málaga, 29071-Málaga, Spain*

Organic semiconductors (OSC) have attracted considerable attention in recent years for applications in electronic and optoelectronic devices such as light-emitting devices (LEDs), field-effect transistors (FETs) and photovoltaic cells.[1] Low processing cost and the mechanical flexibility of organic materials makes them compatible with plastic substrates for lightweight, low cost and foldable products including radio frequency identification tags, portable sensors, electronic paper, flat panel displays, etc.[2] While the charge carrier mobilities achieved for some OSCs already rival that of amorphous silicon, the long term operational and storage stability, which is inherently linked to the molecular structure, is still limiting wide implementation of OFETs. Therefore, design of new stable organic semiconducting materials is of great practical interest. Pentacene and its derivatives, as well as linear oligo- and polythiophenes have been the two most studied classes of materials in OSC.[3]

In this work, we have demonstrated applicability of the first all-heterocyclic octathio[8]circulene (sulflower) and its selenium analogue tetraselenatetrathio[8]circulene (selenosulflower) as a semiconductor through successful fabrication of Organic Thin Film Transistors (OTFT) with these materials. We showed that heterocirculenes can be potentially used as *p*-type semiconductors in nanoelectronics. For vacuum deposited films of both materials, we carried out electronic characterizations in FET configuration. Highest hole mobility of 9×10^{-3} cm^2/Vs and 1×10^{-3} were achieved for sulflower and selenosulflower, respectively. Atomic Force Microscopy (AFM) was used to visualize the morphology of the films grown at different surface coverage and to determine the organization of the molecules. We also employed X-Ray Diffraction (XRD) spectroscopy to reveal information about the crystallographic structure and physical properties of thin films.

---

[1](a) J.H. Burroughes, D.D. Bradley, A.R. Brown, R.N. Marks, K. Mackay, R.H. Friend, P.L. Burn and A.B. Holmes, *Nature*, 1990, **347**, 539; (b) C. D. Dimitrakopoulos and P. R. L. Malenfant *Adv. Mater*., 2002, **14**, 99; (c) I. F. Perepichka, D. F. Perepichka, H. Meng and F. Wudl, *Adv. Mater.*, 2005, **17**, 2281; (d) C. J. Brabec, N. S. Sariciftci and J. C. Hummelen, *Adv. Funct. Mater*., 2001, **11**, 15.

[2] (a) R. Wisnieff, *Nature*, 1998, **394**, 225; (b) B. Crone, A. Dodabalapur, A. Gelperin, L. Torsi, H. E. Katz, A. J. Lovinger and Z. Bao, *Appl. Phys. Lett*., 2001, **78**, 2229; (c) C. J. Drury, C. .M. J. Mutsaers, C. M. Hart, M. Matters and D. M. de Leeuw, *Appl. Phys. Lett.*, 1998, **73**, 108.

[3] (a) J. E. Anthony, *Chem. Rev*., 2006, **106**, 5028; (b) F. Garnier, A. Yassar, R. Hajlaoui, G. Horowitz, F. Deloffre, B. Servet, S. Ries and P. Alnot, *J. Am. Chem. Soc.*, 1993, **115**, 8716; (c) B. S. Ong,; Y. Wu, P. Liu and S. Gardner, *J. Am. Chem. Soc.*, **2004**, 126, 3378; (d) I. McCulloch, M. Heeney, C. Bailey, K. Genevicius, I. MacDonald, M. Shkunov, D. Sparrowe, S. Tierney, R. Wagner, W. Zhang, M. L. Chabinyc, R. J. Kline, M. D. McGehee and M. F. Toney *Nat. Mater*., 2006, **5**, 328.

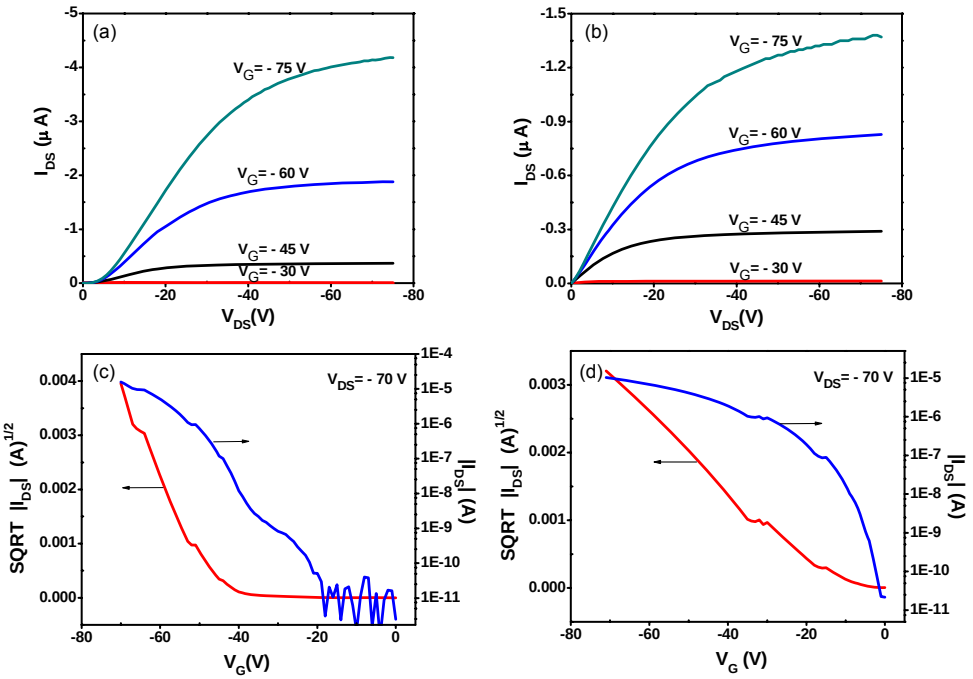

Figure 1: (a) and (b) output characteristics of bottom-contact OFET of sulfower and tetraselenotetrathio[8]circulene, respectively, (c) and (d) transfer characteristics of bottom-contact OFET of sulfower and selenasulflower, respectively. (deposition rate =0.2 Å/s, nominal thickness ~ 36 nm, W/L=1880/6 μm/μm). I_{DS} is the drain-source current and V_{DS} and V_G are the biasing voltages of drain-source current and gate electrodes, respectively.

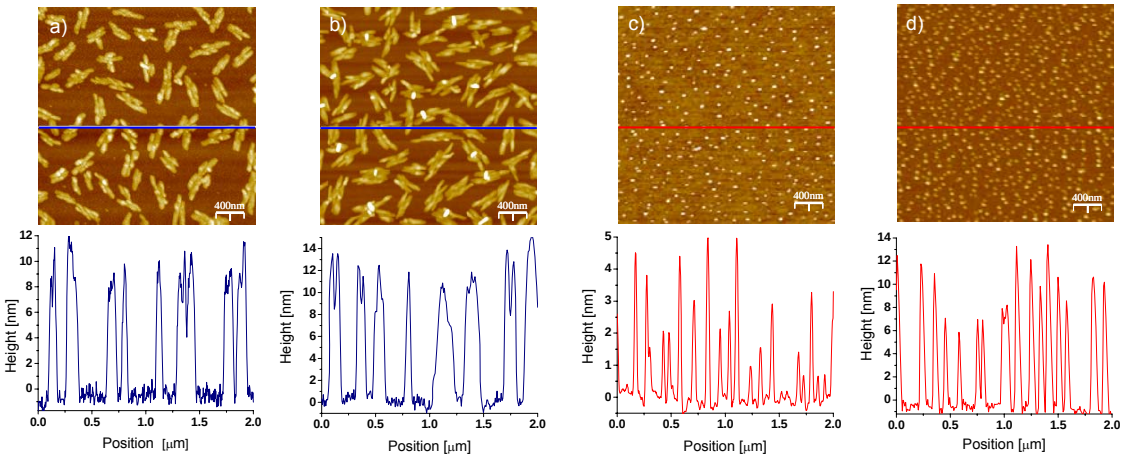

Figure 2: AFM Micrograph (2 μm×2 μm) images of thin films of sulflower (a, b) with the deposition time of 1 min, 2 min, respectively; tetraselenotetrathio[8]circulene (c,d) with the deposition time of 1min, 2 min, respectively. Films grown on SiO_2/Si substrate at room temperature (deposition rate=0.2 Å/s).

Gold Nanocubes: novel photo-synthetic method and morphological characterization

Adelaide Miranda[1], Patrícia A. Carvalho[2], Baltazar de Castro[1], Eulália Pereira[1]

[1]REQUIMTE, Faculdade de Ciências, Universidade do Porto, Rua do Campo Alegre, 687, 4169-007 Porto, Portugal
[2]Departamento de Engenharia de Materiais, Instituto Superior Técnico, Av. Rovisco Pais, 1049-001 Lisboa, Portugal
mariaadelaidemiranda@gmail.com

The development of new synthetic methods to prepare nanoparticles with different morphological characteristics is critical for the successful application of nanotechnology. Nanostructures with a cubic shape are quite interesting as they have larger surface-to-volume ratios and may prove to have significantly different reactivity and selectivity in catalysis.

To our best knowledge no one has reported the preparation of gold nanocubes by a bottom-up approach with mean edge length below 20 nm. Herein we describe a green simple rapid method to obtain nanocubes that have a mean edge length below 20 nm. This method is based on that previously reported by Shelnutt *et al.* for preparing platinum nanostructures[1]. Gold nanocubes were obtained by a light driven/crystal growth process using triethanolamine (TEA) as an electron donor, hexadecyltrimethlyammonium bromide (CTAB) as the capping agent, and a photosensitizer - Sn (IV) meso-Tetra(N-methyl-4-pyridyl) porphine tetra tosylate chloride (SntMepyP).

The formation of nanoparticles was monitored by ultraviolet-visible spectroscopy and the morphological characterization was carried out by transmission electron microscopy (TEM). UV/vis spectra showed one plasmon band at ~530 nm within 60 minutes after starting irradiation, accompanied by a color change from slightly yellow (gold) to red. TEM analysis indicates that the cubes have a mean edge length 16.91±2.54 nm. Electron dispersive spectroscopy and X-ray photoelectron spectroscopy were performed in order to obtain a more accurate chemical analysis of the nanoparticles prepared.

Figures:

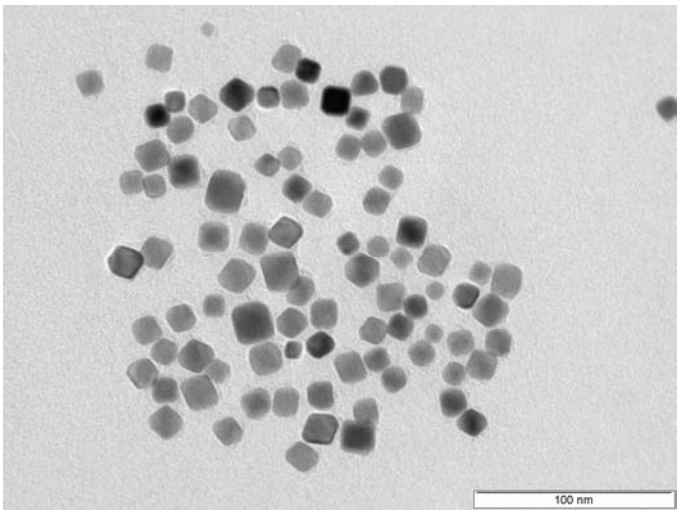

References:

[1] Song, Y.; Yang, Y.; Medforth, C. J.; Pereira, E.; Singh, A. K.; Xu, H.; Jiang, Y.; Brinker, C. J.; van Swol, F.; Shelnutt, J. A., *J. Am. Chem. Soc*. 2004*,* 126*,* 625-635.

Acknowledgments:

Financial support from Fundação para a Ciência e a Tecnologia through project PTDC/QUI/64484/2006. Adelaide Miranda thanks FCT for a Ph.D. grant SFRH/BD/17566/2004.

SIMULATION OF AN ABSORPTION CHILLER DUAL EFFECT OPERATING WITH THE COUPLE H2O/LiBr

Kadiatou Thérèse Dembélé

Centre d'Énergie Matériaux et Télécommunication, Institut National de la Recherche Scientifique 1650, boulevard Lionel-Boulet Varennes (Québec), Canada.

Abstract

We propose in this article an absorption chiller with effect double and two floors, and we evaluate their performance factors. It is an installation using solar energy and operating with environmentally friendly fluids, the lithium bromide and water (H2O/LiBr). This system uses in addition to solar cell, a photovoltaic's sensor for the pumping. It operates with two condensers, and two boilers (or desorbeurs), following three levels of pressure. The production due to cold refrigerant desorbed by the first boiler is free. The structure of these machines can be "working" heat introduced at the hot spring twice, hence the term double effect.

This article considers the coefficient of performance of these types of machine compared with absorption chillers classics.

ISOLATED NANOSCALE PROCHIRAL REACTION ASSEMBLIES ON PT(111)

Vincent Demers-Carpentier and Peter H. McBreen
Département de chimie, Université Laval, Québec (Qc), Canada, G1K 7P4

Chiral surfaces can be used to achieve catalytic chirality transfer. The mechanism through which this occurs is one of very precise nanoscale assembly. In particular, it involves a constraint in which the substrate, prochiral, molecule is forced into contact with the catalyst surface uniquely via a specific enantioface. One method to achieve this is to chemisorb a chiral-modifier so as to form molecular chiral sites. Co-adsorption of the substrate then leads to 1:1 prochiral modifier-substrate complexes. We report a combined STM, HREELS and computational study of such 1:1 prochiral assemblies on Pt(111). The study reveals the existence of chemisorption induced strong C-H to O=C intermolecular hydrogen bonding between co-adsorbed ketones and aromatics on Pt(111). It also shows how this unforeseen interaction may be used to sensitively modulate both chemical reactivity at surfaces and nanoscale assembly at surfaces.

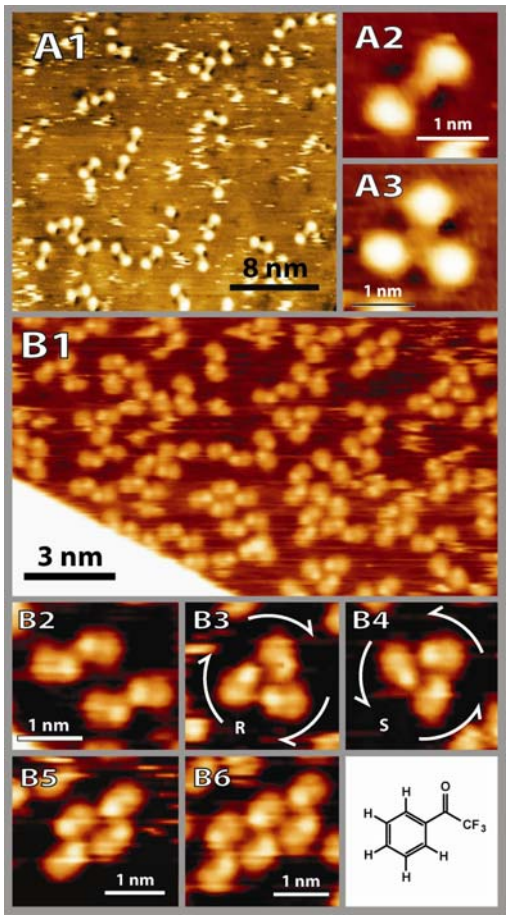

Figure1. STM images of trifluoroacetophenone (TFAP) adsorbed on Pt(111).[1] Panels A and B show well-defined groups of two (A1,A2,B1,B2), three (A3,B1,B3,B4), four (B1,B5) or six (B6) molecules over the entire surface at room temperature. Only dimers were observed (A1) at low coverages, indicating that they are the basic unit for the larger even-numbered clusters. Left and right-handed trimers are also observed as the coverage is increased. In B1-B6, each molecule is imaged as a lobe composed of a broad protrusion and a smaller bright spot at one end. In A1-A3, each molecule is imaged as a bright protrusion with a smaller dark spot at one end. The high-resolution images show that the dimers are formed from counter-aligned molecules. DFT calculations by Hammer *et al.*[1] show that dimer formation is stabilized by hydrogen bond interactions between the carbonyl group of one molecule and the aromatic CH bonds of the other molecule.

Such C-H···O bonded prochiral dimers, and similar systems formed by enol-enol interactions,[2] permit the study of surface reaction chemistry in isolated nanoscale assemblies. The combination of STM and electron energy loss spectroscopy is particularly powerful in this respect.

(1) Laliberté, Hammer *et a*l. *J. Am. Chem. Soc*. 2008, 130, 5386.
(2) Lavoie, Demers-Carpentier *et al. J. Am. Chem. Soc.* 2007, 129, 11668.

DEVELOPMENT OF A NOVEL MAGNETIC-FLUORESCENT COLLOIDAL NANO-CLUSTER

Riccardo Di Corato[†*], *Philomena Piacenza*[†], *Raffaella Buonsanti*[†*], *Roberto Cingolani*[†*], *Giovanna Barbarella*[‡], *Liberato Manna*[†*] *and Teresa Pellegrino*[†*]

[†] *National Nanotechnology Laboratory of CNR-INFM, 73100 Lecce, Italy*
[‡] *CNR, Area di Ricerca, ISOF, I-40129 Bologna, Italy*
* *Unità di Ricerca IIT, Lecce, Italy*

riccardo.dicorato@unile.it

The idea of the present work is to assemble iron oxide nanoparticles to develop super-structures with a faster response to an external magnet. In addition, functionalization of these composites with organic fluorophores, based on oligothiophenes, allows to obtain a final product suitable for a multiplexing cell sorting and for other kinds biomolecule separations.[1]

Magnetic nanocrystals of iron oxide have some well-defined characteristics, like superparamagnetic behaviour and high biocompatibility. However, iron oxide nanocrystals with diameters below 15 nm, have a low magnetization per particle, thus it is difficult to separate them from solution or to promptly accumulate them within few minutes by using moderate magnetic fields. This limits their use in applications such as cell sorting and drug delivery. On the other hand, increasing the nanocrystal size, increases the magnetization of saturation, but also induces the superparamagnetic–ferromagnetic transition (at a dimension of about 30 nm for Fe_3O_4), so that nanocrystals are no longer well disperse in solution.

Recently, our group reported a study on the water-solubilization of monodisperse nanoparticles using poly(maleic anhydride-*alt*-1-octadecene) polymer.[2] By using the same polymer it was possible to induce a partial agglomeration of iron oxide nanoparticles coordinated by the polymer in solution. In this case we have exploited the hydrophobic interaction between the poly(maleic anhydride-*alt*-1-octadecene) polymer and the surfactant coated iron oxide nanoparticles to favour in the reaction conditions, the formation of beads in a controlled way.

In a colloidal cluster the inter-particle distance is reduced to the thickness of the surfactant shell around the single nanocrystals; this feature can simulate the mass effect that determines the speed of the magnetic response in a concentrated sample. Moreover, the advantage to work still with a nano-scale cluster is the high ratio surface area / volume, that allow to have an higher level of functionalization.

The final nano-objects show a layer of polymer that prevents the degradation of the structure and equipped their surface with carboxylic groups that allows to solve the nano-clusters in polar solvent, like ethanol or water, having high stability (Figure 1). To control the size and the shape of the beads we have been changing the parameters that induce the bead formation, such as the solvent for creating the gradient, the gradient time, the amount of polymer added, the nanoparticles concentration and we show we were able to control the total diameter of the beads between 70 and 350 nm but also the thickness of the polymer shell and the core of the inorganic nanoparticles.
Recently, the Parak W.J. group reported a studies on the functionalization of poly(maleic anhydride *alt*-1 octadecene) with different moieties.[3] With a similar approach we functionalized the poly(maleic anhydride *alt*-1 octadecene) with different oligothiophene molecules (OTFs) to obtain a fluorescent polymer able to coordinate the formation of a fluorescent-magnetic cluster. In comparison to the organic dyes commonly used in bio-imaging and more similarly to colloidal quantum dots, OTFs have broad optical absorption spectra, and therefore fluorophores

emitting at different colours can be excited with a single excitation source, allowing for easier multiplexing analysis.
The characterization of the nanocrystals was carried out by means of transmission electron microscope (TEM), spectroscopy analysis (absorption spectra, FT-IR analysis), gel electrophoresis, dynamic light scattering and zeta-potential measurements.

References:

[1] Quarta A., Di Corato R., Manna L., Ragusa A., Pellegrino T., IEEE Transaction on nanobiocience, **6** (2007) 298.
[2] Di Corato R., Quarta A., Piacenza P., Ragusa A., Figuerola A., Buonsanti R., Cingolani R., Manna L. and Pellegrino T., Journal of Materials Chemistry., **18** (2008) 1991.
[3] Lin C.A., Sperling R.A., Li J.K., Yang T., Li P., Zanella M., Chang W.H., Parak W.J., Small, **4** (2008) 334.

Figures:

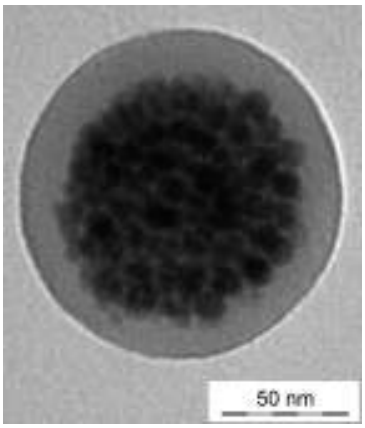

Figure 1. Low resolution TEM image of a magnetic-fluorescent nano-cluster. The synthesis was carried out by assembling γ-Fe_2O_3 nanocrystals (13 nm in diameter) with a poly(maleic anhydride *alt*-1 octadecene) functionalized with oligothiophene fluorophores.

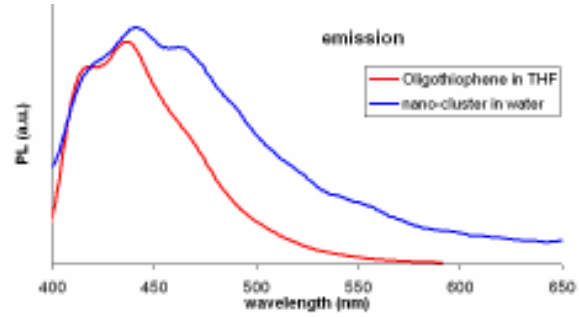

Figure 2. Photo-luminescent spectra of magnetic-fluorescent nano-cluster as compare to free oligothiophene. The red line corresponds to oligothiophene molecules solved in THF while the blue line corresponds to magnetic-fluorescent nano-cluster solved in water.

USE OF CONDUCTIVITY ON SILICON-ON-INSULATOR AS A PROBE OF MOLECULE-SURFACE INTERACTIONS

G.Dubey[1,2], F. Rosei[2], G.P. Lopinski[1]
[1] *NRC, Steacie Institute for Molecular Science, Ottawa, ON, Canada*
[2] *INRS, Energy and Materials, Universite du Quebec, Varennes, QC, Canada*
Gregory.Lopinski@nrc.ca

The surface properties of semiconductor structures are dramatically affected by transverse electric fields, which can penetrate appreciably over sub-micron lengths. Crystalline films scaled to nanometer dimensions are thereby attractive platforms for detecting charged states present at a molecular interface, inducing band-bending. In these systems, surface conduction exhibits distinct behaviour from bulk transport. One critical property of silicon-on-insulator substrates (SOI) is that their top film thickness (50 nm<d<3μm) is comparable to or less than the space-charge width (~1μm) for light doping levels (10^{14}-10^{15}cm^{-3}). Therefore transport is ideally suited as a dynamic probe of events modulating the conductivity such as molecular physisorption[1], chemisorption[2], presence of surface dipoles, and occupation of electrically active gap states.

In this work, conductivity and Hall effect measurements in high vacuum (HV) environments and under ambient conditions have been used to monitor adsorption and reaction events on H-terminated SOI (111) and (100) surfaces. In ambient, the sheet resistance $R_s(t)$ and carrier density $n(t)$ of H-SOI was shown to degrade by 1-2 orders of magnitude in days, attributed to occupation of acceptor-like gap states formed during the early stages of oxidation. Surprisingly in addition to this increase, a thin water layer present was found to lower the resistance on n-type substrates[1].

Controlled adsorption of water confirmed that H_2O causes downward band-bending, inducing accumulation of electrons on n-type and an inversion layer on p-SOI. The latter effect was explored with a range of other gases. In particular, hole trapping molecules such as pyridine and ammonia have been found to mimic the action of a gate in a field effect transistor, biasing p-type surfaces into inversion[3,4]. A change in sign of the Hall voltage supports the formation of this inversion layer. Adsorption of toluene and thiophene vapors however, did not alter the resistance, indicating they weakly couple to electronic states of the silicon. These results demonstrate the potential of SOI substrates as platforms for studies of molecular adsorption and charge transfer effects at surfaces. The observations have significant relevance to the electronic properties of silicon nanowires, which are presently being studied for chemical sensing applications.

References:

1 G. Dubey, G. P. Lopinski, and F. Rosei, Applied Physics Letters **91** (2007), 232111.

2 G. P. Lopinski, B. J. Eves, O. Hul'ko, C. Mark, S. N. Patitsas, R. Boukherroub, and T. R. Ward, Physical Review B (Condensed Matter and Materials Physics) **71** (2005), 125308.

3 H. Statz, G. deMars, L. Davis, and A. Adams, Physical Review **106** (1957), 455.

4 L. Osminkina, A. Vorontsov, E. Konstantinova, V. Timoshenko, and P. Kashkarov, Semiconductors **39** (2005), 458.

THE EFFECT OF SINGLE NANOCRYSTAL BLINKING ON THE LUMINESCENCE DECAY OF ENSEMBLES

K. Dunn, J. Derr, M. Chaker, F. Rosei
INRS-EMT, Université du Québec
1650 Lionel-Boulet, Varennes, Canada
dunn@emt.inrs.ca

Nanocrystal (NC) systems commonly exhibit multiexponential photoluminescence (PL) decays. Though many explanations have been provided that hypothetically explain the manifestation of the stretched-exponential form, there has been little experimental evidence to indicate the success of one model over any other. Interestingly, the influence of single NC intermittence on the decay curves of NC ensembles has so far been overlooked. We suggest that the anomalous curve elongation is intimately liked to the power-law blinking statistics of single NCs.

Figure 1 pictorially summarizes a simple model used to investigate the effect that the single NC blinking phenomenon has on the anomalous multiexponential behaviour of NC ensembles. Using stable distribution theory we derive a simple fitting form for the analysis of PL decay curves which allows the extraction of both intrinsic recombination rates linked to quantum confinement and power-law exponents typifying blinking statistics of single nanocrystals. This approach is then applied to the PL decay curves of a series of silicon NCs embedded in silicon oxide with average sizes within the range 1.5 to 4nms. These results are shown in figure 2a and b; and are compared with parameters extracted using the empirical stretched exponential law figures 2c and d.

A theoretical tendency of recombination rate with emission energy as determined by Delerue et. al. is plotted on figure 2b for comparison. Note that the extracted values represent a much better agreement with theory than the inverse stretched exponential lifetime which is consistently some order of magnitude higher. Remarkably the extracted α values also agree perfectly with the expected values of the blinking exponent which are generally determined experimentally within the range $1<\alpha_{on/off}<2$, and predicted theoretically to be exactly equal to 1.5 for normal diffusion and to fall within the range $1.5<\alpha_{on/off}<2.5$ where anomalous diffusion and reaction is applicable. These results represent a promising development as the the same technique can potentially be applied to the analysis of carrier recombination in a great number of other quantum confined systems and in addition, may provide a simple alternative for the extraction of nanocrystal blinking statistics under a much wider range of conditions than is possible in difficult to execute single nanocrystal spectroscopy experiments.

References:

[1] C. Delerue, G. Allan, C. Reynaud, O. Guillois, G. Ledoux, and F. Huisken. Multiexponential photoluminescence decay in indirect-gap semiconductor nanocrystals. Phys. Rev. B: Condens. Matter. Phys., 73(23):235318, 2006.

[2] Daniel E. Gomez, Marco Califano, and Paul Mulvaney. Optical properties of single semiconductor nanocrystals. Phys. Chem. Chem. Phys., 8:4989–5011, 2006.

[3] O. Guillois, N. Herlin-Boime, C. Reynaud, G. Ledoux, and F. Huisken. Photoluminescence decay dynamics of noninteracting silicon nanocrystals. J. Appl. Phys., 95(7):3677–3682, 2004.

[4] Jan Linnros, Nenad Lalic, Augustinas Galeckas, and Vytautas Grivickas. Analysis of the stretched exponential photoluminescence decay from

nanometer-sized silicon crystals in sio[sub 2]. J. Appl. Phys., 86(11):6128–6134, 1999.
[5] T. Suemoto, K. Tanaka, and A. Nakajima. Interpretation of the temperature dependence of the luminescence intensity, lifetime, and decay pro les in porous si. Phys. Rev. B: Condens. Matter. Phys., 49(16):11005–11009, Apr 1994.
[6] Milan Sykora, Lorenzo Mangolini, Richard D. Schaller, Uwe Kortshagen, David Jurbergs, and Victor I. Klimov. Size-dependent intrinsic radiative decay rates of silicon nanocrystals at large con nement energies. Physical Review Letters, 100(6):067401, 2008.
[7] Jau Tang. Fluorescence intermittency of silicon nanocrystals and other quantum dots: A uni ed two-dimensional di□usion-controlled reaction model. The Journal of Chemical Physics, 127(11):111105, 2007.
[8] P. J Ventura, M. C. do Carmo, and K. P. O'Donnell. Excitation dynamics of luminescence from porous silicon. Journal of Applied Physics, 77, 1995.
[9] J. C. Vial, A. Bsiesy, F. Gaspard, R. H´erino, M. Ligeon, F. Muller, R. Romestain, and R. M. Macfarlane. Mechanisms of visible-light emission from electro-oxidized porous silicon. Phys. Rev. B: Condens. Matter. Phys., 45(24):14171–14176, Jun 1992.

Figures:

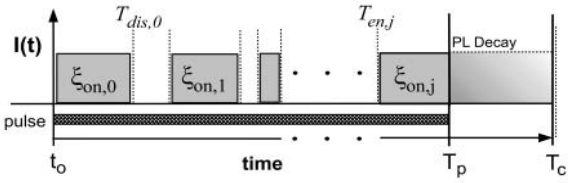

Figure 1: Events contributing to luminescence decay curves for blinking nanocrystal ensembles

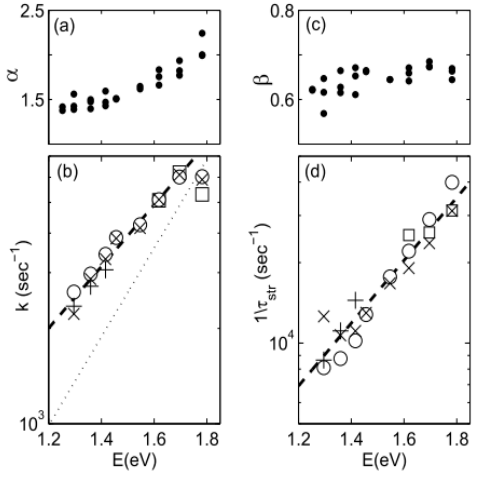

Figure 2: Recombination rates and associated parameters with observation energy resulting either from the derived blinking form (figures a and b) or the conventional stretched-exponential figure (c and d) for silicon nanocrystal samples.

QUANTUM DOTS-BASED FLUORESCENT INMUNOASSAY FOR THE DETERMINATION OF AFLATOXINS

M. T. Fernández-Argüelles, L. Trapiella, J. M. Costa, R. Pereiro and A. Sanz-Medel.
Department of Physical and Analytical Chemistry, Faculty of Chemistry,
University of Oviedo,Oviedo, 33006, Spain.
fernandezteresa@uniovi.es

Luminescent colloidal semiconductor nanocrystals, known as "quantum dots" (QDs), have captivated researchers from multiple areas of the science and technology, owing to their fascinating optical and electronic properties, which are not available from either isolated molecules or bulk solids. These properties include high quantum yields, large extinction coefficients, high photostability, and broad absorption spectra coupled to narrow size-tuneable photoluminescent emission spectra. Unlike conventional dyes, distinct populations of QDs can be simultaneously excited by a single wavelength far from their respective emissions, which suggests they could be especially suited for multiplexing assays *via* simultaneous detection of multiple signals [1]. Due to these favourable optical properties, analytical chemists have started to explore the use of QDs as a new generation of luminescent labels in different biochemical applications, and particularly in the development of luminescence-based immunosensors [2]. In this line, very recently, we have investigated the applicability of QDs as photoluminescent labels in the development of an immunoassay for the detection of the toxic species, Aflatoxin B1, based on the bioconjugation of ZnS-CdSe QDs to anti-aflatoxin antibodies.

Colloidal ZnS-CdSe QDs used as labels in this work were synthesized from organometallic precursors and are inherently hydrophobic. Different approaches have been used to make them hydrophilic and, so, water-soluble and compatible with biological media while preserving their optical properties. In this work we resorted to an approach involving the coating of the surface of the native hydrophobic QDs with an amphiphilic polymer shell. The hydrophilic functions of the polymeric shell provide water-compatibility and can be used for further simple and general bioconjugation of the nanocrystals to appropriate antibodies [3].

Further, bioconjugation of the synthesized polymeric-layered water-soluble QDs to anti-aflatoxin antibodies was performed by a simple method. The formed bio-conjugates were purified from an excess of free antibodies and of free nanoparticles by size-exclusion chromatography and then exhaustively characterized by fluorescence spectroscopy and MALDI-TOFMS. Finally, applicability of the proposed QDs-based immunoassay to Aflatoxin B1 detection was demonstrated by resorting to photoluminescence measurements.

References:

[1] A. Paul Alivisatos, Science, **271** (1996) 933.
[2] R. E. Bailey, A. M. Smith, S. Nie, Physica E, **25** (2004) 1.
[3] M. T. Fernández-Argüelles, A. Yakovlev, R. A. Sperling, C. Luccardini, S. Gaillard, A. Sanz Medel, J. M. Mallet, J. C. Brochon, A. Feltz, M. Oheim, and W. Parak, Nano Lett., **7(9)** (2007) 2613.

COMPETING SUPERPARAMAGNETISM AND EXCHANGE BIAS IN Fe NANOPARTICLES EMBEDDED IN AN AMORPHOUS CARBON MATRIX

M.P. Fernández García[a], *D.S. Schmool*[b], *A.S. Vieira*[b], *M. Sevilla*[c], *A.B. Fuertes*[c], *P. Gorria*[a], *J.A. Blanco*[a].

[a]*Dpto. de Física, Universidad de Oviedo, C/ Calvo Sotelo s/n,33007,Oviedo, SPAIN.*

[b]*IN-IFIMUP in Dpto. de Física, Universidade do Porto, Rua do Campo Alegre, 687, 4169-007, Porto, PORTUGAL.*

[c]*Instituto Nacional del Carbón, CSIC, Ap. 73, 33080, Oviedo, SPAIN.*

fernandezpaz.uo@uniovi.es

Research in magnetic nanoparticles (NPs) continues to have a high impact over the last decade not only for their fundamental scientific knowledge [1], but also for their unique properties and potencial technological applications such as ultrahigh-density recording and medicine. The synthesis of NPs is of key importance [2,3], because the properties of these nanocrystals are strongly dependent on their physical dimensions [4]. As a consequence we have used a commercial and low cost activated carbon (AC) (widely used before as adsorbents, as catalyst support and in Medicine because of their bio-compatible character) for embedding Fe NPs [5].

Another important issue for most applications relies on the magnetic order of NPs being stable with time. Sometimes, NPs loose this required stability (wanted for example in recording media) when the reduction of their sizes comes into conflict with the superparamagnetic (SPM) limit [6]. When this happens, magnetic exchange coupling [7] induced by the core and NP´s surface competes with SPM behaviour leading to magnetization stability. We have studied these and other interesting behaviours by combining structural characterization and physical properties of Fe NPs randomly dispersed in AC.

The sample in powder form, with average grain sizes of several microns, as SEM images reveals, contains around 17 wt.% of Fe. The average crystalline sizes for the Fe-AC NPs, obtained from TEM images (Figure 1), correspond to a broad distribution ranging from 5 to 50 nm with different crystal structures as the X-ray diffraction evidences.

The analysis of the room temperature Mössbauer spectrum of these NPs (Figure 2) was performed with three different contributions: a ferromagnetic α-Fe phase with B_{HF} = 33 T, a paramagnetic γ-Fe phase and an additional doublet, that could be associated with the NP´s shell or with an oxide phase probably located on the surface of the NPs. The relation between the percentage of α-Fe and both γ-Fe and the doublet contribution is $42/58 \approx 0.72(4)$. XRD pattern collected at room temperature confirms the existence of both BCC and FCC crystal structures giving a relative phase percentage of $\alpha - Fe/\gamma - Fe \approx 0.82(5)$ that agrees rather well with that of Mössbauer spectrum.

Magnetization vs. magnetic field curves, *M(H)*, are reversible above 200 K (Figure 3) as expected for a superparamagnetic-like behaviour. In addition $M_{ZFC}(T)$-$M_{FC}(T)$ curves do not overlap in the measuring range 10 - 340 K (Figure 3), suggesting that the whole system has not reached a SPM regime. Moreover, M_{ZFC}, exhibit a broad maximum that leads to a non unique well-defined blocking temperature owing to the broad distribution of NP´s size. Finally, a loop shift in *M(H)* curves indicating the existence of a magnetic exchange bias coupling (Figure 4), seems to suggest the presence of a core/shell morphology that makes Fe-AC NPs remain completely blocked below 60 K.

References:

[1] J.L. Dormann, D. Fioranni, E. Tronc, Magnetic relaxation in fine-particle systems, John Wiley & Sons, (1997).
[2] J. Park, K. An, Y. Hwang, J.-G. Park, H.-J. Noh, J.-Y. Kim, J.-H. Park, N.-M. Hwang, T. Hyeon, Nature materials, **3** (2004) 891.
[3] V.P. Dravid, J. H. Host, M. H. Teng, B. Elliot, J. Hwang, D. L. Johnson, T. O. Mason, J. R. Weertman, Nature, **374** (1995) 602.
[4] X. Battle, A. Labarta, J. Phys. D: Appl. Phys. **35** (2002) R15-R42.
[5] A.B. Fuertes, P. Tartaj, Chem. Mater., **18** (2006) 1675-1679.
[6] V. Skumryev, S. Stoyanov, Y. Zhang, G. Hadjipanayis, D. Givord, J. Nogués, Nature **423** (2003) 850-853.
[7] J. Nogués, J. Sort, V. Langlais, V. Skumryev, S. Suriñach, J. S. Muñoz, M. D. Baró, Physics Reports, **422** (2005) 65-117.

Figures:

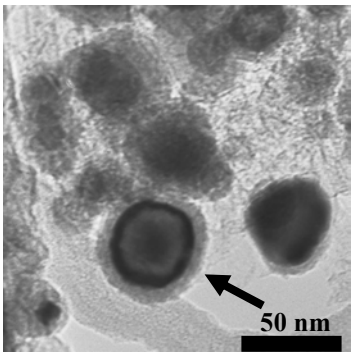

Figure 1. TEM image of Fe-AC NPs. The arrow points a core/shell Fe-AC NP.

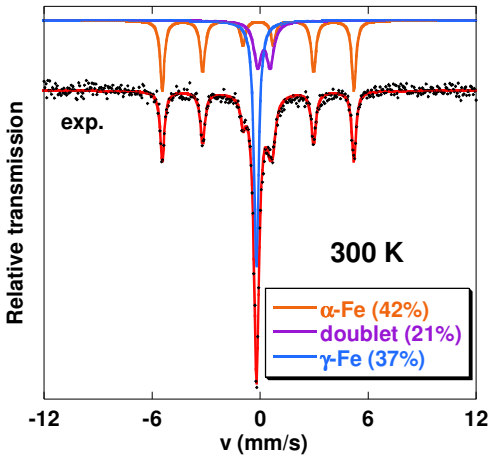

Figure 2. Room temperature Mössbauer spectrum of Fe-AC NPs together with the fit with three different contributions.

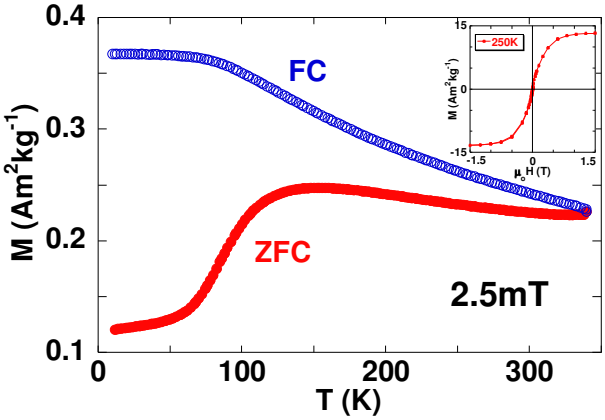

Figure 3. ZFC-FC magnetization variations under an applied field of 2.5 mT measured in the range 10-340K. The inset shows the SPM behaviour for *M(H)* curve at 250 K.

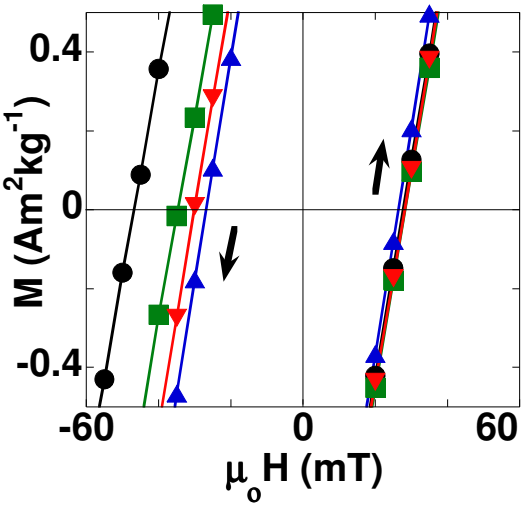

Figure 4. Details of the *M(H)* hysteresis loops around *M=0* under $\mu_o H_{cool}$=1.5T

ON-SITE APPROXIMATION FOR SPIN-ORBIT COUPLING IN LCAO DENSITY FUNCTIONAL METHODS: APPLICATION TO CLUSTERS AND CHAINS

L. Fernández Seivane1, J. Ferrer Rodríguez1
Departamento de Física, Universidad de Oviedo, Oviedo, Spain
quevedin@condmat.uniovi.es

We propose a computational method that simplifies drastically the inclusion of spin-orbit interaction in density functional theory implemented on localised atomic orbital basis sets. Our method is based on a well-known procedure for obtaining pseudopotentials from atomic relativistic ab initio calculations and on an on-site approximation for the spin-orbit matrix elements. We have implemented the technique in the SIESTA code[1], and we show that it provides accurate results for the overall band structure and splittings of group IV and III-IV semiconductors as well as for 5d metals[2]. We also analyze the impact of the magnetic anisotropy on the geometric structure and magnetic ordering of small atomic clusters of palladium, iridium, platinum and gold[3]. Our results highlight the absolute need to include self-consistently the spin orbit interaction in any simulation of the magnetic properties of small atomic clusters, and a complete lack of universality in the magnetic anisotropy of small-sized atomic clusters.

References:

[1] cond-mat/0611624 Predictions for the formation of new atomic chains in Mechanically Controllable Break Junction experiments. Lucas Fernandez Seivane, Victor M. Garcia-Suarez, Jaime Ferrer. *Phys. Rev. B* **75**, 075415 (2007).
[2] cond-mat/0610879 Magnetic anisotropies of late transition metal atomic clusters. Lucas Fernandez Seivane, Jaime Ferrer. Physical Review Letters **99**, 183401 (2007)
[3] cond-mat/0601093 On-site approximation for spin-orbit coupling in LCAO density functional methods. Lucas Fernandez Seivane, Miguel A. Oliveira, Stefano Sanvito, Jaime Ferrer. *J. Phys.: Condens. Matter* 18 7999-8013, 2006.
[4] M. N. Huda, M. K. Niranjan, B. R. Sahu and L. Kleinman, *Phys. Rev. A* 73, 053201 (2006).
[5] F. Aguilera-Granja, J. Ferrer and A. Vega, *Phys. Rev. B*, 74 174416 (2006).

Figures:

Results for Trimers

Equilibrium geometries and spin moments $g \cdot S_i$ of (a) Pd_3, (b) Ir_3, (c) Pt_3 and (d) Au_3.

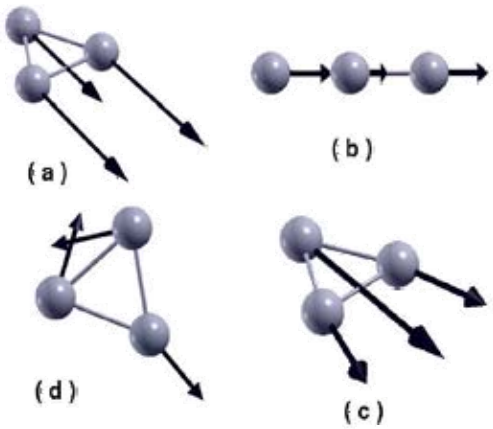

Left to right: (a) Pd2, (b) Ir2, (c) Pt2 and (d) Au2.

Up downwards: (1) Energy, (2) Spin moment per atom times gyromacnetic ratio and (3) Orbital angular moment per atom

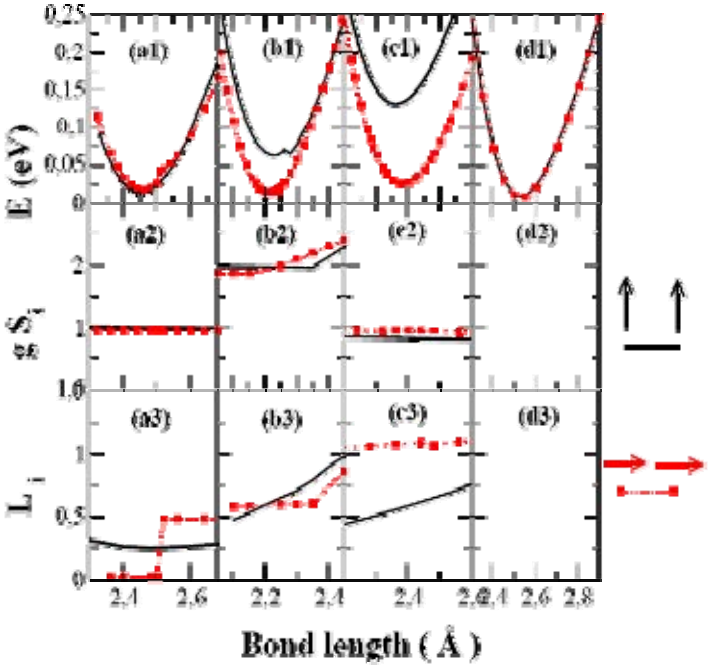

Results for Tetramers

Equilibrium geometries and spin moments $g \cdot S_i$ of (a) Pd_4, (b) Ir_4, (c) Pt_4 and (d) Au_4.

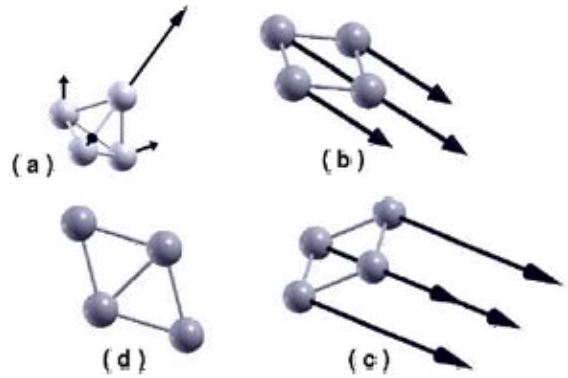

Results for Pentamers

Equilibrium geometries and spin moments $g \cdot S_i$ of (a) Pd_5, (b) Ir_5, (c) Pt_5 and (d) Au_5.

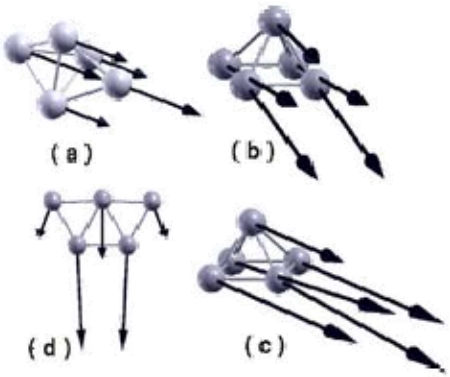

HYBRID NOBLE METAL-FERROMAGNET NANOPARTICLES FOR BIOSENSING APPLICATIONS: A PRELIMINARY STUDY.

J.F. Torrado, E. Ferreiro, J.B. González-Díaz, A. García-Martín, J.M. García-Martín, A. Cebollada, J.V Anguita and G. Armelles
Instituto de Microelectrónica de Madrid, Consejo Superior de Investigaciones Científicas, C\Isaac Newton 8 (PTM) 28760 Tres Cantos, Spain
jftorrado@imm.cnm.csic.es

A. Blanco and C. López
Instituto de Ciencia de Materiales de Madrid, Consejo Superior de Investigaciones Científicas, Ctra. de Colmenar Km. 15, Cantoblanco, 28049 Madrid, Spain

B. Sepúlveda and M. Käll
Chalmers University of Technology, Göteborg, 41296, Sweden

Surface plasmons are collective electronic excitations localized at the interface of a metal and a dielectric and they play a very important role in the optical properties of metallic systems. This physical principle is being successfully exploited to develop biosensing devices since surface plasmons are extremely sensitive to small dielectric modifications close to the metal surface. For instance, functionalized Au nanolayers are the basis of the Surface Plasmon Resonance sensor that has shown a high sensitivity detecting small biological molecules [1]. This sensitivity has been recently enhanced by combining noble metal materials that present plasmonic properties with ferromagnets that give rise to magneto-optical (MO) activity [2]. The origin is that such combination leads to an increased MO response when a surface plasmon is excited and allows the modulation of the optical signal [3].
An alternative and promising approach consists in the use of metallic nanoparticles to develop biosensing applications [4]. They support localized surface plasmons (LSPs) and present considerable advantages with respect to continuous layers. For example, the spectral resonance can be tuned not only by means of the dielectric material surrounding the nanoparticles but also by altering the size, shape, or distance between particles. Another advantage is that the electromagnetic field is strongly localized, a property that might lead to high spatial specificity sensing. In this way, several studies have shown the spectral shift of the optical response when varying the surrounding refractive index of the nanoparticles [5]. Our purpose in this work is to go beyond by introducing MO activity simultaneously to LPS excitation. To do so we will analyze the MO response of a series of Au/Co/Au nanodisks[6] as a function of the surrounding environment. Our preliminary results have shown that the MO measurements are more sensitive to dielectric changes than the optical ones. We expect to improve this result tuning the nanostructure geometrical parameters.

References:

[1] Naimushin AN et al. Biosens. Bioelectron., **17** (2002) 573.
[2] B. Sepúlveda et al. Opt. Lett.**31**, (2006) 1085.
[3] J.B. Gonzalez-Diaz et al. Phys. Rev. B. **76**, (2007) 153402.
[4] Frederix F, Friedt JM, Choi KH, et al. Anal. Chem., **75**, (2003) 6894
[5] K.S. Lee, M.A. El-Sayed, J. Phys. Chem. B. **110**, (2006) 19220.
[6] J.B. Gonzalez-Diaz et al. Small, **4**, (2008) 202.

SEEDED GROWTH APPROACH FOR SYNTHESIS OF SEMICONDUCTOR NANOTETRAPODS

Angela Fiore[a], *Rosanna Mastria*[a], *Davide Cozzoli*[a], *Liberato Manna*[a], *Roberto Cingolani*[a]
[a]*National Nanotechnology Laboratory of CNR-INFM, Distretto Tecnologico ISUFI 73100 Lecce, Italy*
angela.fiore@unile.it

A step forward in the shape control of colloidal nanocrystals is the generation of inorganic nanostructures with deliberately designed branching. The most basic branched crystal is a tetrapod that is formed when four wurtzite-phase arms grow out of four equivalent facets of a zinc blende nanocrystal core. The formation of tetrapods has recently been reported for several II–VI semiconductors,[1-10] because they exhibit zinc blende–wurtzite polytypism. Indeed, their lattice has a common crystal plane, which can be used to achieve branching. The [111] plane of the cubic zinc blende lattice structure is atomically identical to the ±[0001] plane of the wurtzite structure.
In order to form the tetrapods it is possible to separate the nucleation and growth processes by seeded growth approach. According this method preformed nuclei in zinc blende phase are added to the reaction mixture, followed by the growth of the arms in wurtzite structure. In fact the balance of the nucleation and growth processes in a one-pot reaction is hardly achieved and leads to high sensitivity on small variations in reaction conditions.
Talapin and co-workers[11] demonstrated that seeded growth of nanocrystals offers a convenient way to design nanoheterostructures with complex shapes and morphologies by changing the crystalline structure of the seed.
In this contribution, we present a step in this field, demostrating that the seeded growth approach is easily extendible to other combinations of materials. Here, we demonstrate its viability to the synthesis of tetrapod-shaped heterostructures with ZnTe core and CdX (X=S, Te, Se) arms. In addition, by the same approach, we are able to synthetize tetrapods nanocrystals with CdSe as core and CdTe arms. These strategies of synthesis permit to obtain tetrapods with significantly narrow distribution of arm lengths and diameters; in addition, it is possible to tune the size of nanocrystals by changing several reaction parameters.
These heterostructures present a type II character (staggered band), that leads to the formation of an indirect exciton. The relative energy offset can be tuned by controlling the size of the core and the arms, which should allow the further exploitation of these nanocrystals in potential application such as photovoltaic devices.

References:

[1] L. Manna, D. J. Milliron, A. Meisel, E. C. Scher, A. P. Alivisatos, Nat. Mater., **2** (2003) 382.
[2] Y.W. Jun, S. M. Lee, N. J. Kang, J. Cheon, J. Am. Chem. Soc., **123** (2001) 5150.
[3] L. Manna, E. C. Scher, A. P. Alivisatos, J. Am. Chem. Soc.**, 122** (2000) 12700.
[4] Q. Pang, L. Zhao, Y. Cai, D. Nguyen, N. Regnault, S. Wang, W. Ge, R. Ferreira, G. Bastard, J. Wang, Chem. Mater., **17** (2005) 5263.
[5] W. Yu, L. Qu, A. Wang, X. Peng, Chem. Mater., **15** (2003) 4300.
[6] Y. Li, H. Zhong, R. Li, Y. Zhou, C. Yang, Y.F. Li, Adv. Funct. Mater., **16** (2006) 1705.
[7] M. B. Mohamed, D. Tonti, A. A. Salman, M. Chergui, ChemPhysChem., **6** (2005) 2505-2507.
[8] S. Asokan, K. M. Krueger, V. L. Colvin, M. S. Wong, Small, **7** (2007) 1164 – 1169.
[9] Q. Pang, L. Zhao, Y. Cai, D. P. Nguyen, N. Regnault, N. Wang, S. Yang, W. Ge, R. Ferreira, G. Bastard, J. Wang, Chem. Mater., **17** (2005) 5263-5267.

[10] L. Carbone, S. Kudera, E. Carlino, W. J. Parak, C. Giannini, R. Cingolati, L. Manna, J. Am. Chem. Soc. 2006, **128** 2006 748-755.
[11] D. V. Talapin, J. H. Nelson, E. V. Shevchenko, S. Aloni, B. Sadtler, P. Alivisatos, Nano Lett., **10** (2007) 2951-295.

Figure: TEM images of tetrapod shaped nanocrystals formed by seeded growth approach.

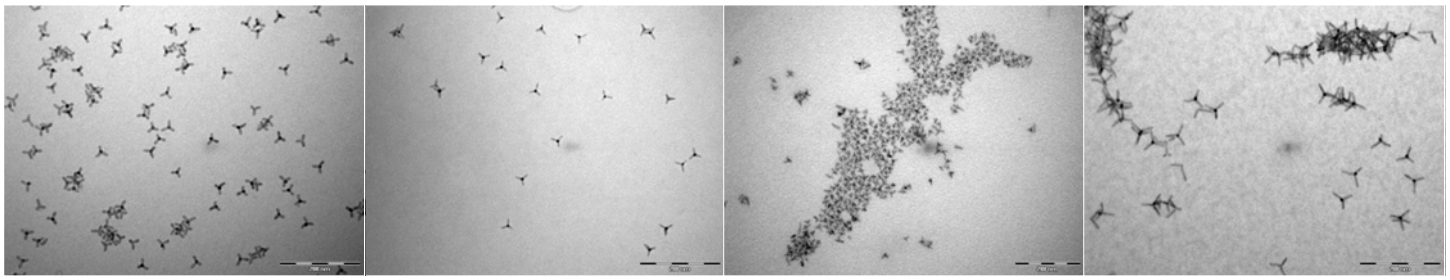

CONTACTS AT THE NANOSCALE: USING SILICON NANOSTENCILS TO MAKE WIRES AND CONTACTS ON ULTRA HIGH VACUUM CLEAVED INSULATORS

S. Fostner, S. Burke, J. Topple, P. Grütter
McGill University, 3600 University St, Montreal, Canada
Email: sfostner@physics.mcgill.ca

The conductance measurement of single molecules has been a focus of many groups for the past decade. Careful measurement of molecular transport would help pave the way for molecular electronic devices with numerous applications. Despite many attempts, rigorous agreement between theory and experiment remains elusive [1]. In order to close this gap, a detailed knowledge of the environment and contacting geometry is required. To this end, ultra high vacuum (UHV) measurements provide a possible route, however making the connection from the macroscopic realm of cables and measurement devices to the nanometer scale of individual molecules requires a creative mixture of micromachining techniques and understanding of the growth processes at atomic scales.

In order to make electrical measurements at the single molecule level, stencil masks based on silicon membranes have been developed to deposit metals onto atomically flat insulating substrates in UHV. Stencil deposition has the advantages of being a resist free deposition process, and compatible with UHV-clean substrates, such as vacuum cleaved KBr, while providing flexibility in both structures and substrates. [2,3]
In order to make contacts at the nanometers scale but have the flexibility of contacting to millimeter or later deposited contacts we chose to use a two mask process. Using two sets of masks allows a separation of length scales, where nanometer scale openings are present solely in the membrane but the interface to the macroscopic is accessed by a simple millimeter scale contact mask. Samples are created using vacuum cleaved substrates with 2 terminal contacts deposited in situ onto the freshly cleaved face using a 50-75 micrometer copper mask [3]. For the smaller features we use stencil masks created using standard micromachining techniques at the McGill Nanotools facility. Smaller features are deposited using openings as small as 50 nm created in thick silicon membranes with regions thinned using the focused ion beam at the University of Sherbrooke, as shown in Fig 1. These masks are now being used to deposit long tantalum and gold contacts and wires on KBr without removing the sample from vacuum, which bridge the gap given by the initial masking step.

One difficulty of using stencil masks is maintaining the pattern integrity in the face of intrinsic and deposited film stress created by depositing thick films of metal or other materials on the stencil. Efforts have been make to create stabilizing structures and patterns for stencil membranes [4], typically using thin silicon nitride membranes. These can suffer from a difficulty of extending the support structures close to the apertures while avoiding disrupting line of sight for the openings and source. Using single crystal silicon membranes greatly helps alleviate the former, but the latter is still a problem for all stencils. We have created a simple form of support structure in the silicon stencil itself

to allow it to resist significant deformation even with high stress metal films while maintaining the aspect ratio near the nanoscale openings.

To further allow the positioning of molecules near electrodes, nanometer size pits have been created in the surface by electron irradiation of the substrate. The pits can be created either the scanning electron microscope (SEM) or the electron beam evaporator. Using the SEM, pits as small as 1-2 nm across have been created and then imaged using atomic force microscopy. These pits can also be used as a template to control the growth of metals and molecules on nanometer length scales. By imaging the metal wires and contact pads with the SEM we can both obtain structural information on the metal contacts and create pits of arbitrary size to which will tend to nucleate near metal structures. Furthermore, as we have also demonstrated, these pits can in turn act as nucleation centers for the growth of molecules and metal clusters, such as gold [5]. Gold clusters will preferentially nucleate on the corners of these pits, and together with the control over the pit size this allows the templating of close proximity metal contacts to individual molecules. .

These techniques give us access to all the relevant length scales in which one would like to control the deposition and position of metals and molecules in order to make well characterized conductance measurements, bringing us closer to being able to close the fundamental gaps in molecular measurements between theory and experiment.

References:

[1] Lindsay, S., Ratner, M., Advanced Materials, **19** (2007) 23.
[2] Deshmukh, M. , Ralph, D. , Thomas, M. , Silcox, J., App. Phys. Lett., **75** (1999) 1631
[3] C. Gärtner et al, Rev. Sci. Instr, **77** (2006) 026101.
[4] Van den Boogaart, M., Doeswijk, L., Brugger, J., J. Microelectromechanical Systems, **15** (2006) 1663.
[5] Mativetsky, J. ,Burke, S., Fostner, S., Grutter, P., Small, **3** (2007) 818.

Figures:

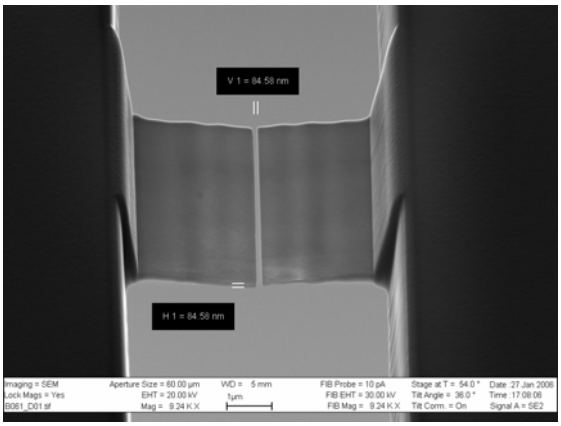

Figure 1: Silicon stencil, 80 nm wire opening

END-TO-END ASSEMBLY OF SHAPE-CONTROLLED NANOCRYSTALS VIA A NANO-WELDING APPROACH.

Isabella R.Franchini [a], Albert Figuerola [a,b], Angela Fiore [a,b], Rosanna Mastria, [b] Roberto Cingolani [a,b], Liberato Manna [a]

[a] National Nanotechnology Laboratory of CNR-INFM, Distretto Tecnologico ISUFI, via per Arnesano km 5, 73100 Lecce, Italy
[b] Scuola Superiore ISUFI, University of Salento, Distretto Tecnologico ISUFI, via per Arnesano km 5, I-73100 Lecce, Italy
isabella.franchini@unile.it

Controlled assemblies of colloidal nanocrystals (NCs) have recently attracted growing interest as a result of their potentially novel electronic, optical and magnetic properties, which might be different from those of a corresponding collection of individual non-coupled NCs or from the bulk solid.

By the literature the formation of one-, two- and three- dimensional assemblies of NCs with different type materials is known.[1-3] A large variety of approaches has been used for their obtaining, using biomolecules as linkers or inorganic templating agents as architectonic platforms for several NCs. One issue that has been mainly addressed in this field is the control of the interparticle distance in the assembly which allows the tuning of the properties of the NC superstructure. Our work is based on a variety of chemically directed chalcogenide-based NC assemblies. By taking advantage of easily processable solution-based reactions at low temperatures, different chalcogenide materials of various sizes and shapes have been assembled without the need of organic linkers giving rise to only inorganic NC-based superstructures with different branching degrees.

One general assembling strategy has been used for the organization of differently sized and shaped Type IV-VI semiconductor nanocrystals, independently of the nature of the chalcogenide atom (S^{2-}, Se^{2-} or Te^{2-}). The NCs utilized were CdSe@CdS asymmetric core@shell nanorods, CdSe nanorods and CdSe@CdTe tetrapods, all of them synthetized by a seeded growth approach.[4] The scope of our work consists in the formation of an inorganic heterojunction between nanocrystals by means of a previous selective nucleation of gold dots on the tips of the semiconductor nanostructures. Infact, state of the art of gold nanoparticles shows the role of the iodide (I^-) to fuse and assemble colloidal gold NCs in solution[5-6]. However, in our experiments, iodine (I_2) seems to have a comparable effect using the previously mentioned semiconductor-Au heterostructures. Actually, the presence of iodine, even in trace amounts, was found sufficient to glue together the Au domains that had nucleated at the tips of the NCs (nanorods or tetrapods) (see Scheme 1).
All reactions take place in relatively short times ($t \leq 30$min) and at room temperatures. The final size of the assembly can be controlled by the ratio between NCs and aggregator agent (I_2) in the solution. The selective nucleation of Au domains in just one or both tips of the chalcogenide crystals introduces preferential anchoring points that allow tuning the assembling freedom degree of the heterostructures. In this way zero-dimensional superstructures, i.e. flower-like (see Figure 1), can be obtained in solution by the reaction of I_2 with only one tip Au-decorated nanorods, while 1D, 2D or 3D superstructures are formed in solution when all tips of the semiconductor structures present an Au domain (see Figure1).
In summary, our work introduces a general approach for the assembly of cadmium chalcogenide semiconductor NCs by means of metallic gold junctions. It yields solely inorganic nanocrystalline assemblies, which are stable in organic solvents and hence should be easily processable for the fabrication of new devices[7, 8,9]. Charge carrier transport should be facilitated across such superstructure of Au-interlinked NCs, and in addition novel structures

with interesting mechanical properties and/or controlled porosity could be realized, which, in the case of TP assemblies, could also serve as “scaffolds”.

References:

[1] Tang Z., Kotov N.A., Adv. Mat., **17** (2005) 951.
[2] Murray C.B., Kagan C.R., Bawendi M.G., Annu. Rev. Mater. Sci., **30** (2000) 545.
[3] Pileni M.P., J. Phys. Chem. B **105** (2001) 3358.
[4] Carbone L., Nobile C., et al., Nano Lett., **7** (2007) 2942.
[5] Wenlong Cheng, Shaojun Dong, Erkang Wang, Angew. Chem. Int. Ed. **42** (2003).
[6] Rai A., Singh A., Ahmad A., Sastry M., Langmuir **22** (2006) 736.
[7] T.Aramoto, S. Kumazawa, et al., Jpn, J. Appl. Phys. **36** (1997) 6304.
[8] Shah A.; Torres, P.; Tscharner, R.; Wyrsch, N.; Keppner, H. Science, **285** (1999) 692.
[9] Gur, I.; Fromer, N.A.; Geier, M.L.; Alivisatos, A.P. Science, **310** 2005 462.

Figures:

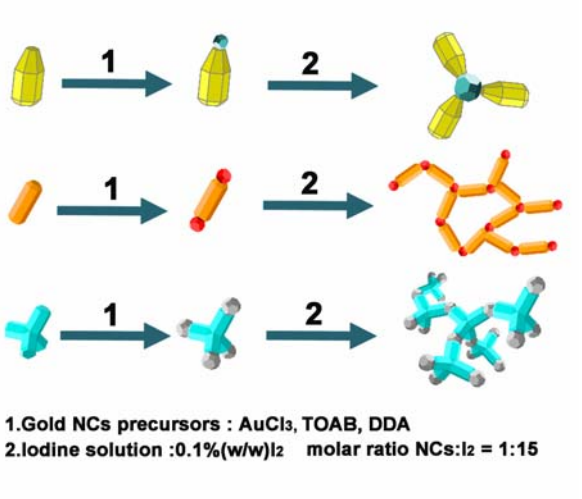

Scheme 1. Assembly of bullet-, rod-, and tetrapod-shaped NCs mediated by coalescence of Au domains grown at their tips and then destabilized with the help of molecular iodine. The reactants for the gold growth are gold chloride ($AuCl_3$), tetraoctylammonium bromide (TOAB) and dodecylamine (DDA).

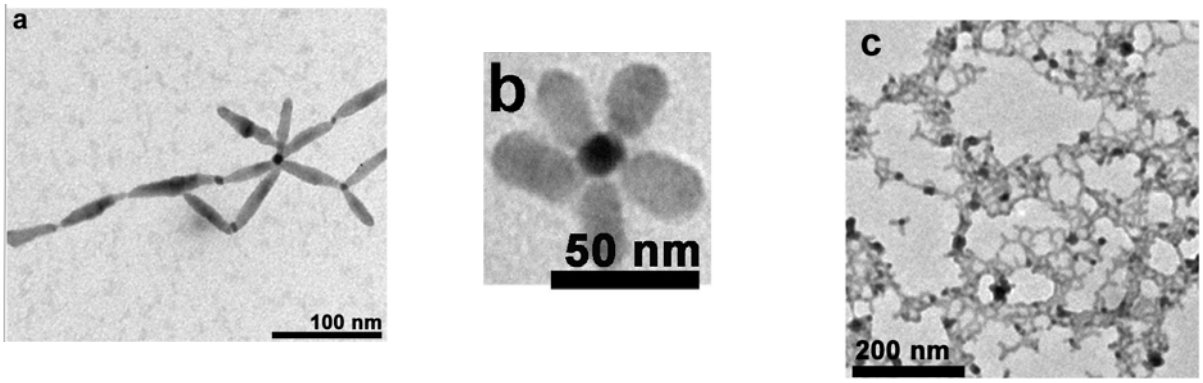

Figure 1. a) CdSe nanorods-based single structures formed at the initial steps of the assembly after reaction with I_2, b) CdSe@CdS core@shell rods decorated with one single Au tip after reaction with I_2, c) CdSe@CdTe tetrapods multibranched networks after reaction with I_2.

ORGANOMETALLIC SILVER COMPOUNDS AS PRECURSORS FOR NANOMATERIALS. USE OF THIOLS AND POLYMERS AS NANOPARTICLE STABILIZERS.

Jorge García-Barrasa,[a] Eduardo J. Fernández,[a] Antonio Laguna,[b] José M. López de Luzuriaga,[a] Miguel Monge,[a] and Katerina Soulantica.[c]

[a]Departamento de Química. Grupo de síntesis química de La Rioja, UA-CSIC. Universidad de La Rioja. Madre de Dios 51. E-26006 Logroño, Spain.
[b]Departamento de Química Inorgánica. Instituto de Ciencia de Materiales de Aragón. Universidad de Zaragoza-CSIC. E-50009 Zaragoza, Spain.
[c]Laboratoire de Physique et Chimie des Nano-Objets. INSA Toulouse. 135, Av. De Rangueil. 31077 Toulouse, France.
Email: jorge.garcia@unirioja.es

There is nowadays a great interest in metal nanoparticles due to their unusual chemical and physical properties that have given rise to new applications in many different areas [1,2]. These properties depend on the the size and the shape of the nanoparticles, that can be controlled, for example, through the synthesis from organometallic compounds. The use of these precursors allows to work under mild reaction conditions.

In order to control the growth of nanoparticles we use different stabilizers like long alkyl-chain thiols or organic polymers. In this way we have obtained arranged silver nanoparticles forming nanocrystal super lattices (NCSs), or silver nanoparticles inserted in materials with possible applications, respectively.

When long alkyl-chain thiols are used as stabilizers against silver (I) organometallic precursors, polymeric sheets of [Ag(SR)] stoichiometry are formed. Decomposition of this already organized silver polymer allows a very good control over the nanoparticle growth leading to highly ordered nanocrystal superlattices (NCSs) using specific reaction conditions.

We have also used different polymers, like cellulose acetate or polyvinylpyrrolidone, as stabilizing agents in the reaction, obtaining in each case silver nanoparticles inserted in cellulose acetate films, highly homogeneous silver nanoparticles using ethylene glycol as solvent, and very small silver nanoparticles (2-3 nm) that have been coated with a silica shell.

References:

[1] Niemeyer, C. M, Angew. Chem. Int. Ed., **22** (2001) 4128-4158.
[2] Kamat, P. V.; Meisel D., Current Opinion in Colloid & Interface Science, **5-6** (2002) 282-287.

Figures:

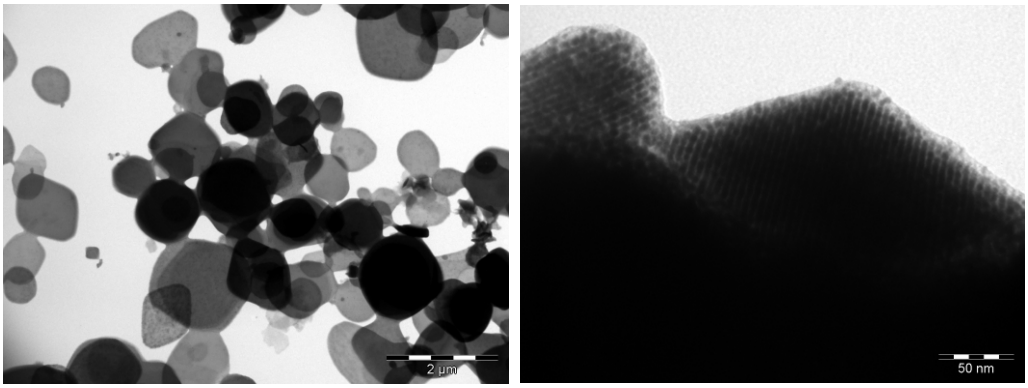

Figure 1. Silver nanoparticles obtained using hexadecanethiol as stabilizing agent.

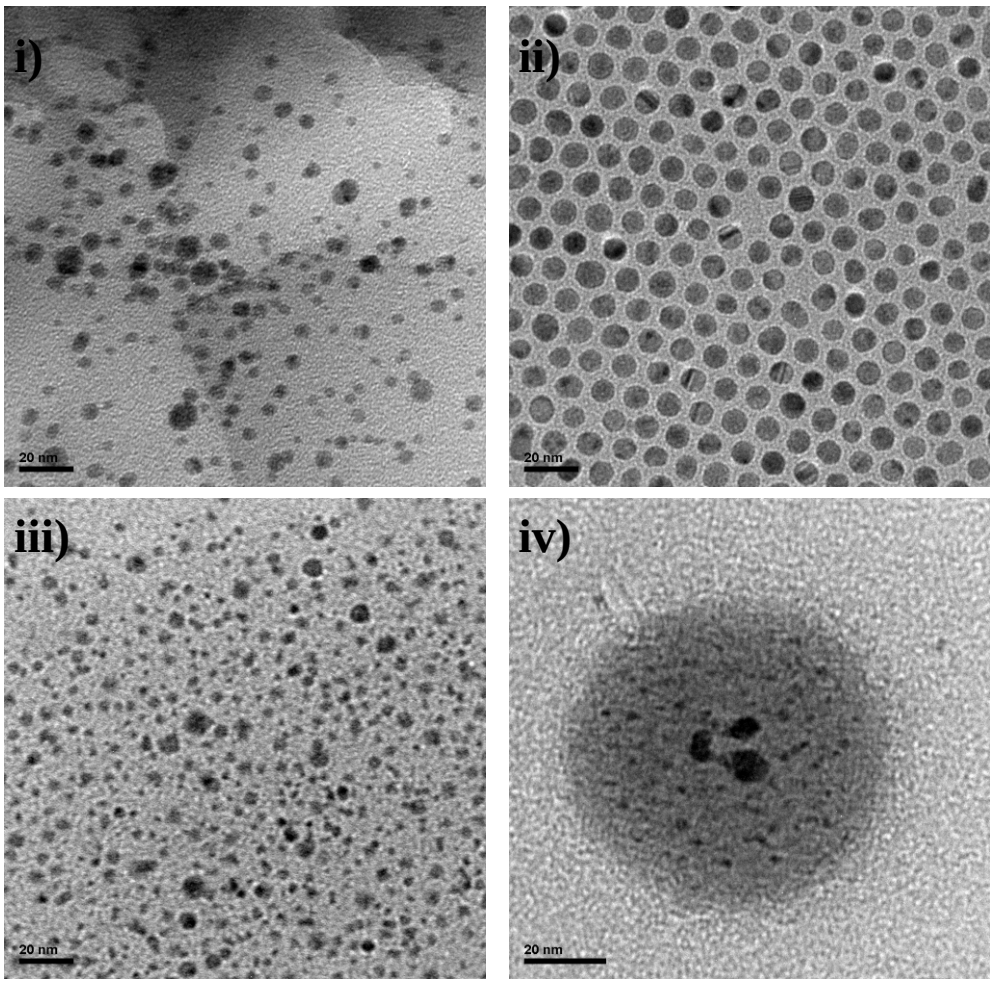

Figure 2. Silver nanoparticles obtained using i) cellulose acetate, ii) polyvinylpyrrolidone in ethylene glycol, and iii) polyvinylpyrrolidone as stabilizing agent, and iv) silver nanoparticles coated with a silica coating.

PROBING MULTIVALENT HOST-GUEST COMPLEXES USING AFM

Alberto Gomez-Casado, Henk H. Dam, Pascal Jonkheijm and Jurriaan Huskens
Laboratory of Molecular NanoFabrication - MESA+, University of Twente
P.O. Box 217, 7500 AE Enschede, The Netherlands

a.gomezcasado@utwente.nl

Multivalent interactions are the biological answer to many problems such as recognition, immune response and structural arrangement[1]. Several artificial systems exploiting this phenomenon have been constructed, trying to mimic cell processes or in the search of new devices and material properties[2]. It is, however, not fully understood yet what the relationship is between the number of host-guest interactions and their combined binding force (i.e. the total binding force has been predicted to scale following from linear to harmonic laws[3-6]).

We aim to probe multivalent host-guest complexes using force spectroscopy (Fig 1)in order to achieve a better understanding of the dynamical properties of these assemblies. To do so, a model system is being developed using cyclodextrin printboards as multivalent receptors and synthetic guest molecules of different valency.

We measured the dissociation force of single adamantane-βcyclodextrin complexes where the adamantane moiety is connected to the AFM tip using different linkers (Fig 2). The magnitude of the measured binding forces is in well agreement with previously reported values[7] for this system. The continuation of this project will be focused on the probing of divalent and trivalent guests and optimization of the experimental conditions in order to control the guest surface density and prevention of unspecific interactions between probe and printboard.

References

[1] Mathai Mammen, et al., Angewandte Chemie International Edition, **37** (1998) 2754.
[2] J. D. Badjic, et al., Acc Chem Res, **38** (2005) 723.
[3] U. Seifert, Phys Rev Lett, **84** (2000) 2750.
[4] T. V. Ratto, et al., Langmuir, **22** (2006) 1749.
[5] P. M. Williams, Analytica Chimica Acta, **479** (2003) 107.
[6] F. J. T. David, et al., The Journal of Chemical Physics, **114** (2001) 7483.
[7] T. Auletta, et al., J Am Chem Soc, **126** (2004) 1577.

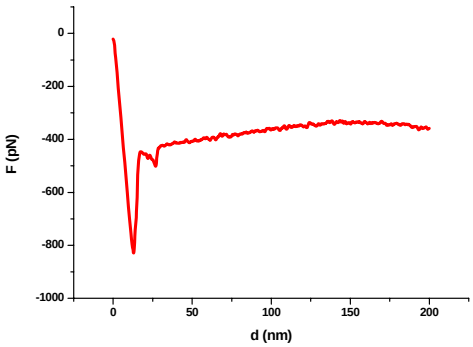

Figure 1: example of force – distance curve

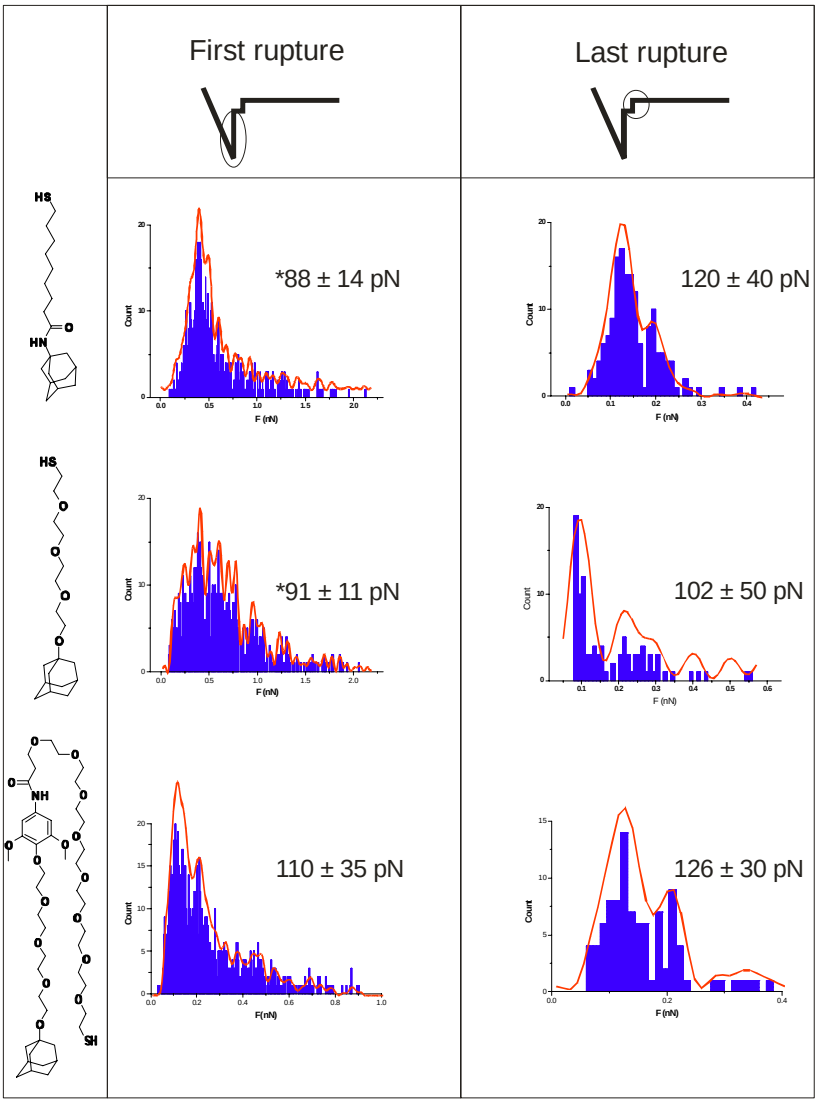

Figure 2: Measured binding forces between adamantane and β-cyclodextrin. (*) Obtained from peak periodicity.

USING COMPLEX POTENTIALS TO DESCRIBE ELECTRON TRANSMISSION THROUGH MOLECULES

Francois Goyer, Matthias Ernzerhof
Department of Chemistry, University of Montréal, Montréal, Canada
francois.goyer@umontreal.com

The understanding of electron transport through molecular electronic devices (MEDs) is essential for the conception of new types of circuits, such as quantum transistors. We present our newly developed Source-Sink Potential (SSP)[1] method for the calculation of the transmission probability.
Using SSP we explore simple relationships between molecular structure and conductance to analyze and predict experiments. The systems studied range from small aromatic compounds to nanotubes. In these systems, phenomena, such as destructive interference, are studied to provide insight on their impact on the conductance of MEDs.
We also present an approach to include correlation effects in the description of MEDs. A generalization of density functional theory (DFT) has been proposed[2] to allow for the use of complex (SSP) potentials. We apply the SSP method in the framework of this complex DFT. The implementation of this new DFT[2] is explained, as well as preliminary results of the conductance of model MEDs.

References:

[1] Goyer, Ernzerhof, and Zhuang, *The Journal of Chemical Physics* ***126,*** (2007) p. 144104.
[2] Ernzerhof, *The Journal of Chemical Physics* ***125,*** (2006) p. 124104.

Characterizing contact formation at the atomic scale: A combined Scanning Tunneling Microscopy (STM) and Atomic Force Microscopy (AFM) study

Till Hagedorn, Mehdi El Ouali, Yoichi Miahara, Peter Grutter
McGill Unversity, Montreal, Canada
email: hagedorn@physics.mcgill.ca

We are investigating contact formation at the atomic scale, in particular the interplay of forces and conductivity. It is well known that the contact geometry in scanning probe microscopy plays a key role in understanding tunneling junctions [1,2], molecular electronics junctions [2] and dissipation[3]. In order to investigate these phenomena, we use a combined ultra high vacuum (UHV) scanning tunneling microscope (STM) and atomic force microscope (AFM) to measure metal-metal junctions between STM tips and metallic STM samples. In addition to obtaining the simultaneous tunneling current (STM) and force (AFM) information we are also able to image the STM tip before and after the experiments with field ion microscopy (FIM) [4]. All these methods are applied in situ in the same microscope. Therefore we see atomic changes of the STM tip that happen during scanning and distance spectroscopy.

There are many possible ways to make use of our setup. The most obvious would be to use it to make atomic contacts (the contact between an atomically sharp STM tip as one electrode and an atomically flat STM sample as counter electrode). This is the aim of the current work.

Figure 1 shows our setup and the way we are using the system to do atomic contact experiments. We use FIM to image the STM tip (part a). The STM tip is facing a screen unit. Both of them are biased at several kV in opposite polarity while the tip has to be on posivitve potential to ionize the imaging gas (He). The ionized He follows the field lines between screen and tip and produces a magnified image of the tip on the screen. The image we obtain consists of bright spots representing the atoms at the edges of crystalline planes. By identifying the crystalline orientation the hole STM tip can be reconstructed as a ball model. Therefore we know the real space structure of our tip. After the tip imaging we introduce the sample and approach the tip towards the sample as shown in figure 1 b). We take care not to crash the tip during the approach. Once the tip is in tunneling contact, we do STM scans and approach curves with various distance ranges.

These distance ranges refer to different processes:

- contact formation: few nm of tip sample separation to contact (tunneling current saturates and cantilver shows onset of linear force distance relation (Hook's law)) [1]
- nano indentation: from contact to 3 nm further in (see [5])
- dissipation: the hole range that shows a hysteresis in the force channel and structure changes of the STM tip (future work)

[1] Sun et. al. PRB 71 193407, 2005
[2] De Menech et. al. PRB 73, 155407, 2006
[3] Ghasemi et. al. PRL 100, 236106 2008
[4] Lucier et. al. PRB 72, 235420, 2005
[5] Cross et. al. Nature Materials vol 5, p. 370, 2006

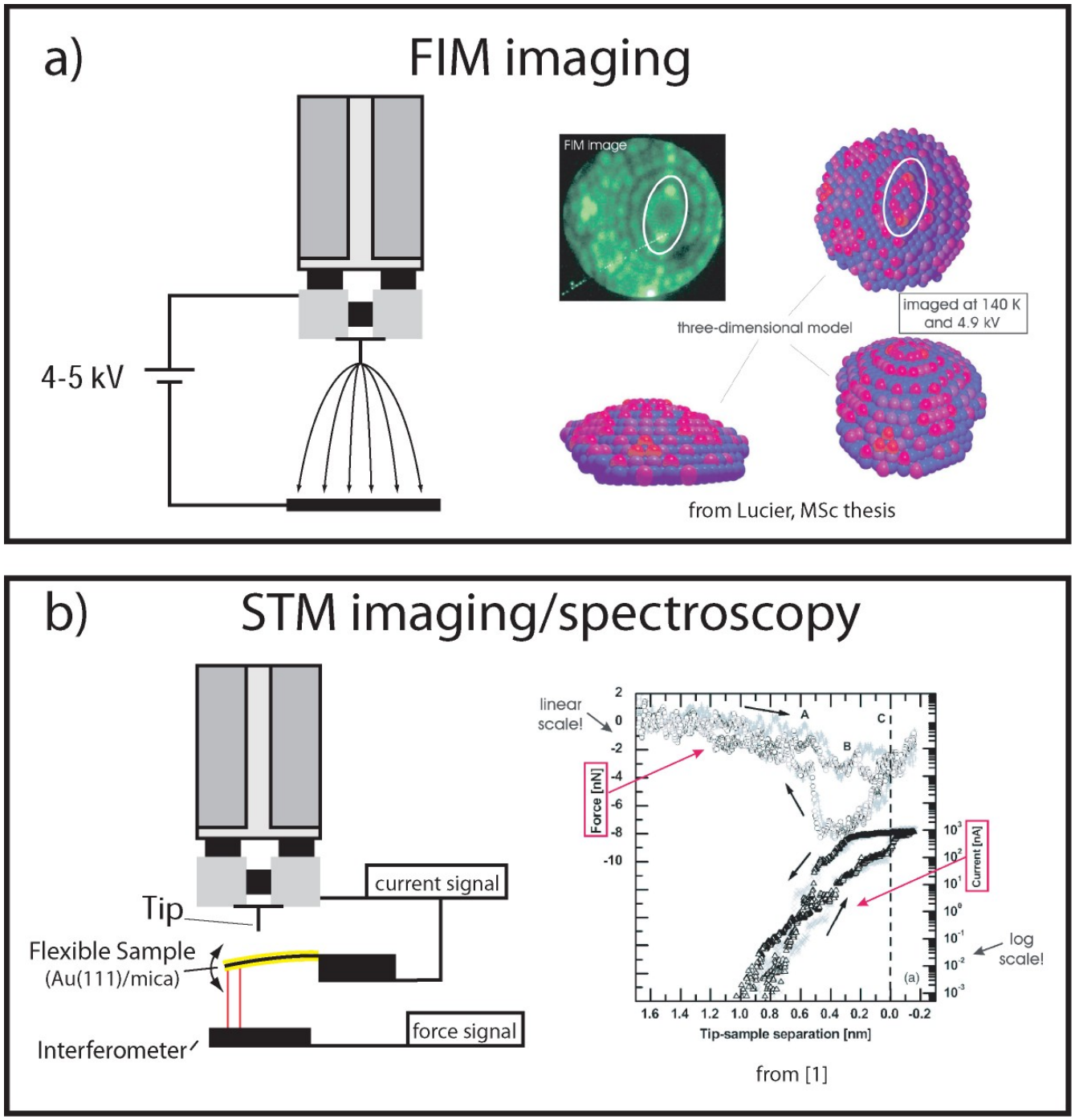

Figure 1: The UHV STM/AFM with FIM capability. (a) shows the FIM process and (b) shows how we acquire simultaneous STM/AFM data

EVALUATION OF HYDRODYNAMIC PARAMETERS OF FLUIDIZED BED ADSORPTION ON PURIFICATION OF NANOBIOPRODUCTS

Mohsen Jahanshahi[*]*, Ghasem Najafpour, Melika Ebrahimpour, Solmaz Hajizadeh*
Nanobiotechnology Research Laboratory, School of Chemical Engineering, Babol University of Technology, Babol, Iran. mjahan@nit.ac.ir,mmohse@yahoo.com

The majority of biotechnology processes for producing pharmaceutical or diagnostic products involve the purification of proteins and peptides from a variety of sources. Typically, such purification schemes contain multiple unit operations, including a number of chromatographic steps to ensure the safe removal of critical impurities and contaminants. Each step in the recovery process will affect the overall process economy by increasing operational cost and process time

Nanoparticles are of colloidal size and they are generally sophisticated biological structures composed of one or more types of proteins, lipid and/or nucleic acids and subsequently various problems are associated with their recovery and purification. Nanoparticle sizes are defined from 10 to 1000 nm. Protein nanoparticles generally vary in size from 50-300 nm.

Expanded bed adsorption (EBA) is a novel primary recovery technology allowing the adsorption of target proteins directly from unclarified feedstock without the risk of blocking the bed which innovatively combines solid-liquid separation with an adsorption step in a single unit operation .Expanded bed adsorption is based on controlled stable fluidization, thus combining the hydrodynamic properties of a fluidized bed with the chromatographic properties of a packed bed. Physical parameters are the parameters related to the hydrodynamics and stability of a homogeneous fluidization in the expanded bed. The **Residence Time Distribution** (RTD) analysis was used to acquire hydrodynamic information from changes bed expansion and column diameter, settled bed height to the shape of a tracer pulse as it passed from the expanded bed .The adsorption of **bovine serum albumin (BSA) nanoparticle** on STREAMLINE DEAE, were used to examine how adsorption behaviour was affected by the hydrodynamics of bed by changing bed condition (degree of expansion). In the present work, protein nanoparticles fabricated from bovine serum albumin (BSA) was purified by expanded bed adsorption on the streamline DEAE adsorbent.

- The material was used in this work: BSA, Tween-20, ethanolamine, glutaraldehyde (25% solution), supplied by Sigma Aldrich. Streamline DEAE was provided by Amersham bioscience. Sodium azide from Merck (Germany).all other chemicals were of analytical grade from local sources.
- Preparation of BSA nanoparticle: The bovine serum albumin nanoparticles (BSANPs) were prepared by a coacervation method and chemical cross-linking with glutaraldehyde.
- Glass columns (1.3cm×25 cm, 1.6cm×20cm, 2cm×15cm) were used, which had a top adaptor and a bottom flow distributor. The Liquid from the outlet of the column was transferred through the UV detector. The particle size range for adsorbent is100-300µm.the approximate mean particle size is 200µm and the approximate mean particle density is1.2g/ml.
- Estimation of bed voidage and RTD study, bed expansion characteristics and axial dispersion calculation: Tris-Hcl buffer at a 10mM concentration and at pH 7.6 were used as fluidizers .Acetone solution (10%, w/w) as a tracer was injected at the bottom of the column. : Bed voidage(ε), number of theoretical plates (N) of the column, (HETP) obtains from following equations:

$$\varepsilon = 1-\frac{V_P}{V_L} = 1-\frac{V_P}{A_T.H} = 1-\frac{m_p}{\rho_p A_T.H} \quad (1), \quad N = \frac{t_r^{\,2}}{\sigma_t^{\,2}} = \frac{L}{H} \quad (2), \quad HETP = \frac{t^2}{\sigma^2}\times H \quad (3)$$

It was known that the Richardson–Zaki equation Eq.4 conducted an extensive investigation of the expansion behavior of particles at different velocity. The Bodenstein number (Bo) is a dimensionless term that is often used to relate the convective transport of liquid to dispersion Eq.5. Bo number can be calculated from Eq.6.results show in fig.1.

$$\frac{u}{u_t} = \varepsilon^{n} \quad (4), \quad B_0 = \frac{UH}{D_{axl}.\varepsilon} \quad (5), \quad \frac{1}{N} = \frac{2}{B_0} + \frac{8}{B_0^{\,2}} \quad (6)$$

- The bed expansion characteristics for the streamline DEAE in 1.3cm×25cm column was shown in fig.2. *H*/*H*0 increases linearly at the same flow rate with increasing buffer viscosity. The experimental value of n, 4.77 was obtained fig.3. Results show a good agreement between the experimental and theoretical value of n and u_t.
- The time courses of BSA nanoparticle purification were carried by the EBA on columns with different degree of expansion. Yield of BSA nanoparticle recovery in expanded bed adsorption with different degree of expansion was showed in fig.4.
- The RTD study showed that HEPT, axial dispersion increased with bed height, bed voidage and linear velocity. At 6cm of bed height, it is the best system for BSA nanoparticle recovery by the expanded bed chromatography in streamline DEAE adsorbent. The Best yield of recovery of BSA nanoparticle in optimal condition 80.71% was achieved.

References:

[1]Jahanshahi M.,Williams S., Lyddiatt A.,Shojaosadati S.A. Journal of IEE Nanobiotechnology, 151, 2004, 176-182.

[2] Rhaese .S. Briesen.H., Rübsamen-Waigmann. H, Kreuter. J., Langer .K., Journal of Controlled Release, 92, 2003, 199-208.

[3] Lin.D.O., Miao.Z.J. Yao.S.J Journal of Chromatography A, 1107, 2006, 265–272.

[4] Zhang. L, Hou .S, Mao. S, Wei .D, Song .X, Lu. Y, International Journal of Pharmaceutics, 287, 2004,155-162.

[5] Jahanshahi. M., Najafpour .Gh., Rahimnejad .M.,African Journal of Biotechnology, 7, 2008, 362-367.

Figures:

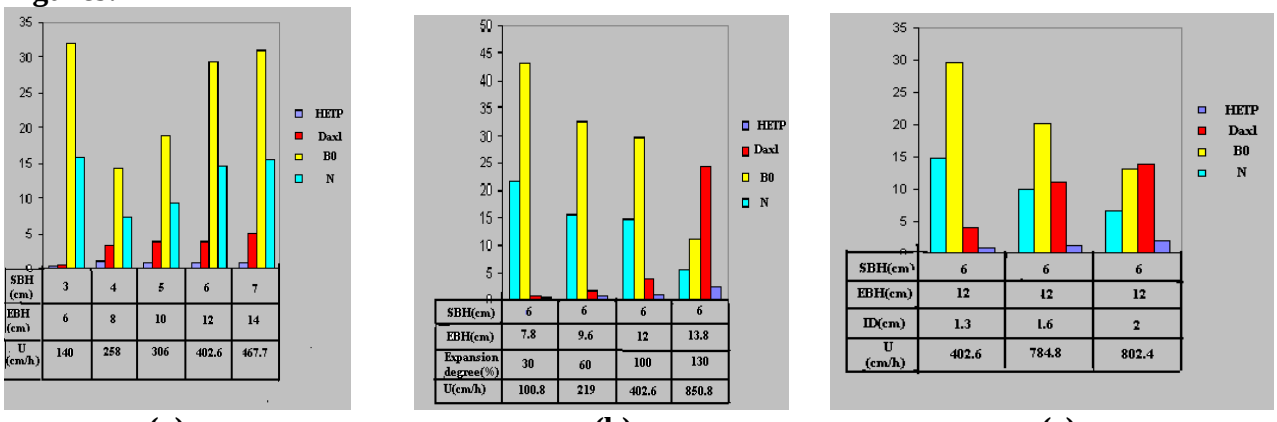

(a) **(b)** **(c)**

Fig1 .Hydrodynamic parameters of the liquid phase estimated expanded bed operations (a) The effect of the settled bed height (b) The effect of optimum bed expansion (c) The effect of column diameter

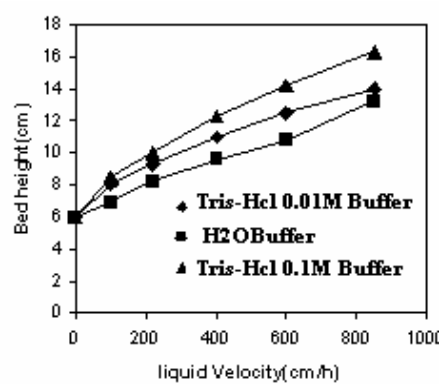

Fig.2.Expanded bed height of streamline DEAE(SBH=6cm) with varying flow rate in a Tris/Hcl buffer system

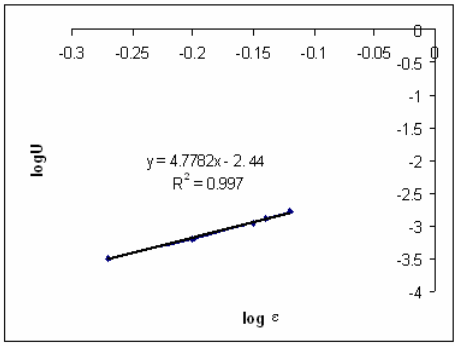

Fig.3.Richardson-Zaki correlation between flow velocity and bed voidage For experimental calculation of n and u

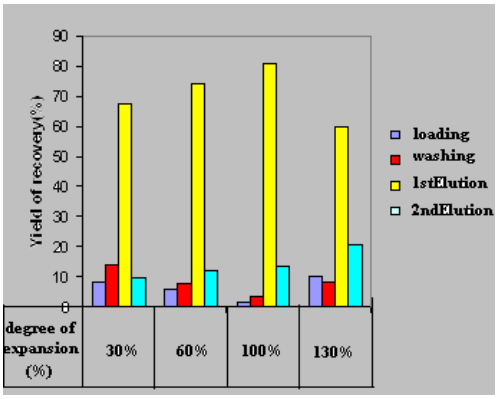

Fig.4. Yield of BSA nanoparticle recovery in expanded bed adsorption

CATALYSTS EFFECTS ON THE PRODUCTION OF CARBON NANOTUBES BY AN AUTOMATIC ARC DISCHARGE SET UP

Mohsen Jahanshahi [1,], Jahan B. Raoof [2], Solmaz Hajizadeh [1], Razieh Jabari Seresht [1]*

[1] Nanobiotechnology Research Laboratory, Faculty of Chemical Engineering, Babol Noshirvani University of Technology, PO. Box 484. , Babol, Iran. . mjahan@nit.ac.ir, mmohse@yahoo.com

[2] Electroanalytical Chemistry Research Laboratory, Department of Chemistry, Faculty of Basic Science, Mazandaran University, Babolsar, Iran

Abstract

Carbon nanotubes (CNTs) represent an important group of nanomaterials with attractive geometrical, electrical and chemical properties. CNTs can be synthesized using a variety of techniques. In this study CNTs were fabricated by electric arc discharge method in liquid which does not require vacuum equipment, heat exchange system, active or inert gases. The effect of the kind of catalyst on quantity of synthesized CNTs was studied in this paper. Carbon nanotubes were fabricated between two graphite electrodes which are submerged in the LiCl 0.25N as a plasma and with a voltage of 25v while for comparative studies, Ni, Mo, Fe, Ni-Mo were used in synthesis as metallic or bimetallic catalysts and the results then were analyzed, compared and discussed. The arc discharge set up which used in this study was full automatic that enables the controlling of gap between the two electrodes. Then for purification purpose a modified acid treatment method were applied. To analyze the morphology of the synthesized products a scanning electron microscopy (SEM) and transmission electron microscopy (TEM) study were employed. A Raman spectroscopy was utilized for investigation on amount of purity. A High-crystalline and alonged multi walled carbon nanotubes (MWCNTs), single walled carbon nanotubes (SWCNTs) and springy carbon nanotubes (SCNTs) can be synthesized using this technique with carbon electrode including 5% Mo-Ni as catalysts.

References

[1] S. Iijima; “Helical Microtubules of Graphitic Carbon”, Nature 354 , 56-58 (1991)

[2] S. Iijima, T. Ichihashi; “Single Carbon Nanotube of 1-nm Diameter”, Nature 363, 603-605 (1993).
[3] W. Thomas, “Carbon Nanotubes” University of Washington (2007).
[4] X. Zhao, M. Ohkohchi, H. Shimoyama, Y. Ando “Morphology of carbon allotropes prepared by hydrogen arcdischarge” Crystal Growth 198/199 ,934-938(1999).
[5] C. D. Scott, S. Arepalli, P. Nikolaev, R.E. Smalley “Growth mechanisms for single-wall carbon nanotubesin a laser-ablation process”, Appl. Phys. A 72, 573–580 (2001).
[6] Flahaut, et.al, “Gram-Scale CVD Synthesis of Double–Walled Carbon Nanotube” , Chemical Communications , 1442-1443(2003).
[7] M. Daenen, R. D. de Fouw, B. Hamers, P. G. A. Janssen, K. Schouteden, M.A.J. Veld; “The Wondrous World of Carbon Nanotubes”, Eindhoven University of Technology (2003).
[8] H. Molavi, M. Shariaty-Niassar, M. Jahanshahi; “Comparative Study of CNT Synthesis by Arc Discharge in Solution”, Proceedings of the International Conference on Bio-Nanotechnology: Future Prospects in the Emirates November 18-21, Al Ain, United Arab Emirates (2006).
[9] R. B. Mathur, S. Seth, Ch. Lal, R. Rao, B. P. Singh, T. L. Dhami, A. M. Rao; “Co-synthesis, purification and characterization of single- and multi-walled carbon nanotubes using the electric arc method,” carbon, 45, 132-140 (2007).
[10] H. Lange, M. Sioda, A. Huczko, Y. Q. Zhu, H. W. Kroto, D. R. M. Walton; "Nanocarbon production by arc discharge in water", Carbon 2003;41:1617–23.
[11] R. David Lide; "CRC Handbook of Chemistry and Physics", 85th ed., p.938, New York, U.A.S. (2005).

GROWTH OF SITE-CONTROLLED InAs QUANTUM DOTS ON PREPATTERNED GaAs (001) SUBSTRATES BY AFM LOCAL OXIDATION

J. Martín-Sánchez, Y. González, P. Alonso-González, B. Alén, D. Fuster, L. González, J. Herranz and F. Briones.
Instituto de Microelectrónica de Madrid, C/Isaac Newton 8 (PTM) 28760 Tres Cantos, Spain
G. Muñoz-Matutano, J. Canet-Ferrer and J. Martínez-Pastor.
ICMUV, Instituto de Ciencia de Materiales, Universidad de Valencia, P.O. Box 22085, 4607 Valencia, Spain
jesus@imm.cnm.csic.es

The precise location of quantum dots is a critical step towards the development of single photon emitters, where a single quantum dot should be located at a specific site within an optical micro cavity [1]. In this work, we present a fabrication process combining AFM local oxidation nanolithography and molecular beam epitaxy (MBE) growth techniques to control the nucleation of InAs quantum dots (QD) on prepatterned GaAs (001) substrates [2].

Our approach basically involves three steps: i) Fabrication of patterned GaAs(001) substrates by AFM local oxidation lithography: The pattern consist of a 2D array of nanometric size oxide dots (see Fig. 1a). The GaAs oxide dots are removed by FH selective etching obtaining 2D arrays of nanometric holes (see Fig. 1b). The design of the pattern can be freely modified to control the final QD density; ii) Preparation of GaAs(001) patterned substrates for further epitaxial growth by a process that preserves the pattern. This process includes GaAs native oxide desorption and GaAs buffer layer growth; iii) InAs deposition on patterned substrates.

Our experimental results show that a high selectivity of InAs nucleation in the nanoholes can be achieved when appropriate growth conditions are used. Therefore, the QD nucleation sites are defined by the pattern (Fig. 2). The number of QD obtained inside each nanohole depends on the geometrical shape of the oxide dot and can be chosen by varying the shape of the oxide dot.

Finally, in order to validate our whole fabrication process, micro-photoluminescence characterization of a single InAs QD obtained by this process will be presented.

This work was financed by Spanish MEC (TEC2005-05781-C03-01, NAN2004-09109-C04-01, Consolider-Ingenio 2010 CSD2006-00019), CAM (S 0505ESP 0200) and by the SANDIE Network of excellence (Contract nº NMP4-CT-2004-500101 group TEP-0120). JMS and PAG thanks to the I3P program.

References:

[1] A. Badolato, K. Hennessy, M. Atatüre, J. Dreiser, E. Hu, P.M. Petroff, and A. Imamoglu, Science **308** (2005) 1158.

[2] J. Martín-Sánchez, Y. González, L. González, M. Tello, R. García, D. Granados, J.M. García, and F. Briones, J. Cryst. Growth **284** (2005) 313

Figures:

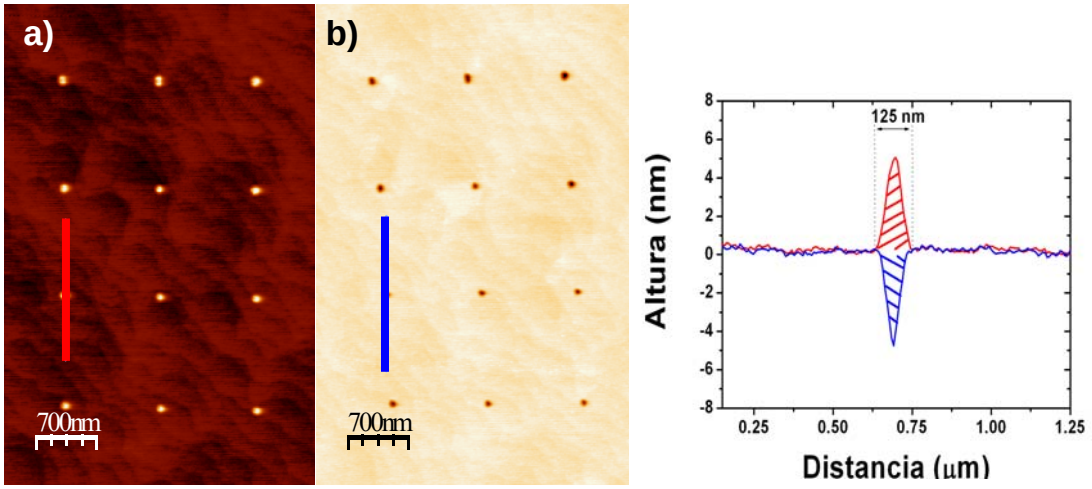

Fig 1: a) Atomic Force Microscopy (AFM) images of oxide dots fabricated by AFM local oxidation nanolithography. b) 2D array of nanoholes obtained after selective FH chemical etching of oxide dots . Notice on profiles shown on the right that the volume of emerging oxide dots are similar to that of the resulted holes.

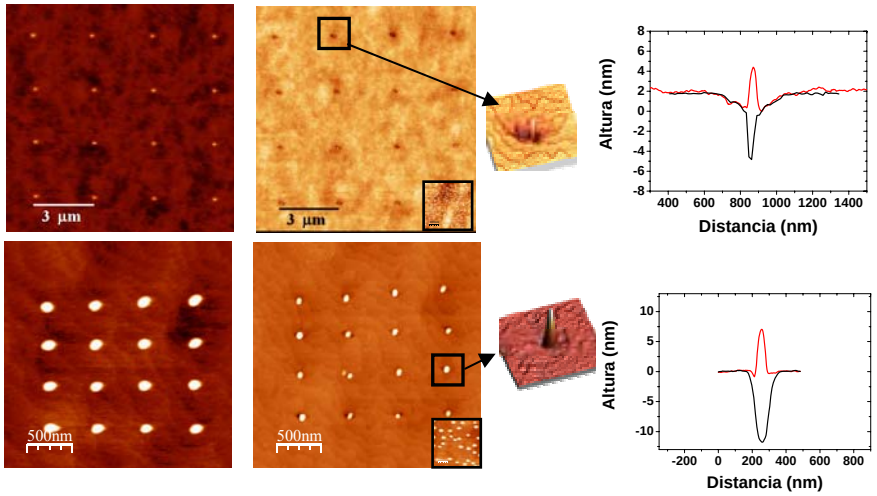

Fig. 2: AFM images of 2D arrays of oxide dots fabricated by AFM local oxidation technique (left) and resulting InAs QDs after growth process (right). Density of QDs can be controlled as desired varying the pattern design.

GROWING UP OF MAGNETIC NANOSTRUCTURES BY EBL USING DOUBLE LAYER RESIST SYSTEM AND CHARACTERIZATION BY AFM AND MAGNETO OPTICAL SNOM.

A.Hierro-Rodríguez, L.M. Álvarez-Prado, M.Vélez, A.Pérez-Junquera, J.I.Martín, J.M.Alameda
Departamento de Física, Universidad de Oviedo, Av. Calvo Sotelo, 33007 Oviedo, Spain,
aurehr@condmat.uniovi.es

The fabrication of patterned thin films with nanometric structures using electron beam lithography (EBL) has problems with the sharpness and the form of the defined nanoelemets. It occurs because the edges of the patterns are touching the resist used to write the form, so that, when the resist is removed in the lift-off process, some times it cannot be completely cleaned as it is adhered to the nanostructures edges. To solve this problem samples can be prepared with a "two layer system" of different resists. The sensibility of both resins to electrons is different and, as a consequence, when the deposition is performed, the edges of the nanostructures are not in contact with the resin, avoiding the adhesion effects.

In this work we have evaluated this technique applying it to fabricate rings grown-up with cobalt. The study of these nanometric magnetic systems has now a great interest from their possible applications in memories, and from basic research point of view as they present several stable magnetic configurations.

The structural characterization has been done using AFM and SEM techniques (Fig.1). These images shows that, actually, the fabricated nanostructures do not present particles of resist remaining at the edges of the rings. Also, the profiles across the ring section have been analyzed by AFM in order to obtain the appropriate dose in the EBL process for fabrication of high quality edges. The magnetic properties of the rings[1] were studied using a Scanning Near Optical Microscopy (SNOM)[2] system that allows to perform transversal magneto optical Kerr effect (TMOKE [3]) measurements. The hysteresis loops show the great difference between the coercive field of continuous film and the Co rings, as the former has about 5 times lesser coercive field than the latter (Fig.2).

Work supported by Spanish CICYT (grants NAN2004-09087 and FIS2005-07392). A.H-R acknowledges the predoctoral fellow from FICYT of Principado de Asturias.

References:

[1] M.Kläui, C.A.F.Vaz, L.Lopez-Díaz and J.A.C.Bland
J.Phys.:Condens.Matter **15** R985 (2003)

[2] L.M.Álvarez-Prado, J.Schoenmaker, A.D.Santos, T.Fournier and Y.Souche.
Phys.Stat.Sol (a)**203**, No.6, 1425 (2006)

[3] L.Blanco-Gutierrez, M.Vélez, J.Díaz, L.M.Álvarez-Prado and J.M.Alameda
Phys.Rev.B **64,** 024417 (2001)

Figures:

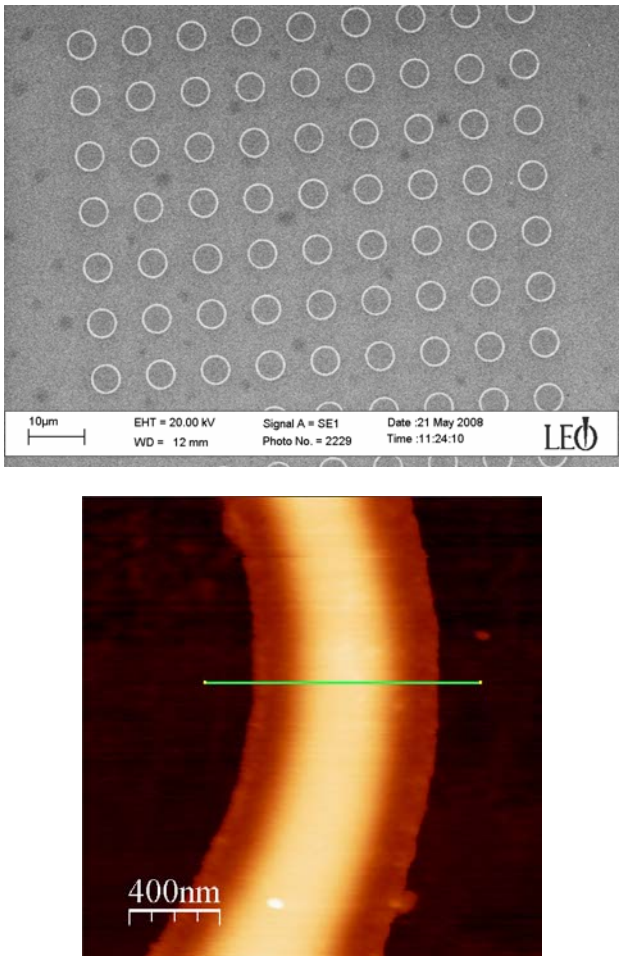

Fig. 1 The top left image shows a general view of the patterned Co film using SEM. The other two images are measures of the ring crown section obtained by AFM technique.

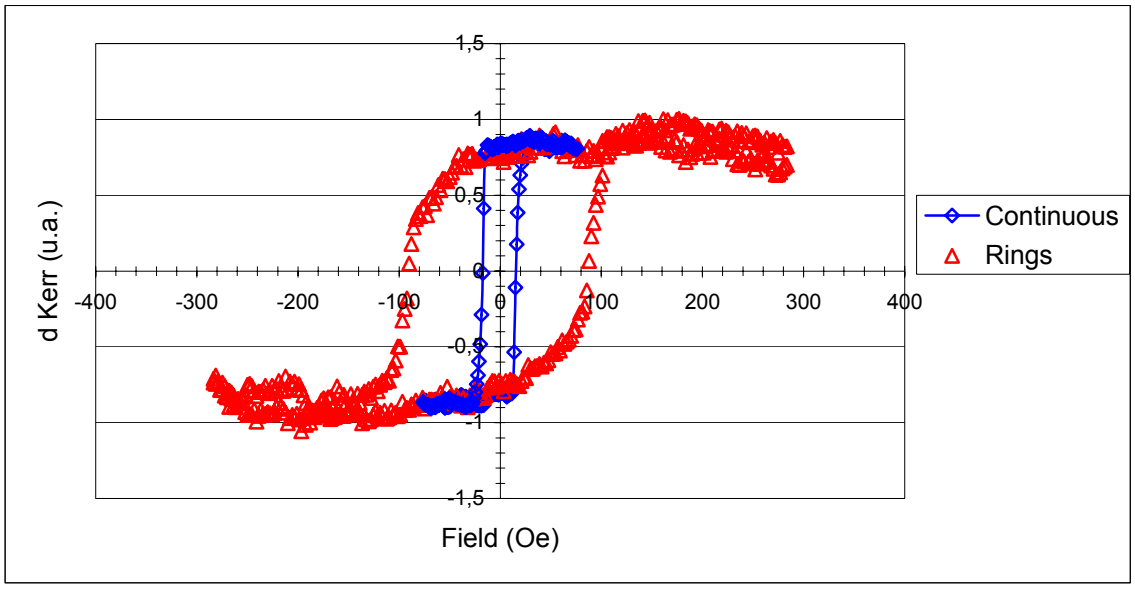

Fig. 2 TMOKE measurements performed by SNOM in the continuous thin film (diamonds) and the Co nanostructured rings (triangles).

EFFECT OF DIFFERENT MICROWAVE-BASED TREATMENTS ON MULTI-WALLED CARBON NANOTUBES

Pejman Hojati-Talemi, George P. Simon
Department of Materials Engineering, Monash University,
Clayton, Victoria 3800, Australia
Pejman.hojati@eng.monash.Edu.au

Since carbon nanotubes (CNTs) are insoluble and inert, oxidative treatments of these materials have been frequently used for many purposes [1,2]. Many different wet and dry methods based on different oxidizing agents have been developed, but most are time consuming, expensive and require accurate control of temperature, atmosphere and reaction time. The other problem with these techniques is the lack of control of formation of the wide variety of functional groups that are introduced to CNTs [1,2].

There have been some reports about modification of CNTs with water as a mild reactive agent that selectively introduces hydroxyl groups to the CNTs [3-5]. although a high energy source is required for preparation of the reactive radicals. Absorption of MW irradiation by CNTs, for example results in such an intense heat release that the temperature can rise to close to 2000 °C in a few seconds [6]. Such interactions can be enough for preparation of reactive species for modification of nanotubes. [3].

In this work, we report the comparative effect of three different straightforward methods for modifying CNTs using a "kitchen microwave oven" and water as a reactive agent that can be easily replicated in most laboratories. In the first method, the effect of application of MW irradiation on CNTs dispersed in deionized water was studied. The second method made use of application of MW radiation to CNTs in a water vapor atmosphere. We also developed a new technique for producing plasma using an unmodified "kitchen microwave oven" and standard laboratory glassware. This method operates at relatively low pressures (~10^{-2} Torr) of a residual gas (water vapor in this report) after evacuation of the plasma chamber. In such environment water molecules disintegrate into various active hydrogen and oxygen compound radicals and can be used for functionalization of CNTs [7].

We compared results of these methods with results of thermal oxidation in controlled atmosphere and acid treatment, as two conventional methods for the functionalization and modification of CNTs. The TEM, XPS, Raman spectroscopy results, demonstrate that in comparison to acid treatment and thermal oxidation (two conventional methods for oxidative treatment of CNTs), our methods result in lower damage to the structure (Figure1.(a-f)) and more uniformity in chemical functionalization of CNTs. For example the concentration of oxygenated groups in CNTs after microwave treatment in steam was similar to thermally treated samples (most in form of hydroxyl groups) with less notable structural damage or cutting of CNTs. Although long exposure times in microwave-plasma treatment resulted in formation of amorphous carbon materials, short exposure times appeared to transform other existing oxygenated functional groups to hydroxyl groups which are useful for further chemical reactions in many applications. We also observed that the heat release in the MW-plasma method was high enough to soften even borosilicate glass, as well as soda-lime glass; therefore we successfully used this

technique for welding carbon nanotubes on a range of surfaces such as polystyrene, borosilicate glass and soda-lime glass (Figure1. (g, h)) (Such microwave welding has previously been reported only for polymeric surfaces [8]).

Refrences:

[1] Hidefumi H, Ebbesen TW and Tanigaki, K. Advanced Materials. **3**, 1995, 275.
[2] Najafi E, Kim J-Y, Han S-H, Shin K. Colloids and Surfaces A: Physicochemical and Engineering Aspects. **284-285**, 2006,373.
[3] Raghuveer MS, Agrawal S, Bishop N, Ramanath G. Chemistry of Materials. **6,** 2006, 1390.
[4] Imasaka K, Suehiro J, Kanatake Y, Kato Y, Hara M. Nanotechnology, **14,** 2006, 3421.
[5] Yu G, Gong J, Wang S, Zhu D, He S, Zhu Z. Carbon. **7**, 2006, 1218.
[6] Imholt TJ, Dyke CA, Hasslacher B, Perez JM, Price DW, Roberts JA, et al. Chem Mater. **21**, 2003, 3969.
[7] Uhm HS, Kim JH, Hong YC. Physics of Plasmas. **7**, 2007, 073502.
[8] Wang CY, Chen TH, Chang SC, Cheng SY, Chin TS. Advanced Functional Materials. 12, 2007,1979.

Figures:

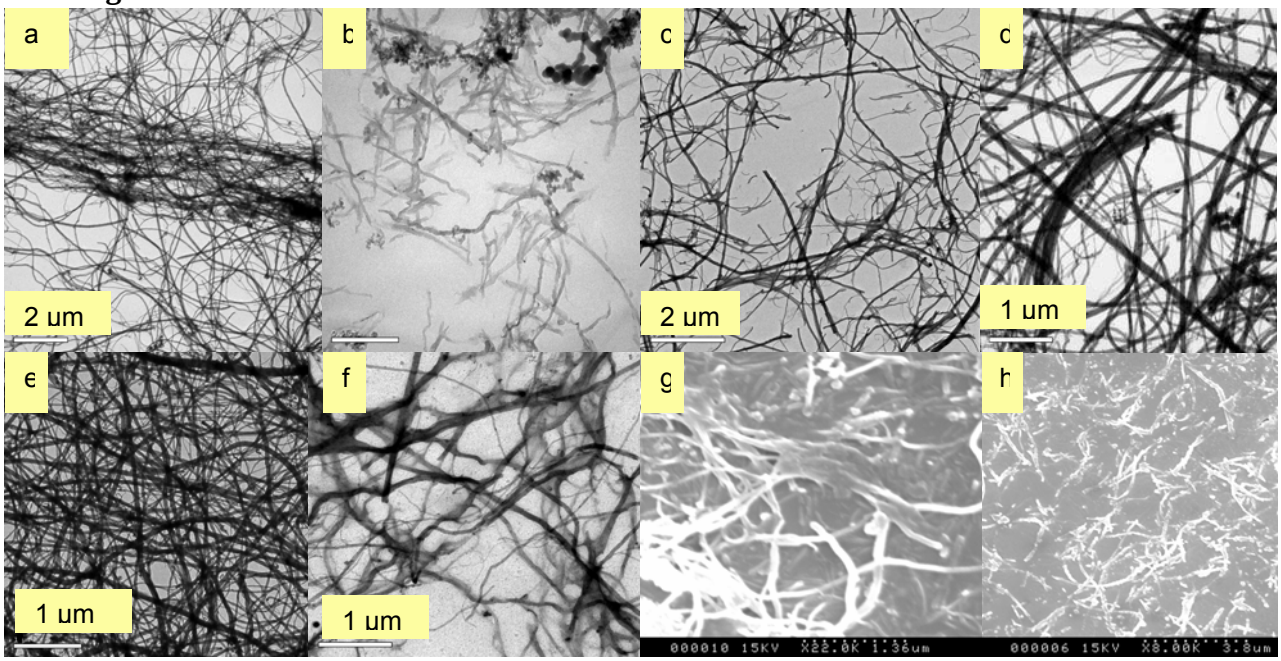

Figure 1. a) as received CNTs, b) acid treated CNTs, c) Thermally treated CNTs, d) MW treated in water, e) MW-Treated in vapor, f) MW-plasma treated after 120s, g) CNTs welded on lime-soda glass, h) CNTs welded on borosilicate glass.

Detection of Ureasa Enzyme Analysis Using Electrode Modified with Vertically Aligned Ni Nanopillars

Radim Hrdy[1], Dalibor Huska[2], Vojtech Adam[2], Ales Horna[3], Jaromir Hubalek[1], Rene Kizek[2]
[1]Department of Microelectronics, Faculty of Electrical Engineering and Communication, Brno University of Technology, Udolni 53, CZ-602 00 Brno, Czech Republic
[2]Department of Chemistry and Biochemistry, Faculty of Agronomy, Mendel University of Agriculture and Forestry, Zemedelska 1, CZ-613 00 Brno, Czech Republic
[3]Radanal Ltd., Okruzni 613, CZ-530 03, Pardubice, Czech Republic
hubalek@feec.vutbr.cz

Urease, enzyme catalyzing the hydrolysis of urea into carbon dioxide and ammonia, was firstly isolated from *Cannavalia enzyformis* (*Fabacae*) in 1926 [1]. Afterward it has been shown that urease (EC 3.5.1.5, amidohydrolases) is abundant enzyme in plants and, moreover, it can be found at numerous of eukaryotic microorganisms and bacteria [2-5]. The existence of this enzyme at higher organisms has not been shown yet. The highest activity of urease was determined in embryonic plant tissues, first of all, in seeds of *Fabaceae* and *Curcubitaceae* species [6-12]. In addition, a highly active isoenzym of urease was found at developing embryos. The activity of this enzyme is very dependent on nickel presence in its active centre [13]. This enzyme is substrate-specific, which means that the enzyme catalyzes the hydrolysis of urea only [14]. This feature is a basic diagnostic criterion used in the determination of many bacteria species, which produce highly active urease. *Helicobacter pylori* belong to such bacteria species. Many cases of peptic ulcers, gastritis, and duodenitis are caused by *H. pylori* infection. The presence of urease is used in the diagnosis of Helicobacter species [15-20]. The aim of this work is to use nickel nanoelectrode for selective and sensitive detection of urease

Nanoelectrodes preparation

The formation of nanostructures (nanopillars) is based on using an alumina template (Whatman Anodisc with pore diameter 100 nm) with hexagonally arrayed nanopores. One of the template sides is sputtered by metal (Au) which forms a conductive layer on the surface of the template to a cathode in an electroplating cell. During the electroplating process under galvanostatic conditions the selected metal fills the nanopores of the template. As an electrolyte, Watts Bath (250 g/l $NiSO_4$, 50 g/l $NiCl_2$, 34 g/l H_3BO_3) was used. The temperature of the solution was 55 °C, the pH was usually ranging between 3 and 3.5. The current density was 15 mA/cm^2.The circular electrode was prepared on the bottom of alumina template using fotolitography and etching of gold layer. Cu wire was fixed to the gold layer for electrode interconnection.) and the system has been sealed using epoxy resin (Cyborbond) and curred in UV light. After dissolving the template the required vertically aligned and ordered nanopillars (nanoelectrodes) on the gold layer are obtained.

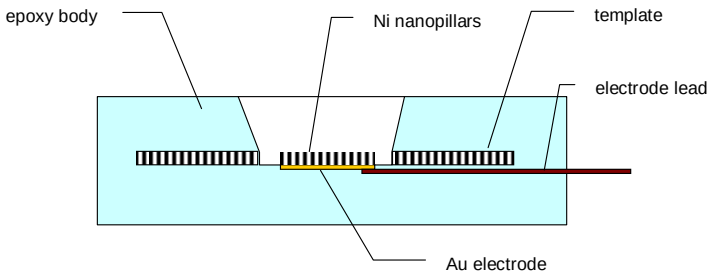

Figure 1. Coross-sectional view of the gold electrode construction with Ni nanoelectrodes for urease detection.

The Ni nanoelectrodes were utilized for a detection of urease. Measurements were carried out in acetate buffer (pH 4.6). Urease (10 µl) was accumulated at the surface of Ni nanoelectrode for various times (from 30 s to 10 min). The optimal time of accumulation was 240 s. Under these experimental conditions urease gave oxidative signal at 0.8 V. Previously we investigated the influence of various denaturing conditions (physical and chemical) on signals of various proteins (lactoferrin, protein p53) [21, 22]. However, we have not utilized the stationary electrochemical instrument to measure denaturation of protein yet. Therefore we were interested in the issue whether we were able to observe a difference between signal of native and heat denatured urease. The protein was denatured for 30 min at 99 °C. Subsequently the urease was measured at the Ni nanoelectrode. The voltammograms obtained are shown in Fig. 8 (red curve – native protein, blue curve – denatured protein). Based on the results obtained the native urease gave approximately six times lower signal compared to the denatured protein.

Acknowledgements: This work was supported from the grant of the Grant Agency of Academy of Sciences of the Czech Republic No. GAAV IAA401990701, and GAAV 1QS201710508, and from the Czech Ministry of Education within the framework of Research Plan MSM 0021630503.

References:

[1] J. B. Sumner, *J. Biol. Chem.* **1926,** *69*, 435.
[2] M. L. Mobley, R. P. Hausinger, *Microbiol. Rev.* **1989,** *53*, 85.
[3] C. P. Witte, M. G. Rosso, T. Romeis, *Plant Physiol.* **2005,** *139*, 1155.
[4] C. P. Witte, S. Tiller, E. Isidore, H. V. Davies, M. A. Taylor, *J. Exp. Bot.* **2005,** *56*, 91.
[5] C. P. Witte, S. A. Tiller, M. A. Taylor, H. V. Davies, *Plant Physiol.* **2002,** *128*, 1129.
[6] J. C. Polacco, R. G. Winkler, *Plant Physiol.* **1984,** *74*, 800.
[7] W. J. de Melo, P. D. Aguiar, G. M. P. de Melo, V. P. de Melo, *Soil Biol. Biochem.* **2007,** *39*, 1341.
[8] A. K. Thoren, *Microb. Ecol.* **2007,** *53*, 221.
[9] S. Kojima, A. Bohner, N. von Wiren, *J. Membr. Biol.* **2006,** *212*, 83.
[10] J. Kohler, F. Caravaca, L. Carrasco, A. Roldan, *Appl. Soil Ecol.* **2007,** *35*, 480.
[11] V. H. Varel, J. E. Wells, D. N. Miller, *J. Appl. Microbiol.* **2007,** *102*, 472.
[12] Z. X. Yang, S. Q. Liu, D. W. Zheng, S. D. Feng, *J. Environ. Sci.* **2006,** *18*, 1135.
[13] N. E. Dixon, C. Gazzola, R. L. Blakeley, B. Zerner, *J. Am. Chem. Soc.* **1975,** *97*, 4131.
[14] J. Zehnalek, V. Adam, R. Kizek, *Chem. Listy*. **2006,** *100*, 508.
[15] J. Robotis, *Gastroenterology*. **2003,** *124*, A176.
[16] R. Vilaichone, V. Mahachai, P. Nunthapisud, D. Thong-Gyam, P. Kullavanijaya, *Gut*. **2002,** *51*, A111.
[17] M. Wisniewska, H. O. Nilsson, L. Bak-Romaniszyn, T. Rechcinski, W. Bielanski, I. Planeta-Malecka, M. Plonka, S. Konturek, T. Wadstrom, W. Rudnicka, M. Chmiela, *Microbiol. Immunol.* **2004,** *46*, 657.
[18] H. H. X. Xia, B. C. Y. Wong, *J. Gastroenterol. Hepatol.* **2002,** *17*, 629.
[19] Y. K. Yee, K. T. Yip, T. L. Que, K. K. Chang, K. F. Li, C. K. Lee, S. W. Wong, S. F. Lau, M. L. Szeto, *Aliment. Pharmacol. Ther.* **2002,** *16*, 1739.
[20] J. Berdoz, B. Corthesy, *Mol. Immunol.* **2004,** *41*, 1013.
[21] D. Potesil, R. Mikelova, V. Adam, R. Kizek, R. Prusa, *Protein J.* **2006,** *25*, 23.
[22] O. Zitka, A. Horna, K. Stejskal, J. Zehnalek, V. Adam, L. Havel, L. Zeman, R. Kizek, *Acta Chim. Slov.* **2007,** *54*, 68.

ZnO NANOWIRES FOR NANOCOMPOSITE ORGANIC THIN FILM TRANSISTORS

Chien-Wen Hsieh[1], *Flora M. Li*[2], *Husnu Emrah Unalan*[1], *Sharvari Dalal*[1], *William I. Milne*[1]

[1]*Engineering Dept., University of Cambridge, 9 JJ Thomson Avenue, Cambridge CB3 0FA, UK*
[2]*Electrical and Computer Eng., University of Waterloo, Waterloo, Ontario N2L 3G1, Canada*
cwh31@cam.ac.uk

Large area and flexible electronics is a rapidly expanding research area, where much attention has been focused on the use of organic semiconductors. These have attracted much interest by virtue of their solution processability. However, the performance of the field effect mobility and conductivity of organic thin film transistors (TFTs) limits their application. While organic TFTs often exhibit reasonably high ON/OFF current ratios, attempts to improve their mobilities (typically < 0.1 cm^2/Vs) and stability, remain a subject of ongoing research [1-2]. The limitations of organic materials have thus prompted the pursuit of alternative material systems/options for use in large area and flexible electronics.

One-dimensional nanostructures, such as carbon nanotubes (CNTs) and nanowires, present feasible alternatives; these nanostructures can be used as the sole material in a device structure, or can be implemented as a complement to organic semiconducting material to form nanocomposite-based devices [3,4]. Several groups have recently considered CNTs for fabrication of solution-processed p-type composite TFTs; they were incorporated into poly(3-hexyl-thiophene) (P3HT) and poly[5,5'-bis(3-dodecyl-2-thienyl)-2,2'-bithiophene] (PQT-12) which are organic semiconducting polymers [5,6]. However, there are few reports concerning solution-processed n-type organic TFTs with high field effect electron mobility [7-9]. Here we report a means of enhancing n-type organic TFT devices by introducing random arrays of stamped semiconducting zinc oxide (ZnO) nanowires (Figure 1). An n-type solution-processed organic semiconductor, [6,6]-phenyl C_{61}-butyric acid methyl ester is utilized as the organic host matrix in this study, where PCBM exhibits typical field effect electron mobility of 10^{-3}-10^{-2} cm^2/Vs [8,9]. The performance of these composite ZnO-PCBM TFTs is presented alongside that of the pristine organic PCBM TFTs.

Our preliminary results reveal that the effective field effect mobilities of ZnO nanowire-PCBM composite TFT devices are increased by 20-40 times compared to pristine PCBM organic TFT, while the ON/OFF current ratio is maintained in the range of 10^5. Figure 2 shows the transfer characteristics of pristine PCBM TFT and ZnO-PCBM TFT. In the saturation regime (V_{DS} = 40V), the saturation field effect mobility of the ZnO-PCBM TFT is increased to 0.561 cm^2/Vs, representing an improvement of > 17 times over pristine PCBM TFT (0.034 cm^2/Vs). The ON/OFF current ratio remains in the same order for both composite and pristine TFTs. When the measured transfer characteristics are close to the linear regime (V_{DS} = 10V), the field effect mobility is improved markedly by 40 times, by incorporating ZnO nanowires into the organic matrix (Table 1). We suggest that the increase in the field effect mobility is due to the superior semiconducting properties of the ZnO. The nanowires can be viewed as conducting bridges which serve to enhance electron transport between crystals in the PCBM film. There may also be an increased number of charge carriers in the transport channel. For a better understanding of the role of each material, further experiments will examine the effect of different network densities of ZnO nanowires on the field effect characteristics.

References:

[1] H. Sirringhaus, T. Kawase, R.H. Friend, T. Shimoda, M. Inbasekaran, W. Wu, E.P. Woo, Science **5499** (2000) 2123.

[2] C.D. Dimitrakopoulos and P.R.L. Malenfant, Adv. Mater. **2** (2002) 99.

[3] S.H. Hur, C. Kocabas, A. Gaur, O.O. Park, M. Shim, and J.A. Rogers, J. Appl. Phys. **11** (2005) 114302.

[4] S. Liu, S.C.B. Mannsfeld, M.C. LeMieux, H.W. Lee and Z. Bao, Appl. Phys. Lett. **5** (2008) 053306.

[5] X.-Z. Bo, C.Y. Lee, M. S. Strano, M. Goldfinger, C. Nuckolls, and G.B. Blanchet, Appl. Phys. Lett. **86** (2005) 182102.

[6] P. Beecher, P. Servati, A. Rozhin, A. Colli, V. Scardaci, S. Pisana, T Hassan, A.J. Flewitt, J. Robertson, G.W. Hsieh, F.M. Li, A. Nathan, A.C. Ferrari and W.I. Milne, J. Appl. Phys. **4** (2007) 043710.

[7] C.R. Newman, C.D. Frisbie, D.A. da Silva Filho, J.-L. Bredas, P.C. Ewbank and K.E.Mann, Chem. Mater. **23** (2004) 4436.

[8] C. Waldauf, P. Schilinsky, M. Perisutti, J. Hauch and C.J. Brabec, Adv. Mater. **24** (2003) 2084.

[9] M. Chikamatsu, S. Nagamatsu, Y. Yoshida, K. Saito, K. Yase and K. Kikuchi, Appl. Phys. Lett. **20** (2005) 203504.

Figures:

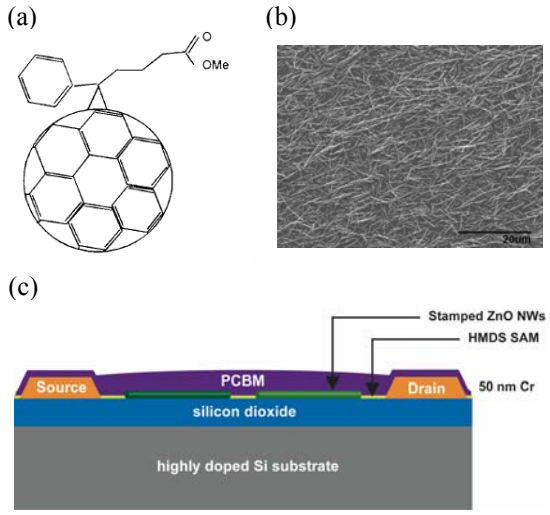

Figure 1. (a) Chemical structure of [6,6]-phenyl C_{61}-butyric acid methyl ester (PCBM). (b) Network of stamped ZnO nanowires (c) Schematic cross-section of the composite ZnO-PCBM TFT structure employed in this study.

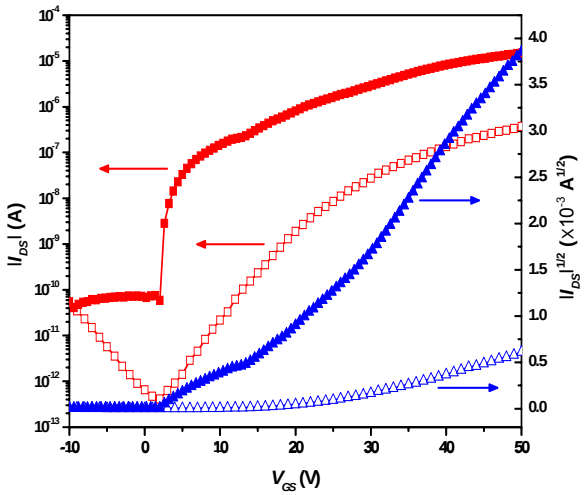

Figure 2. Transfer characteristics I_{DS}-V_{GS} and $I_{DS}^{1/2}$-V_{GS} of pristine PCBM and ZnO-PCBM TFT devices in the saturation regime at V_{DS} = 40 V.

Table 1. Field effect mobility (μ_{FE}), ON/OFF current ratio, OFF current (I_{OFF}), threshold voltage (V_T) and subthreshold swing (V/dec) of pristine PCBM and ZnO-PCBM TFT devices at V_{DS} = 40V and at V_{DS} = 10V, respectively.

Bias Regime	TFT	μ_{FE} (cm^2/Vs)	*ON/OFF Current Ratio*	I_{OFF} (A)	V_T (V)	S (V/dec)
V_{DS} = 40V (saturation)	Pristine PCBM	0.0334	9×10^5	4×10^{-13}	~ 12	4.606
	ZnO-PCBM	0.561	4×10^5	5×10^{-11}	~ 4	0.356
V_{DS} = 10V (linear)	Pristine PCBM	0.0071	9×10^4	1×10^{-13}	~ 15	2.810
	ZnO-PCBM	0.285	1×10^5	6×10^{-11}	~ 5	0.898

COMPARISON OF ELECTRO AND AIR-BLAST SPRAY DEPOSITION FOR PREPARING LANTHANUM STRONTIUM MANGANITE FILMS

Jongmo Im, Inyu Park, Seungun Jang, and Dongwook Shin*

Division of Material Science & Engineering, Hanyang University
17 Haengdang-dong, Seongdong-gu, Seoul, 133-791, Korea

**Corresponding author: dwshin@hanyang.ac.kr*

Electro spray deposition (ESD) and air-blast spray deposition (ASD), using liquid droplets atomized by electric field and gas pressure respectively, are based on the aerosol technique. These techniques have shown many advantages over several conventional deposition techniques, such as a simple set-up, inexpensive and nontoxic precursors, high deposition rate and, in particular, easy control of the surface morphology of the deposited layers. These methods also enable the thin film deposition in ambient atmosphere even if an additional heat treatment is required to obtain film with high degree of crystallinity [1,2].

In this work, air-blast spray deposition and electro-spray deposition were applied to prepare porous lanthanum strontium manganite (LSM) films on silicon substrate in the submicron range for the cathode application in solid oxide fuel cell (SOFC). The precursor solution was prepared by dissolving lanthanum nitrate hydrate, manganese nitrate hexahydrate and strontium chloride hexahydrate into methanol. The morphology of LSM film was dependant on the process parameters such as substrate temperature, liquid flow rate, air flow rate, nozzle-substrate distance, deposition time, and DC voltage. The effects of heating temperature on the crystal structure of films were investigated with X-ray diffraction (XRD) in the heating temperature range of 600 to 1000 ^{o}C. The microstructure of the LSM film was also studied by scanning electron microscopy (SEM). The porous LSM film was successfully prepared in the solution flow rate range of 1 l/min to 6 l/min, the substrate temperature of 200 ^{o}C to 600 ^{o}C, the nozzle-substrate distance range of 1 cm to 6 cm, the air flow rate range of 0.1 Mpa to 0.5 Mpa, and the DC voltage range of 1 kV to 20 kV.

References:

[1] I. Taniguchi, R.C. van Landschoot and J. Schoonman, Solid State Ionics. **160** (2003) 271.
[2] D. Beckel, A Dubach, A. R. Studart, and L. J. Gauckler, J. Electroceram.. **16** (2006) 221.

Acknowledgements

This work was supported by the Seoul Research and Business Development Program (Grant No.10583).

Figures:

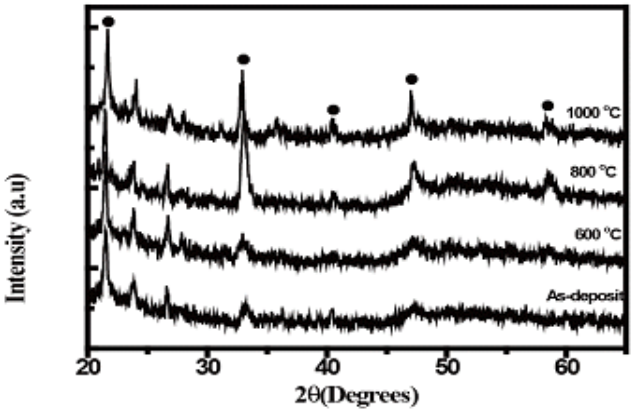

Fig. 1. X-ray diffraction patterns of LSM layers heated in the sintering temperature range of 600 ^{o}C to 1000 ^{o}C

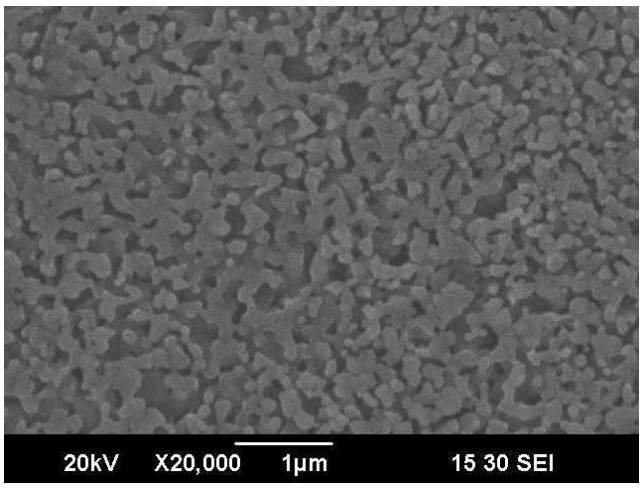

Fig. 2. Surface SEM image of sintered LSM films on Si deposited by electro spray deposition at argon pressure 0.45 Mpa, substrate temperature 325 ^{o}C, deposition time 10 min, solution flow rate 4.5 ml/h, and precursor solution concentration 0.05M at nozzle-substrate distance 4 cm

SINGLE NANOHOLES WITH GOLD NANOPARTICLES A NOVEL TOOL IN NANOOPTICS

N. Jahr [1] , A. Csaki [1], A. Steinbrück [1], S. Schröter [1], J. Popp [1,2], W. Fritzsche [1]

[1] Institute of Photonic Technology (IPHT) Jena, PO Box 100239, D-07745 Jena
[2] Friedrich Schiller University Jena, Institute of Physical Chemistry, D-07743 Jena

Nanoholes, small optical apertures with diameters below the wavelength of light; represent interesting optical properties caused by diffraction at the surface and plasmon resonance of the surface conductive electrons. The optical behaviour of these nanoscale structures are usually discussed as a setting of nanoholes in an array[1] with small period between the holes. This leads to integral optical effects, which investigated for the use in nanooptics. Our goal of research is to observe the optical effects of single nanoholes in combination with metal nanoparticles.

Nanoholes and metal nanoparticles are known for their unique optical properties. Metal nanoparticles, especially gold nanoparticles, have a strong absorption and scattering in the visible range of light. Nanoholes in plasmonic materials instead are known for extraordinary transmission of light. The combination both nanostructures have interesting novel characteristics, like the enhanced transmission of light through nanoholes with gold nanoparticles in comparison to nanoholes without particle[2]. This enhancement not only appears in the optical near field, but also in the far field and therefore in can be detected by standard optical methods. Here we present our results obtained by different methods of investigation. The methods for this investigation are optical microscopy, optical spectroscopy and ultramicroscopic methods, like atomic force microscopy (AFM), near field scanning microscopy (SNOM). This all is use to understand the process of light enhancement by nanoparticles, which are located in the nanoholes. This method gives use different kind of information we use to build a physical model of the process.

The understanding of the process is necessary for the targeted application. In the future, combination such nanostructures can maybe using for the cost-effective and highly parallel detection of single molecule binding reactions in bioanalytics.

References:

1. Ebbesen, T. W., Lezec, H. J., Ghaemi, H. F., Thio, T. & Wolff, P. A. Extraordinary optical transmission through sub-wavelength hole arrays. *Nature* **391**, 667-669 (1998).
2. Csáki, A., Steinbrück, A., Schröter, S. & Fritzsche, W. Combination of Nanoholes with Metal Nanoparticles-Fabrication and Characterization of Novel Plasmonic Nanostructures. *Plasmonics* **1**, 147-155 (2006).

Figures:

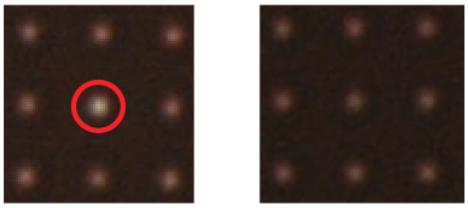

Fig. 1. : Transmission images of nanoholes. Left nanoholes filled with different values of nanoparticles, right holes without particles

FABRICATION OF Ni-YSZ ANODE FOR SOFC BY ESD

*Sungeun Jang, Jongmo Im, Inyu Park, Dongwook Shin**
Division of Material Science and Engineering, University of Hanyang,
17 Haengdang-dong, Seongdong-gu, Seou1 133-79l, KOREA
E-mail: dwshin@hanyang.ac.kr

The commonly used Ni-YSZ cermet is known to have many desirable properties for use in SOFC anodes, such as high electronic and ionic conductivity, high electrochemical activity, and good microstructural stability. ESD(Electrostatic Spray Deposition) was applied to fabricated a thin-layer of yttria-stabilized zirconia(YSZ) electrolyte on a solid oxide fuel cell(SOFC) anode substrate consisting of NI-YSZ cermet.

In this work, a solution of Ni-YSZ(Ni- 8 mol% yttria stabilized zirconia) in methanol was sprayed onto the substrate anode surface at 600-800□ by ESD. After sintering the deposited layer at 1100-1300□ for 5h depending on temperature, analyzed SEM images and XRD data.
A Ni-YSZ composite material was used for the anode, with porosity and pore size, designed to ensure a large enough effective surface area for electrochemical oxidation. The studied deposition parameters were deposition temperature, distance between nozzle and substrate, solution flow rate and DC voltage.

The goal was to obtain porous and continuous 8YSZ coatings by ESD. We have checked the efficiency of this system by SOFC measuring apparatus. Solid Oxide Fuel Cells (SOFCs) are interested as an energy conversion system of future with high efficiency and environmental cleanness. We have checked the efficiency of this system by SOFC measuring apparatus.

References:

[1] Hiroshi Nomura, Sandeep Parekh, J. Robert Selman and Said Al-Hallaj: Fabrication of YSZ electrolyte for intermediate temperature solid oxide fuel cell using electrostatic spray deposition: □-Cell performance. Journal of Applied Electrochemistry, 35(2005) 1121-1126
[2] A.H.M. Esfakur Rahman, Jong-Hee Kim, Kap-Ho Lee, Byong-Taek Lee: Microstructure characterization and electrical conductivity of electroless nano Ni coated 8YSZ cernets. Surface & Coatings Technology, 202(2008) 2182-2188

Figures:

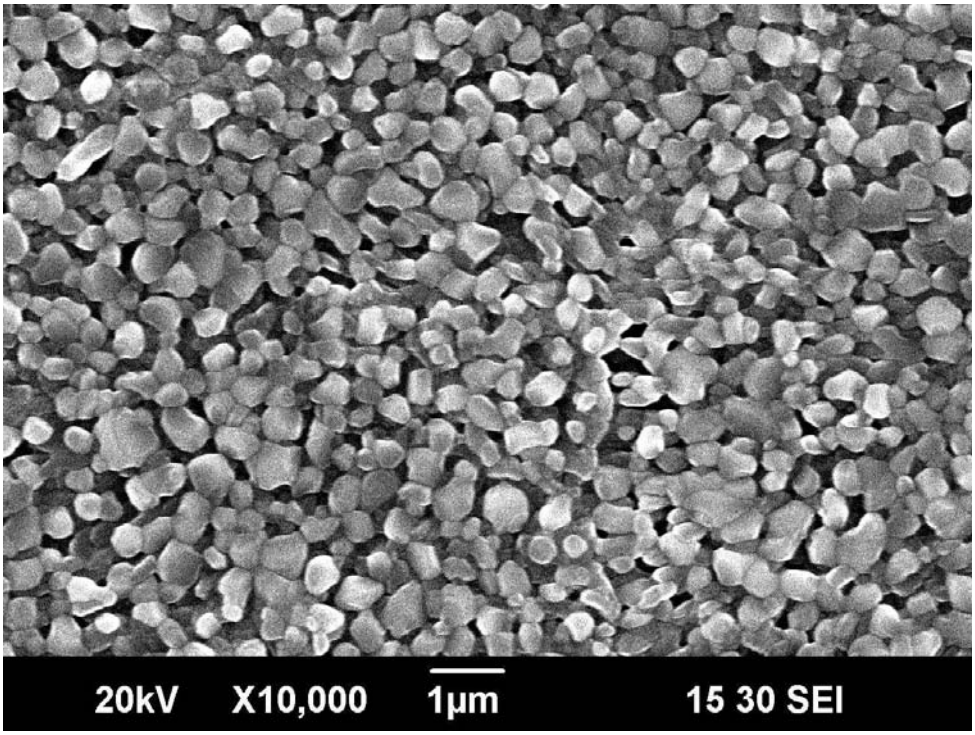

Figure 1. SEM image of a SOFC anode substrate. After sintering 1300 -5hr, Porous and continuous composition observed.

CHEMICAL ACTIVATION OF FISH-BONE TYPE CARBON NANOFIBERS

V. Jiménez*, J.L. Valverde, P. Sánchez, A. Romero.

Chemical Engineering Department. University of Castilla- La Mancha. Avenida Camilo José Cela 12, 13071, Ciudad Real. **Telephone:** +34926295300, Ext. 3509. Fax number: 926-295256. **e-mail:** Vicente.Jimenez@uclm.es

Carbon nanofibers (CNFs) are recognized as one of very promising materials based on its nanostructure and particular properties, being expected in various applications such as, catalysts or catalyst supports, selective adsorption agents and energy storage devices such as, lithium ion second battery or electric double layer capacitor [1].

The most principal disadvantage of CNFs is its low surface area and porosity (around 10-200 m^2/g). This fact restrict the applications of these materials like hydrogen (or energy) storage or catalyst support; therefore is necessary increase the surface area to improve the yield in these materials.

The surface area can be modifying by means of activation process in which a part of structural carbon atoms are eliminated (mainly, the most reactive) by an activate agent. As consequence, the porosity and surface area increase and so, their applications as hydrogen storage or catalyst support improve.

Comparatively to nanotubes, nanofibers present a nanostructure made of grapheme layer stacking which is favourable to activation. There are mainly three types of carbon nanofibers: the fishbone in which the graphene layers are stacked obliquely with respect to the fiber axis; the platelet in which the graphene layers are perpendicular to the fiber axis; and the ribbon in which the grapheme layers are parallel to the growth axis [4].

Chemical activation is an effective method to prepare activated carbon with high surface area from a wide variety of carbon precursors. Chemical activation is characterised by advantages and disadvantages when compared to physical activation by stream or carbon dioxide. To consider advantages, higher yields and more porosity are obtained, and less time is typically required to activate the samples. Key disadvantages include the corrosiveness of the activating compound and the washing stage required.

The present study was aimed to investigate the influence of different activate agents and different inert gases used in the chemistry activation process over the increase of the surface area and porosity of fishbone type CNFs. KOH, $KHCO_3$, K_2CO_3, NaOH and $Mg(OH)_2$ were the chemistry agents used and N_2, Ar and He the inert gases. The structural changes of the CNFs were investigated by using BET, XRD, TGA and TEM.

Table 1 shows the surface area of the different activated CNFs using helium like inert gas. It can be observed that the KOH increase the surface of CNFs more than other agents (almost 3.3 times the initial area). Mainly, micropores are formed during the activate process. A higher increase in the surface area, lower yield is obtained, due to the collapse and rearrangement of grapheme layers (fibrous form was destroyed) during the activate process [1,2]. Figure 1 shows the micropore size distributions of the different activated CNFs (KOH, NaOH and $Mg(OH)_2$). It can be observed that the

surface area always increase after the treatment. On the other hand, cations such as K, Na and Mg have a stronger effect on the development of the surface area because their size (K: 0.22 nm Na: 0.18 nm, Mg: 0.15) [3] permit the intercalation into the interlayer space of the carbon network structure. Finally, the basic character of the activate agents has also a great influence over the surface area increase ($pH_{KOH:}$ 14.7, pH_{K2CO3}: 12.0 and pH_{KHCO3}: 8.1).

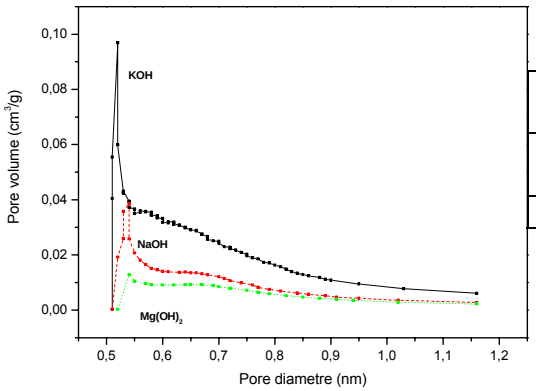

Table 1. Surface area and yield to different agents with He

Activate agent[a]	initial CNFs	KOH	NaOH	K2CO3	KHCO3	$Mg(OH)_2$
Surface area (m^2/g)	127	407.5	177.0	261.0	233.0	173.8
Yield (%)	-	55.1	76.2	62.7	67.2	77.5

[a]The activate process was made to 850 ºC during 1 h [4].

Figure 1. Micropore size distribution of the different activated CNFs

The two XRD analysis parameters, namely the average interlayer spacing d_{002} and the average stacking height of carbon planes $Lc_{(002)}$, have been showed in Table 2. The d_{002} showed just a little change, whereas the $Lc_{(002)}$ decrease when surface area increase. It shows that the mean number of grapheme plans in the crystallites decrease with increasing activation yield [4].

Table 2. Surface area and XRD analysis parameters

Activate agent	initial CNFs	KOH	NaOH	K2CO3	KHCO3	$Mg(OH)_2$
Surface area (m^2/g)	127	407.5	177.0	261.0	233.0	173.8
d_{002} (nm)	3.44	3.51	3.46	3.48	3.47	3.46
Lc (nm)	37.25	28.70	35.13	32.59	33.60	35.41

References:

[1] S. Yoon, S. Lim, Y. Song, Y. Ota, W. Qiao, A. Tanaka, I. Mochida. Carbon, 42 (2004) 1723-1729.
[2] J. M. Blackman, J. W. Patrick, A. Arenillas, W. Shi, C. E. Snape. Carbon, 44 (2006) 1376-1385.
[3] K. Okada, N. Yamamoto, Y. Kameshima, A. Yasumori, Journal of Colloid and Interface Science, 262 (2003) 179-193.
[4] D. Luxembourg, X. Py, A. Didion, R. Gadiou, C. Vix-Guterl, G. Flamant. Microporous and Mesporous Material, 98 (2007), 123-131.

POLARIZATION EFFECTS IN GaN/ALN SHORT-PERIOD SUPERLATTICES FOR INTERSUBBAND OPTOELECTRONICS

P. K. Kandaswamy[a,*], *C. Bougerol*[b], *D. Jalabert*[a], *E. Bellet-Amalric*[a] *H. Machhadani*[c], *M. Tchernycheva*[c], *F. H. Julien*[c], *and E. Monroy*[a]

[a] *CEA-Grenoble, INAC/ SP2M/ NPSC, 17 rue des Martyrs, 38054 Grenoble, France*

[b] *Institut Néel, CNRS, Département Nano, 25 Avenue des Martyrs, 38042 Grenoble, France*

[c] *Action OptoGaN, IEF, Université Paris-Sud, 91405 Orsay, France*

[*] Corresponding author: prem-kumar.kandaswamy@cea.fr

In the last several years, there has been phenomenal progress in the field of nitride semiconductor technology. The wide band gap of these materials motivated a huge international effort to develop light emitters, photodetectors, modulators and lasers in the visible and UV spectral regions. Recently, the extremely large conduction band offset of ~1.7eV in the GaN/AlN system impelled research in nitride-based intersubband (ISB) devices, with potentially interesting applications in the near-IR spectral region, covering the fibre optics telecommunications window (1.3 μm -1.55 μm) [1]. ISB transitions occur between the confined states of the conduction band in nitride nanostructures. The performance of ISB devices depends upon the ultra-fast ISB carrier relaxation time (150-300 fs in GaN/AlN quantum wells) attributed to Fröhlich (electron-LO phonon) interaction dominant in ionic materials. Along with operating speed, ISB devices also offer other advantages such as temperature insensitivity and large dipole moment. However, the large electron effective mass in GaN demands extremely thin (1-1.5 nm) QWs to reach 1.55 μm wavelength, which currently is only achieved by molecular beam epitaxy (MBE). Futhermore, spontaneous and piezoelectric polarization in nitride semiconductors induces an intrinsic electric field in the QWs. Therefore, strain management becomes a powerful design parameter which controls piezoelectric phenomena and defect formation, in a material system with huge piezoelectric constants (3-5 times those of GaAs(111)) and a significant lattice mismatch (~2.5%).

In this contribution we will present our latest achievements in terms of MBE growth of Si-doped GaN/AlN short-period superlattices (SL) for ISB optoelectronics [2]. We will discuss the effect of various growth and design parameters on the device performance, paying particular attention to the strain and polarization effects in the structures. The influence of the buffer and cap layers on the electronic profile and ISB absorption properties will be analyzed. Experimental results are interpreted by comparison with theoretical calculations of the electronic structure using a self-consistent 8-band-**k.p**-Schrödinger-Poisson solver.

All the samples show pronounced TM-polarized absorption in the near-IR, positioned at 1.55 μm (0.8 eV) for GaN/AlN (1.5 nm / 3 nm) quantum well. No shift of the absorption spectra was observed irrespective of the lattice parameter of the substrate, in disagreement with theoretical calculations which predict a blue shift under tensile strain. To clarify these odds, the structural properties were characterized with reflection high energy electron diffraction (RHEED), x-ray diffraction (XRD), transmission electron microscopy (TEM) and medium energy ion scattering (MEIS). Results point to periodic relaxation of the SL, which evolves to an average in-plane lattice parameter independent of the substrate and closer to that of AlN than predicted by elastic energy minimization.

In contrast with the observed insensitiveness to the buffer layer, the magnitude of ISB absorption depends drastically on the Al mole fraction of the cap layer. This behavior is attributed to the depletion or accumulation of charge in the QWs induced by the electric field due to difference in polarization between the cap layer and the SL. We demonstrate that polarization-

induced doping can result in a significant, and even dominant, contribution to the IR absorption in GaN/AlN MQW structures.

[1] M. Tchernycheva et al., Phys. Rev. B, **73** (2006) 125347
[1] P. K. Kandaswamy et al., submitted to Phys. Rev. B

Figures:

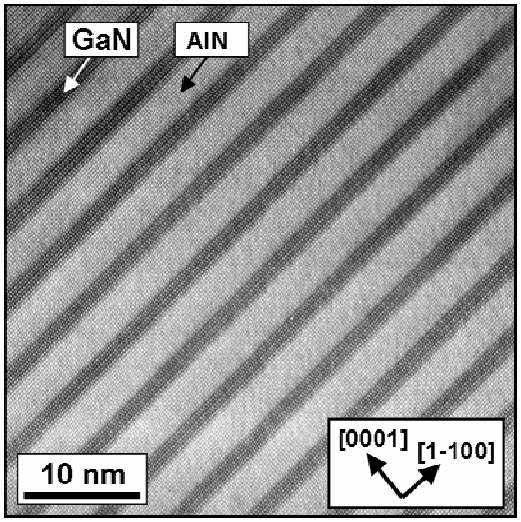

Fig. 1. High-resolution TEM image of a Si-doped GaN/AlN (1.5 nm / 3 nm) multi-QW structure (ISB absorption peak at 1.55 μm).

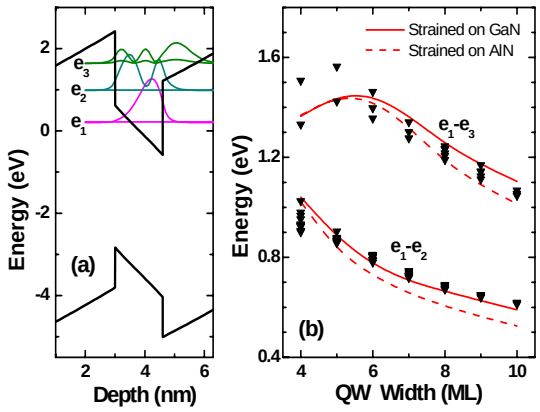

Fig. 2. (a) Band diagram of a GaN / AlN (1.5 nm / 3 nm) QW. (b) Variation of e_2-e_1 and e_3-e_1 transition energy for different QW thickness. Solid and dashed lines represent the ISBTs for SLs strained on GaN and AlN, respectively. Triangles correspond to experimental data.

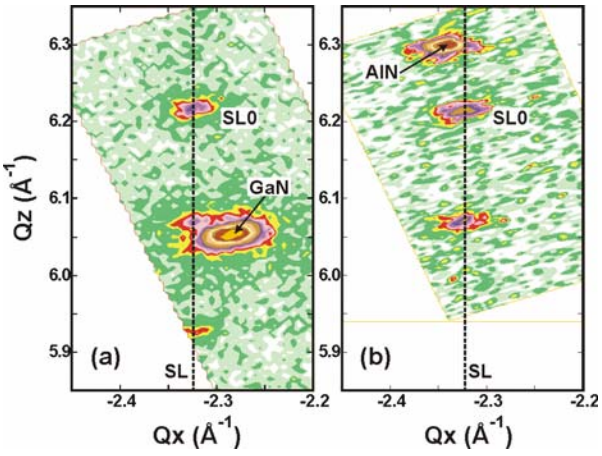

Fig. 3. Reciprocal space map around the (10-15) x-ray reflection of GaN/AlN MQW structures grown (a) on GaN and (b) on AlN templates. The average lattice parameter –i.e. the strain state- of the superlattice remains the same irrespective of the substrate.

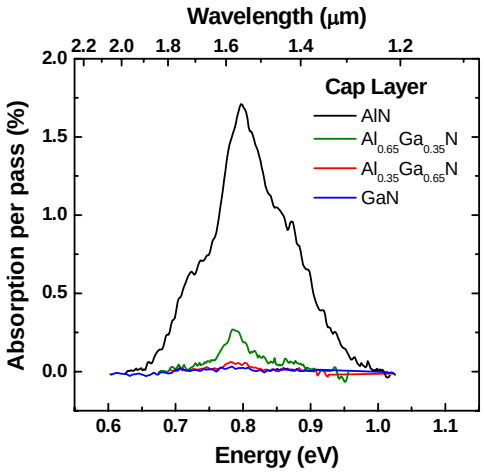

Fig. 4. Room temperature TM-polarized ISB absorption spectra of non-intentionally doped GaN/AlN (1.5 nm / 1.5 nm) MQW structures finished with a 50 nm thick $Al_xGa_{1-x}N$ cap layer with different Al content. The magnitude of the absorption increases with the Al mole fraction of the cap layer as a result of polarization-induced doping.

DESIGN AND RECTIFICATION STUDY OF DIFFERENT AVIRAM-RATNER MODEL MOLECULES .

Mykola Kondratenko, D.F. Perepichka
McGill University, Chemistry Department, 801 Sherbrooke Street West, Room 322
Montreal, Quebec, Canada
H3A 2K6
mykola.kondratenko@mail.mcgill.ca

The interest in molecular electronics began in the 1970s with the work of Aviram and Ratner. It was proposed that a covalent donor-acceptor diad, such as TTF–σ–TCNQ molecule (TTF – tetrathiafulvalene, σ – nonconjugated bridge, TCNQ – tetracyanoquinodimethane) could resemble the electric properties of a p-n junction, acting as a unimolecular rectifier [1]. The reason of such behavior lies in asymmetrically distributed electronic levels, and very low HOMO-LUMO gap (0.3 eV) was imposed for the model molecule. Up to date, numerous donor-acceptor diads have been investigated as candidates for molecular rectifiers (diodes), which include some D–σ–A diads with weak donor moiety, numerous D–π–A and also molecules without obvious asymmetry in the structure. However, neither the original TTF–σ–TCNQ molecule nor any other molecule with similar HOMO–LUMO gap have been studied in molecular electronics applications, which was due to synthetic unavailability of such molecules.

Recently we reported the synthesis and study of D–σ–A diads, based on TTF-σ-fluorene **1**, with HOMO–LUMO gap below 0.3 eV and unimolecular rectification ratio 1:18 [2]. Having asymmetrically distributed HOMO/LUMO orbitals with low energy gap, this compound present an ideal model for studying the original Aviram-Ratner concept of molecular electronics. The molecule **1** was specially designed with long alkyl chains for Langmuir-Blodgett type of deposition on the surface, where a polar dicyanomethylenefluorene fragment of **1** is exposed to the polar water phase, whereas the hydrophobic trialkylTTF moiety is stretched into the air. Using such amphilic character of molecule **1**, monolayer can be transferred onto different surfaces such as gold, Si etc.

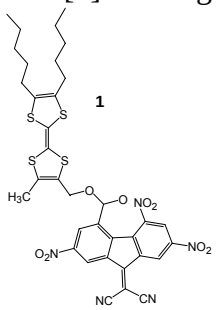

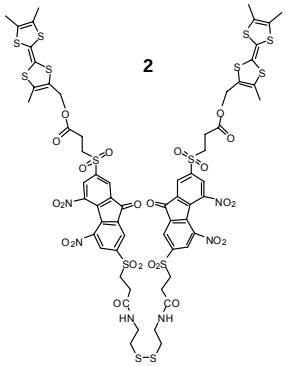

Furthermore, study on construction of molecular rectifying devices that based on self-assembly technique was also done, in which thiol-terminated molecules **2** could be bound to the electrode surface (Au, Pt) by chemical S-Au bond [3].

To study the rectification behavior of the molecule, molecular junction devices (M/D–σ–A/M) were fabricated, where the D and A moieties were put in contact with metal electrodes (M). Careful contact with the organic monolayer was made by mercury drop, covered with alkyl thiol monolayer, affording Au/A–σ–D/Hg junction. The choice of Hg and Au as electrodes was made as their work-functions match well the energy levels of the molecule and also by the fact that Hg, with alkyl thiol monolayer on the surface, does not penetrate deep in the organic layer thus preventing direct contact between two metal electrodes.

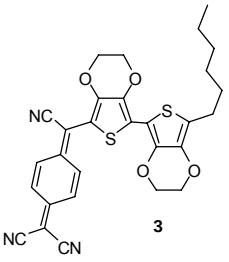

Another series of molecular rectifiers have been synthesised which are based on EDOT-3CNQ diad **3**. EDOT is a widely used nowadays in the field of molecular electronics due to its good stability. Moreover, by increasing the number of EDOT species in the chain it is possible to tune donor property of the molelcule. In contrast with original Aviram-Ratner model, molecule **3** has conjugated bridge between donor and

acceptor, but geometry calculations exhibit torsion angle between EDOT and TCNQ planes, thus HOMO of donor and LUMO of acceptor are separated. Also, donor moiety has been functionalized with long alkyl chain for the purpose of Langmuir-Blodgett deposition of the molecules on the electrode surface for further rectification study.

To conclude our study of the rectification of different molecular structures we have designed diodes made of asymmetrically structured single walled carbon nanotubes [4]. SWNTs are promising materials for future nanoelectronic technologies, and chemical functionalization of CNs by attaching various substances to side walls and oxidized ends have been extensively investigated, mostly with the aim to improve the solubility and processability of SWNTs. On the other hand, an asymmetric functionalization of a highly polarizable SWNT with electron donor substituents at one end and electron acceptors at the other should yield a highly dipolar molecule for which interesting electronic properties, including current rectification, can be expected. Our synthetic strategy is based on surface-confined reaction at one end of the tubes (yielding a film of SWNTs covalently linked to the gold surface), followed by functionalization of the "top" end of the tubes via solution chemistry. To address the induced asymmetry of the SWNTs, the conductance of the prepared film was studied in mercury drop junction experiment (fig. 1, left). The typical IV characteristics of the studied junctions (fig. 1, right) exhibit highly asymmetric behavior, with rectification ratio of $\geq 10^3$. This work describs the first asymmetric functionalization of SWNTs and demonstrate modulation of the current rectification by the modified nanotubes, self-assembled on the gold surface.

1. A. Aviram, M.A. Ratner, *Chem. Phys. Lett.* **1974**, 29, 277.
2. G. Ho, J. Heath, M. Kondratenko, et al, *Chem. Eur . J.* **2005**, 11 , 2914–2922.
3. D.F.Perepichka, M.Kondratenko, M.R.Bryce , *Langmuir* **2005** , 21, 8824–8831.
4. Z.Wei, M.Kondratenko, D.F.Perepichka, et al, *J. Am. Chem. Soc.* **2006**, 128, 3134-3135.

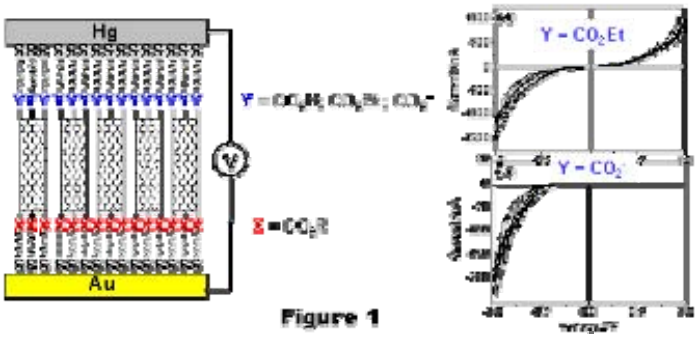

Figure 1

ATOMIC-SCALE FRICTION OF GOLD AND COPPER IN PERCHLORIC ACID

Aleks Labuda[1], *Brendan Pietrobon*[2], *Bruce Lennox*[2], *Peter Grutter*[1], *and Roland Bennewitz*[1,3]

[1]*Department of Physics, McGill University, Montreal, QC, H3A 2T8, Canada*
[2]*Department of Chemistry, McGill University, Montreal, QC, H3A 2K6, Canada*
[3]*INM–Leibniz Institute for New Materials, Campus D2 2, 66123 Saarbrücken, Germany*

labuda@physics.mcgill.ca

With the advent of nanotechnology, and more specifically nanomechanical devices, the scaling of friction down to the nanoscopic scale carries significant technological importance. Laws of friction breakdown on such scales because of the dominance of single asperity contacts rather than an ensemble average of them. Nanotribology aims to explain this phenomenon.

In this study, a home-built friction force microscope was used to measure tribological differences between two metal surfaces in a solution of perchloric acid. Electrochemical control of the Au(111) sample allowed to quickly and reversibly switch the surface from copper to gold via an underpotential deposition (UPD) process. The sustained stick-slip imaging of both surfaces confirms the switch by the change in lattice constant. Ramping up and down the normal load (while continuously alternating between both surfaces) yields reversible plots demonstrating the non-linear behavior of friction at such scales. More importantly, friction contrast between gold and copper is consistent throughout the many experiments performed using different AFM tips.

Keywords: Friction, atomic force microscope, stick-slip, copper UPD, gold.

ELECTROCHEMICALLY GROWN PEDOT ON NANOTUBE FILMS FOR TRANSPARENT ELECTRODES

Tobias Lockwood

McGill University, Department of Chemistry

801 sherbrooke st W, Montreal (Canada)

In order to further the development of important organic electronic devices such as solar cells and LEDs, a transparent electrode material is required to replace indium tin oxide, which is rapidly decreasing in availability and poses stability problems for devices. Films of carbon nanotubes on glass or plastic substrates have shown promising conductivities and transparencies which could make them a highly suitable alternative to ITO. Poly(ethylene dioxythiophene) is a semi-transparent conductive polymer which is frequently used to aid electron transport between the electrode and active organic layers of a device, yet due to its high insolubility it is normally mixed with a nonconductive polymer such as PSS to enable processing; significantly impeding its performace. The research described here proposes the use of carbon nanotube films as a conductive scaffold on which to grow PEDOT films by electrochemical oxidation of the monomer, thus forming a pure PEDOT layer on the electrode. The resulting electrode benefits from both the high conductivity and surface area of the nanotubes, and the work function of the polymer layer, which also serves to fill the space between nanotubes. The mechanical stability and charge transport properties of the electrodes can be enhanced by covalently binding the two materials. This is achieved by functionalisation of the nanotubes with EDOT monomer prior to the formation of the electrodes, thus instigating PEDOT growth directly from the nanotube surface.

DETERMINATION OF MOLECULAR ORIENTATIONS IN SINGLE POLYFLUORENE NANOWIRES USING POLARISATION DEPENDENT NONLINEAR MICROSCOPY

Pierre Lovera, *Gareth Redmond*
Tyndall National Institute, Lee Maltings, Prospect Row, Cork, Ireland
pierre.lovera@tyndall.ie

One-dimensional (1D) nanostructures based on molecular and polymeric materials are attracting significant research interest due to the many novel chemical, physical and electronic properties that may arise in such systems and the possibility for exploitation of their properties in a variety of applications. In terms of useful polymeric materials, polyfluorene based π-conjugated polymers are attractive due to their excellent charge transport properties, high photoluminescence (PL) quantum efficiencies and chemically tuneable emission wavelengths. Poly(9,9-dioctylfluorene) (PFO) is a prototypical main chain liquid crystalline homopolymer that emits in the blue and can exhibit a variety of different phases. Incorporation of PFO into 1D nanostructures would be an important advance since it would offer the potential to exploit the diverse benefits of this unique polymer in nanowire based photonic and electronic devices. To this end, we developed a novel way to synthesise PFO nanowires with semi-crystalline internal morphologies by exploiting the method of melt-assisted template wetting. The resulting wires exhibited regular cylindrical morphologies with well-defined end facets allowing nanowire active waveguiding, Fabry-Pérot microcavity behaviour and optically pumped lasing to be achieved [1-3].

More recently, we extended these studies to demonstrate that PFO nanowires can also be synthesized by solution-assisted template wetting and that these wires also exhibit attractive properties [4]. For example, investigation using linear optical methods revealed that the wires contained a significant fraction of β-phase PFO, in which polymer chain segments adopt a planarised and extended conformation, and that, as a consequence, the wires essentially acted as self-doped 1D nanostructures in which the β-phase dominated the luminescence behaviour following optical, electrochemical or electrical excitation. However, given the diverse range of potential applications available to these novel structures, one topic of great importance merits significant attention, namely, the development of an understanding of the effects of processing conditions on the extent of internal molecular organisation within PFO nanowires.

To address this challenge, we selected β-phase containing PFO nanowires as model 1D organic nanostructures and, for the first time, studied the internal molecular arrangements within single wires using a combination of third harmonic generation (3HG) and three photon excited luminescence (3PEL) imaging and spectroscopy. The dependence of three photon effects on the cube of the incident laser intensity provides for higher spatial resolution as compared with one photon methods and the use of a

near-IR laser as the excitation source (1064 nm) minimises both optical damage and scattering backround at the sample. These advantages are critical for imaging potentially fragile organic nanostructures. Another benefit is that three photon methods may show superior sensitivity to molecular anisotropy, relative to linear methods, as a result of the directionality induced by the multiphoton interaction.

In this talk, I will present results that demonstrate, for the first time, 3HG in single conjugated polymer, PFO, nanowires. Notably, by measuring polarisation dependent 3HG spectra, a pronounced dependence of excitation polarisation angle on 3HG signal intensity is observed. When the polarisation of the excitation beam is parallel to the long axis of a nanowire, the magnitude of the 3HG signal is found to be about 20 times greater than when the polarisation of the excitation beam and the nanowire long axis are mutually orthogonal. By assuming that $\chi_{\parallel}^{(3)}$, i.e., the component of the third-order susceptibility tensor with all indices parallel to the direction of the internal polymer molecular chains, dominates the 3HG signal response, a fit which incorporates a Gaussian distribution of polymer chain orientations about a net alignment direction may be made to the measured angular variation in 3HG signal intensity. A best fit to the data is found to correspond to a distribution of chain orientations about the long axis of the nanowires with a FWHM of 19° indicating that the polymer molecules within the wires are predominantly axially oriented.

I will also demonstrate 3PEL in PFO nanowires for the first time and show that, by analysing the dependence of 3PEL intensity images and spectra on both excitation and collection polarisations at the single nanowire level, values for the spread in molecular orientations about the nanowire long axis similar in magnitude to those obtained by 3HG methods, may be obtained. Importantly, by measuring both excitation and collection polarisation dependent data independently, it is possible to identify distinct orientation distributions for the populations of molecules that absorb the three photon excitation light and that subsequently emit the resulting luminescence, i.e., the nature of energy transfer processes within the wires may be probed. To conclude my talk, the implications of these results for the design of new optical methods to monitor nanowire internal structure and, also, for tailoring synthetic methods to achieve specific wire morphologies will be discussed.

References:

[1] Physica E, DOI: 10.1016/j.physe.2007.10.009.
[2] Small, **3** , 1178 (2007)
[3].Nat. Nanotech., **2**, 180 (2007).
[4] Adv. Mater. **20**, 42 (2008).

BAND-ALIGNMENT ENGINEERING OF ORGANIC PHOTOVOLTAIC MATERIALS

Arnaud Maillard and Alain Rochefort
Département de génie physique, École Polytechnique de Montréal,
and Regroupement Québécois sur les Matériaux de Pointes (RQMP), Montréal, Canada
arnaud.maillard@polymtl.ca

Organic solar cells have attracted a great deal of interest for their foreseen possibility of producing low-cost energy from light. Devices with power conversion efficiency near 5% have been reported in the literature [1]. Although the actual market for solar cell is dominated by polycrystalline silicon based devices, the use of highly efficient organic materials will become significant once the 10% power conversion efficiency mark is reached. One of the approaches to reach the 10% power conversion efficiency is to increase the charge carrier mobility. Indeed, the structural organization in organic materials for field effect transistors has been demonstrated to play a significant role in carrier mobility [2-4]. However, more efforts are needed to understand such structural effects in donor-acceptor blends used in high performance organic photovoltaic devices.

The present paper is a computational study on the structural and electronic properties of regioregular head-to-tail poly(3-hexylthiophene-2,5-diyl) (rrP3HT). We have also investigated a promising donor-acceptor blend composed of buckminsterfullerene (C_{60}) for acceptor and rrP3HT for donor. The rrP3HT polymer has been chosen for its tendency to self-assemble into microcrystalline domains, for its good mobility (up to 0.1 cm^2/Vs [2]) and processability. First principles DFT calculations were performed using the SIESTA software package [5] within local density approximation (LDA) and periodic boundary conditions. Norm-conserving Troullier-Martins pseudopotentials were used with a linear combination of numerical atomic orbitals basis set. Molecular geometries were fully optimized following a Broyden algorithm on the DFT calculated forces and stresses. The different parameters defining the pseudopotentials and basis set were validated by comparing the optimized molecular geometry and known calculated band structure of isolated polythiophene (PT) chains [6-7].

The structural and electronic properties of rrP3HT crystal were thoroughly investigated in order to be used as reference for the donor-acceptor blend. Multiple configurations of rrP3HT crystal were considered to find the most stable configuration (Fig. 1) which compares favorably to the structure observed experimentally [8-10]. Analysis of the wavefunctions symmetry was used to unfold the band structure and to determine the bandwidths. An increasing dispersion of the HOMO and LUMO bands and a reduction of the band gap energy are observed when a pressure in the π-stacking direction is applied to the system (Fig. 1).

Bulk donor-acceptor heterojunctions were studied by introducing C_{60} into the rrP3HT network. The insertion of C_{60} reduces the bandwidth of the polymer states in the π-stacking and the backbone directions. The nature of the HOMO in the blend is similar to the HOMO in the rrP3HT crystal but with some electron delocalization over the C_{60}s, while the LUMO is strongly localized on the C_{60} (Fig. 2). The results obtained clearly indicate that the structural order between the two phases in the donor-acceptor bulk heterojunction strongly influences the resulting electronic properties. These results for the donor-acceptor blend, along with those for the rrP3HT network,

suggest that their electronic properties can be tuned by engineering the material structure properties. Indeed, the displacement of the band levels with structural organization calculated for these materials can be used to optimize the band alignment in the organic photovoltaic device.

References:

[1] N. S. Sariciftci , Materials Today, 7, (2004), 36.

[2] H. Sirringhaus, et al., Nature, 401, (1999), 685.

[3] R.J. Kline, M.D. McGehee, M.F. Toney, Nature Materials, 5, (2006), 222.

[4] A. Salleo, Materials Today, 10, (2007), 38.

[5] J.M. Soler et al., Journal of Physics: Condensed Matter, 14, (2002), 2745.

[6] G. Brocks, Journal of Physical Chemistry, 100, (1996), 17327.

[7] A.M. Asaduzzaman, et al., Physical Chemistry Chemical Physics, 7, (2005), 2714.

[8] M. Brinkmann and P. Rannou, Advanced Functional Materials, 17, (2007), 101.

[9] K. Tashiro, M. Kobayashi, T. Kawai and K. Yoshino, Polymer, 38, (1997), 2867.

[10] T. J. Prosa, M. J. Winokur and R. D. McCullough, Macromolecules, 29, (1996), 3654.

Figures:

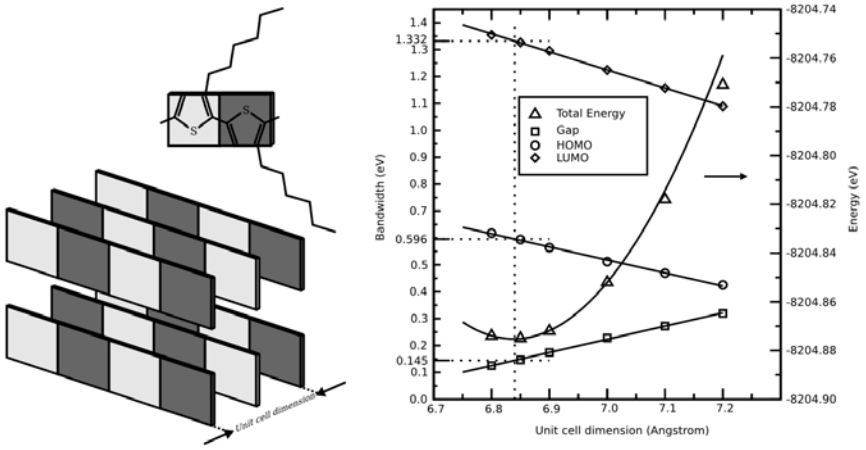

FIG. 1 – Left : Schematic optimal configuration of rrP3HT crystal. Right : Graph of the influence of the unit cell dimension on different electronic properties of the rrP3HT crystal.

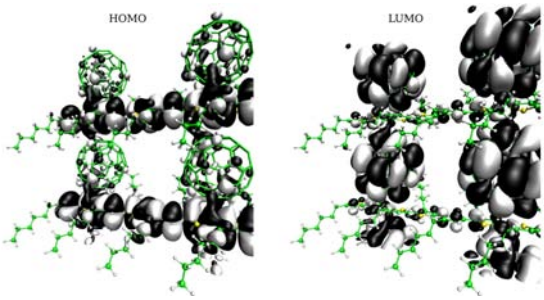

FIG. 2 – HOMO (left) and LUMO (right) wavefunctions of a rrP3HT/C_{60} bulk heterojunction.

1.06 μm → 532 nm SECOND HARMONIC GENERATION BY FERROELECTRIC NANOPARTICLES OF STRONTIUM BARIUM NIOBATE

E. Martín Rodríguez[1], A.Speghini[2], F. Piccinelli[3], L. Nodari[3], M. Bettinelli[3], D. Jaque[1] and J. García Solé[3]

[1]Departamento de Física de Materiales, C-IV, Universidad Autónoma de Madrid, c/ Francisco Tomás y Valiente 7, 28049, Madrid, Spain

[2]DiSTeMeV, Università di Verona, Via della Pieve 70, 37029 San Floriano, Verona, Italy

[3]Dipartimento Scientifico e Tecnologico, Universita di Verona and INSTM, UdR Verona, Cá Vignal, Strada Le Grazie 15, I-37134 Verona, Italy

Contact:emma.martin@uam.es

There is an increasing interest in optical imaging for biomedical applications under infrared light excitation (multi-photon illumination). The main advantages of these imaging methods are a much better spatial resolution and less scattering of the excitation radiation. This has strongly encouraged the study of new infrared to visible up converting nanoparticles which can be easily incorporated in biological systems. Recent efforts have been made on dielectric crystals doped with pairs of trivalent rare earth optically active ions, such as Pr^{3+} and Yb^{3+} in $Gd_3Ga_5O_{12}$ nanocrystals [1]. These systems can produce visible fluorescence under infrared excitation by means of different up-conversion processes. Alternatively infrared excited optical images can be produced by means of second harmonic generation, using suitable non-linear crystals. Strontium Barium Niobate, $Sr_xBa_{1-x}Nb_2O_6$ (abbreviated SBN), is a family of ferroelectric crystals of great interest from the basic and applied viewpoints. This has been recently considered as a "photonic glass", because it is able to efficiently produce multi-directional second and third harmonic generation for a variety of geometries and in a broad wavelength range [2]. Moreover SBN can be doped with a variety of luminescent ions. In fact, a self-frequency doubling SBN:Nd solid state laser has been recently demonstrated [3]. Thus SBN appears as an excellent candidate for the production of nanoparticles, having the possibility of incorporation in biomedical samples for optical imaging purposes.

In this work congruent (x=0.6) SBN nanoparticles of different sizes have been produced by different synthetic techniques [4, 5]. Then second harmonic 532 nm green light has been generated from SBN powdered crystals of different sizes, from bulk (microcrystals) to 40 nm nanoparticles, using the 1.06 μm pulsed radiation of a Nd:YAG laser as a fundamental wave. It is demonstrated that SBN nanoparticles are still ferroelectric (and so non-linear) materials, so that 532 nm green radiation can be produced because of random phase matching processes.

Figure 1 show, for the sake of comparison, the second harmonic spectra obtained for different SBN particle sizes. It can be seen that the efficiency is clearly reduced as the particle size decreases (notice that the SH signal is almost unobserved for 40 nm SBN particles). This fact is due to the absence of ferroelectric microdomains that contribute to second harmonic generation by quasi phase matching and to the shorter length of the active material. However the green signal generated by the nanoparticles is

still measurable and can be increased by using more powerful infrared lasers, such as fs lasers.

The stability of the SBN nanoparticles to laser fluence and input laser power has been systematically investigated. The SH intensity remains constant with fluence for those samples having a single SBN phase. However in the way of preparation it is often observed the presence of two phases: SBN and Strontium Niobate. In those cases the SH intensity diminishes with laser fluence and optical damage is observed.

References:

[1] R. Naccache, F. Vetrone, A. Speghini, M. Bettinelli and J. A. Capobianco, J. Phys. Chem. C, **112** (2008) 7750.
[2] P. Molina, M.O Ramírez and L.E. Bausá, Adv. Funct. Mat. **18**, (2008) 709.
[3] M.O. Ramírez, D. Jaque, L.E. Bausá, J. García Solé and A.A. Kaminskii, Phys. Rev. Lett. **95**, (2005) 267401.
[4] Y. Li, J. Zhao and B. Wang, Mat. Res. Bull. **39** (2004) 365.
[5] M. Daldosso, A. Speghini, P. Ghigna, M. O. Ramirez, D. Jaque, L.E. Bausá, J. García Solé and M. Bettinelli, J. Alloys and Comp. **451** (2008) 12–17

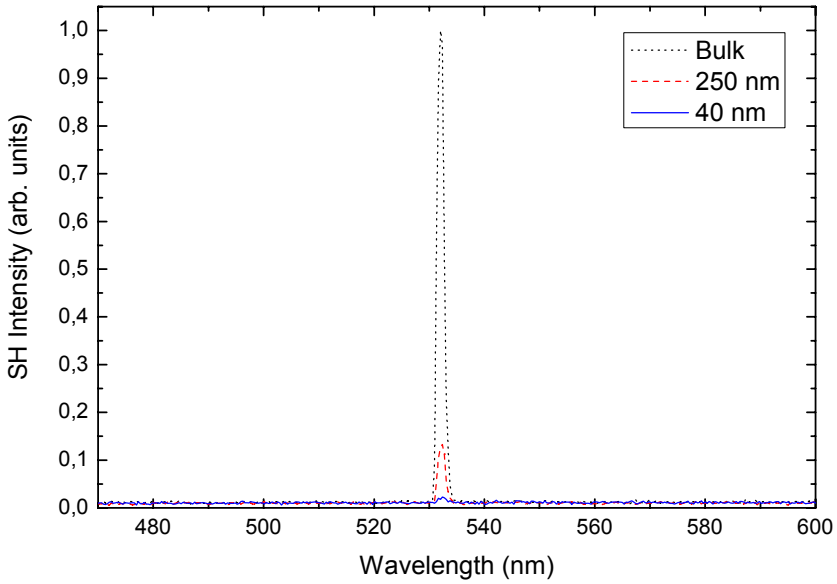

Figure1.- SH spectra for three different SBN particle sizes.

CONJUGATED POLYMER NANOFIBERS: EFFECTS OF NANOSTRUCTURATION ON PHOTOEMISSION PROPERTIES

Florian Massuyeau, Jean-Luc Duvail, Jean-Marc Lorcy, Han Athalin, Eric Gautron, Serge Lefrant, Eric Faulques and Jany Wéry
Equipe de Physique des Matériaux et Nanostructures, Institut des Matériaux Jean Rouxel, UMR6502 CNRS-Université de Nantes, 2 rue de la Houssinière,44322 Nantes, France
Florian.Massuyeau@cnrs-imn.fr

The controlled elaboration of well-defined nanostructures made of conjugated photo-electroluminescent organic polymers is very challenging for the fields of organic light emitting diodes (OLEDs), optoelectronics, photonics, and sensors. One of the most studied electroluminescent and photoconductive polymer in photonics is poly-(*p*-phenylene-vinylene) (PPV) which is the insoluble archetype of the π-conjugated polymers now used in OLEDs. The fabrication of thin films and the bulk optical properties of PPV and its related derivatives are at present quite well documented. Nanoscale systems make possible to integrate and tune desirable attributes of molecular and bulk regimes, through confinement effects, localization versus delocalization, exciton binding energy, exchange interaction and exciton fine structure, exciton-vibration coupling and dynamics of excitons.

Nanowires and nanotubes of poly-(*p*-phenylene-vinylene), a prototypical photo- and electroluminescent pi-conjugated polymer, have been prepared by the wetting template method in nanoporous membranes with an easy all-in-solution polymer precursor route. Both nanowires and nanotubes were obtained by varying the dilution of the polymer precursor in methanol prior to thermal conversion, as shown by a morphological study by scanning and transmission electron microscopies (fig.1). The effect of dilution has been addressed for PPV thin film in previous studies [1] and is compared to the case of PPV nanostructures. A polarized infra-red absorption spectroscopy (PIRAS) study indicated a preferential orientation of the PPV chains along the wire axis (fig.2). Nanofibers are highly luminescent (fig.3). Photoemission properties have been determined by steady-state and time-resolved photoluminescence (PL) spectroscopies. The time-resolved PL set-up is equipped with a confocal nanoprobe equipment, which results in a very small probe size. PPV nanotubes exhibit blue-shifted emission, higher quantum yield, and longer fluorescence lifetime with respect to PPV films. Interestingly, a new band appears at higher energy (447 nm) for the PPV nanotubes (fig.4) [2]. These effects are attributed to the cancellation of interchain interactions, that are consistent with nanoscale tubular structures formed from isolated short polymer chain segments.

References:

[1] Optical properties of poly(para-phenylene vinylene) and single-walled carbon nanotube composite films: Effects of conversion temperature, precursor dilution, and nanotube concentrations.
F. Massuyeau, H. Aarab, L. Mihut, S. Lefrant, E. Faulques, J. Wery, E. Mulazzi and R. Perego, J. Phys. Chem. C, **111** (41), 15111 (2007).

[2] Controlling shape of conjugated polymer nanofibers for tunable photoemission properties. F. Massuyeau, J.L. Duvail, H. Athalin, J.M. Lorcy, , S. Lefrant, J. Wery and E. Faulques, Advanced materials, in submission.

Figures:

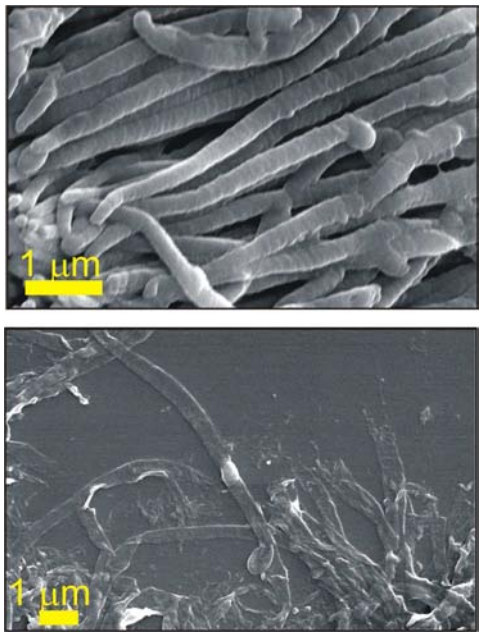

Figure 1: up: nanowires ; down : nanotubes.

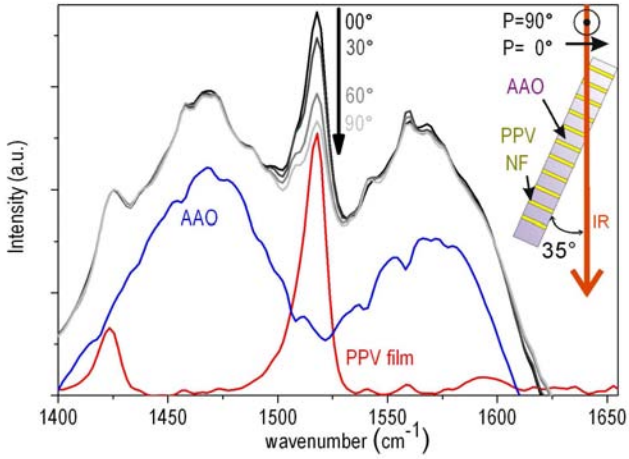

Figure 2: Micro-PIRAS recorded on PPV nanowires for different orientations of polarization.

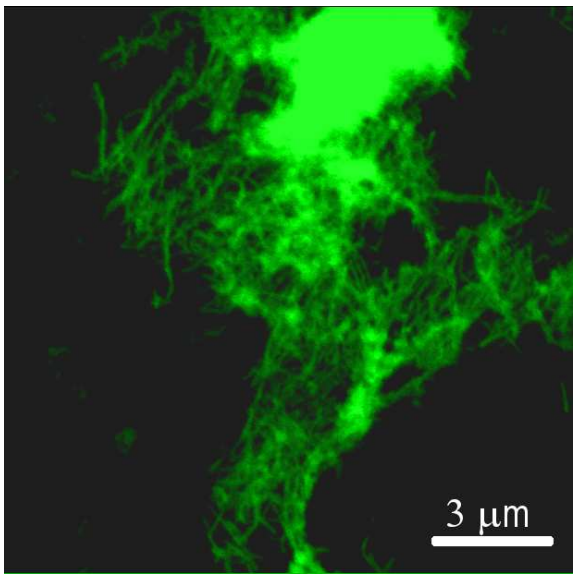

Figure 3 : Epifluorescence image of PPV nanowires.

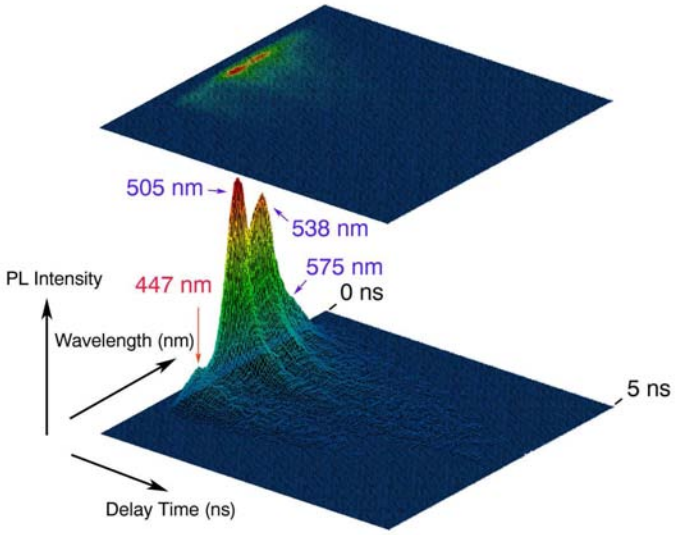

Figure 4: 3D time-resolved PL image of PPV nanotubes.

AB-INITIO CALCULATIONS OF CORE-SHELL CDSE/ZNS NANOWIRES

M. Mohr and C. Thomsen
Inst of solid state physics, TU Berlin
Germany

We present ab-initio calculations of CdSe nanowires with a surrounding ZnS shell. The influence of a ZnS shell on the structural, electronic and vibrational properties is investigated. The ZnS shell leads to a shortening of the CdSe bond length. The electronic band gap is reduced by the presence of the ZnS shell. In the present study, the CdSe/ZnS multistructure forms a type-II heterojunction, in contrast to plane CdSe/ZnS superlattices forming type-I heterojunctions. The effect of the shell on the Raman-active radial breathing mode (RBM) is analyzed. A comparison with experimental RBM-frequencies will be given.

TOWARDS THE CONTROLLED NANOMECHANICAL ACTUATION OF MICROCANTILEVERS USING REDOX REACTIONS IN ELECTROACTIVE SELF-ASSEMBLED MONOLAYERS

Lana L. Norman and Antonella Badia

FQRNT Center for Self-Assembled Chemical Structures and Department of Chemistry, Université de Montréal, C.P. 6128 succursale Centre-Ville, Montréal, QC H3C 3J7 Canada
Lana.norman@gmail.com

The vertical bending or deflection of surface-functionalized microcantilevers provides an ideal platform for nano- and micro- mechanical actuation and highly sensitive sensing technologies.[1] The basic principle arises from a chemical or physical event occurring on one face of the microcantilever generating a differential surface stress change that is manifested as a bending away from the equilibrium position. The transduction event can be monitored in real-time with considerable sensitivity via an optical beam reflected from the free end of the microcantilever. The deflection is directly proportionally to the surface stress through a modified form of the Stoney's equation and by definition a *compressive stress* (negative surface stress) corresponds to an expansion of the microcantilever, whereas a *tensile stress* (positive surface stress) corresponds to a contraction.[2,3] Over the last decade, a number of nanomechanical systems that employ microcantilevers have been successful in transferring molecular phenomena into macroscopic-scale motion. One of the first and ground breaking examples was the translation of DNA hybridization into nanomechanical motion by Fritz et al.[4] While biomolecular interactions are highly specific and evolve under mild aqueous conditions, their inherent complexity renders the exact origin of the surface stress difficult to ascertain. Key to the development and implementation of microcantilever-based technologies is the ability to control the directional motion with known precision and amplitude. In turn, this requires a comprehensive understanding of the parameters which dictate the origin of the surface stress. To this end, we have investigated the mechanism of the redox-induced deflection of microcantilevers using model self-assembled monolayers (SAMs) of electroactive ferrocene-terminated alkylthiols.

Ferrocenylalkylthiol SAMs are probably the most studied electroactive monolayers and their faradaic electrochemistry is extensively documented in the literature. This is largely because ferrocene SAMs exhibit relatively straightforward electrochemistry meaning that with the appropriate experimental parameters every surface-tethered ferrocene can undergo a one-electron reversible redox reaction. Furthermore, for a compact ferrocene SAM, the dense molecular packing confines the electrogeneration of ferrocenium cations and their complexation with the counterions to the monolayer/solution interface and non-specific ion/solvent permeation across the dielectric monolayer is predominantly inhibited. Electrochemical transformations of surface-confined ferrocenylalkylthiols have previously been shown to elicit dramatic changes in interfacial properties through molecular reorganization or ion complexation controlled/triggered by small external changes in the applied potential.[5,6] In our study, gold coated microcantilevers are functionalized with the redox-active ferrocenylalkylthiols and the origin of the dynamically controlled actuation and surface stress properties are investigated. It is well-known that the selectivity and sensitivity of microcantilever systems rely heavily on the reproducible formation of a functional layer on one surface of the microcantilever,[7] chemically well-defined SAMs provide a relatively simple and versatile system where the amplification of conformational transformations to macroscopically measured deflection can readily be tuned. We clearly demonstrate that the

electrochemical transformation of a redox moiety (ferrocene) in the *monomolecular* organic film can generate a surface stress change of a sufficient magnitude to deflect a microcantilever. A characteristic cyclic voltammogram and microcantilever stress profile observed for the redox reaction of the ferrocene-terminated monolayer in a typical electrolyte solution is shown in Figure 1A. Also illustrated in Figure 1B is a schematic representation of the redox reaction that results in the ferrocenium-bearing alkyl chain reorientation giving rise to a lateral force which we propose drives the microcantilever deflection. We will also show that small changes in molecular structure, anion composition and surface concentration of the electroactive redox centers can be used to drive a much larger micromechanical motion in a well-defined and controlled manner, which could have broad implications in micro/nano-electro-mechanical systems.

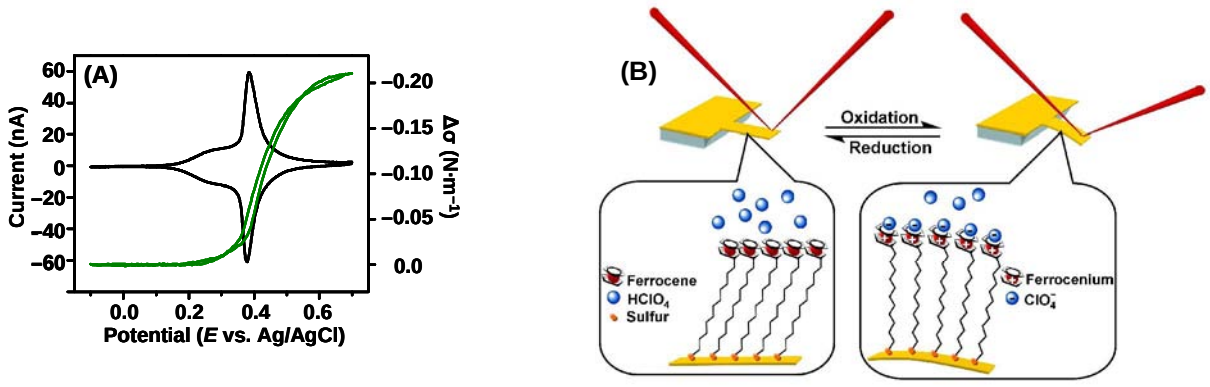

Figure 1. **(A)** Typical CVs (—) and corresponding differential surface stress, $\Delta\sigma$, (—) response for a $FcC_{11}SAu$ modified microcantilever substrate in perchlorate solution. **(B)** Schematic representation of the proposed mechanism for the $FcC_{11}SAu$ microcantilevers during a redox reaction in perchlorate solution.

[1] Singamaneni, S.; LeMieux, M. C.; Lang, H. P.; Gerber, C.; Lam, Y.; Zauscher, S.; Datskos, P. G.; Lavrik, N. V.; Jiang, H.; Naik, R. R.; Bunning, T. J.; Tsukruk, V. V., Advanced Materials, **20**, (2008), *20*, 653.

[2] Haiss, W., Reports of Progress in Physics, **64** (2001) 591.

[3] Godin, M.; Tabard-Cossa, V.; Grütter, P., Applied Physic Letters, **79** (2001) 551.

[4] Fritz, J.; Baller, M. K.; Lang, H. P.; Rothuizen, H.; Vettiger, P.; Meyer, E.; Güntherodt, H.-J.; Gerber, C.; Gimzewski, J. K., Science, **288** (2000) 316.

[5] Sondag-Huethorst, J. A. M.; Fokkink, L. G. J. Langmuir, **10** (1994) 4380.

[6] Luk, Y.-Y.; Abbott, N. L., Science, **301** (2003) 623.

[7] Tabard-Cossa, V.; Godin, M.; Burgress, I. J.; Monga, T.; Lennox, R. B.; Grütter, P., Analytical Chemistry, **79** (2007) 8136.

FABRICATION OF $SM_{0.5}SR_{0.5}COO_3$ CATHODE THIN FILMS FOR IT-SOFCS BY ELECTROSTATIC SPRAY DEPOSITION

*Inyu Park, Jongmo Im, Sungeun Jang and Dongwook Shin**

Division of Material Science & Engineering, Hanyang University
17 Haengdang-dong, Seongdong-gu, Seoul, 133-791, Korea
**Corresponding author:* dwshin@hanyang.ac.kr

Abstract

Strontium-doped samarium cobaltite ($Sm_{0.5}Sr_{0.5}CoO_3$, SSC) has good electrochemical properties for intermediate-temperature solid oxide fuel Cells (IT-SOFCs) because it has mixed-conduction characteristics which are electronic and ionic conductivities. It has higher ionic conductivities than other cathode materials for SOFCs such as LSM and LSC. Electrostatic Spray Deposition (ESD) method has some advantages such as simple apparatus, convenience of controlling microstructure of thin films and variety of choice of precursor solution.

In this study, the ESD method was applied to fabricate porous SSC thin films for a SOFC cathode. Samarium chloride hexahydrate ($SmCl_3 \cdot 6H_2O$), strontium chloride hexahydrate ($SrCl_2 \cdot 6H_2O$), cobalt nitrate hexahydrate ($Co(NO_3)_2 \cdot 6H_2O$) as starting materials and methyl alcohol as solvent were used to make precursor solution. The porous SSC films were deposited on Si substrate and the microstructure was dependent on processing parameters such as substrate temperature, distance from nozzle to substrate, applied voltage and flow rate of a syringe. Scanning Electron Microscope (SEM) and X-ray Diffractometer (XRD) measurement were used to investigate the microstructure and crystallinity of the SSC films. The ESD technique is shown to be an efficient method in which SOFCs' cathode film can be fabricated with tailoring of the desired phases and microstructure.

References:

[1] Changrong Xia, William Rauch, Fanglin Chem, Meilin Liu, Solid State Ionics, 149 (2002) 11-19
[2] Chun-Liang Chang, Ching-Shiung Hsu, Bing-Hwai Hwang, Journal of Power Sorces, 179 (2008) 734-738
[3] Zhaolin Tang, Yongsong Xie, Howard Hawthorne, Dave Ghosh, Journal of Power Sources 157 (2006) 385-388

Figures:

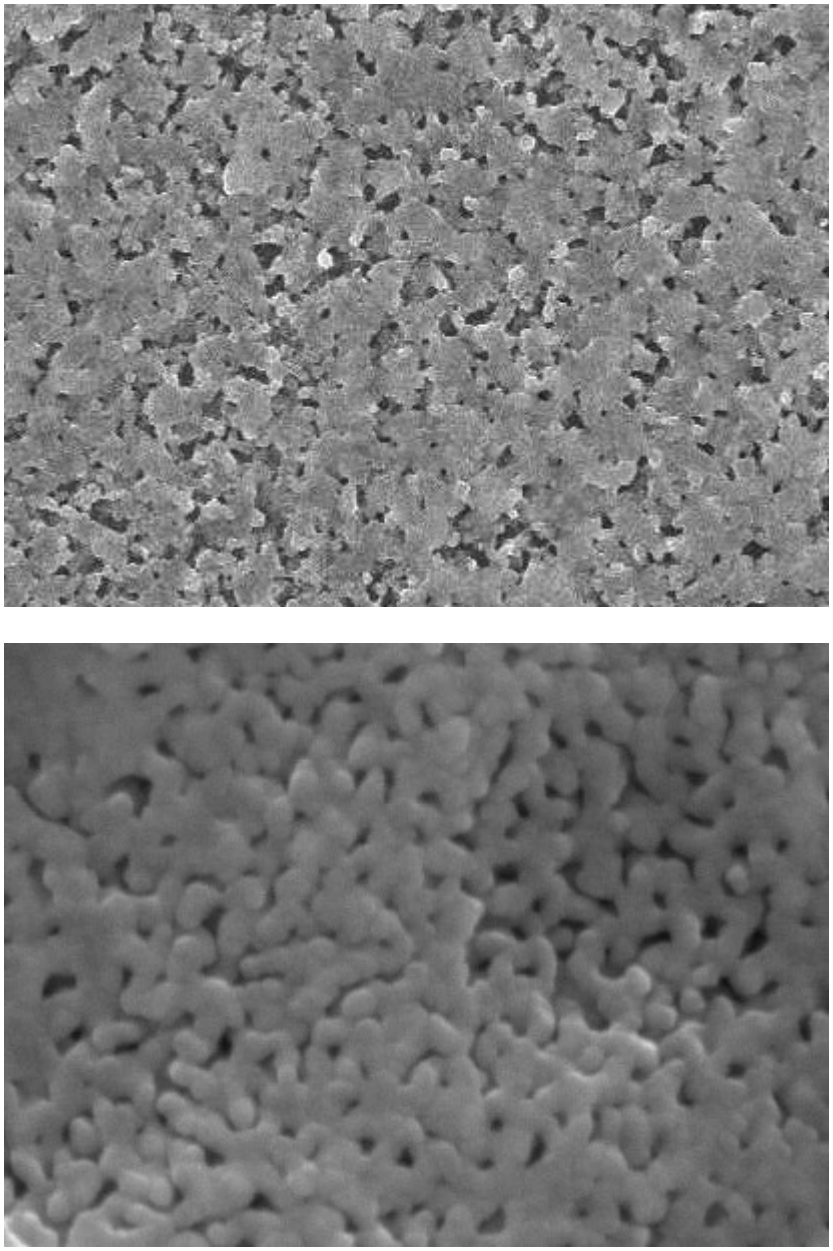

Fig.1. Surface morphologies of SSC films prepared by ESD deposited onto a silicon substrate at 350 ^{o}C and a distance of nozzle to substrate is 40 for 5min. (a) as-deposit, (b) sintered at 800 ^{o}C for 2 hrs.

MECHANICAL PROPERTIES AT THE NANOSCALE: THE DEPENDENCE OF YOUNG'S MODULUS OF NANOWIRES ON THE SHAPE AND AXIAL ORIENTATION.

S. Peláez, P. A. Serena*
Consejo Superior de Investigaciones Científicas
Instituto de Ciencia de Materiales de Madrid
c/Sor Juana Inés de la Cruz 3, Cantoblanco 28049-Madrid
**email: spelaez@icmm.csic.es*

Nanotechnology covers a broad variety of basic and applied studies aiming at the control of different properties at the nanometer level for their use in promising applications. In particular, metallic nanowires are very interesting systems for the basic point of view as well as within the context of future nanoelectronics and sensors industry [1]. The mechanical behaviour of metallic nanowires under stress has been intensively studied in order to understand their deformation and fracture mechanisms [2-5]. More recently, several studies have focussed on the dependence of the elastic constants on the nanowire size [6], neglecting the role of the orientation and shape of the nanowire. In this work we present the dependence of the Young's modulus of Al and Ni nanowires on three different parameters: cross-section shape and size, as well as the nanowire crystallographic orientation.

We have studied the tensile stress of Al and Ni nanowires by intensive computer simulations. The Embedded Atom Method (EAM) interatomic potential [8,9] is used to describe the energetic of the nanowires. Periodic boundary conditions are used to simulate infinite nanowires. For each nanowire under study we have carried out a conjugate gradients minimization of the cohesive energy in order to obtain its optimal relaxed structure. We have already used this methodology for calculating edge energies in these systems [10]. From this equilibrium condition we contract or stretch the nanowire by imposing compressive and tension loads (see Figure 1a and 1b). The nanowire atomic positions are optimized again for the stressed situation, and from these optimized coordinates the local (microscopic) stress as well as the total energy are calculated. From the total energy *versus* strain curve we determine the Young’s modulus.

We have considered nine different sets (or families) of crystalline FCC nanowires. Each family is characterised by a particular cross sectional shape (rectangular, hexagonal or octagonal) and its main axis orientation (parallel to the [100], [110] or [111] crystallographic direction). For each family several nanowires of different size (cross sectional area) have been taken into consideration in order to describe size effects.

We present results on the distribution of the stress inside the nanowire. We show that surfaces, and specially edges, accumulate a high tensile stress when compared with bulk regions. Young's modulus tends to the expected bulk limit value in the corresponding direction when the nanowire cross-section area increases. However interesting size effects are observed for thinner nanowires. Young's modulus of [100]-oriented nanowires becomes smaller than the limit bulk value as thinner nanowires are considered (see Figure 2). However, for [110]- and [111]-oriented nanowires the Young's modulus grows for decreasing nanowire

diameters. This general trend is slightly dependent on the kind of cross-section shape. This trend agrees with that observed for thin slabs.

The change of the elastic constants when modifying the nanowire radius opens a way to tailor mechanical properties of future nanoscale devices.

REFERENCES:

[1] N. Agraït, A. Levy-Yeyati and J.-M. van Ruitenbeek, Phys. Rep. **277**, 81 (2002).
[2] Referencias a Landman (articulos seminales)
[3] I.-L. Chang, and Y.-C. Chen, Nanotech. **18** 315701 (2007).
[4] A. Hasmy, E. Medina, and P. A. Serena, Phys. Rev. Lett. **86** 5574 (2001).
[5] P. García-Mochales, S.Peláez, P. A. Serena, E. Medina, and A. Hasmy, Appl. Phys. A **81** 1545 (2005).
[6] J. Diao, K. Gall, M. L. Dunn, J. Mech. Phys. Sol. **52** 1935 (2004).
[7] C. Q. Chen, Y. Shi, Y. S. Zhang, J. Zhu, and Y. J. Yan, Phys. Rev. Lett. **96**, 075505 (2006).
[8] M. S. Daw and M. I. Baskes, Phys. Rev. Lett. **50**, 1285 (1982); S. M. Foiles, Phys. Rev. B **22**, 2409 (1985).
[9] Y. Mishin, D. Farkas, M. J. Mehl, and D. A. Papaconstantopoulos, Phys. Rev. B **59**, 2292 (1999).
[10] S. Peláez and P. A. Serena, Surf. Sci. **601** 4163 (2007).

FIGURES:

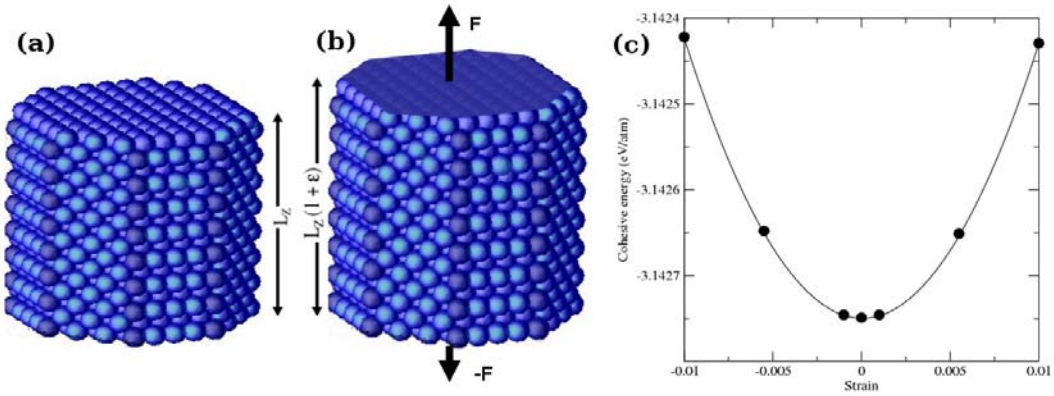

Fig 1. Schematic view of an octogonal nanowire along the [100] crystallographic orientation. Left: original configuration. Right: a strain ε is applied.

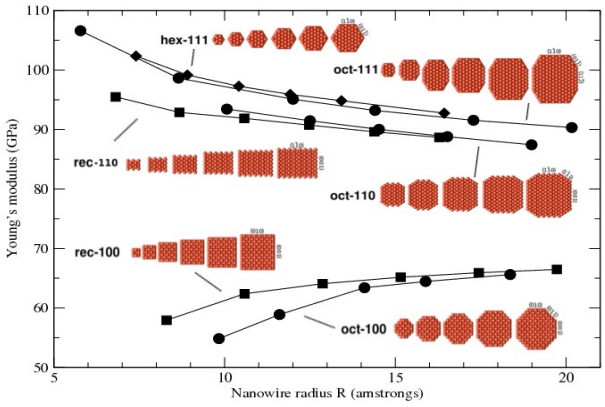

Fig 2. Young's moduli for several families of Al nanowires.

P3OT SURFACE CHARACTERITATION AS A FUNCTION OF TEMPERATURE BY VARIABLE TEMPERATURE SCANNING FORCE MICROSCOPY.

Beatriz Pérez-García[1], Elena López-Elvira[1], Jose Abad[1], Elisa Palacios-Lidón[1,2] and Jaime Colchero[1].
[1]CIOyN, Dept. de Física, Campus Espinardo, Universidad de Murcia, E-30100 Murcia,Spain
[2] CINAM-CNRS, Campus de Luminy, case 913, 13288 Marseille Cedex 09 France 3 CRHEA
beatrizp@um.es

The study of π-conjugated polymers plays an important role nowdays due to their different aplication in (opto)electronic devices, plastic solar cells[1], light emision diodes[2], etc. It is well known that polymers present a very rich molecular dynamic at temperatures raging between 0 and 100^0C such as crystalline phase transition, glass transition and melting. Therefore the study of these phenomena as a function of temperature is of vital importance. In addition, Scanning Force Microscopy (SFM) techniques have shown to be powerful tools for determining the polymer mechanical properties in the nanoscale.

In this work we study the dependence of topography and mechanical properties as a function of temperature in different crystalline and amorphous phases in the poly(3-octylthiophene) (P3OT), thin films[3] by variable temperature SFM. By ranging the temperature between 5^0C and 115^0C, the topograpy images (Fig.1,2) show that the crystalline regions disappear and all the polymer become amorphous. In parallel, local force spectroscopy has been performed at each temperature to determine the variation of stiffness of the two phases. It has been found that in both phases stiffness decreases with temperature increase, reaching a minimum at the phase transition temperature (Fig. 3).

References:

[1] Brabec C J, Sariciftci N S and Hummelen J C, Adv. Funct. Mater,. **11** (2001) 15

[2] Friend R H *et al.* Nature **397** (1999) 121

[3] Abad, J. Pérez-García, B**.** Urbina, A. Colchero, J. and Palacios-Lidón, E. , European Polymer Journal**,** *in press.*

Figures:

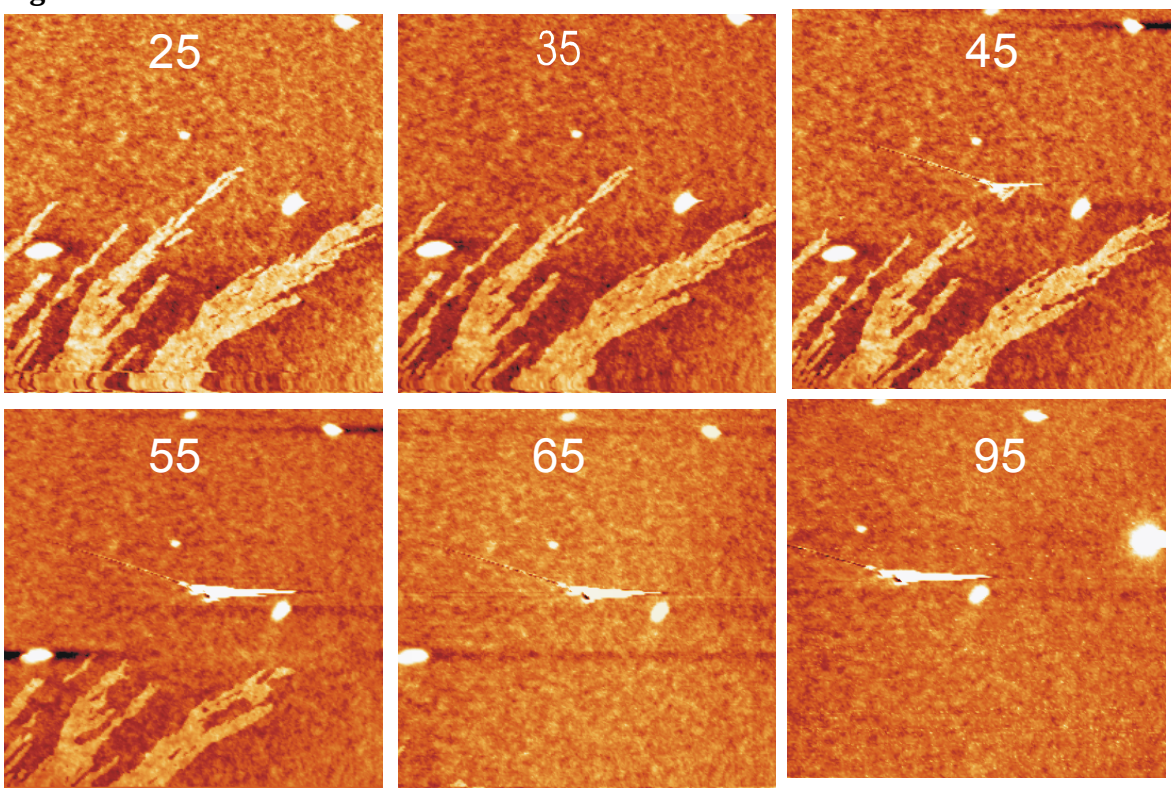

Figure 1. P3OT topography images (11.5 μm^2) in an increasing range of temperatures between 25ºC and 95ºC. Crystalline phase (brighter zones) disappears when temperature increases.

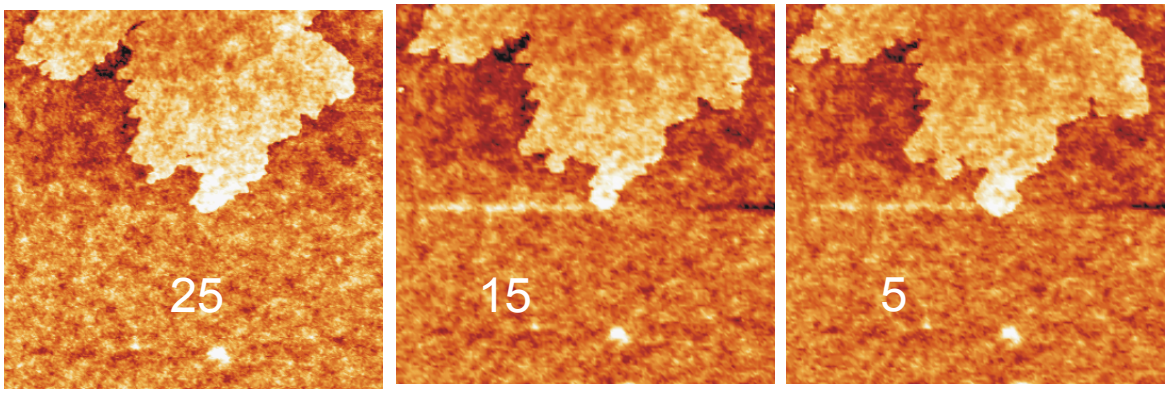

Figure 2. P3OT topography images (7.2 μm^2 **)** in a decreasing range of temperatures between 25ºC and 5ºC). Crystalline phase (brighter zones) increases when temperatue decreases.

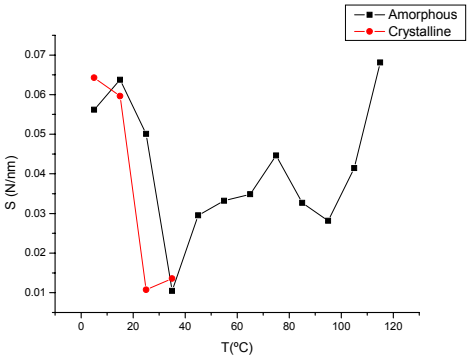

Figure 3. Stiffness determination as a fuction of temperature by local spectroscopy mearurements.

Spin contamination in quantum dot RHF states: a phase diagram

Miquel Pons Viver, Antonio Puente
Dep. de Física, Universitat de les Illes Balears,
Ctra. De Valldemossa km. 7.5, 07122 Palma de Mallorca, Spain
miquel.pons@uib.es

In recent years, semiconductor heterostructures, such as quantum dots and rings, have been the subject of many experimental and theoretical investigations. The success in controlling several system parameters, including shape, size or electron number encourages its potential use in future applications as nanoscale electronic devices. From a theoretical point of view the electronic structure of these systems has been studied using different methods [1]. Quantum Monte Carlo (QMC), configuration interaction (CI) or exact diagonalization (ED) have proved to give quite accurate results for moderate number of electrons $N \leq 13$. For larger electron numbers all these methods become exceedingly demanding for computational purposes and the electronic properties must be analyzed by resorting to simpler approximate methods such as Hartree-Fock (HF) or density functional theory (DFT). Depending on the relative strength of electron-electron interaction versus confinement, represented by the Wigner parameter (R_W), space restricted (RHF, RDFT) or unrestricted (UHF, UDFT) formalisms are more suitable to describe the state of the system [2,3]. In either case the many body wave function is represented by a single Slater determinant which in general is not an eigenstate of the total spin operator $\hat{S}^2$, thus breaking an exact symmetry of the hamiltonian. This failure to describe an adequate spin wave function can be important when trying to explain the dependence of spin properties, like singlet-triplet transitions, with the intensity of an applied magnetic field, as the mixing or *contamination* of different total spin states may result in wrong predictions for these quantities. Methods of spin restoration, pioneered by Löwdin [4] in the 1950s, (see [5] for a recent application to quantum dots), provide a useful way to solve this problem by projecting the mixed spin wave function onto different eigenstates of the total spin operator. In this work we analyze in detail the spin properties of the RHF ground states for parabolically confined quantum dots as a function of two parameters: the intensity of an applied magnetic field (B) and the relative strength of interaction over confinement (R_W). The (B-R_W) spin phase diagram is presented for quantum dots containing different number of electrons, clearly identifying regions where the spin dispersion varies from zero to its maximun allowed value. The same method can also be applied to analyze UHF or DFT states with arbitrarily high number of electrons.

References:

[1] S M Reimann and M Manninen, Rev. Mod. Phys., **74** (2002) 1283 and references therein.
[2] B Reusch and H Grabert, Phys. Rev. B, **68** (2003) 045309.
[3] C Yannouleas and U Landman, Phys. Rev. B **68**, (2003) 035325.
[4] P-O Löwdin, Phys. Rev., **97** (1955) 1509; P-O Löwdin, Phys. Rev., **97** (1955) 1474.
[5] U Giovannini, F Cavaliere, R Cenni, M Sassetti and B Kramer, New J. Phys., **9** (2007) 93.

ON-LINE MONITORING OF CYTOTOXIC EFFECTS USING EIS BASED CELL-CHIPS

Elisabetta Primiceri*, Maria Serena Chiriacò*, Rodica.Elena Ionescu*, Eliana D'Amone*, Michele Maffia§, Ross Rinaldi*, Giuseppe Maruccio*
*National Nanotechnology Lab of CNR-INFM, Lecce, Italy, § Laboratory of General Physiology, Department of biological and environmental Science and technology, University of Salento, Lecce, Italy
elisabetta.primiceri@unile.it

An important goal of biomedical research is the development of tools for high throughput evaluation of drugs effects and cytotoxicity tests. In this respect, electrochemical impedance spectroscopy (EIS) is an emerging technique for the fabrication of sensitive and specific biosensors and lab-on-chips since the immobilization/adhesion of biomolecules or cells on biofunctionalized electrodes alters the capacitance C and interfacial electron transfer resistance R_{ET}. In particular, for cell layers, R_{ET} and C are correlated to cell viability, adhesion and cytoskeleton organization and this approach has been demonstrated to be a successfull strategy to monitor cell behaviour (cells micromotion, cells attachment and spreading, cell concentration and growth or apoptosis [1-5]). In the future such EIS devices are expected to replace *in vivo* tests on animals.

Here we demonstrate EIS cell chips able to monitor cell growth, morphology, adhesion and their changes as a consequence of treatment with drugs or toxic compounds. As a case study, we investigated the uptake of copper ions and its effect on HeLa cells. For further understanding, we also carried out in parallel an AFM characterization of cells and Cu effects and monitored them in real-time using an inverted microscope during the EIS experiments.

Specifically, our chips consist of a cell culture chamber made of PDMS with integrated interdigitated electrodes (with a line-space period of 40 μm and covering a 2 x 2.5 mm^2). ITO and Cr/Au (respectively 100 nm and 3/10 nm thick) electrodes were fabricated by optical lithography, lift-off and etching on glass substrates. The PDMS cell culture chamber was realized by replica molding from a hard master. The whole device is made using transparent (or semitransparent) and biocompatible materials (fig. 1) in order to be mounted on an inverted microscope for real-time monitoring of cells during measurements to correlate cell growth, status and detachment to changes in the EIS signal.

In fig. 2, we show typical AFM images of HeLa cells in physiological conditions **(a)** and after treatment with copper ions (500 μM) for 2h and 4h **(b-c)**. Experimental results indicate that at the beginning of the treatment the toxic effect of copper causes a spreading of cells (they become thinner, fig 2b). Then after a longer treatment some of them start to acquire a round shape (see for example the cell indicated by narrow) and detach as a consequence of cell death. These cytotoxic effects can be easily identified in our chips. Both the Nyquist and Bode plots reported in fig.3 change significantly. Cell attachment and growth onto the electrodes induces an increasing impedance compared with the empty device. Looking at EIS spectra (Nyquist plot in fig 3a) is possible to distinguish two different semicircles (not present in the empty device). The semicircle at higher frequencies can be ascribed to round shape cells, while the portion at lower frequencies to adhering and spreading cells into the same device. The equivalent circuit is shown in fig3b, where the Warburg impedance Z_W consists of a resistance R_W and a capacitance C_W in parallel. During the treatments R_W increases from 50 to 160 kΩ while C_W decreases from 330 nF to 180 nF.

In conclusion, these results reveal that our cell chips provide an easy and real-time tool to study cells attachment/spreading and to perform viability and cytotoxicity tests. They are cheap and reusable and join a great sensitivity and low cost both for fabrication and usage, since they do not require any additional reagent. Moreover, they can be easily multiplexed to monitor in parallel the effect of different drugs/compounds. In the future such devices will be useful to perform drug screening without animal sacrifice and to achieve this goal we are integrating in such devices new modules for temperature regulation and drug delivery.

1. E.Katz and I.Willner, Electroanalysis **15**, 913-947, 2003.
2. X. Cheng et al., Lab on a Chip, **7**, 746–755, 2007.
3. C.Xiao et al., Anal. Chem., **74**, 1333-1339, 2002.
4. R. Ehret et al., Biosens. Bioelectron., **12**, 29–41, 1997.
5. S. Arndt et al., Biosensors and Bioelectronics, **19**, 583–594, 2004

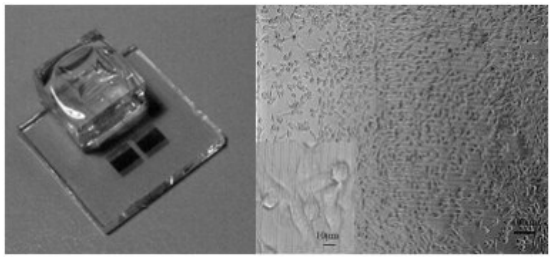

Fig. 1: Adhesion of Hela cells on ITO interdigitated electrodes on glass and picture of the whole device.

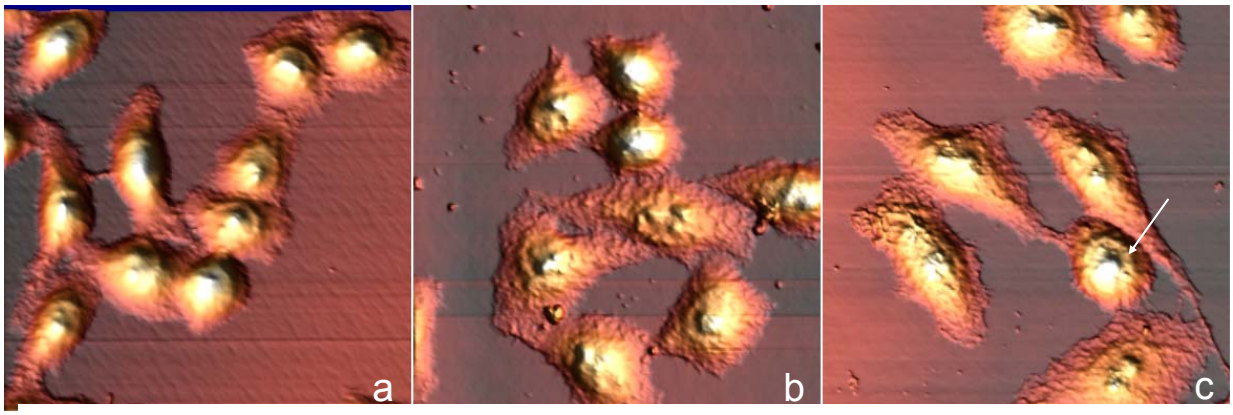

Fig.2: 3D AFM images (area 100 μm^2) of HeLa cells after different time of incubation with copper: **A**) control **B**) 2h at $CuCl_2$ 500µM **C**) 4h at $CuCl_2$ 500µM

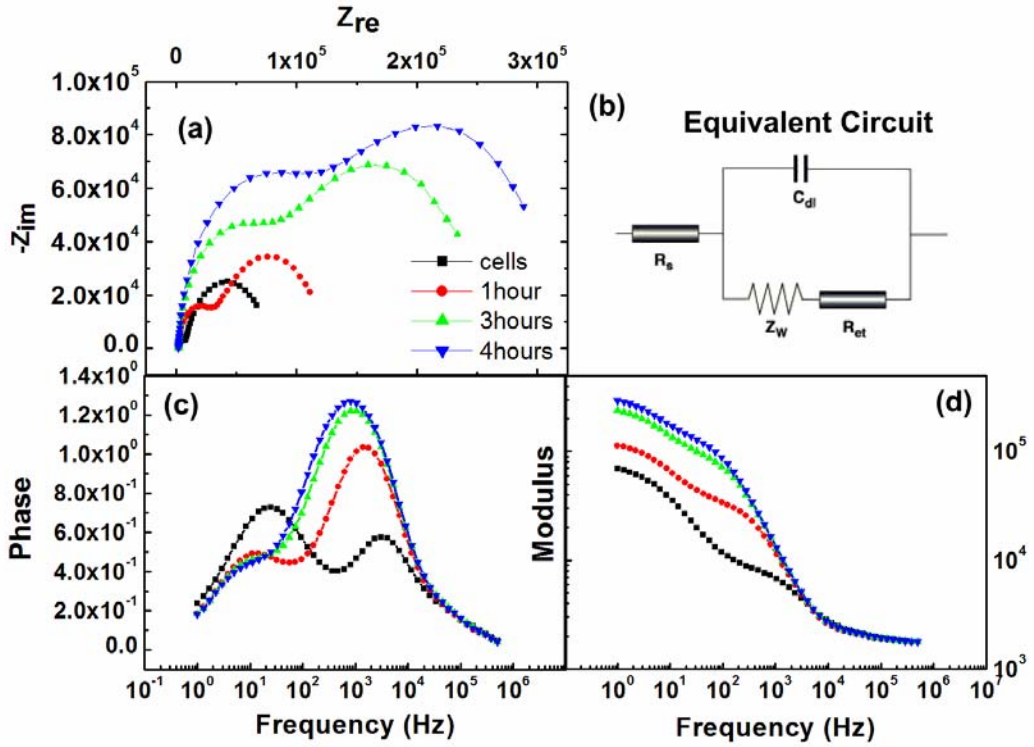

Fig. 3: Nyquist (Z_{re} vs Z_{im}) and Bode plots from chips with HeLa cells after treatment with copper for different time (0-4 hours). The data were recorded at 0V in culture medium in the presence of $K_3[Fe(CN)_6]/K_4[Fe(CN)_6]$ (1:1), 10 mM. The equivalent circuit is also reported in (b).

DESIGN OF PEPTIDES NANOSTRUCTURES HAVING ANTIMICROBIAL ACTIVITY

Marie-Ève Provencher [1], *Mariza Gattuso*[2], *Mathieu Noël*[1], *Aurélien Lorin*[1], *Barbara Collignon*[1], *François Malouin*[2], *Patrick Lague*[1], *Michèle Auger*[1], *Normand Voyer*[1], [1]*PROTÉO, Département de chimie, Université Laval, Québec, Canada,* [2]*Département de biologie, Université de Sherbrooke, Sherbrooke, Canada*
marie-eve.provencher.1@ulaval.ca

Many people receive health care every day in hospitals.(1) These individuals may be more vulnerable to infection, or may themselves be carrying a transmissible infection. The following bacteria that cause nosocomial infections are currently of particular concern: *C. difficile* (*Clostridium difficile*), VRE (Vancomycin-resistant *Enterococci*) and MRSA (Methicillin-resistant *Staphylococcus Aureus*) and many more gram negative bacteria. In Québec, 80,000 to 90,000 people in health institutions, or 10% of admissions, are thought to have a nosocomial infection. The prevention and control of nosocomial infections is nothing new in Québec. For many years, health professionals, particularly microbiologists, infectious disease specialists and infection prevention and control nurses, have been devoting time and energy in this area at health network institutions, which form the front line in the battle against these infections and have the main responsibility for preventing and controlling them. Our role is to create new antimicrobial generations which will use different mechanism of action that won't develop any resistance mechanism. On that basis, our group devotes efforts to develop novel peptide nanostructures for such purposes.

Cationic antimicrobial peptides (AMPs) have become important candidates as potential therapeutic agents. Cationic AMPs are found in organisms that are evolutionarily quite distant, ranging from plants and insects to birds, animals (including molluscs, crustaceans, amphibians, fish, and mammals), and humans.(3; 4) Cationic AMPS have usually broad spectra of "antimicrobial" activity, which include an ability to kill or neutralize bacteria (gram-positive and gram-negative), fungi, parasites, cancer cells, and even viruses like HIV and herpes simplex virus.(5)

Although the exact mode of action of AMPs has not been established, it is generally accepted that the cytoplasmic membrane is the main target of many AMPs, whereby peptide accumulation in the membrane causes increased permeability and a loss of barrier function, resulting in leakage of cytoplasmic components and cell death. The development of resistance to membrane active peptides whose sole target is cytoplasmic membrane is tought to be considerably reduced when compared with that of many current antibiotics, which have more specific molecular targets. The prediction has been substantiated in several studies.(2; 6; 7) However, the major barrier for the use of AMPs as antibiotics is their toxicity or ability to lyse eukaryotic cells, normally expressed as haemolytic activity (toxicity to human red blood cells). This is the main reason preventing their applications as injectable therapeutics.

Although numerous studies on AMPs have been done on their biological and structural activity, the amount of information about their actives structures and their molecular determinants responsible for their various biological activities is poor. Among the reasons to explain this lack of information we find the chemical and structural complexity. In fact, the minor molecular modifications on those peptides result in enormous modifications on their conformation, structure, solubility and auto-association.

In our previous studies about peptide nanostructures with membrane activity, our group has demonstrated that neutral non-natural peptide composed of 14 residues (10 leucines and 4 phenylalanines modified with crown ether acts similarly to some cationic peptides. Preliminary biophysical studies suggested that peptide nanostructure in **Figure 1** was a unique structural model to identify the molecular determinants responsible of the biological activity of natural cationic peptide.

In this presentation, we will describe the design rational and the synthesis of a library of analogous crown peptide nanostructures. The results obtained about the antibiotic activity and the effect of these compounds on the transcriptome of *Escherichia coli* ATCC 25922 to acquire detailed information on their mode of action will be described also. Moreover, we will present the results of various biophysical and biochemical studies, including circular dichroism (CD), fluorescence spectroscopy to explore the properties of such peptide nanostructures and their interactions with various bacteria and model membranes.

References :

[1]http:// www.msss.gouv.qc.ca/sujets/prob_sante/nosocomiales/index.php?situation_in_ quebec

[2] YG Ge, DL MacDonald, KJ Holroyd, C Thornsberry, H Wexler and M Zasloff, *Antimicrobial Agents and Chemotherapy*, **43** (1999) 782-788.

[3] REW Hancock and DS Chapple, *Antimicrobial Agents and Chemotherapy*, **43** (1999) 1317-1323.

[4] REW Hancock and R Lehrer, *Trends in Biotechnology*, **16** (1998) 82-88.

[5] SH Marshall and G Arenas, *Electronic Journal of Biotechnology*, **6** (2003) 271-284.

[6] DA Steinberg, MA Hurst, CA Fujii, AHC Kung, JF Ho, FC Cheng, DJ Loury and JC Fiddes, *Antimicrobial Agents and Chemotherapy*, **41** (1997) 1738-1742.

[7] LJ Zhang, J Parente, SA Harris, DE Woods, REW Hancock and TJ Fallal, *Antimicrobial Agents and Chemotherapy*, **49** (2005) 2921-2927.

Figures :

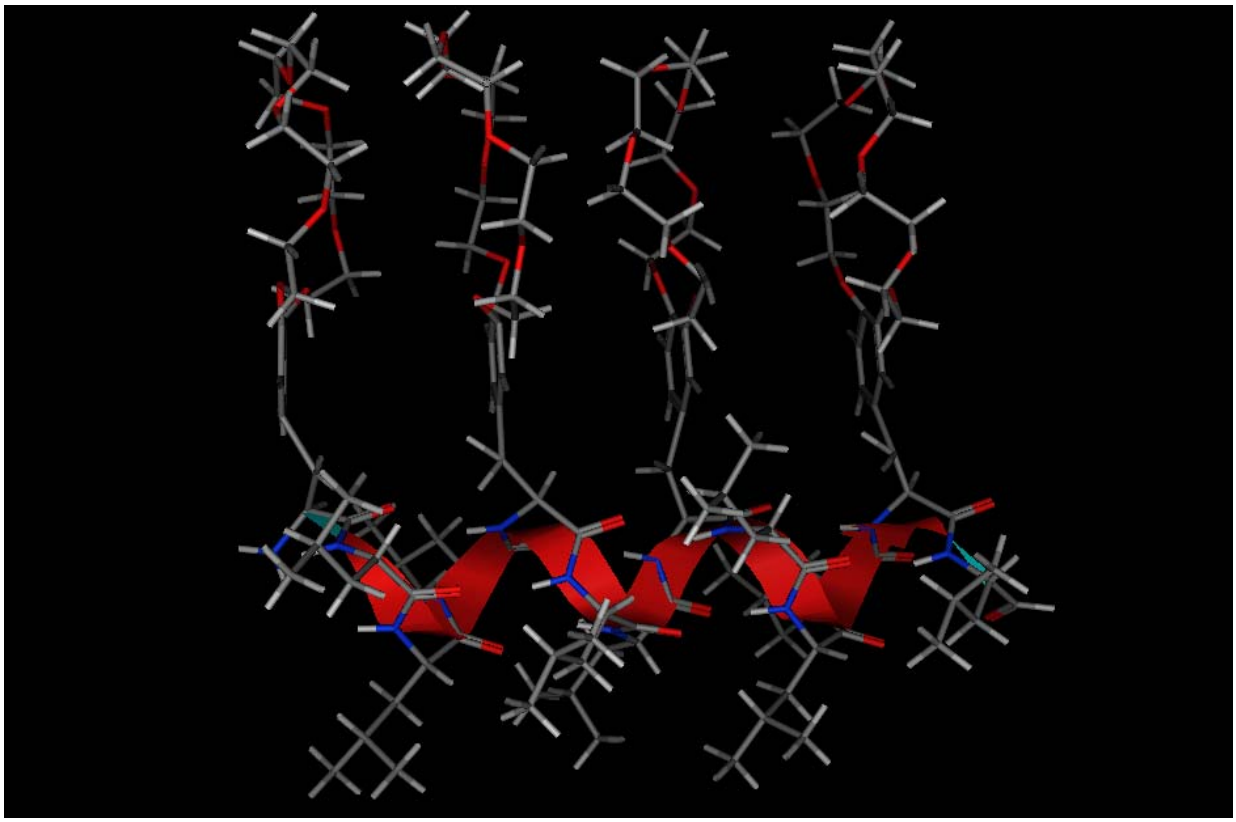

Figure 1

GROWTH STUDY OF SILICON NANOWIRES USING GOLD AND GALLIUM AS CATALYST BY IN SITU SCANNING ELECTRON MICROSCOPY

Alan REGUER, , Arnaud HOUEL[*]*, Pierre SUDRAUD*[*]*, Hervé DALLAPORTA*
CINaM - Campus de Luminy case 913 - 13288 Marseille cedex 9 – France
[*] Orsay Physics Za St Charles Chemin des Michels 13710 Fuveau France
reguer@cinam.univ-mrs.fr

We present a method that allows the synthesis, in a scanning electron microscope (SEM), of silicon nanowires (Si NWs) using Au or Ga as catalyst solvent. In situ SEM nanowire growth offers the ability to observe, film, and record events as they occur in real time. To get in situ growth conditions, we induced a localized heating by flowing current through a tungsten submicronic wire. The Vapor-Liquid-Solid (VLS) Si NWs synthesis is obtained by exposing the heated catalyst solvent to an atmosphere of silane[1-4]. For the two different catalyst solvents used (Au and Ga), we have studied the growth mechanism and determined the structure and the composition of the Si NW's by electron microscopies characterizations.

Experiments were carried out in a nanofabrication station and in a transmission electron microscope (TEM- 2000FX – Jeol) equipped with an energy dispersive x-ray (EDX) analyser. The nanofabrication station is a vacuum chamber containing a cross beam system coupling a scanning electron microscope (SEM -JSM 5910 - Jeol)) and a focused ion beam (FIB – Canion 31^+ - Orsay Physics). The nanofabrication station is also equipped with a gas injection system (GIS) and an in-situ electrical module (current-voltage source, picoammeter). For this study, we have developed two original sample devices suitable for in situ SEM localized growth of Si NWs. The first device is based on an Al pattern deposited on a SiO_2 substrate using conventional microelectronic processes (Figure 1.a.). The second device is based on four Au electrodes thermally evaporated, through a mask, on a Si_3N_4 auto supported membrane (Figure 1.b.c.). This membrane is transparent to high energy electrons (thickness 50nm) allowing subsequent analysis in a TEM. Conductive micronic tungsten wires are fabricated, on both sample devices between the macroscopic electrodes, by Focused Ion Beam Induced Deposition (FIBID) from organometallic precursor $W(CO)_6$. Structural, chemical and electrical properties of the tungsten wire deposited by FIBID as fully described in previous works[5,6]. The devices can be mounted on the in-situ electrical module allowing the heating of the tungsten wires by Joule effect. The local pressure of silane in the vicinity of the heated wire is obtained using the gas injection system while the base pressure in the chamber is in the $1.5.10^{-5}$ Torr range.

The reaction temperature is a key parameter in the VLS Si NWs synthesis. Based on recent results on nanoscale thermal properties in solid[7-9], we have developed a simulation method to get the temperature profile for different heating conditions of the tungsten wire (Figure 2). The results of temperature simulation can be compared with our experimental results obtained by SEM and TEM observations of Au nanoparticules evaporation. These profiles were useful to estimate the temperature condition for VLS Si NWs synthesis.

We have followed the nucleation and the growth of Si NWs and observed that two very different growth mechanisms are obtained depending on the catalyst solvent (Au or Ga). For Au as solvent (Figure 3-4), the growth mechanism is the classical VLS process, the catalytic droplet is on the top of the Si NW and the growth stops when the temperature of the droplet is below the eutectic temperature. For Ga as solvent (Figure 5-6), only one nanowire grows from its bottom in the vicinity of the gallium droplet, the decomposition of silane is induced by the high temperature of the tungsten wire providing silicon for the VLS synthesis. We have observed that the catalytic droplet remains at the base of the Si NW so that this particular growth mechanism leads to the formation of a unique and very long nanowire.

References:

1 L. X. Mu, W. S. Shi, J. C. Chang et al., Nano Lett. **8** (1), 104-109 (2008).
2 A. I. Boukai, Y. Bunimovich, J. Tahir-Kheli et al., Nature **451** (7175), 168-171 (2008).
3 Y. Cui, Q. Q. Wei, H. K. Park et al., Science **293** (5533), 1289-1292 (2001).
4 Y. Cui and C. M. Lieber, Science **291** (5505), 851-853 (2001).
5 A. Reguer, F. Bedu, D. Tonneau et al., J. Vac. Sci. Technol. B **26** (1), 175-180 (2008).
6 M. Prestigiacomo, F. Bedu,, H. Dallaporta et al., Appl. Phys. Lett. **86**, 1 (2005).
7 E. Pop, D. A. Mann, K. E. Goodson et al., J. Appl.Phys. **101** (9), (2007).
8 G. E. Begtrup, K. G. Ray, B. M. Kessler et al., Phys. Rev. Lett. **99** (15), (2007).
9 R. Prasher, Nano Lett. **5** (11), 2155-2159 (2005).

Figures:

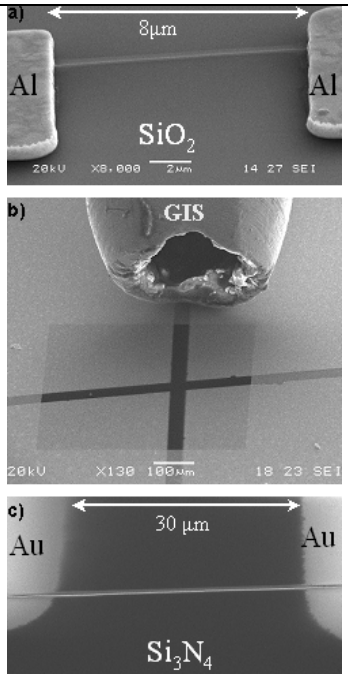

Figure 1. SEM images of the SiO_2 (a) and Si_3N_4 (b,c) sample devices

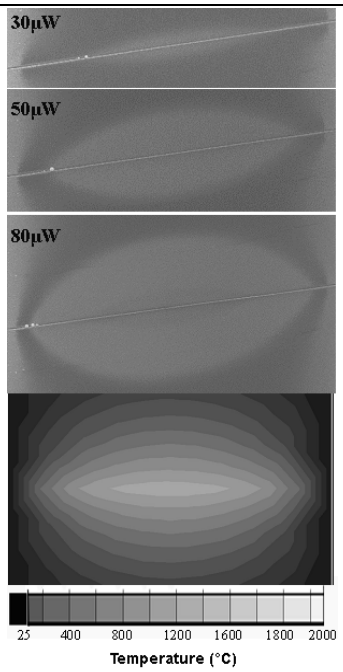

Figure 2. SEM images for different heating conditions and the associate temperature profile for a heating at 80µW.

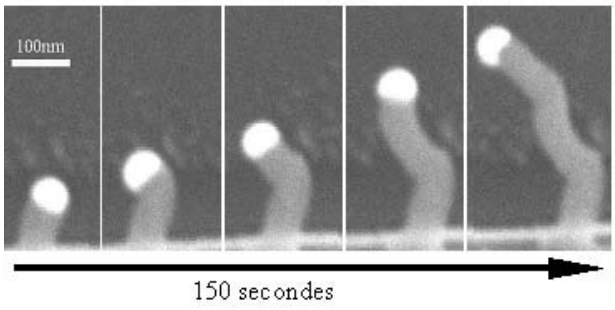

Figure 3. Sucessive SEM images of Si NWs on Si_3N_4 sample device using Au as catalyst solvent.

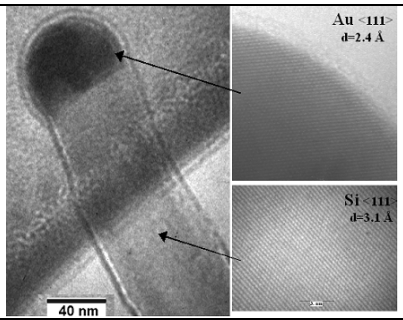

Figure 4. TEM images of Si NW on Si_3N_4 sample device

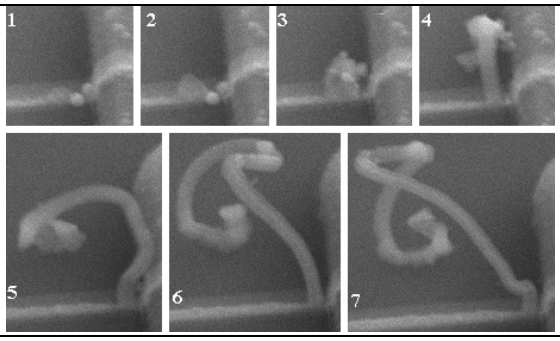

Figure 5. Successive SEM images of Si NW growth on SiO_2 sample device using Ga as catalyst solvent.

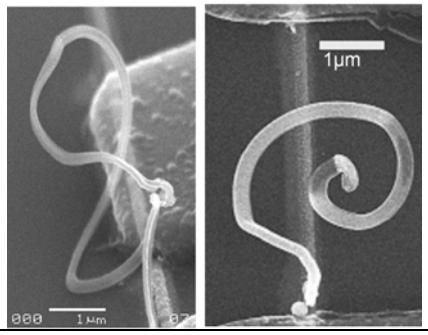

Figure 6. SEM images of Si NWs on SiO_2 sample device using Ga as catalyst solvent

MANIPULATION, ASSEMBLY AND CHARACTERIZATION OF OPTICALLY FUNCTIONAL 1-D ORGANIC NANOSTRUCTURES

Ken Reynolds, *Pierre Lovera, Daniela Iacopino, Marko Pudas, Phil Jones and Gareth Redmond.*

Tyndall National Institute, “"Lee Maltings", Prospect Row, Cork, Ireland.

One-dimensional (1-D) nanostructures based on organic materials are attracting significant research interest due to the many novel chemical, physical and electronic properties that may arise in highly anisotropic systems and the possibility for exploitation of such properties in a wide variety of applications. In particular, the potential of semiconducting polymer nanowires and nanotubes is now being explored for realisation of sub-wavelength photonic devices such as photodetectors, lasers and electroluminescent diodes. Successful realisation of such devices relies upon the ability to precisely manipulate and assemble these nanostructures so they can be successfully interconnected and integrated onto chips. While there has been significant research published on the assembly of inorganic nanostructures[1-2] there has been very limited research carried out in relation to the assembly of organic nanostructures.[3-4] To this end, we have explored a range of manipulation and assembly methods. In this talk I will present recent results in our consortium concerning nanowire manipulation and assembly by probe manipulation, magnetic fields, optical trapping, and “shear alignment”.

A probe-based system was successfully developed to manipulate nanowires and assemble them into complex mesostructures for possible device applications as a step towards a nanostructure prototype test platform. AFM analysis was carried out to confirm minimal damage was done to the nanowires. Epi-fluorescence microscopic imaging indicated that the nanowires luminesced under UV excitation with intense blue light emission. Far-field fluorescence microscopy allowed for characterisation of the functionality of whole nanowires while polarized optical microscopic studies of nanowire birefringence indicated axial alignment of the polymer molecules within the wires.

To magnetically manipulate organic nanowires, 30 nm Fe_3O_4 nanocrystals were doped into the wires and were successfully aligned when placed in an external

magnetic field. A demonstration of a doped polymer nanowire as a nanoroter undergoing 360° rotation under the influence of a rotating NbFeB magnet while clocking its polarized flouresence will be presented. We will also introduce a novel optical trapping system using a Laguerre – Gaussian laser beam as a new tool for manipulation, assembly and characterization of organic nanostructures. We will demonstrate for the first time successful trapping of number of organic nanowires and nanotubes and present data concerning the nanostructures physical properties while in the beam. Finally a method to successfully align random nanowire mats has been developed by drop-depositing nanowires from suspension onto a substrate where aligned nanowire mats were achieved by the method of shear alignment.

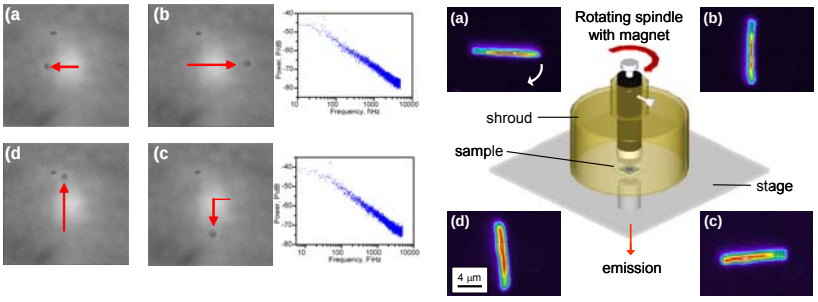

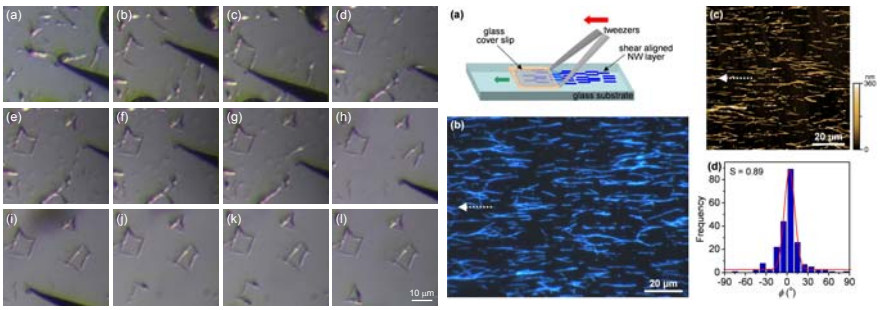

[1] W. Lu and C.M. Lieber, "Nanoelectronics from the bottom up", Nature Mater. 6, 841, 2007.

[2] P. Pauzauskie and P. Yang, “Nanowire Photonics”, Materials Today**,** 9, 36, 2006.

[3] J. Kjelstrup-Hansen, P. Bogild, H-G. Rubahn, ”Mechanical properties of organic nanofibers”, SMALL, 660, 2006.

[4] J. Kjelstrup-Hansen, P. Bogild, J. Hvam, A. Majcher, H-G. Rubahn, “Micromanipulation of organic nanofibers for blue light emitting microstructures”, Phys. Stat. Sol.A, 1459, 2006.

CARBON NANOTUBES AS ELECTRODES FOR MOLECULAR ELECTRONICS: FROM SAMs TO SINGLE-MOLECULE CONNECTION

G. Robert[1], F. Moggia[2], N. Lidgi-Guigui[1], S. Streiff[1], V. Derycke[1], A. Filoramo[1], S. Campidelli[1], M.G. Goffman[1], B. Jousselme[2], S. Palacin[2], S. Lenfant[3], D. Vuillaume[3], and J-P. Bourgoin[1]

[1]Laboratoire d'Electronique Moléculaire, SPEC (CNRS URA 2464), CEA Saclay, 91191 Gif sur Yvette (France) - [2]Laboratoire de Chimie des Surfaces et Interfaces, SPCSI, CEA Saclay, 91191 Gif sur Yvette (France) - [3]Molecular Nanostructures and Devices Group, IEMN, CNRS, BP60069, Avenue Poincaré, 59652 Villeneuve d'Ascq (France)

gael.robert@cea.fr

While the use of molecules as building blocks for the development of new electronic devices has attracted a lot of attention for the past 25 years, one of the main challenges of the molecular electronics field remains the efficient connection of small assemblies of organized molecules and, ultimately, of individual molecules. For fundamental studies, several techniques to address either self-assembled monolayers (SAMs) on a nanometer-scale or single molecules have demonstrated their high potential, in particular those with adjusting electrode distances such as STM, Conducting-Probe AFM and mechanical break-junctions. From a device point of view vertical structures (such as nanopores) have been used but suffer from severe limitations related to the top contact formation - direct metal evaporation on top of SAMs usually resulting in the deterioration of the molecules. Even if a few methods were derived to limit this problem (indirect evaporation, conducting polymer inter-layer deposition…), the spatial resolution of the final device is limited by the patterning technique, which implies the connection of a very large number of molecules. Horizontal structures have also been developed, in particular micro-fabricated nanogaps, which have lead to fascinating results. In this geometry, the challenges concern both the control of the inter-electrodes distance and the reliable insertion of a known number of molecules, ideally a single one.

In this context, using carbon nanotubes (CNTs) as electrodes to connect molecules is very attractive with respect to their intrinsic nanoscale size, exceptional electronic properties and compatibility with most fabrication processes and substrate types (including flexible ones). Our work demonstrates the use of individual CNTs as electrodes in two configurations.

In the first one, an individual single wall CNT is used as top electrode in nanoscale metal-SAM-nanotube junctions (Fig 1.a). We first use a metallic CNT and compare the transport properties of a simple octadecanethiol (ODT) SAM with the more complex case of sigma-pi-sigma molecules with a terthiophene core (T3). The simple tunnelling regime of the first case corresponds to a barrier height of ~2.4 eV in strong contrast with the structured I-Vs of the second type of SAM, which includes hysteretic Negative Differential Resistance (NDR) behaviour (Fig 1.b,c).
Most interestingly, when a semiconducting CNT is used, the proposed device geometry combined with the insulating character of the ODT SAM enables the study of carbon nanotube field-effect transistors, in which the SAM serves as ultrathin and organic gate dielectric. These p-type transistors display excellent performances (very steep subthreshold slope, greatly reduced hysteresis and band-to-band tunneling) and allow the direct and quantitative determination of the efficiency of such molecular gate dielectric (Fig 1.d). Moreover, when converted into n-type transistors, these devices show an absence of gate modulation, which emphasizes the key role of the electrical dipole of the SAM in controlling the device switching behavior [1]. The tunability of this parameter associated with the high level of performances open new ways towards the realization of fully organic nano-scale transistors.

Very recently, nanotubes were also used by the Nuckolls group as electrodes for single molecule devices [2]. However the oxygen-plasma cutting technique results in the statistical fabrication of

different gap sizes, which are difficult to adjust to a specific class of molecules.

In a second step, we have thus studied and optimized a quantitative and selective chemistry route to covalently connect single molecules between CNTs, with preferential connection at the end of the CNTs [3] (Fig 2.a). We then show that the CNT-molecule-CNT junctions produced in solution can withstand the following process steps all the way to the device realization. We perform electrical measurements in the case of ethylenediamine (EDA) (Fig 2.c), which give conductance values in reasonable agreement with previous results from the STM-break junction technique [4]. The richness of the nanotube electronic properties together with the possible choice of the connected molecules offers a wide range of possibilities to study self-assembled single-molecule devices.

References :

[1] G. Robert et al, *Self-assembled molecular monolayers as ultrathin gate dielectric in carbon nanotube transistors*, submitted.
[2] X. Guo et al, *Science* **311**, (2006), 356.
[3] J.-P. Bourgoin et al, *Electron Devices Meeting 2006, IEDM '06 Technical Digest* (2006), 435.
[4] L. Venkataraman et al, *Nano Letters* **6**, (2006), 458.

Figures :

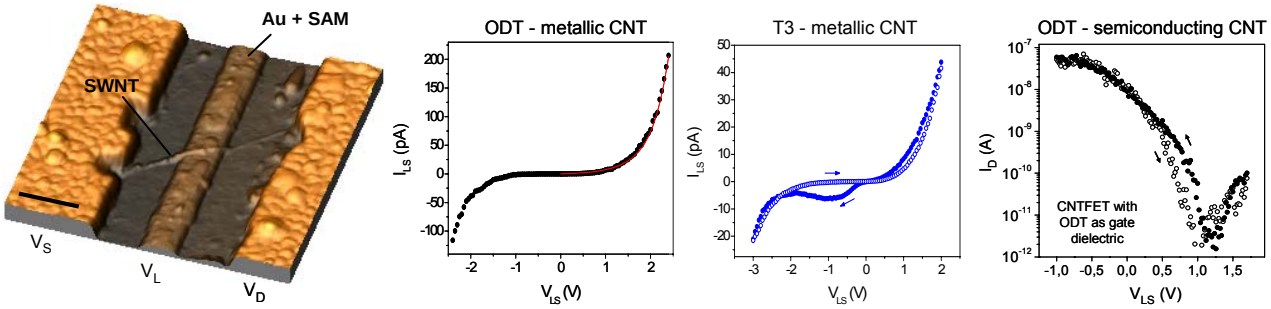

***Figure 1** : **a)** AFM picture of a CNT-SAM device (scale bar 200 nm). **b)** I(V) characteristic of a metallic nanotube-ODT SAM-gold junction and associated Simmons fit (red line). **c)** I(V) characteristic of a metallic nanotube-T3 SAM-gold junction, forward and backward sweeps. **d)** ODT-SAM CNFET: $I_D(V_{LS})$ characteristic through the tube in both sweep directions showing the reduced hysteresis.*

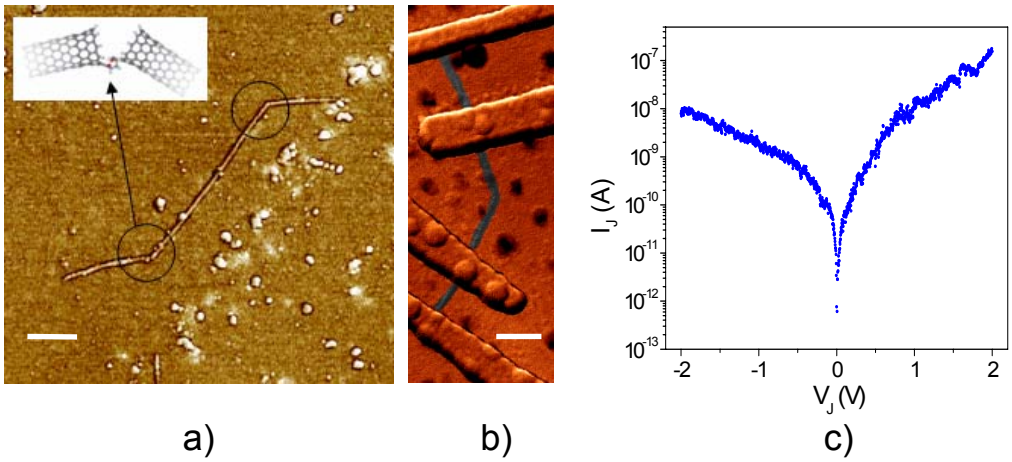

***Figure 2** : **a)** AFM picture of multiple CNT-EDA-CNT junctions (scale bar is 200 nm). **b)** AFM picture of a connected CNT-EDA-CNT junction (the tubes have been colored for clarity – scale bar is 200 nm). **c)** $I_J(V_J)$ characteristic through the CNT-EDA-CNT junction*

MOLECULAR CONDUCTANCE IN TERMS OF ORBITAL DENSITIES AND POLARIZABILITIES

Philippe Rocheleau and Matthias Ernzerhof
Département de Chimie, Université de Montréal, Montréal, Québec, Canada
philippe.rocheleau@umontreal.ca

In molecular electronics, molecules are connected to macroscopic contacts. In our work we focus on modeling the transmission of electrons through a molecular electronic device (MED). We use conventional perturbation theory (where the contacts are represented by a perturbing potential[1]) to calculate the transmission probability T(E) for an electron to pass through the molecule. This allows us to express T(E) in terms of properties of the bare molecule. We show that, in general, it is the electron density (first-order contribution) on the atoms that connect to the contacts that contributes the most to the transmission probability of the MED. The second-order correction, determined by the orbital polarizability, adds little improvement on the first-order results for the system studied. Using this approach, we obtain a simple qualitative answer to the question why the molecule studied by M. Mayor[2] shows orders of magnitude difference in the conductance by changing the contact attachment points in the molecule. We outline an extension of our method that accounts for correlation effects.

References:

[1] F. Goyer, M. Ernzerhof and M. Zhuang, J. Chem. Phys., **126**, (2007) 144104
[2] M. Mayor *et al.*, Angewandte Chemie Int. Ed., **42**, (2003) 5834

Micromagnetic simulation of MFM tip hysteresis and stray field

Rodríguez-Rodríguez,G. [1,2], *Velez, M*[1]., *Chubykalo-Fesenko, O*[2] *and Alameda, J.M*[1]
[1]*Depto. de Física; Facultad de Ciencias; Universidad de Oviedo – CINN; Avda. Calvo Sotelo s/n 33007, Oviedo, Spain*
[2] *Instituto Nacional del Carbón (INCAR), CSIC c/Francisco Pintado Fe 26, 33011, Oviedo, Spain*
[3]*Instituto de Ciencia de Materiales de Madrid, CSIC, Cantoblanco, 28049 Madrid, Spain*
fxx@condmat.uniovi.es

The stray field of MFM tips can be strong enough to compromise the characterization of soft-magnetic materials based nanostructures. On the other hand, this stray-field can be used to alter the magnetic state of the system, getting involved in magnetization reversal of magnetic nanoparticles[1],[2], as well as being used to modify the domain walls, dragging or pushing them away [3],[4],[5] in order to interact with the nanostructured system.

In this work, micromagnetic simulations of a generic MFM tip and its stray field have been performed using MAGPAR in order to obtain, not only the tip-to-sample interaction magnitude[7], but all the three components of the stray-field as a function of the retrace height. This allows us to fit the tip stray-field in terms of simple monopole, dipole and second order multipole expansion, as well as to determine each applicability height range.

We have simulated the complete hysteresis loop of the MFM tip in order to obtain the remanence state and to explore de different states of the tip under external field applied parallel to the Z axis.

Finally, we can appraise the effects of the tip-sample interaction in CoSi and CoZr based thin films systems, which are in good agreement with MFM measurements.

This work was supported in part by Spanish Ministerio de Educación y Ciencia under grants NAN2004-09087, FIS2005-07392, R-R.,G. acknowledges financial support from MERG-2004-513625 and I3P grants program.

References:

[1] M. Kleiber, F. Kümmerlen, M. Löhndorf and A. Wadas
Physical Review B, **59** (1998) 5563-5567 DOI: 10.1103/PhysRevB.58.5563

[2] Xiaobin Zhu, P. Grütter, V. Metlushko and B. Ilic,
J. Appl. Phys. **91,** 7340 (2002); DOI:10.1063/1.1452683

[3] Xiaobin Zhu, Dan A. Allwood, Gang Xiong, Russell P. Cowburn, and Peter Grütter
Applied Physics Letters **87**, 062503 (2005), DOI: 10.1063/1.2009050

[4] J. M. Garcia, A. Thiaville, J. Miltat, K. J. Kirk, J. N. Chapman, and F. Alouges,
Appl. Phys. Lett. **79**, 656 (2001), DOI:10.1063/1.1389512

[5] G Rodríguez-Rodríguez, A Pérez-Junquera, M Vélez, J V Anguita, J I Martín, H Rubio and J M Alameda**,**
J. Phys. D: Appl. Phys. **40** (2007) 3051–3055, DOI:10.1088/0022-3727/40/10/006

[6] W. Scholz, J. Fidler, T. Schrefl, D. Suess, R. Dittrich, H. Forster, V. Tsiantos,
Comp. Mat. Sci. **28** (2003) 366-383. doi:10.1016/S0927-0256(03)00119-8

[7] A.Carl, J. Lohau, S. Kirsch and E.F. Wassermann
Journal of Applied Physics **89** (2001) 6098-6104

Figures:

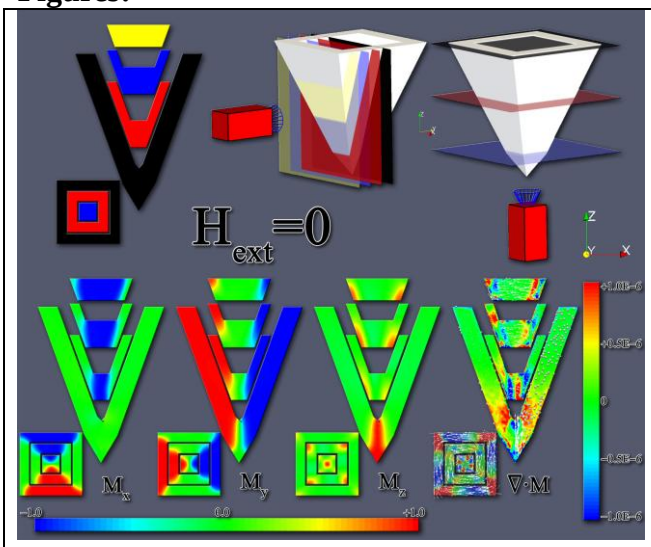

Fig 1: Slices of the MFM-tip model showing the magnetization configuration at remanence state.

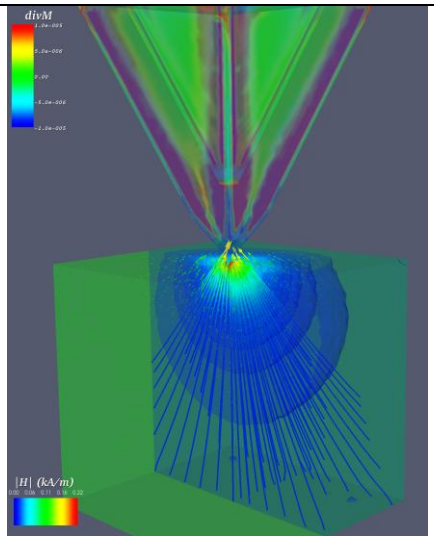

Fig 2: MFM tip magnetic poles distribution and associated stray field.

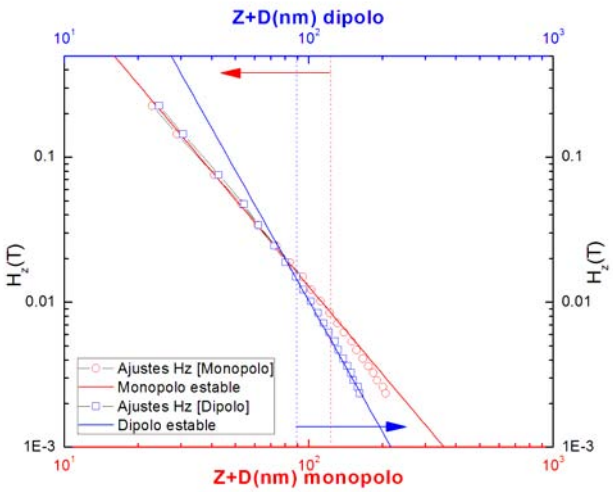

Fig 3: Applicability height ranges for the monopole and dipole fittings.

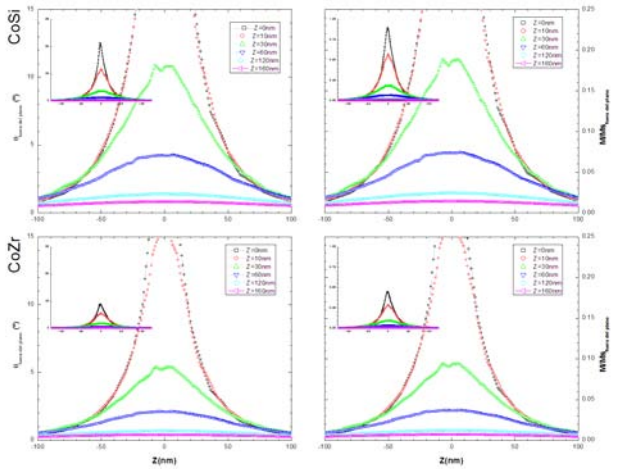

Fig 4: Magnetization *off-plane* displacement due tip-sample interaction in CoSi and CoZr thin films according the simulated H_{tip}.

SYNTHESIS OF METALLIC ATOM CLUSTERS BY SOFT METHODS. CHARACTERIZATION AND PROPERTIES.

María J. Rodríguez-Vázquez, Beatriz Santiago, Noelia Vilar, Eldara Rodríguez-Cobo, David Buceta, Ana Ledo, Mercedes Torneiro, Mª Carmen Blanco, Carlos Vázquez-Vázquez, José Rivas and Arturo López-Quintela

Laboratory of Nanomaterials and Magnetism. Institute of Technological Research. Departments of Physical Chemistry, Organic Chemistry, and Applied Physics. University of Santiago de Compostela
mary268@usc.es, qfarturo@usc.es

The main goal of the research carried out was to optimize the synthesis of atomic clusters and their purification; it means the control of the number of metallic atoms per cluster. Clusters were prepared by means of selective synthesis. It is observed that the sizes, geometry, and composition depend very much on synthesis conditions. A novel procedure for the production of metallic clusters based on a patent will be presented.

Our study has been based on the synthesis and study of the properties of atomic clusters of the following metals. A novel procedures for the production of this metallic clusters based on a patent will be presented. Several kinds of synthesis strategies were employed for production of these metallic atom clusters. Right now, we are able to tailor the clusters size by choosing suitable synthesis parameters. These parameters are different for each method. For example, the conditions that we can use to have a control of size of the clusters for electrochemical method are working electrode, electrolyte, solvents, current and time of synthesis, and the kind of ligands. With this method of synthesis we obtain sizes of clusters between 2 y 25-30 atoms per clusters. As an example of the possibilities offered by those techniques the preparation of specific clusters with interesting optical, fluorescent, and magnetic properties will be show.

References:

[1] M.A. López Quintela and J. Rivas. "Procedure for the preparation of atomic quantum clusters". Spanish patent application No.P200402041, 2005. PCT/ES2006/070121, 2006.
[2] M.L. Rodríguez-Sánchez, M.J. Rodríguez, M.C. Blanco, J. Rivas, M.A. López-Quintela *J.Phys.Chem.B* **109** (2005), 1183-1191.
[3] M.L. Rodríguez-Sánchez, M.C. Blanco, M.A. López-Quintela. *J.Phys.Chem.B* **104** (2000), 9683-9688.
[4] A. Ledo-Suárez, J. Rivas, C.F. Rodríguez-Abreu, M.J. Rodríguez, E. Pastor, A. Hernández-Creus, S.B. Oseroff, M.A. López-Quintela. *Angew. Chemie Ed. Int. **46** (2007)*, 1-6.
[5] O.Guillén-Villafuerte, G. García, B. Anula, E. Pastor, M.C. Blanco, M.A. López-Quintela, A. Hernández-Creus, G.A. Planes. *Angew. Chemie Ed. Int.* **45** (2006), 4266-4269.
[6] M.J. Rodríguez, J. Rivas, M.A. López-Quintela, A. Mouriño, M. Torneiro. Nanomaterials for Application in Medicine and Biology. M. Giersig (ed) (Springer Verlag, 2008, 113).

Figures:

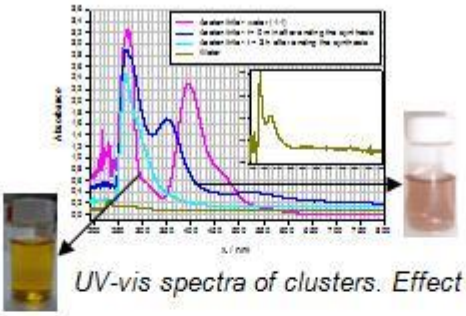

UV-vis spectra of clusters. Effect of change of solvent

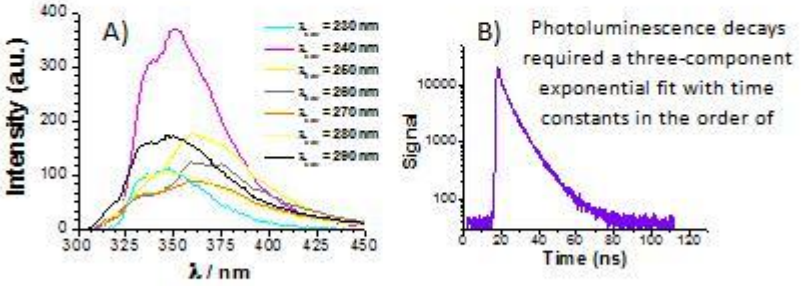

Fluorescent properties of Au clusters. A) Fluorescent spectra of the electrochemically synthesized Au clusters at different excitation wavelengths. B) Time-resolved photoluminescence spectrum of Au

Hydrogen Storage in Thin Metallic Films

Loránd Románszki, Nicola Naujoks, Michael Zäch and Bengt Kasemo
Chalmers University of Technology, Fysikgränd 3, F5112, 41296 Göteborg, Sweden
Lorand@chalmers.se

Hydrogen is a high energy density, environmentally ideal energy carrier in electric cars, a promising alternative of the conventional fossil fuels gradually being exhausted. For such applications, the problem of the hydrogen storage must be solved. High pressure hydrogen gas tanks onboard are not the best option and liquid hydrogen has its own disadvantages too. It has been known for long time, that certain metals can reversibly absorb hydrogen, however, none of these is perfect [1]. Palladium is an excellent hydrogen absorber metal, the kinetics being fast in both absorption and desorption way at room temperature, however, the storage capacity is less than 0.6 wt% and the metal is expensive. In contrast, magnesium is relatively cheap, with more than 7.6 wt% storage capacity, but the reversibility is poor and the decomposition temperature is too high (330 °C) for the polymer electrolyte membrane of the fuel cell. Therefore a lot of effort has been put in the research for the right metal, alloy or catalyst [2, 3].

Our contribution to this field consists in the study of hydrogenation/dehydrogenation processes in (nanostructured) thin metallic films with the quartz crystal microbalance technique. The experimental setup and some recent results will be presented.

References:

[1] Schlapbach L, Züttel A, Nature, **414** (2001) 353.
[2] Grochala W, Edwards PP, Chem. Rev., **104** (2004) 1283.
[3] Orimo S, Nakamori Y, Eliseo JR, Züttel A, Jensen CM, Chem. Rev., **107** (2007) 4111.

Intermatrix synthesis of polymer-copper nanocomposites with predetermined parameters by using coproportionation reaction.

P.Ruiz[1,2], M. Muñoz[2], J. Macanás[3] and D.N. Muraviev[1]

[1] Grup de Sensors i Biosensors (GSB), Unitat de Química Analítica, Departament de Química, Universitat Autònoma de Barcelona, 08193 Bellaterra, Barcelona, Spain
[2] Grup de Tècniques de Separació (GTS), Unitat de Química Analítica, Departament de Química, Universitat Autònoma de Barcelona, 08193 Bellaterra, Barcelona, Spain
[3] Laboratoire de Génie Chimique, Université Paul Sabatier, CNRS UMR 5503, 118 Route de Narbonne, 31062 Toulouse Cedex 4, France
Patricia.Ruiz.Nicolas@uab.cat

Synthesis and characterization of metal nanoparticles (MNPs) is one of the hottest topics in Nanoscience and Nanotechnology. The physical and chemical properties of MNPs substantially differ from those of both bulk material and single atoms that can be in certain instances purposely used to improve the properties of MNP-containing materials. The main drawback, which still limits wide application of MNPs, is their insufficient stability due to the high trend to aggregation. Stabilization of MNPs during their growth allows for preventing their aggregation (e.g., by Oswalt Rippening mechanism) and allow for their dissolution/dispersion in some solvents. Stabilization of MNPs in polymeric matrices is one of the most promising ways to solve MNPs stability problem [1-3]. Electroanalytical applications of MNPs (e.g., in sensors and biosensors) are based in many instances on the use of noble metals due to their unique catalytic properties. The decrease of the noble metal loading without a change in the sensitivity of electroanalytical devices is one of the important problems, which still is unsolved. A possible solution in this case can be the use of core-shell MNPs composed by a cheap metal core (e.g., Cu) coated with a thin noble metal shell. In this context optimization of the synthesis of core-MNPs stage is of particular interest.

In this presentation we report the results obtained by the study of the intermatrix synthesis (IMS) of Cu-MNPs, which is based on the use of functional polymer (sulfonated polyetherether ketone, SPEEK, in our case) as a nanoreactor. The Cu-MNPs were synthesized by using either one or two sequential copper-loading-reduction cycles when varying copper concentration in the loading solution and the loading time. The second loading of SPEEK membrane with pre-formed Cu-MNPs has been shown to result in the copper coproportionation reaction [4] what allows for doubling the quantity of Cu-MNPs in the membrane. The characterization of Cu-MNPs and SPEEK-metal nanocomposite membranes was done by TEM and ICP-OES techniques.

The results obtained indicate that both the metal concentration and the time of second loading can be use as "tuning parameters" to optimize both the MNPs size and the number of nanoparticles in the membrane (N_{np}). The synthesis of Cu-MNPs is the first step in the synthesis of core-shell nanoparticles (e.g. Pt@Cu-MNPs), and optimization of this particular step can be used for the posterior optimization of core-shell MNPs.

References:

[1] D.N. Muraviev, Contrib. Sci. 3(1), 19 (2005).
[2] D.N. Muraviev, J. Macanas, M.J. Esplandiu, M. Farre, M. Muñoz, S. Alegret, Phys. Stat. Sol. (a) 204, 1686 (2007).
[3] J. Macanas, J. Parrondo, M. Muñoz, S. Alegret, F. Mijangos, D.N. Muraviev, Phys. Stat. Sol. (a) 204, 1699 (2007).
[4] D.N. Muraviev, J. Macanás, J. Parrondo, M. Muñoz, A. Alonso, S. Alegret, M.Ortueta, F.Mijangos, Reactive& Functional Polymers, 67, 1612 (2007)

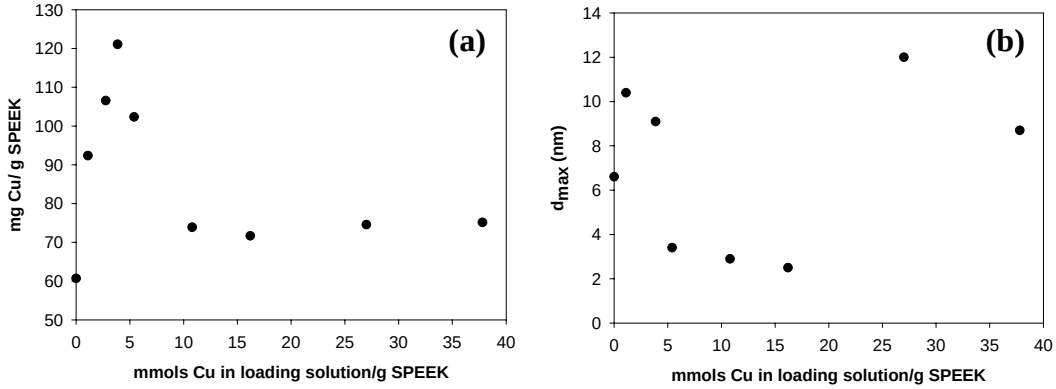

Figure 1: Copper content (a) and diameter of Cu-MNPs (b) in samples of Cu-SPEEK nanocomposite membranes after second loading with different copper concentrations.

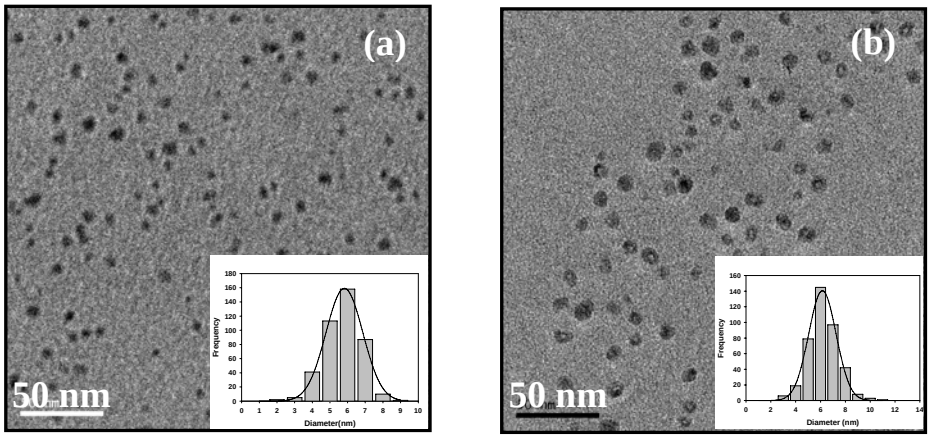

Figure 2: TEM images and corresponding size-distribution histograms (see inserts) of Cu-MNPs obtained after second loading with 4.5 (a) and 8.4 mmols Cu/g SPEEK (b), respectively.

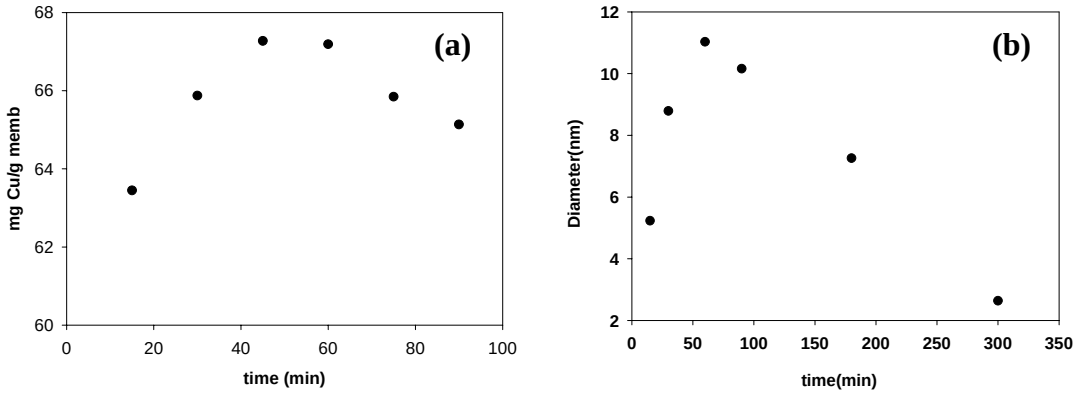

Figure 3: Copper content (a) and diameter of Cu-MNPs versus time of second metal loading at copper concentration in loading solution of 1.46 mmols Cu/g SPEEK.

Diffraction gratings embedded in bulk fused silica by laser ablation

Francisco Javier Salgado-Remacha, Isidoro Jimenez-Castillo,
Luis Miguel Sanchez-Brea, Eusebio Bernabeu
Universidad Complutense de Madrid, Applied Optics Complutense Group,
Facultad de Ciencias Físicas, Ciudad Universitaria s.n., 28040, Madrid, Spain
fjsalgado@fis.ucm.es

Diffraction gratings are one of the most used optical components [1], [2]. The gratings are normally amplitude or phase gratings [3], [4] although there exist some other possibilities such as polarization grating [5] or gratings formed by strips with different micro-topographic roughness [6]. In all this cases, the gratings are manufactured superficially, which can be problematic in some applications with dirty industrial environments.

In this work we develop a new kind of diffraction grating that is not engraved at the surface of the sample, but it is placed inside a bulk part of fused silica. Microtubes with a nano-size rough surface are formed (Fig. 1). We use a nanosecond Q-switched laser so that we can study, depending on the laser pulse width, not only the pure ablation regime, but also the thermal effects of radiation ([7], [8], [9]).

Moreover, we can study the differences between the gratings engraved in bulk and the gratings engraved in surfaces (front and rear), due the electronic process that appears in the ablation regime ([10], [11]), Fig. 2 and Fig. 3.

This kind of gratings can be employed in industrial environments since embedded gratings present several characteristics such as robustness, stability against surfaces flaws and easy cleaning process. Besides, the study of the diffraction due the nano-size roughness of the engraved cylinders is a quite new field of research in which meet two of the lasts advances of our group: the study of the diffraction by a cylinder with and without surface defects [12], [13], and the study of the effect of the roughness in a diffraction grating [14]. The theoretical analysis of this kind of diffraction gratings is not yet developed, according to our knowledge, Techniques based in statistical optics are required in order to analyze the optical behavior of this gratings. Therefore, we have experimentally analyzed the optical behaviour of this gratings, such as far field diffraction pattern and Talbot self-images (Fig. 4).

Salgado-Remacha is employed by the Universidad Complutense de Madrid, with the participation of the Ministerio de Educacion y Ciencia and the European Social Fund. This work has been supported by the DPI2005-02860 project of the Ministerio de Educación y Ciencia of Spain and the "Tecnologías avanzadas para los equipos y procesos de fabricación de 2015: e-eficiente, e-cológica, e-máquina" CENIT project of the Ministerio de Industria, Turismo y Comercio.

References:

[1] E.G. Loewen, E. Popov, Diffraction gratings and applications (Marcel Dekker, New York, 1997).
[2] C. Palmer, Diffraction Grating Handbook (Richardson Grating Laboratory, New York, 2000).

[3] M. Born, E. Wolf, Principles of Optics (Pergamon Press, Oxford, 1980).
[4] J.W. Goodman, Introduction to Fourier Optics (McGraw-Hill, New York, 1968).
[5] C.G. Someda "Far field of polarization gratings" Opt. Lett. 24 1657- 1659 (1999).
[6] L.M. Sanchez-Brea, F.J. Torcal-Milla, E. Bernabeu "Far field of gratings with rough strips" J. Opt. Soc. Am. A 25 828-833 (2008).
[7] M. D. Feit, A. M. Komashko, A. M. Rubenchik, Applied Physics A **79**, (2004) 1657-1661
[8] D. Ashkenasi, G. Müller, A. Rosenfeld, R. Stoian, I. V. Hertel, N. M. Bulgakova, E. E. B. Campbell, Appl. Phys. A **77** (2003) 223-228.
[9] R. Bernath, C. G. Brown, J. Aspiotis, M. Fisher, M. Richardson, Proc. Of SPIE **Vol. 6219**, (2006), 62190A
[10] S. Juodkazis, K. Nishimura, H. Misawa, Applied Surface Science, **253 (15)** (2007), 6539-6544
[11] Zhaoxin Wu, Hongbing Jiang, Quan Sun, Henchang Guo, Hong Yang, Qihuang Gong, J. Opt. A.: Pure Appl. Opt. **6,** (2004) 671-674
[12] L. M. Sanchez-Brea, Journal of the Optical Society of America A **21 (6),** (2004), 1102-1108
[13] L. M. Sanchez-Brea, Journal of the Optical Society of America A **22(7),** (2005), 1402-1407
[14] F. J. Torcal-Milla, L. M. Sanchez-Brea, E. Bernabeu, IEEE: 5th Topical Meeting on Optoelectronic Distance/Displacement Measurements and Application A, (2006) 171-175

Figures:

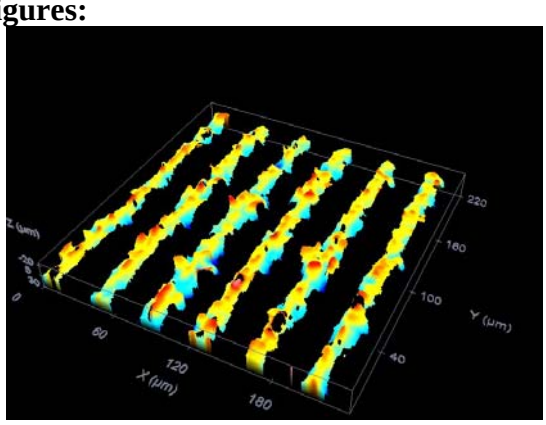

Fig. 1: Confocal image of an embedded diffraction grating with submicron roughness

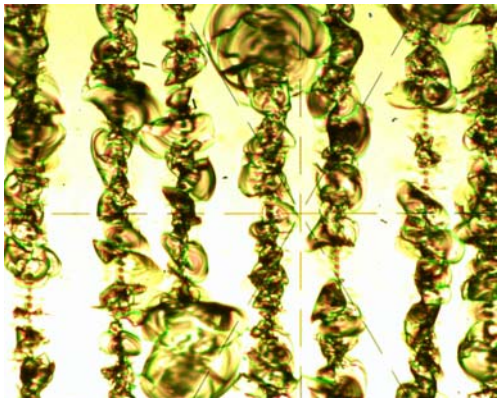

Fig. 2: Optical Microscopy Imaging of a diffraction grating engraved at the surface

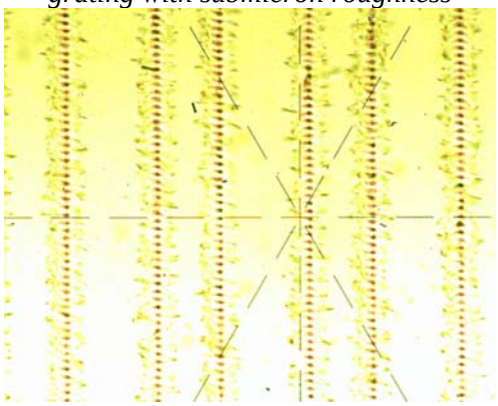

Fig. 3: Optical Microscopy Imaging of a diffraction grating engraved in bulk.

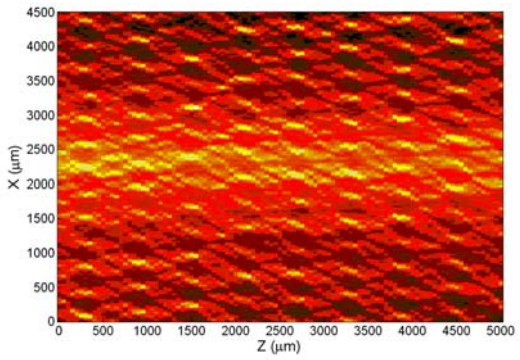

Fig. 4 : Talbot self-images of an embedded diffraction grating.

PHTHTALOCYANINE DERIVATIVES ON (111) NOBLE METAL SURFACES – MULTIPHASE BEHAVIOR AND CAPABILITY OF HOSTING OTHER MOLECULES

Tomas Samuely (a), Shi-Xia Liu (b), Nikolai Wintjes (a),Mihaela Enache (a), Marco Haas (b), Silvio Decurtins (b), Thomas A. Jung (c), Meike Stöhr (a)
(a) Institute of Physics, University of Basel, Klingelbergstrasse 82, 4056 Basel, Switzerland
(b) Department of Chemistry and Biochemistry, Freiestrasse 3, University of Bern, 3012-Bern, Switzerland
(c) Laboratory for Micro- and Nanostructures, Paul-Scherrer-Institute, 5232 Villigen, Switzerland
tomas.samuelyt@unibas.ch

Symmetrically substituted phthalocyanines (Pcs) with eight peripheral di-(tert-butyl)phenoxy (DTPO) groups[1] self-organize on (111) noble metal surfaces into various assembly structures (Fig. 1a). The rotational degrees of freedom allow all the DTPO substituents to be arranged above the plane of the Pc core, forming a bowl-like structure, which in turn enables the interaction of the Pc core with the metal substrate. The structural phases can coexist due to a significant retardation of the thermodynamic optimization of the conformations, caused by the proximity of the Pc core to the metal substrate together with the steric entanglement between neighbouring DTPO substituents.[2] Moreover, a substitution of a dipyrido[3,2-f:2',3'-h]quinoxaline (DPQ) in place of two adjacent DTPO groups results in an asymmetric structure of the Pc derivative.[1] Such a variation induces even more assembly structures by further expanding the plethora of conformational possibilities. (Fig. 1b)

The specific conformation with the DTPO groups arranged above the plane of the Pc core predetermines such assemblies to serve as hosts accommodating other guest molecules. This can be of great importance for the construction of possible future applications by the bottom-up approach. As an example, C_{60} molecules, upon deposition on the densest ordered layer of the symmetric Pc derivatives, bind to two clearly distinguishable sites (Fig. 2), exhibiting different morphologic and electronic properties. The electronic structure of the adsorbed C_{60} molecules, revealed by tunnelling spectroscopy investigations, are in good agreement with the proposed model of the adsorption and with the expected charge transfer in the Pc- C_{60} complex.

All measurements were carried out at various temperatures, with a scanning tunneling microscope housed in an ultra high vacuum system, consisting of different chambers for sample preparation and characterization.

References:

[1] Haas, M.; Liu, S. X.; Kahnt, A.; Leiggener, C.; Guldi, D. M.; Hauser, A.; Decurtins, S., **20** (2007) 7533.

[2] Samuely, T.; Liu, S. X.; Wintjes, N.; Haas, M.; Decurtins, S.; Jung, T. A.; Stohr, M., Journal of Physical Chemistry C, **15** (2008) 6139.

Figures:

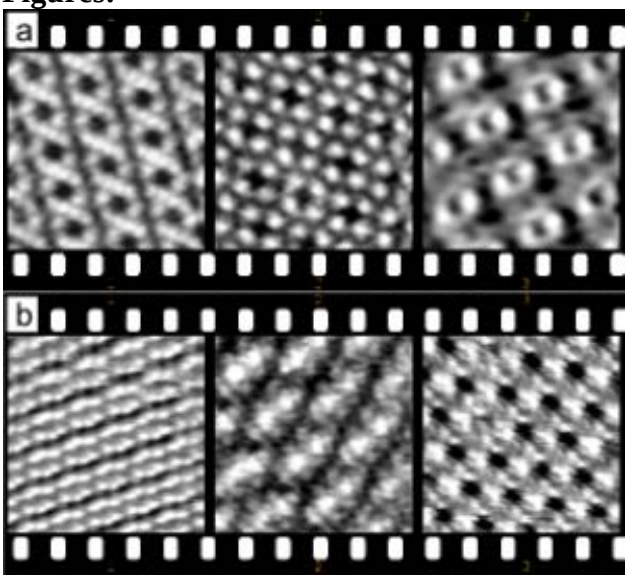

Figure 1 . STM images (10 x 10 nm^2) of Pc derivatives self-organized on (111) noble metal surfaces. a) Various assemblies of the symmetric DTPO-Pc b) Various assemblies of the asymmetric DTPO-DPQ-Pc

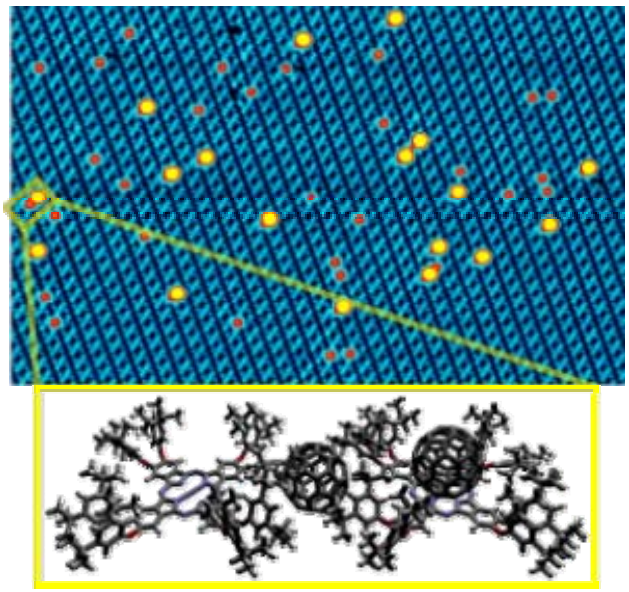

Figure 2. Top: STM image (80 x 50 nm^2) of C_{60} molecules adsorbed onto the densest ordered layer of the symmetric Pc derivatives. Bottom: 3D model of the molecules marked by the yellow rectangle in the STM image.

FRIEDEL OSCILLATIONS IN CARBON NANOTUBE QUANTUM DOTS

H.Santos[a] , *A. Ayuela*[b], *L. Chico*[a], *W. Jaskólski*[c] *and M. Pelc*[c]
[a]*Universidad de Castilla-La Mancha, 45071 Toledo, Spain*
[b]*Centro Mixto CSIC-UPV/EHU, 20080 Donostia, Spain*
[c]*Instytut Fizyki UMK, Grudziadzka 5, 87-100 Torun, Poland*
hernan.santos@uclm.es

Recently, important advances in the controlled synthesis of carbon nanotube intramolecular junctions during growth have been reported [1]. This may open the possibility to control the production of carbon nanotube quantum dots (QDs) and superlattices (SLs).

We have studied the interface states of all-metallic carbon nanotube quantum dots and superlattices using a tight-binding approach and a Green function matching technique. We have focused on systems made by connecting (n,n) and (2n,0) tubes, in which the interface states appear due to n pairs of pentagon/heptagon topological defects [2,3,4]. The M(2n,0) quantum dots are formed by sandwiching M unit cells of (2n,0) tube between two semi-infinite (n,n) leads, whereas the N(n,n) dots consist of N unit cells of the (n,n) tube between two (2n,0) leads. The superlattices are made by a periodic sequence of N(n,n) and M(2n,0) tubes.

When the armchair length N is increased in both, QD and SL, the energy of the interface states oscillates with N. However, when the size of the zigzag part M is increased, the energy of interface states shows a monotonic behavior with M. We attribute this effect to a Friedel-like oscillation. We have successfully fitted the interface energies to the expression

$$f(d) \propto \frac{\sin(2k_F(d+\delta_0))}{d^{\alpha}} \quad , \qquad (1)$$

where d is the length of QD, δ_0 is the surface shift, and α is the exponent decay. All the cases studied have an unusual decay (>1). For zigzag NTs, $k_F = 0$, so the dependence is monotonic (Fig. 1), and for armchair tubes, with nonzero k_F, oscillations appear (Fig. 2).
In order to see this oscillating behavior more clearly, we have plotted and fitted the second derivative of the energy with respect to the system size, as shown in Fig. 3 [5].

The reported oscillatory changes of the separation energy between the interface states should be seen in optical experiments. We also expect this interaction to be important for the understanding of other physical processes, such as selective dot growth and magnetic interaction of transition metal contacts through carbon nanotubes.

References:

[1] Y. Yao, Q. Li, J. Zhang, R. Liu, L. Jiao, Y. T. Zhu, and Z. Liu, Nature Mater. **6**, (2007) 283.
[2] L. Chico and W. Jaskólski, Phys. Rev. B **69**, (2004) 085406.
[3] W. Jaskólski, L. Chico, Phys. Rev. B **71**, (2005) 155305.
[4] A. Ayuela, L. Chico, and W Jaskólski, Phys. Rev. B **77**, (2008) 085435.
[5] A. Ayuela, W. Jaskólski, M. Pelc, H. Santos, and L. Chico 'Friedel Oscillations in Carbon nanotube Quantum Dots, (submitted 2008).

Figures:

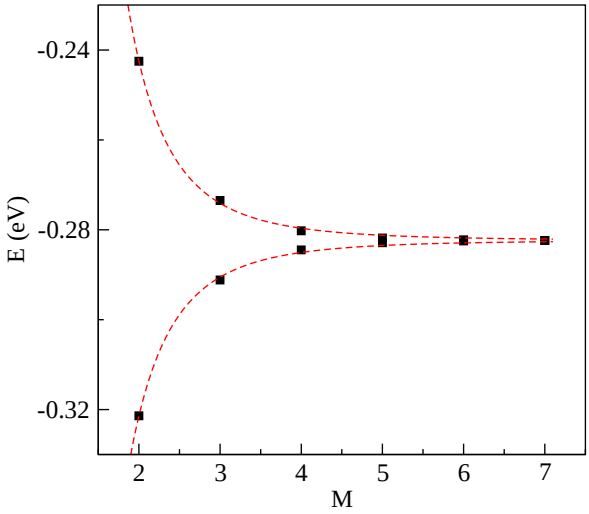

Fig. 1. Interface states energies for the M(18,0) quantum dot vs dot size M corresponding to the series which converges to E = -0.2824 eV. The dashed line shows the fits to $\propto 1/d^{\alpha}$.

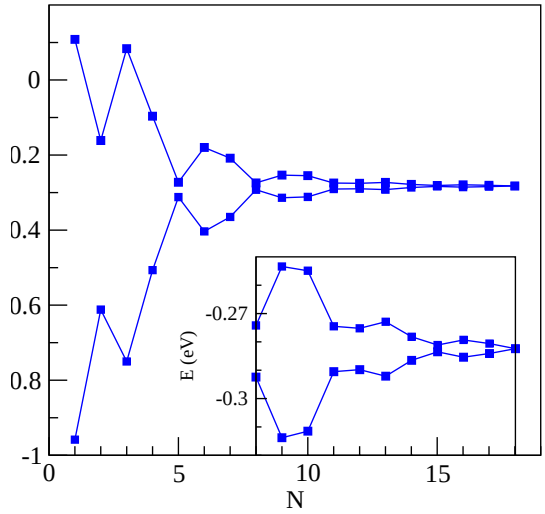

Fig. 2. Interface states energies for the N(9,9) quantum dot as a function of dot size N corresponding to the series which converging to E = -0.2824 eV. Lower inset: zoom in the region of large N.

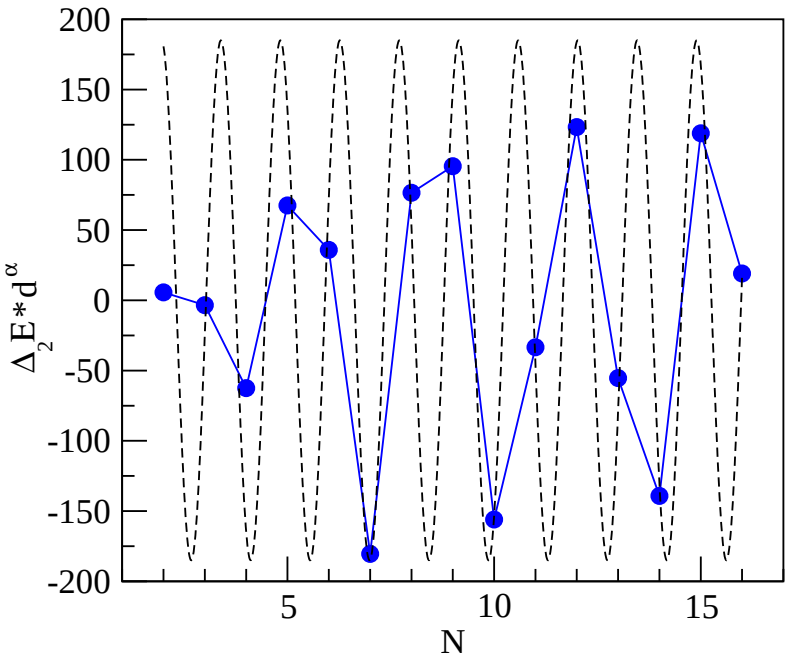

Fig 3. Second derivative of the lowest interface state energy series (shown in Fig. 2) with respect to the system size N. The dashed line is the fit to the function given by Eq. (1).

ELECTROCHEMICAL SYNTHESIS AND CHARACTERIZATIONS OF VERSATILE NANOWIRES

Sirilak Sattayasamitsathit[a,b,d], *Panote Thavarungkul*[a,c], *Joseph Wang*[d*], *Jared Burdick*[d], *Rawiwan Laocharoensuk*[d], *Andrea Bulbarello*[e,d] *and Proespichaya Kanatharana*[a,b*]

[a]*Trace Analysis and Biosensor Research Center,* [b]*Department of Chemistry,* [c]*Department of Physics Faculty of Science, Prince of Songkha University, Hat Yai, Songkhla, 90112 Thailand*

[d]*Biochemistry and Biodesign Institute, Arizona State University, Tempe, Arizona, 85287 USA*

[e]*Department of Food Science and Technology, Universita'degli di Milano, Milano, 20133 Italy*

joseph.wang@asu.edu and proespichaya.K@psu.ac.th

Introduction and objective

Multisegment nanowires are interested because of their potential applications, e.g. chemical sensor, catalyst, products identification and biotechnology. However, the preparation process is time-consuming involving multiple plating steps from different metal solutions. This work proposed the use of single plating solution for single- and multi-segment alloy nanowires. In addition step-like porous gold nanowires were also prepared from etching electro-active component of multi-segment alloy nanowires. These nanowires showed the ability to be applied for product tracking. Composite material of step-like porous gold and polymer was also synthesized leading to attractive material for nano-hardware.

Methods

Alloy nanowires were prepared using template-assisted electrodeposition technique of the metal-mixture plating solution. Mixture of cobalt (Co), nickel (Ni) and copper (Cu) was used for single-segment nanowires by applying a constant deposition potential at -1.4 V and changing metal concentration to synthesize alloy nanowires of various compositions. Silver (Ag) and gold (Au) were used for multi-segment and step-like porous gold nanowires. By changing deposition potential between -0.5 to -1.2 V various compositions of Au/Ag in each segment can be achieved. For step-like porous gold nanowires the deposition potential was varied from -0.9 to -1.1 V followed by the dealloying of silver composition via acid etching to obtain porous structure. Finally, for all nanowires preparation, the template was dissolved to obtain free standing nanowires. Composition profile of single-segment alloy nanowire, qualitatively and quantitatively, was detected by X-ray fluorescence (XRF) whereas optical reflectivity was used to qualify the multi-segment alloy nanowires. These can be interpreted to be coding pattern. Energy dispersive X-ray fluorescence (EDX) was used to study the % atom of gold and silver at different deposition potential for multi-segment and porous gold nanowires. Scanning electron microscope (SEM) was used to study the pore distribution, the diameter of porous gold at different composition of gold/silver and the characteristic of all nanowires.

Results

In single-segment alloy nanowires, different concentrations of Co, Ni and Cu in the plating solution provided different distinguishable XRF signatures corresponding to the metal concentrations. In case of multi-segment alloy nanowires, tuning the deposition potential from -0.5 to -1.2 V provided different Au-Ag compositions resulting in different light reflectivity. From EDX study silver decreased from 92 to 53% in the studied range. The reflectivity of multi-segment alloy nanowires can be distinguished up to 5 intensity levels. Thus, various encoding patterns can be generated for product tracking. For the step-like porous gold nanowires, applying different deposition potential from -0.9 to -1.1 V changed the composition of Au-Ag from 15% atom of gold (-0.9 V) to 85% (-1.1 V). Different diameters were obtained at different % atom of gold. The normalized diameter of step-like porous gold was calculated with respect to solid gold segment and ranged from 65.0 to 88.7%. Nanowires containing composite material between porous gold and polypyrole were also synthesized. The SEM images in Figure 1 presented the single- (A) and multi- segment (B) alloy nanowires, the step-like porous gold (C) and step-like porous gold/polymer composite nanowires (D). These micrographs illustrated the ability to tailor the composition and shape of the nanowires for bar-codes application and nano-devices.

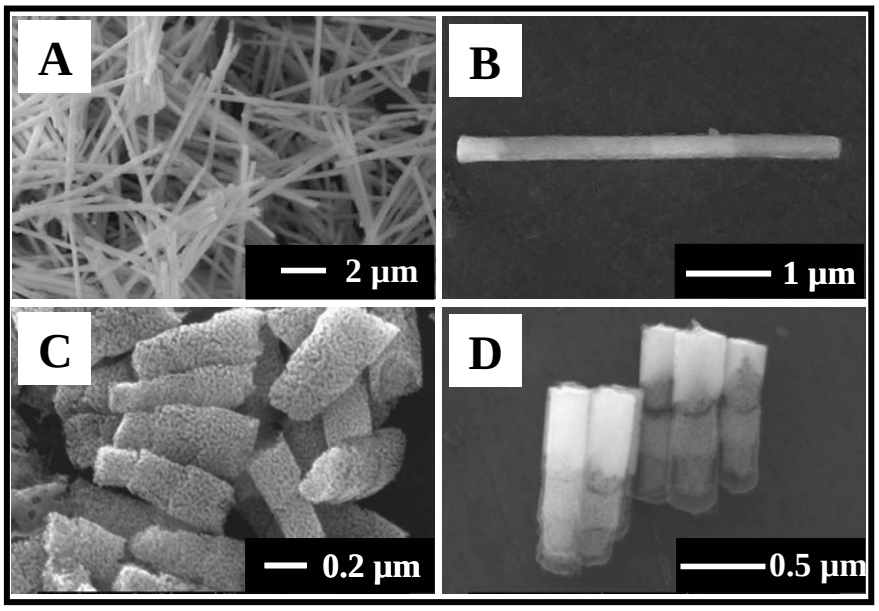

Figure 1 SEM images of nanowires prepared from single plating solution (A) single segment alloy nanowires (B) multisegment alloy nanowires (C) step-like porous gold nanowires (D) step-like porous gold/polymer composite nanowires

Conclusions

The template-assisted electrochemical technique with a single plating solution was successfully developed for single- and multi-segment alloy nanowires barcodes and step-like porous gold nanowire. XRF and optical reflectance are effective readout techniques of alloy nanowires. SEM illustrated the step-like porous gold and also composite material. These versatile composition- and shape- tailored concept can be extended to nanowires which have diverse properties based on different metals and also composite material. These production can be used for a wide range of application *i.e.,* product tagging and nano-devices.

Keywords: Alloy nanowire barcodes, Step-like porous gold, Composite Au/PPy, Electrodeposition

Selected References:

1. Ji C, Searson PC. J Phys Chem B 107 (2003) 4494-4499.
2. Keating, C.D. and Natan, M.J. Adv. Mater. 15 (2003) 451-454.
3. Wang, J. and Liu, G. Anal. Chem. 78 (2006) 2461-2464.

CVD ROUTES TO CARBON NANOTUBE SYSTEMS WITH HIGHLY ANISOTROPIC NANOMAGNETS

F. Schäffel, *C. Schünemann, Ch. Täschner, M. H. Rümmeli, A. Gebert, D. Pohl, C. Kramberger, A. Leonhardt, B. Rellinghaus, B. Büchner, L. Schultz*

IFW Dresden, P.O. Box 270116, D-01171 Dresden, Germany
f.schaeffel@ifw-dresden.de

The preparation of nanoparticles in the gas phase through inert gas condensation is a very versatile method to fabricate catalyst particles that act as catalytic templates for carbon nanotube (CNT) synthesis since the method allows for easy control of the catalysts' elemental composition and their morphology. Chemical vapour deposition (CVD) as a synthesis route for CNT is by far the most popular synthesis mode to its potential for up-scaling. Various CVD systems exist and two of the more popular are thermal CVD [1,2] and plasma enhanced CVD [3,4].

In this contribution we report on the synthesis of carbon nanotubes via two distinct chemical vapour deposition routes, thermal and plasma enhanced chemical vapour deposition, using such gas phase prepared elemental Fe catalyst particles as well as binary FePt nanoparticles. The gas phase preparation of nanoparticles is very versatile when it comes to the preparation of predefined nanoparticles. The particle material is simply changed through variation of the sputtering target thus enabling to synthesize not only elemental particles, but also alloy particles such as the binary FePt particles shown in this contribution. This alloy, which has so far rarely been used for CNT synthesis, was applied to a thermally activated CVD process. Homogenous and clean CNT were grown. Further gas phase prepared elemental FePt particles were also applied to a plasma-enhanced CVD process. Here CNT with a bamboo-like structure and a conical particle at each tip were grown.

Although FePt is rarely used as a binary catalyst it is of great interest due to the special character of the chemically ordered $L1_0$ phase of FePt. The super structure reflex (001) of the FePt-$L1_0$ phase exhibits a very high magnetic anisotropy. This makes such FePt nanoparticles interesting in terms of their potential for storage media. The combination of such nano-magnets with carbon nanotubes also open up exciting possibilities. For example, the tailored growth of CNT with a hard magnetic particle at their tip is very promising for the realization of functional devices, for example magnetically actuated nanoelectronic systems. Hence, we conducted systematic studies on the synthesis of CNT via FePt catalysts using both thermal and plasma CVD routes to explore their potential in the controlled synthesis of carbon nanotube systems with highly anisotropic nanomagnets. The studies not only exploit the potential for CVD for the single step synthesis of CNT-nanomagnet systems but also open up the opportunity to gain deeper understanding of CNT growth mechanisms.This is important if CNT are to fulfil their promise in CNT based molecular electronics. While efforts are undertaken to reach this goal, optimised device architectures are still emerging and the basic understanding of the physics of CNT-FETs is steadily expanding. However, one of the key weaknesses is the lack of understanding of CNT growth, particularly via supported catalyst routes, which are anticipated to provide easier access for CNT based molecular electronics into current microelectronics systems.

Our systematic studies provide deeper insight into the growth mechanisms at play within thermal and plasma CVD and show new and interesting in roles of the catalyst particles. In thermal CVD we show the supported catalyst is key to nucleate the growth of CNT, however continued growth takes place from the oxide support [5]. In plasma CVD we show the so called "tip-growth" mode dominates and is suited to the formation of chemically ordered $L1_0$ phase of FePt.

References:

[1] W. Z. Li, S. S. Xie, L. X. Qian, B. H. Chang, B. S. Zou, W. Y. Zhou, R. A. Zhao, and G. Wang, *Science* **274**, 1701 (1996).
[2] F. Schäffel, C. Kramberger, M. H. Rümmeli, R. Kaltofen, D. Grimm, A. Grüneis, E. Mohn, T. Gemming, T. Pichler, B. Büchner, B. Rellinghaus, L. Schultz, *phys. stat. sol. (a)* (2007), DOI 10.1002/pssa.200675339; F. Schäffel, C. Kramberger, M. H. Rümmeli, D. Grimm, E. Mohn, T. Gemming, T. Pichler, B. Rellinghaus, B. Büchner, L. Schultz, *Chem. Mater* **19**, 5006 (2007).
[3] H. Murakami, M. Hirakawa, C. Tanaka, and H. Yamakawa, *Appl. Phys. Lett*. **76**, 1776 (2000).
[4] Z. F. Ren, Z. P. Huang, J. W. Xu, J. H. Wang, P. Bush, M.P. Siegal, and P. N. Provencio, *Science* 282, 1105 (1995).
[5] M. H. Rümmeli, F. Schäffel, C. Kramberger, T. Gemming, A. Bachmatiuk, R. J. Kalenczuk, B. Rellinghaus, B. Büchner, and T. Pichler, *J. Am. Chem. Soc*. **129**, 15772 (2007).

Figures:

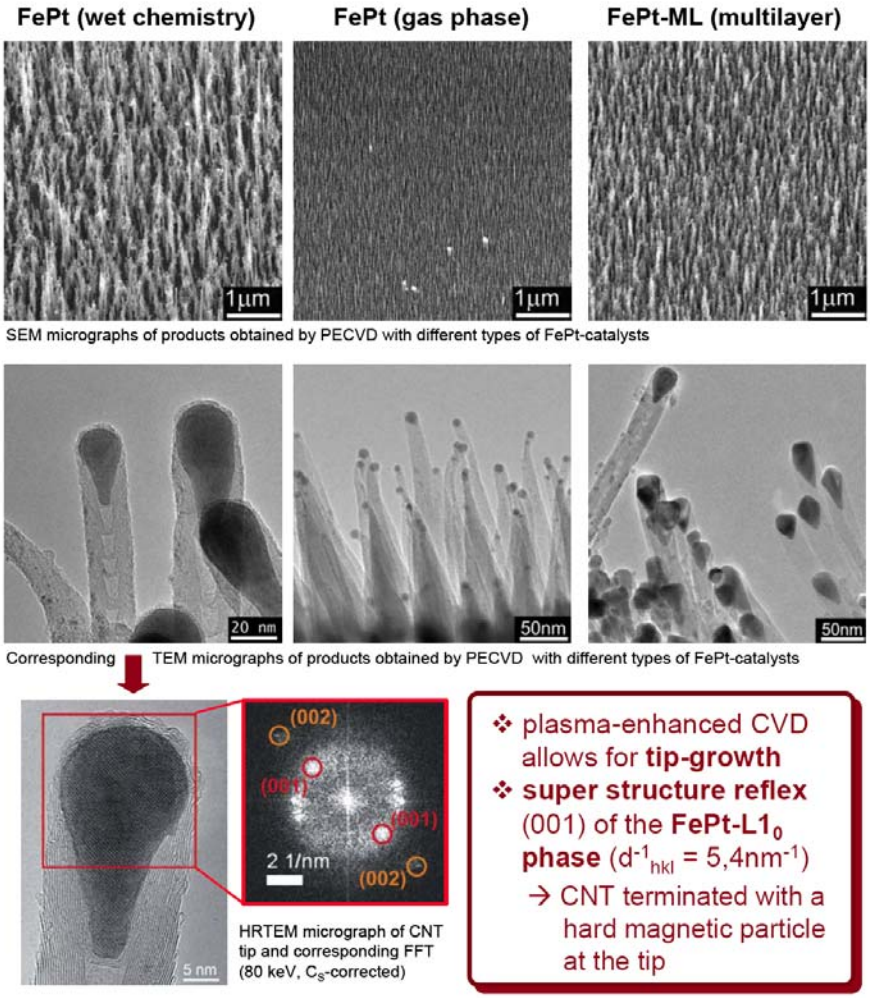

TEMPERATURE AND VOLTAGE TMR DEPENDENCIES FOR HIGH PERFORMANCE MAGNETIC JUNCTIONS

H. Silva[1,2], *Y. Pogorelov*[1]
[1]*IFIMUP-IN, Universidade do Porto, Porto 4169-007, Portugal* [2]*CEOT, Universidade do Algarve, Faro 8005-139, Portugal*
huggsil@gmail.com

Recent spintronics magnetic junctions with ultra-thin MgO barriers attained as high tunnel magnetoresistance (TMR) as ~600% [1] at room temperature which makes them ideal for non-volatile high-density memories. Amazingly, TMR even reached ~1200% at low temperatures, but it can be also sensibly degraded with voltage [2], hence a detailed study of its temperature and voltage dependencies is fundamental for future device applications.

For nano-size junctions, a fully quantum description is required to take a proper account of specific coherency effects. The commonly used Green's functions in the Kubo formula framework [3] are not easy enough to include the electrical field (E) effect in an analytic way [4]. Here a tight-binding dynamics [5] is generalized to describe this effect on the spin-dependent quantum transmission for magnetic junctions with ultrathin non-magnetic spacers. Starting from the n-site atomic chain with on-site energies ε_0, locally shifted under E, and nearest-neighbour hopping amplitudes t, we write down the Hamiltonian in terms of local Fermi operators $\hat{c}_i$ and $\hat{c}_i^{\dagger}$ as:

$$H = \sum_{i=1}^{n}(\varepsilon_0 - iE)\hat{c}_i^{\dagger}\hat{c}_i + t\sum_{i=1}^{n-1}\left(\hat{c}_i^{\dagger}\hat{c}_{i+1} + \hat{c}_{i+1}^{\dagger}\hat{c}_i\right), \quad (1)$$

and obtain the local (non-normalized) amplitudes for the eigen-state with energy ε as:

$$p_i(x) = \xi^i \sum_{j=0}^{[i/2]} C_j^{i-j}(-\xi^2)^{-j}(j + x/\xi)_{i-2j}, \quad (2)$$

where $x = (\varepsilon - \varepsilon_0)/t$, $\xi = E/t$, C_m^n is the binomial coefficient, $[u]$ is the entire part of u, and $(u)_n = u(u + 1)\ldots(u + n - 1)$ is the Pochhammer symbol. Next this finite chain (called the gate, g) is attached to semi-infinite chains (source, s, and drain, d), with respective on-site energies ε_s, ε_d and hopping parameters (see Fig. 1, supposing that the electrical voltage drop between the sites in s, d elements is negligible), to generate a collective electronic state with energy ε. This defines the 1D transmission coefficient (spin-dependent through the Stoner shifts in ε_s, ε_d) for given electrical field as $T(\varepsilon) = -2i(t_{sg}t_d|\gamma_s|\sin q_s)/(t_s t_{gd} D)$ where the characteristic denominator:

$$D = \varphi\left[p_n(x_g) - p_{n-1}(x_g + \xi)\gamma_s\right] - p_{n-1}(x_g)\gamma_d + p_{n-2}(x_g + \xi)\gamma_s\gamma_d, \quad (3)$$

with $q_i = \arccos[(\varepsilon - \varepsilon_i)/2t_i]$, $\varphi = 1 + (n+1)\xi e^{iq_d}$, $\gamma_i = e^{iq_i} t_{gi}^2/(t_g t_i)$ for $i = s$, d and $x_g = (\varepsilon - \varepsilon_g)/t_g$, allows for up to n resonance spikes in the Landauer conductance formula. Its 3D generalized and temperature dependent form reads as

$$G = (e^2/h) \sum_{\boldsymbol{k}} f_s(\boldsymbol{k})[1 - f_d(\boldsymbol{k})]|T(\boldsymbol{k})|^2,$$

with the Fermi function $f_i(\boldsymbol{k}) = \{\exp[\beta(\varepsilon_i(\boldsymbol{k}) - \mu_i)] + 1\}^{-1}$ for a dispersion law $\varepsilon_i(\boldsymbol{k})$, chemical potential μ_i ($i = s,d$) and inverse temperature β. The calculated behaviour for a characteristic choice of model parameters (Fig. 2) shows an intriguing possibility of further enhancement of TMR efficiency by a proper choice of applied voltage on the quantum coherent device, as an alternative/addition to the previously suggested adjustment of its elemental composition [5]. Moreover, this voltage effect proves to be temperature stable, permitting to compensate the common temperature degradation of TMR.

References:

[1] S. Ikeda, J. Hayakawa, Y. Lee, K. Miura, H. Hasegawa, F. Matsukura, H. Ohno, "Intermag Europe 2008"
[2] S. Yuasa, A. Fukushima, H. Kubota, Y. Suzuki, K. Ando, Appl. Phys. Lett 89, 042505 (2006).
[3] J. Mathon, M. Villeret, H. Itoh, Phys. Rev. B **52**, R6983 (2005).
[4] C. Heiliger, P. Zahan, B. Yavorsky and I. Mertig, Phys. Rev. B **72**, 180406(R) (2005).
[5] H. G. Silva and Yu. G. Pogorelov, arXiv:0802.1436v1 [cond-mat.mtrl-sci].

Figures:

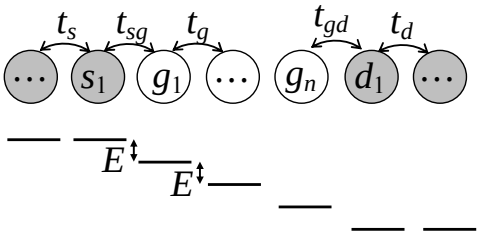

Fig.1 – On-site amplitudes, hopping parameters, and spatial distribution of electrical voltage in the composite chain system.

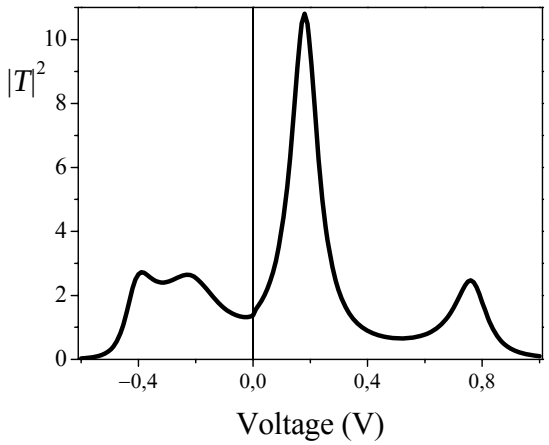

Fig.2 – 1D transmission coefficient $|T|^2$ (at zero temperature) of the composite chain system with parameters $\varepsilon_s = -0.5$eV, $\varepsilon_d = -1.0$ eV, $\varepsilon_g = 0.2$ eV (ε_F=0), $t_s = t_d = 0.5$ eV, $t_g = t_{sg} = t_{gd} = 0.25$ eV and $N_g = 4$ (number of planes) in function of the bias voltage.

NANOPARTICLE CONSTRUCTS OF METALLIC AND CORE-SHELL NANOPARTICLES BASED ON DNA-HYBRIDIZATION

Andrea Steinbrück[1], *Andrea Csaki*[1], *Kathrin Ritter*[2], *Martin Leich*[2], *Michael Wartbüchler*[1], *J. Michael Köhler*[2], *Wolfgang Fritzsche*[1]

1 Institute of Photonic Technology; Nanobiophotonics Department; PO Box 100 239; D-07702 Jena

2 Technical University Ilmenau; Institute for Micro and Nanotechnology, Department of Physical Chemistry and Microreaction Technology; PO Box 100 565; D-98684 Ilmenau

andrea.steinbrueck@ipht-jena.de

Nanoparticles represent versatile building blocks for nanotechnology and material science. Therefore, the defined assembly of nanostructures is of significant importance. Short DNA sequences bound to the nanoparticles' surface enable highly specific DNA hybridization-driven events that direct the formation of nanoparticle constructs. The well-established system based on thiolated DNA was thereby complemented with amino-functionalized DNA.
Examples for the defined formation of gold and gold/silver nanoparticle constructs are demonstrated. Further, gold-silver core-shell nanoparticles are introduced as further building blocks for the hybridization-controlled formation of nanoparticle constructs. The resulting plasmonic properties of the particles are studied using ensemble as well as single particle spectroscopic characterization, even during the process of metal shell growth. The optical properties are determined by the outermost layer when a certain shell thickness is reached. In addition, the formation of constructs of gold and silica nanoparticles is demonstrated including core-shell structures of gold and silica.
The results demonstrate the potential of the combination of different particle sizes, compositions as well as coupling chemistry in order to realize controlled nanoparticle constructs.

References:

[1] A. Steinbrück, A. Csaki, G. Festag, W. Fritzsche, Plasmonics, **1** (2006) 79-85.
[2] A. Steinbrück, A. Csaki, K. Ritter, M. Leich, J. M. Köhler, W. Fritzsche, J Nanoparticle Research (2008) in press.
[3] A. Steinbrück, A. Csaki, K. Ritter, M. Leich, J. M. Köhler, W. Fritzsche, J Biophotonics **1** (2008) 104-113.

EPITAXIAL p & n ZnO THIN FILMS GROWN BY PULSED LASER DEPOSITION

C. S. Steplecaru[1], M. S. Martín-González[1], D. Alegre[1], I. Lorite[2], J. F. Fernández[2], J. L. Costa-Krämer[1]

1. *Instituto de Microelectrónica de Madrid, CSIC, c/Isaac Newton 8, 28760 Tres Cantos, Madrid, Spain*
2. *Instituto de Cerámica y Vidrio, CSIC, c/Kelsen 5, 28049 Madrid, Spain*

Contact E-mail: kramer@imm.cnm.csic.es

Although diluted magnetic semiconductors (DMSs) and carrier induced ferromagnetism are attracting considerable attention because of the possibility of incorporating magnetic degrees of freedom in traditional semiconductor materials[1] the origin of magnetism in oxide mixtures is still not clear, and a clear relationship between doping and the exchange interaction is still lacking.

Since the recent theoretical prediction by Dietl *et al.*[2] of Curie temperatures above room temperature (RT FM) in ZnO and GaN containing 5% of Mn, several experimental studies have reported ferromagnetic like behaviour in these compounds[3]. Several theories exist about the mechanism responsible for ferromagnetism. In order to clarify if magnetism is due to doping, to an interfacial phenomenon, or to a surface reduction of the Co_3O_4 due to the presence of zinc oxide, epitaxial ZnO thin film and ZnO-Co_3O_4 multilayers have been grown by pulse laser deposition (PLD) and characterized structurally, electrically and optically.

While previous work of our group has been obtained polycrystalline ZnO thin films[4], recently we have obtained epitaxial ZnO films on (0001) Al_2O_3 substrates at a relatively low temperatures (300-600ºC). These films are used to correlate transport and optical properties in the absence of grain boundary effects. Results are also shown for ZnO/Co_3O_4[5,6] multilayers and compared with the properties of individual ZnO and Co_3O_4 layers.

References:

[1] Ohno, H., *Science* 1998, **281**, 951-956.

[2] Dietl, T., Ohno, H., Matsukura, F., Cibert, J., Ferrand, D., *Science* 2003, **287**, 1019-1022.

[3] García, M. A., Ruiz-Gonzalez, M. L., Quesada, A., Costa-Krämer, J. L., Fernández, J. F., Khatib, S. J., Wennberg, A., Caballero, A. C., Martin-Gonzalez, M. S., Villegas, M., Briones, F., Gonzalez-Calbet, J. M., Hernando, A., *Phys. Rev. Lett.* 2005, **94**, 217206 and references within.

[4]E. Lopez-Ponce, J.L. Costa-Krämer, M.S. Martín-González**,** F. Briones, J.F. Fernandez, A.C. Caballero and M. Villegas, *Physica Status Solidi* (a) 2006, 203, 1383–1389

[5]M. S. Martín-González, J. F. Fernández, F. Rubio-Marcos, I. Lorite, J. L. Costa-Krämer, A. Quesada, M.A. Bañares, J. L. G. Fierro., *J. Appl. Phys.* 2008,

[6]E. López-Ponce, A. Wennberg, M. S. Martín-González, J. L. Costa-Kramer, F. Briones, M. García, A. Quesada, A. Hernando, J. F. Fernández, A.C. Caballero, M. Villegas, S. J. Khatib, M. A. Bañares, J. L. García –Fierro, *Jpn. J. Appl. Phys*. 2006, 45, 7667-7671

[7]A. Quesada, M.A. García, M. Andrés, A. Hernando, J.F. Fernández, A.C. Caballero, M.S. Martín-González and F. Briones, *J. Appl. Phys*., 2006, 100, 113909 (1-4)

CONTROLLED CHARGE TRANSPORT MEASUREMENTS THROUGH SHORT DSDNA USING CONDUCTIVE AFM

Lev Tal-Or, Maya Gottlieb, Daniela Ullien and Danny Porath
Physical Chemistry Department, The Hebrew University of Jerusalem, Israel.
lev.tal-or@mail.huji.ac.il

Complementary, single-strands of DNA (ssDNA), one bound to an ultra flat gold electrode and the other to a gold nanoparticle (GNP) were hybridized on the surface to form a double stranded (ds)DNA bridge between the two gold electrodes. The adsorption of a ssDNA monolayer at each gold interface eliminates non-specific interactions of the dsDNA with the surface, allowing bridge formation only upon hybridization. The technique used, in addition to providing a good electrical contact, offers topographical contrast between the GNP and the non-hybridized surface and enables accurate location of the bridge for the electrical measurements[1].

Electrical measurements, as well as topography images, were performed using conductive Atomic Force Microscope system (C-AFM). Generally**,** the tip is approached to the nanoparticle and then current-voltage (IV) measurement is performed. Previously, we reported currents of up to 220 nA flowing through the dsDNA at a bias voltage of 2 V, while the surrounding ssDNA monolayer was found to be insulating at a bias voltages up to 2.5V and even at 4 V.[2,3,4]

In the present work we report the results of additional and highly controlled measurements of the same system. We have developed the experimental measurement method, using special codes that were incorporated with the measurements system to enable full control over the measurement parameters. This control allows following and verifying all the measurement parameters at all measurement stages. In particular the codes we developed enable us to monitor the tip deflection and the current simultaneously at all the measurement stages and to perform measurements with a wide range of action sequences and parameters, e.g., times and repetitions.

Here we report the results of two measurement methods. In the first method (Method I) we form a contact between the AFM tip and the GNP, and then measure I-V every 0.5 nm of withdrawal while monitoring the deflection. In the second method (Method II) we form a contact between the AFM tip and the GNP, and then ramp the bias and withdraw the tip at fixed bias voltage while monitoring the current and deflection. Using Method I we show that significant currents flows through the dsDNA when the GNP is raised 2-3 nm above the ssDNA monolayer while the monolayer itself is insulating. Using Method II we show that almost no current is measured up to a bias of ~2 V, while at a bias of 2-2.5 V the current first rises and then falls upon withdrawal of the tip from the surface. Both methods show that the current peaks when raising the GNP to 2-3 nm above the ssDNA monolayer (possibly improving the dsDNA configuration).

In conclusion, we reconfirm, in a controlled way, that short dsDNA is able to transport electrical charge, while the ssDNA monolayer is insulating at bias voltages of up to 2.5V. Additionally, we find that the GNP raising has an effect on the conductivity, and the conductance peaks at a ramp of 2-3 nm. We believe that these measurement methods will enable us to get further important information on the electrical properties of dsDNA and on the relation between the measured current and the mechanical properties of the DNA.

References:

[1] Nogues C., Cohen S.R., Daube S.S. & Naaman R., Phys.Chem.Chem.Phys. 6, ***Electrical properties of short DNA oligomers characterized by conducting atomic force microscopy*** (2004) 4459–4466

[2] Cohen H., Nogues C., Naaman R., Porath D., Proc. Nat. Acad. Sci. USA 102, ***Direct measurement of electrical transport through single DNA molecules of complex sequence*** (2005) 11589.

[3] Cohen H., Nogues C., Ullien D., Daube S., Naaman R., Porath D., Faraday Discussions 131, ***Electrical characterization of self-assembled single- and double-stranded DNA monolayers using conductive AFM*** (2006) 367

[4] Ullien D., Cohen H., Porath D., Nanotechnology 18, ***The effect of the number of parallel DNA molecules on electric charge transport through 'standing DNA'*** (2007) 424015

Figures:

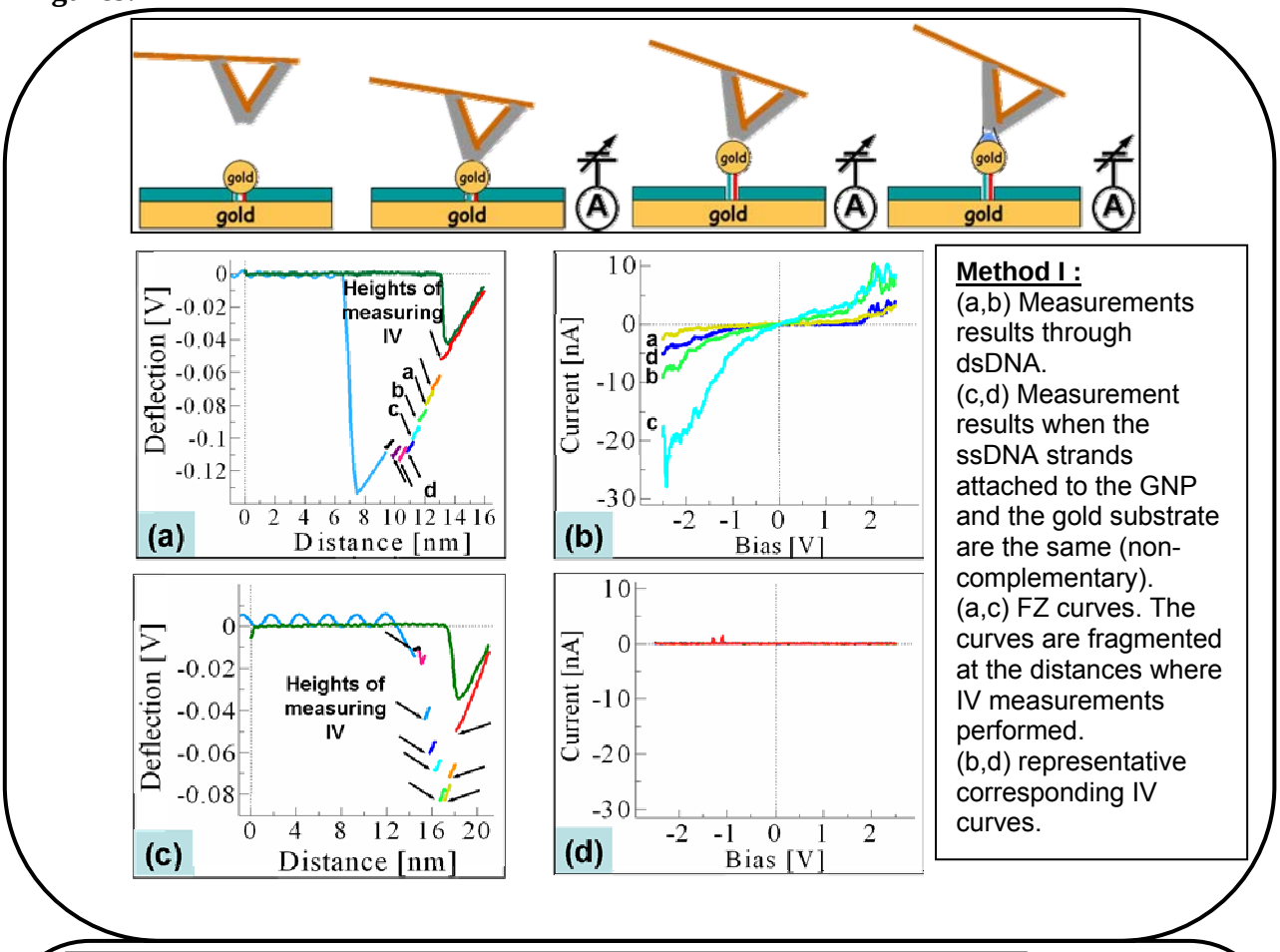

Method I :
(a,b) Measurements results through dsDNA.
(c,d) Measurement results when the ssDNA strands attached to the GNP and the gold substrate are the same (non-complementary).
(a,c) FZ curves. The curves are fragmented at the distances where IV measurements performed.
(b,d) representative corresponding IV curves.

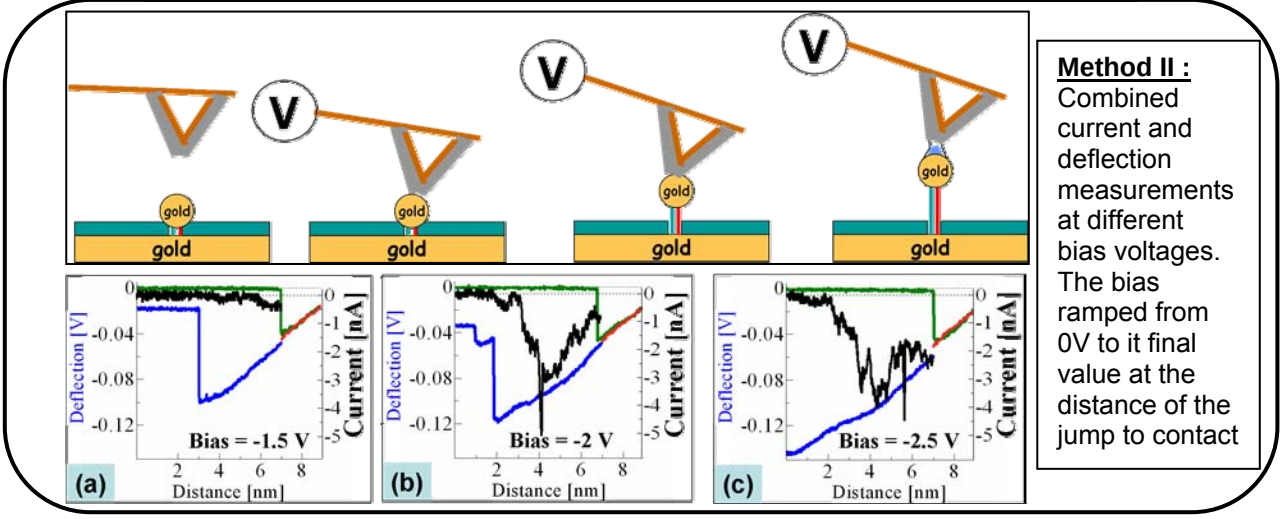

Method II :
Combined current and deflection measurements at different bias voltages. The bias ramped from 0V to it final value at the distance of the jump to contact

ENZYME-ASSISTED ATTACHMENT OF GOLD NANOPARTICLES ONTO PATTERNED ORGANIC SURFACES

N. Y.-W. Tang and A. Badia
FQNRT Center for Self-Assembled Chemical Structures and Department of Chemistry, University of Montreal, Montreal, Qc, H3T 1J4
nathalie.tang@umontreal.ca

The current fascination with nanoscale materials and surface patterns is due to the novel physico-chemical properties that these can exhibit. Integrating nanoscale features into organic and hybrid organic/inorganic thin films are vital for applications in the areas of nano-microelectronics, optoelectronics, nano-microfluidics, biosensing and biomaterials. Conventional serial approaches in nanofabrication include electron-beam lithography and scanning probe lithography, which are both very expensive and tedious. Hence, novel parallel methods that are compatible with organic materials must be developed.

In this poster, the spatially-directed attachment of gold nanoparticles (NPs) by an enzyme will be demonstrated. Phospholipase D (PLD) is part of the phospholipase enzyme family which is specific to phospholipids. PLD is capable of a transphosphatidylation reaction in which the phosphatidyl moiety of a phospholipid is transferred to a primary alcohol, releasing the choline group of the phospholipid. We are using the PLD transphosphorylation reaction to attach alcohol-functionalized gold NPs to laterally structured phospholipid monolayers.

First, the preparation of the phospholipid substrate will be presented. The phospholipid used is an analogue of DPPC with a methyl-disulfide functionality at the end of one of the alkyl chain (Figure 1).

This disulfide functionality allows us to form a self-assembled monolayer of phospholipid with a thiol-gold bond between the alkyl chains and a gold substrate. In this conformation, the surface exposed phospholipid head is accessible to the enzyme for biochemical processing. This monolayer was characterized by ellipsometry (thickness of 3 nm) and by polarization modulation infrared reflection absorption spectroscopy (PM-IRRAS) which indicated the presence of ordered alkyl chains. Tof-SIMS also confirms the presence of an exposed phosphate head at the gold surface. The creation of a mixed surface pattern was achieved by microcontact printing. The pattern consists of 10 μm circular dots of inert tetradecanethiol monolayer in a matrix of phospholipids. This pattern will serve as a template to spatially direct the selective attachment of gold NPs.

The synthesis of water-soluble hydroxy-capped gold nanoparticles (NPs) will also be presented. Up to date, very few hydroxy-terminated water-soluble gold NPs have been reported. A short ethylene glycol ligand, $OH(CH_2CH_2O)_3CH_2CH_2SH$, was prepared and used to form monolayer-protected gold NPs that are soluble in aqueous solution. The synthesis of the gold NPs was performed using the Brust and Schiffrin method with the addition of dioctylamine [1] . The particles were characterized by TEM and measured 2 nm in diameter. These were small enough to be characterized by ^{1}H and ^{13}C NMR.

Finally, preliminary results obtained for the PLD catalyzed attachment of the gold NPs to the phospholipid monolayer will be presented (Figure 2).

In this work, the combination of biology and surface chemistry is being exploited to functionalize the surface with gold NPs. This enzymatic modification of solid-supported biomimetic monolayers will allow us to establish the true scope and utility of enzymes as nanostructuring tools.

References:

[1] P. Scrimin *et al. Langmuir*, 24 (**2008**) 120.

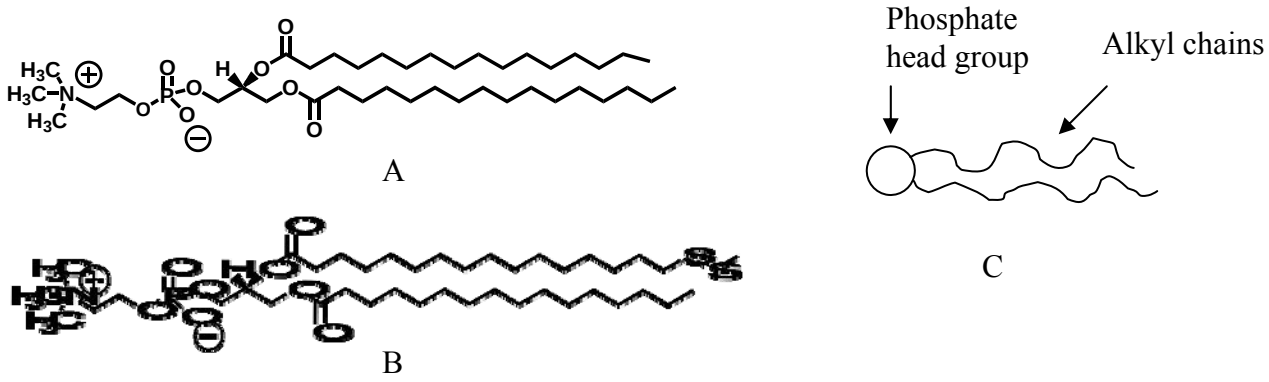

Figure 1. Structure of phospholipids A) 1,2-dipalmitoyl-sn-glycero-3-phosphocholine, DPPC B) 1-Palmitoyl-2-(16-(S-methyldithio)hexadecanoyl)-sn-glycero-3-phosphocholine DS-DPPC C) cartoon of a phospholipid.

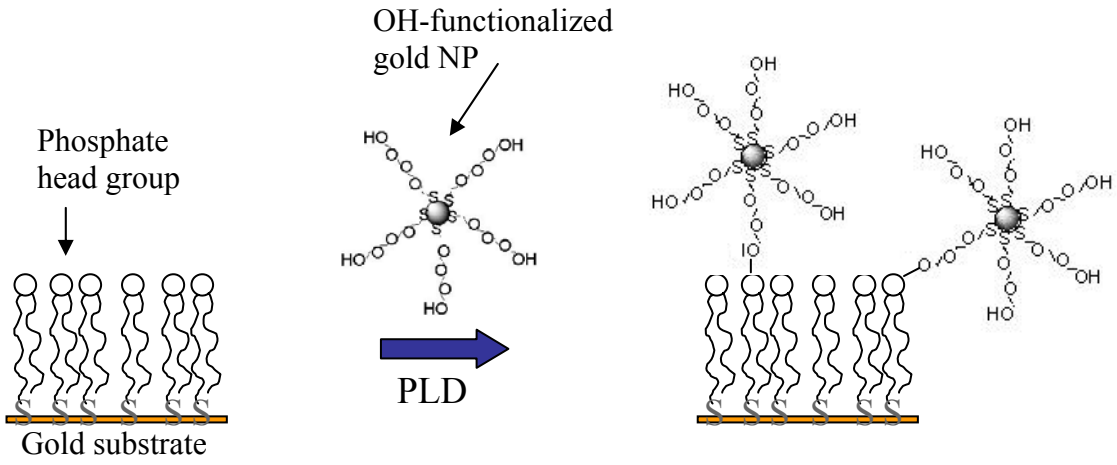

Figure 2: PLD catalyzed attachment of gold NPs onto a phospholipid monolayer.

TEMPERATURE DEPENDENT TRANSPORT PROPERTIES OF MgO-BASED ULTRA-THIN MAGNETIC TUNNEL JUNCTIONS: EXPERIMENT AND MODELING.

J. M. Teixeira, J. Ventura, J. P. Araújo, J. B. Sousa, P. Wisniowski, and P. P. Freitas
IFIMUP and Faculty of Sciences U. Porto, Rua do Campo Alegre 687, Porto, Portugal
jmteixeira@fc.up.ptl

Magnetic tunnel junctions (MTJs), constituted by two ferromagnetic (FM) layers separated by an insulating barrier, are currently used as magnetic sensors in high density recording media. The characteristics of the tunnel junctions implemented in read heads include a low resistance-area product ($R \times A$), to achieve a high readout speed, and a high enough sensitivity to read the ever smaller magnetic bit. To achieve the desired $R \times A$-values, the thickness of the insulating barrier is decreased to less than one nanometer, towards a few atomic planes thick. This leads to the possible existence of metallic paths across the insulating barrier (pinholes), with consequences in device reproducibility, performance and reliability. Furthermore, the presence of pinholes can have important impact on the MTJ-spin transfer driven magnetization dynamics, or on the MTJ-magnetoresistance sign.

Recently, tunnel junctions with crystalline MgO(001) barriers displaying very large tunnel magnetoresistive (TMR) ratios were successfully fabricated, opening new opportunities to develop read heads for ultrahigh density hard drives. The large TMR ratio of crystalline MgO tunnel junctions arises from the different symmetry-related decay rates of the Bloch waves for majority and minority spin channels. For sensor applications, MTJs with tunnel magnetoresistance above 50% and $R \times A$ as low as 0.4 $\Omega\mu m^2$ were recently obtained using thin MgO barriers.[1] However, a significative TMR-decrease is usually observed with decreasing MgO thickness,[2] showing the importance of studying the impact of pinholes on the magneto-transport properties of ultra-thin magnetic tunnel junctions.

To probe the absence of pinholes in MTJs one usually uses the three applicable Rowell criteria. However, both the exponential dependence of resistance with insulator thickness and the non-linear current-voltage characteristics were found to be non-reliable even in high resistance tunnel junctions ($R \times A \geq 1$ kΩm^2).[3] On the other hand, the third criteria [the weak insulating-like temperature dependence of the electrical resistance ($dR/dT<0$)], although insensitive to the presence of few or small pinholes in low resistance MTJs (≤ 10 $\Omega\mu m^2$),[4] can be used to probe if sizeable pinholes are present in the barrier.[5]

Here we study the temperature dependence (300-20 K) of the transport properties of low resistance magnetic tunnel junctions with an ultra-thin MgO barrier (7.5 Å). Our samples display $R \times A \geq 40$ $\Omega\mu m^2$ and TMR ~ 60-75% at room temperature. Temperature dependent electrical resistance measurements [R(T)] allowed us to observe different behaviors depending on the MTJ-magnetic state. The studied samples showed positive dR/dT for the parallel (P) state (Fig. 1), indicating a metallic-like behavior, so that pinholes are already present in the barrier. However, in the antiparallel (AP) state, the R(T) curves exhibit a mixed character, with dR/dT negative at sufficiently high temperatures but changing to positive at low temperatures (Figs. 1 and 2b). These results show an interesting competition between tunnel and metallic transport in the studied samples.

In order to understand this transport behavior, we propose a simple model of two conducting channels, metallic and tunnel, acting in parallel. We assume a linear temperature variation of the electrical resistance for both conducting channels, as observed experimentally over a broad temperature range. The model also takes into account the experimentally observed dependence of the linear coefficients on the MTJ-magnetic state (parallel and antiparallel). According to the model, the sign of the *dR/dT* derivative does not illustrate the dominant conductance mechanism and the crossover temperature (T^*) at which *dR/dT* changes sign in the

AP state depends strongly on the linear temperature coefficients. Fittings performed to the experimental *R*(*T*) data, using the developed model, reproduce the data quite well, illustrating the validity of the model.

References:

[1] Y. Nagamine *et al*, Appl. Phys. Lett., **89** (2006) 162507.
[2] K. Tsunekawa *et al*, Appl. Phys. Lett., **87** (2005) 072503.
[3] B. J. Jönsson- kerman *et al*, Appl. Phys. Lett., **77** (2000) 1870.
[4] J. Ventura *et al*, J. Phys. Cond. Matt., **19** (2007) 176207.
[5] J. Ventura *et al*, Appl. Phys. Lett., **90** (2007) 032501.

Figures:

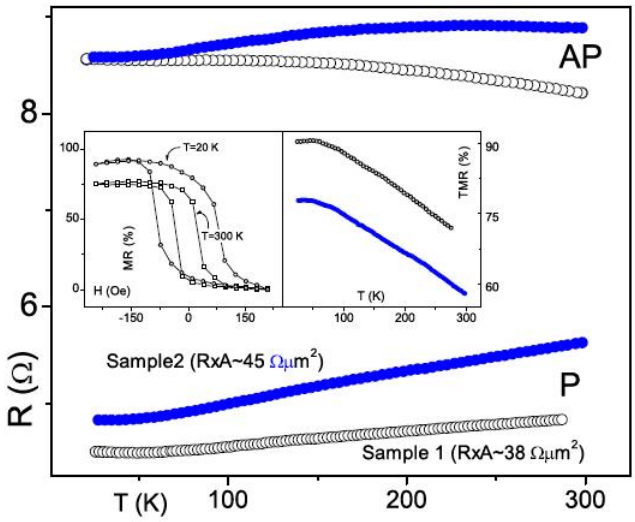

Fig. 1: Temperature dependence of the electrical resistance of samples 1 and 2 in the parallel and antiparallel states. Insets: Room and low temperature magnetoresistance cycles (sample 1) and MR-temperature dependence.

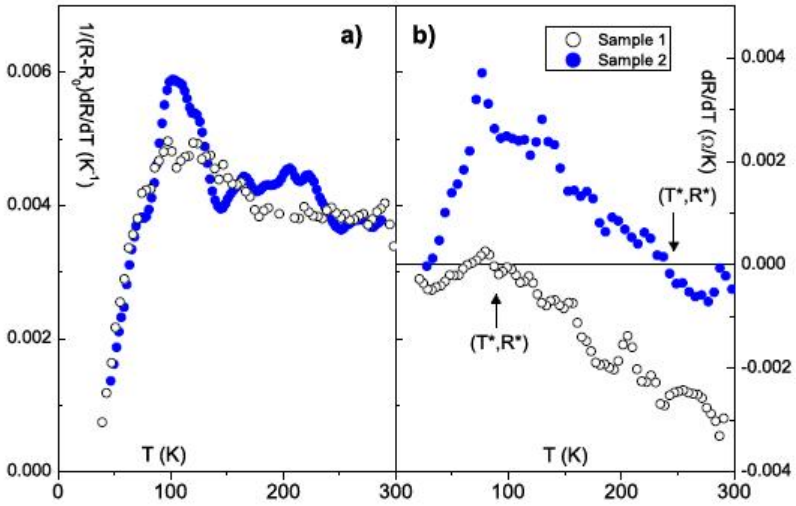

Fig. 2: Temperature derivative of (a) the normalized electrical resistance in the parallel state and (b) the electrical resistance in the antiparallel state.

MOLECULAR CONTACTS THROUGH INDUCING SURFACE INITIATED POLYMERIZATION OF NANOWIRES ON MOLYBDENUM CARBIDE

Israel Temprano Fariña, Peter H. McBreen
Université Laval, G1K 7P4, Québec, Canada
Israel.Temprano@chm.ulaval.ca

The ability to develop new methods to enhance electrical contact between organic molecules and electrodes is fundamental to the design of devices that require electron flow between an organic and a metallic component. Examples of such devices are organic thin film field effect transistors, where electrons flow from the source to drain electrodes through the organic film. The metal-organic contacts are the 'electrical plugs' in such a system. Metal-organic contacts using double or triple bonds is a promising approach in that they combine four advantages. They display very high transmission coeficients; [1,2] high thermal stability;[3,9-10] well defined contact geometries, and they show activity for olefin-metathesis add-on chemistry[1].

The dissociative adsorption of carbonyl compounds leads to the formation of C=Mo double bonds on the surface of molybdenum carbide[3-6]. These metal alkylidenes are mimics of well defined homogeneous metathesis catalysts, and present similar activity for transalkylidenation and ring-openining polymerization (ROMP)[8] reactions (figure 1). The data to be presented will emphasize surface initiated metathesis polymerization with the objective of growing conjugated molecular wires from the surface of a conducting material. from sites. In particular, results will be presented for the initial steps in the growth of polyaceylene from the surface of molybdenum carbide.

This study of surface olefin-metathesis opens a new method to interconnect electrodes in nanodevices, using molecular wires with great control and precission. Self-assembly of conjugated polymers may allow their targeted insertion into electronic and electrooptical devices.

References:

[1] Tulevski, G.S., Myers, M.B., Hybertsen, M.S., Steigerwald, M.L., Nuckolls C., Science, **309** (2005) 591.

[2] J. Ning, Z. Qian, R. Li, S. Hou, A. R. Rocha, S. Sanvito. *J. Chem. Phys*., **126** (2007), 174706

[3] Zahidi, E-M., Oudghiri-Hassani, H., McBreen, P.H., Nature, **409** (2001), 1023

[4] Siaj, M., Reed, C., Oyama, T., Scott, S.L., McBreen, P.H., J. Am. Chem. Soc, **126** (2004) 9514

[5] Siaj, M., Oudghiri-Hassani, H., Zahidi, E-M., McBreen, P.H., Surf. Sci., **579** (2005) 1

[6] Oudghiri-Hassani, H., Zahidi, E-M., Siaj, M., McBreen, P.H., App. Surf. Sci., **212-213** (2003) 4

[7] Siaj, M., McBreen, P.H., Science, **309** (2005) 588

[8] Siaj, M., Temprano, I., Dubuc, N., McBreen, P. H., J. Organomet. Chem. 691 (2006) 5497-5504

[9] Oudghiri-Hassani, H., Siaj, M., McBreen, P.H., J. Phys. Chem. C, 111, (2007), 5954-5962

[10] Siaj, M., Oudghiri-Hassan, H., Maltais, C., McBreen, P.H., J. Phys. Chem. C., 111 (2007), 1725-1732

[8] http://nobelprize.org/nobel_prizes/chemistry/laureates/2005/chemadv05.pdf

[9] http://nobelprize.org/nobel_prizes/chemistry/laureates/2000/adv.html

Figures:

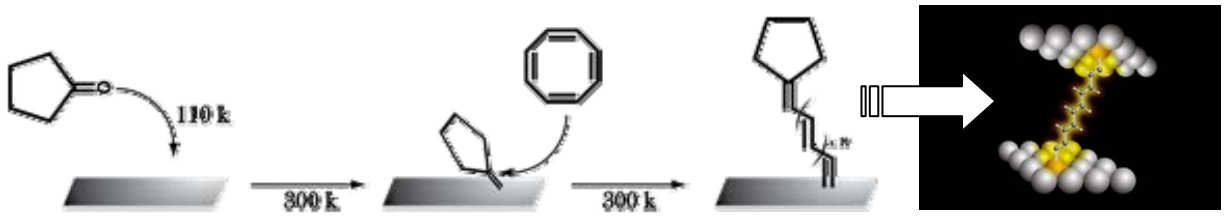

Figure 1: Schema of polyacetylene formation on molybdenum carbide and a representation of how it would be interconected between two electrodes.

PROPERTIES OF CdS And CdSe NANOPOARTICLES IN POLY(2-(DIMETHYLAMINO)ETHYL METHACRYLATE-CO-ACRYLIC ACID) CO-POLYMER MATRIX

L. V. Trandafilović[1], *N. Bibić*[1], *J. Blanuša*,[1] *M. K. Georges*[2], *T. Radhakrishnan*[2], *V. Djoković*[1]

[1]*"Vinča" Institute of Nuclear Sciences P.O. Box 522, 11001 Belgrade, Serbia*

[2]*Department of Chemistry, University of Toronto at Mississauga, Mississauga, Ontario, L5L 1C6, Canada*

lidija@vin.bg.ac.yu

CdS and CdSe nanoparticles were synthesized in poly(2-(dimethylamino) ethyl methacrylate-co-acrylic acid (pDMAEMA-AA) co-polymer. Poly(2-(dimethylamino)ethyl methacrylate-co-acrylic acid) has been synthesized by free radical polymerization in different co-monomer mol ratios (1:1, 1:2, 2:1; DMAEMA:AA; P11, P12, P21). The obtained nanocomposites were investigated using structural and optical methods. XRD measurements showed the cubic crystal phase of the CdS and CdSe nanoparticles. TEM analysis revealed the presence of the spherical nanoparticles well dispersed in the co-polymer matrix. Size of the particles was calculated from the UV VIS absorption spectra using Brus equation. The results were compared to the particle size distribution obtained from the TEM micrographs. A possible interaction between semiconductor nanoparticles and the polymer matrices was studied by means of FTIR spectroscopy.

References:

[1] L. V. Trandafilovic, V. Djokovic, N. Bibic, M. K. Georges, T. Radhakrishnan, Opt. Mater. **30** (2008) 1208
[2] L. Brus J.Chem. Phys. **90** (1986) 2555
[3] L.Brus J.Chem. Phys. **80** (1984) 4403

Figures:

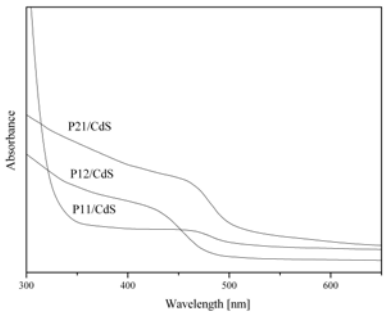

FIGURE 1. Absorption spectra of CdS nanocomposites

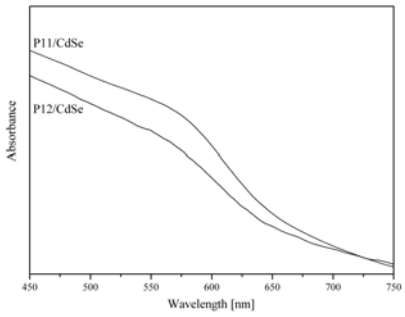

FIGURE 2. Absorption spectra of CdSe nanocomposites

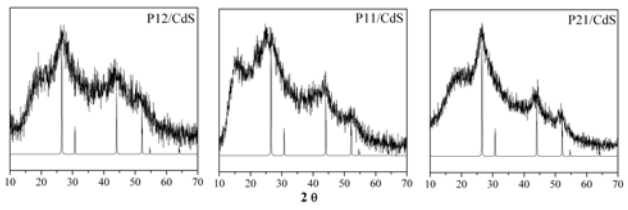

FIGURE 3. XRD spectra of CdS nanocomposites.

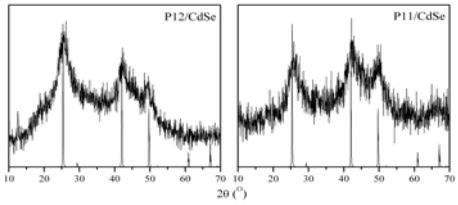

FIGURE 4. XRD spectra of CdSe nanocomposites.

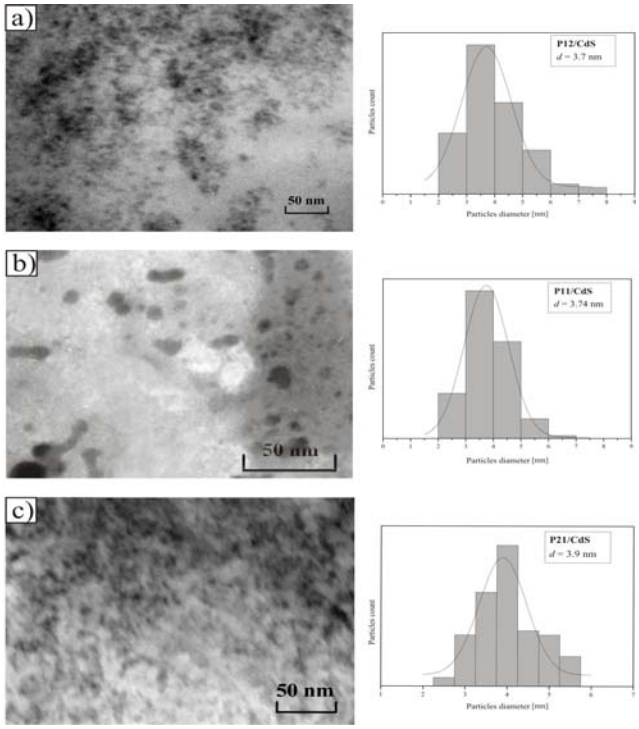

FIGURE 5. TEM micrographs and corresponding size distribution histograms of CdS nanoparticles

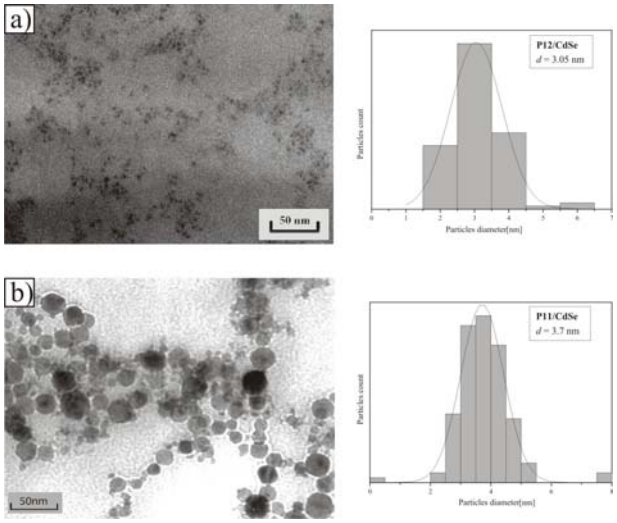

FIGURE 6. TEM micrographs and corresponding size distribution histograms of CdSe nanoparticles

THE INFLUENCE OF SURFACE MODIFICATION OF NANOPARTICLES ON THEIR STRUCTURING IN A LIQUID MEDIUM

Igor Valtsifer
Institute of Technical Chemistry
3, Akademika Koroleva Street - 614013, Perm (Russia)

Nanosized particles find a wide application in different fields of industry, they are used as components of nanocomposites, catalytic base of catalysts etc.

Introduction of nanosized particles into oligomer binding agent at definite process conditions promotes their structuring and formation of continuous clusters, penetrating the bulk. Nanoparticles, uncluding carbon ones, have pronounced ability to structuring into chain clusters. This ability provides obtaining of materials with different rheological properties and uniform distribution of the particles in an olygomer medium at relatively low filling degrees.

The main processing factors, influencing on formation of continuous structures of carbon-containing catalyst based on nanodispersed copper, nickel and led oxides within the polymer matrix have been studied. Among these are such parameters as temperature, volume filling, shear rate, structurization time; the influence of medium viscosity and surface modification of nanodispersed components on structurization processes of nanocarbon polymer systems has been studied too. Experimental studies of nanodispersed particles structurization in the polymer medium has been carried out using rotational viscometer with the method of dynamic vibrations.

The regularities, connected with structurization and rheological properties of filled olygomer systems depending on the surface modification of carboncontaining catalysts by metal oxides have been established.

MAGNETIZATION REVERSAL PROCESS IN SPIN SPRING MAGNETS. ELECTRONIC STRUCTURE CALCULATIONS

A. Vega[1], *V.M. Uzdin*[2]

1. Dep. de Física Teórica, Atómica y Óptica, University of Valladolid, 47005 Valladolid, SPAIN
2. St. Petersburg State University, Universitetskaya nab. 7/9, St. Petersburg, 199178 RUSSIA

vegat@phenix.fam.cie.uva.es

One of the nanostructures in which a non-collinear magnetic structure can be continuously and reversibly tuned by an external magnetic field is the spin spring permanent magnet which consists of exchange-coupled hard and soft magnetic bilayers or multilayers. Exchange spring media are of technological interest as permanent magnets but are also promising nanostructures for magnetic recording[1,2]. Various experimental methods have been used for the investigation of magnetic ordering in spring magnets[3,4], which in turn became a model system for benchmarking different methods to study non-collinear magnetism. Due to their complexity, the interpretation of experimental data has been made so far with the help of phenomenological models[3,4].

For the description of the magnetization reversal process in exchange spring magnets with Fe (and Fe capped by Cr or V) as the soft phase, we developed an atomic-scale quantum-mechanical theory for itinerant magnetism based on a realistic non-collinear Tight-Binding formulation of the Hamiltonian with universal parameters for each chemical element. Therefore, the behaviour of the soft magnetic films as a function of the intensity and orientation of an external magnetic field is described in the framework of fully self-consistent electronic structure calculations. Our results reproduce qualitatively all the main trends experimentally observed.

In Fig.1 we show the calculated spin-configuration for the 100ML thick Fe slab in an external magnetic field applied in the film plane. Fig. 2 illustrates the angle between the magnetic moment of the Fe layers and the easy axis of the hard magnet for different external fields applied opposite to this easy axis. In Fig. 3 we plot the reversible part of the hysteresis loop. The critical intensity of the external field required for the onset of the non-collinear spiral formation depends on both the thickness of the soft magnetic phase and on the orientation of the field, and the spin spiral structure undergoes a change of chirality in rotating fields. Our theoretical approach opens new prospects for investigating the response of other nanostructures to external magnetic fields, beyond the usual phenomenological models.

References:

[1] R.H. Victora and X. Shen, IEEE Trans. Mag. **41** (2005), 537.
[2] D. Suess, App. Phys. Lett. **89** (2006), 113105.
[3] E.E. Fullerton et al., Phys. Rev. B **58** (1998), 12193.
[4] R. Rhölsberger et al., Phys. Rev. Lett. **89** (2002), 237201.

Figures:

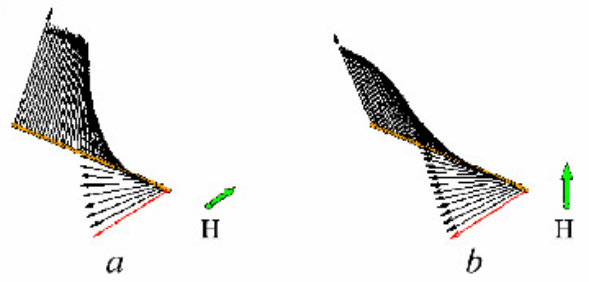

FIG. 1: Calculated spin configuration of the 100 ML thick Fe slab in an external magnetic field ($h = 3.0 \times 10^{-5}$), applied in the film plane opposite (a) and perpendicular (b) to the easy axis of the substrate (hard magnet). The direction of the lower (red) Fe moment is fixed along this easy axis. The arrows are proportional to the local magnetic moments. Only each second layer is shown. See also [21].

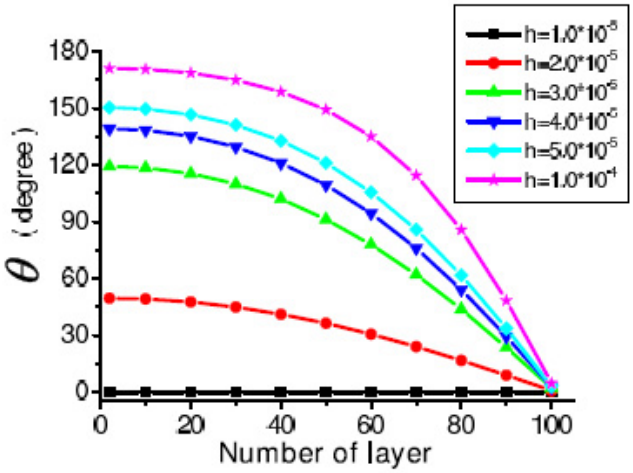

FIG. 2: Layer dependence of the angle θ_i between the magnetic moment and the easy axis of the hard magnet for different values of the external magnetic field applied opposite to the easy axis. The surface layer has number 1.

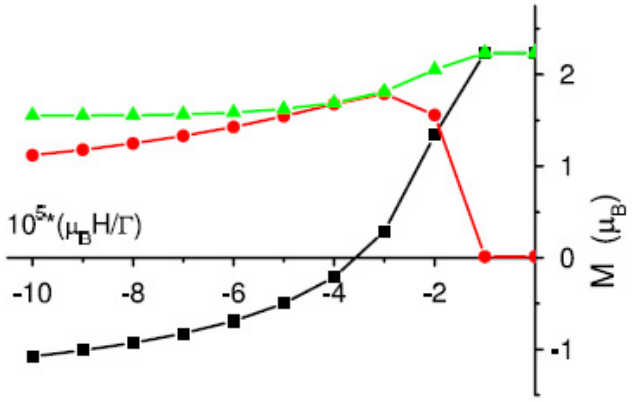

FIG. 3: Average modulus (triangles), longitudinal (squares) and transverse (circles) components of the magnetic moment (see text) as a function of the external magnetic field applied opposite to the easy axis of the hard magnet. See also [21].

STRUCTURE AND UP-CONVERSION LUMINESCENCE IN TRANSPARENT Er^{3+}-Yb^{3+} Co-Doped SiO_2-PbF_2 SOL-GEL DERIVED NANO-GLASS-CERAMICS

J. del-Castillo[a], A.C. Yanes[a], J. Méndez-Ramos[b], J.J. Velázquez[b]
V.K. Tikhomirov[c] and V.D. Rodríguez[b]

[a] Departamento de Física Básica
[b] Departamento de Física Fundamental y Experimental, Electrónica y Sistemas
Universidad de La Laguna, La Laguna, Tenerife, Spain
[c]INPAC- Institute for Nanoscale Physics and Chemistry, Katholieke Universiteit Leuven, Belgium

josvel@ull.es

Rare-earth doped materials have been extensively investigated due to their potential applications in photonic devices, such as laser and optical amplifiers [1, 2]. In particular, rare-earth doped oxyfluoride glass-ceramics have attracted much attention because they combine the low phonon energy environment of fluoride crystal with the chemical, mechanical and thermal stability of oxide glasses [3]. Different results in these glass-ceramics containing PbF_2 nanocrystals can be found in the literature [4,5]. In order to avoid technical difficulties of conventional melting techniques, sol-gel method can be used to prepare high purity glasses, with ease in the composition and homogeneity control and lower processing temperature [6].

In the present work, Er^{3+}-Yb^{3+} co-doped silica based transparent glass-ceramics containing PbF_2 nanocrystals were successfully obtained by adequate thermal treatments of sol-gel precursor glasses with composition $90SiO_2$-$10PbF_2$ codoped with 0.3 Yb^{3+} and 0.1 Er^{3+} (mol %). The structural analysis by XRD and TEM has shown the precipitation of cubic β-PbF_2 nanocrystals with radii between 5-10 nm, calculated by using Scherrer's equation. Up-conversion luminescence pumped at 980 nm has been observed and studied, some spectra are shown in Fig. 1. Up-conversion emission bands show well-resolved Stark components confirming the incorporation of the rare-earth ions into precipitated nanocrystals. Colour tuneability of up-conversion luminescence by varying pump power has been analyzed in terms of standard chromaticity diagram. This tuneability opens the way to applications for up-conversion phosphors and three-dimensional optical recording.

References:

[1] D.J. Norris, A.L. Efros and S.C. Erwin, Science **319** (2008) 1776; V. I. Klimov, Nature **447** (2007) 441.
[2] V.D. Rodríguez, V.K. Tikhomirov, J. Méndez-Ramos and A.B. Seddon, Europhys. Lett. **69** (2005) 128.
[3] Y.H. Wang and J. Ohwaki, Appl. Phys. Lett. **63** (1993) 3268.
[4] M. Mortier, A. Bensalah, G. Dantelle, G. Patriarche, D. Vivien, Opt. Mater. **29** (2007) 1263.
[5] Zhongchao Duan, Junjie Zhang, Weidong Xiang, Hongtao Sun, Lili Hu, Mater. Lett. **61** (2007) 2200.
[6] J. del-Castillo, V.D. Rodríguez, A.C. Yanes, J. Méndez-Ramos and M.E. Torres, Nanotechnology **16** (2005) 300.

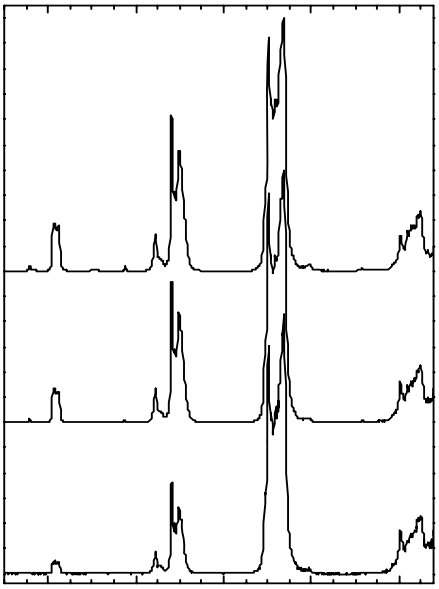

COLOR TUNEABILITY AND WHITE LIGHT GENERATION IN Yb^{3+}-Ho^{3+}-Tm^{3+} DOPED SiO_2-LaF_3 NANO-GLASS-CERAMICS PREPARED BY SOL-GEL METHOD

J.J. Velázquez[1*], A.C. Yanes[2*], J. del-Castillo[2], J. Méndez-Ramos[1] and V.D. Rodríguez[1]

[1]Departamento Física Fundamental y Experimental, Electrónica y Sistemas

[2]Departamento Física Básica

Universidad de La Laguna, 38206 La Laguna, Tenerife, Spain

josvel@ull.es ayanesh@ull.es

There is a great interest in the tuneability of the infrared-to-visible up-conversion phosphor for general lighting appliances and integrated optical devices [1]. In this sense, rare-earth doped oxyfluoride nano-glass-ceramics (GCs) appear as ideal luminescent materials for active optical devices, combining spectroscopic advantages of the fluoride hosts, due to their low phonon energies, and the good mechanical and chemical properties of the oxide glasses [2,3]. Special attention has been paid to sol-gel derived nano-glass-ceramics, since the sol-gel process is an alternative synthesis method without the difficulties of conventional melt-quenching techniques [4,5]. In particular, LaF_3 is an excellent fluoride host material due to high solubility for rare-earth ions and very low phonon energy (300-400 cm^{-1}), reducing non-radiative loss by multiphonon relaxation [6].

In this work, we report a transparent nanostructured glass-ceramics with composition $95SiO_2$-$5LaF_3$ co-doped with 0.3 Yb^{3+}, 0.1 Tm^{3+} and 0.1 Ho^{3+} (mol%) synthesized by thermal treatment at 800 ºC of precursor sol-gel derived glasses prepared in a similar way as Fujihara et al. [4]. Precipitation of LaF_3 nanocrystals, with an estimated size of 9 nm, during ceramming process was confirmed by X-ray diffraction and TEM and HRTEM analysis. Simultaneous efficient up-conversion luminescence comprising of blue, green and red emission bands under infrared excitation at 980 nm was observed, like shown in Fig. 1. Color tuneability and white light generation has been achieved varying the ratio between up-conversion emission bands by changing pump power of infrared excitation as indicated in the CIE diagram in Fig. 2. This leads the way for applications in 3-D colour optical recording/displays, white light generation for ambient lighting and biological labels [7].

References:

[1] C.Feldmann, T.Justel, C. R. Ronda and P. J. Schmidt, Adv. Func Mater. 13, (2003), 511.

[2] Y.H. Wang and J. Ohwaki, Appl. Phys. Letters **63**, (1993), 3628.

[3] J. Méndez-Ramos, V.K. Tikhomirov, V.D. Rodríguez and D. Furniss, J. Alloys Compd. **440**, (2007), 328.

[4] S. Fujihara, C. Mochizuki and T. Kimura, J. Non Crist. Solids **244**, (1999), 267.

[5] J. del-Castillo, V. D. Rodríguez, A. C. Yanes, J. Méndez-Ramos and M. E. Torres, Nanotech. **16**, (2005), 300.

[6] J.J. Velázquez, A.C.Yanes, J. del-Castillo, J. Méndez-Ramos and V.D. Rodríguez, *Physica Status Solidi (a)* **204**, (2007), 1762.

[7] J. del-Castillo, J. Méndez-Ramos, A. C. Yanes and V. D. Rodríguez, J. Nanopart. Res. in press, (2008).

Figures:

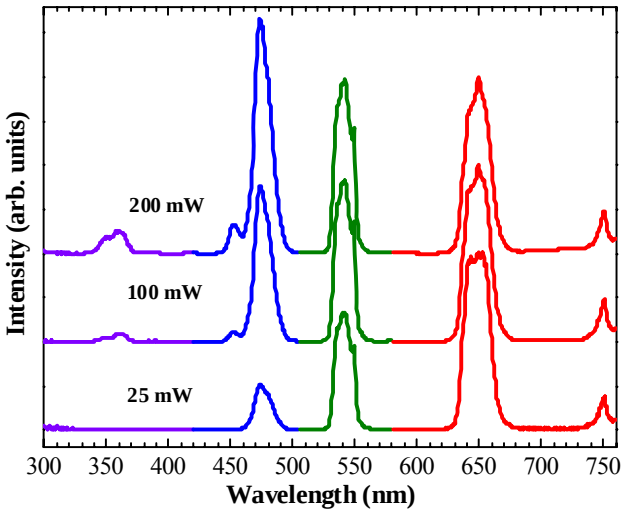

Fig. 1. Simultaneous up-conversion emission spectra under infrared excitation at 980 nm at 25, 100 and 200 mW pump power of $95SiO_2$-$5LaF_3$ doped with 0.3 Yb^{3+}, 0.1 Ho^{3+} and 0.1 Tm^{3+} (mol%) nano-glass-ceramics heat treated at 800 ºC. Spectra have been normalized to the maximum of the 660 nm red emission.

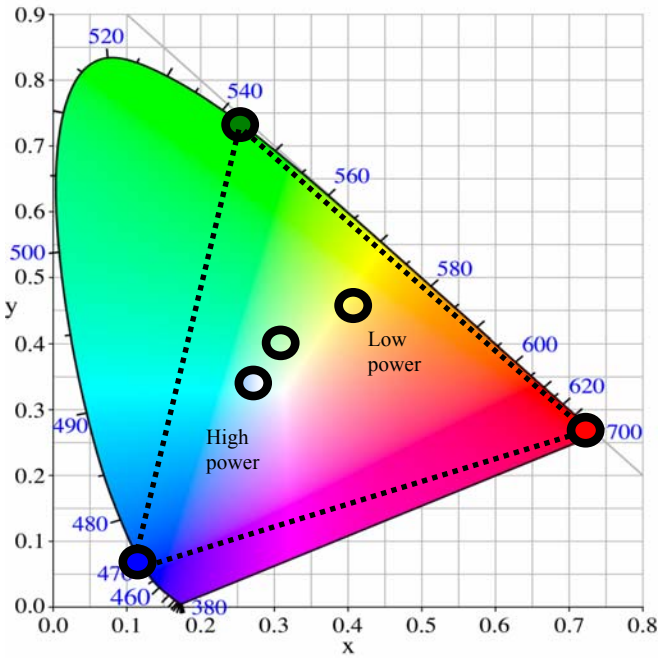

Fig. 2. Comission Internationale d'Eclairage (CIE) coordinates of $95SiO_2$-$5LaF_3$ doped with 0.3 Yb^{3+}, 0.1 Ho^{3+} and 0.1 Tm^{3+} (mol%) nano-glass-ceramic under excitation at 980 nm from high (200 mW) to low pump power (25 mW). Internal dotted triangle shows the wide colour gamut covered by the emission of sample.

ATOMISTIC SIMULATIONS OF CATALYTIC CARBON NANOTUBES GROWTH

JinJin Wang, John Robertson

Department of Engineering, University of Cambridge, Cambridge CB3 0FA, United Kingdom
jw528@cam.ac.uk

Carbon nanotubes (CNTs) have remained an attractive topic since their discovery in 1991. [1] The interests of their potential applications largely arose from their unusual structural and electronic properties. It is crucial to have a full understanding of the formation mechanisms of the CNTs in order to yield a limited distribution of nanotube chiralities. Besides experiments, the CNTs growth can also be studied theoretically using Density Functional Theory (DFT). [2-4] In this report, we investigate how different catalysts would change the growth of SWNTs.

The SIESTA ab-initio code [5] within the PBE parameterization of the generalized gradient approximation (GGA) was used to calculated the total energy of nanotube caps on different transition metal (Fe, Co, Au, Mo, Ti) surfaces. All the surfaces were built from the (111) surface. We described the valence electrons of C and the metal by a double-ζ and single-ζ polarized basis set, respectively. Caps were relaxed with the metal atoms fixed. The energy of the cap was found by joining two identical caps into a fullerene. Excess energies were corrected for the basis set superposition error.

Our studies of the nucleation stage of the CNTs growths strengthen the idea that selectivity must start during nucleation. [6] Our preliminary results show that for all transition metals the energy of the C-M bonds for the armchair edges are higher than those with zigzag edges by 30% in average; this indicates that the armchair CNTs are more favourable than the zigzag ones. For the same cap, the total energy is also affected by the position of where it was placed. In generally, a more stable structure can be achieved when the edge atoms were above the metal bonds. Fig. 1 shows how the structures of the same cap vary depending on their position. However, the relative stability varies according to metal catalysts. From our calculations, Ti offers the most stable structures, while Mo and Co provide a less strong bond with those edge carbon atoms.

References:

[1] S. Iijima, Nature, 354 (1991) 56.
[2] W.Deng et al., Nano Lett. 4, (2004). 2331
[3] X. Fan et al., Phys. Rev. Lett. 90, (2003) 145501-1
[4] Y. H. Lee et al., Phys. Rev. Lett. 78, (1997) 2393
[5] J.M. Soler et al., J. Phys. Condens. Matter. 14 (2002) 2745.
[6] S. Reich, L. Li, and J. Robertson, Chem. Phys. Lett. 421, (2006) 469

Figures:

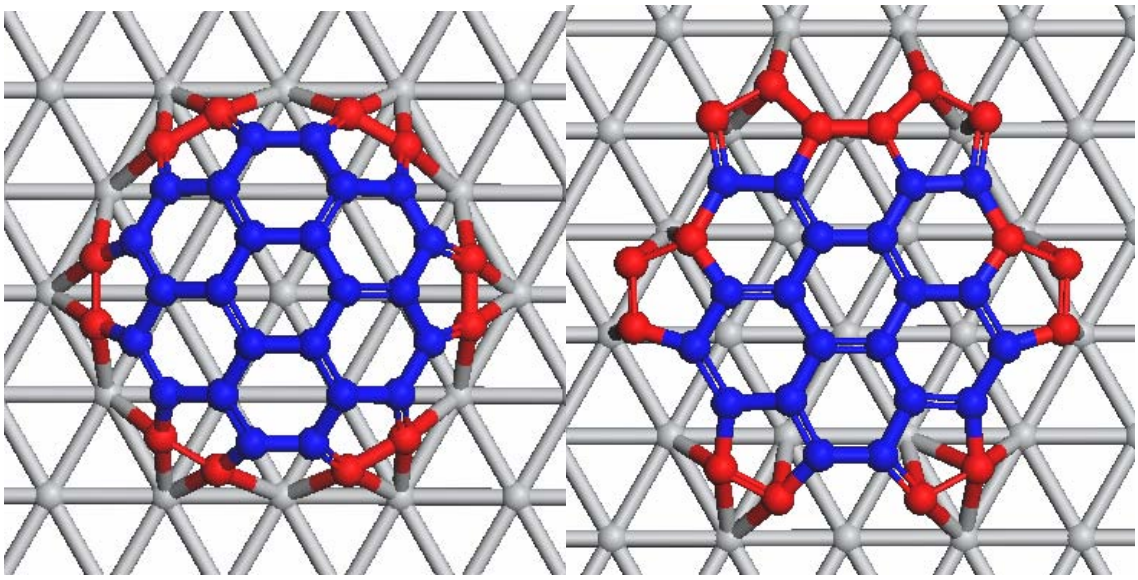

(a) (b)

Fig. 1 Relaxed (6, 6) cap on Ti (1 1 1) with the centre hexagon above (a) Ti atom (b) Ti hole site

FABRICATION OF Fe-Pt AND AU MONODISPERSED NANOPARTICLE COLLOIDS BY KrF EXCIMER LASER IRRADIATION

Masato Watanabe[1,2], Hitoshi Takamura[1] and Hiroshi Sugai[2]
[1]Tohoku University/CRESS and [2]3R Corporation
301-2-2, 6-6-11, Aza-Aoba Aramaki, Sendai 980-8579, Japan
4-10-3, Chuo, Aoba-ku, Sendai 980-0021, Japan
masato33@ceram.material.tohoku.ac.jp

In recent years, lots of research works have been devoted to Fe-Pt alloy nanoparticles due to their diverse potentials such as ultra-high density magnetic recording[1] and biomedical uses[2]. A synthesis technique based on thermal decomposition and chemical reduction of metal complexes has been mainly applied[3], while from the complexity of process and the toxicity of iron complex, more simple and enviornmental process has been expected. In this work, we propose a synthesis technique in which nanoparticles can be easily prepared only by ultraviolet laser irradiation to precursor solutions. This technique has also been applied for synthesis of Au nanoparticles with wide-ranged applications.

A schematic diagram of the experimental configuration for laser irradiation is shown in Fig. 1. A KrF excimer pulsed laser generation system (λ = 248nm) was used as the laser light source. The conditions of laser power, pulse frequency and irradiation time were varied up to 30W, 50Hz and 60min, respecviely. The precursor solutions were methanol (Fe-Pt) and water (Au) solutions into which iron (III) and platinum (II) acetylacetonates for Fe-Pt and hydrogen tetrachloroaurate (III) hydrate for Au, respectively. Polyvinylpyrrolidone (average molecular weight ~10,000) were added to the solutions for preventing aggregation. After laser irradiation, the resulting solutions were centrifuged for the Fe-Pt and Au cases and dissolved into hexane for removal of decomposed or undecomposed matters for the Fe-Pt case.

Figure 2 shows the typical bright field transmission electron microscopic (TEM) image of the Fe-Pt nanoparticles with laser conditions of 15W and 30min using a Hitachi HF2000 with an acceleration voltage of 200kV. Very fine nanoparticles with the diameters of 1-3nm have been observed. Lattice fringes characteristic of crystallinity can be partly observed on the naoparticles. Fine nanoparticles with the same size range were always obtained independent of the laser and/or precursor conditions. Micro energy dispersive Xray spectroscopic (EDXS) measurements were carried out on the Fe-Pt nanoparticles, which indicates the alloying of iron and platinum in the nanoparticles. Irradiated laser power dependence of evaluated Fe compositions in the nanoparticles is shown in Fig.3. The lower laser power is found to cause a lower iron composition, which may indicate that the iron complex in precursor solution is harder to be decomposed compared with the platinum one. Figure 4 shows absorption spectra in ultraviolet and visible light regions for the Au nanopaticle colloids with varying laser pulse frequency. The absorption peaks characteristic of surface plasmon resonance on gold nanoparticles were observed at the wavelengths of 530-540nm. The higher pulse frequency of 20Hz is found to cause broadening in the resonance peak, considered to be due to some microstructual change.

We succeeded in fabricating Fe-Pt alloy and Au nanoparticles monodispersed in methanol or water solutions only by UV laser irradiation to precursor solutions. The further results will be discussed in the session.

References:

[1] D.Weller; A.Moser, L.Folks, M. E.Best, W.Lee, M F.Toney, M.Schwickert,; J-U.Thiele and M.F.Doerner, IEEE Trans. Magn. **36** (2000**)** 10.
[2] R.Hong, N.O.Fischer, T.Emrick and V.M.Rotello, Chem. Mater. **17** (2005**)** 4617.
[3] S.Sun, C. B.Murray, D.Weller, L.Folks and A.Moser, *Science* **287** (2000) 1989.

Figures:

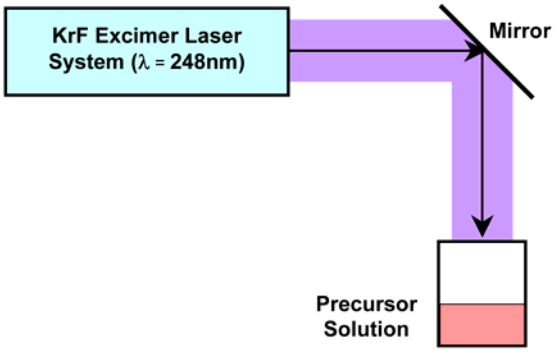

Fig.1. Schematic diagram for nanoparticle fabrication by KrF excimer laser irradiation to precursor solution

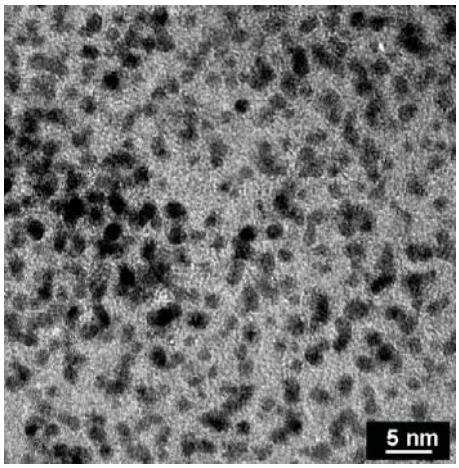

Fig.2. Transmission electron microscopic image of the Fe-Pt nanoparticles with the laser conditions of 15W and 30min.

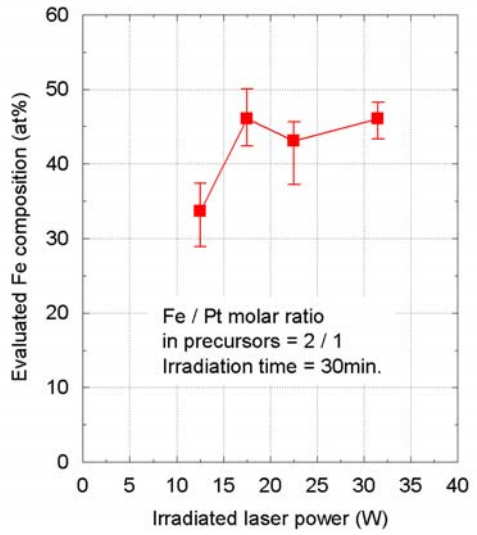

Fig.3. Irradiated laser power dependence of evaluated Fe compositions in the Fe-Pt nanoparticles

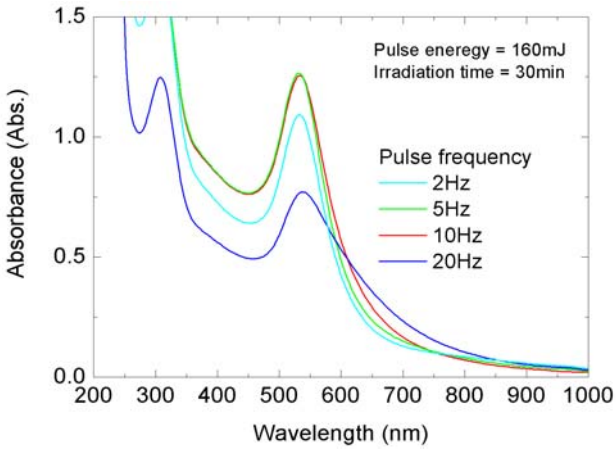

Fig.4. Ultraviolet and visible light absorption spectra of the Au nanoparticles with varying pulse frequency.

FABRICATION OF METAL-ION PATTERNS BY μCP AND DPN FOR PROTEIN IMMOBILIZATION

C.C.Wu[1,2], K. van der Werf[1], D. N. Reinhoudt[2], C. Otto[1], A.H. Velders[2], and V. Subramaniam[1]

[1]Biophysical Engineering Group, [2] Laboratory of Supramolecular Chemistry and Technology. MESA+ Institute for Nanotechnology. University of Twente, P.O. Box 217, 7500 AE Enschede, the Netherlands

c.wu@tnw.utwente.nl

We have demonstrated that calcium and copper ions can be transferred onto fluorescent SAMs using dip-pen nanolithography (DPN) at μm and sub-μm scale[1]. Subsequent modulations of the fluorescent signal were visualized in situ by using a hybrid atomic force fluorescence microscope (AFFM). This approach enables several applications, including the selective and controlled immobilization of proteins via a specific metal–protein interaction.

Nitrilotriacetic acid (NTA)-terminated SAMs are particularly suitable for protein immobilizaton experiments, because they allow the oriented binding of His-tagged proteins via the complexation with metal ions (Ni^{2+}, Cu^{2+}, or Co^{2+})[2]. We present data using two lithography techniques, microcontact printing (μCP) and DPN, to fabricate nickel ion patterns on NTA-functionalized glass slides as templates for the immobilization of His-tagged enhanced green fluorescent protein (EGFP) (Figure 1).

We demonstrate that His-tagged EGFP patterns at μm scale can be achieved by microcontact printing of Ni^{2+} ions (Figure 2-a). The protein and complexed Ni^{2+} patterns can be removed easily by using EDTA solution (Figure 2-b). To demonstrate that the functionalized surfaces can be re-used, a PDMS stamp with a different feature size was used for microcontact printing of Ni^{2+} ions for immobilization of His_6-EGFP (Figure 2-c). The difference of fluorescence intensities in Figure 2-a and c may result from the varied amount of Ni^{2+} ions adsorbed onto the surface of PDMS stamp.

In order to obtain protein patterns at smaller scale, a cleaned Si_3N_4 tip dipped in $NiCl_2$ solution was used to write metal ion patterns. Figure 3-a and c depict fluorescence images of His-tagged EGFP line and dot patterns, respectively. Protein patterns with line width about 1.2 μm are presented. The smallest diameter of the dots in Figure 3-c is ~ 0.6 μm which is close to the resolution limit of the confocal fluorescence microscope. AFM topography experiments yield further information about the exact sizes of the nanofabricated protein patterns.

References:

[1] L. Basabe-Desmonts, C.-C. Wu, K. O. van der Werf, M. Peter, M. Bennink, C. Otto, A. H. Velders, D. N. Reinhoudt, V. Subramaniam, and M. Crego-Calama, ChemPhysChem, (2008), in press.
[2] M. J. W. Ludden, A. Mulder; R. Tampé, D. N. Reinhoudt and J. Huskens, Angew. Chem. Int. Ed., **46** (2007), 4104.

Acknowledgement:

This work was supported by the MESA+ Institute for Nanotechnology and NanoNed.

Figures:

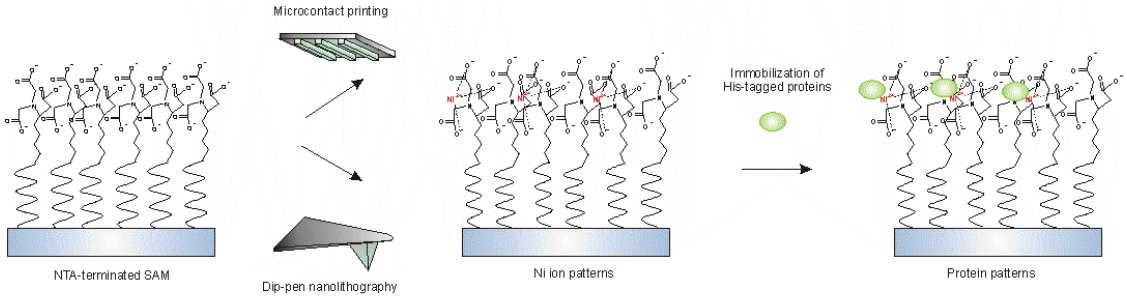

Figure 1 *Illustration of fabricating nickel ion patterns on a NTA-functionalized surface with microcontact printing and dip-pen nanolithography techniques for immobilization of His-tagged proteins.*

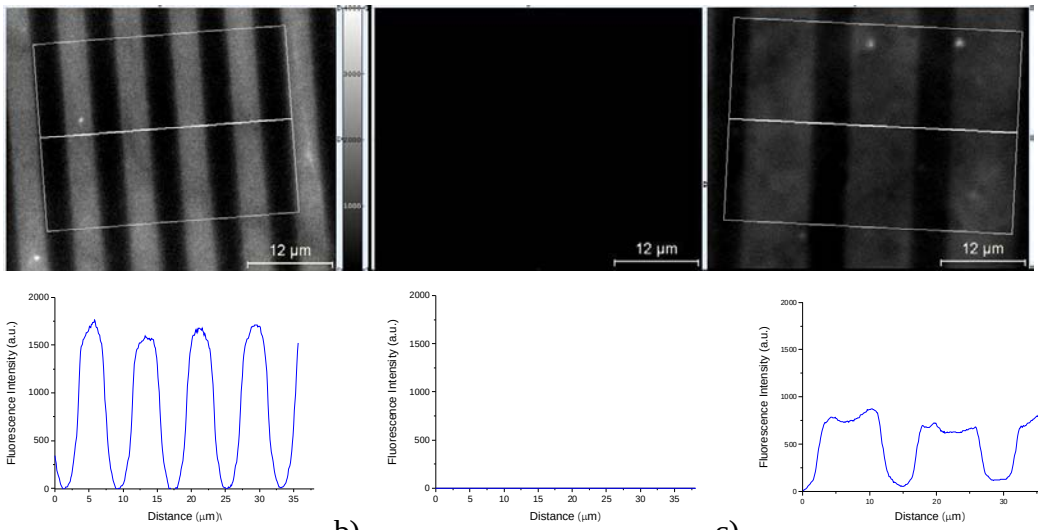

Figure 2 *Fluorescence images in gray scale and average fluorescence intensity profiles of the area inside the rectangle of His_6- tagged EGFP immobilized on Ni^{2+} patterns created after a) 1st µCP, b) after rinsing with 0.1M EDTA solution and c) after 2nd µCP). The integration time of (a), (b) and (c) is 200 ms, 200ms and 800ms, respectively. The printing time of 1st and 2nd µCP is 2 minutes without applying extra load.*

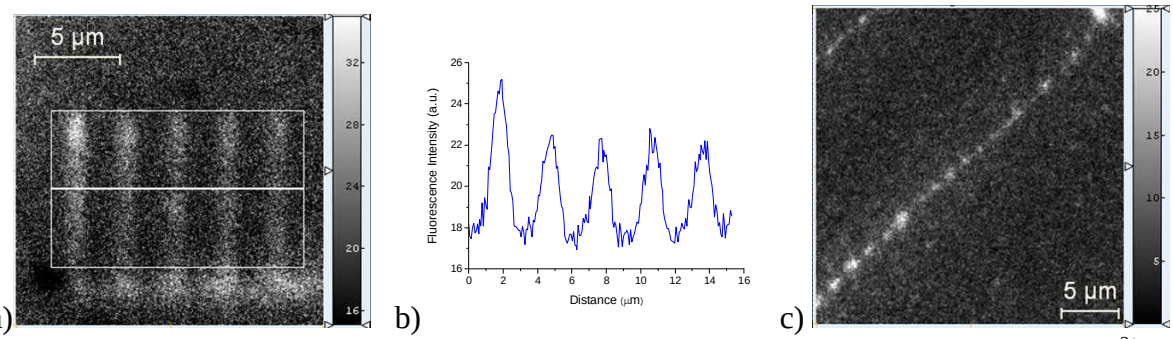

Figure 3 *a) and c) Fluorescence images in gray scale of His_6- tagged EGFP immobilized on Ni^{2+} line and dot patterns created by DPN. b) Average fluorescence intensity profile of the area inside the rectangle indicated in (a).*

Magnetocapacitance in Fe_3O_4@SiO_2 nanocomposite

S. Yáñez-Vilar[1], *M. Sánchez-Andújar*[1], *S. Castro-García*[1], *J. Rivas*[2], *M. A. Señarís-Rodríguez*[1]
[1]*Dept. Química Fundamental, Univ. da Coruña, A Zapateira s/n, 15071 A Coruña, España*
[2]*Dept. Física Aplicada, Univ. de Santiago de Compostela, 15781 Santiago de Compostela, España*
syanez@udc.es

Nowadays, there is a growging interest in materials in which their dielectric constant can be modified by the application of a magnetic field [1]. Unluckily, relatively few compounds display such a magnetocapacitive (MC) behavior and many efforts have been devoted in the last years to search for new alternatives.

Recently, several authors have reported magnetocapacitive response in magnetic nanoparticles systems such as ε-Fe_2O_3 [2], $MnFe_2O_4$ and γ-Fe_2O_3 [3]. Therefore, nanoparticle technologies open a new route to obtain materials with such a behavior.

In this contribution, we study the influence of the SiO_2 coating on the dielectric and magnetocapacitive response of one of the most studied magnetic compounds among the iron oxides: the magnetite, Fe_3O_4. This compound is a very well known material that shows a ferrimagnetic transition around T_C ~ 850 K and nearly full spin polarization at room temperature [4], both properties of great potential for applications in giant magnetoelectronic and spin-valve devices.

For this purpose, the Fe_3O_4 nanoparticles (ϕ~ 20 nm) that constitute the cores were prepared following the solvothermal method described by Pinna et al. [5], and the Fe_3O_4@SiO_2 core-shell nanocomposites (Figure 1) were synthesized using the Stöber method [6]. The obtained samples were morphologically and structurally characterized by means of X-ray powder diffraction, scanning electron microscopy and transmission electron microscopy. Its complex dielectric permittivity, $\varepsilon_r = \varepsilon_r' - i\varepsilon_r''$, was measured as a function of frequency ($20 \leq \nu\ (Hz) \leq 10^6$) and temperature ($90 \leq T\ (K) \leq 300$). Dielectric measurements as a function of a magnetic field, H_{max}= 0.5 T, were aditionally performed in the temperature range $200 \leq T\ (K) \leq 300$.

The frequency dependent behavior of the two materials are compared in Figure 2. As it can be seen the dielectric constant shows higher values in the case of the Fe_3O_4 nanoparticles, even if those of the core-shell nanocomposite do not decrease so markedly with frequency. Very interestingly in the coated sample the loss tangent has decreased as compared to the uncoated sample by at least a factor of 10 (Figure 3).

Moreover, a magnetocapacitive (MC) response is observed at room temperature in the Fe_3O_4 nanoparticles, $MC = [\varepsilon'_{r(H=0.5T)} - \varepsilon'_{r(H=0T)}]/\varepsilon'_{r(H=0T)}$~ 6 %, that slighly decreases, but maintains values ~ 1 % in the case of the Fe_3O_4@SiO_2 nanocomposite.

Acknowledgments:

The authors are grateful for financial support from Xunta de Galicia under project PGIDIT06PXB103298PR and from Consolider-Ingenio 2010 under poject CSD2006-00012. S. Yáñez-Vilar want to thank to MEC of Spain for her FPI fellowship and M. Sánchez-Andújar acknowledges to Xunta de Galicia for support under program Parga Pondal.

References:

[1] G. Catalan, *Appl. Phys. Lett*. **88** (2006) 102902.
[2] M. Gith, C. Frontera, A.Roig, J. Fontcuberta, E. Molins, *Nanotechnology* **17** (2006) 687.
[3] G. Lawes, R. Tackett, O. Masala, B. Adhikary, R. Naik, R. Seshadri, *Appl. Phys. Lett*. **88** (2006) 687.
[4] J. M. D. Coey, A. E. Berkowitz, Ll. Balcells, F. F. Putris, F. T. Parker, *Appl. Phys. Lett.* **72** (1998) 734.
[5] N. Pinna, S. Grancharow, P. Beato, P. Bonville, M. Antonetti, M. Niederberger, *Chem. Mater*. **17** (2005) 3044.

[6] W. Stöber, A.Fink, E. Bohn, *J. Colloid Interface Sci.* **26** (1968) 62.

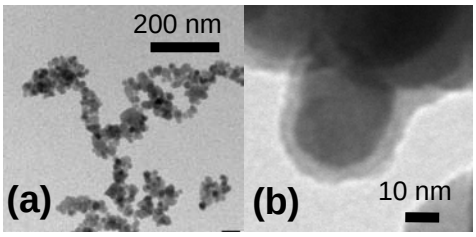

Figure 1. TEM micrographs of: (a) the Fe_3O_4 nanoparticles, (b) the Fe_3O_4@SiO_2 core-shell composite (thickness of the SiO_2 nanocoating ~ 6 nm).

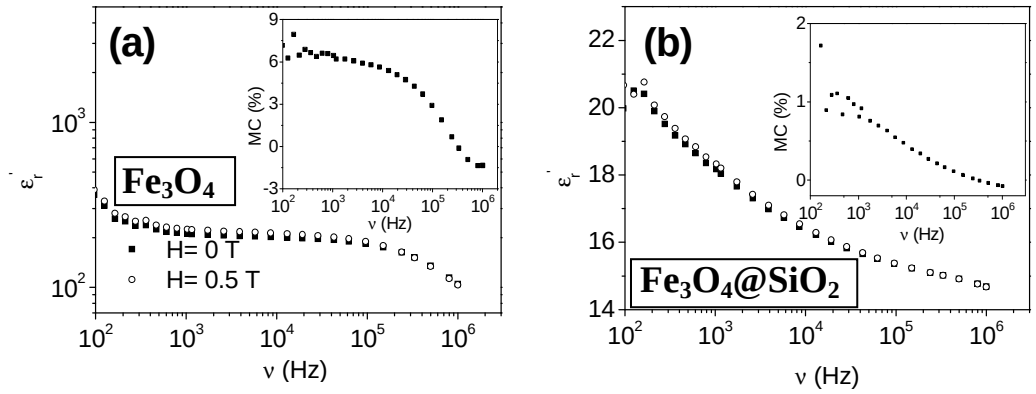

Figure 2. Frequency (ν) dependence of the dielectric constant (ε'_r) for: (a) Fe_3O_4 nanoparticles and (b) Fe_3O_4@SiO_2 nanocomposite, measured at T= 295 K in the absence and presence of magnetic field.
Inset on Figures 2a and 2b: Magnetocapacitive effect, where $MC=[\varepsilon'_{r(H=0.5T)}-\varepsilon'_{r(H=0T)}]/\varepsilon'_{r(H=0T)}$.

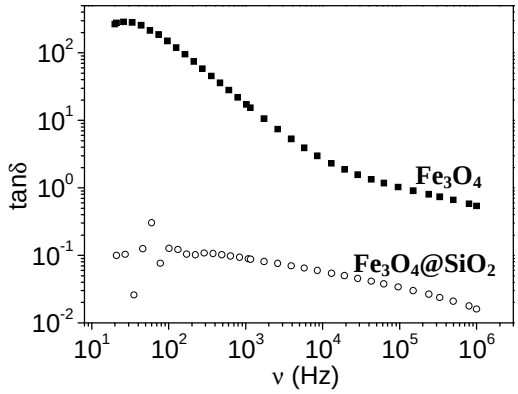

Figure 3. Plot of the loss tangent (tanδ) versus frequency ($20 \leq \nu$ (Hz) $\leq 10^6$) corresponding to both the Fe_3O_4 nanoparticles and the Fe_3O_4@SiO_2 nanocomposite measured at T= 300 K.

INDEX

POSTERS

ALPHABETICAL ORDER SESSION PB

Session B (PB) is dedicated to Doctors

FABRICATION OF IMPEDIMETRIC GAS SENSOR WITH Au/TiO_2 ORDERED STRUCTURE ON MICROHOT-PLATE SYSTEM

Martin Adámek, Radim Hrdy, Marina Voroskova, Jana Drbohlavova, Jaromir Hubalek
Department of Microelectronic, Faculty of Electrical Engineering and Communication, Brno University of Technology, Udolni 53, Brno, Czech Republic
hubalek@feec.vutbr.cz

Recent research showed the availability of atmospheric pollutant monitoring using a gas sensor with a nanostructured surface of sensing electrode which can be prepared through anodisation process [1]. The use of the anodisation technique for obtaining oxide porous material which can be used e. g. as nano-template was firstly reported in the work of Masuda *et al.* [2]. The aim of presented work is a fabrication of Au nanorods further modified with TiO_2 layer for the improving of electrode sensing properties due to increasing its specific surface.

The impedimetric microsystem, which represents microhot-plate gas sensors, was prepared by the deposition of $POCl_3$ doped polysilicon heater and gold comb-like microstructures. The thin aluminum film (2 μm) was deposited by evaporation method on the gold microstructures. The thin porous anodic alumina template was prepared by one-step oxidation process under potentiostatic voltage (40 V) in 0.3 M oxalic acid [3, 4]. The anodisation process ran to point where the current density started to increase. The pore diameter was in the range of 30–80 nm and thickness was 2 μm. The original porous structure can be seen on the steps break (Fig. 1). Close to the base layer the porosity and ordering grow up. SEM analysis showed several advantage of this technique. First, the porous alumina grew up only on a conducted micro system, despite the theory of growing on all surface of aluminum layer [5, 6]. This fact was caused by differences between the thickness of aluminum on conductive layer and on the other areas (Fig. 2). The porous alumina started to grow on whole surface. After few seconds, the current density was higher in aluminum on conductive layer in comparison with the other space and therefore the porous alumina was obtained only on small conductive areas.

The second advantage is a skip phasing of oxide barrier chemical etching. The oxide barrier was successfully removed by continual anodization under a constant potential. Despite the previous experience, it is not necessary to use a phosphoric acid for dissolving of oxide barrier [7, 8]. The barrier is very thin. Since all aluminum is consumed, the oxide barrier starts to be dissolved due to high electric potential on interface conductor – oxide.

Finally, the alumina template was used for the galvanic deposition of gold nanowires with the same length and diameter as pore sizes of the template [9]. The cross section image (Fig. 3) shows the gold nanowires after dissolution of alumina in 5 % NaOH.

Next step was aimed to immobilization of TiO_2 coatings by sol-gel technology starting from titanium tetrapropoxide precursor, ethanol as solvent and acetyl-acetone as stabilizing agent. The concentration of Ti was 0.35 mol dm^{-3}. The sol was simply dropped onto Au nanomachined surface of comb-like structure, then dried at 110 °C in oven and finally annealed at 450 °C in a furnace. Raman spectroscopy was employed to characterize TiO_2 phase constitution (Fig. 4).

References:

[1] Klosová K., Hubálek J., Phys. Stat. Sol. A 205 (2008) 1435
[2] Masuda H., Fukuda K., Science, **268** (1995) 1566.
[3] Jessensky O., Müller F., Gösele U., Appl. Phys. Lett., **72** (1998) 1173.
[4] Li A.P., Müller F., Bimer A., Nielsch K., Gössele J., J. Appl. Phys., **84** (1998) 11.

[5] Dickey C. E., Oomman K. V., Sensors, **2** (2002) 91.
[6] Wang A., Wahite R.M., presented at the IEEE Ultrasonic Symposium, Seattle, WA, Nov. 7–10 , 1995.
[7] Masuda H., Yada K., Osada A., J. Appl. Phys., **37** (1998) L1340.
[8] Nielsch K., Choi J., Schwirn K., Wrespohn R. B., Nanoletters, **2** (2002) 7
[9] Oropeza C., *A New Approach to Evaluate Fracture Strength of UV-Liga Fabricated Nickel Specimen,* Louisiana, State University, 2002

Acknowledgment: This research was supported by Grant Agency of the Czech Republic under the contract GA102/06/1624. The CNM of Barcelona is also acknowledged for support delivery of the microhot-plate microsystems.

Figures:

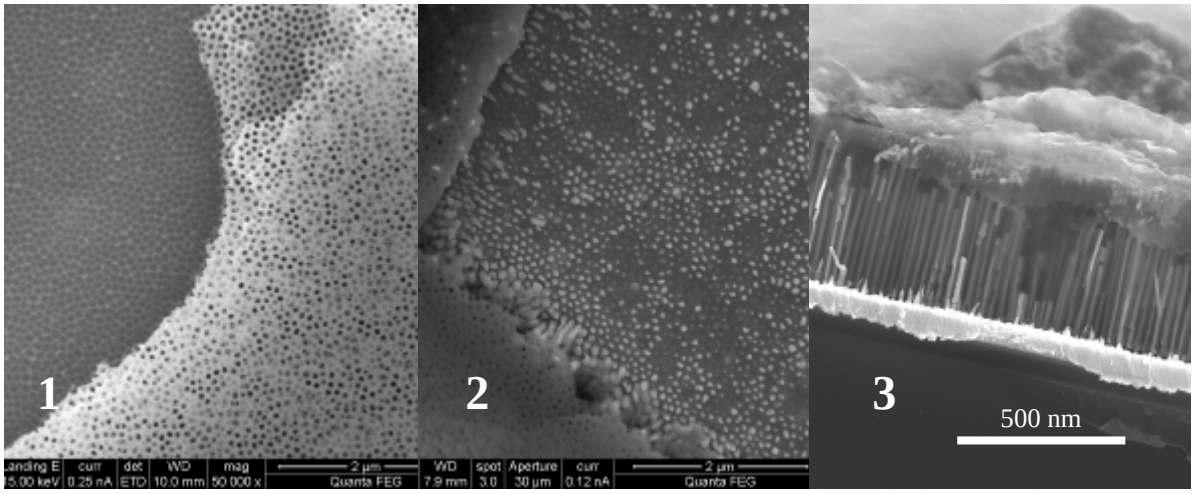

Fig. 1-3 *SEM analysis of nanomachined microelectrodes*

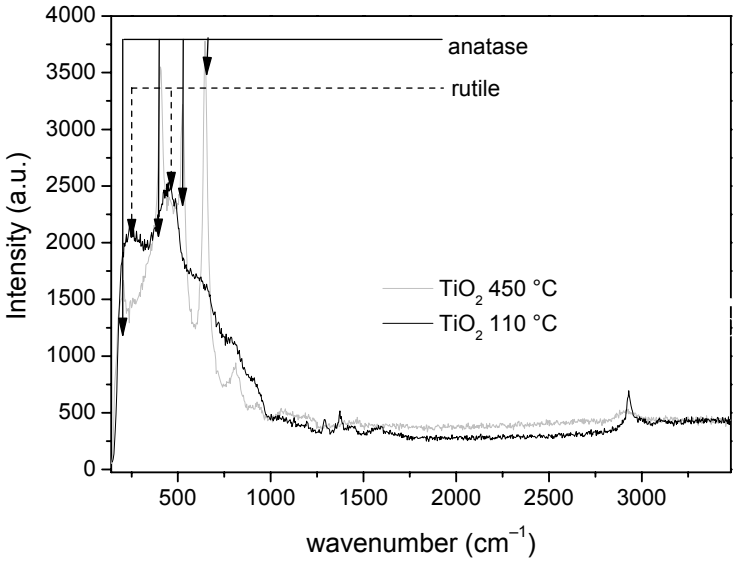

Fig. 4 *Raman spectra of TiO_2 annealed at 110 °C and 450 °C*

CHARACTERIZATION OF DNA IMMOBILIZATION AND HYBRIDIZATION COMBINING NANOMECHANICAL AND ELECTROCHEMICAL BIOSENSORS

M. Arroyo-Hernández, J.L. Costa-Krämer, M. Martín-González and J. Tamayo
Instituto de Microelectrónica de Madrid, IMM-CNM-CSIC,
Isaac Newton 8, PTM, 28760 Tres Cantos Madrid
marroyo@imm.cnm.csic.es

The development of highly sensitivity and inexpensive DNA biosensors is of great interest for medical analysis, forensics, genomics etc. While conventional methods achieve most of the requirements, sample labelling has some disadvantages: it is time-consuming, there is interference with the molecular recognition process and an unspecific background signal. On the other hand, nanomechanical[1,2] and electrochemical[3,4] biosensors are label free detection schemes that can be combined to characterize the mechanisms involved in the immobilization of thiolated ss-DNA onto gold surfaces. The sensitivity of a DNA biosensor depends on the hybridization efficiency, which is in turn related to the DNA orientation and the surface coverage, and on the detection signal. Local measurements of the displacement along the cantilever position give information about the homogeneity of the DNA adsorption and about the surface stress induced by DNA adsorption and hybridization. The electrochemical measurements give information about the electron transfer through the monolayers. This is relevant to accurately determine the molecule sites involved in the interaction with the gold surface and with other molecules: 5´-thiolated end, the phosphate backbone (negative charge) or the amines on the bases (positive charges). The dynamics of the absorption mechanism and the resulting coverage pattern depend on the chemical environment, the deposited species, and presumably on the charge state of the metallic surface on which the DNA strands deposit.

Cantilever deflexion measurements show a clear relation between the gold surface charge and the mechanism of DNA adsorption and intermolecular interactions at the nanometer scale. The experiments show how the cantilever bending is modified drastically depending on the initial surface charge state. Remarkably, the cantilever bends downward or upwards after DNA immobilization (figure 1) depending on the initial charge state. This is probably related to differential population of DNA strands standing up and laying down on the gold surface.. (Further support of this assumption comes from white light reflectivity measurements that show a different DNA apparent thickness depending on the surface charge.

In situ measurements of the electric currents during both immobilization and hybridization processes in an electrochemical cell allow to optimize the conditions for nanomechanical translation of hybridization events. Moreover it allows a deeper understanding of the mechanism of surface stress generation under self-assembly of DNA on gold and subsequent hybridization.

References:

[1] Hansen KM, Thundat T. Methods **37** (2005) 57-64.

[2] J. Mertens, C. Rogero, M. Calleja, D. Ramos, J.A. Martín-Gago, C. Briones and J. Tamayo, Nature Nanotechnology **3**, 301 - 307 (2008)

[3] Palecek E., Fotja M, Tomschik M, Wang J. Biosensors and Bioelectronics **13** (1998) 621-628

[4] Mascini M, Palchetti I, Marrazza G. Fresenius' journal of analytical chemistry **369** (2001) 15-22

Figures:

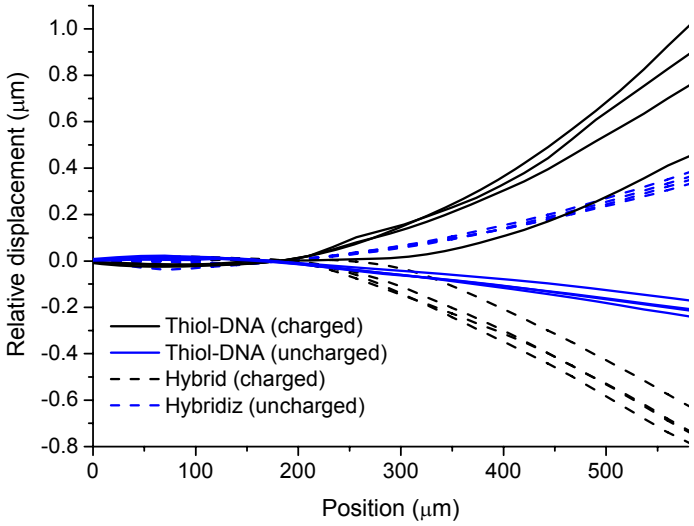

Figure 1: Cantilever profile measurements of two arrays of cantilevers DNA coated with charged (black lines) and uncharged (blue lines) gold. The cantilever displacement was measured after thiolated-DNA immobilization (solid lines) and hybridization with complementary DNA (dotted lines).

Fe/MgO NANOPARTICLES DEPOSITED ON NANOSTRUCTURED $La_{2/3}Sr_{1/3}MnO_3$ THIN FILMS

Z. Konstantinović, C. Martinez-Boubeta, Ll. Balcells, B. Martinéz
Institut de Ciència de Materials de Barcelona, CSIC, Campus UAB, 08193 Bellaterra, Spain
zorica@icmab.es

The appearance of new functionalities and devices arising from size- and shape-dependent properties has triggered the interest in creating well-defined structures at nanometric scale. However, the fabrication of artificial nanostructures appears to be a very difficult task requiring sophisticated technologies. The self-organized processes offers an alternative route to generate nanometric-scale objects of controlled size and shape together with long-range ordered, required for most practical applications. Growth conditions that cause the well-defined nanostructured surface have gained wide-spread interest for the implementation of self-assembled 1D and 0D nanostructures.

Oxides are one of the largest families of new materials which attract great attention due to their rich physics. Among them, the manganese perovskites showing colossal magnetoresistance and half metallic characteristics have emerged as good candidates for miniature spintronic devices. Complex oxide thin films are often elastically strained and this lattice strain can, in some cases, select preferential growth modes leading to the appearance of different self-organized morphologies. On the other hand, self assembly of magnetic nanoparticles on top of technological substrates (such as manganese perovskites) becomes a very useful technique for the fabrication of nanostructured materials.

In this work we report preliminary results on the controlled fabrication of self-assembled nanostructures in $La_{2/3}Sr_{1/3}MnO_3$ (LSMO) thin films grown on top of $SrTiO_3$ (100) and MgO (100) oriented substrates. On top of these films, a new nanostructured system, made of crystalline Fe particles covered by a uniform 2-3 nm thick MgO epitaxial shell, is spread. The magnetic properties of these heterosystems are discussed.

‘Spring-Like’ Molecular Junctions: An Avenue to Store Energy in Molecules to Power Molecular-Machines

Kabeer Jasuja, Vikas Berry*
Chemical Engineering Department, Kansas State University, Manhattan, Kansas - USA
vberry@ksu.edu

ABSTRACT:

Incorporation of the inherent molecular elasticity into molecular electronics (*1-6*) would enable development of next-generation molecular electromechanical systems like energy storage devices, molecular timers and actuators, which could be integrated to build self-sustaining molecular machines. However, the major challenges in achieving such molecular-mechanics are (a) applying confined and precise forces on the molecular-junction, (b) fabricating a molecular-junction with strong (multiple) bonds which can sustain mechanical deformation and (c) having a non-rigid system at molecular scale with sufficient mobility to achieve unrestrained mechanics. Such molecular mechanics cannot be achieved in a device construct where molecular junctions are incorporated between rigid electrodes.

As a part of this presentation, we will demonstrate (a) a working “molecular-spring” nanodevice, (b) a mechanism to controllably apply confined forces on molecular junctions, and (c) a molecular system which can store compression and stretching energy. Here, the molecular spring system is built with crosslinked polyallylamine-hydrochloride (cPAH) molecules sandwiched between 30 nm gold nanoparticles (GNP), where cPAH molecular-junctions are reversibly compressed and stretched by applying electrically and centrifugally induced forces respectively, while GNPs play a dual role (a) of movable connectors to apply forces and (b) of nanoelectrodes to measure molecular deformation via change in electron tunneling conductivity(*7-9*). The system functions like a ‘molecular-spring’, where the compression and stretching energy of the junctions can be stored and used to apply forces on the nanoparticles to bring them back to their native state. The dynamics of both externally and internally induced molecular motion fits well with the equation of spring in viscous media.

In the second part of the presentation, we will present a light-actuated molecular junction built by incorporating azo-group containing molecular junctions between metal-nanoparticles. Here, the mechanical actuation of azo-group is induced via exposure to light of wavelength 365 nm and 420 nm and is used to controllably manipulate the attached nanoparticles. The dynamics of reversible light-induced-actuation of nanoparticles (by ~0.2 nm) will also be demonstrated.

As an enabling technology, the outcome of these results will benefit a wide range of scientific disciplines and push the frontier of molecular-mechanics and nanotechnology. The ability to store compression energy in a molecular-device-architecture has the potential to power future molecular devices by stored molecular-energy. Further, the azo-group mechanics could be used to manipulate nanoparticles, thus controlling properties of nanocomponent based devices.

Reference List

1. D. Dulic *et al.*, *Physical Review Letters* **91**, (2003).
2. J. E. Green *et al.*, *Nature* **445**, 414 (2007).
3. A. M. Brouwer *et al.*, *Science* **291**, 2124 (2001).
4. N. Koumura, R. W. J. Zijlstra, R. A. van Delden, N. Harada, B. L. Feringa, *Nature* **401**, 152 (1999).
5. A. Aviram, M. A. Ratner, *Chem. Phys. Lett.* **29**, 277 (1974).
6. S. Yasuda, T. Nakamura, M. Matsumoto, H. Shigekawa, *J. Am. Chem. Soc.* **125**, 16430 (2003).
7. V. Berry, S. Rangaswamy, R. F. Saraf, *Nano Letters* **4**, 939 (2004).
8. V. Berry, A. Gole, S. Kundu, C. J. Murphy, R. F. Saraf, *Journal of the American Chemical Society* **127**, 17600 (2005).
9. V. Berry, R. F. Saraf, *Angewandte Chemie-International Edition* **44**, 6668 (2005).

Figures:

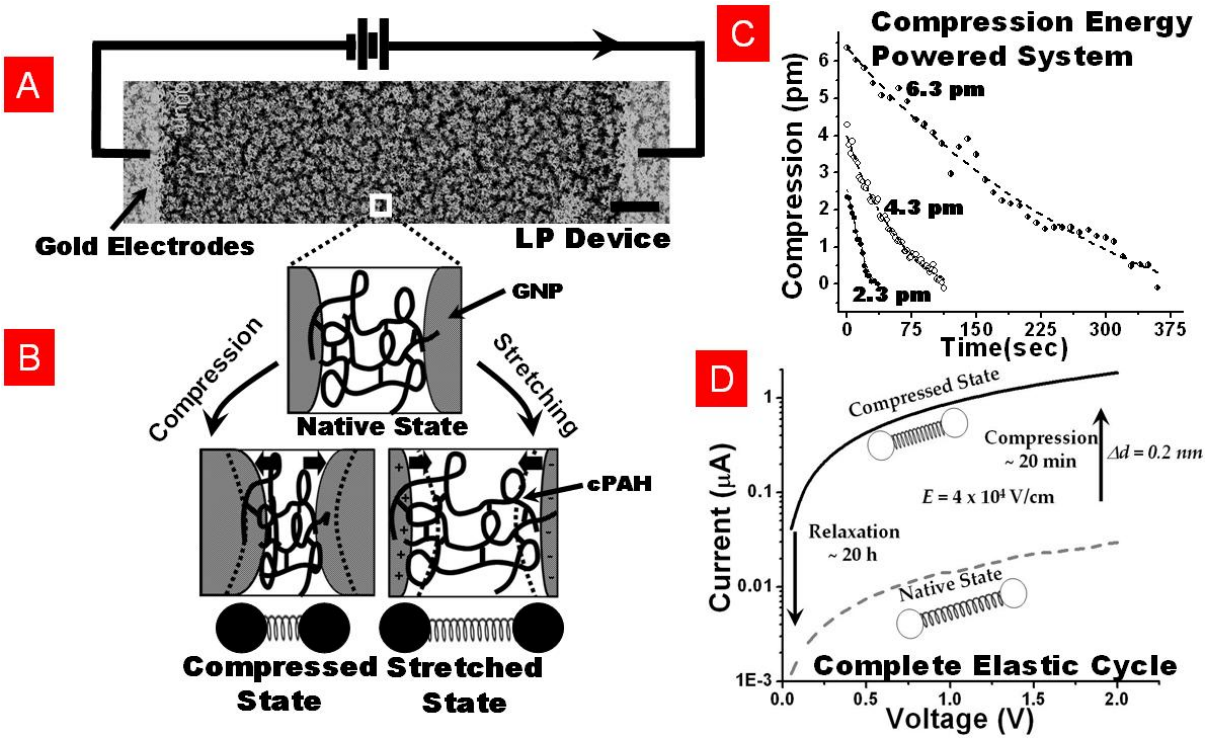

Figure A. FESEM micrograph of a typical molecular-spring device between gold electrodes connected to a power supply. Scale bar = 100 nm. **B.** Schematic representation of compression and stretching of cPAH junctions between GNPs. **C.** Compressed molecules upon release of forces use the stored compression energy to push nanoparticles back to their native state with the rate of relaxation governed by the magnitude of the stored compression energy. Molecules compressed by ~2.3 pm, ~4.3 pm and ~6.3 pm, relaxes back to its original state in ~0.5 min, ~2 min and ~6 min respectively. **D.** Complete compression-relaxation cycle of a molecular spring device with the two conductivity states is shown.

POROUS MATERIALS BASED IN LAMINAR AND PILLARED ZIRCONIUM PHOSPHATES FOR THE EFFICIENT STORAGE OF HYDROGEN

Ernesto Brunet, Carlos Cerro, Olga Juanes and Juan Carlos Rodriguez-Ubis
Department of Organic Chemistry, Faculty of Sciences C-I-207, Universidad Autónoma de Madrid, 28049-Madrid (Spain)
ernesto.brunet@uam.es

Hydrogen is a very appealing energy vector: the release of its energy does not involve the noxious carbon dioxide. Yet, it is becoming a well known fact by our society that two problems must be solved if hydrogen is to be efficient and safely used as the clean energy carrier of the future: *i*) its environmental-friendly production and *ii*) its safe storage and transportation. Although there are already many reasonably useful technical approaches, neither of the two problems is nowadays at a level of resolution which would make the use of hydrogen routinely possible. Besides, the technical solutions to these problems must be quite robust in order to make a smooth transition to the "hydrogen culture" from the actual fossil-fuel civilization, whose economic moguls are far too powerful to be convincingly counterfeited. Therefore, a lot of research is being performed and even new institutions are being created to accomplish the aforementioned double task. Concerning the second one, hydrogen storage (**HS**) may be attained by at least four main methods: *i*) in high-pressure cylinders, *ii*) as a liquid in cryogenic tanks, *iii*) in ionic or covalent compounds (chemisorption), and *iv*) by *physisorption* in porous matrices.[1] This communication will give a critical quick view of the visible state-of-the art of the latter method (*physisorption*) and report our approach and progress in the use of porous organic-inorganic solids based in Al and Zr and various phosphonates.

A thorough revision of the literature (Figure 1) shows that the materials with very large specific surface areas (the record is well above 3000 m^2/g) are not suitable for efficient HS at room temperature and low pressures, as common sense would have been anticipated. The free energy of interaction among the hydrogen molecules and the scarce matter of these systems is very low similarly as it is in an empty cylinder. Therefore, to increase that interaction energy, closer contact H_2-material and thus much smaller pores are needed. It is now considered that a material bearing micropores or even ultramicropores would be more efficient for HS.[2] Many reported materials fall within this category. However, the average HS capacity (A and B in Figure 1) is around 2 wt% (77K and 1 atm) and a barrier of 3-4 wt% appears to be by far insurmountable. The average enthalpy of interaction H_2-material is around 6-7 KJ/mol. It seems clear that higher enthalpies are needed (15-20 KJ/mol) to achive HS at room temperature and atmospheric pressure. It should be noted that a record enthalpy of interaction (17.5 KJ/mol) was reported in faujasite-type (Mg,Na)-Y zeolite[3] but, unfortunately, the HS was low due to a strong entropic compensation. The existence of ions, specially Li^+, and/or the presence of metals with open coordination sites in microporous organic-inorganic scaffolds are considered quite favourable features to increase HS.[4] Also, the presence of aromatic moieties in these scaffolds, probably with the idea of building kin

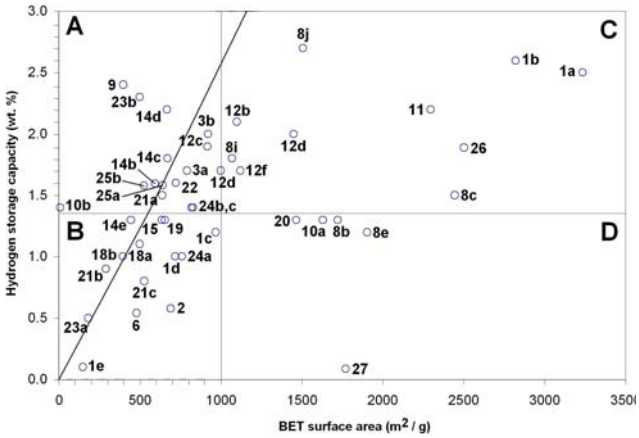

Figure 1

structures to superactivated carbon, graphenes and carbon nanotubes, is also a coveted architectural characteristic.

We are investigating the possibilities that organic-inorganic scaffolds based in phosphonates and Al and Zr have in this field. Although our preliminary results have been only quite modest,[5] we believe that we have a set-up of conceptual and material tools,[6] similar to that reigning organic chemistry, which could lead to the design of an endless number of structures and interesting results. For instance, the use of $Al_2(HPO_3)_x$ $(C_{12}H_8P_2O_6)_{1.5-x/2}$ allows the easy control of the HPO_3/diphenyl-phosphonate ($C_{12}H_8P_2O_6$) ratio. The resulting materials displayed a good correlation between wt% HS and the HPO_3 content (UAM-150 $\rightarrow$ 152: *cf.* Figure 2), probably due to the increasing internal area caused by the increment of latter.[7]

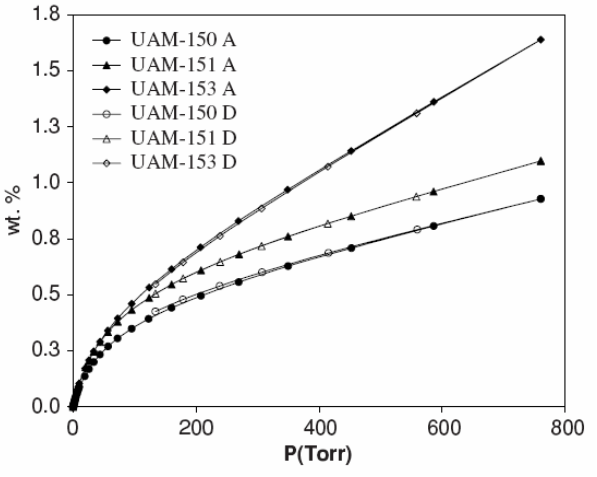

Figure 2

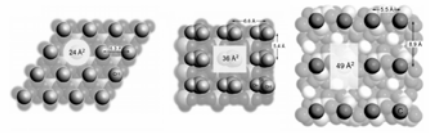

Figure 3

The Zr derivatives, in which we have a larger experience, seem to be even much more flexible. Three phases (α, γ and λ; Figure 3) of quite different structures are known for Zr phosphates which easily allow the inclusion of a variety of species, comprising various organic components (carboxylic acids, amines, phosphonates, etc), various phosphorous acids and metal ions. Preliminary results in the building of these structures with the phosphonates of Scheme 1 will be reported in this communication.

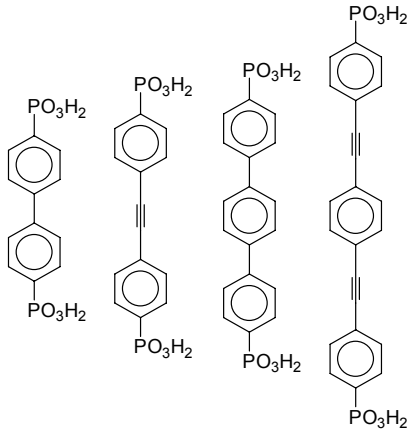

Scheme 1

References

[1] See for example: Zuettel, A. *Naturwissenschaften* **2004**, *91*, 157-172.

[2] Bhatia, S. K.; Myers, A. L**.** *Langmuir* **2006**, *22*, 1688-1700.

[3] Turnés, G.; Llop, M. R.; Otero, C. *J. Mater. Chem.*, **2006**, *16*, 2884–2885.

[4] Sun, Q.; Jena, P.; Wang, Q.; Marquez, M. J. Amer. Chem. Soc. **2006**, *128*, 9741-9745.

[5] Brunet, E.; Alhendawi, H. M. H.; Cerro, C.; de la Mata, M.J.; Juanes, O.; Rodríguez-Ubis, J.C. *Angew. Chem. Int. Ed.* **2006**, *45*, 6918-6920.

[6] Brunet, E.; de la Mata, M.J.; Alhendawi, H. M. H.; Cerro, C.; Alonso, M.; Juanes, O.; Rodríguez-Ubis, J.C. *Chem. Mater*. **2005**, *17*, 1424-1433.

[7] Brunet, E.; Cerro, C.; Juanes, O.; Rodríguez-Ubis, J.C.; Clearfield, A. *J. Mater Sci.* **2008**, *43*, 1155-1158

ENDOHEDRAL METALLOFULLERENES AS IMPROVED ACCEPTOR MATERIALS FOR ORGANIC SOLAR CELLS

Martin Drees, Claudia Cardona, Brian Holloway
Luna Innovations Incorporated,
521 Bridge Street
Danville, VA 24541

Russel Ross, Ed VanKeuren
Georgetown
37th and O st. NW
Washington, DC 20057

Dirk Guldi
Friedrich-Alexander-Universität Erlangen-Nürnberg
Egerlandstr. 3
91058 Erlangen, Germany

Cost factors in inorganic solar cells have opened up a new path to less expensive manufacturing techniques using bulk heterojunction polymer/fullerene based solar cells. Using empty cage fullerene derivatives as the acceptor material, state-of-the-art organic photovoltaics currently display ~5% overall conversion efficiency. One of the main factors limiting the efficiency in organic solar cells is the low open circuit voltage. The open circuit voltage is governed by the molecular orbitals of the donor and acceptor material; therefore better matching of the orbitals will lead to improved voltages. Here we present a novel acceptor material based on Trimetasphere® carbon nanomaterials (TMS). Trimetaspheres® are endohedral metallofullerenes that consist of a trimetal nitride cluster enclosed in a C_{80} cage. First-generation Trimetasphere® carbon nanomaterial derivatives have been synthesized and show behavior consistent with C_{60} but with improved molecular orbitals. Electrochemical data suggests a maximum voltage increase of up to 280 mV over C_{60}-PCBM-based devices and photophysical characterization of shows efficient and stable charge separation. Initial bulk-heterojunction devices have been synthesized with open circuit voltages that are 280 mV higher than reference devices using C60-PCBM and state-of-the art (>3.4%) conversion efficiencies.

CHARACTERIZATION OF METALLIC NANOPARTICLES OBTAINED BY BIOMASS REDUCTION

Laura Castro
Department of Material Science and Metallurgic Engineering, Complutense University of Madrid, Avda. Complutense s/n 28040 Madrid, Spain.
mailto:lauracr84@hotmail.com
mlblazquez@quim.ucm.es

Nowadays precious metal recovery technologies use harmful chemicals that may represent a risk to the environment and public health. This is the reason why it is necessary to develop clean, non-toxic and environmentally friendly procedures to recover precious metals. The use of biological organisms in synthesis and assembly of nanoparticles has received an increasing interest. In these experiments, dead brown and red seaweeds (*Ascophyllum nodosum* and *Chondrus crispus*) have shown to be efficient for gold (III) reduction. Seaweeds reduce gold (III) to gold (0) and produce nanoparticles. The reduction process was found to be dependant on pH, time, temperature and concentration of biomass. UV-vis spectrums and transmission electron micrographs showed nanoparticles of several shapes and sizes. In order to resolve the mechanism of reduction of gold (III), the evolution of pH and potential was measured.

References:

Bhattacharya, D., y Grupta, R. K.: Nanotechnology and potential of microorganisms. Critical reviews in biotechnology, **25** (2005), pp. 199-204.

Gadea-Torresday, J. L., Parsons, J.G., Gomez, E., Peralta-Videa, J., Troiani, H. E., Santiago, P., Yacaman, M. J.: Formation and growth of Au nanoparticles incide live alfalfa plants. Nano Letters, **2** (4) (2003) pp. 397-401.

Mukherjee, P., Senapati, S., Mandal, D., Ahmad, A., Khan, M. I., Kumar,R, Sastry, M.: Extracellular synthesis of gold nanoparticles by the fungus *Fusarium oxysporum*. Chem. Biol. Chem. 3 (2002), pp. 461-463.

Figures:

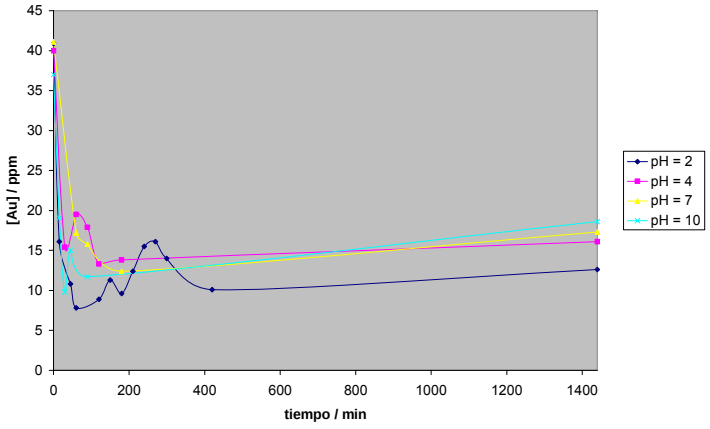

Fig. 1. Influence of initial pH in reduction of $AuCl_4^-$ with 2 g/L *Ascophyllum nodosum*.

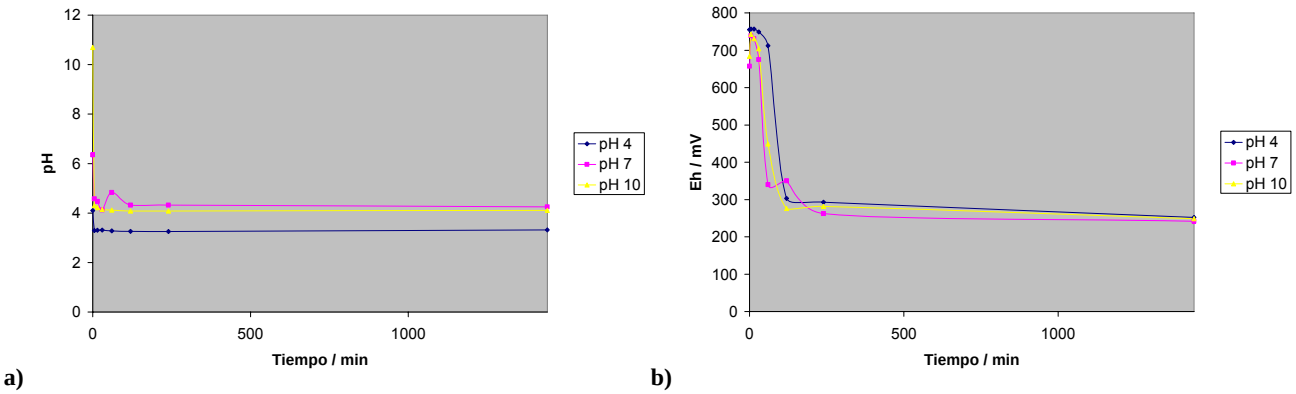

a) b)

Fig. 2. Evolution of pH (a) and potential (b) in reduction of $AuCl_4^-$ with 5 g/L *Ascophyllum nodosum* for different values of initial pH..

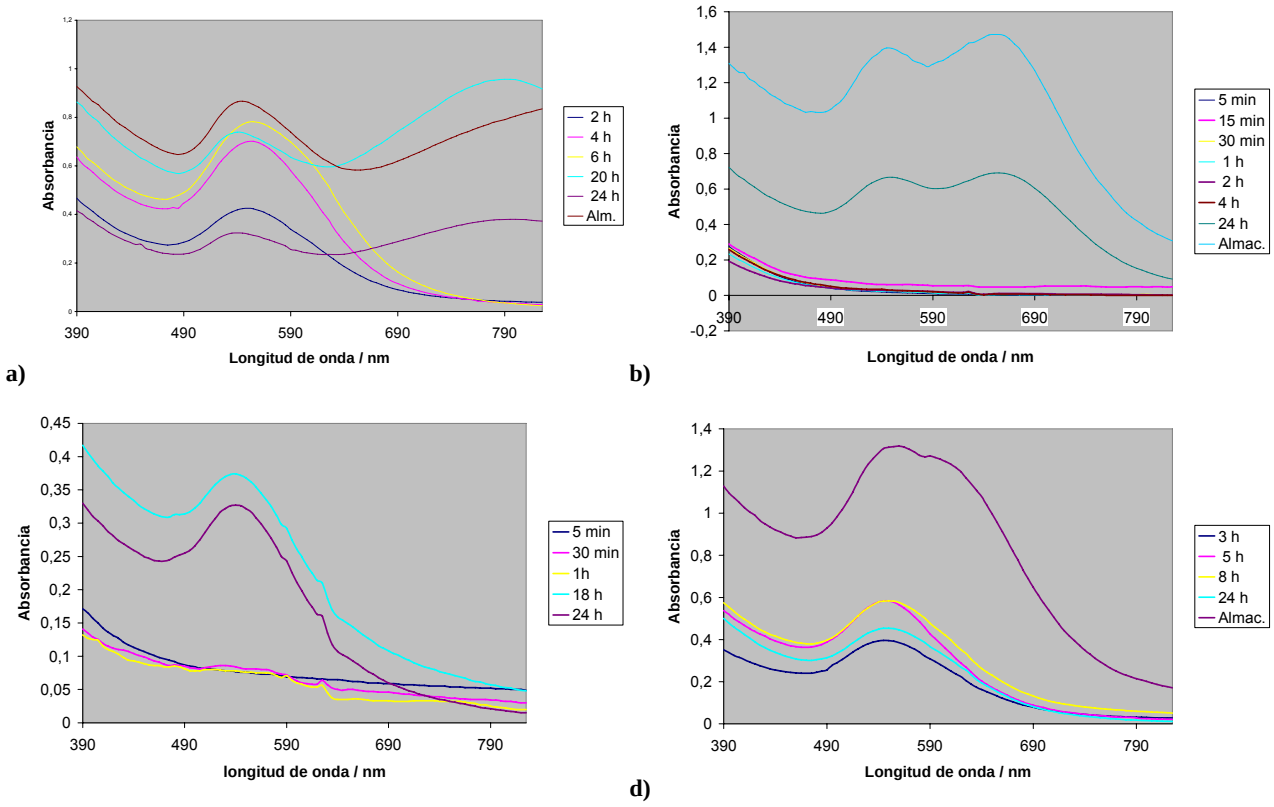

a) b)

c) d)

Fig. 3. UV-vis spectrums of Au nanioparticles dissolutions produced with 5 g/L *Chondrus Crispus* with different values of initial pH: a) pH = 2, b) pH = 4, c) pH = 7, d) pH = 10.

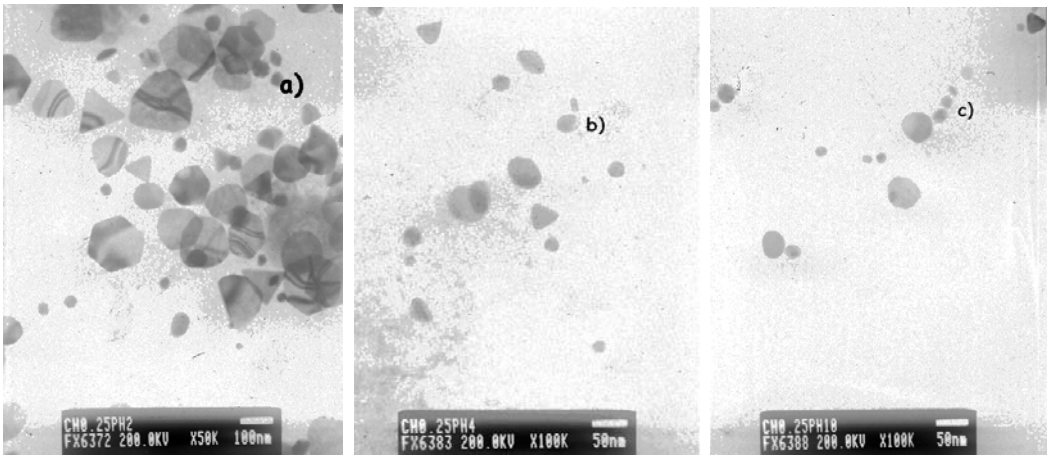

Fig. 4. Photographs of Au nanoparticles obtained with 5 g/L *Chondrus crispus* observed by TEM: a) pH 2, b) pH 4, c) pH 10.

III-V SEMICONDUCTOR QUANTUM DOTS WITH A MAGNETIC IMPURITY

Sucismita Chutia and A. K. Bhattacharjee

Laboratoire de Physique des Solides, UMR du CNRS, Université Paris-Sud
91405 Orsay, France
chutia@lps.u-psud.fr

A single transition-metal impurity in a semiconductor quantum dot (QD) seems promising for spintronics and quantum information processing. The $sp-d$ exchange interaction between the magnetic ion and the carriers, well characterized in bulk diluted magnetic semiconductors, is strongly enhanced by quantum confinement leading to a zero-field splitting of the exciton [1]. The excitonic photoluminescence (PL) in Mn-doped CdTe/ZnTe self-assembled QDs was indeed found to split into six components [2]. More recently, a strikingly different zero-field splitting pattern of the PL has been reported [3] in Mn-doped InAs/GaAs QDs, which arises from the difference in the nature of the Mn impurity in II-VI and III-V semiconductors.

We present a theoretical model for the electronic structure of GaAs and InAs quantum dots (QDs) containing a single substitutional Mn impurity. The Mn impurity in these compounds is known to be a shallow acceptor in the configuation $d^5 + h$. Our model for the hole states is based on the Luttinger Hamiltonian and the Coulomb potential with a central cell correction that accounts for the observed binding energy in the bulk. The total binding energy as well as the exchange contribution are found to increase with decreasing QD size. The effect is more pronounced in spherical nanocrystals (NCs) than in lens-shaped self-assembled QDs, because of the highly anisotropic confinement in the latter. With an on-center impurity, NCs retain the bulk T_d symmetry and the ground state is a $j = 3/2$ - like Γ_8 level. In self-assembled QDs it splits into two doublets: $\Gamma_6(|j_z| = 1/2)$ and $\Gamma_7(|j_z| = 3/2)$ of D_{2d}, which mix in the presence of in-plane asymmetry, both belonging to Γ_5 of the reduced symmetry C_{2v}. The order and the splitting between the doublets depend on the degree of confinement and the strain-induced separation between the light- and heavy-hole bands. In lattice-matched GaAs/(Ga,Al)As QDs the ground-state doublet is $|j_z| = 3/2$ - like in the low-confinement limit; as the QD size decreases there is a rapid cross-over to a $|j_z| = 1/2$ - like ground state in QDs of typical sizes. On the other hand, in strained InAs/GaAs QDs the ground state is always $|j_z| = 3/2$ - like and the splitting relatively large. The exchange coupling with the Mn spin $S = 5/2$ finally leads to a set of doubly degenerate energy levels, rather close to one another. Our results invalidate the previously adopted perturbative picture based on the bulk level scheme. We also study the lowest two-hole states: The ground state is a singlet almost uncoupled to the Mn spin. We deduce the zero-field fine structure of the excitonic transitions and compare our results with the experimental photoluminescence spectra [3] in Mn-doped InAs/GaAs QDs.

[1] A. K. Bhattacharjee and J. Pérez-Conde, Phys. Rev. B **68**, 045303 (2003); A. K. Bhattacharjee, *ibid.* **76**, 075305 (2007).
[2] L. Besombes *et al.*, Phys. Rev. Lett. **93**, 207403 (2004).
[3] A. Kudelski *et al.*, Phys. Rev. Lett. **99**, 247209 (2007).

SORPTIVE BEHAVIOUR OF NANOPOROUS MATERIAL AS MOLECULAR SIEVE FOR COMPRESSOR APPLICATIONS: A COMPUTATIONAL STUDY

B. Coto, A. Marcaide, G. Beobide, A. Aranzabe
Tekniker-IK4, Otaola 20,Eibar, Spain
bcoto@tekniker.es

Although esters are used as base oil for lubricants in applications as hydraulic and chainsaw oils and metalworking fluids, no biolubricants are known for compressor applications except for food industry. One of the main concerns of biolubricants is their performance which is improved using additives. The use of additives allows to increase the performance and physical properties of an oil but they also increase the cost of lubricants an may even be harmful to health or environment[1].

Our research aims to avoid the use of antioxidant additives in biolubricants for compressor applications by replacing them with a nanoporous material able to trap the oxidation products. In this way the development a nanoporous material based filter may lead to obtain a cost effective and environmentally friendly alternative to antioxidant additives.

Computational methods have become a tool to study absortive systems[2][3]. In this work Monte Carlo (MC) and Molecular Dynamics (MD) simulations have been carried out to study the absorption of oxidation products of an ester based biolubricant.

The ability of the material to absorb the oxidation products was obtained from the absortion isotherms and absortion isobars calculated by means of a configurational bias grand canonical monte carlo (CB-GCMC) method used to simulate the absortion of oxidation molecules at temperatures and pressures ranging from room conditions to the working conditions of a real compressor. Both surface and bulk sorption were studied. Isosteric heats, preferred absortion sites and minimum energy configurations have also been obtained. The configurations obtained from CB-GCMC were used as input for MD calculations in the NPT ensemble in order to study the dynamical behaviour of the system under compressor working conditions. Berendsen methods[4] were used to control temperature an pressure during simulations. The results obtained from MD simulations were used to calculate the diffusion coefficients of the molecules.

References:

[1] F.L. A. Lee; J.W. Harris. Lubricant additives. (2003) 575-577.
[2] S. Chempath, J. F. M. Denayer, K. M. A. De Meyer,G. V. Baron, R. Q. Snurr. Langmuir **20 (**2004), 150-156
[3] I. Daems, G. V. Baron, S. Punnathanam, R. Q. Snurr, and J.F. M. Denayer. J. Phys. Chem. C **111** (2007), 2191-2197
[4] Berendsen, H. J. C.; Postma, J. P. M.; van Gunsteren, W. F.; DiNola, A.; Haak, J. R., J. Chem. Phys., **81** (1984), 3684-3690.

Figures:

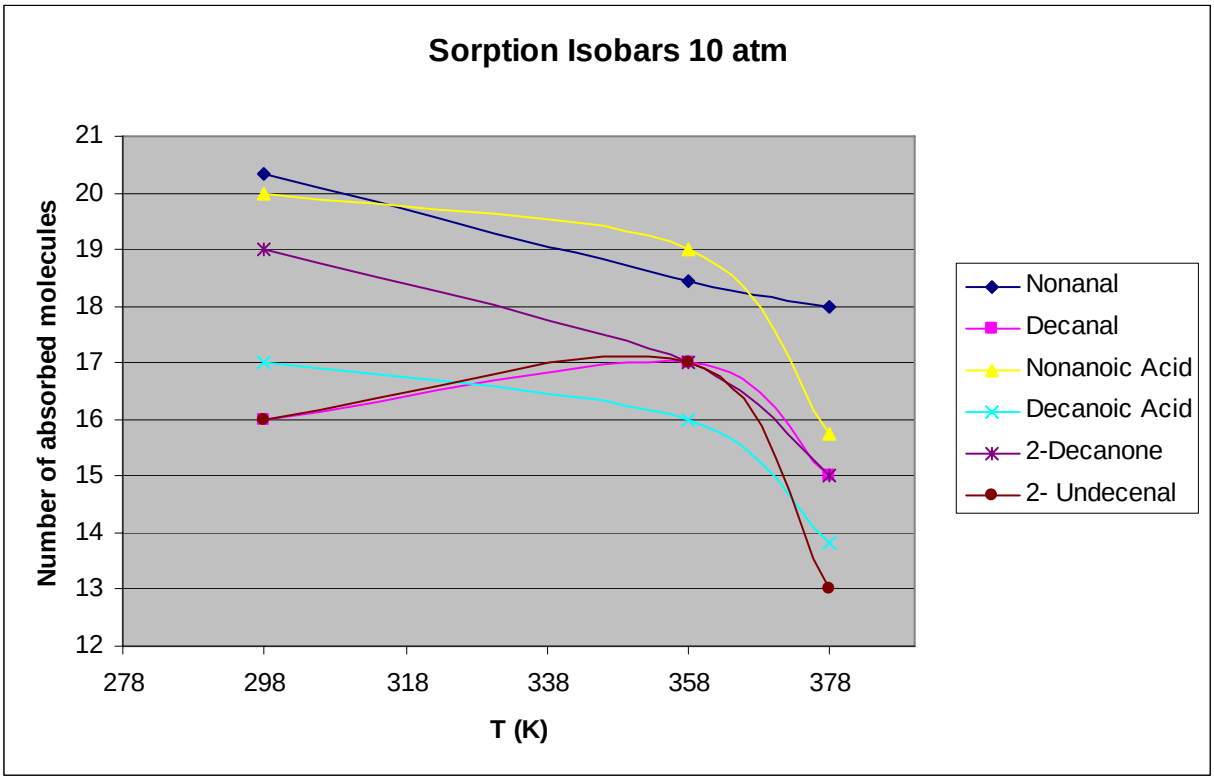

Figure 1. Sorption isobars for different oxidation products

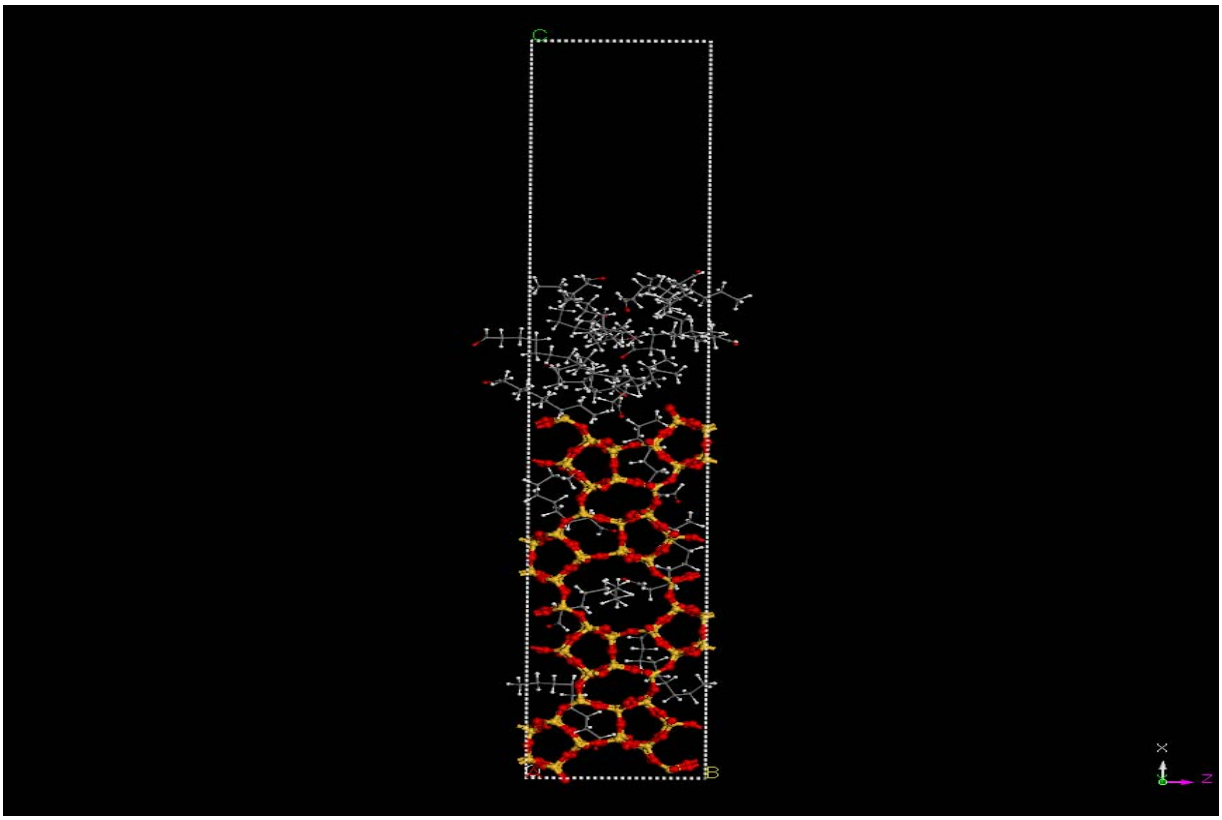

Figure 2. Minimun energy configuration from CB- GCMC calculations

THE EFFECTS OF EMBEDDING MEDIUM AND SIZE ON OPTICAL PROPERTIES OF II-VI CORE/SHELL NANOCRYSTALS

R.M. de la Cruz[1], C. Kanyinda-Malu[1,2], J. Iñarrea[1], F.J. Clares[1] and S.N. Santalla[1]

(1) Departamento de Física, EPS, Universidad Carlos III de Madrid, Av. de la Universidad 30, 28911 Leganés (Madrid), Spain.

(2) Departamento de Economía Financiera y Contabilidad II, FCJS, Universidad Rey Juan Carlos, Paseo de los Artilleros s/n, 28032 Madrid, Spain.
E-mail: rmc@fis.uc3m.es

Recently, a family of water-soluble quantum dots (QDs) that exhibit low nonspecific binding to cells, small hydrodynamic diameter, tunable surface charge, high quantum yield, and good solution stability across wide range of pH has been reported [1]. The choice of these high-yield QDs is based on their sizes, optical properties and toxicity. For imaging applications, the QD emission wavelength should ideally be in a region of the spectrum where blood and tissue absorb minimally but detectors are still efficient (approximately 700-900 nm) in the near-infrared. In addition, the hydrodynamic size of the QD should be appropriately matched to the biological molecules. To find good fluorescent labels for biological macromolecules, II-VI quantum dots enclosed in a II-VI semiconductor shell and both surrounded by organic or inorganic medium have been developed for a large number of applications (see for example ref. [2]).
The aim of this work is to investigate the optical properties (absorption, scattering and extinction) of II-VI core/shell nanostructures in a wide range of visible and near-infrared spectrum of light. In dipole approximation, the Mie scattering theory is applied to nanoshell systems to calculate the absorption, scattering and extinction coefficients [3]. To implement the calculations, Mie theory requires the dielectric function to be clearly defined. So, in this work an explicit expression of frequency-dielectric function for both the core and shell is used and it includes the phonon and plasmon contributions as defined in reference [4] i.e.,

$$\varepsilon_i(\omega)=\varepsilon_i(\infty)\left[1+\frac{\omega_{LO,i}^2-\omega_{TO,i}^2}{\omega_{TO,i}^2-\omega^2-i\gamma_i\omega}-\frac{\omega_{p,i}^2}{\omega^2+i\gamma_{p,i}\omega}\right] \qquad (i=1,2). \qquad (1)$$

In eq. (1), $\varepsilon_i(\infty)$ are the high-frequency dielectric constants of core (1) and shell (2) respectively; $\omega_{TO,i}$ and $\omega_{LO,i}$ the transverse and longitudinal frequencies of the polar modes and γ_i their damping constants; $\omega_{p,i}$ and $\gamma_{p,i}$ are respectively the frequencies and the damping constants of the plasmons for core and shell materials.
The system under investigation is described in figure 1 with its respective geometric sizes. Core and shell are embedded by an insulating medium with dielectric constant ε_3 (see figure 1).
Effects of shell-size and insulating media on the optical properties are investigated. As an example, we show in figure 2 the scattering coefficient of CdS/ZnS/glass nanoshell as a function of the wavelength for three different sizes of the shell. Clearly, the scattering coefficient is greater for increasing size of core/shell nanostructure and it decreases for increasing wavelength as it is predicted by experiments.

References:

[1] Kim, S.; Lim, Y. T.; Soltesz, E. G.; De Grand, A. M.; Lee, J.; Nakayama, A.; Parker, J. A.; Mihaljevic, T.; Laurence, R. G.; Dor, D. M.; Cohn, L. H.; Bawendi, M. G.; Frangioni, J. V. Near-infrared fluorescent type II quantum dots for sentinel lymph node mapping. *Nat. Biotechnol.* **22** (2004**)**, 93.
[2] Sullivan, S. C.; Woo, W.-K.; Steckel, J. S.;
Bawendi, M. and Bulovic, V., *Organic Electronics* **4** (2003), 123.
[3] Averitt, R.D.; Westcott, S. L. and Halas, N.J., *J. Opt. Soc. Am. B* **16** (1999) 1824.
[4] Demangeot, F.; Frandon, J.; Renucci, M.A.; Meny, C.; Briot, O. and Aulombard, R.L., *J. Appl. Phys*. **82** (1997) 1305.

Figures:

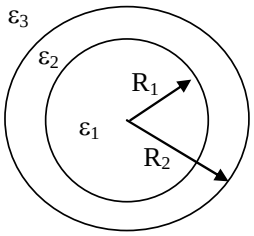

Figure 1: Scheme of a core/shell nanocrystal: ε_1 and ε_2 are frequency-dependent dielectric functions of the core and shell, R_1 and R_2 their respective radii .

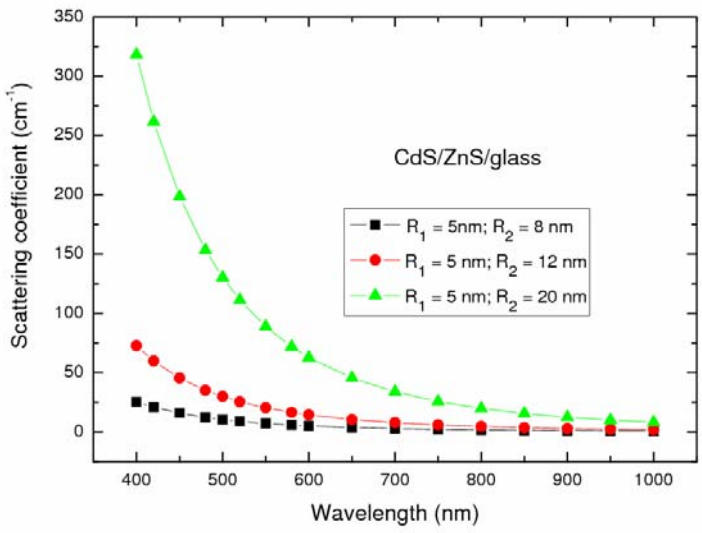

Figure 2: Scattering coefficient of CdS/ZnS/glass nanoshell versus λ (wavelength) for different values of shell-sizes.

GENERAL SOLUTION FOR INTERFACE OPTICAL PHONON MODES IN A DOUBLE NANOSHELL SYSTEM

F.J. Clares[1], C. Kanyinda-Malu[1,2], and R.M. de la Cruz[1]

(1) Departamento de Física, EPS, Universidad Carlos III de Madrid, Av. de la Universidad 30, 28911 Leganés (Madrid), Spain.

(2) Departamento de Economía Financiera y Contabilidad II, FCJS, Universidad Rey Juan Carlos, Paseo de los Artilleros s/n, 28032 Madrid, Spain.
E-mail: rmc@fis.uc3m.es

The study of electron-phonon interactions in low-dimensional quantum structures have attracted much interest [1] since this interaction plays a key role in many physical processes, such as transport or electron relaxation processes in confined systems. Due to the rapid progress in semiconductor nanotechnology, sophisticated systems such as multi-layer planar CQWs, multi-layer coupling quantum well wire (CQWW) and multi-shell coupling quantum dots (CQDs) [2] can be fabricated. Along with devices fabrication, the works on phonon modes were extended to these new systems. In fact, recently a study on interface optical phonon modes in a double nanoshell system has been reported [3].
Thus, the aim of this work is to generalize the solution of the electrostatic potentials generated by the interface optical modes in a double nanoshell system which was obtained in our previous work [3]. For this, we use the dielectric continuum model. To illustrate our results, typical II-VI semiconductors are used as constitutive polar materials of the nanoshells. In figure 1, we show the scheme of the investigated system. Resolution of Laplace´s equation in bispherical coordinates for the general potentials derived from the interface vibration mode is made. By imposing the usual electrostatic boundary conditions at the surfaces of the two-nanoshell system, recursion relations for the coefficients appearing in the potentials are obtained, which entails infinite matrices. The problem of deriving the interface frequencies is reduced to the eigenvalue problem on infinite matrices. A truncating method for these matrices is used to obtain the interface phonon branches. As an example, in figure 2 we show the interface frequencies for CdS/ZnS/polyethylene as a function of the geometrical parameter D/R_1 and a fixed value of D/R_2. Clearly, we obtain a clustered band-like phonon modes, feature appearing in other low-dimensional heterostructures such as superlattices.

References:

[1] Zhang, L.; Xie, H.J. and Chen, C.Y., *Phys. Rev.* B **66** (2002) 205326.
[2] Eychmüler, A.; Mews, A. and Weller, H., *Chem. Phys. Lett*. **208** (1993) 59.
[3] Kanyinda-Malu, C.; Clares, F.J. and de la Cruz, R.M., *Nanotechnology* **19** (2008) 285713.

Figures:

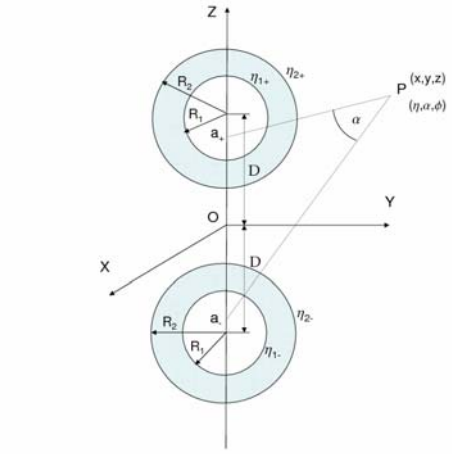

Figure 1: Scheme of the double coupled nanoshell system and the bispherical coordinates employed in the analysis with their respective parameters.

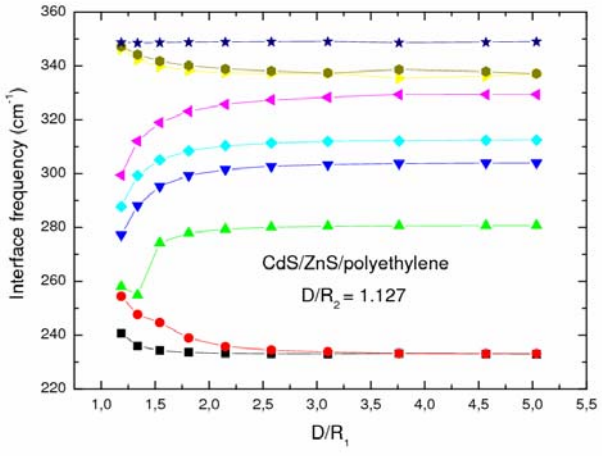

Figure 2: Interface frequencies of CdS/ZnS/polyethylene as a function of D/R_1.

Direct electrochemical detection of gold nanoparticles: application in magnetobiosensors

Alfredo de la Escosura-Muñiz [1,2], *Adriano Ambrosi* [2], *Marisa Máltez* [2], *Arben Merkoçi* [2]
[1] *Instituto de Nanociencia de Aragón, Universidad de Zaragoza, Zaragoza, Spain*
[2] *Institut Català de Nanotecnologia, Campus UAB, Barcelona, Spain*
alfredo.escosura.icn@uab.es

Nanobiotechnology can be defined as the branch of nanotechnology that uses its tools, components and processes for biosystem studies and applications. It is an interdisciplinary field, that integrates physical sciences, molecular engineering, biology, chemistry and biotechnology.

The development of nanobiosensors is one of the main research areas of nanobiotehcnology. In this context, electrochemical biosensors based on the use of nanoparticles (NPs) as electroactive labels offer several advantages in terms of sensitivity, selectivity, cost and time of analysis, etc. compared with the traditional methods of bioanalysis, such as ELISA or PCR.

Gold nanoparticles (AuNPs) stand out from the variety of nanoparticles used as labels in biosensing, due to their simple synthesis, narrow size distribution, optical and electrochemical properties and easy bioconjugation. These advantageous properties have given rise to an explosive growth of AuNP-based immuno and DNA electrochemical assays in the last years. The vast majority of these electrochemical methods have been based on chemical dissolution of AuNPs in a hydrobromic acid/bromine mixture followed by accumulation and stripping analysis of the resulting Au^{3+} solution. The HBr/Br_2 solution is highly toxic and therefore methods based on direct electrochemical detection of AuNPs tags, which would replace the chemical oxidation agent, are needed.

In the present work, a direct electrochemical detection route for detect AuNPs, without previous dissolving is used. This route consists in the in-situ electrochemical oxidation of AuNPs to $AuCl_4^-$ on the electrode surface, followed by immediate electro-reduction and registering the reduction process current [1]. This AuNPs detection strategy is approached for the determination of DNA [2] and proteins [3] in magnetobioassays, using micromagnetic beads (MBs) as support of the bioassays, and AuNPs as labels. These biosensors take advantage of the properties of the MBs as platforms for the bioreactions, in terms of selectivity and time of analysis, together with the electro-detection inherent advantages.

The developed biosensors are instrumentally simple to use, with low cost and portable instrumentation, and the samples volumes required are lower than those used in the traditional methods. The low levels of AuNPs detected with the electrochemical method allow the obtaining of biosensors with low protein and ss-DNA target detection limits, with special interest for further applications in clinical analysis, food quality and safety as well as other industrial applications.

References:

[1] Pumera, M.; Aldavert, M.; Mills, C.; Merkoçi, A.; Alegret, S. *Electrochim. Acta* **50** (2005) 3702-3707.
[2] Castañeda, M.T.; Merkoçi, A.; Pumera, M.; Alegret, S. *Biosens. Bioelectron*. **22** (2007) 1961-1967.
[3] Ambrosi, A.; Castañeda, M.T.; Killard, A.J.; Smyth, M.R.; Alegret, S.; Merkoçi, A. *Anal. Chem*. **79** (2007) 5232-5240.

THE EFFECT OF ELECTROCHEMICAL POTENTIAL ON CONDUCTANCE OF Au NANOCONTACTS

M. Díaz[1,2], M. Martín-González[1] and J.L. Costa-Krämer[1]

[1]*Instituto de Microelectrónica de Madrid, CSIC, Isaac Newton 8 PTM, 28760 Madrid, Spain*
[2]*Centro de Física, Instituto Venezolano de Investigaciones Científicas, Apartado 20632, Caracas 1020A, Venezuela*

marisel@ivic.ve

Conductance quantization of metal nanocontacts mechanically formed at RT has been studied recently in several electrochemical environments [1-5]. In these experiments, different reactions (i.e. adsorption or desorption of molecules or ions) at the metal surface can take place that can be controlled by the electrochemical potential of the nanocontact relative to a reference electrode in the electrolyte. At positive potentials, well defined peaks at integer multiples of G_0 ($2e^2/h$) are observed in the conductance histograms of Au (much like in air or vacuum), while under the hydrogen evolution reaction (negative potentials), a well defined fractional conductance peak appears near $0.5G_0$. In order to explain this fractional conductance several mechanisms (i.e. hydrogen incorporated wire, dimerized wire) have been proposed. However, the actual origin is not clear at present.

In this work we present conductance measurements on Au nanocontacts formed at room temperature in several solutions and under electrochemical potential control. Fig.1 shows the cyclic voltammogram of Au in the 0.1 M HNO_3 solution. The hydrogen evolution proceeds at potentials lower than ~ -0.3 V, while the double layer regime proceeds between ~ -0.3 V and 0.8V. Fig.2 shows the histograms of Au in this electrolyte at different electrochemical potentials. At 0.25V (double layer regime, Fig. 2c) the histogram shows peaks near integer values of G_0, but when the potential decreases (hydrogen evolution, Fig.2b and 2a), the width of these peaks and the background in the histograms increase and peaks appear at fractional values of G_0 (the most important at $0.3G_0$). At $0.5G_0$ a shoulder is observed in the histogram at -0.5V (Fig.2a) in contrast with the intense peak reported in previous works [1-5]. Similar results are found using different electrolytes. At negative electrochemical potentials is expected that cations, such as H^+ (H_3O^+) accumulate at the nanocontact, and they may act as impurities or disorder centers. This behavior could explain the increase in the width and background in the histograms with the negative potential in agreement with theoretical works [6].

References:

[1] C. Shu, C.Z. Li, H.X. He, A. Bogozi, J.S. Bunch and N.J. Tao, Phys. Rev. Lett., **84** (2000) 5196.
[2] B. Xu, H.X. He, S. Boussaad and N.J. Tao, *Electroch. Acta*, **48** (2003) 3085.
[3] M. Kiguchi, T. Konishi, S. Miura and K. Murakoshi, *Trans. Mater. Res. Soc. Jpn.*, **30** (2005) 1215.
[4] M. Kiguchi, T. Konishi, S. Miura and K. Murakoshi, *Phys. Rev. B*, **73** (2006) 125406.
[5] M. Kiguchi, T. Konishi, S. Miura and K. Murakoshi, *Nanotechnology*, **18** (2007) 424011.
[6] P. García-Mochales and P.A. Serena, *Phys. Rev. Lett.*, **79** (1997) 2316.

Figures:

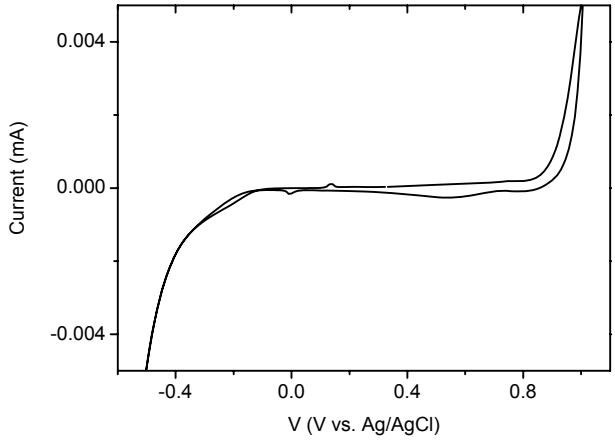

Fig.1. Cyclic voltammogram of Au electrode in 0.1 M HNO_3.

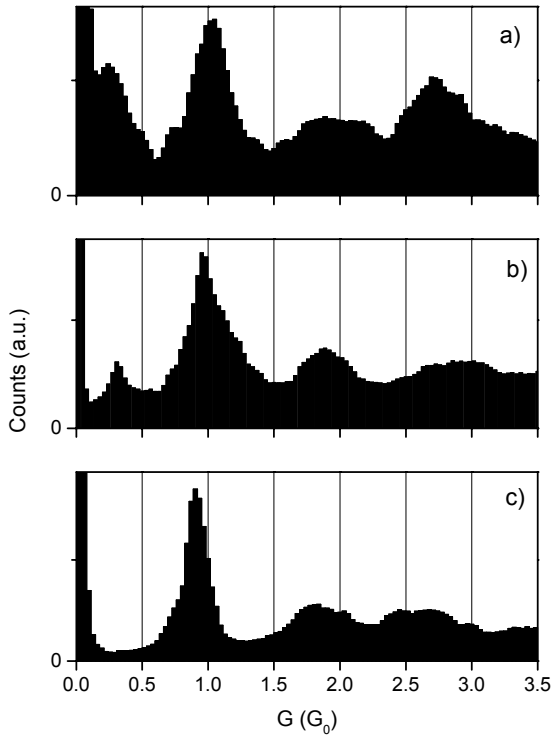

Fig2. Conductance quantization histograms of Au nanocontacts in 0.1 M HNO3 solution. The electrochemical potentials are: a) -0.5V, b) -0.3V and c) 0.25V.

STUDY OF COMPOSITIONAL INHOMOGENEITIES IN MAGNETIC Fe-Si AND Co-Si AMORPHOUS FILMS BY GRAZING INCIDENTE SMALL ANGLE SCATTERING (GISAXS)

Javier Díaz[(a)], Carlos Quirós[(a)], Francois Fauth[(b)], Alessandro Mirone[(b)] and Jose María Alameda[(a)]

[(a)]Departamento de Física, Universidad de Oviedo, Avenida de Calvo Sotelo s/n, 33007 Oviedo, Spain

[(b)]European Synchrotron Radiation Facility, 6 rue Jules Horowitz, BP 220, Grenoble Cedex, France

javidiaz@condmat.uniovi.es

GISAXS is a powerfull technique to determine density inhomogeneities at the nanometer scale in a medium like amorphous alloys, where borders between grains are extremely undefined due to the important diffusion between alloy components. Inhomogeneities in this kind of films have typical sizes of the order of tens of nanometers, resulting to be elusive to regular microscopical techniques like SEM, TEM, STM or AFM. However, they are easy to detect and measure by GISAXS. In the present work, the distribution, average size and shape of density inhomogeneities were extracted from the GISAXS spectra of magnetic Fe-Si and Co-Si amorphous films 20 nm thick by reproducing the experimental data (figure 1), calculating the x-ray scattering of alloy islands with different shapes embedded in Si using the Distorted Wave Born Approximation (DWBA). Fe-Si and Co-Si amorphous thin films owe their excellent soft magnetic properties to their extraordinary atomic disorder, which has been demonstrated by EXAFS spectroscopy [1]. Despite this atomic disorder, they have uniaxial magnetic anisotropy when Si is deposited at oblique incident angles, with the magnetic easy axis in the plane, and with anisotropy energies two orders of magnitud smaller than bcc Fe [2]. The same EXAFS studies showed the precipitation of Si rich transition metal environments. GISAXS demonstrated that the distribution of these environments was anisotropic, with their anisotropy axis linked to the magnetic easy axis found in the films. Si rich regions were observed mainly at the side of the islands exposed to the incident Si, resulting in a columnar growth of that side of the island with the magnetic silicide columns leaning toward the Si evaporator. This effect was stronger in the Co-Si films as a consequence of the lower interdiffusion of their elemental components as compared to Fe-Si [1]. Their magnetic easy axis was always parallel to this side of the islands. In the case of the Fe-Si films, the homogeneity of the films tested by GISAXS was significantly higher along their magnetic easy axis than in the hard axis direction.

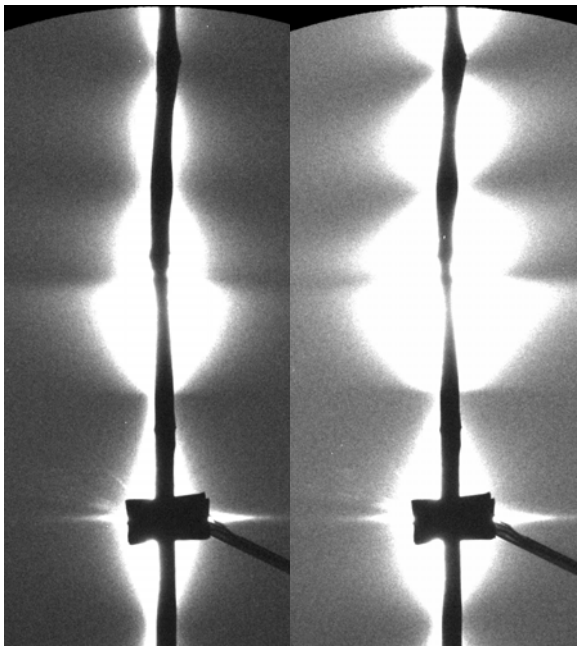

Figure 1. GISAXS images from a Co-Si amorphous 20 nm thick film. Left image, incident x-ray beam was perpendicular to the magnetic easy axis of the film. Right image, incident x-ray beam was parallel to the magnetic easy axis of the film.

References

[1] J. Díaz, R. Morales, M. Valvidares, and J. M. Alameda. Phys. Rev. B 72 (2005) 144413.1-15
[2] J. Díaz, M. Valvidares, R. Morales, and J. M. Alameda. Phys. Status Solidi A 203 (2006) 1409-1414

VARIOUS MAGNETIC NANOPARTICLES PREPARATION AND COMPARISON REGARDING BIOMEDICAL APPLICATION

Drbohlavová Jana [a], *Hrdý Radim* [a], *Adam Vojtěch* [b], *Kizek René* [b], *Hubálek Jaromír* [a]
[a] *Brno University of Technology, Faculty of Electrical Engineering and Communication, Department of Microelectronics, Údolní 53, Brno, Czech Republic*
[b] *Mendel University of Agriculture and Forestry, Faculty of Agronomy, Department of Chemistry and Biochemistry, Zemědělská 1, Brno, Czech Republic*
drbohla@feec.vutbr.cz

In few past years, magnetic nanoparticles (MNPs) have gained the great attention in medical and pharmaceutical applications due to their ability of drug delivery or various biomolecules separation [1, 2]. Iron oxide based-nanoparticles belong among most widely used materials in this field. Recently, more sophisticated Fe_2O_3 nanoparticles were synthesized by surrounding the magnetic core by amorphous silica shell, which could be further modified for better conjugation with various biological molecules [3]. SiO_2 protecting coating was found to be useful also in the case of paramagnetic gadolinium nanoparticles designed for multimodal contrast agent with optical and magnetic properties. However, the synthesis of such products is often time-consuming, so there is a demand to use rather a simple way of magnetic nanoparticles fabrication. This study is aimed to comparison of magnetic properties of silica coated samples with non-coated one prepared by simple precipitation method.

Next to previously reported techniques of Fe_2O_3/SiO_2 [4] and Gd/SiO_2 [5] preparation, we employ an easy co-precipitation method to fabricate Fe_2O_3 magnetic particles. $FeCl_2.4H_2O$ was mixed with K_2CO_3 under constant stirring up to pH 7, which results in the formation of black precipitate. After separation, the precipitate was dried for 15 min at 80 °C, then finely crushed in agate mortar and finally thermally treated for 4 hours at 200 °C in the oven. The obtained Fe_2O_3 powder was redish-brown in colour. These nanoparticles revealed the magnetic properties in water suspension when external magnetic field was applied. The resulting pH value of product was equal to 5.5.

SEM analysis showed that nanoparticles in all prepared samples tended to form the agglomerates with particle size less than 100 nm (Fig. 1). According to XRD measurement, haematite crystallographic form was observed as majority phase in the case of Fe_2O_3/SiO_2 annealed for 4 hours at 800 °C. We suppose, there are also very small maghemite or magnetite particles but they were not detected in XRD spectra probably due to “hiding” of their peaks in amorphous ones of SiO_2. Gd^{III}/SiO_2 nanoparticles were found to be completely amorphous. Fe_2O_3 powder consisted of 60% iron oxide and 30% of sylvite (KCl). Since X-ray powder diffraction cannot distinguish between maghemite and magnetite nanoparticles, Mössbauer spectroscopy analysis was performed in order to better determine Fe_2O_3 sample. The results showed the maghemite phase as dominant one (36%) with small portion of magnetite (6%) and some amorphous or very small iron oxide nanoparticles but for their more precise identification, a measurement in external magnetic field should be done. Moreover some superparamagnetic or paramagnetic component was detected in this sample. All three samples behaved as a very weak ferromagnetic material as can be seen from Fig. 2.

References:

[1] Lu A.-H., Salabas E. L., Schüth F., Angew. Chem. Int. Ed., **46** (2007) 1222.
[2] Arruebo M., Fernández-Pacheco R., Ibarra M. R., Santamaría J., Nanotoday, **2** (2007) 22.
[3] Ichiyanagi Y., Moritake S., Taira S., Setou M., J. Magn. Magn. Mater., **310** (2007) 2877.
[4] Ichiyanagi Y., Kimishima Y., J. Ther. Anal. Calor., **69** (2002) 919.
[5] Santra S., Bagwe R. P., Dutta D., Stanley J. T., Walter G. A., Tan W., Moudgil B. M., Mericle R. A., Adv. Mater., **17** (2005) 2165.

Acknowledgement: The financial support from the grant KAN 208130801 is highly acknowledged. The authors also gratefully thank to Dr. Oldrich Schneeweiss from Institute of Physics of Material of the Academy of Sciences of the Czech Republic for magnetization measurement.

Figures:

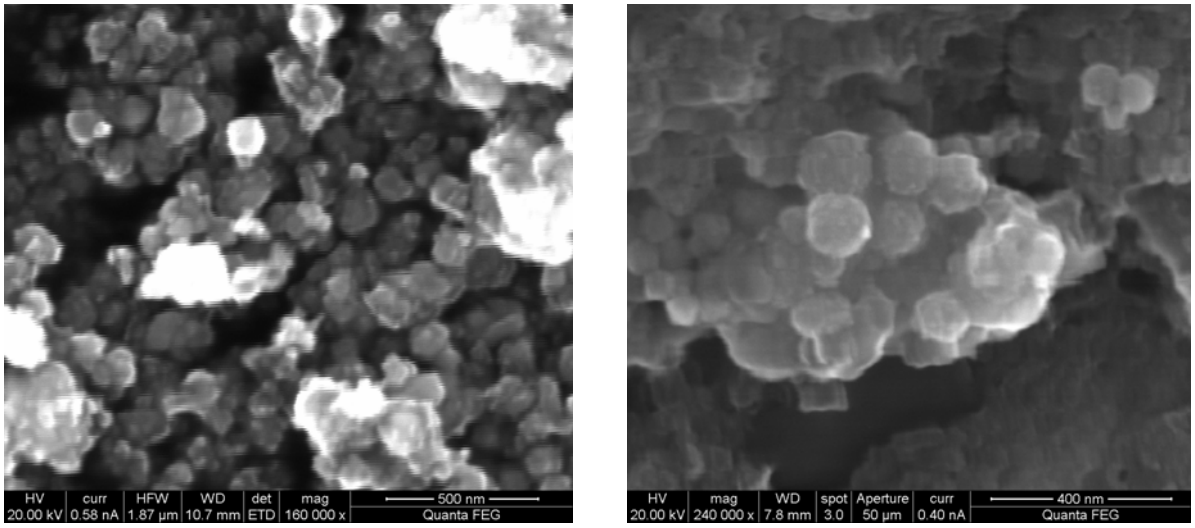

Fig. 1 *SEM image of Fe_2O_3 (left) and Gd^{III}/SiO_2 (right)*

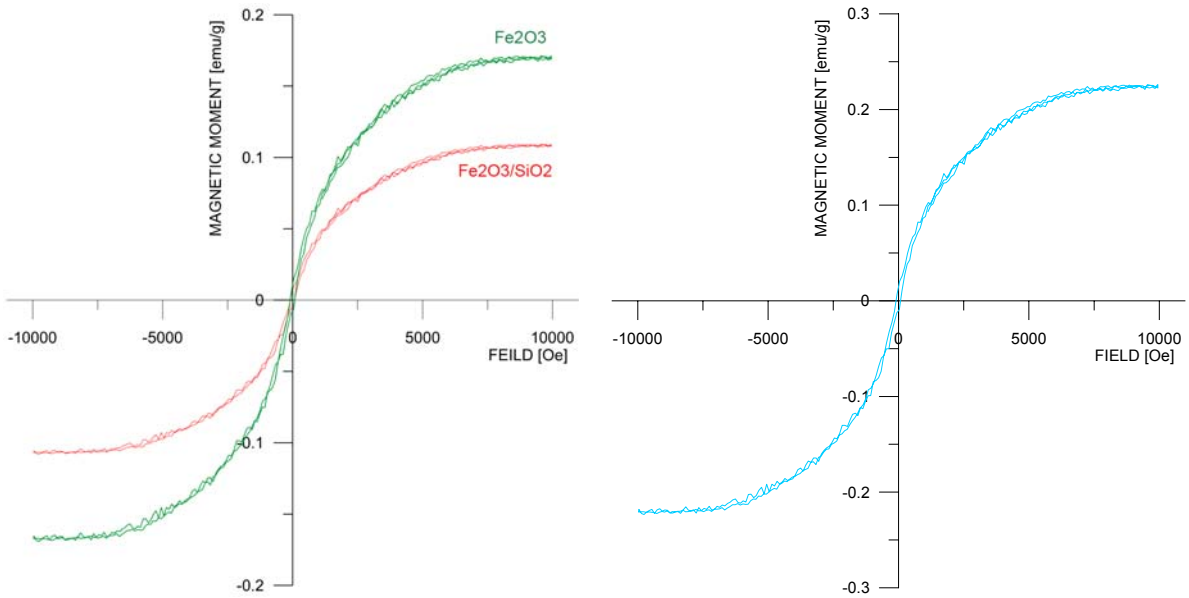

Fig. 2 *Magnetization curves of Fe_2O_3 and Fe_2O_3/SiO_2 (left) and Gd^{III}/SiO_2 (right)*

NANORODS GROWTH FROM SOLUTION BY A TEMPLATE APPROACH

M. Enculescu[1*], *R. Neumann*[2]
[1] *National Institute for Materials Physics, PO Box MG-7, 77125, Magurele, Romania;*
[2] *Gesellschaft fur Schwerionenforschung (GSI), Planckstr. 1, D-64291, Darmstadt, Germany.*
* Corresponding author: mdatcu@infim.ro

Fabrication of nanostructures with tailored morphology attracted an increased interest during the last decade, due mainly to the wide field of potential applications [1]. In order to achieve the goal a large number of preparation techniques ware developed. One such fabrication approach is represented by the so called template technique [2]. Thus, nanoporous membranes such as ion track polymer foils or anodic alumina are used as templates; by filling the pores with the desired material nanowires or nanotubes are obtained. Various techniques were applied for filling the pores such as electrochemical deposition or electroless plating [3, 4].
In this paper we present our results regarding solution growth of nanorods by employing a template approach.
Polycarbonate foils (30 and 100 micrometers thick) were prepared by swift heavy ions irradiation (e.g. Au with 11.4 MeV/nucleon) and subsequent etching. We employed an aqueous 5M NaOH etching bath at 50 °C, conditions which have as a result cylindrical pores with the diameter as a function of etching time (2 micrometers/hour etching rate).
These foils were further used as templates using a solution growth approach for filling the pores. We grew different types of rods of water soluble materials such as alkali-halides (NaCl, KCl) or potassium acid phthalate (KAP) both pure and doped with luminescent dyes.
The algorithm for preparation was extremely simple and consisted in dipping the membrane in a solution close to saturation. Slow evaporation resulted in complete saturation being obtained. In order to observe the rods by electron microscopy the foils were partially dissolved in dichlormethane. The growth of the material took place both inside the pores and onto the membranes surface. In Fig. 1 rods of alkali halides are presented. As one can see in Fig. 1 (b) the membranes are faceted showing the single crystalline growth tendency.
In Fig. 2 rods of potassium acid phthalate, also grown from solution are presented. Again it can be observed that the rods present facets, a consequence of single-crystalline growth.
The approach allowed the preparation of such KAP rods doped with fluorescent dyes such as rhodamine, dyes which are typically employed for dye lasing. The fluorescence properties of these dye doped nanorods were measured. Due to the combination between the lattice of the host (KAP) and the luminescence of the dye, up conversion phenomena were evidenced.
Such nanorods can be successfully employed as ultraminiaturized light sources for a wide field of applications ranging from communications and optoelectronics to life sciences.

Acknowledgments

The authors gratefully acknowledge the financial support of the Romanian Ministry of Education and Research (Projects CEEX 2/2006 and PNII 30/2007).

References:

[1] Cui, Y., Lieber, C., Science, **291** (2001) 851
[2] Martin, C. R., Science, **266** (1994) 1961
[3] Enculescu, I., Siwy, Z., Dobrev, D., Trautmann, C., Toimil Molares, M.E., Neumann, R., Hjort, K., Westerberg, L., Spohr, R., Copper nanowires electrodeposited in etched single-ion track templates, Appl. Phys. A, **77** (2003) 751
[4] Bercu, B., Enculescu, I., Spohr, R., NIM B, **225/4** (2004) 502

Figures:

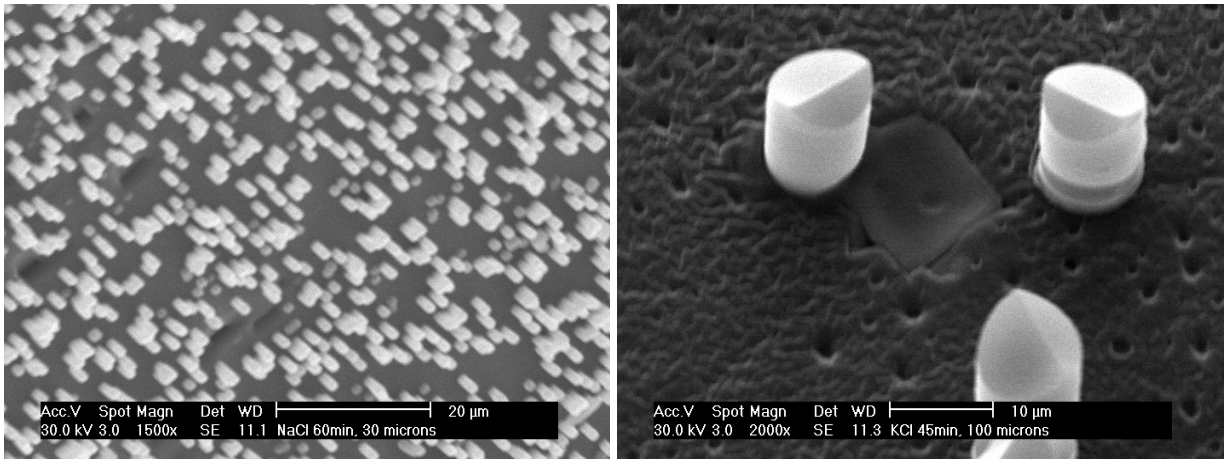

Figure 1. Alkali halide rods (a) NaCl and (b) KCl grown by the template method.

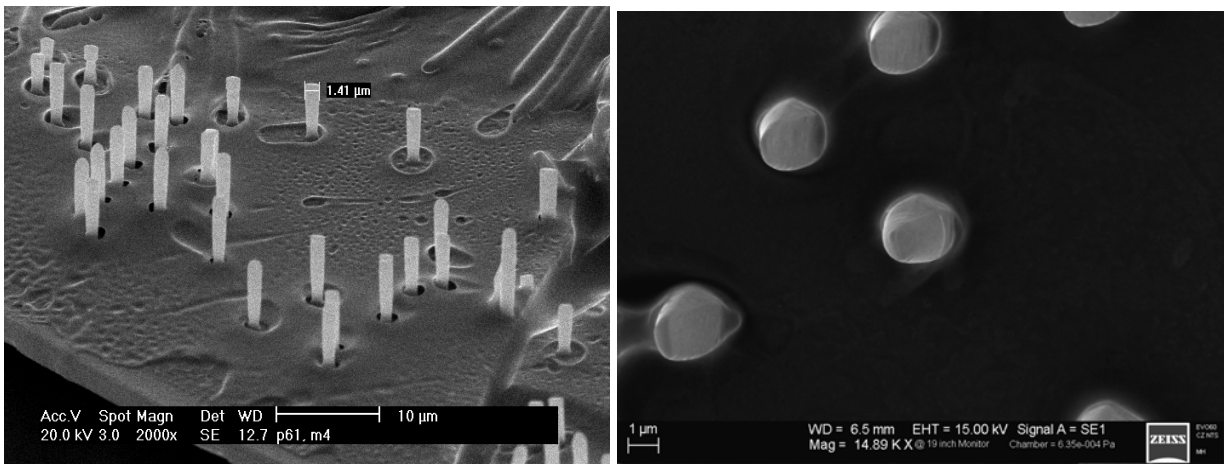

Figure 2. KAP rods grown from solution.

NANOCONES ON (a-C:H):Si FILMS: BASIC CONDITIONS FOR PROCESSING AND OPTICAL PROPERTIES

V.D. Frolov[1], *A.V. Khomich*[2], *V.V. Kononenko*[1], *V.A. Gerasimenko*[1], *S.M. Pimenov*[1], *G.G. Kirpilenko*[3], *V.I. Kovalev*[2], *E.Y. Shelukhin*[3]

[1] *A.M. Prokhorov General Physics Institute of RAS, 38 Vavilov str., Moscow, Russia*

[2] *Institute of Radiotechnics and Electronics of RAS, 1 Vvedensky sq., Fryazino 141190, Russia*

[3] *Patinor Coatings Ltd., NIIMV, Zelenograd, Moscow 103460, Russia*

Contact e-mail: frolov@ran.gpi.ru

Amorphous (a-C:H):Si thin films attract great interest due to unique combination of mechanical, electrical, optical and thermal properties. Functional and technological opportunities of micro-electromechanical systems (MEMS) and optoelectronic systems (OES) can be broadened significantly with genesis of thermally stable resistive micro-heaters and emitters on the base of metal-containing (a-C:H):Si films [1]. Recently a new effect of Scanning Probe Microscopy (SPM) -based nanostructuring, namely the electric field–assisted growth of nanocones, was observed in metal-free (a-C:H):Si films [2]. The SPM process was found to be highly reproducible thus realizing nanocone arrays with a preassigned configuration.

In the present work, we report the inner properties (atomic content and structure, sp^2/sp^3 bond ratio, surface morphology and energy) and external conditions, in the presence of which the metal-free (a-C:H):Si films show ability for the nanocone growth. The experiments were done with the 50-200 nm thick (a-C:H):Si films, deposited on Si substrates by CVD method, where silicon-organic liquid was used as a plasma-forming substance of the open plasmatron. Under optimal conditions, the electric field-induced SPM actions on the film surface lead to the formation of nanocones up to 100 nm in height. Special emphasis is paid for optical parameters of the (a-C:H):Si films before and after the SPM actions. It is distinctive that for the untreated region the refraction index is n=2.15-2.2 (in the spectral range of 400 – 700 nm), and decreases to n~ 1.6 after the SPM-actions. In the same spectral range the extinction coefficient inside the modified region becomes close to zero. Raman spectra evidence about ordering the film atomic structure under the SPM actions.

Possible mechanism of the SPM-based nanostructuring is discussed.

The work was supported by the Russian Foundation for Basic Research, project no. 07-02–12090.

References:

[1] V.K. Dmitriev, V.N. Inkin, G.G. Kirpilenko, B.G. Potapov, E.A. Ilyichev, E.Y. Shelukhin, Diamond and Related Materials **10** (2001) 1007.
[2] G.G. Kirpilenko, E.Y. Shelukhin, V.D. Frolov, E.V. Zavedeev, S.M. Pimenov, Diamond and Related Materials **15** (2006) 1147.

CHARACTERIZATION OF ICOSAHEDRAL METALLIC NANOWIRES FORMED UNDER STRETCHING

S. Peláez [1], P.A. Serena [1], P. García-Mochales [2,], R. Paredes [3], C. Guerrero [4]*

[1] *Instituto de Ciencia de Materiales de Madrid, Consejo Superior de Investigaciones Científicas, c/ Sor Juana Inés de la Cruz 3, Cantoblanco, E-28049-Madrid, Spain*

[2] *Dept. Física de la Materia Condensada, Facultad de Ciencias, Universidad Autónoma de Madrid, c/ Tomas y Valiente 7, Cantoblanco, E-28049-Madrid, Spain*

[3] *Centro de Física, Instituto Venezolano de Investigaciones Científicas, Apto. 20632, Caracas 1020A, Venezuela*

[4] *Departamento de Física, Facultad Experimental de Ciencias, La Universidad del Zulia, Maracaibo, Venezuela*

[*] *e-mail: pedro.garciamochales@uam.es*

Icosahedral or pentagonal nanowires are formed by subsequent staggered parallel pentagonal rings (with a relative rotation of $\pi/5$) connected with single atoms, showing a characteristic -5-1-5-1- ordering. These structures have been found on simulated nanowires of different species [1-5]. However, the statistical study of their formation has been only addressed for Ni up to date [4,5]. It has been shown that that [100] and [110] stretching direction favour the appearance of long pentagonal nanowires [4,5], and that there exist an optimal temperature at which the pentagonal nanowire yield is maximized [5].

In [4,5] a method based on the time that the breaking nanowire lasts with a cross section S_m~5 (close to that corresponding to a pentagonal ring) was used to detect the formation of -5-1-5- structures. This measure gives a qualitative value of the length of the pentagonal nanowire formed, but not its actual value (deformations of non-pentagonal regions of the simulated nanowire can increase the total nanowire length without an increase the pentagonal zone length). This method can not determinate either the number of pentagonal rings that form the tubular structure. In order to overcome its limitations, in this paper we present an algorithm that allows the automatic identification of pentagonal rings structures as well as the determination of the actual pentagonal nanotube length L_p. With this new tool we have revisited the Ni case, and extended to Al and Cu the statistical analysis of the formation of pentagonal nanowires.

The algorithm is based in the determination of the angular distribution of the nearest-neighbors atoms and provides a parameter α that measures such angular distribution. The average of α ($\langle\alpha\rangle$) over a 1Å thickness slabs differentiates between pentagonal and non-pentagonal structures. If the parameter $\langle\alpha\rangle<0.5$, the set of atoms inside the slab forms a structure similar to that of a pentagonal ring. On the contrary, if $\langle\alpha\rangle>0.5$ the structure presents another structure (bulk like or disordered). Figure 1 illustrates the use of the α-parameter for a nanowire with pentagonal structures.

We have obtained for different conditions (crystalline orientation, initial size and temperature), the distribution of lengths of the pentagonal wire L_p as well as the probability distribution of the number of pentagonal rings n_p before the nanowire breaking. An example of these distributions is shown in the left panel of Figure 2. In order to summarize the large amount of computed data we have constructed the cumulative probability of finding a tubular nanowire containing at least a given number (n_p) of pentagonal rings. From this figure it can be conclude that, for aluminium and this initial size, the optimal temperature for obtaining longer pentagonal nanowires is close to 300K, where we have found nanowires with up to 16 pentagonal rings.

References:

[1] H. Mehrez and S. Ciraci, Phys. Rev. B **56**, 12622 (1997); O. Gülseren, F. Ercolessi and E. Tosatti, Phys. Rev. Lett. **80**, 2775 (1998); J. C. González, V. Rodrigues, J. Bettini, L. G. C. Rego, A. R. Rocha, P. Z. Coura, S. O. Dantas, F. Sato, and D. S. Galvao, and D. Ugarte, Phys. Rev. Lett. **92**, 126102 (2004).

[2] H. S. Park and J. A. Zimmerman, Scripta Materialia **54**, 1127 (2006).

[3] P. Sen, O. Gülseren, T. Yildirim, I.P. Batra, and S. Ciraci, Phys. Rev. B **65**, 235433 (2002).

[4] P. García-Mochales, R.Paredes, S. Peláez and P.A. Serena, Journal of Nanomaterials **2008**, 361464 (2008); P. García-Mochales, R.Paredes, S. Peláez and P.A. Serena, Nanotechnology **19**, 225704 (2008)

[5] P. García-Mochales, R.Paredes, S. Peláez and P.A. Serena, Phys. Stat. Sol. (a) **205**, 1317 (2008)

Figures:

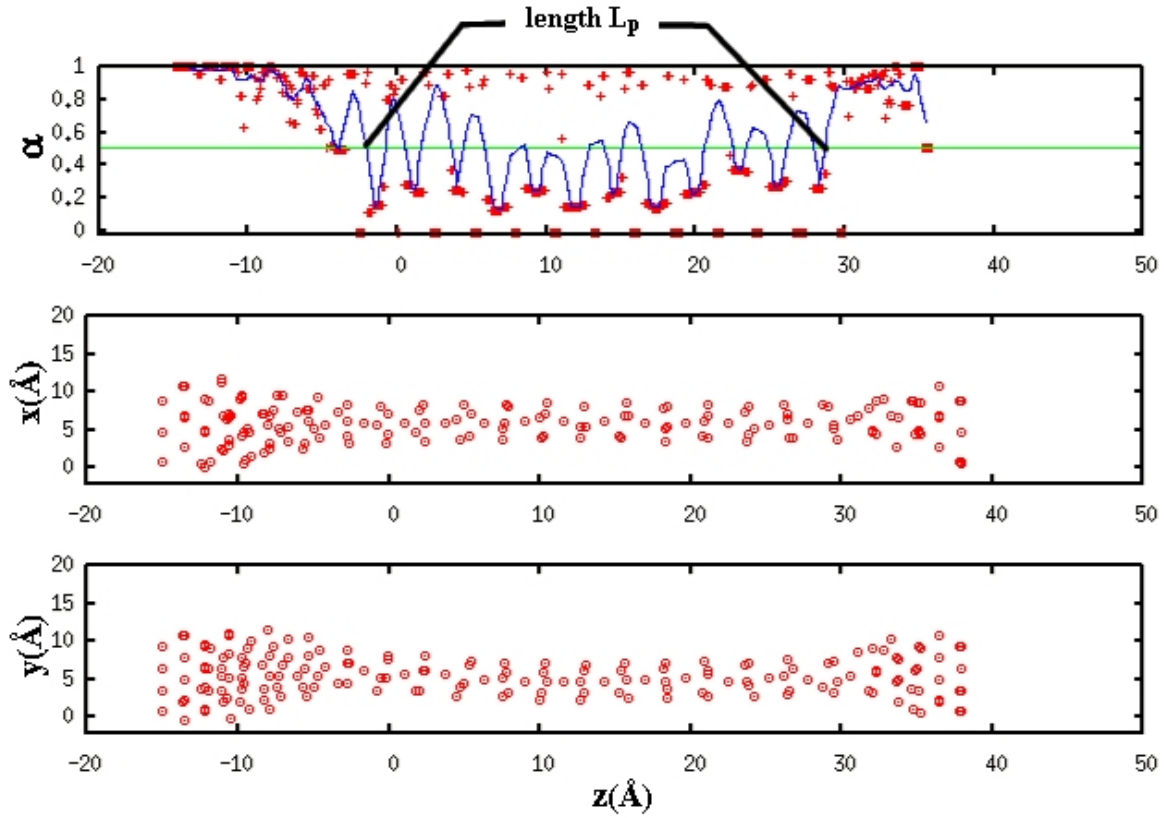

Figure 1: xz (middle) and yz (bottom) projections of the atomic coordinates of a test configuration of a simulated Al nanowire with 204 atoms stretched along the [100] direction at 300K. (top) Value of the α -parameter (red dots) and its average ‹α› (blue line) along the nanowire. The green line is the reference value ‹α›=0.5. L_p is the pentagonal nanotube length as defined from the maximum and minimum z coordinates satisfying ‹α›=0.5.

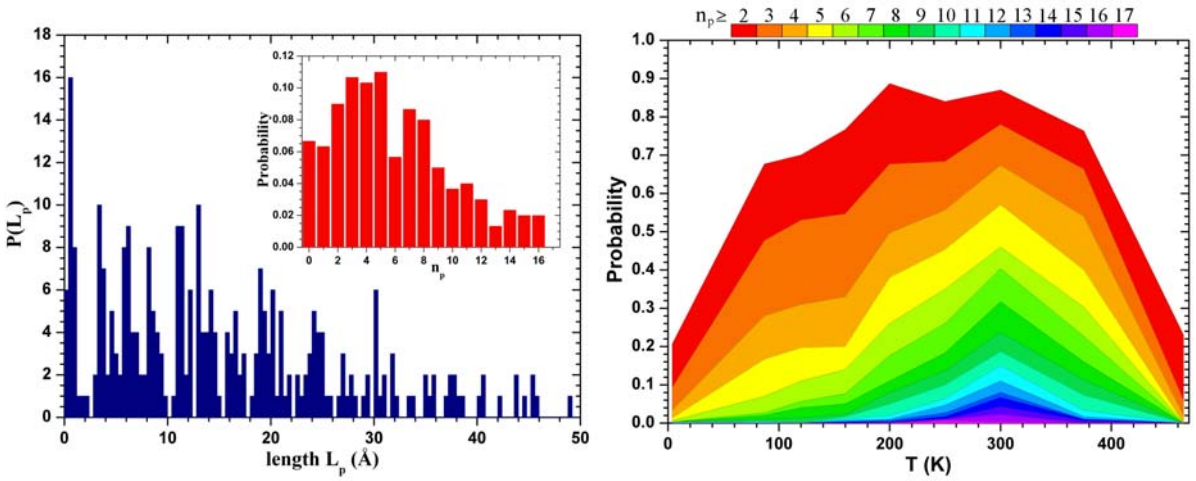

Figure 2: (Left) Pentagonal tube length distribution $P(L_p)$ and probability distribution of the number of pentagonal rings n_p for nanowires of Al stretched along the [110] direction and 204 atoms at 300K. (Right) Temperature dependence of the probability of finding a pentagonal nanotube with n_p or more pentagonal rings for Al nanowires containing 204 atoms stretched along the [110] direction.

GROWTH OF IAs AND InP NANOSTRUCTURE ON GaP SUBSTRATE FOR PHOTONICS ON SILICON

W. Guo, A. Bondi, B. Alsahwa, C. Cornet, A. Létoublon, N. Chevallier, H. Folliot, A. Le Corre, J. Even and S. Loualiche
CNRS UMR 6082 FOTON, INSA, 20 Avenue des Buttes de Coësmes, CS 14315, 35043 RENNES Cedex FRANCE
Weiming.guo@insa-rennes.fr

Realizing active nanostructure on GaP substrate (nearly the same lattice parameter with the silicon) which emits in the transparency region of the Silicon is the first step to achieve a light-emitter monolithically grown on Silicon.[1] This would lead to reach the so-called electronic-optical very large scale integration. In(As)P nanostructure embedded on GaP substrate is attractive because of its predicted direct low bandgap energy, and also because large lattice mismatch between InAs and GaP (≈ 11%) ensures quantum dots formation. For these reasons, the InAsP/GaP system is interesting for practical use, but also for theoretical understanding.

First, growth of InAs QDs on GaP has been performed and structural datas were extracted from Atomic Force Microscopy (AFM) measurements. The amount of deposited InAs is changed to observe the influence of thickness on structural properties of InAs QDs (diameter and density). An increase of density and a decrease of diameter with increasing of thickness deposited is observed. The critical thickness for the formation of InAs Qds is measured to be 1.2-1.5ML, assuming a stransky-krastanov growth mode, as shown in fig. 1(a). These results are in opposition with those found by Leon et al. [2]

From these pictures, it is also shown that the measured volume of quantum dots is larger than the deposited InAs Volume (fig. 1(b)), which tends to prove that QDs are not pure InAs dots. However, photoluminescence has not been observed from these quantum dots. It is interpreted in term of partial plastic strain relaxation in QDs.

We also tried to grow InP QDs on GaP with a variation of thickness changed from 2 to 6 ML, without any capping layer for AFM measurements (cf. Fig. 2). Critical thickness is determined to be between 2 and 2.3 ML. Structural properties are extracted from theses datas. Comparison is also made with the work presented by Hatami et al. [3] The question of growth mode is discussed. [4]

Finally, photoluminescence is performed using a CW 405 nm, 50 mW laser from 10 K to room temperature. While no signal can be found on the rich variety of various samples performed on the InAs/GaP system, a clear signal can be extracted until 140 K for both GaP substrate and InP nanostructures. The structures defined for the AFM on previous samples (with 2, 3, 4, 5 and 6 ML), are capped. However, no shift of the wavelength can be measured, raising the question of the nature of optical emission, that could be due to the wetting layer, to QDs constant shape, or to energy levels due to interfaces. Further experiments will be performed to understand this behavior.

In conclusion, InAs and InP nanostructures have been grown on GaP substrate by MBE. AFM images confirm the formation of InAs and InP QDs and photoluminescence signal has been detected in the InP/GaP system.

References:

[1] I. Hayashi, "Optoelectronic devices and material technologies for photo-electronic integrated systems", Jpn. J. Appl. Phys. **32,** 266 (1993).
[2] R. Leon, C. Lobo, T. P. Chin, J. M. Woodall, S. Fafard, S. Ruvimov, Z. Liliental-Weber, M. A. Stevens Kalceff. "Self-forming InAs/GaP quantums dots by direct island growth", Appl. Phys. Lett. **72**, 1356 (1998).
[3] F. Hatami and W. T. Masselink, "radiative recombination from InP quantum dots on (100) GaP", Applied Physics Letters **78**, 2163 (2001).
[4] István Daruka and Albert-László Barabási, Phys. Rev. Lett. **79**, 3708 (1997).

Figures:

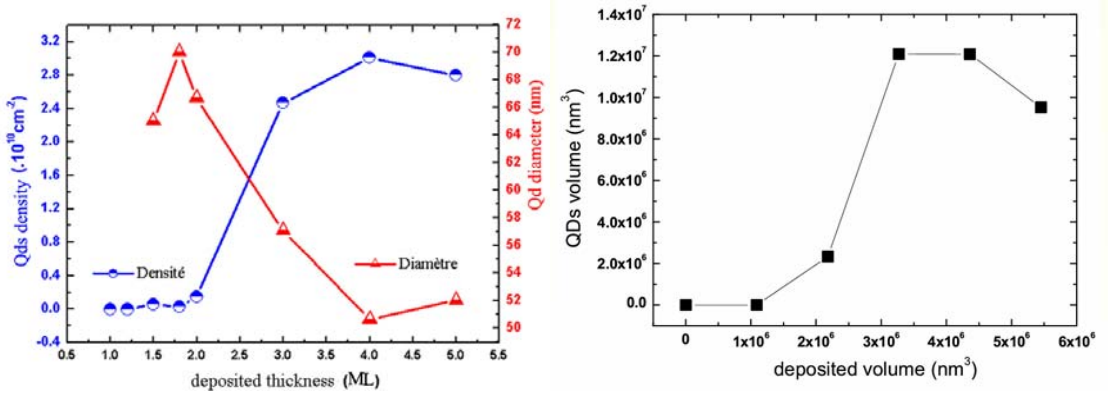

Fig. 1 : (a) Evolution of the density and diameter of InAs/GaP QDs with thickness (grown under 0,3 SCCM AsH_3 et 450°C) and (b) estimation of the QDs volume as a function of the deposited InAs volume

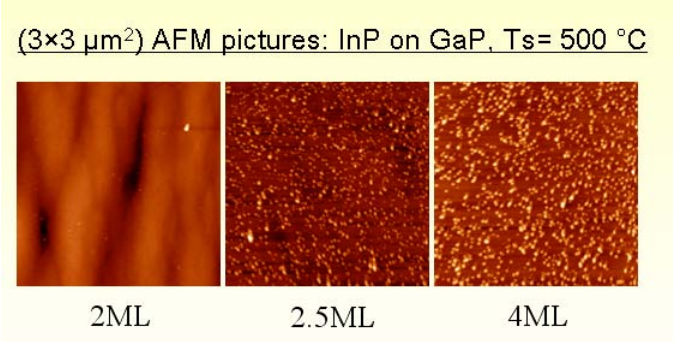

Fig. 2 : 3*3 µm² AFM pictures from InP/GaP quantum dots with respectively 2, 2.5 and 4 ML deposited

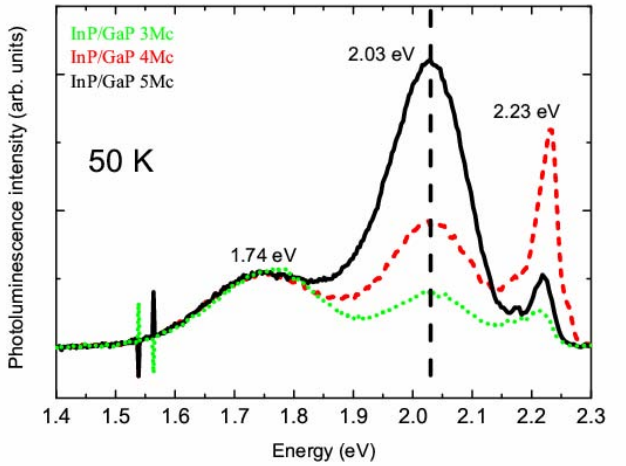

Fig. 3 : Photoluminescence emission from InP deposited on GaP with respectively 2, 2.5 and 4 ML of InP grown

Highlighting excitonic optical properties of bundled carbon nanotubes to tailor novel nanomaterials-based devices

M. Gicquel-Guézo[(1)], H. Nong[(1)], C. Labbé[(1)], A. Moréac[(2)], S. Loualiche[(1)]

[(1)]FOTON, UMR CNRS 6082, INSA, Avenue des Buttes de Coësmes CS 14315 35043 Rennes Cedex, France
[(2)]IPR, UMR CNRS 6251, Université Rennes1, 263 avenue du Général Leclerc, 35 042 Rennes Cedex, France
maud.gicquel@insa-rennes.fr

The original excitonic optical properties of carbon nanotubes (CNT) [1,2] confer great potential on these 1D-nanomaterials for direct telecommunications applications around 1,55µm. Nowadays, all-optical regeneration of telecom signal, in high-bit-rate optical fibre transmission systems, need still more efficient optical devices, such as saturable absorbers (SA) with ultrafast optical response time and great ratio between ON/OFF states. Excitonic optical properties of nanomaterials- based SA, such as quantum wells (QW) nanostructures (2D-nanomaterials), have already demonstrated huge potential for such signal regeneration [3], in comparison to bulk materials. However, fabrication of these ultrafast 2D-nanostructures-based SA need complex and expensive growth technique, and QW-doping [4] or QW-irradiation [5] techniques have been developed to reduce typical nanosecond QW nanostructures optical response time down to subpicosecond range, required for high-bit-rate signal regeneration. Thus, ultrafast absorption dynamics and large 1D-excitonic nonlinearities of bundled CNT [6] make them intrinsically and potentially as prime candidate to replace QW-based SA. In this way, we have deposited CNT on glass, Si or photolithographied-InP substrates, from nitrogen-brushed NMP-dispersion containing CNT. We also extend the well-controlled microtechnology techniques developed for III-V semiconductor nanostructures-based devices (quantum wells, wires and dots) to CNT-based SA realization. Quality of technological process used for CNT deposition is analyzed by Scanning Electron Microscopy (SEM). Vibrational properties of CNT-based SA are characterized by Raman spectroscopy using 785nm-pump laser diode, and will be presented too. This invasive and useful optical experiment reveals vibrational modes and typical features of CNT [7]: radial breathing mode (RBM), defect-mode D and tangential modes G. The position of RBM mode provides first useful information, as it depends inversely to CNT-diameter [8]. This estimation of CNT-diameters provides first optical Van-Hove transition energy of semiconductor CNT, thanks to Kataura plot, which can be exploited for telecom applications near 0,8eV (1,55µm). Furthermore, the Raman spectra and SEM pictures show a relatively good reproductibility of our CNT-based SA, from fabrication (HiPCO from CNI *Inc.*) to deposit technological process.

Dynamics of nonlinear optical properties of CNT-based SA are highlighted by femtosecond-pulses cross-polarized degenerate pump-probe experiment. Figure 1 shows temporal evolution of normalized differential transmissions ($\Delta T/T_0$) of CNT-based and doped-QW-based SA for comparison (see ref [4] for details on doped-QW SA). A significant reduction of monoexponential response time by

using CNT as efficient and relatively low-cost nanomaterials instead of doped-QW for SA applications is demonstrated (divided by ten factor), keeping an encouraging good contrast ratio for CNT–based SA. Studies on power and wavelength dependence of these excitonic nonlinear optical properties in telecom wavelength range (ultrafast response time and contrast ratio) are in progress.
This project is labeled by french “Image et Réseaux” competitiveness pole and supported by french “Agence Nationale de la Recherche”.

References:

[1] Ma *et al.*, Phys. Rev. Lett., **94** (2005) 157402.
[2] Korovyanko *et al.*, Phys. Rev. Lett., **92** (2004) 017403.
[3] Gay *et al.*, IEEE Photon. Technol ; Lett., **18** (2006) 1273.
[4] Guézo *et al.*, Appl. Phys. Lett., **82** (2003) 1670.
[5] Mangeney *et al.*, Appl. Phys. Lett., **76** (2000) 1371.
[6] Lauret *et al.*, Appl. Phys. Lett., **85** (2004) 3572.
[7] Dresselhaus *et al.*, Phys. Rep., 409 (2005) 47.
[8] Bachilo *et al.*, Sience, **298** (2002) 2361.

Figure:

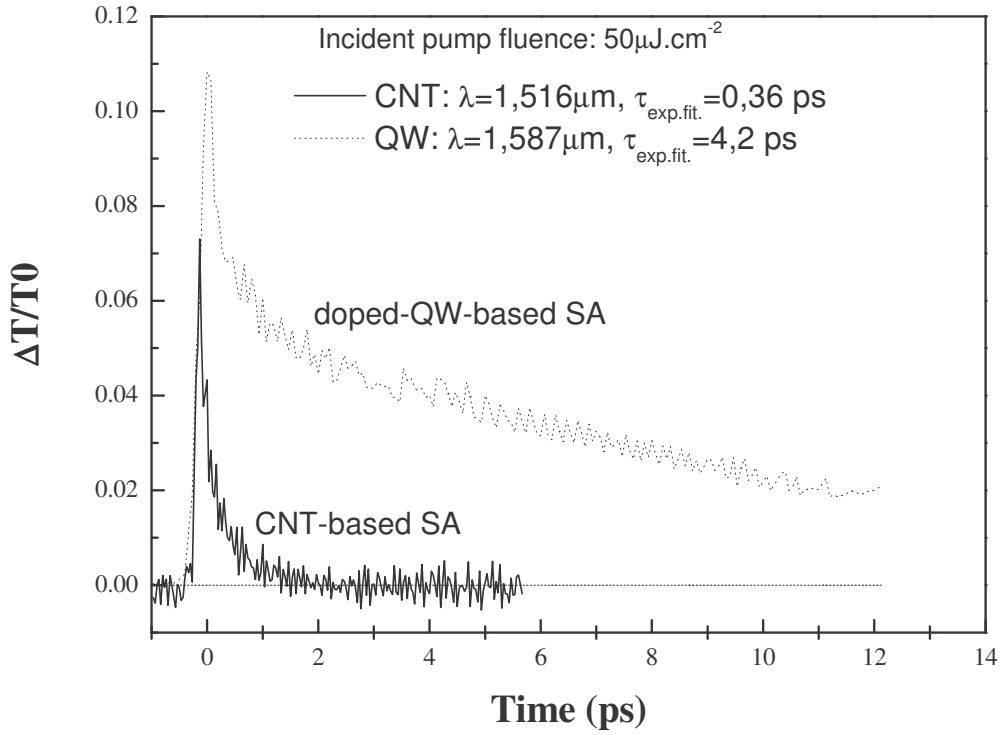

Figure 1: Ultrafast dynamics of CNT-based and doped-QW-based-SA. Degenerate pump and probe wavelengths, in resonance with first semiconductor nanomaterials optical transition, and fitted monoexponential response times are mentioned. Dashed line at zero level is a guide for the eye.

LIGHT EMITTING DIODES ON SILICON SUBSTRATES: PRELIMINARY RESULTS

A. BONDI, W. GUO, L. PEDESSEAU, S. RICHARD, H. FOLLIOT, C. CORNET, C. LABBE, M. GICQUEL, A. LE CORRE, J. EVEN, A. MOREAC, S. LOUALICHE*
CNRS UMR 6082 FOTON, INSA, 20 Avenue des Buttes de Coësmes, CS 14315, 35043 RENNES, France
**I.P.R. UMR-CNRS n°6251, Université Rennes1, Campus de Beaulieu - 35042 Rennes, France*
Alexandre.Bondi@ens.insa-rennes.fr

Silicon is the most widely used semiconductor in microelectronics industry but it presents an indirect bandgap unable to produce photons efficiently. GaP is almost lattice matched to silicon but it also has an indirect bandgap which does not allow photon emission in the transparency region of silicon. We therefore propose to grow quantum dot (QD) or quantum well (QW) light-emitting diodes by molecular beam epitaxy to obtain direct band gaps on GaP grown onto Si (**Fig. 1**). The major challenge for a GaP-based diode (**fig 1-a**) is to process a good active zone. For the GaP/Si-based diode (**fig 1-b**), the interface quality between GaP and Si is thus very important. Finally, we theoretically consider the use of InAs QDs as emitters with the help of Ab initio calculations.

First, the active zone is made of QDs or QWs. To test the efficiency of this active zone, photoluminescence (PL) measurements have been performed. Figure 2.a shows the GaAsP / GaP QWs PL spectra variation with temperature. Luminescence appears up to 281K (almost room temperature). This PL peak shift with temperature is in agreement with the gap variation determined by Varshni law (**figure 2.b**).

The second goal to achieve is the growth of GaP on Si [1]. To characterize the interface, Raman spectroscopy was performed to obtain a strong evidence for the determination of the bonding nature of the cristal (Ga-Si or P-Si, …). The first Raman Spectra (**fig. 3**) show Si and GaP characteristic peaks. A mapping of a GaP/Si pseudo-substrate is performed.

We have compared the band line-ups of InAs/GaP thanks to the classical calculations [2] with Ab initio method (**fig.4**). We consider InAs and GaP bulk crystals with the Local Density Approximation (LDA) [3] as pseudopotential plus GW correction using the many-body perturbation theory included in ABINIT package [4]. The *d* electrons effect has been taken into account because they play an important role to describe the correct behaviour of these semiconductors. We do not include spin-orbit (SO) splitting in both calculations. There is a good agreement between both methods. The same study will be done for InP/GaP.

We have observed GaAsP/GaP QW photoluminescence up to room temperature. This kind of active zone is promising for light emitters integration onto Si substrate. GaP growth onto Si substrate has successfully been achieved and characterized by Raman scattering. Future works will be conducted to insert these active zones (QWs or QDs) into a diode.

References:

[1] V. K. Dixita1, Tapas Gangulia, T. K. Sharmaa, S. D. Singha , Ravi Kumara, S. Porwala, Pragya Tiwaric, Alka Ingaleb, and S. M. Oak, “Effect of two step growth process on structural, optical and electrical properties of MOVPE grown GaP/Si”, India, 2008.

[2] Chuang S L "Physics of optoelectronic devices. Wiley Series in pure and Applied Optics." Joseph W. Goodman, Series Editor, 1995.
[3] Troullier N and Martins J L 1991 Phys. Rev. B 43, 1993.
[4] Gonze X, Beuken J M, Caracas R, Detraux F, Fuchs M, Rignanese G M, Sindic L, Verstraete, M, Zerah G, Jollet F, Torrent M, Roy A, Mikami M, Ghosez Ph, Raty J Y, and Allan D C Comput. Mater. Sci. 25 478, 2002.

Figures:

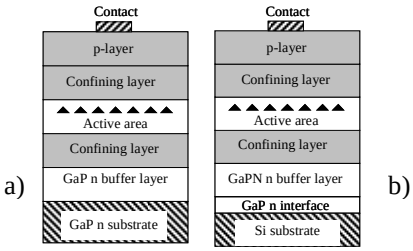

Fig. 1: (a), structure of the future DEL with QDs or QWs on GaP substrate. (b), structure of the DEL with QDs or QWs on GaP deposited on silicon substrate.

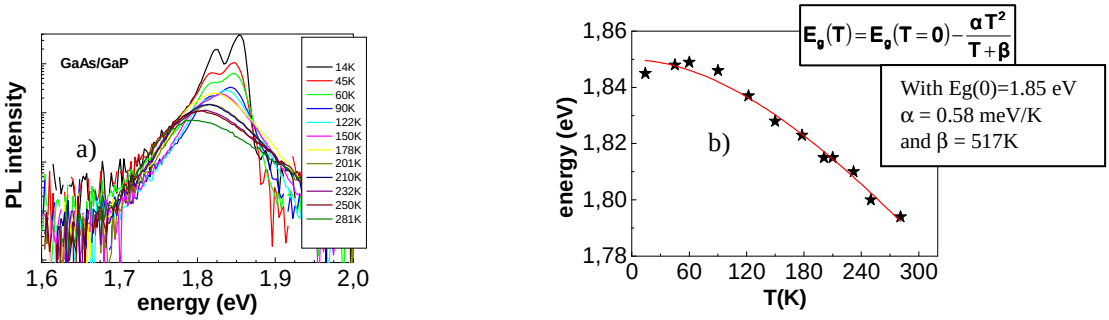

Fig. 2: (a), PL spectra of GaAsP/GaP for several temperatures. (b), experimental datas following Varshni Law variation.

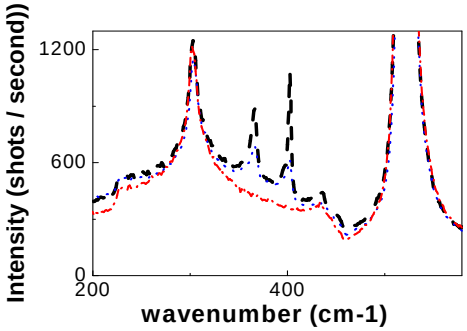

Fig. 3: Raman spectra performed on HR800 system (ONIS, University Rennes1). Dash dots indicate silicon Raman spectrum; Dashes, GaP on silicon Raman spectrum; Dots, an intermediate zone.

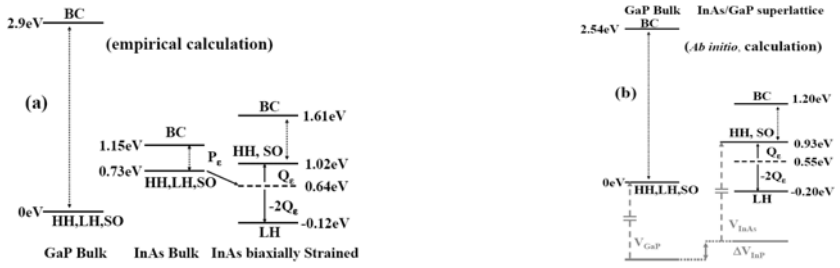

Fig. 4: Band line-ups at Γ point calculated without SO coupling for both the classical empirical method (a) and Ab initio calculation (b).

Magnetic Particles for Fully Automated Nucleic Acids Isolation and Their Application in Nanomedicine

Jaromir Hubalek[1], Jana Drbohlavova[1], Dalibor Huska[2], Vojtech Adam[2], Ales Horna[3], Libuse Trnkova[4], Rene Kizek[2]
[1]Department of Microelectronics, Faculty of Electrical Engineering and Communication, Brno University of Technology, Udolni 53, CZ-602 00 Brno, Czech Republic
[2]Department of Chemistry and Biochemistry, Faculty of Agronomy, Mendel University of Agriculture and Forestry, Zemedelska 1, CZ-613 00 Brno, Czech Republic
[3]Radanal Ltd., Okruzni 613, CZ-530 03, Pardubice, Czech Republic
[4]Department of Chemistry, Faculty of Science, Masaryk University, Kamenice 5, CZ-625 00 Brno, Czech Republic
hubalek@feec.vutbr.cz

Electrochemical DNA recognition has already known and described [1-3].Technologies based on ferro- and paramagnetic particles seem to be very perspective in isolation of RNA or DNA sequence for studying DNA-protein or DNA-medicament interaction in medicine [4,5]. The technique employs a modification of the magnetic micro- and nanoparticles surface by biomolecules. The most frequent techniques for nucleic acids capture are shown in Fig. 1. In the work the modification of magnetic particles surface coated by streptavidin is presented. This protein exhibit a high affinity to low-molecular compound as biotin. These particles can be used for recognizing a specific DNA or RNA sequences and its consequent identification.

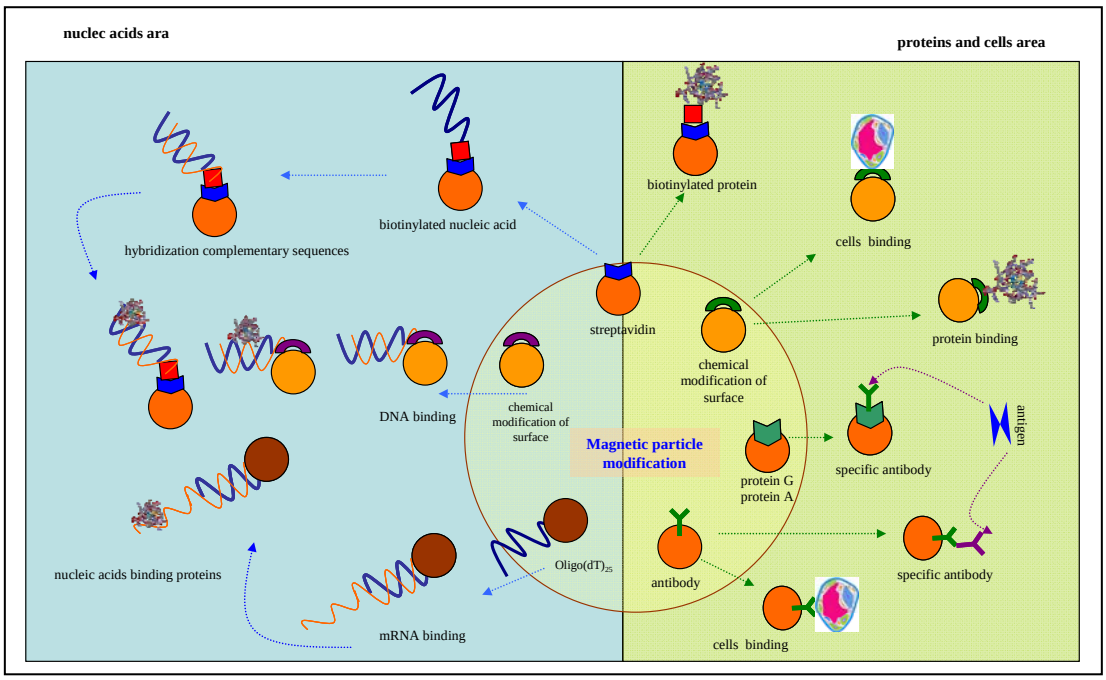

Figure 1. Possibilities in magnetic particles surface modification for capture of various biological molecules.

In our experiments superparamagnetic particles Fe_2O_3 were fabricated (Fig. 2). Paramagnetic properties are needed because magnetization disappears when magnetic field break off. Therefore the particles can be reused again after RNA capture. According X-ray diffraction measurement, the prepared sample consisted of 60% maghemite (γ-Fe_2O_3) and 30% of sylvite (KCl). Modified particles were added to the mRNA sample and hybridized [6-9] for 30 min at 25°C. After the removal of unspecific bound molecules the captured nucleic acid was released by temperature denaturation [6-9] lasting for 8 min at 85°C. The solution is then transferred

into a pure microplate and electrochemically analyzed. The electrochemical analysis was performed in the presence of acetate buffer at carbon printed electrodes containing carbon nanoparticles.

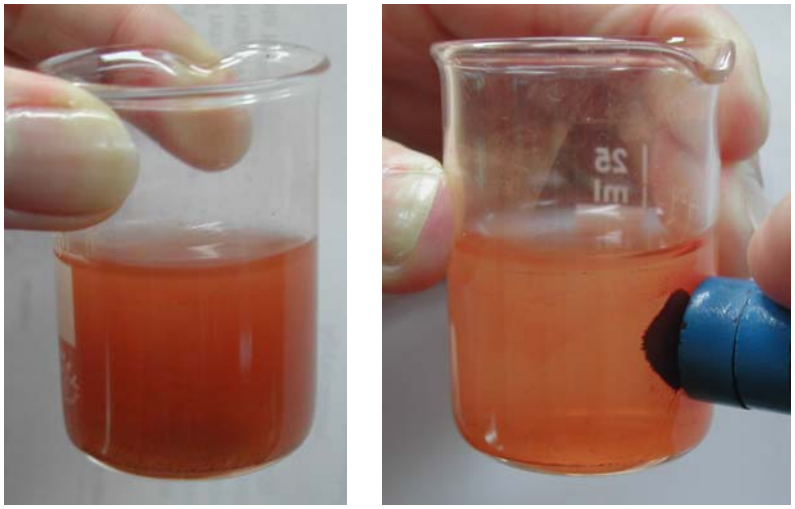

Figure 2. Illustration of magnetic properties of Fe_2O_3 nanoparticles.

The relative standard deviation of the proposed procedure based on the paramagnetic particles is 11 %. The efficiency of the nucleic acid capture during the hybridization process varied from 40 to 60 %.

Acknowledgement: The financial support from the grant KAN 208130801 is highly acknowledged.

References:

1. Drummond T. G., Hill M. G., Barton J. K.: Nature Biotech., *21*, 1192 (2003).
2. Palecek E.: Talanta, *56*, 809 (2002).
3. Wang J., Polsky R., Merkoci A., Turner K. L.: Langmuir, *19*, 989 (2003).
4. Palecek E., Fojta M., Jelen F.: Bioelectrochemistry, *56*, 85 (2002).
5. Wang J.: Anal. Chim. Acta, *500*, 247 (2003).
6. Fojta M., Havran L., Kizek R., Billova S., Palecek E.: Biosens. Bioelectron., *20*, 985 (2004).
7. Kizek R., Havran L., Fojta M., Palecek E.: Bioelectrochemistry, *55*, 119 (2002).
8. Palecek E., Kizek R., Havran L., Billova S., Fojta M.: Anal. Chim. Acta, *469*, 73 (2002).
9. Palecek E., Billova S., Havran L., Kizek R., Miculkova A., Jelen F.: Talanta, *56*, 919 (2002).

Effect of stack number on the threshold current density in Quantum Dash/Dot lasers

D. Zhou, R. Piron, M. Dontabactouny, E. Homeyer, O. Dehaese, T. Batte, F. Grillot, K. Tavernier, J. Even, S. Loualiche
CNRS UMR6082 FOTON, INSA, 20 Avenue des Buttes de Coësmes,
CS 14315, 35043 RENNES Cedex FRANCE
Dayong.zhou@insa-rennes.fr

Abstract : We demonstrate the achievement of multiple stacked InAs quantum dash and quantum dot lasers. The threshold current density reaches a minimum value of 680 A.cm^{-2} for quantum dash lasers on InP (100) and 170 A.cm^{-2} for quantum dot lasers on InP (311)B. The wavelength varies from about 1.49µm to 1.58µm.

Experiment: The lasers were grown by gas source molecular beam epitaxy (GSMBE) on n-type (100) and (311)B InP wafers for QDH and QD respectively. The active region comprises multiple layer stacked QDHs (QDs) with a nominal deposition thickness of 0.6 nm InAs per layer. The QDH (QD) layers are separated by relatively thin barriers of 30 nm lattice-matched $In_{0.8}Ga_{0.2}As_{0.43}P_{0.57}$ quaternary ($Q_{1.18}$; λ_g=1.18 µm). The active region is embedded into the centre of a 320 nm $Q_{1.18}$ waveguide, providing optical confinement in the transverse direction by the refractive index contrast to the cladding layers. The core structure is surrounded by 500 nm low doped InP cladding layers on both sides. The top cladding is followed by a highly doped 2.5 µm InP and capped with a 150 nm InGaAs contact layer. All layers, except the QDH (QD) layers, are lattice matched to InP. The growth process of QDH (QD) was optimized by using the double-cap technique as well as controlling the arsenic flux[1]. The double-cap technique consists of a capping procedure in two steps. The first capping step is the deposition of a fixed small thickness, and the maximum height of the QDH (QD) is therefore controlled easily and reproducibly by the thickness of this first capping layer, thus allowing a reduction of the height dispersion. The QDH (QD) formation is followed by a growth interruption under group As_2 and P_2 fluxes, resulting in planarization of the surface due to effective As/P exchange. The second capping step is then carried out to complete the spacer layer. The reduction of the arsenic flux results in better morphology. Therefore, the emitting wavelength of the laser can be easily tuned in the range of 1.55 µm telecommunication wavelength. Moreover, a sharper gain curve can consequently be expected for the structure, which greatly eases the losses compensation. Figure 1 is a 1 × 1 µm^2 atomic force microscopy (AFM) image of uncapped QDHs structure containing 3 stacked layers. The morphology shows elongated QDHs with a mean height, width, and length of 2.2, 20, and 300 nm respectively. The surface density is 2×10^{10} cm^{-2}.

The broad area lasers were processed by a standard laser processing technique. The stripes of QDH lasers on InP (100) were patterned along [011] direction which is perpendicular to the dash elongated direction, with a width of 100 µm. The direction is chosen to obtain higher modal gain and thus lower threshold [2]. For QD lasers on InP (311)B, the stripes were along [01-1], as (01-1) planes are the only ones that can be cleaved to obtain cavity mirrors. The cavity length of QDH and QD lasers are 1.2 and 3.0 mm respectively, with both cleaved facets uncoated. The lasers were mounted on a copper block using silver epoxy. The laser diodes showed turn-on voltages at 0.7 V. The laser diodes are electrically injected by pulsed current with 500 ns pulse width and 2 kHz repetition rate.

Results: The lasing wavelengths of QDH lasers increase with stack number from 1.49 to 1.58 µm, resulting from inhomogeneous morphology during stacking. A gradual decrease of J_{th} with reduced stack number is confirmed, and a minimum J_{th} of 680 A.cm^{-2} is obtained for a double layer stacked QDH laser, depicted in Figure 2. Similar J_{th} trend is predicted in quantum wells [3]. For quantum dot lasers on (311)B, double stacked QD laser with ultra low J_{th} of 170 A.cm^{-2}

was demonstrated[4]. Moreover, lasing from a single QD layer as active region was obtained with a QD density of higher than 10^{11} cm^{-2} [5]. Unfortunately, the single QDH structure didn't give lasing at room temperature, probably due to the very low optical confinement factor and relatively low surface density of QDHs. For a very small number of stacked layers, the low value of optical confinement factor implies a strong increase of the threshold carrier density, and thus high pumping level is required to reach lasing. On the other side, for larger number of stacked layers, threshold carrier concentration approaches transparency carrier concentration, and J_{th} thus increases linearly with the number of stacks. At the minimum of the curve, a further reduction of J_{th} in QDH laser could be possible after optimizing the size fluctuation and surface density of the quantum structure.

Conclusion: Threshold current density and wavelength as a function of stack number are investigated in quantum dash and quantum dot lasers. The results show that the lowest J_{th} can be obtained at an intermediate stack number. This is attributed to the behaviour from the sum of current density in active region and in the waveguide region.

References:

[1] **P. Caroff, N. Bertru, C. Platz, O. Dehaese, A. Le Corre and S. Loualiche, J. Cryst. Growth 273, 357 (2005)**

[2] **R. H. Wang, A. Stintz, P. M. Varangis, T. C. Newell, H. Li, K. J. Malloy, and L. F. Lester, IEEE Photon. Technol. Lett. 13, 767 (2001)**

[3] **Quantum Well Lasers, edited by Peter S. Zory, Jr. (Academic Press, New York, 1993)**

[4] **E. Homeyer, R. Piron, F. Grillot, O. Dehaese, K. Tavernier, E. Macé, A. Le Corre and S. Loualiche, Jpn. J. Appl. Phys. 46, 6903 (2007)**

[5] **E. Homeyer, R. Piron, F. Grillot, O. Dehaese, K. Tavernier, E. Macé, A. Le Corre and S. Loualiche, Semicond. Sci. Technol. 22 827-830 (2007)**

Figures:

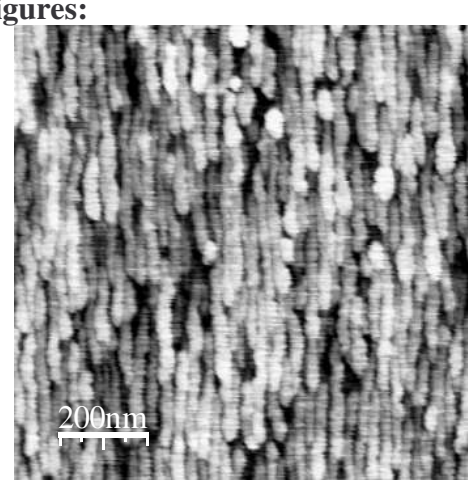

Figure 1

1 × 1 μm² AFM image of an uncapped three-fold stacked QDH layer.

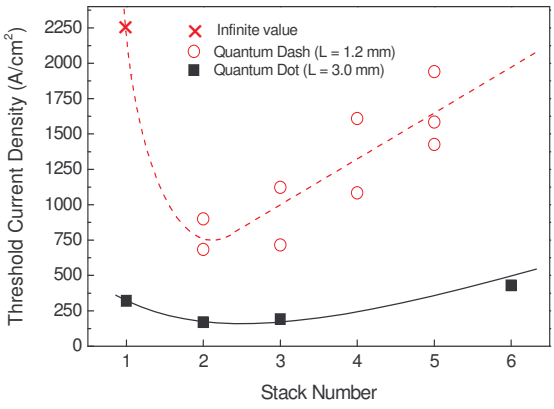

Figure 2

Threshold current density as a function of stack number for QDH (open circle) and QD (filled square). (The continuous line is a guide to eyes). For single stacked QDH laser, no lasing was observed, as J_{th} reaches infinite value.

NOVEL POLYMER-METAL PRECURSOR ROUTE FOR SIMPLE AND MASS PRODUCTION OF ITO NANOPARTICLES

Sung-Ho Hwang,[1] *Sang Kyoo Lim*[1] *and Sanghee Kim*[2]
[1]*Advanced Nano-Materials Research Team, Division of Nano & Bio Technology, Daegu Gyeongbuk Institute of Science & Technology(DGIST), Daegu, 704-230, Korea*
[2] *Department of Chemistry, Kyungpook National University, Daegu, 702-701, Korea*
hsungho@dgist.ac.kr

Sn-doped In_2O_3 [indium tin oxide (ITO)] is a promising type of transparent conducting oxide material, and has been used in wide fields such as optoelectronic devices, solar cells, liquid crystal displays and sensors.[1] Over the past decades, much research effort has been made on the synthesis of ITO films. Several effective techniques have been reported to obtain these coatings including d.c. magnetron sputtering,[2] highly dense plasma assisted electron beam evaporation,[3] and sol–gel method.[4] These films may also be prepared by dispersing ITO nanoparticles with desirable optical properties in a polymer binder. For these applications, small particle size or large specific surface area is essential to high performance. In this work, we describe the synthesis of monodisperse ITO nanoparticles less than 20nm in average particle diameter in mass production through novel simple two-step method using the coordinating chemistry between the electron donating polymeric ligands and the metal ion, which offers several advantages over other methods, including simple procedure, lower processing temperature, and better homogeneity. We have proceeded to the measurement of physico-chemical properties such as surface area, particle characteristics, crystal structure and etc. of ITO nanoparicles that were prepared by this novel synthetic method.

The synthesis of ITO nanoparticles was carried out by simple scheme in Figure 1, which contains the mixing of 10 wt % and 5 wt % PEO solutions and In and Sn compounds such as $In(NO)_3 \cdot 3H_2O$, $In(Ac)_3$, $SnCl_2 \cdot 2H_2O$, or $Sn(C_2O_4)$, then followed by thermal decomposition at 450□, and 600□, respectively, where the molar ratio of metal precursor was 9:1(In/Sn) and that of PEO monomer was 1:1 to moles of total metal ions. The morphologies of the nanoparticles were observed using a Hitach H-7600 transmitted electron microscope (TEM) under an acceleration voltage of 100kV. The XRD patterns were obtained from the X-ray diffractometer (Rigaku D/MAX-2500, 18kV) using Cu $K_{\alpha 1}$ radiation (λ = 1.5405 Å). Nitrogen adsorption-desorption isotherms were collected at -196 °C using Micromeritics ASAP 2020 equipment. Figure 2 displays the experimental XRD patterns of the ITO samples. Except for the difference in intensities, the as-synthesized ITO nanoparticles were highly crystalline and all the diffractograms correspond to the cubic bixbyite structure of indium oxide(ICDD PDF No. 6-416) without any indication of crystalline SnO_2 as an additional phase. This observation points to the formation of solid solutions rather than the mixture of indium oxide and tin oxide. On the other hands, the morphologies of ITO nanoparticles appeared to be a little different in size according to the average molecular weight of PEO (Figure 3) and thermal decomposition temperature. It may be understood due to the difference of coordination length in metal-polymer precursor. And it will be discussed in relation with other physico-chemical properties such as specific surface area and so on.

References:

[1] I. Hambergend and C. G. Granquist, *J. Appl. Phys., 60*, R123 (1996); B. J. Luff, J. S. Wilkinson, and G. Perrone, *Appl. Opt., 36,* 7066 (1997).
[2] H. Morikawa, M. Fujita, *Thin Solid Films, 359*, 61, (2000).
[3] I.A. Lauf, *Mater. Lett., 18* 123, (1993).
[4] T.F. Stoica, V.S. Teodorescu, M.G. Blanchin, T.A. Stoica, M.Gartner, M. Losurdo, M. Zaharescu, *Mater. Sci. Eng., B101*, 222, (2003).

Figures:

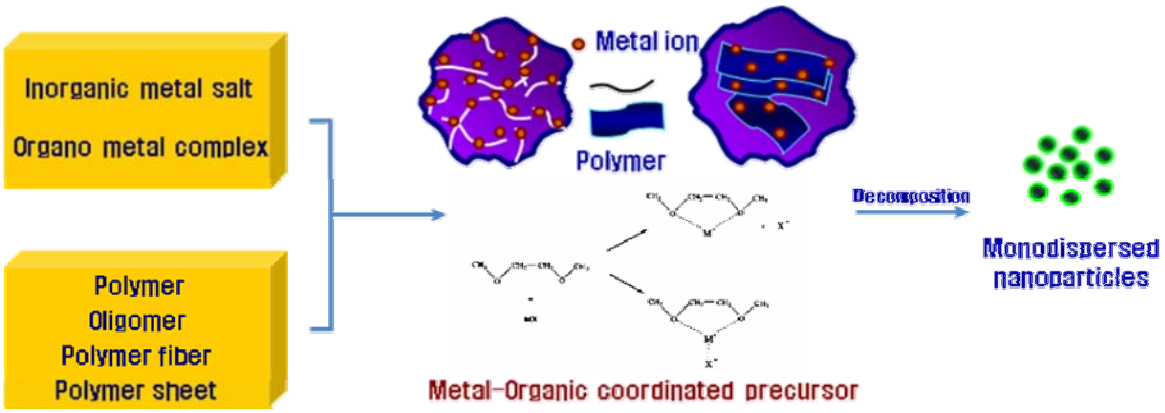

Figure 1. Schematic representation of this synthetic strategy.

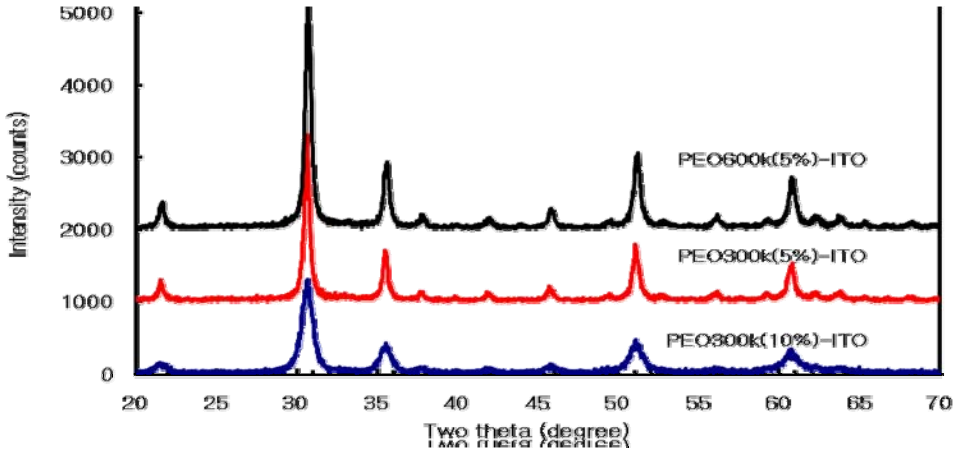

Figure 2. XRD patterns of the ITO nanoparticles according to the synthetic conditions.

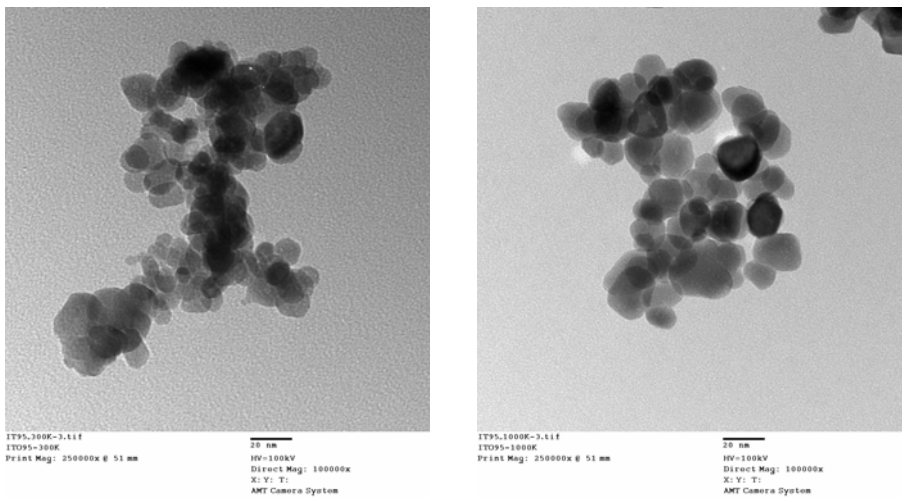

(a) (b)

Figure 3. TEM images of the ITO nanoparticles synthesized with PEO of different average molecular weight : (a) M.W. 300,000 and (b) M.W. 1,000,000

FERROELECTRIC MATERIALS TO THE AID OF LOW-POWER SWITCHING

David Jiménez

Departament d'Enginyeria Electrònica, Escola Tècnica Superior d'Enginyeria, Universitat Autònoma de Barcelona, 08193-Bellaterra, Barcelona, Spain
(*) david.jimenez@uab.es

One of the most severe problems in the field of microelectronics is the evacuation of heat dissipated during data processing [1]. Although a single semiconductor device produces a tiny amount of heat (around 10^{-16} J), integrated circuits today contain about 10^9 devices. The problem has led to a power crisis in manufacturing of semiconductor devices, which could well end up with Moore's law. To achieve the integration of 10^{12} devices, which would enable new features not yet imagined, and a significant reduction of integration cost, some radical new solution that allows handle the problem of heat dissipation is required. One possibility is to dissipate less power (P_{active}) during transistor switching. The most effective way to reduce power is to reduce the supply voltage (V_{dd}), as $P_{active} \propto CV_{dd}^2 f$ (where C is the total equivalent capacitance to be charged and discharged in a clock cycle, and f is the frequency of the clock). For high-performance digital applications –e.g, microprocessors for personal computers- reducing V_{dd} must be accompanied by a reduction of the threshold voltage (V_{th}), for not to worse the delay time. However, reducing V_{th} implies an exponential increase of dissipated power in the OFF state (P_{off}). Accordingly, downscaling of V_{dd} can not be applied without limit as a strategy to reduce power consumption, as P_{off} would grow uncontrollably. The reason is that the subthreshold slope (a figure of merit that describes the goodness of the transition OFF-ON/ON-OFF) of a conventional transistor is not scalable and presents a fundamental thermodynamic limit of S=60 mV/decade at room temperature. This limit is known as the *Boltzmann tyranny* and is widely accepted by the scientific community that is not possible to obtain S<60 mV/decade without changing the principle of operation of the transistor.

In this project I will explore a change in the design of conventional transistor in order to achieve subthreshold slopes below 60 mV/decade. The proposal is replacing the conventional gate insulator (a dielectric material) with a ferroelectric material [2-4]. This type of material presents a region of negative capacitance in its Q-V curve (charge vs. applied voltage) (Figure 1a). A negative capacitance means that by increasing the applied voltage then the stored charge decreases. This region of negative capacitance is not directly observable in experiments but, if the ferroelectric material is associated in series with a small enough capacitance, the conditions for its observation should be fulfilled. The role of this capacitance is played by the channel-substrate capacitance. The negative capacitance provides a mechanism for amplifying the surface potential (Figure 1b). The gain (G) could be around 4, although this limit is an issue that should be further explored. The amplification of the surface potential is the key ingredient for increasing the current in more than one order of magnitude for every 60 mV increase in gate voltage (Figure 1c).

[1] *International Technology Roadmap for Semiconductors. Available: public.itrs.net*
[2] S. Salahuddin and S. Datta, *Nano Letters* **2008**, no. 2, 405-410.
[3] J. F. Scott and C. A. Paz de Araujo, *Science* **1989**, 246, 1400-1405.
[4] J. F. Scott, *Science* **2007**, 315, 954-959.

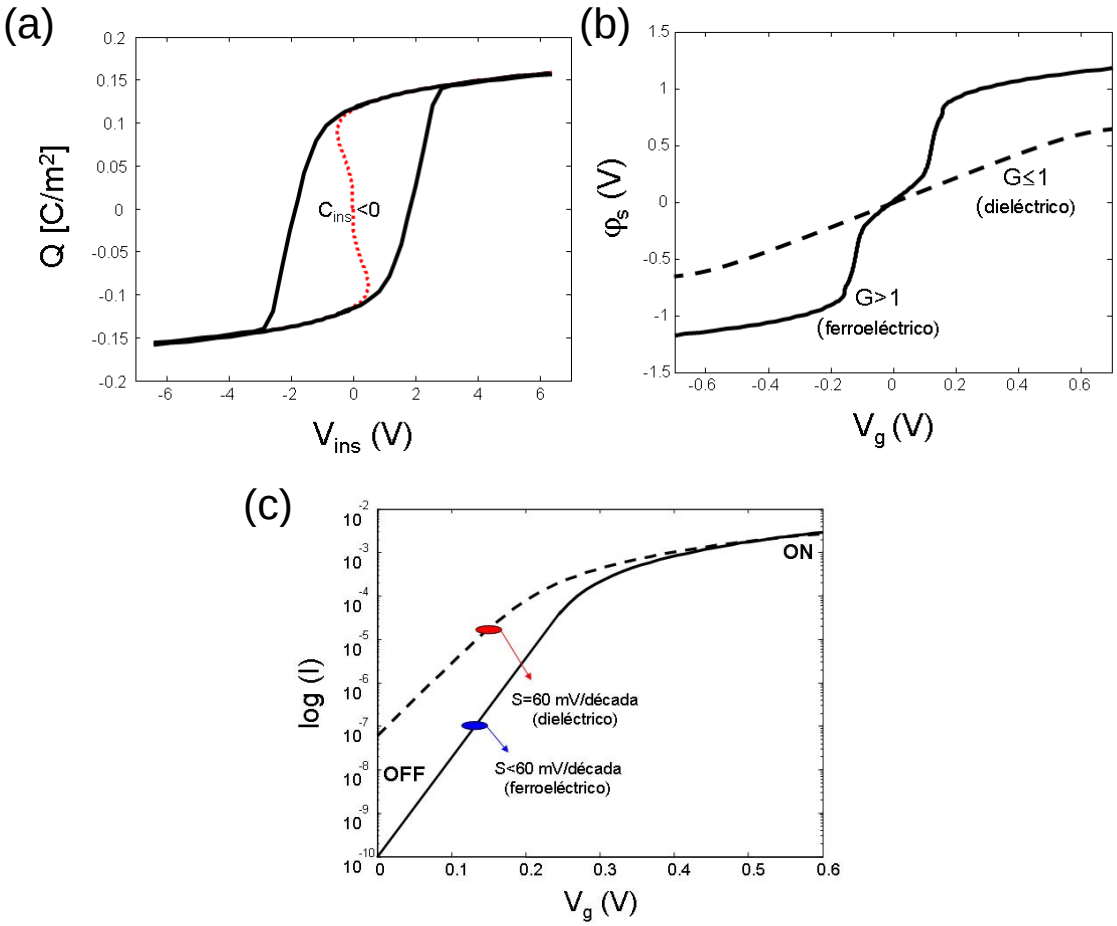

Figure 1. (a) Stored charge (Q) vs applied voltage (V_{ins}) for a typical ferroelectric material. Dashed line shows the **negative capacitance region** (C_{ins}<0). (b) Dielectric insulators exhibit positive capacitance (C_{ins}>0) and the surface potential (φ_s) follows the gate voltage (V_g) with a gain G ≤1 (dashed line). Ferroelectric insulators, operated in the negative capacitance region, could result in surface potential amplification (G>1) (solid line). (c) A gain G=1, which is the maximum gain with a dielectric insulator, results in a subthreshold slope S=60 mV/decade (dashed line). If we replace the insulator by a ferroelectric material operated in the negative capacitance region, then G>1 and S<60 mV/decade (solid line).

Ozone analyzer for Air quality monitoring based in nanotechnology: A real industrial application

A. Pérez-Junquera, A. Ayesta, L. García and J. Blanco
***Ingenieros Asesores S.A**., Parque Tecnológico de Asturias, nº 39; 33428, Llanera (Asturias), Spain*
ajp@ingenierosasesores-sa.es

The development of gas sensor devices with optimized selectivity and sensitivity has received much interest in recent years as they provide the ability to detect, for example, the presence of a non healthy gas concentration with low cost and low power energy. Furthermore, due to the rapid progress in micro and nanofabrication processes, some companies in this field have developed semiconductor oxide sensors in low range, i.e. sensors for air quality monitoring [1-3]. In order to reduce the cost, the best manufacturing process is the use of a semiconductor fabrication line. However, fundamental materials and processing issues, which are critical for a high-performance gas sensor, need to be assessed, as well as the influence of cross sensitivities with other gases or parameters. In particular, in this work we show the importance of the temperature in the ozone monitoring using this technique.

During the last two years, Ingenieros Asesores S.A has been developed an ozone analyzer for air quality monitoring, based on semiconductor oxide sensor (see fig. 1). The main part is the sensor, where a sensing layer, made of a metal oxide, generally SnO_2, is heated by a heater structure (see inset in fig. 1 (c)). When chemicals, in this case O_3, are absorbed on its surface, its electrical conductivity changes locally; this leads to a change of its electrical resistance. Analysing the modifications of the resistance over time, compared with reference values, information about variable gas concentrations is available. With the aim of registering the values of the resistance and to obtain the concentration ozone level conversion (Ohms to ppb) we have developed a micro data logger with mobile GSM communication and 12 V power supply which is possible to work with a small solar panel. In this way, the Ozone monitor has free mobility which makes it possible to install practically everywhere. The data of the analyzer are downloading using specifically developed software in a PC with a modem connexion.

The calibrated commercial sensor that we have used was first checked with good results in the laboratory (Temperature = 25ºC and Relative Humidity = 50%). For the conversion between electrical resistance and ozone level, the sensor applied a temperature correction at 25ºC following the equation: $R^{sensor}_{Tcorrection} = R^{sensor}_{original} * EXP\left[0.05 * \left(T_{offset} + T_{real} - 25\right)\right]$. This manufacturing temperature correction is good for laboratory conditions but what happens in a real case?

We have installed the system on the top of an air quality station in Toledo (Spain), to compare our results with the validated Ozone data on this place (UV absorbing Vs Semiconductor Gas sensor). We can see (fig. 2) the real importance of and extra temperature correction in the calculus of Ozone final value, with big differences with or without this new correction. We can clearly appreciate how the original temperature correction is only valid for temperatures lower than 25 ºC, not valid for a real monitoring case where temperatures can be higher. Other parameters as humidity or cross sensitivities with other gases are now under investigation.

*Work supported by own I+D+i Ingenieros Asesores S.A project.

References:

[1] A.M. Azad et al. (Review), *J. Electrochem. Soc.,* **139** (1992), pp. 3690-3704.
[2] W. Gopel, *Sensors and Actuators B,* **18-19** (1994), pp. 1-21.
[3] G. Sberveglieri, *Sensors and Actuator B,* **23** (1995), pp. 103-109.

Figures:

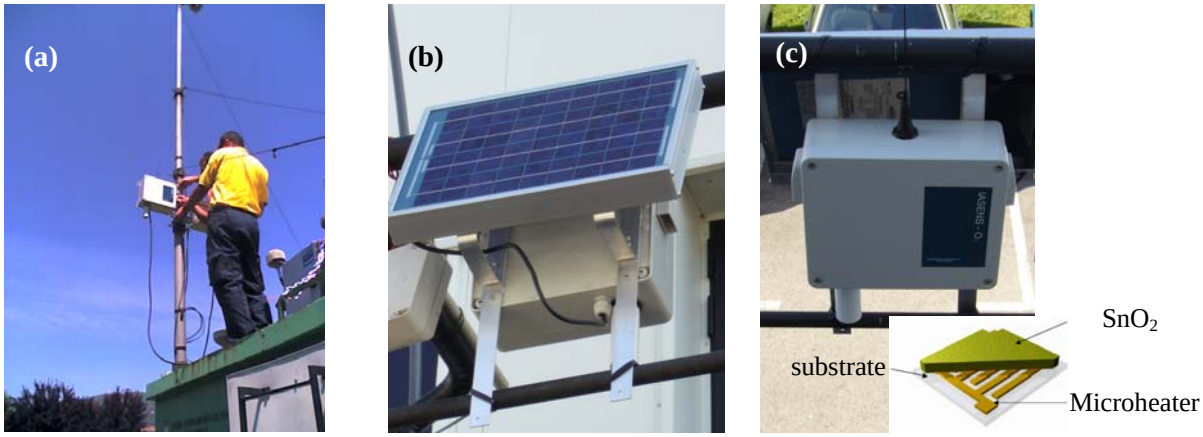

Fig. 1: (a) Ozone analyzer based on nanotechnology (IASens O_3) developed by Ingenieros Asesores S.A., being installed on the top of an air quality monitoring station. (b) and (c) back and front side respectively of an IASens O_3 system. We can see the Solar Panel for power supply and the antenna for GSM communications. Inset in (c), typical internal structure of the sensors.

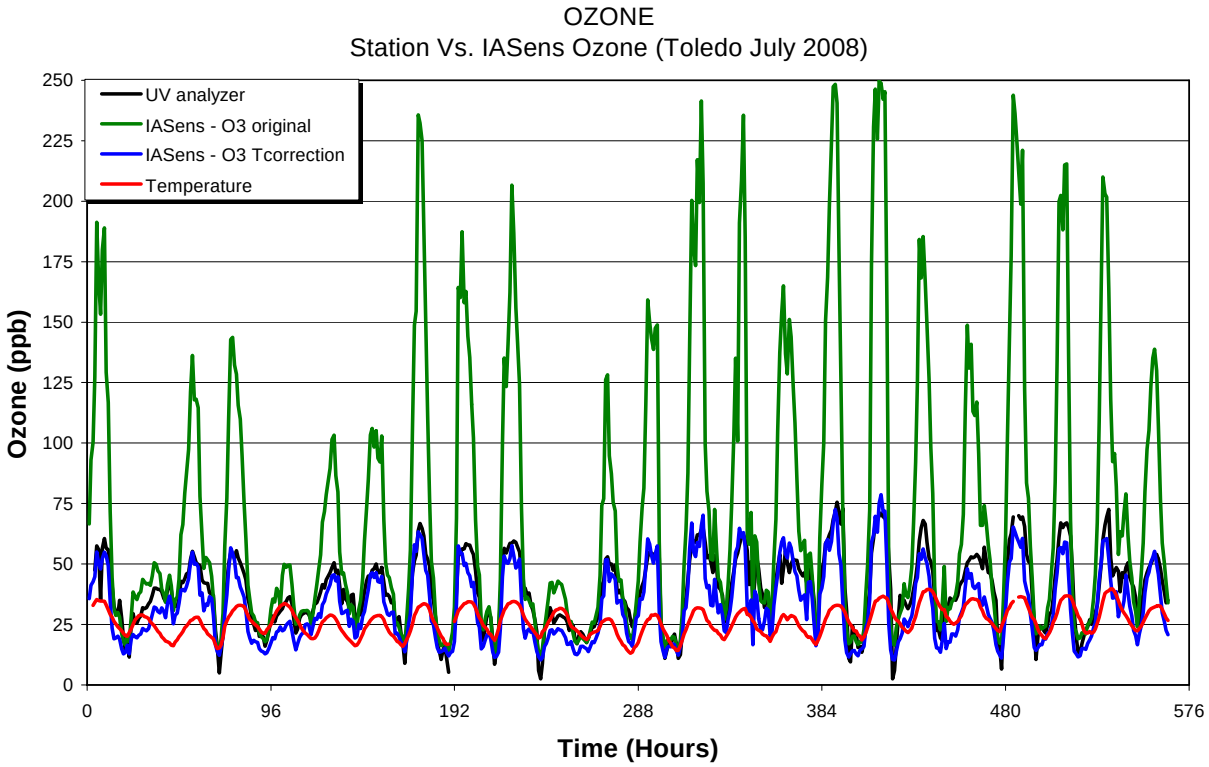

Fig. 2: Plot of the ozone concentration and temperature versus time in 24 days of July 2008. Ozone concentration measured by UV analyzer (black line); IASens original value with temperature correction at 25 ºC (green line); IASens corrected value depending of the temperature (blue line) and ambient temperature values in Toledo during this period (red line).

A Localized Quantum Spin Reversal by Spin Injection in A Spin Quantum Dot: Effect of Spin Relaxation

Satoshi Kokado[1], *Kikuo Harigaya*[2], *and Akimasa Sakuma*[3]
[1]*Faculty of Engineering, Shizuoka University, Hamamatsu, Japan*
[2]*Nanotechnology Research Institute, AIST, Tsukuba, Japan*
[3]*Graduate School of Engineering, Tohoku University, Sendai, Japan*

tskokad@ipc.shizuoka.ac.jp

The single-atom memory is expected to be an ultimate microscopic element of the data storage device. Recently, towards development of such a memory, single quantum spin systems with bistable states have been studied extensively [1-3]. In particular, it has been experimentally reported that a single atomic spin (S=2) of an Fe atom on CuN surface has the uniaxial anisotropy energy, $-|D|S_z^2$, which shows the bistable potential between $Sz=-S$ and S, and $|D|$ is evaluated to be 1.55 ± 0.01 meV [1].

For the spin system with $-|D|S_z^2$, we consider the manipulation of spin states. As a method, we propose "a quantum spin reversal induced by spin injection in a spin quantum dot", where the transition from $S_z=-S$ to S is induced by the spin injection [2, 3]. It should be noted here that atomic vibration may give strong influence to the spin reversal, because the energy of the atomic vibration is usually in the range of 0.4 meV - 40 meV (100 GHz - 10 THz) which is close to the energy-level spacing of spin systems, and then the spin relaxation may be enhanced.

On the other hand, we expect that the other bistable spin systems such as S=1, 3/2, 5/2 will be synthesized in the future. An obvious difference of energy levels between the integer spins and half-integer ones, which is shown in Fig. 1, may make some sort of difference to the reversal.

In this paper, we study the spin reversal induced by the spin injection for electrode/spin quantum dot/electrode junctions, in which the dot has a localized spin $\boldsymbol{S}$ with S=1, 3/2, 2, 5/2 (see Fig. 1) [2, 3]. Furthermore, $\boldsymbol{S}$ shows $-|D|S_z^2$, and it is coupled to the vibration of the dot (VOD). Here, the spin relaxation time due to the $\boldsymbol{S}$-VOD interaction, τ, is introduced. For the initial state of $S_z=-S$, we consider a situation in which up-spin electrons exhibit the spin-flip tunnelling from the left electrode to the right one and then an exchange interaction acts between the electron spin and $\boldsymbol{S}$. Using the master equation and the Fermi golden rule, we investigate the time t dependences of the expectation value of the localized spin $\langle S_z \rangle$, the current, and the expectation value of the number operator of the VOD for any τ's.

As a result, we find that spin systems of S=3/2, 5/2 tend to exhibit the spin reversal compared to systems of S=1 and 2. In Fig. 2, we show t dependence of $\langle S_z \rangle$ of S=1, 3/2, 2, 5/2, at temperature T=10 K, where $|D|$ is 1 meV, and the voltage between the electrodes is 5 meV. The systems of S=3/2, 5/2 give rise to the spin reversal irrespective of τ, while the systems of S=1, 2 do not exhibit the reversal for τ=0.1 ns and 0.01 ns.

This behavior can be explained by taking into account the transition rates from $S_z=-S$ to S, where the transition rate due to "the conduction electron spin-$\boldsymbol{S}$" interaction (due to the $\boldsymbol{S}$-VOD interaction) is represented by $W^{\text{el-}\boldsymbol{S}}$ ($W^{\boldsymbol{S}\text{-VOD}}$), with $W^{\boldsymbol{S}\text{-VOD}}$ being a function of τ. Roughly speaking, $W^{\text{el-}\boldsymbol{S}}$ contributes to the spin reversal, while $W^{\boldsymbol{S}\text{-VOD}}$ tends to suppress the reversal. The magnitude of the ratio of transition rates $|W^{\boldsymbol{S}\text{-VOD}}/W^{\text{el-}\boldsymbol{S}}|$ of S=3/2, 5/2 is much smaller than that of S=1, 2, because the transition due to the $\boldsymbol{S}$-VOD interaction between $S_z=-1/2$ and 1/2 is

forbidden. Therefore, the systems of S=3/2, 5/2 are apt to exhibit the spin reversal compared to S=1, 2.

References:

[1] C. F. Hirjibehedin *et al*., Science **317** (2007) 1199.

[2] S. Kokado *et al*., preprint.

[3] As a related literature, see S. Kokado *et al*., Phys. Rev. B **76** (2007) 054451.

Figures:

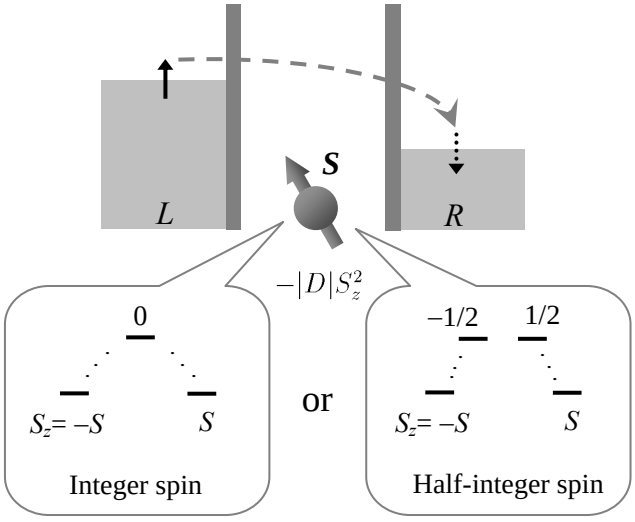

Fig. 1 Schematic illustration of electrode/spin quantum dot/electrode junctions. The quantum spin ***S*** has the uniaxial anisotropy energy, $-|D|S_z^2$, where energy levels for the integer spin (the half-integer spin) are shown in left frame (right frame). The spin ***S*** is connected to the left electrode (L) and the right one (R), where the L has conduction electrons with up spin, while the R has those with down spin. Furthermore, ***S*** is coupled to the vibration of the dot.

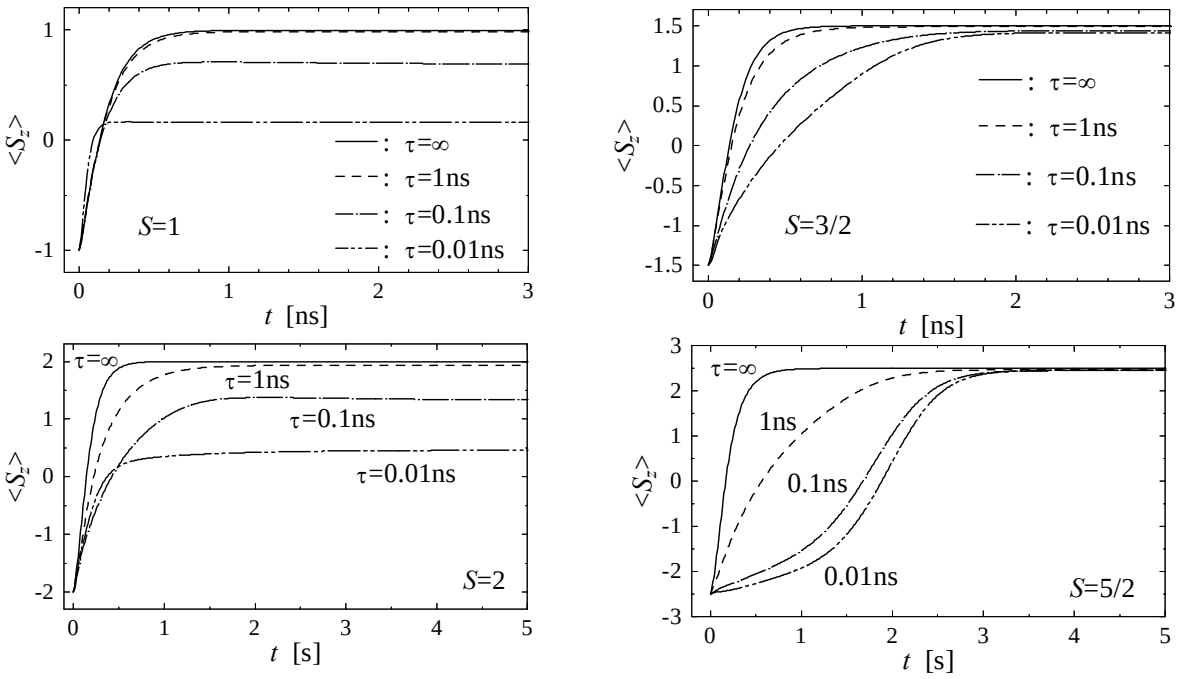

Fig. 2 Time t dependence of the expectation value of the z-component of the spin $\langle S_z \rangle$ for each S.

EXPERIMENTAL OBSERVATION OF THE RADIAL BREATHING MODE IN NANORODS

Holger Lange, Mikhail Artemyev, Ulrike Woggon, Marcel Mohr, and Christian Thomsen

Institut fuer Festkoerperphysik, TU Berlin, Germany

We present an experimental investigation of the radial breathing mode in CdSe nanorods of various sizes. We employ low-temperature Raman scattering experiments to determine the size dependence of the modes frequency. The radial breathing mode is, as predicted by ab initio calculations, highly diameter sensitive and can be used to estimate the nanorods diameter via Raman scattering experiments and is especially useful to estimate diameter variations of very small structures.

MODIFIED ELECTRODES BASED ON FERROCENE ATTACHED TO MULTI-WALLED CARBON NANOTUBES: APPLICATION TO GLUCOSE BIOSENSING

A. Le Goff[a], *R.Métayé*[a], *V. Artero*[b], *B. Jousselme*[a], *M. Fontecave*[b], *S. Palacin*[a]
[a] *CEA/DSM/IRAMIS/SPCSI, F-91191 Gif-Sur-Yvette Cedex, France*
[b] *CEA/DSV/iRTSV/LCBM, Université Joseph Fourier, 17 rue des Martyrs, 38054 Grenoble*
alan.legoff@cea.fr

Since their characterization in 1991[1], carbon nanotubes (CNT) have revealed fascinating properties. Their great conductivity, wide surface area and ease of modification make them great candidates for building nanostructured electrodes in a wide variety of applications. In particular, immobilizing organometallic molecules on CNT gives access to modified electrodes for sensing and electrocatalysis applications.

Immobilizing a redox probe like ferrocene is extensively studied to build up new glucose sensors; indeed ferrocene plays the role of an electron mediator in the biocatalytic oxidation of glucose to gluconolactone by glucose oxidase[2]. Hence, functionalizing CNT with ferrocene derivatives can lead to very sensitive nanoelectrodes for glucose sensing[3].
In this way, we compared two original methods for immobilizing ferrocene groups on a Multi-Wall CNT electrode. The first one is based on the π-stacking properties of pyrene towards CNT. Electrochemical studies indicate the robust immobilization of 2-pyrenylethyl 2-ferrocenylethanoate on a CNT electrode (figure **A**). The second method is based on the modification of CNT by the electrogeneration of aryl radicals from the reduction of diazonium salts[4]. The electroreduction of amine-functionalized aryldiazonium salts was performed at an ITO/MWCNT electrode. A post-fonctionalization step reaction achieved the immobilization of the ferrocene moiety (figure **B**). Both modified CNT-based materials were characterized by electrochemistry and XPS measurements. The efficiency of the two synthetic methods and the activity of the resulting modified electrodes towards glucose biosensing were compared.

References:

[1] S. Iijima, Nature, **354**(1991), 56.
[2] A. Heller, B. Feldman, Chem. Rev., ASAP.
[3] B. Sljukic, C. E. Banks, C. Salter, A. Crossley, R. G. Compton, The Analyst, **131**(2006), 670.
[4] J. Pinson, F. Podvorica, Chem. Soc. Rev., **34**(2005), 429.

Figures:

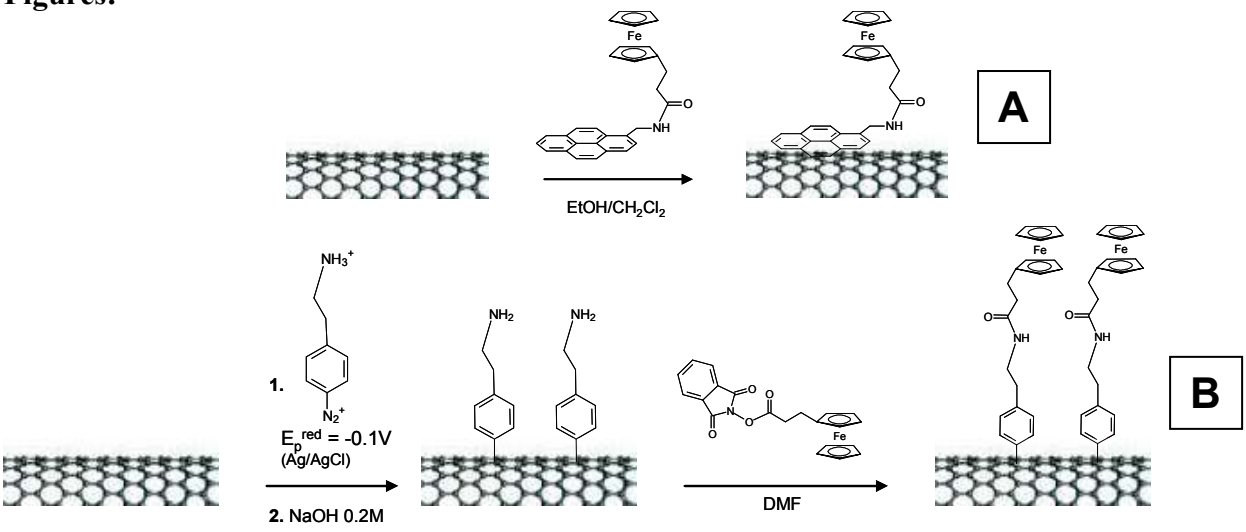

NITRIDATION OF Pt-TiO_2 NANOPARTICLE AND THEIR CHARACTERISTICS AS A VISIBLE LIGHT PHOTOCATSYST

Soo-Keun Lee, Soonhyun Kim
Division of Nano-Bio Technology, Daegu Gyeongbuk Institute of Science and Technology (DGIST), Samsung Financial Plaza, Duksan-dong 110, Jung-gu, Daegu 700-010, Korea
laser@dgist.ac.krl

TiO_2 photocatalyst has been extensively studied with regard to its application in degradation of various organic pollutants [1-3]. However, because of the size of its band gap, TiO_2 is active only under UV irradiation, which accounts for less than 5 % of solar light energy. Therefore, there have been many efforts to make a TiO_2 photocatalyst that would be active under visible irradiation. One approach is to prepare impurity doped TiO_2 [4]. Impurity doping material would substitute the Ti^{4+} ion or O^{2-} ion in the TiO_2 lattice and form the intraband states, which could be responsible for the visible absorption of impurity doped TiO_2. Previously, Kim et al. [5] investigated that Pt-ion-doped TiO_2 photocatalysts showed the efficient photocatalytic activities under visible irradiation. In that case, the Pt ions substituted in the TiO_2 lattice were present mainly in the Pt(IV) state. In this work, the nitrided Pt-TiO_2 nanoparticle was prepared for the enhancement of photocatalytic activity under visible irradiation. We have investigated the physicochemical properties and photocatalytic activities of nitrided Pt-TiO_2 for 4-chlorophenol (4-CP) and dichloroacetate (DCA) degradation.

Pt-TiO_2 was prepared by a sol-gel method as reported previously [5]. 2.5 ml of TTIP dissolved in 50 ml of ethanol was dropwise to 450 ml of chloroplatinic acid solution (0.08 mM for 0.5 atom% Pt doping) whose pH was adjusted at 1.5 with nitric acid. The resulting colloidal suspension was stirred overnight. For nitridation, Pt-TiO_2 or TiO_2 nanocolloid solution was directly mixed with an excess of TEA and vigorously stirred [6]. The nanocolloid solution rapidly forms a yellowish mixture. All nanocolloid solution was evaporated at 40 °C using a rotavapor. The obtained powder was calcined at 673 K for 3 hr under air atmosphere. The photocatalytic activities were evaluated for the photocatalytic degradation of 4-CP and DCA. TiO_2 was dispersed in distilled water (0.5 g/L) and an aliquot of the substrate stock solution (1 mM) was subsequently added to the suspension to give a desired substrate concentration. Photoirradiation employed a 300-W Xe arc lamp (Oriel) as a light source. Light passed through a 10-cm IR water filter and a UV cutoff filter (>420 nm for visible irradiation), then the filtered light was focused onto a 30-mL Pyrex reactor with a quartz window. The degradation of 4-CP was monitored using a high performance liquid chromatograph (HPLC: Agilent 1100 series) equipped with a UV detector and a ZORBAX 300SB C18 column (4.6×150 mm).

Nitridation treatment changed the physicochemical properties of TiO_2 and Pt-TiO_2. The primary particle size of nitrided samples was slightly smaller than that of unnitrided samples(Fig. 1) and the anatase to rutile phase transformation was seem to be retarded by the nitridation treatment. The visible light absorption of n-Pt-TiO_2 was more extended than that of Pt-TiO_2 and Pt ion state of n-Pt-TiO_2 was higher than that of Pt-TiO_2. Furthermore, surface area of nitrided samples was more than twice that of unnitrided samples. From these changes of physicochemical properties, we expected the enhanced photocatalytic activities of nitrided samples. However, their photocatalytic activities were restrictively enhanced and significantly affected by the kind of substrates. For 4-CP degradation, n-Pt-TiO_2 showed the enhanced photocatalytic activity under visible irradiation. For DCA degradation, the enhancement effect of nitridation treatment was not observed under visible irradiation. Above observations indicate that photocatalytic degradation activities of photocatalysts are depended on the kind of substrate as reported by Ryu and Choi [7]. Although they compared the photocatalytic activities

under UV irradiation their conclusions could apply to the photocatalytic activities under visible irradiation. In our case, the synergetic effect of n-Pt-TiO_2 was showed in 4-CP degradation but it was not observed in DCA degradation. The synergetic effects of n-Pt-TiO_2 for 4-CP degradation under visible irradiation seem to be due to enhancement of surface area by nitriding. For DCA degradation, surface area enhancement of TiO_2 might not affect on the visible activity of TiO_2. Although nitridation treatment significantly affected the physiochemical properties of Pt-TiO_2 and we expected the enhanced visible activities for the degradation of organic substances, as previously discussed, its positive effects were limited to the degradation of 4-CP.

This work was supported by DGIST basic research program of the MOST.

References:

[1] A. Mills and S. -K. Lee, J. of Photochem. & Photobiol., A: Chemistry, **152** (2002) 233-247.
[2] M. R. Hoffmann, S. T. Martin, W. Choi, D. W. Bahnemann, Chem. Rev. **95** (1995) 69-96.
[3] W. Choi, Catal. Surv. Asia **10** (2006) 16-28.
[4] R. Asahi, T. Morikawa, T. Ohwaki, K. Aoki, Y. Taga, Science **293** (2001) 269-271.
[5] S. Kim, S.-J. Hwang, W. Choi, J. Phys. Chem. B **109** (2005) 24260-24267.
[6] J. L. Gole, J. D. Stout, C. Burda, Y. Lou, X. Chen, J. Phys. Chem. B **108** (2004) 1230-1240.
[7] J. Ryu, W. Choi, Environ. Sci. Technol. **42** (2008) 294-300.

Figures:

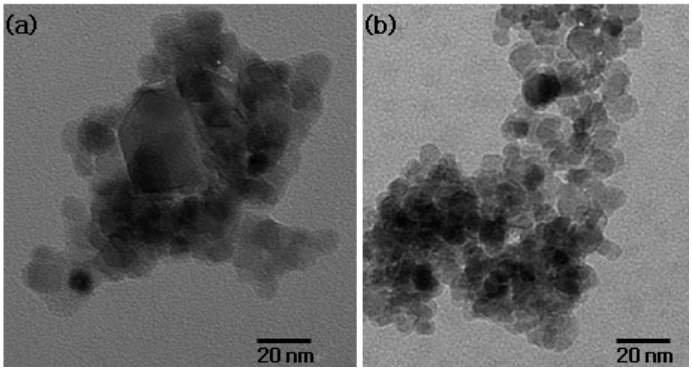

Fig. 1 TEM images of various TiO_2 samples. (a) TiO_2, (b) *n*-Pt-TiO_2.

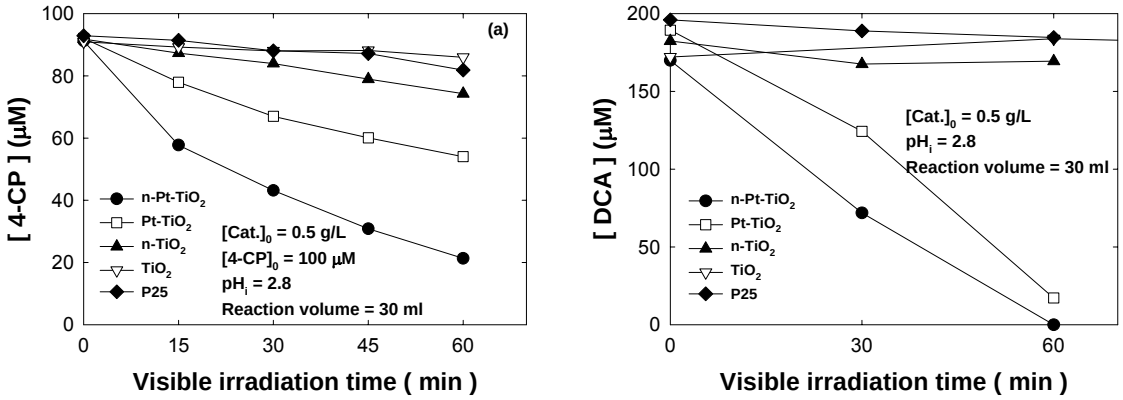

Fig. 2 Photocatalytic degradation of 4-chlorophenol (a) and DCA (b) under visible irradiation.

ZnO NANORODS FABRICATED BY A WET CHEMICAL METHOD

Sang Kyoo Lim and Sung-Ho Hwang
Advanced Nano-Materials Research Team, Division of Nano & Bio Technology, Daegu Gyeongbuk Institute of Science & Technology, 5th Floor, Daegu Technopark Venture 2 Plant, 75 Gongdanbuk2gil, Dalseo-gu, 704-230, Daegu, Republic of Korea
limsk@dgist.ac.kr

In recent years, one-dimentional (1D) nanostructures in the form of nanorods, nanowires or nanotubes, appear as an exciting research area for their great potential of applications. Zinc oxide is a versatile material with many applications including transparent electrode in solar cells, gas sensors and photo-luminescence devices [1-3]. Recently, strong efforts have been made to fabricate one-dimensional ZnO synthesized, for example, by the high-temperature physical evaporation, the micro emulsion hydrothermal process and the template induced method [4-6]. Among all these methods, the solution-based synthesis, by thermal treatment of reactants in different solvents, maybe the most simple and effective way to prepare sufficiently crystallized materials at relatively low temperatures. Also, the benefits of utilizing solution-based method have also involved a basic understanding upon the substantial influence of reaction species on the size and morphology as well as effective and economic preparation. In this aspect, many of the previous investigations on ZnO prepared by solution based method, mainly utilized zinc hydroxide or salt as precursors and water or organic solvent as reaction media. Only few publications reported the relationship between amphiphile structure and ZnO nanorods morphologies. Herein, we present microemulsion method toward the growth of well-proportioned and crystallized ZnO nanorods using two types of amphiphiles in figure 1 as the modifying and protecting agents to evolve the morphological changes upon the difference of amphiphiles. The synthesis of ZnO nanorods was carried out in microemulsions, which consisted of 5g of each amphiphile such as isopropyl naphthalene sulfonate or sodium lauryl sulfonate and 2 mmol of $ZnAc_2 \cdot 2H_2O$ dispersed in 60 ml xylene by stirring until a homogenous slightly-turbid appearance of mixture was obtained. Then, hydrazine monohydrate 2 ml and ethanol 8 ml mixture solution was added drop-wisely to the well-stirred mixture at room temperature by simultaneous agitation. The resulting precursor-containing mixture was subsequently heated to the 140□ for refluxing. After refluxing for 5 hours, a milky-white suspension was obtained and centrifuged to separate the precipitate, which was rinsed with absolute ethanol and distilled water for several times and dried in vacuum oven at 70□ for 24 hours. These as-prepared products were used for characterization. X-ray powder diffraction (XRD) analysis was conducted on a Rigaku D/max-2500 X-ray diffractometer. Room temperature fluorescence measurement was carried out on a JASCO FP-6500 fluorescence spectrophotometer at room temperature with a Xe lamp as the excitation light source. The excitation wavelength used was 325nm. The sample morphology was examined by field emission scanning electron microscopy (FE-SEM). On the basis of XRD patterns (Figure 2), the crystallographic phase of both samples belongs to the Wurtzite-type($P6_3mc$), reflecting that all the samples are well-synthesized to single phasic ZnO. On the other hands, the morphologies of both ZnO nanorods appeared to be quite a little different in length, aspect ratio and aggregations according to the type of amphiphiles (short aromatic amphiphile and long aliphatic surfactant) in Figure 3. It may be understood due to the fact that the difference of structural and chemical properties between two amphiphiles leads to the difference in emulsion phases and it will be discussed.

References:

[1] Z. W. Pang, Z. R. Dai and Z. L.Wang, *Science*, *291*, 1947, (2001).

[2] E. Comini, D. Faglia, G. Sberveglier, Z. Pan and Z. L. Wang, *Appl. Phys. Lett. 81*, 1869, (2002).
[3] W. C. Shih and M. S. Wu, *J. Cryst. Growth*, *137*, 319, (1994).
[4] M. H, Huang, S. Mao, H. Feick, H. Q. Yan, Y. Y. Wu, H. Kind, R. Russo and P. D. Yang, *Science, 292*, 1897, (2001).
[5] Z. W. Pang, Z. R. Dai, Z. L. Wang, *Science*, *291*, 1947, (2001).
[6] L. Guo, Y. L. Ji and H. Xu, *J. Am. Chem. Soc*., *124*, 14864, (2002).

Figures:

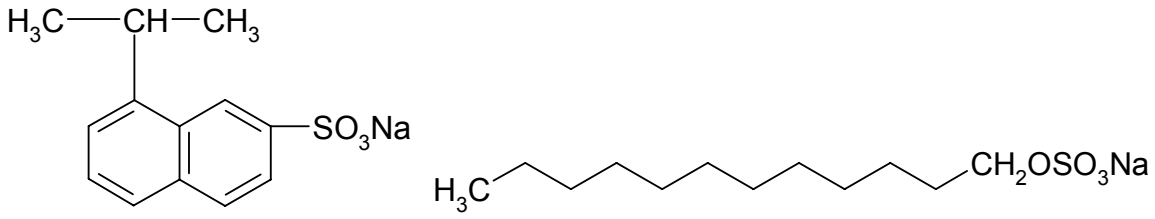

(a) (b)

Figure 1. Molecular structures of the amphiphiles: (a) isopropyl naphthalene sulfonate, (b) sodium lauryl sulfonate.

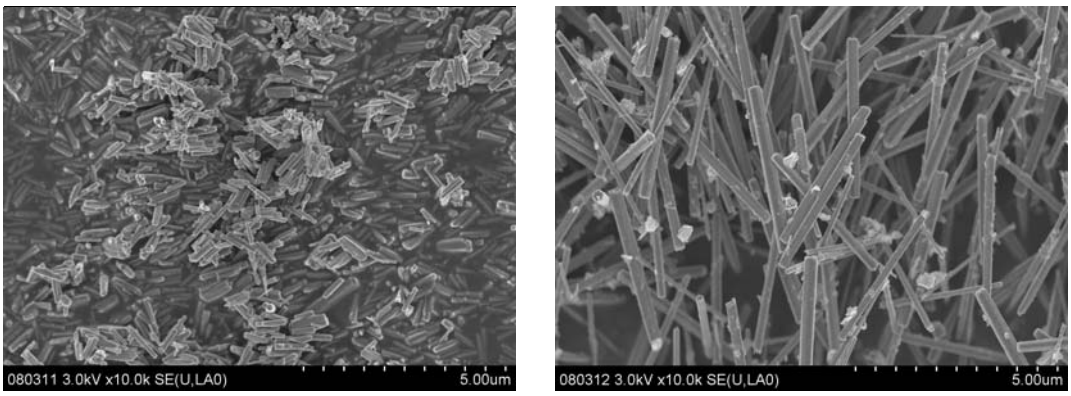

(a) (b)

Figure 3. FE-SEM images of the ZnO nanorods at different amphiphiles: (a) isopropyl naphthalene sulfonate, (b) sodium lauryl sulfonate.

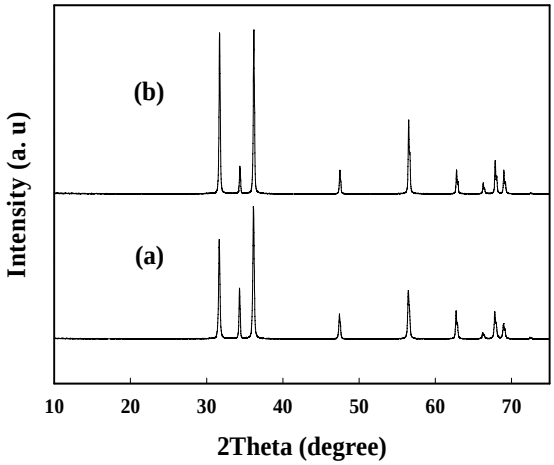

Figure 2. XRD patterns of the ZnO nanorods at different amphiphiles: (a) isopropyl naphthalene sulfonate, (b) sodium lauryl sulfonate.

TRANSPORT IN HYBRID DOUBLE KONDO DOTS

Rosa Lopez[(1)], Minchul Lee[(2)], M-S Choi[(2)], Ramón Aguado[(3)], Rok Zitko[(4)]

[(1)]Department of Physics, University of Balearic Islands, Crta Valldemossa Km 7.5 E-7122, Mallorca (Spain)
[(2)]Department of Physics, Korea University, Seoul 136-701
[(3)]Teoría de la Materia Condensada, Instituto de Ciencia de Materiales de Madrid, Cantoblanco 28049, Madrid (Spain)
[(4)]J. Stefan Institute, Ljubljana, Slovenia
rosa.lopez-gonzalo@uib.es

We investigate electronic transport through a serially-coupled double quantum dot in the Kondo regime coupled to normal-metals and superconducting leads. For the first case we calculate the linear conductance and for the superconducting one we compute the Josephson current. We employ different techniques, slave boson expansions and NRG calculations and we discuss the range of validity of these approaches. Surprisingly for the normal case we find that the dependence of the linear conductance on the interdot coupling varies with the strength of the lead-dot tunneling amplitude [see Fig. 1] when the exchange interaction is negligible. However when magnetic correlations play an important role the linear conductance presents a scaling behaviour independently on the magnitude of the interdot tunneling rate [see Fig.2]. For the Josephson current we obtain a non monotonous behaviour with the interdot tunneling [see Fig.3] that can be explained in terms of the formation of coherent Kondo states similar to the behaviour found in carbon nanotubes attached to superconducting contacts.

References:

[1] R. Lopez, M-S Choi, R. Aguado Phys. Rev. B 75, 045132 (2007).
[2] P. Jarillo-Herrero et al., Nature 439, 953-956 (23 February 2006).

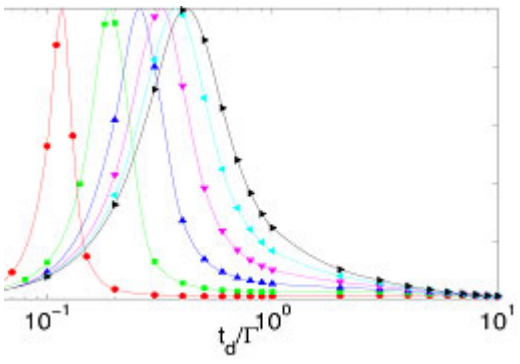

Fig.1 Linear conductance for different values of the lead-dot tunneling coupling

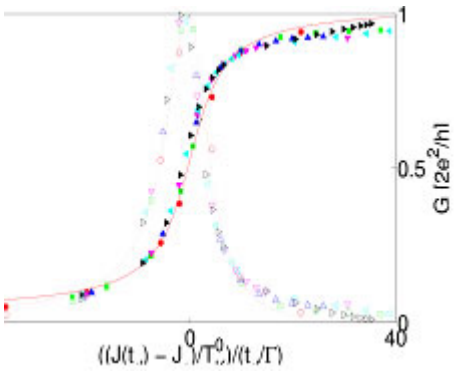

Fig.2 Linear conductance behavior for different lead-dot couplings

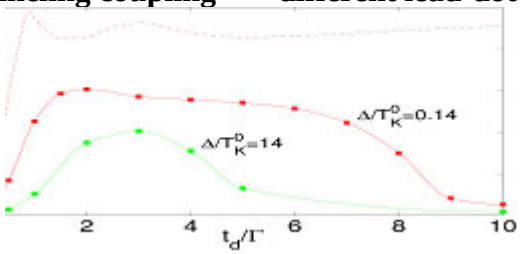

Fig3. Non monotonous behavior of the Josephson current as a function of the interdot tunneling amplitude

Mode II loading behaviour of intergranular nanocracks lying on a Σ17(530) symmetrical tilt boundary in copper

A. Luque, J. Aldazabal, J.M. Martínez-Esnaola, J. Gil Sevillano
CEIT and TECNUN (University of Navarra)
Paseo Manuel de Lardizábal, 15. 20018 San Sebastián, Spain
Contact e-mail: aluque@ceit.es

Recently the phenomenon of the grain boundary (GB) movement as a consequence of applied mechanical load has attracted much attention [1–4]. Shear-coupled migration (SCM) of tilt boundaries has been acknowledged as a particular plastic strain mechanism that can complement or compete with the other intra– or inter–granular mechanisms in a wide temperature range. SCM is diffusion–less but thermally activated. The shear strain effectiveness of the migration of a tilt boundary can be characterized by a shear coupling factor, β, the ratio of the shear displacement parallel to the GB surface to the GB migration normal to its surface. The factor β is determined by the tilt GB misorientation, θ, either $\beta = 2\ \mathrm{tg}(\theta/2)$ ("small" misorientations) or $\beta = -2\ \mathrm{tg}(\varphi/2)$, $\varphi = \pi/2 - \theta$ ("large" misorientations).

In this work MD simulations of SCM of a Σ17(530)/[001] symmetrical tilt boundary ($\theta = 61.9^{\circ}$, $\beta = -0.5$) in copper have been carried out aiming to compare the behaviour of a perfect boundary with that of a boundary containing nanocracks lying on its surface. Details of the MD technique, the Embedded Atom Method and the copper potential employed in the simulations are given elsewhere [5]. The Nosé-Hoover thermostat [6] was implemented for temperature control. Simulations have been carried out at $T = 300$ K using time increments $\Delta t = 2.5\times10^{-15}$ s.

Prior to sample virtual testing, the cracked or uncracked bicrystals of $14.8\times2.2\times21.0$ nm^3 of size were constructed at 0 K, the cracks being formed by removing the atoms located in a band of 0.55 nm centred in the GB along 1/3 of the specimen size in the x direction. They were relaxed during 5 ps at 0 K and during 12.5 ps at 300 K under no constraints, for the GB to acquire its metastable configuration. Surface tension leads to some global and geometrical distortion of the initial shape of the bicrystals. In all of the tested cases, the Σ17(530) symmetrical tilt boundary showed negative shear coupling, in agreement with the reported negative coupling for $\theta \geq 35^{\circ}$ in [001] tilt boundaries [3]. After relaxation, two rigid zones 0.55 nm thick were established in the upper and lower layers of the samples. During the virtual shear test, the lower rigid zone remained fixed, the upper part being displaced at a constant rate of 2.12 m·s^{-1} ($\dot{\gamma} \approx 10^8$ s^{-1}). Periodic boundary conditions were set along the x and y axes.

Figure 1 shows the nominal shear stress, τ_{nom}, as a function of the nominal shear strain, γ_{nom}. The average shear stress in the ligament of the cracked specimens is 1.5 times higher than that value. For the uncracked tilt boundary the result reproduces the behaviour observed at similar homologous temperature by other authors [3, 4], characterized by a stick–slip phenomenon associated to the GB migration when certain shear stress (≈ 0.3 GPa) is overcome. The slopes of the intermittent elastic loading stages are 27 GPa. The presence of a crack affects the mechanical response of the samples. The cracked specimen shows similar stick–slip behaviour but the shear stress increases monotonically with strain till a value of 1.5 GPa at $\gamma_{nom} \approx 0.12$, when a sudden drop of the stress occurs.

The bicrystal is thus strengthened by the presence of intergranular cracks. The situation is similar to the strengthening of a crystal by a dispersion of nanovoids in dislocation-mediated plasticity. The shear strain–induced structural changes explain this anomalous behaviour (Fig. 2). Although the crack strongly amplifies the shear stress in the vicinity of the tip, the GB of the

cracked bicrystal is pinned by the crack. SCM occurs away from the crack tip, the GB bowing out (downwards as $\beta < 0$). The shear stress applied on the GB surface close to the crack tip weakens because of the progressive GB misorientation. Migration of the GB progressively becomes more difficult until GB depinning from the crack (small $|\beta|$) helped by partial dislocation emission from the crack tip.

Acknowledgements
Work supported by the Department of Industry, Commerce and Tourism of the Basque Government and the Provincial Council of Gipuzkoa (projects UET 1210/06 and ETORTEK inanoGUNE). A. Luque also acknowledges the Spanish Ministry of Science and Innovation and the European Social Fund (Torres Quevedo Programme).

References

[1] C.H. Li, E.H. Edwards, J. Washburn, E.R. Parker, Acta Metall., **1**, (1953) 223.
[2] M. Winning, G. Gottstein, L.S. Shvindlerman, Acta Mater., **49**, (2001) 211.
[3] J.W. Cahn, Y. Mishin, A. Suzuki, Acta Mater., **54**, (2006) 4953.
[4] H. Zhang, D. Du, D. Srolovitz, Philos. Mag., **88**, (2008) 243.
[5] A. Luque, J. Aldazabal, J.M. Martínez-Esnaola, J. Gil Sevillano, Fatigue Fract. Engng. Mater. Struct., **30**, (2007) 1008.
[6] S. Nosé, J. Chem. Phys., **81**, (1984) 511.

Figures

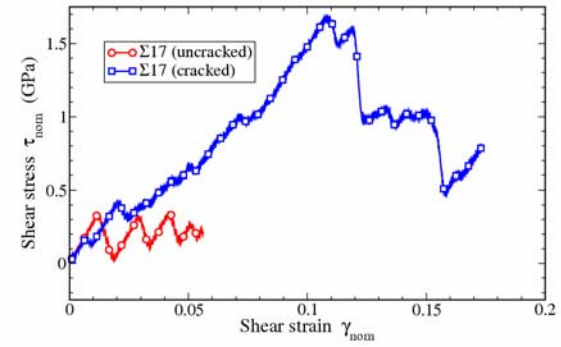

Figure 1. Nominal shear stress, τ_{nom}, vs. nominal shear strain, γ_{nom}, curves of the un-cracked and the cracked bicrystals of the Σ17(530) symmetrical tilt boundary.

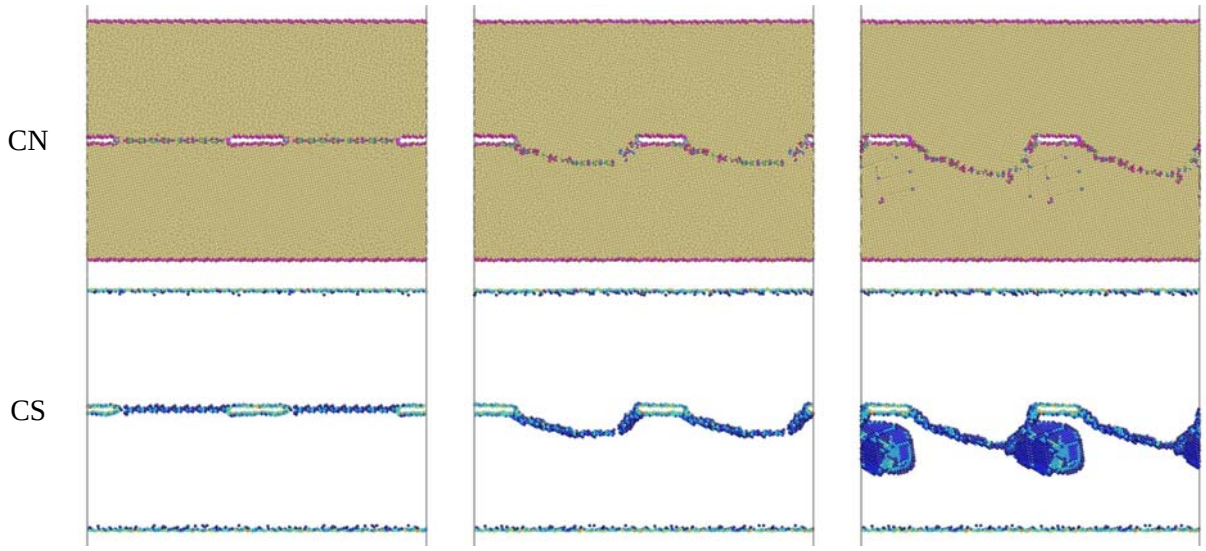

Figure 2. Copper bicrystal (Σ17(530)/[001] tilt boundary) under imposed shear displacement parallel to the boundary plane. The tilt axis is perpendicular to the figure. The bicrystal contains periodically spaced through–thickness intergranular cracks. Images are snapshots at macroscopic strain (a) γ_{nom} = 0,

(b) $\gamma_{nom} = 0.08$ and (c) $\gamma_{nom} = 0.12$. Depinning of the GB occurs shortly after that strain. Coordination number (CN) makes visible the GB and partial dislocations, centro-symmetry (CS), the stacking faults.

RESPONSE OF Mn OVERLAYERS ON Fe SUBSTRATE TO EXTERNAL MAGNETIC FIELDS

Eduardo Martínez[1], *Huahai Tan*[1], *Andrés Vega*[2], *Roberto Robles*[3] *and Valery Uzdin*[4]

[1] *Fachbereich Physik, Universität Osnabrück, Osnabrück, Germany*
[2] *Departamento de Física Teórica, Atómica y Óptica, Universidad de Valladolid, Valladolid, Spain*
[3] *Department of Physics, Virginia Commonwealth University, Richmond, VA 23284, USA*
[4] *St. Petersburg State University, Universitetskaya nab. 7/9, St. Petersburg, Russia*

Email: edmartin@uos.de

The magnetism of a large variety of nanostructures has been investigated in the last decades from both the experimental and theoretical sides [1]. The full understanding of the magnetic properties of a given system requires not only knowing its intrinsic properties but also its response to external fields. Moreover, many of the technological applications on magnetism are based on the possibility of engineering the system by applying external fields [2]. Experimentally, increasing the level of locality of applied fields is a challenge which will improve the density of information storage in recording media and consequently the device miniaturization. Most of the previous studies concentrated on collinear magnetism, which does not allow the local magnetic moments to rotate freely. Here we employed a semiempirical Tight-Binding method [3,4,5,6], which allows calculations in systems with large inequivalent sites within a noncollinear framework and includes the interaction with external magnetic fields. The system we studied is composed of 6 Mn overlayers deposited on a Fe substrate. In the collinear framework, we obtained various couplings in Mn overlayers. As a general trend, we found that those metastable configurations energetically close to the ground state have antiparallel couplings between Mn surface and subsurface layers as well as between Mn layers adjacent to the Fe interface, and a parallel coupling at the Mn/Fe interface. The hysteresis loop in the collinear case shows both smooth and sharp changes of the average magnetic moment of the Mn slab depending on the external field. The smooth changes correspond to reversible variations of a magnetic configuration of the system while the sharp changes are the result of a magnetic transition to a configuration with different local exchange couplings. In contrast, a reversible cycle is obtained in the noncollinear framework for the full range of applied fields. Therefore the response of the system is markedly different in both approaches. Due to the non-reversibility obtained in the collinear framework, the external magnetic field can be used to switch the system between different metastable configurations, some of them having very different average magnetic moment. We have found that the magnetic couplings in the central layers are weaker than those at the interface region and at the surface.

References:

[1] S. D. Bader, 2006 *Rev. Mod. Phys*. **78** 1
[2] D. Suess, 2006 *Appl. Phys. Lett.* **89** 113105
[3] E. Martínez, A. Vega, R. Robles and A. L. Vázquez de Parga, 2005 *Phys. Lett. A* **337** 469
[4] T. K. Yamada, E. Martínez, A. Vega, R. Robles, *et al.* 2007 *Nanotechnology* **18** 235702
[5] R. Robles, E. Martínez, D. Stoeffler and A. Vega, 2003 *Phys. Rev.B* **68** 094413
[6] E. Martínez, R. Robles , D. Stoeffler and A. Vega, 2006 *Phys. Rev.B* **74** 184435

Sol-gel derived nano-glass-ceramics containing Eu^{3+}- doped $NaYF_4$ nanocrystals

A. C. Yanes[1], A. Santana-Alonso[1], J. Méndez-Ramos[2], J. del-Castillo[1] and V. D. Rodríguez[2]

[1] Departamento de Física Básica
[2] Departamento de Física Fundamental y Experimental, Electrónica y Sistemas
Universidad de La Laguna, La Laguna, Tenerife, Spain
jmendezr@ull.es

Transparent glass-ceramics containing rare-earth doped nanocrystals emerge as new class of materials presenting enhanced physical and optical properties with potential applications in optoelectronic technology [1, 2]. On the other hand, $NaYF_4$ crystal is an excellent luminescence host material for rare-earth ions with relevance in a wide range of fields such as lighting, displays, photo-electronic devices, biological labels, solar cells and tuneable infrared phosphors for 3D optical recording [3, 4]. Furthermore, highly transparent nanostructured rare-earth doped glass-ceramics can be obtained by thermal treatment of precursor glasses prepared by the easy and low cost room-temperature sol-gel method [5]. In this sense nano-glass-ceramics containing Eu^{3+}-doped $NaYF_4$ nanocrystals have been successfully developed for the first time by thermal treatment of precursor sol-gel derived glasses with composition $95SiO_2$- $5NaYF_4$: 0.1 Eu^{3+} (mol %).

X-ray diffraction patterns of samples heat treated at temperatures ranging from 550 to 650 ºC confirmed the precipitation of $NaYF_4$ nanocrystals. Moreover, nanocrystal mean radii were calculated by using Scherrer's equation obtaining values ranging from 4.3 to 9.6 nm corresponding to treatment temperatures of 550 and 650 ºC, respectively. Addionally, TEM and HRTEM analysis were carried out for the 650 ºC heat treated sample, see Fig. 1. The precipitated nanocrystals are clearly visible as nearly spherical dark spots homogeneously dispersed in the amorphous silica network. Using HRTEM we can also observe a simple nanocrystal where direct image was filtered by using FFT pattern. A complete spectroscopic study has been carried out. Changes in the luminescence spectra with the temperature of the heat treatment have been analyzed and related to the degree crystallinity of the sample. Luminescence features are indicative of higher incorporation of Eu^{3+} ions into precipitated nanocrystals with increasing heat treatment temperature. In particular, emission spectra have been obtained for different excitation wavelengths discerning between the fraction of the rare-earth partitioned into $NaYF_4$ nanocrystals and those remaining in the amorphous silica glassy phase, see Fig. 2

References:

[1] Y. Ying and A.P. Alivisatos, Nature **437** (2005) 664.
[2] Y.H. Wang and J. Ohwaki, Appl. Phys. Lett. **63** (1993) 3268.
[3] Y. Guangshun, L. Huachang, Z. Shuying, G. Ye, Y. Wenjun, C. Depu and G. Liang-Hong, Nano Letters **4** (2004) 2191.
[4] A. Shalav, B. S. Richards, and T. Trupke, K. W. Krämer and H. U. Güdel, Appl. Phys. Lett. **86** (2005) 013505; J.F. Suyer, J. Grimm, M.K. van Veen, D. Biner, K.W. Krämer and H.U. Güdel, J. Lumin. **117** (2006) 1.
[5] A.C. Yanes, J. Del Castillo, M. Torres, J. Peraza, V.D. Rodríguez and J. Méndez-Ramos, Appl. Phys. Lett. **85** (2004) 2343; J. Del Castillo, V.D. Rodríguez, A.C. Yanes, J. Méndez-Ramos and M.E. Torres, Nanotechnology **16** (2005) S300.

Figure:

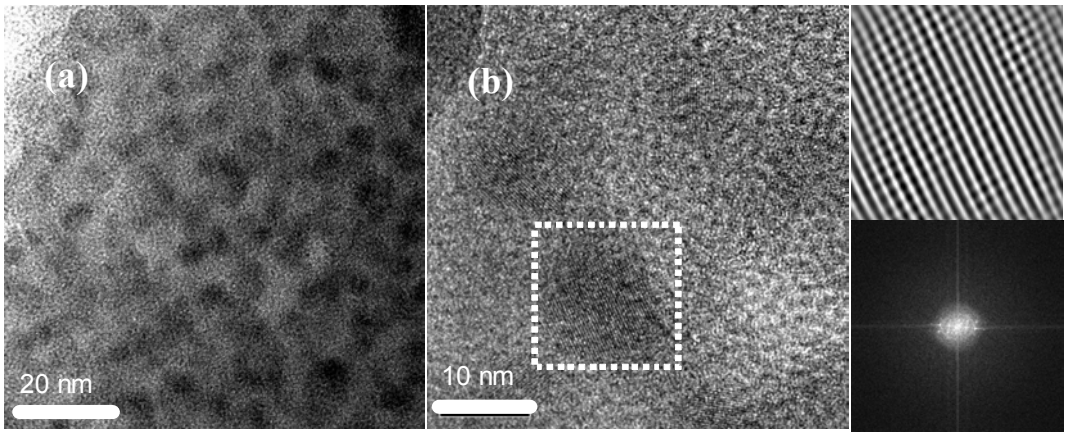

Fig. 1. TEM bright field image shows the presence of $NaYF_4$ nanoparticles in dark contrast (a). HRTEM microphotograph with $NaYF_4$ nanocrystals squared in white (b). The right-bottom image corresponds to the power spectrum obtained from the squared region. The right-up image shows a magnified detail of the same squared region revealing the crystalline pattern of a $NaYF_4$ nanoparticle.

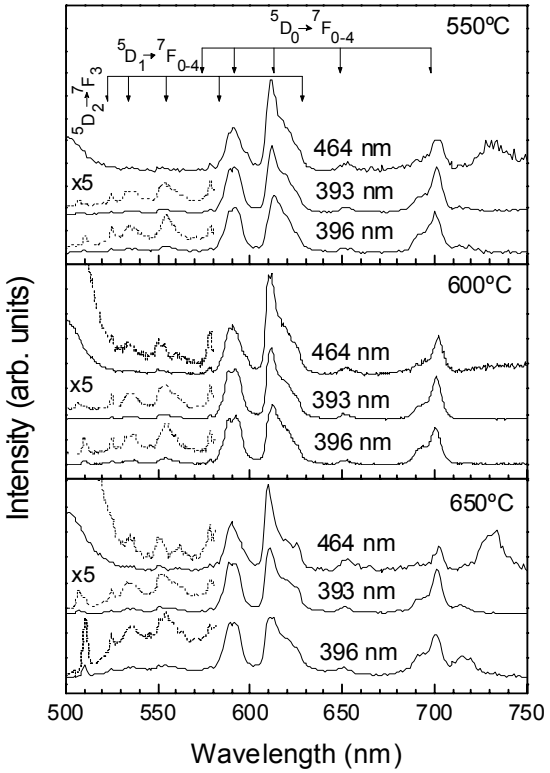

Fig. 2. Emission spectra exciting at 393, 396 and 464 nm, normalized to the maximum intensity at 590 nm. The intensity ratio R between the transitions at 590 and 613 nm increases with heat treatment temperature, indicative of a higher degree of crystallinity. Crystalline-like environment (higher R values) is favoured when exciting at 396 nm.

Tuneable up-conversion phosphor based in sol-gel derived nano-glass-ceramics containing Yb^{3+}-Er^{3+} co-doped $NaYF_4$ nanocrystals

A. Santana-Alonso[a], A. C. Yanes[a], J. Méndez-Ramos[b], J. del-Castillo[a] and V. D. Rodríguez[b]

[a] *Departamento de Física Básica*
[b] *Departamento de Física Fundamental y Experimental, Electrónica y Sistemas*
Universidad de La Laguna, La Laguna, Tenerife, Spain
jmendezr@ull.es

Enhanced physical and optical properties of rare-earth doped nanocrystals make transparent nano-glass-ceramics a promising class of materials with potential applications in optoelectronic technology [1, 2]. $NaYF_4$ crystal is known to be one of the most efficient rare-earth ions host for near infrared to visible up-conversion [3]. Rare-earth doped $NaYF_4$ up-converting phosphors have been found to be useful for enhanced responsivity in the near-infrared for silicon solar cells [4], bioimaging and fluorescent probe labelling, sensitive detection of DNA and tuneable infrared phosphors for 3D optical recording [5]. Furthermore, highly transparent nanostructured rare-earth doped glass-ceramics can be obtained by thermal treatment of precursor glasses prepared by the easy and low cost room-temperature sol-gel method [6]. In this work nano-glass-ceramics containing Yb^{3+}-Er^{3+} co-doped $NaYF_4$ nanocrystals have been successfully developed for the first time by thermal treatment of precursor sol-gel derived glasses with composition $95SiO_2$-$5NaYF_4$ co-doped with 0.3 Yb^{3+} and 0.1 Er^{3+} (mol %). X-ray diffraction confirms the precipitation of $NaYF_4$ nanocrystals during heat treatment and their corresponding sizes have been calculated by using Scherrer's equation, obtaining values in the range 4.1–9.6 nm, corresponding to 550 and 650 ºC treatment temperatures, respectively.

Visible up-conversion luminescence has been obtained under infrared excitation at 980 nm, see Fig. 1. Up-conversion emission bands present sharp structure with well-resolved Stark components indicative of the incorporation of the rare-earth ions into precipitated nanocrystals. A remarkable change in the intensity ratio of the red to green up-conversion bands as a function of heat treatment temperature can been observed, resulting in colour tuneable up-conversion phosphors with applications in optical integrated devices. Colour tuneability has been also analyzed and quantified in terms of CIE standard chromaticity diagram where the colour gradually changes from reddish to greenish part of the diagram, as shown in Fig. 1.

References:

[1] Y. Ying and A.P. Alivisatos, Nature **437** (2005) 664.
[2] Y.H. Wang and J. Ohwaki, Appl. Phys. Lett. **63** (1993) 3268.
[3] J.F. Suyer, J. Grimm, M.K. van Veen, D. Biner, K.W. Krämer and H.U. Güdel, J. Lumin. **117** (2006) 1.
[4] A. Shalav, B. S. Richards, and T. Trupke, K. W. Krämer and H. U. Güdel, Appl. Phys. Lett. **86** (2005) 013505;
[5] S. F. Lim, R. Riehn, W.S. Ryu, N. Khanarian, C.K. Tung, D. Tank and R.H. Austin, Nano Letters **6** (2006) 169.
[6] A.C. Yanes, J. Del Castillo, M. Torres, and J. Peraza, V.D. Rodríguez and J. Méndez-Ramos, Appl. Phys. Lett. **85** (2004) 2343; J. Del Castillo, V.D. Rodríguez, A.C. Yanes, J. Méndez-Ramos and M.E. Torres, Nanotechnology **16** (2005) S300.

Figures:

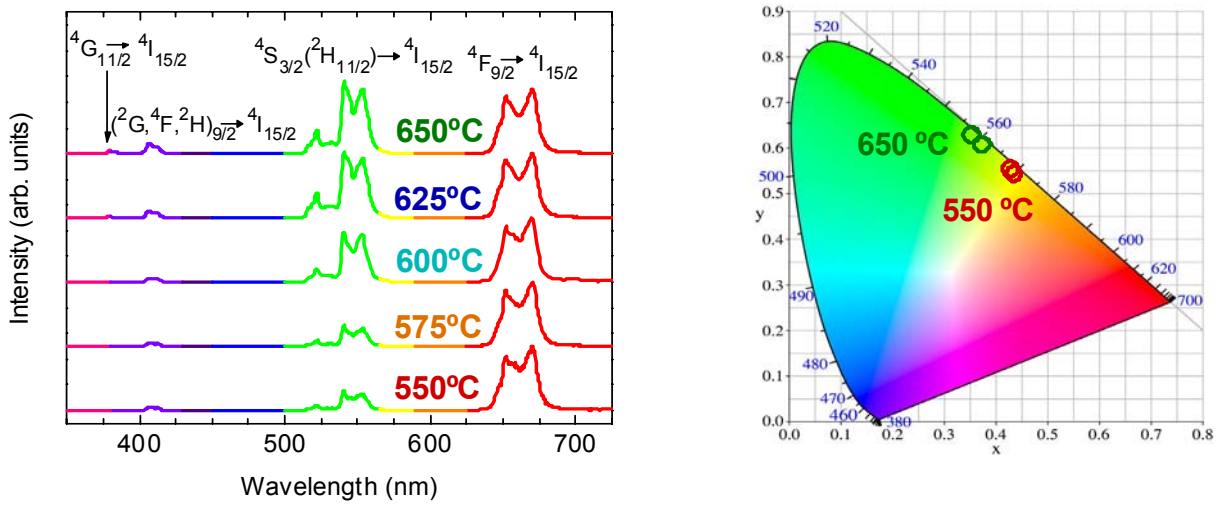

Fig. 1. Up-conversion emission spectra under 980 nm excitation at 200 mW as a function of heat treatment temperature, normalized to the maximum at 660 nm (left). Corresponding colour coordinates in the CIE chromaticity diagram of visible up-conversion emission for different heat treatment temperatures (right).

PLASMA PROCESSING OF POLYPYRROLE-HEPARIN THIN FILMS ON TITANIUM SUBSTRATES FOR BIOMEDICAL APPLICATIONS

Adina Morozan, Florin Nastase, Anca Dumitru, Claudia Nastase, Silviu Vulpe
Polymer Science Group, University of Bucharest, P.O. Box MG-40 Magurele, Bucharest, 077125, Romania
adina@psg.unibuc.ro

Many structural materials have been placed in the live body in attempt to aid the body in repairing processes of diseases. The predominantly used materials in the treatment of various diseases have been and still are metals and polymers. The materials that can function intimately with the living cells tissue, with minimal adverse reaction, must be manufactured as multiple metallic or nonmetallic phases.

Titanium and its alloys are considered to be the most attractive metallic materials for biomedical applications because of their excellent mechanical properties, corrosion resistance and biocompatibility [1]. In recent years, many methods have been applied to improve the biocompatibility and biofunctionality of titanium-based implants.

Conducting polymers such as polypyrrole (PPy) offer a new class of material for trial use in biological applications. PPy has been chosen as coating polymer to protect the metal implant against corrosion and could be surface modified with biologically active molecules able to stimulate positive interactions with bone tissue [2, 3]. Surface modification of these materials with biological moieties is desired to enhance the biomaterial-tissue interface and to promote desired tissue responses. Heparin (HE) is a potent anticoagulant that can be immobilized on biomaterial surfaces to increase their hemocompatibility.

Many ingenious and useful techniques have been evolved for modifying the surface structure, while keeping the bulk structure unchanged. The plasma polymerization is the process mostly used for the deposition of thin polymer and polymer-based composite films with a variable amount of functionalities available for reaction with biomolecules [1, 4, 5].

In this context, the strategy followed was based on a plasma deposition of PPy and PPy-HE films onto Ti substrate. Heparin was immobilized on/in the PPy films using plasma processing. Heparin was chosen because it is a component of the extracellular matrix of blood vessels and has anticoagulant properties.

The chemical composition and the morphology of the polymeric films PPy and Ppy-HE films deposited onto Ti substrate were investigated using Fourier transform infrared (FT-IR), Raman spectroscopy and atomic force microscopy (AFM). Results showed that HE was incorporated into the PPy matrix and is presented on particle surface.

References:

[1] Xuanyong Liu, Ray W. Y. Poon, Sunny C. H. Kwok, Paul K. Chu and Chuanxian Ding, Surface and Coatings Technology, Volume 186, Issues 1-2, 2 August 2004, Pages 227-233

[2] E. De Giglio, M. R. Guascito, L. Sabbatini and G. Zambonin, Biomaterials Volume 22, Issue 19, 1 October 2001, Pages 2609-2616

[3] W. Khan, M. Kapoor, N. Kumar, Acta Biomaterialia, 3(4), (2007) 541.

[4] Eun-Deock Seo, Macromolecular Research, Vol. 11, No. 5, pp 387-392 (2003)

[5] B. D. Ratner, Journal of Photopolymer Science and Technology, Vol. 8, No.3 (1995), Pages 481-494

PLASMA PROCESSING OF PMMA FILMS FOR BIOMEDICAL APPLICATIONS

Claudia Nastase,[1] Anca Dumitru,[1] Florin Nastase,[1] Adina Morozan,[1]
Silviu Vulpe,[1] and Dan Batalu[2]
[1]Polymer Science Group, University of Bucharest,
P.O. Box MG-40 Magurele, Bucharest, 077125, Romania
[2]Center for Research and Expertise of Special Materials,
University Politehnica of Bucharest, Splaiul Independentei 313,
Bucharest, 060032, Romania

nastasec@psg.unibuc.ro

The polymer thin films have been used as biomaterial in medicine area from cardiovascular to plastic surgery. When a biomaterial implanted into a living tissue generate a cascade of host reactions occur at interface between tissue and material [1,2]. These reactions are known as inflammatory response. Proteins and blood cells from body fluids interact with the surface of the biomaterial; therefore the adsorption of proteins at the surface of the biomaterial is an important issue in its design [3,4]. Hence, an important goal in the design of biocompatible materials is to create surfaces that minimize unspecific interactions with biological material such as proteins and (blood) cells.

The different studies showed that plasma deposition processes could enhance the compatibility with blood of vascular grafts with small diameter. Plasma processing can be used to introduce desired functional groups or chains onto the surface of materials with particular application for improving the polymer film biocompatibility [5]. In this way a multitude of chemical substance, including that can not be polymerized by conventional methods, can be used for introducing specific functional groups on substrate. Moreover, the plasma treatment is a unique and powerful method for modifying polymeric materials without altering their bulk properties.

In this purpose we are using the plasma processing to enhance the properties of PMMA films for biomedical applications. Plasma processed PMMA thin films have been obtained in a DC glow discharge from polymer solution at different plasma powers. The results are compared with that for PMMA films obtained by deep coating method.

The structure and composition of the films have been characterized by Fourier Transform Infrared Spectroscopy (FTIR), Raman spectroscopy and atomic force microscopy (AFM). The surface modifications of PMMA films obtained with both methods proposed above have been evidence by noncontact mode AFM images (figure 1). It has also shown that the topography of PMMA surface was influenced by plasma parameters.

References:

[1] J.M. Anderson et al., in: B.D. Ratner, et al. (Eds.), Biomaterials—an Introduction into Materials in Medicine, Academic Press, San Diego (1996) p. 165.

[2] J.I. Gallin, R. Snyderman (Eds.), D.T. Feraon, B.F. Haynes, C. Nathan (assoc. Eds.), Inflammation: Basic Principals and Clinical Correlates, third ed., Lippincott Williams and Williams, Philadelphia (1999).
[3] C.R. Jenney, J.M. Anderson, J. Biomed. Mater. Res. 44 (1999) 206.
[4] Z. Xu, R.E. Marchant, Biomaterials 21 (2000) 1075.
[5] A. Karkhaneh, H. Mirzadeh, and A.R. Ghaffariyeh, Proceedings of the Fifth IASTED International Conference on Biomedical Engineering, BioMED 2007, pp.433-438, Innsbruck, Austria, February 14 – 16 (2007).

Figures:

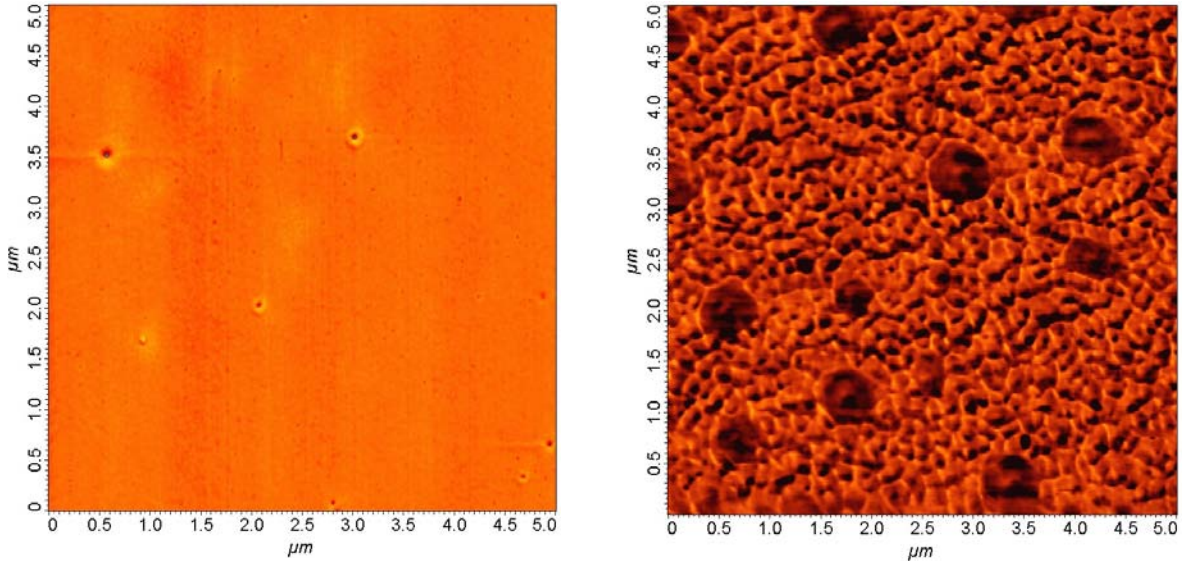

a b

Figure 1. Noncontact AFM images of (a) deep coating PMMA film and (b) plasma processed PMMA film

FILMS CONSISTING OF GRAPHITE-LIKE SHEETS SUITABLE FOR INTERCONNECTS WITH HIGH ELECTRICAL AND THERMAL CONDUCTIVITY

J. G. Partridge, D. Lau, M. Taylor, A. Moafi and D. G. McCulloch
RMIT University, 124 LaTrobe Street, Melbourne, Victoria, Australia
D. R. McKenzie and N. A. Marks
School of Physics, University of Sydney, NSW 2006, Australia

jim.partridge@rmit.edu.au

The graphite sheet is the strongest two-dimensional structure known and has high in-plane thermal and electrical conductivity. As a result, arrays of carbon nanotubes have been proposed as heat sinks and electrical interconnects [1]. Fully oriented sp^2 sheets [2] as described in this work are equally suited to these applications and as shown, they can be produced in a FCVA system with no requirement for high deposition temperatures or catalyst layers.

Carbon films with thicknesses in the range 20-80 nm were fabricated using a Filtered Cathodic Vacuum Arc (FCVA) deposition system and a sputtering system. By varying the substrate bias (in the FCVA only) as well as the background Ar gas pressure, films with different intrinsic stress were produced at room temperature. Following deposition, through-film I(V) characteristics were measured for each film. Figure 1 shows the normalised through-film resistance/nm (calculated at 1V) plotted against the intrinsic stress for sixteen carbon films. In the films deposited with low stress (1-5 GPa) asymmetric, current-voltage characteristics resembling those of a Schottky contact were observed (inset A) and the resistance-per-nm was of the order of 10^3 Ω/nm. In films with higher intrinsic stress (>7 GPa), ta-C was formed and while the non-linear behaviour was maintained, the resistance-per-nm exceeded 10^4 Ω/nm. In films deposited using a substrate bias of approximately 400 V (corresponding to an incident ion energy of approximately 300 eV) and with intrinsic stress of approximately 6 GPa, very different I(V) characteristics were observed. The high resistance non-linear current-voltage behaviour was replaced by a low resistance linear (Ohmic) current-voltage characteristic (inset B).

Figure 2(a) shows a cross-sectional bright field high resolution TEM image of a film with stress in the transition region located on the return path (dashed line) in Figure 1, where Ohmic behaviour was observed. The diffraction pattern (not shown) revealed localised graphitic {002} reflections aligned with the plane of the film and the microstructure consists entirely of graphite-like sheets aligned normal to the film surface. This orientation is preferred on the basis of energy minimisation of turbostratic graphite in a biaxial stress field. Films with this preferred orientation exhibit low resistance and Ohmic behaviour and are indicated by filled squares in Figure 1(a) on the dashed trajectory. Figure 2(b) shows how vertically aligned graphite-like sheets may be used in vertical interconnects.

References:

[1] P. Avouris, Z. Chen and V. Perebeinos, Nature Nanotechnology 2 (2007) 605
[2] D. W. M. Lau, D. G. McCulloch, M. B. Taylor, J. G. Partridge, N. A. Marks, D. R. McKenzie, E. Teo and B. K. Tay, Physical Review Letters 100 (2008) 176101

Figures:

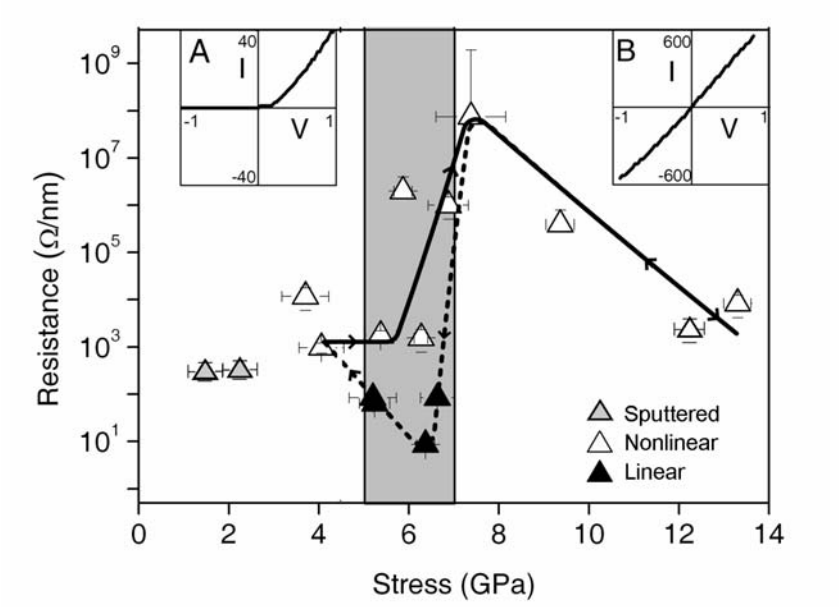

Figure 1. The through-film resistance per nanometre plotted against intrinsic stress for sixteen carbon films. Insets A and B show examples of non-Ohmic and Ohmic current-voltage characteristics obtained from these films. The experimental transition region is shown in grey. The solid and dashed thick lines show the trajectories through the transition region when the ion energy is increased.

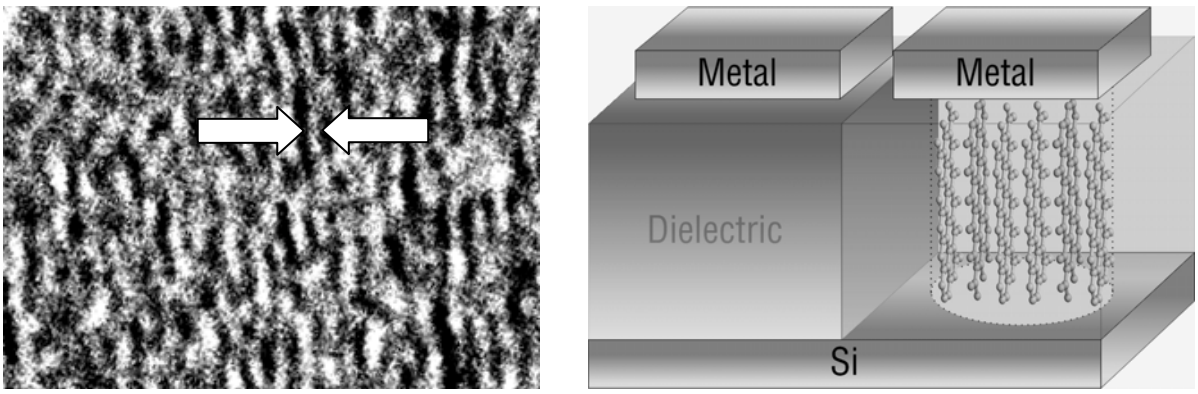

(a) **(b)**

Figure 2. (a) A high-resolution TEM image of the 0.335nm graphite-like planes (indicated by arrows) aligned perpendicular to the surface of the film and (b) a schematic diagram showing vertically oriented graphite-like sheets as a vertical interconnect material.

Stress-strain curves of aluminum nanowires: fluctuations in the plastic regime and absence of hardening

L. Pastor-Abia[1], M.J. Caturla[1,2], E. SanFabián[1,3,4], G. Chiappe[1,2], E. Louis[1,2,3]

[1] *Instituto Universitario de Materiales de Alicante (IUMA), Universidad de Alicante San Vicente del Raspeig, E-03690 Alicante, Spain*
[2] *Departamento de Física Aplicada, Universidad de Alicante San Vicente del Raspeig, E-03690 Alicante, Spain*
[3] *Unidad Asociada of the Consejo Superior de Investigaciones Científicas, Universidad de Alicante, San Vicente del Raspeig, E-03690 Alicante, Spain*
[4] *Departamento de Química Física, Universidad de Alicante, San Vicente del Raspeig, E-03690 Alicante, Spain*
Corresponding author: L. Pastor-Abia luis.abia@ua.es

One of the most subtle issues in the increasingly broad area of nanoscience concerns the mechanical response of small systems. Mechanical devices are getting so small that quantum limits are already reachable [1]. Understanding how materials respond at such small scales is a need for the design of novel electromechanical devices.

Although technical difficulties inherent to the measurement of the mechanical response of small systems are enormous, nowadays tools are allowing to investigate both inorganic [2–5] and organic (biological) [5, 6] systems. Several issues are particularly attracting the interest of researchers, among which we mention the size dependence of mechanical moduli (Young modulus, yield stress, ...) [5], fracture at the nanoscale [3], and whether small systems do or do not harden [4]. No complete agreement has yet been attained on any of these questions.

We have carried out molecular dynamics calculations of stress-strain curves of aluminum nanowires using the interatomic potential proposed by Ercolessi and Adams [7]. Nanowires were stretched along the [001] direction at a constant rate of 0.01 Å/ps at 4.2 K, using as initial conditions fixed atomic positions and velocity at each atom randomly distributed according to Maxwell distribution. The stress tensor can be easily derived from molecular dynamics calculations as:

$$\sigma_{\alpha\beta} = \frac{1}{V}\left(\sum_{i=1}^{N} m_i v_{i\alpha} v_{i\beta} + \frac{1}{2}\sum_{i\neq j}^{N} r_{ij\beta} F_{ij\alpha}\right) \quad (1)$$

where V is the volume of the sample, $v_{i\alpha}$ is the component α of the velocity vector at atom i, $r_{ij\beta}$ is the component β of the vector that joins atoms i and j, and $F_{ij\alpha}$ is the component α of the force that atom i exerts on atom j. V was replaced by its initial value, thus giving the engineering stress.

Fig. 1 shows the results for a nanowire of 2645 atoms and an ab-initio result for a small cluster of 22 atoms. Both approaches show short quasi-elastic events followed by sudden drops of the total energy associated to major atomic rearrangements. Averaging over at least 1500 realizations on the streching of a 463 atoms nanowire allows to unambiguously conclude that, beyond the yield point, the system does not harden (see Fig. 2).

Another outstanding issue, is how fluctuations in the plastic, non-linear, regime are distributed [6]. Experimental data obtainedon polymers indicate that the work probability distribution has a Gaussian component plus long non-Gaussian tails. The origin of this deviation from the Gaussian distribution predicted by the Central Limit Theorem (CLT) is a matter of fundamental interest that is being intensively investigated. Whether this kind of deviations from the CLT is a characteristic common to any small system is something that has not yet been settled. The analysis over the around 1.5 million data indicate the presence of non-gaussian tails in the heat probability distribution but not in the engineering stress (Fig. 3).

[1] K.C. Schwab, M.L. Roukes, Physics Today, july 2005, p. 36, and references therein.
[2] G. Rubio-Bollinguer, S.R. Bahn, N. Agrait, K.W. Jacobsen, S. Vieira, Phys. Rev. Lett. 87, 026101 (2001).
[3] D. Wang, J. Zhao, S. Hu, X. Yin, S. Liang, Y. Liu, and S. Deng, Nano Letters **7**, 1208 (2007).
[4] B. Wu, A. Heidelberg, anj J. Bolland, Nature Mater. **4**, 526 (2005).
[5] S. Suenot, S. Demoustier-Champagne, C. Frétigny and B. Nysten, Nanotech, **3**, 549 (2003).

[6] C. Bustamante, J. Liphardt, F. Ritort, Physics Today, july 2005, p. 43, and references therein.
[7] F. Ercolessi and J. B. Adams, Europhys. Lett. **26**, 583 (1994).

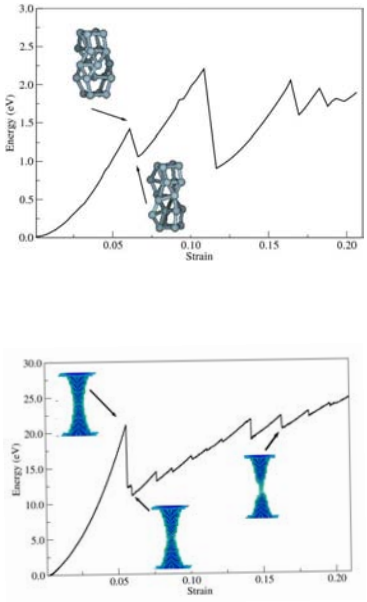

FIGURE 1: Energy vs engineering strain, calculated using either Density Functional Theory (upper panel) or molecular dynamics (lower panel), for aluminum nano-wires containing 22 and 2645 atoms, respectively: Actual atomic arrangements are also shown at different stages of the stretching process. The results correspond to single a realization (initial distribution of velocities)

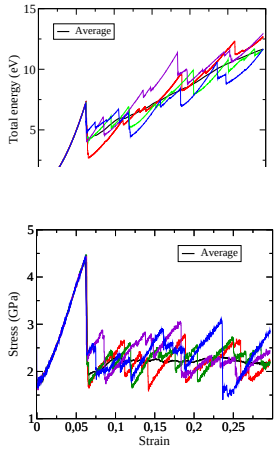

FIGURE 2: Total energy (upper panel) and stress (lower panel) versus engineering strain, as derived from molecular dynamics calculations on aluminum nanowires containing 463 atoms stretched at a constant strain rate. The results correspond to three individual realizations (different initial distributions of atomic velocities) and to an average that includes over 1500 (thick black line).

FIGURE 3: Probability distributions of the engineering stress and the heat evolved (ΔQ) in the non-linear (plastic) regime derived from molecular dynamics calculations on aluminum nanowires, containing 463 atoms, stretched at a constant strain rate. The distribution contains more than 1.5 million counts (1500 realizations by at least one thousand points along the stress-strain curve). The (red) continuous curves are Gaussian fits to the numerical data over the stress range [-0.5,0.5] GPa or the heat range [-0.02,0.02] eV.

NANORECTIFIERS BASED ON SUPERCONDUCTING/MAGNETIC HYBRIDS

D. Perez de Lara[1], E. M. Gonzalez[1], J. V. Anguita[2], J. L. Vicent[1]
[1]Departamento Física de Materiales, Facultad Ciencias Físicas, Universidad Complutense, 28040 Madrid, Spain
[2]Instituto de Microelectrónica, Centro Nacional de Microelectrónica, Consejo Superior de Investigaciones Científicas, Tres Cantos, 28760 Madrid, Spain
dperezla@fis.ucm.es

Films of superconducting Nb have been grown on top of arrays of Ni nanotriangles. In the superconducting mixed state of this hybrid system, the vortex lattice dynamics shows rectification effects [1]. The array of nanotriangles acts as pinning centers for the superconducting vortex lattice. The vortex lattice motion on these asymmetric potentials shows rectification effect. That is, an input ac current applied on the nanodevice yields an output dc voltage. There are two possible rectification effects: longitudinal effect, when the input current is injected perpendicular to the triangle reflection symmetry axis and transverse rectification when the input current is injected parallel to the triangle reflection symmetry axis effect the output voltage drop occurs perpendicular to the triangle reflection symmetry axis [2].

References:

[1] J. E. Villegas, S. Savelev, F. Nori, E. M. Gonzalez, J. V. Anguita, R. Garcia, J. L. Vicent, Science, **302** (2003) 1188.
[2] E. M. Gonzalez, N. O. Núñez, J. V. Anguita, J. L. Vicent, Applied Physics Letters, **91** (2007) 062505.

COMPOSITION AND STRUCTURE OF Si(001)/CaF_2 INTERFACES

Henry P. Pinto[1], *Franco Chiaravalloti*[2], *Damien Riedel*[2], *Adam S. Foster*[1] *and Gérald Dujardin*[2]

[1]Laboratory of Physics, Helsinki University of Technology, P.O.Box 1100, FI-02015 TKK, Finland
[2]Laboratoire de Photophysique Moléculaire, Université Paris-Sud 91405 Orsay, France
hpp@fyslab.hut.fi, franco.chiaravalloti@u-psud.fr

The development of practical molecular electronics relies on the identification of molecule-surface combinations where the molecule is bound to the surface without being electronically coupled. A possible approach is to consider molecules on insulating thin films on conducting substrates. This film is meant to isolate the molecule, while allowing controlled contact to the conducting substrate if wanted. Demonstrating the potential of such a setup requires complete characterization of both the atomic structure of the molecule-surface interface and the its electronic structure.

Calcium fluoride has always been considered as an interesting and prototypical insulating material to be grown epitaxially on silicon single-crystal surfaces. Due to the small lattice mismatch between the two materials 0.6% at room temperature, CaF_2 films of good crystal quality can be grown by molecular beam epitaxy MBE on silicon. CaF_2 has very good insulating properties and optical transmission in the range of infrared and visible radiation. Stimulated by the number of potential applications, extensive studies of the growth of CaF_2 on silicon have been mainly carried out on Si (111) [1]. Only a few attempts have been undertaken up to now to investigate the initial stages of CaF_2 growth on the technologically important Si(001) surface [2], and detailed studies in high resolution remain absent.

In this study, we use an ultra thin film of CaF_2 grown on the top of a Si(001) substrate as a prototype substrate for molecular adsorption. The film is grown using molecular beam epitaxy in ultra high vacuum at a substrate temperature of about 750 K. The films were characterized at several stages of their growth via low temperature scanning tunneling microscopy (LT-STM) and spectroscopy measurements. Using a plane-wave density functional theory, we compute the electronic and energetic properties of several structural candidates, and calculate the Gibbs free energy to determinate the most stable structures of the Si(001)/Ca_xF_y interface in thermodynamic equilibrium with a CaF_2 gas environment. We perform multiple scattering theory STM simulations on the most stable interface structures, and resolve the actual structure of the interface by comparison of theoretical and experimental linescans. Finally, the electronic and structural properties of the interface are discussed in the light of the experimental molecular adsorption results.

[1] E. Rotenberg, J. D. Denlinger, M. Leskovar, U. Hessinger, and M. A. Olmstead, Phys. Rev. B **50**, 11052 (1994).
[2] L. Pasquali, S. M. Suturin, V. P. Ulin, N. S. Sokolov, G. Selvaggi, A. Giglia, N. Mahne, M. Pedio, and S. Nannarone, Phys. Rev. B **72**, 045448 (2005)

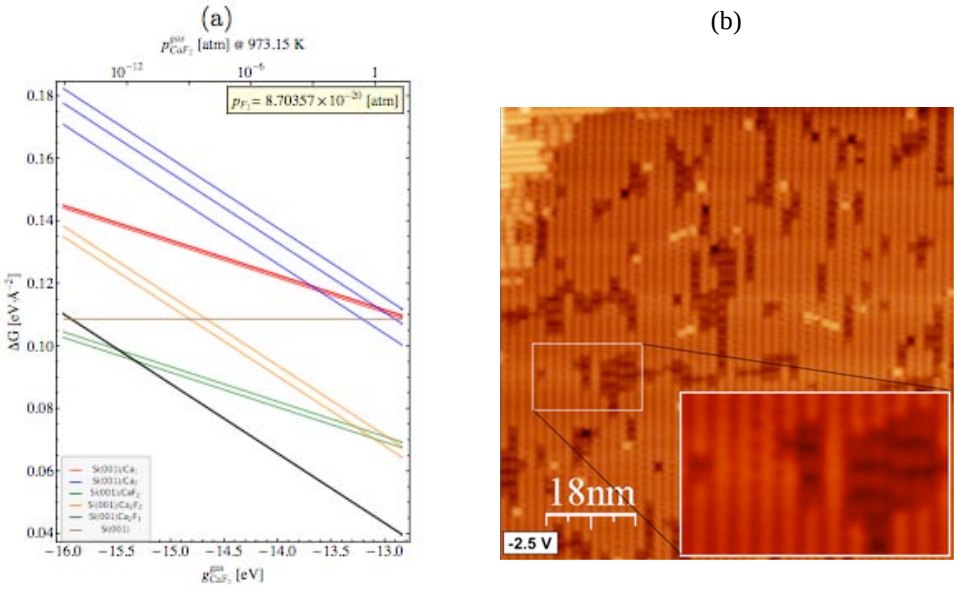

Figure 1: (a) Interfacial energy for various structures as a function of the free energy of the CaF_2 source. (b) STM image of the CaF_2 wetting layer on Si(001)

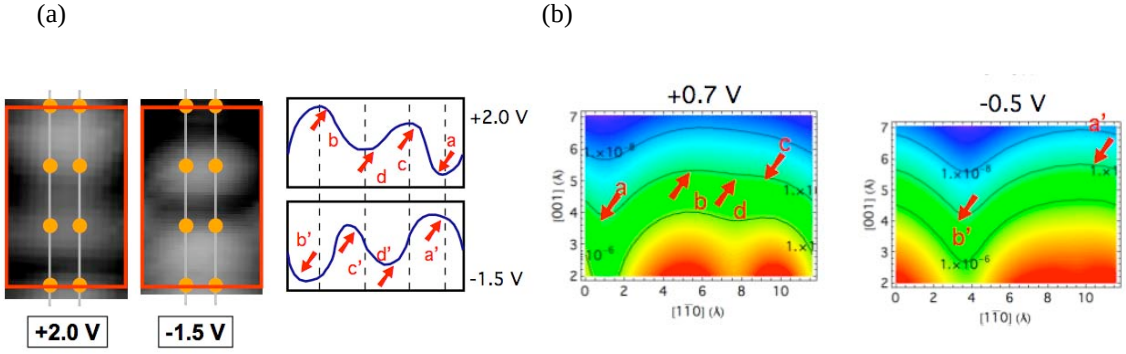

Figure 2: (a) Experimental images and scanlines, and (b) simulated STM scanlines of the interface at different bias voltages.

USE OF NANOPARTICLES FOR PREPARATION OF RARE-EARTH DOPED SILICA FIBERS

Ondrej Podrazky, Ivan Kasik, Marie Pospisilova, Vlastimil Matejec
Institute of Photonics and Electronics AS CR, v.v.i.,
Chaberska 57, 182 51 Prague, Czech Republic
podrazky@ufe.cz

Rare-earth doped optical fibers are used in fiber lasers and fiber amplifiers. Erbium-doped fiber amplifiers (EDFA) for C-band are commercially available today, but new methods for improving their performance are still developed, since emission of the Er^{3+} ions in silica is affected by multi-phonon relaxations and ion-ion interactions. Fibers based on fluoride, telluride or chalcogenide glasses offer low-phonon matrix with good solubility of Er^{3+} ions, but their chemical and physical properties are quite different from silica fibers used in telecommunications. An alternative approach can be preparation of silica fibers co-doped with erbium and nano-structured aluminium oxide (alumina) in its core, since alumina has lower phonon energy and better solubility of Er^{3+} ions compared to silica.
The work deals with preparation of aluminium-erbium co-doped silica fibers. The MCVD method[1] with solution-doping technique[2] were used for preparation of preforms for fiber drawing. At first a porous silica frits were deposited on the inner walls of silica substrate tubes and the frits were soaked either by dispersion of alumina and erbium(III) oxide nanoparticles in water or by aqueous solution of aluminium chloride and erbium chloride. The soaked frits were dried in a flow of dry oxygen and then they were sintered and the tubes were collapsed into preforms. The preforms were analyzed by confocal-microscopy and refraction-index profiler and fibers with diameter of 125 μm were drawn. Fluorescence emission spectra of Er^{3+} ions in the fibers were measured using 980 nm pigtailed laser diode as the excitation source.
It was found that the distribution of Er^{3+} ion concentration is more homogeneous in preforms prepared from dispersions of nanoparticles compared to the preforms prepared using solutions of chlorides (see the fig.1). The fluorescence intensity of Er3+ ions in fibers in range from 1500 nm to 1650 nm was found to be approx. 2.5 times higher in "nanoparticle-doped" fibers compared to the fibers prepared conventionally (see fig.2).
This work was supported by the Czech Science Foundation, contract No.102/07/P507.

References:

[1] Nagel S.R., Macchesney J.B., Walker K.L., IEEE J. Quantum. Elect. **18** (1982) 459-476.

[2] Townsend J.E., Poole S.B., Payne D.N., Electron. Lett. **23** (1987) 329-331

Figures:

Figure 1: Emission of Er^{3+} ions in preform cores at 505-550 nm, excited by argon laser (λ=488 nm) scanned by confocal microscope (left - nanoparticle doped fiber, right - "conventionally" doped fiber).

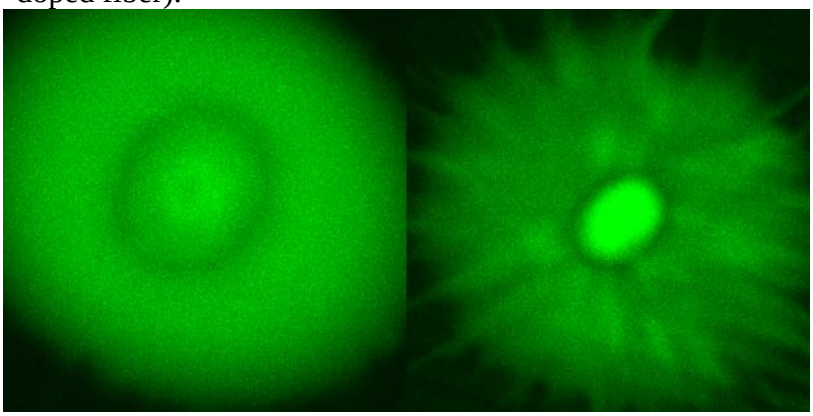

Figure 2: Fluorescence emission spectra of Er^{3+} ions in prepared fibers. (λ_{EX}=980 nm)

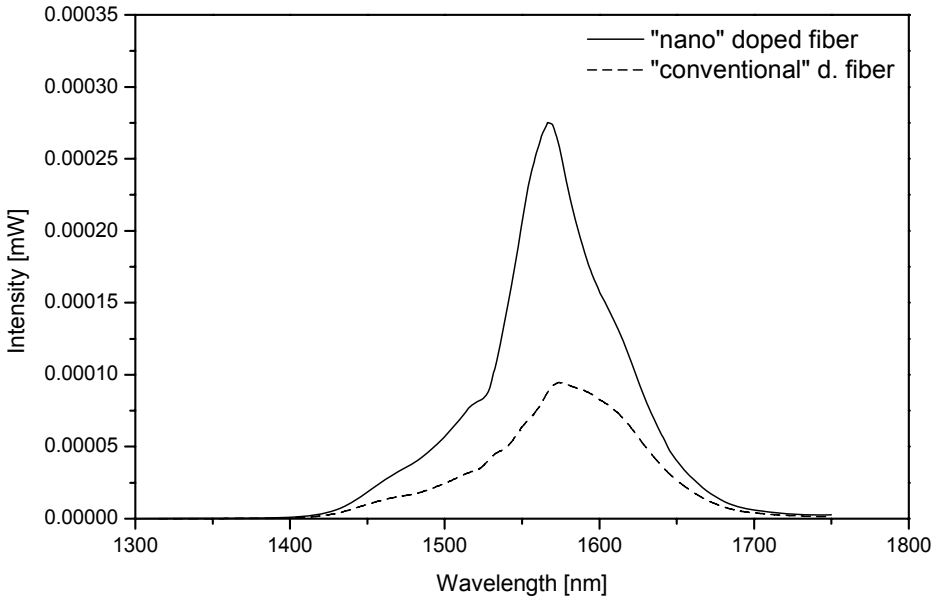

Using of Carbon Nanotubes for Fabrication of Printed Electrodes and Their Employing in DNA Analysis

Jan Prášek[1], Radim Hrdý[1], Jan Sileny[1], Violetta Shestivska[2], Dalibor Huska[2], Vojtech Adam[2], Jaromir Hubalek[1], Ales Horna[3], Libuse Trnkova[4], Rene Kizek[2]
[1]Department of Microelectronics, Faculty of Electrical Engineering and Communication, Brno University of Technology, Udolni 53, CZ-602 00 Brno, Czech Republic
[2]Department of Chemistry and Biochemistry, Faculty of Agronomy, Mendel University of Agriculture and Forestry, Zemedelska 1, CZ-613 00 Brno, Czech Republic
[3]Tomas Bata University, T.G. Masaryka 275, CZ-762 72 Zlin, Czech Republic
[4]Department of Chemistry, Faculty of Science, Masaryk University, Kamenice 5, CZ-625 00 Brno, Czech Republic
hubalek@feec.vutbr.cz

In the beginning of the 21st century the complete structure of human genome was recognized. Since then the importance of the rapid testing of DNA nucleotide sequences is increasing. Except specialized genetic tests, rapid detection of biological weapons, environmental monitoring and forensic medicine the quick DNA analysis is approaching to common use. In contemporary numerous scientific institutions are searching for low cost, rapid and easy-to-use tools for such purposes. Electrochemistry belongs to promising methods in DNA analysis. The electrochemical behaviour of nucleic acids has been studied for more than 40 years. The first publication describing the nucleic acids determination by using the mercury electrode was published in 1960 [1, 2]. The measurement on mercury electrodes allow the determination of small amount both unmodified and electrochemically labeled nucleic acids. Nucleic acids gave two signals: i) redox signal of adenine and cytosine, and ii) oxidative signal of guanine. Moreover, electroactivity of all four nucleic bases was observed by using of carbon electrodes [3-5]. The aim of this work was to find and optimize the electrochemical methods for DNA detection on nanocarbon screen printed electrodes.

Chemicals
DNA and standards of nucleic acid bases was obtained from Reanal. The other chemicals were purchased from Sigma-Aldrich, unless stated otherwise. Materials for electrodes fabrication: the carrier substrate was from ceramic (Alumina-96% Al_2O_3), pastes 5545, 9635-HG, 4460 (ESL) and 5874, 7105, BQ221 (DuPont). Multiwalled carbon nanotubes (Sigma Aldrich) mixed with organic binder and homogenized to thixotropic paste.

Screen-printed electrodes fabrication
For fabrication of printed electrodes the semi-automatic screen-printing machine UL-1505A Tesla, laser AUREL AUTOMATION ALS 300L, hot-flow furnace HS 62A and inline furnace BTU were utilized. The used materials were: working electrode – carbon, reference electrode – Ag/AgCl, auxiliary electrode – Pt, isolation – dielectric paste, leads and pads – AgPd. The area of the working electrode was 0.5 mm^2.

Electrochemical measurements
The electrochemical measurement was carried out with multi-mode potentiostat BioStat (ESA, Inc. USA). It is four-channel system with three operating modes per channel (amps, volts, and temp). The system is connected through data bus USB to personal computer. To the first channel of the potentiostat the home made apparatus was connected. This apparatus consists of basic plate on which the connector TX721 1115 with pins spacing 2.54 and the connector 0039532035 from the manufacturer Molex with pins spacing 1.25 mm are placed. The connectors are designed for connection of two different screen-printed electrodes. For data processing the software BioStat and MS Excel was used. The parameters of the analysis were

as follows: channel number 1, sampling frequency 20 sps (samples/s), filter order 5. The working electrode potential was set according to previous analyses at carbon paste electrode. Phosphate buffer pH 6.0 was used as supporting electrolyte. All experiments were carried out at room temperature.

Measurement itself was performed according to the following scheme. For base lane establishing 10 µl of the supporting electrolyte was introduced on the electrodes surface, then 2 µl of the sample was added and the changes of current were determined. The electrode surface was mechanically polished with redistilled water and filter paper. Primarily we optimized experimental conditions for determination of nucleic acid bases by using of carbon paste electrodes. Under the optimal conditions (0.1 M phosphate buffer, pH = 6.0, frequency of 50 Hz and time of accumulation 120 s) we analyzed all four nucleic acid bases – adenine, guanine, cytosine and thymine using nanocarbon screen printed electrodes and well repeatable data were obtained (Fig. 1). Potentials of certain bases were as follows: cytosine C ~ 1.3 V; thymine T ~ 1.2 V; adenine A ~ 1.0 V; guanine G ~ 0.7 V. The detection limits evaluated at the fabricated electrodes were 0.2 µM for cytosine, 1.5 µM for guanine, 0.8 µM for thymine and 1.5 µM for adenine. The optimized procedure was further used for DNA analysis, where the signals of single bases were distinguished. When the denatured and native DNA was measured, it was observed, that the signals of temperature denatured DNA was of about 40 % higher in comparison to native DNA. The detection limit of native DNA was of about 1.5 µg/ml and the detection limit of denatured DNA was 0.5 µg/ml. The surface of the working electrode was enhanced by using of the carbon nanotubes created in plasma with nickel catalyst. The using of nanotubes increased the electrochemical response of 40 % and the detection limit was markedly lowered.

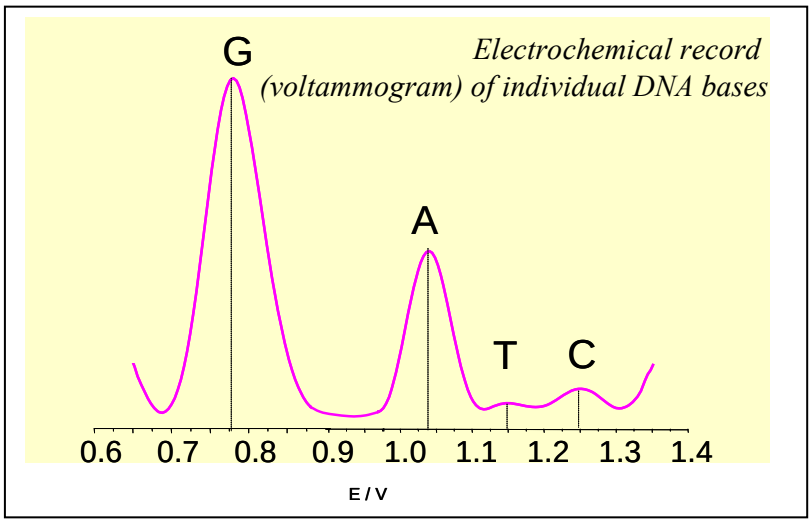

Acknowledgement: The financial support from the grant KAN 208130801 is highly acknowledged.

References:

[1] E. Palecek, *Collect. Czech. Chem. Commun.* **1960,** *25*, 2283.
[2] E. Palecek, *Biochem.-Moscow.* **1960,** *25*, 619.
[3] V. C. Diculescu, A. M. C. Paquim, A. M. O. Brett, *Sensors*. **2005,** *5*, 377.
[4] A. M. O. Brett, A. M. Chiorcea, *Electrochem. Commun.* **2003,** *5*, 178.
[5] F. C. Abreu, M. O. F. Goulart, A. M. O. Brett, *Biosens. Bioelectron.* **2002,** *17*, 913.

Spin projection energies in RHF: application to quantum dots

Antonio Puente, Miquel Pons Viver
Dep. de Física, Universitat de les Illes Balears,
Ctra. De Valldemossa km. 7.5, 07122 Palma de Mallorca, Spain
toni.puente@uib.es

In the last years both Hartree-Fock (HF) and density functional theory (DFT) have been extensively applied to study different properties in a variety of electronic nanostructures with occupations that range from moderate to large number of electrons, for which more exact methods, such as exact diagonalization, quantum Monte Carlo or configuration interaction, are not feasible. The importance of correlations in circular quantum dots depends on the so-called Wigner parameter (R_W), which is a measure of the relative strength between electron-electron interaction and external confinement. Whereas for high density (weak interaction) a single-particle picture is valid and the system can be adequately described within a space restricted mean field formalism (RHF, RDFT), for low density (strong interaction) the electronic structure is more adequately described by allowing the electrons to localize, forming a so-called Wigner molecule, similar to that found in the 2D electron gas in the strong correlation limit [1]. In this latter case it has been shown that a space unrestricted formalism (UHF, UDFT) can provide a better description of the electronic structure [2,3]. A common drawback in all mean field calculations lies in its failure to work with good total spin states, *i.e.* eigenstates of the $\hat{S}^2$ operator. Spin symmetry, as well as rotational symmetry for UHF, restoration methods have proved to be a valuable technique, which led to improved energy estimates and at the same time is able to provide predictions for total spin and orbital angular momentum [3,4].

In this work we concentrate on the spin symmetry restoration technique [5], based on the evaluation of the spin projection operator acting on a Slater determinant (SD) with the help of the Sanibel coefficients [3,6]. This total spin eigenstate is simply expressed as a linear combination of a big new set of SD's obtained by performing all possible spin-exchange operations over the initial state. This state can then be used to estimate different physical quantities through the calculation of appropriate expectation values. We apply this formalism to circularly confined quantum dots, described within RHF, and show how the corresponding expectation values for the total energy and several other observables can be efficiently computed for an arbitrary number of electrons. The predictions for the total spin projection (S, S_z) corresponding to the lowest energy solution are discussed as a function of R_W and the strength of a vertically applied magnetic field. The projected total energies are also compared with their RHF counterparts, and explicit expressions for the evaluation of expectation values of arbitrary, but spin-independent, one- and two-body operators are provided. As an example we compute the particle density variation in the different spin channels.

References:

[1] E P Wigner, Trans. Faraday Soc. **34** (1938) 678.
[2] C Yannouleas and U Landman, Phys. Rev. B **68**, (2003) 035325; A Puente, L Serra and R G Nazmitdinov, Phys. Rev. B **69** (2004) 125315.
[3] U Giovannini, F Cavaliere, R Cenni, M Sassetti and B Kramer, New J. Phys. **9** (2007) 93.
[4] C Yannouleas and U Landman, J. Phys.: Condens. Matter **14**, (2002) L591-L598;
C Yannouleas and U Landman, Rep. Prog. Phys. **70** (2007) 2067.
[5] P-O Löwdin, Phys. Rev. **97** (1955) 1509; P-O Löwdin, Phys. Rev. **97** (1955) 1474.
[6] F Sasaki and K Ohno, J. Math. Phys. **4** (1963) 1140.

NANOPARTICLES IN $YBa_2Cu_3O_7$ SUPERCONDUCTING THIN FILMS

Susagna Ricart
ICMA (CSIC)
Campus de la UAB, Bellaterra 08193

There is a large number of functional materials were the possibility to have a high contact surface between two dissimilar materials by means of a nanometric structure, give them a high added value. Nanoparticles are considered as essential materials in nanotechnology. Physical and chemical properties of nanoparticles can be varied by changing its size and morphology .In particular, the use of metallic nanoparticles approach has been applied to nanocomposite superconducting layers having high critical currents.

The present communication deals with the preparation of nanocomposite superconducting layers by Chemical Solution Deposition (CSD) using the Metal Organic Decomposition approach (MOD).

There is a close relationship between the composition and shape of nanometric structures and their effectiveness in enhancing the properties of the superconducting material.

There are very few procedures described for the preparation of these nanocomposite materials and, mainly, the first approaches have been recently achieved by physical methods such as Pulsed Laser Deposition (PLD). [2] .

In this communication we present a new approach based in an “all chemical” process using the methodologies for the preparation the superconductor solution precursors. The goal of the present work is to obtain a nanocomposite thin film containing previously or simultaneously synthesized nanoparticles of a non-superconducting second phase (Au, Ag, BZO, CeO_2) in the YBCO matrix using the Metal Organic Decomposition. The general principle of the MOD process is the decomposition of metal organic precursors at 310ºC to obtain a mixture of fluorides, oxides and oxifluorides which are subsequently thermally treated at 795-810ºC to obtain the desired superconductor oxide phase

[1] X.Obradors et al, *Supercond. Sci. Technol*., **2004**, *17*, 1055.
[2] J. L. MacManus-Driscoll et al, *Nature Mat.,* **2004**, *3*, 439.

FERROELECTRIC BEHAVIOR OF POLYCRYSTALLINE ULTRATHIN LEAD TITANATE FILMS

J. Ricote[1], R. Fernández[1], R. Jiménez[1], S. Holgado[2] and M.L. Calzada[1]
[1]Instituto de Ciencia de Materiales de Madrid, CSIC
[2]Escuela Politécnica Superior, Universidad Autónoma de Madrid,
Cantoblanco, E-28049 Madrid, Spain
jricote@icmm.csic.es

Ferroelectric lead titanate based thin films have extensively been studied for their applications as active elements in non-volatile ferroelectric random access memories (NV-FeRAM) and microelectromechanical systems (MEMS). The miniaturization trends followed by the electronics industry results in a drastic reduction of the dimensions of the devices and their elements, which has stimulated an increasing number of studies on the preparation of ferroelectric nanostructures and their properties. For example, regarding the Nanoelectromechanical Systems (NEMS), one of the major challenges they face now is related to the search of alternative transduction elements [1], as most of the techniques used in MEMS reach their limits in the nanoscale. A promising solution is the use of piezoelectric transduction with ferroelectric films. To this aim, high quality ultrathin capacitors need to be prepared. Among the different methods used for the fabrication of films, Chemical Solution Deposition methods have the advantages of their low cost, good compositional control and large deposition areas, but it has traditionally regarded as useless for the preparation of very thin films. Recently, we have shown that lead titanate based continuous films down to 13-18 nm thickness can successfully be prepared by CSD [2,3], by a careful control of the precursor solutions and deposition parameters. Deposits are made on Si-based substrates, on which most of the current microelectronics technology is based. Even the thinnest films show significant piezoelectric activity (Fig. 1), which made them promising for applications as transducer elements in the complex structures of NEMS.

The following step towards their integration in real devices is that the capacitors obtained are macroscopically addressable. Electrical characterization of ferroelectric ultrathin films in most studies is carried out by scanning probe microscopy, with only few recent exceptions [4]. We present results of our dielectric, ferroelectric results on capacitors down to ≈40 nm thick, and the strategies we are following to push down this limit, mainly focused on the improvement of the microstructural quality of the films.

Properties are of course affected by the size reduction. The use of polycrystalline Pt bottom electrodes, easily integrated on Si-based substrates and resistant to the thermal treatments that ferroelectrics usually need during processing, results in the fabrication of films polycrystalline in nature. Although there is extensive work devoted in the literature to study the effect of grain size on the ferroelectric domain configuration of ferroelectrics, these studies have mostly been carried out in bulk ceramics. Alternatively, thickness effects that include electrode charge screening, parasitic interfacial layers or strain gradients have primarily been studied in epitaxial films. In this work we try to elucidate which of these two types of size effects is more important for the different thicknesses. We observe an abrupt decrease of the remnant polarization (Fig. 2) which we attribute to the disappearance of 90º-type ferroelectric domains with grain size reduction, as observed by Piezoresponse Force Microscopy (Fig. 3). However, the piezoelectric behaviour of the thinnest films observed on their local piezoelectric loops (Fig. 1) is strongly dependent on the strain gradients produced by the clamping of the substrate. From the results obtained we draw conclusions for the improvement of the properties of these ferroelectric ultrathin films.

References:

[1] K.L. Ekinci, *Small* **1** (2005) 786.
[2] J. Ricote, S. Holgado, P. Ramos, M.L. Calzada, IEEE Trans. Ultrason. Ferroel. Freq. Control **53** (2006) 2299.
[3] J. Ricote, S. Holgado, Z. Huang, P. Ramos, R. Fernández, M.L. Calzada, J. Mater. Res. **in press** (2008).
[4] G.L. Brennecka, B.A. Tuttle, J. Mater. Res. **22** (2007) 2868.

Figures:

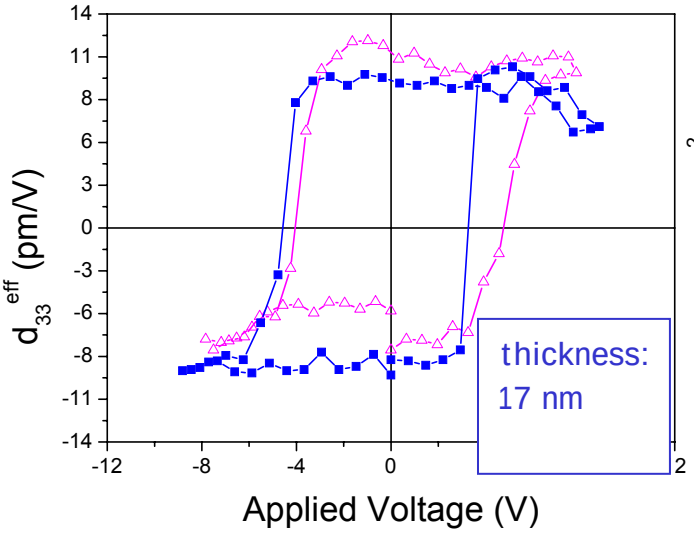

Fig. 1. Local piezoelectric loops of an ultrathin lead titanate film.

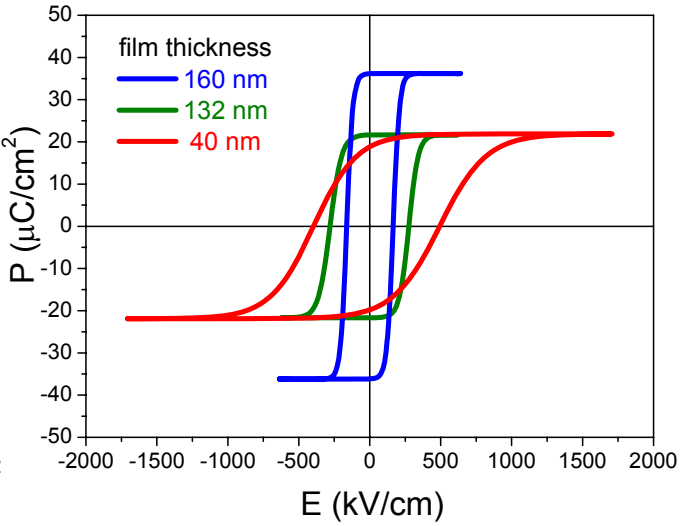

Fig. 2. Corrected P-E hysteresis loop of films with decreasing thickness.

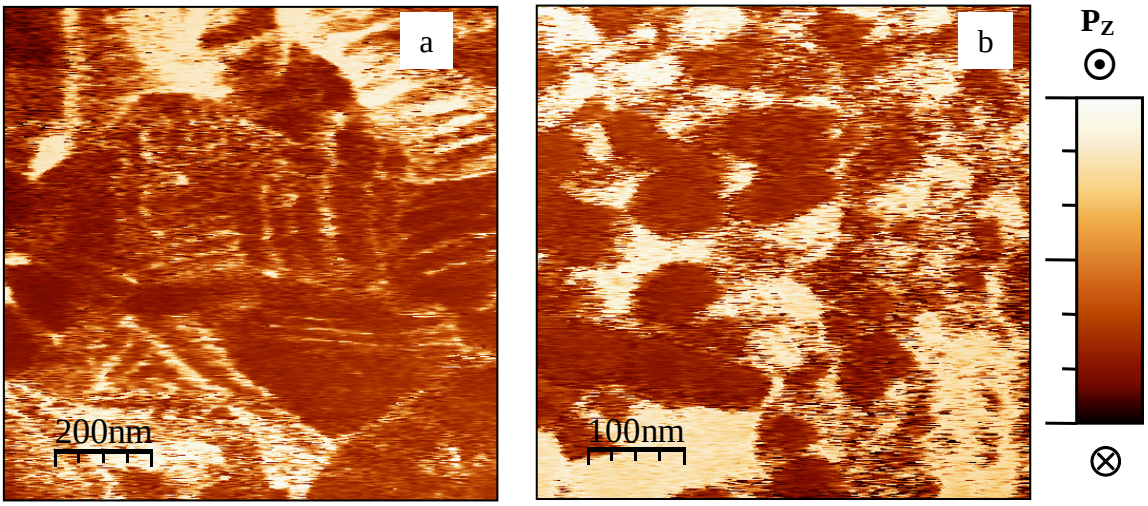

Fig. 3. Phase piezoresponse force microscopy images that show the sense of the out-of plane polarization vector of films with (a) 132 nm and (b) 40 nm thickness. Banded twin domains corresponding to 90º-type ferroelectric domains are observed in (a).

TEMPERATURE DEPENDENCE OF A TWOFOLD MAGNETIC BEHAVIOUR OF A NANOSCOPIC METAL/SILICON HYBRID SYSTEM – A COMPARISON BETWEEN Ni/Si AND Co/Si

K. Rumpf[1], *P. Granitzer*[1], *P. Poelt*[2], *H. Krenn*[1]
[1]*Institute of Physics, Karl Franzens University Graz, Universitaetsplatz 5, 8010 Graz, Austria*
[2]*Institute for Electron Microscopy, University of Technology Graz, Steyrerasse 17, 8010 Graz, Austria*
klemens.rumpf@uni-graz.at

The investigated hybrid nanocomposite consists of a porous silicon template with electrochemically embedded Ni or Co nanostructures and offers magnetic characteristics which can be tailored by the electrochemical process parameters [1]. The magnetic behaviour of the nanocomposite strongly differs from the magnetic properties of the according bulk materials and is not only a consequence of nanostructuring of the semiconductor and the metals, respectively but also of their special combination within the nanoscopic silicon/metal hybrid system.
A twofold magnetic behaviour can be observed, a first one due to the spinmagnetism at magnetic fields below the saturation magnetization of the deposited metals and a second non-saturating term at higher fields above the saturation magnetization.
Tailored magnetic properties as coercivities, squareness and magnetic anisotropy can be achieved by tuning the process parameters during fabrication. The coercivities strongly depend on the geometry of the deposited metal structures, whereas the shape can be modified between spheres, ellipsoids and wires. The maximum elongation of the metal structures is a few microns and the diameter corresponds to the pore-diameter of the templates which can be varied between 30 nm and 100 nm leading to needle-like structures with an aspect ratio of about 100.
The temperature dependence of the coercivity of the Ni-filled samples shows an exponential decay with increasing temperature (4.2 K up to 300 K) whereas the curve progression of the coercivities of Co-filled samples shows a non-monotonous decrease within the same temperature interval. Between 4.2 K and 100 K the values differ less than 10% and at higher temperatures between 100 K and 250 K the coercivity drops of about half the value.
At high magnetic fields (> 1 T up to 7 T) above the saturation magnetization of the deposited metal the nanocomposites offer a non-saturating term additionally to the ferromagnetic spinmagnetism. In case of Ni deposited within the pores this term shows a paramagnetic characteristic and follows exactly the Curie-Weiss law (Fig. 1), whereas for Co/porous silicon samples the temperature dependent magnetization shows some deviations from the Curie Weiss law. Also in the high field region a difference in the temperature dependence between Ni and Co can be observed whereas the non-saturating term does not depend on the geometry of the embedded nanostructures in contrast to the ferromagnetic behaviour at lower fields.
Applications of the hybrid system can not only be found in magnetic sensor technology but the fabricated system is also a promising candidate to detect spin injection from a ferromagnetic metal into silicon. The investigated composite material merges semiconducting and ferromagnetic properties on one level and represents a kind of “ferromagnetic semiconductor” deployable at room temperature.

References:

[1] P. Granitzer, K. Rumpf, P. Pölt, A. Reichmann, H. Krenn, Physica E **38** (2007) 205.

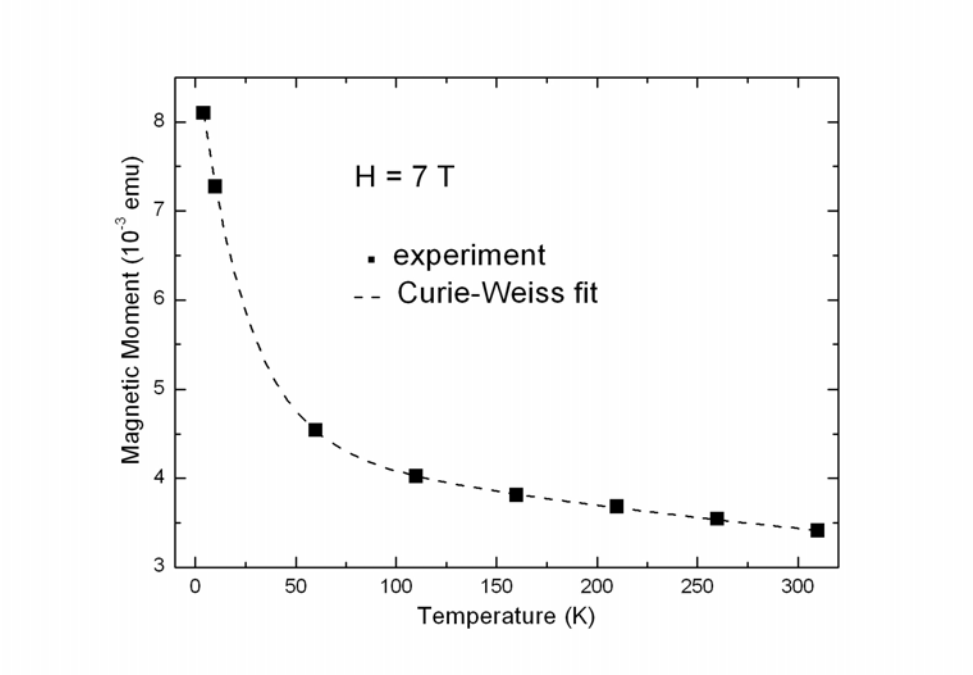

Figure 1: Temperature dependence of a Ni-filled porous silicon sample measured at a magnetic field of 7 T. The decreasing magnetic moment follows exactly the Curie Weiss law.

GRAPHENE NANOCONSTRICTION AS A SINGLE-LEVEL QUANTUM DOT

A. Rycerz[1,2,⋆], J. Wurm[2], M. Wimmer[2], I. Adagideli[2], and K. Richter[2]

[1]*Marian Smoluchowski Institute of Physics, Jagiellonian University, Reymonta 4, PL–30059 Kraków, Poland*

[2]*Institut für Theoretische Physik, Universität Regensburg, D–93040, Germany*

[⋆]*Contact e-mail: Adam.Rycerz@physik.uni-regensburg.de*

Quantum dot having a single relevant electronic level, that shows only spin degeneracy, is widely considered as a key ingredient for solid-state quantum information processing. Recently, such a single-level quantum dot (SQD) was proposed to be realized in graphene constrictions with predominantly *armchair* edges [1, 2] in order to exploit the superior spin coherence expected in carbon nanostructures.

This is the theoretical proposal to build SQD by using graphene nanoconstriction with *zigzag* edges only. The work was motivated by recent experiment by Li *et al.* [3] reporting fabrication of a 120-degree graphene kink with zigzag edges, and partly by an analytical finding by Akhmerov and Beenakker [4] that the zigzag-boundary condition applies generically to the terminated honeycomb lattice of any crystallographic orientation of the edge, except the case of a perfect armchair edge. Therefore, the armchair-boundary condition constitutes an academic, experimentally inaccessible situation. On the other hand, in the existing proposals to build SQD in graphene [1, 2] the sections of an insulating-armchair nanoribbon are used to trap an electron in the device [5].

Earlier, we have shown [6] using tight-binding calculations, that the *asymmetric* kink consists of two nanoribbons with zigzag edges rotated to form a 120-degree kink, blocks the lowest propagating mode. Here, we first briefly discuss the evolutions of the kink conductance with its geometrical parameters W_1 and W_2 to show the blocking mechanism works effectively except from the *symmetric* case $W_1 \approx W_2$, when the resonant tunneling may appear. The analysis is extended to the case of nonzero edge magnetization, which may appear in nanoribbons with zigzag edges [7].

Then, the two kinks are joined together to form a *double kink*, which shows narrow conductance peaks associated with a charge density localized in a central section. The decay rates of such localized states comparable as of their counterparts in the system of Ref. [2]. This indicates each kink traps an electron as effectively as an insulating-armchair nanoribbon of the similar size and, subsequently, the double kink operates as SQD in graphene. We also consider a *double quantum dot* (DQD), formed in nanostructure containing *four* kinks, to illustrate the scalability of the proposed device. The work is complemented with estimation of the Coulomb-interaction integrals for the localized states, and of the subsequent effective parameters, like the Heisenberg-type exchange and the Kondo couplings in different situations.

References:

[1] B. Trauzettel, D.V. Bulaev, D. Loss, and G. Burkard, *Nature Physics* **3** (2007) 192.

[2] Z.F. Wang, Q.W. Shi, Q. Li, X. Wang, and J.G. Hou, *Appl. Phys. Lett.* **91** (2007) 053109.

[3] X. Li, X. Wang, L. Zhang, S. Lee, H. Dai, *Science* **319** (2008) 1229.

[4] A.R. Akhmerov, C.W.J. Beenakker, *Phys. Rev. B* **77** (2008) 085423.

[5] Dirac fermions cannot be confined by solely using the potential barier due to Klein paradox, see M.I. Katsnelson, K.S. Novoselov, and A.K. Geim, *Nature Physics* **2** (2006) 620.

[6] A. Rycerz, *phys. stat. sol. (a)* **205** (2008) 1281.

[7] M. Wimmer, I. Adagideli, S. Berber, D. Tomanek, and K. Richter, *Phys. Rev. Lett.* **100** (2008) 177207.

Figures:

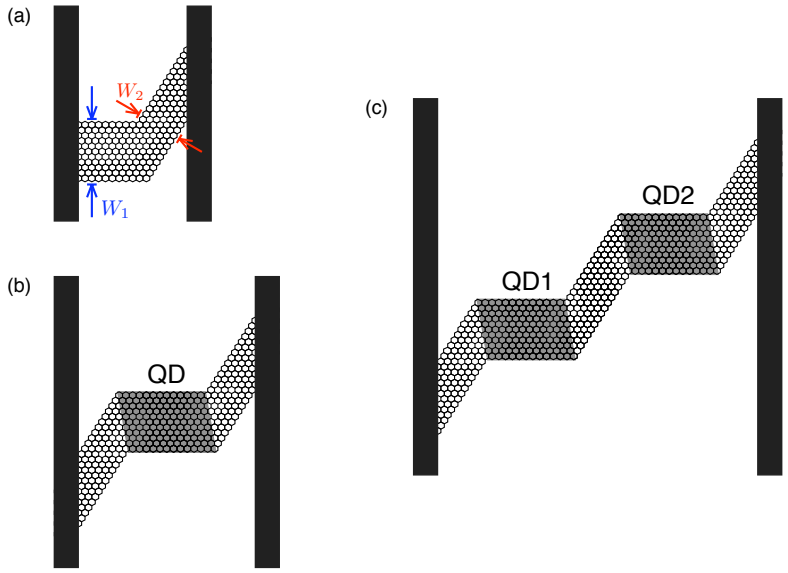

Graphene nanoconstrictions with zigzag edges studied in the present work. 120-degree kink (a) blocks the current at low bias for $W_1 \neq W_2$. Double kink (b) traps an electron in the *shadow* area and thus operates as a single-level quantum dot, whereas constriction with four kinks (c) operates as a double quantum dot. Each of the devices is connected to heavily-doped graphene leads marked with the dark bars.

NANOMETER LOCALIZATION AND IDENTIFICATION OF DNA REPAIR PROTEINS BY COMBINED AFM-FLUORESCENCE ANALYSIS

Humberto Sanchez[1], *Roland Kanaar*[1,2] *and Claire Wyman*[1,2]
[1]Department of Cell Biology & Genetics and [2]Department of Radiation Oncology, Erasmus MC, P.O.Box, 2040, 3000 CA Rotterdam, The Netherlands
h.sanchezgonzalez@erasmusmc.nl

Imaging of processes at the single-molecule level has revealed information otherwise inaccessible by "bulk" experiments. Atomic force microscopy is a powerful technique for studying biomolecular structures with nanometer resolution without necessity of external contrast agents. However, complex genetics transactions require the orchestrated action of different proteins, which would be undistinguishable by conventional AFM. On the other hand, fluorescence techniques can successfully localize proteins *in vivo* and *in vitro*, also for dynamic studies. However, optical resolution limits the details of structural studies in single molecule approaches. We show here the localization with nanometer resolution of recombination proteins using a combined atomic force and fluorescence microscope. Our experiments reveal the versatility of the system in the recognition and simultaneous localization of different fluorescent-tagged proteins on DNA. Moreover, we present the use of fluorescence polystyrene micro-spheres for a reliable alignment of the optical and the topographical images, which together with the DirectOverlay^{TM} system (JPK instruments) have allowed us to precisely localized different proteins with nanometer resolution.

STRONG CURRENT MODULATION IN QUANTUM WIRES WITH LOCALIZED RASHBA INTERACTION

David Sánchez[1], Llorenç Serra[1,2], and Rosa López[1]
1. Departament de Física, Universitat de les Illes Balears, E-07122 Palma de Mallorca, Spain
2. IFISC, Instituto de Física Interdisciplinar y Sistema Complejos (CSIC-UIB), E-07122 Palma de Mallorca, Spain

The Rashba interaction is a salient spin-orbit interaction in semiconductors which occurs due to interfacial electric fields in asymmetric heterostructures [1]. This removes the spin degeneracy of conduction electron states and the resulting splitting can be tuned with external gates [2]. When the Rashba interaction is localized in a one-dimensional (1D) channel, the injected spins in the Rashba region perform a spin precession, leading to a modulated transmission when the leads are ferromagnetic [3]. Recently, we have predicted strongly modulated transmission lineshapes when the quasi-1D wire is attached to *normal* leads, see Fig. 1. These antiresonances originate from the interference between a direct channel through the Rashba region and a channel that interacts with a quasibound state formed by the Rashba potential in the region (the Rashba *dot*). We demonstrated that the Rashba intersubband coupling controls the coupling between the continuum and discrete states and that the lineshape is of the Fano form [4].

When electron-electron interaction is taken into account, our results show that considerable repulsion energy results from charging the dot [5]. The conductance resonances in the Coulomb blockade regime have a Fano form, while in the strong coupling regime we predict an oscillating conductance as a function of the Rashba strength. Furthermore, in the presence of an external magnetic field an energy pseudogap develops in the wire spectrum. We find abrupt changes in the transmission curves when the Fermi energy lies within the pseudogap [6]. The lineshapes are narrow and asymmetric and the transmission reaches zero for energies near the gap closing.

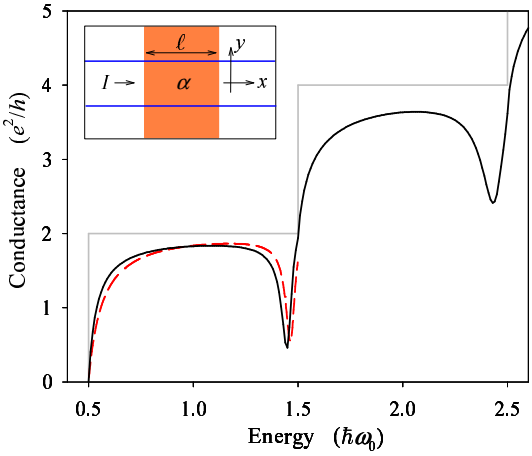

Fig. 1 Characteristic linear conductance curve of a quantum wire with local Rashba interaction (solid line). We show with dashed line the result from a coupled channel model that captures the main ingredients of the effect. We include the case without Rashba interaction (gray line) for comparison. Note the strong conductance modulation close to the onset of the second conductance plateau.

The system discussed here could work as a current modulator device. For slight variations of the Fermi energy, which can be externally controlled, we show that the transmission changes dramatically between two limit values across the antiresonance. Importantly, the current modulation is robust against intersubband mixing, magnetic field changes, and smooth variations of the wire interfaces,

References

[1] E.I Rashba, Fiz. Tverd. Tela (Leningrad) **2**, 1224 (1960). [Sov. Phys. Solid State **2**, 1109 (1960)].
[2] J. Nitta, T. Akazaki, H. Takayanagi, and T. Enoki, Phys. Rev. Lett. **78**, 1335 (1997).
[3] S. Datta and B. Das, Appl. Phys. Lett. **56**, 665 (1990).
[4] D. Sanchez and Ll. Serra, Phys. Rev. B **74**, 153313 (2006).
[5] R. Lopez, D. Sanchez, and Ll. Serra, Phys. Rev. B **76**, 035307 (2007).
[6] D. Sanchez, Ll. Serra, and M.-S. Choi, Phys. Rev. B **77**, 035315 (2008).

MAGNETIC MOLECULES DERIVED FROM HYDROGENATION OF POLYCYCLIC AROMATIC HYDROCARBONS

J.A. Vergés[1], G. Chiappe[2], L. Pastor-Abia[3], E. Louis[2] and E. SanFabián[3*]

[1]Departamento de Teoría de la Materia Condensada, Instituto de Ciencias de Materiales de Madrid (CSIC), Cantoblanco, Madrid 28049, Spain
[2]Departamento de Física Aplicada, Unidad Asociada del Consejo Superior de Investigaciones Científicas and Instituto Universitario de Materiales, Universidad de Alicante, San Vicente del Raspeig, Alicante 03690, Spain
[3]Departamento de Química Física, Unidad Asociada del Consejo Superior de Investigaciones Científicas and Instituto Universitario de Materiales, Universidad de Alicante, San Vicente del Raspeig, Alicante 03690, Spain
[*]Corresponding author: E. SanFabián. E_mail: sanfa@ua.es

The quest for spin polarized organic molecules is since long attracting a great deal of attention. Actual routes to produce magnetic organic-based materials commonly adopt a similar strategy: the addition of magnetic species (atoms, polyradicals, etc.). Here we explore an alternative approach that consists of hydrogenation of Polycyclic Aromatic Hydrocarbons (PAH). The proposal is illustrated by carrying out extensive mono- (Hartree Fock and DFT) and multi-determinantal (CISD and MCSCF) calculations on hexa-hydrogenated coronene $C_{24}H_{18}$ and hexahydrogenated corannulene $C_{20}H_{16}$ (see Fig. 1). The results indicate that high spin species (S=3 or S=2) are stable, its formation being favorable provided that the reaction involves atomic hydrogen. An attempt is made to rationalize these results in terms of Lieb's theorem for bipartite lattices [1], which states that the spin multiplicity of their ground states is $|NA - NB| + 1$, NA and NB being the number of atoms in each sublattice. C atoms in most PAHs, corannulene being an exception, actually form clusters of a bipartite lattice, i.e., graphene (such PAH are also known as alternant hydrocarbons). The spin of the ground state of hydrogenated coronene is in accordance with Lieb's theorem (S=3 in one of the molecules) in spite of the significantly different topologies of ab initio and Lieb's Hamiltonians. This is somehow compatible with results showing that spin states of PAH (corannulene included) (benzene, anthracene and twelve-fold hydogenated coronene) can be nicely fitted by means of Lieb (or Hubbard) Hamiltonian with a Coulomb repulsion of U = 3.3 eV and a hopping of t = 2.71 eV (charge states, however, cannot be fit with this Hamiltonian). Such a low value of U/t gives, notwithstanding, significant antiferromagnetic correlations in the molecules. Based on the strong antiferromagnetic correlation obtained in

PAHs, and in order to handle frustrated topologies, we suggest an extension of Lieb's theorem. ***According to the proposed alternating rule, the number of AB pairs should be maximized in order to optimize energy.*** On the other hand, such simple interacting models cannot describe the energies of the charged molecules; this suggests the need of a critical

The authors are grateful to J. Feliu, A. Guijarro and M. Yus for useful suggestions and remarks. Financial support by the spanish MCYT (grants FIS200402356, MAT2005-07369-C03-01 and NAN2004-09183-C10-08), and the Universidad de Alicante is gratefully acknowledged. GC is thankful to the spanish MCYT for a Ram\'on y Cajal grant.

References:

[1] E.H. Lieb, Phys. Rev. Lett. **62**, 1201 (1989).

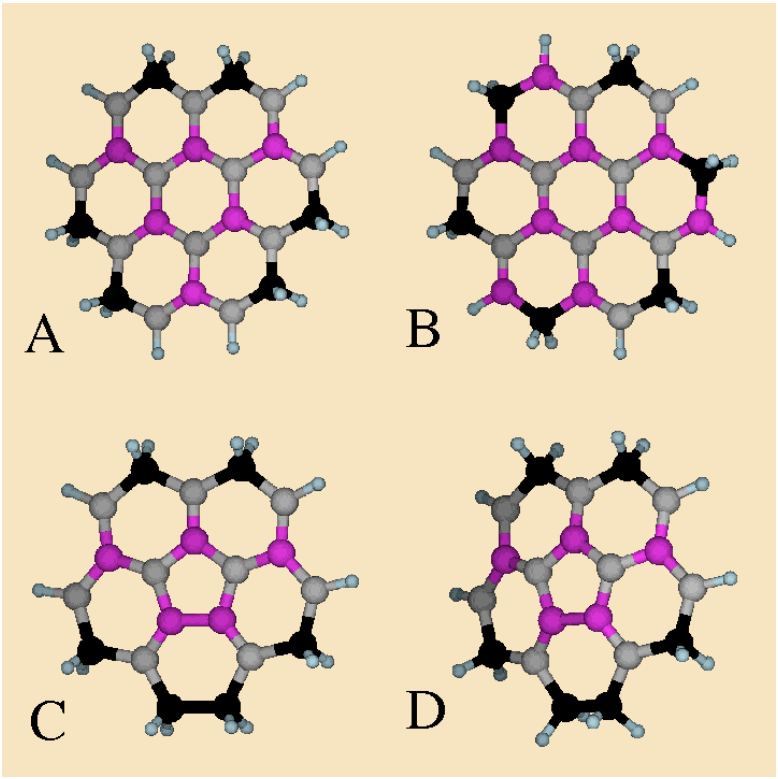

Fig. 1: 1,4,5,8,9,12-hexahydrocoronene (A, hereafter referred to as D_{3h} according to its symmetry group), 1,3,5,7,9,11-hexahydrocoronene (B, hereafter referred to as C_{3h}) and 1,4,5,6,7,10-hexahydrocorannulene (C planar and D curved, hereafter referred to as C_{2v}). Saturated carbons are represented by black symbols while dark grey (magenta) and light grey symbols correspond to carbons in one of the two sublattices. Note that corannulene is a non-alternant hydrocarbon, or, alternatively, a frustrated cluster of carbon atoms (note the fully magenta bond between two magenta atoms)

SUBSTRATE ORIENTATION EFFECTS ON THE LATTICE PARAMETER PROFILES IN THE STRANSKI-KRASTANOV GROWTH MODE

S.N. Santalla[1], C. Kanyinda-Malu[1,2] and R.M. de la Cruz[1]

(1) Departamento de Física, Universidad Carlos III de Madrid, EPS, Av. de la Universidad 30, 28911 Leganés (Madrid), Spain.

(2) Departamento de Economía Financiera y Contabilidad II, FCJS, Universidad Rey Juan Carlos, Paseo de los Artilleros s/n, 28032 Madrid, Spain.
E-mail: silvia.santalla@uc3m.es

One of the factors which greatly influences the Stranski-Krastanov (S-K) growth mode in low-dimensional strained heterostructures is the substrate orientation. A change in the Miller indices of the substrate allows to control the strain relaxation in the heteroepitaxial systems and consequently induces modifications in the onset of the S-K growth mode. For instance, when InAs epitaxial layers were grown on high index substrates such as (113) and (115) GaAs, the PL spectra indicated a delay in the three-dimensional mode onset [1]. Besides, appropriate changes of substrate orientation induce different morphologies of the islands for the same epitaxial film. This phenomenon is observed by STM in Ge/Si (001) and Ge/Si (111) quantum dots (QDs) [2]. Theoretical studies to investigate the substrate orientation effects on S-K growth mode and electronic properties of Ge/Si (111) and InAs/GaAs (11n) QDs were also reported [3, 4].
In our previous work, we reported analysis of the parameter profile using elasticity continuum theory in Ge/Si (001) and InAs/GaAs (001) QDs for different values of the aspect ratio [5]. Following that theoretical treatment, we will investigate the substrate orientation effects on the lattice parameter profiles in Ge/Si (111) and InAs/GaAs (11n) QDs. As in the previous works, we assume that a small fraction of the substrate ($0 < \alpha < 1$) participates in heterostructure relaxation in the non rigid approximation. Minimization of the free energy by the Euler-Lagrange method allows to analyse the evolution of the lattice parameter with the film coverage. In both rigid and non-rigid approximations, a sigmoidal-like profile is obtained for the lattice parameter. The figure 1 shows the lattice parameter profile for Ge/Si (111) QDs with aspect ratio of $r = 0.6$ and we compare it with Ge/Si(001) in non-rigid approximation. Comparison with the profiles obtained with the smaller Miller indices in InAs/GaAs QDs [5] will also discussed.

References:

[1] Sanguinetti, S.; Chiantoni, G.; Grilli, E.; Guzzi, M. ; Henini, M. ; Polimeni, A. ; Patané, A. ; Eaves, L. and Main, P.C., *Mater. Sci. Eng. B* **74** (2000) 239.
[2] Voigtländer, B., *Surf. Sci. Rep.* **43** (2001) 127.
[3] Santalla, S. N. ; Kanyinda-Malu, C. and de la Cruz, R. M., *Nanotecnology* **15** (2004) S215.
[4] Santalla, S. N.; Kanyinda-Malu, C. and de la Cruz, R.M., *Physica E* **25** (2005) 456.
[5] Santalla, S. N.; Kanyinda-Malu, C. and de la Cruz, R. M., *Nanotechnology* **18** (2007) 315705-1.

Figures:

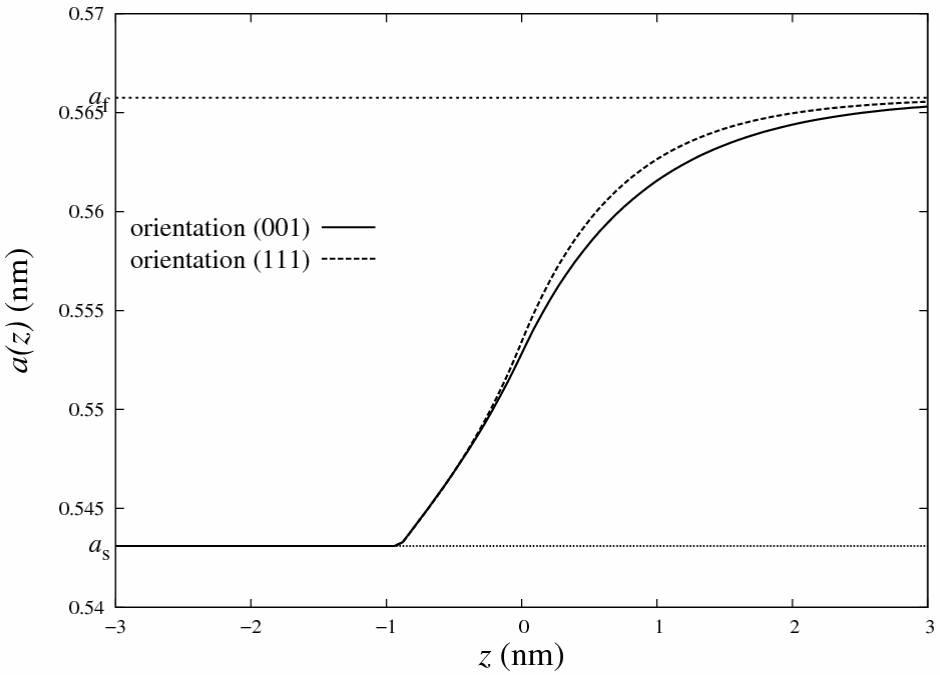

Figure 1: Lattice parameter profiles as a function of film coverage in Ge/Si (001) and Ge/Si (111) QDs for $\alpha = 0.3$ and $r = 0.6$.

MC SIMULATION OF WATER MENISCUS IN NANOCONTAINERS: EXPLAINING THE COLLAPSE OF VIRAL PARTICLES DUE TO CAPILLAR FORCES.

P.A. Serena[1*], *M. Douas*[2], *M.I. Marqués*[2], *C. Carrasco*[3], *P. J. de Pablo*[3], *R. Miranda*[4], *J. L. Carrascosa*[4], *M. Castellanos*[5], *M. G. Mateu*[5]

[1]*Instituto de Ciencia de Materiales de Madrid, Consejo Superior de Investigaciones Científicas, Campus de Cantoblanco, 28049 Madrid, Spain..*

[2]*Departamento de Física de Materiales, C-IV, Facultad de Ciencias, Universidad Autónoma de Madrid, 28049 Madrid, Spain.*

[3]*Departamento de Física de la Materia Condensada C-III, Facultad de Ciencias, Universidad Autónoma de Madrid, 28049 Madrid, Spain.*

[4]*Departamento de Estructura de Macromoléculas, Centro Nacional de Biotecnología, Consejo Superior de Investigaciones Científicas, Campus de Cantoblanco, 28049 Madrid, Spain...*

[5]*Centro de Biología Molecular Severo Ochoa, Consejo Superior de Investigaciones Científicas-Universidad Autónoma de Madrid, Campus de Cantoblanco, 28049 Madrid, Spain..*

**e.mail: pedro.serena@icmm.csic.es*

The study of properties of water confined in complex systems is relevant to many important processes ranging from industrial applications (water membranes, filtering, etc) to biological processes (protein folding, ionic transport through membranes,...) [1]. Changes in thermodynamics, phase behavior and the molecular mobility of water have been observed upon confinement [2]. These changes are strongly dependent on the nano-container properties. In particular, very recently [3] we have reported, using atomic force microscopy (AFM), that remarkable structural modification takes place during the desiccation processes on individual particles of the bacteriophage ϕ29 and the minute virus of mice (MVM). In both cases the genomic DNA was ejected from the viral capsid (see Figure 1). However, while the structural integrity of the minute virus of mice was essentially preserved, the ϕ29 capsid underwent a wall-to-wall collapse. These results points towards the important role played by the capillary forces of water confined inside the viruses. In fact, the desiccation process of an empty viral particle (nano-container) is associated to the formation of internal water menisci with shape (exposed area and curvature) determined by the capsid geometry.

In order to study the way in which the water menisci evolves during the desiccation process of viral particles we have simulated the water+capsid system using a lattice gas model that mimics the gas-liquid phase transition in water. This model has been previously used to study the geometry of the water meniscus formed between an atomic force microscope tip and a substrate [4]. Averaged Monte Carlo (MC) simulations of the water meniscus evolution have been carried out for two types of viruses' cavities: an asymmetric one with a single channel and a symmetric one with pores at every fourfold symmetry axis. The MC simulations describe the formation of an asymmetric water meniscus for the virus with a single hole (ϕ29) whereas, for the virus with a symmetric location of the pores (MVM), the water bridge formed is symmetric and capillary forces could cancel one another (see Figure 2). These differences could explain the wall-to-wall collapse noticed for ϕ29 viral capsids.

References:

[1] Special issue on nanoconfined water. J. Phys.: Condens. Matter 16 (2004) pp.S5257-S5470.
[2] See f.i. M. Rovere (ed.) J. Phys.: Condens. Matter 16, (45), (2004) 1.
[3] C. Carrasco et al. (submitted).
[4] J. Y. Jang, G.C. Schatz, M.A. Ratner, *Phys. Rev. Lett.* 92, (8), (2004) 085504.

Figure 1. (a) MVM and (b) ϕ29 viral particles after de-wetting processes with their respective DNA ejected from the capsids.

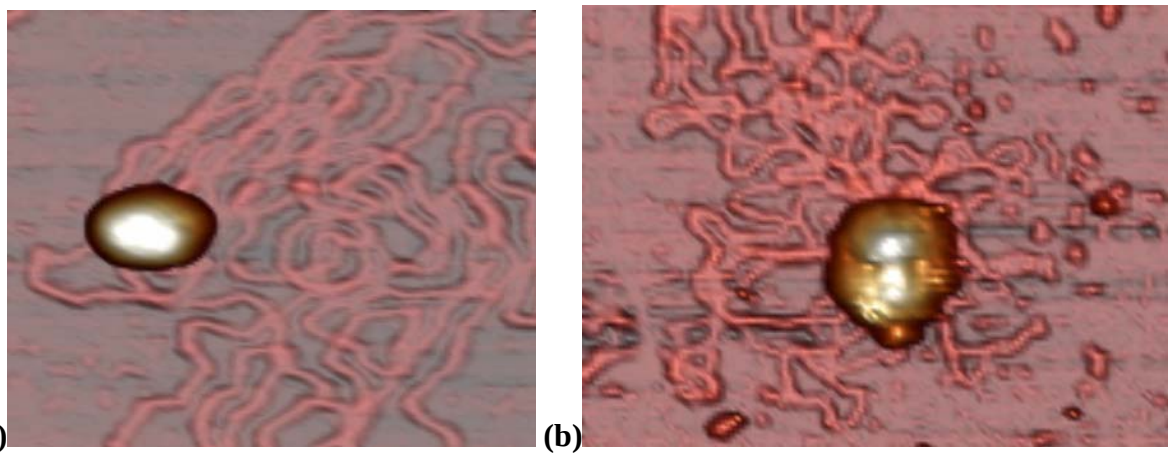

Figure 2. Numerical simulation of a desiccation process for asymmetric (upper panel) and symmetric (lower panel) virus cavities. Monte Carlo steps considered are 200, 600, 800, 1100 (upper panel from left to right) and 200, 400, 500, 700 (lower panel from left to right). Every lattice site with averaged water occupation probability n(i,j)>0.5 is represented with a blue point. Points belonging to the virus cavity are represented with a black line.

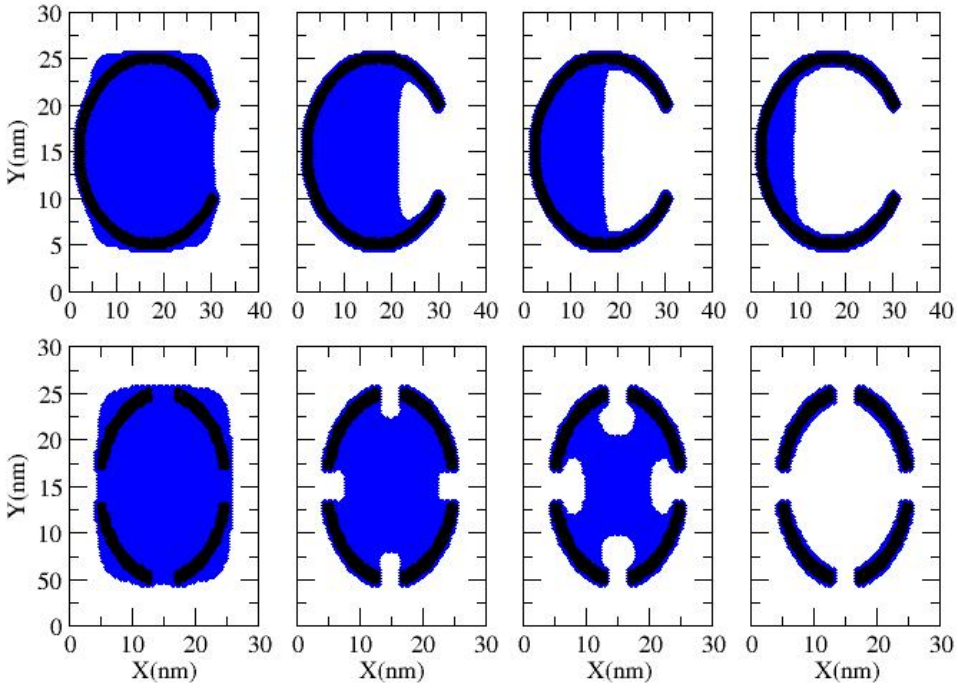

COATING OF PURE TITANIUM WITH TiN/Ti MULTI-LAYERED FILMS BY SPUTTER-DEPOSITION FOR IMPROVING BLOOD COMPATIBILITY

T. Sonoda[1], K.Ogawa[2], K.Furukawa[3], T.Ushida[3], K.Mizuara[2] and T.Yamane[1]
[1]National Institute of Advanced Industrial Science and Technology(AIST), Nagoya / Tsukuba, Japan
[2]Department of Mechanical Engineering, Tokyo Denki University, Tokyo, Japan
[3]Department of Mechanical Engineering, University of Tokyo, Tokyo, Japan
tsutomu.sonoda@aist.go.jp

Titanium-based materials have been utilized as biomaterials in dental or orthopedic field such as denture clasps and artificial dental roots or artificial joints, fixing plates and screws for broken bone, and its prostheses or implants exhibit excellent biocompatibility [1,2]. However, the pure titanium is not suitable for the medical materials exposed to the blood stream such as artificial heart valves, because titanium is poor in the blood compatibility [3]. Therefore, it is necessary to improve both the hardness and the blood compatibility of the barrier layer. Y.Mitamura, et al. reported the good blood compatibility of titanium nitride films [4]. In the present work, we performed the coating of pure titanium substrates with TiN/Ti multi-layered films using sputter-deposition in Ar gas atmosphere, aiming at the application of pure titanium to the material for totally implantable artificial hearts, in order to improve not only the blood compatibility of pure titanium but also the adhesion between the deposited TiN(titanium nitride) coating and the pure titanium substrate. The effects of the thickness of the Ti(pure titanium) layer on adhesion of TiN coatings to the pure titanium substrate were investigated. Furthermore the effects of the TiN coating obtained in this study on blood compatibility were also investigated.

A planar magnetron sputtering system (ANELVA Corp. type L-332S-FHS) with 2 cathodes was used. The planar targets used for this study were a pure titanium disk and a titanium nitride disk of 80mm-diameter, respectively. Pure titanium substrates (14mm diameter disk with 0.50mm thick) were mounted on the water-cooled substrate holder. TiN/Ti multi-layered films were deposited onto the pure titanium substrates by sputtering in sequence the pure titanium target and the titanium nitride one using the planar magnetron sputtering system. The sputter-deposition of the multi-layered films was carried out in the atmosphere of argon (Ar). The sputtering conditions examined in this study were as follows. The electric power source supplying to each sputter cathode with the pure titanium target or the titanium nitride one was of DC (direct current). The discharge voltage and current for sputtering the pure titanium target were 380V and 0.78A respectively. On the other hand, the discharge voltage and current for sputtering the titanium nitride target were 520V and 0.58A respectively. A Ti layer and a Ti-N layer were deposited onto the same pure titanium substrate in sequence by sputtering pure titanium target and titanium nitride one respectively. Thus the Ti-N/Ti multi-layered films were formed through the accumulation of these layers during the sputter-deposition. For the investigation of the effects of the thickness of Ti (pure titanium layer) on adhesion of TiN coatings to the pure titanium substrate, the thickness of pure titanium layer was varied from 0 to 200nm, while that of TiN layer was fixed at 200nm. Thereby the multi-layered film might be from 200nm thick to 400nm thick in total.

To investigate the blood compatibility of the obtained TiN/Ti multi-layered films, their surface thrombogenicity was evaluated by a cone-stirring-type platelet adhesion test with plasma of the blood drawn from health volunteers. The number of platelets adhered to the surface of the TiN/Ti multi-layered film for 15min was compared with that of the pure titanium substrate, where an acrylic resin was used as a negative control.

Under visual observation, the obtained multi-layered films with the pure titanium layer 200nm thick looked yellow gold and appeared to be uniform and adhesive, while both TiN monolithic films deposited directly onto the titanium substrate under the same sputtering conditions and the multi-layered films with the pure titanium layer 100nm thick peeled off partly. Thus the formation of TiN (titanium nitride) layer at the surface was assumed because of their color tone, and it was found that the TiN/Ti multi-layered film with a Ti layer more than 200nm thick was adhesive to the pure titanium substrate. I. Tsyganov et al. reported that TiN showed higher blood compatibility than pure titanium or titanium oxides [5]. Thus it was expected that the obtained Ti-N/Ti multi-layer film coatings could improve the blood compatibility of titanium-based materials. Figure 1 shows the result of the platelet test for the acrylic resin and for the TiN/Ti multi-layered film for 15min. Figure 2 shows the result of the platelet test for the acrylic resin and for titanium substrates for 15 minutes in the same way. And besides, the number of platelets adhered to the surface of the titanium substrates for 15 minutes was the factor of 0.34, comparing to that of the acrylic resin used as and negative control. On the other hand, the number of platelets adhered to the surface of the obtained TiN/Ti films for 15 minutes was the factor of 0.22, comparing to that of the acrylic resin used as a negative control. Based on these results of the platelet test, the ratio of the number of adhered platelets for the obtained TiN/Ti film to that for the titanium substrate was estimated to be 0.65. Thus it was found that the platelet adhesion of the obtained TiN/Ti film was much smaller than the pure titanium, concluding that the TiN/Ti multi-layer coating improved the blood compatibility. Therefore it was found that both the blood compatibility of pure titanium and the adhesion between the deposited TiN coating and the pure titanium substrate were improved by this method.

References:

[1] L. Sennerby and P. Thomsen, **Biomaterials** 14(1993)413.
[2] L. Chou, **Biomed. Mater. Res.** 31(1996)209.
[3] Y. Mitamura, **J. Surface Finishing Society of Japan** 43(1992)739.
[4] Y. Mitamura, T. Yuhta and T. Mikami, **High Tech. Ceramics** 1(1987)127.
[5] I. Tsyganov, M.S. Maitz and E. Wieser, **Applied Surface Science** 235(2004)156.

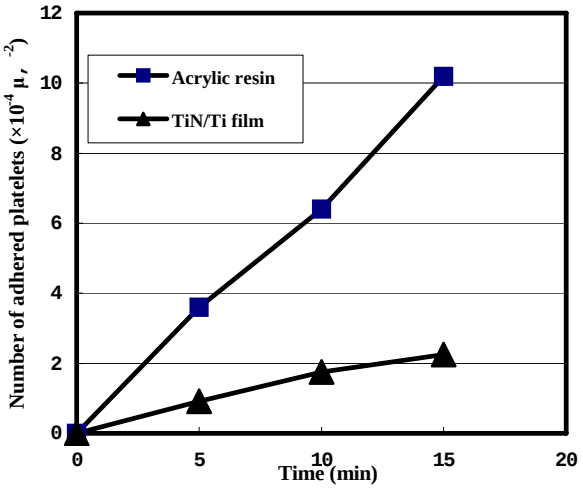

Fig.1. Result of the platelet test for the acrylic resin and for the TiN/Ti multi-layered film.

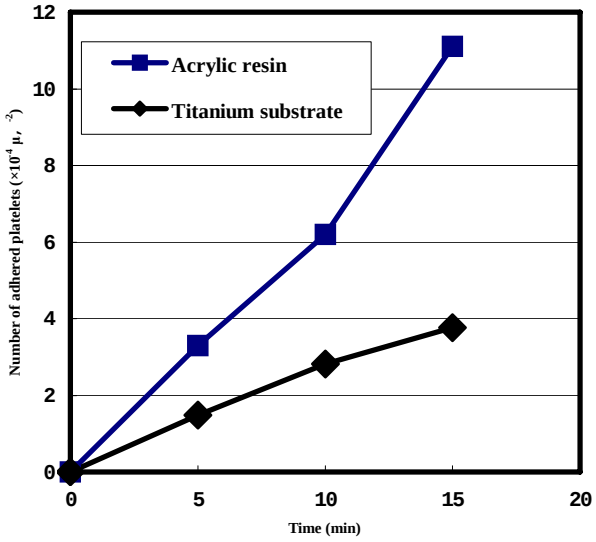

Fig.2. Result of the platelet test for the acrylic resin and for the titanium substrate.

Zn-Al_2O_3 ELECTRODEPOSITED NANOCOMPOSITES

Stancu R., Nicolae A., Raducanu C.
Mechanical Engineering and Research Institute, sos.Oltenitei 103, Bucharest, Romania
das@ictcm.ro

INTRODUCTION:

The presence of oxides, carbides, sulfides and graphites dispersed particles in metallic matrix improve the chemical and mechanical properties.Thus, the metallic coatings' application areas are enlarging.

Much expensive than the classical coatings, nanocomposite depositions have perfect characteristics that transcend their prices.

Three important application areas can be distinguished in metalo-ceramic nanocomposite materials case: nanocomposites hardening, wear and corrosion resistance.

In automotive industry, with the purpose of corrosion resistance increasing, it is recomanded the use of Zn-Al_2O_3 and Zn-SiO_2 nanocomposite coatings.

EXPERIMENTAL:

Zn-Al_2O_3 coatings have been obtained through electrodeposition on steel samples. The deposition was realised using an alkaline electrolyte, with a zinc oxide concentration of 10-12 g/l. In the electrolyte was added Merck Al_2O_3 nanoparticle suspension.

Salt spray tests corrosion have been effectuated according to ASTM B117 standard.

The linear polarization measurements of layers in 5% NaCl solution were also performed using a Radiometer PGP 201 potentiostat. The potential range was ±20 mV referring to E_{corr} and the scan rate was kept constant at 0,150 mV/s. All tests were carried out in aerated solutions.

From the obtained values for polarization resistance, R_p, the corrosion currents (i_{corr}) were calculated using Stern-Geary equation:

$$R_p = \frac{B}{i_{corr}} \quad (1); \qquad B = \frac{b_a b_c}{2{,}3(b_a + b_c)} \quad (2);$$

were b_a and b_c are the Tafel slopes.

The values of b_a and b_c were determined separately in an aerated, stagnant, 5% NaCl solution, from potentiodynamic polarization curves.

RESULTS:

The layers' structure was studied by scanning electron-microscopy (SEM).

In Figure 1. and Figure 2. are presented the micrographies of zinc composite electrodeposition with 10 ml/l alumina, 5 A/dm^2 and with 20 ml/l alumina, respectively.

CONCLUSIONS:

1. Non-passivated zinc depositions have 172 hours salt spray resistance, until the basic corrosion appears, in comparison with non-passivated Zn-Al_2O_3 composite depositions, with 72 hours (20 ml/l suspension) and 96 hours (10 ml/l suspension) salt spray resistance, until the the basic corrosion appears.
2. Passivated zinc depositions in hexavalent chromium ions solutions have 172 hours salt spray resistance, until the the basic corrosion appears, in comparison with passivated Zn-Al_2O_3 composite depositions in the same solution, which have 264 hours (20 ml/l suspension) and 288 hours (10 ml/l suspension) salt spray resistance, until the basic corrosion appears.
3. Passivated zinc depositions in trivalent chromium ions solutions have 172 hours salt spray resistance, until the the basic corrosion appears, in comparison with passivated Zn-Al_2O_3 composite depositions in the same solution, which have 144 hours (20 ml/l suspension) and 264 hours (10 ml/l suspension) salt spray resistance, until the basic corrosion appears.

REFERENCES:

1. J. Fransaer, J.P. Celis, J. R. Roos; J. Electrochem. Soc., 139 (1992) 413;
2. P. R. Webb, N. L. Robertson; J. Electrochem. Soc., 141 (1994) 669.

FIGURES:

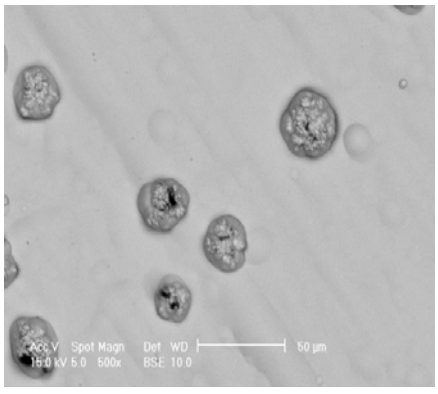

Figura 1. Micrography of Zn composite electrodeposition with 10 ml/l alumina.

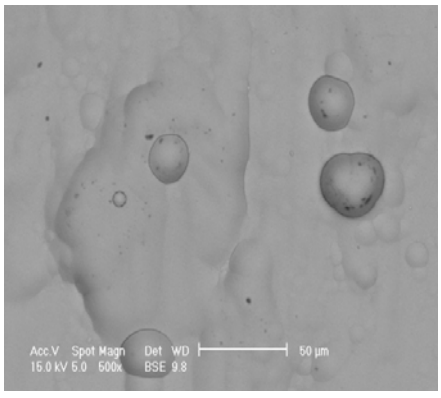

Figura 2. Micrography of Zn composite electrodeposition with 20 ml/l alumina.

DYNAMICS IN POLYMER-CLAY NANOCOMPOSITES AS STUDIED BY FTIR, XRD, TEM, TSDC AND DSC TECHNIQUES

Nery Suárez[1], Norkis Salazar Serge[2], José Luis Feijoo[3], María Hernandez[1]
[1]Departamento de Física, [2]Departamento de Química, [3]Departamento de Materiales
Universidad Simón Bolívar, Caracas, Venezuela
nsuarez@usb.ve

This work is related to the preparation of polymer-clay nanocomposites (PCNs) by the exfoliation-adsorption technique, from atactic poly(methyl methacrylate) (PMMA) in solution, using Bentonite (B) as a layered-silicate natural clay. To optimize the intercalation of B with PMMA, it has been organically modified (OB) with a quaternary ammonium salt that helps the interchange of cations, and thus converting its hydrophilic surface to an organophilic one. An investigation of the morphology and molecular motions or dynamics of the net polymer film as well as the PCN final films was performed by X-ray diffraction (XRD), Transmission Electron Microscopy (TEM), Infra-Red Spectroscopy (IR), Thermally Stimulated Depolarization Currents (TSDC), and Differential Scanning Calorimetry (DSC) techniques. One of our interests was to discuss the solvent influence on the polymeric matrix. Herein, comparative studies of the effects of different solvents on the thermal and dielectric properties of the net PMMA films are reported. Four solvents were used to prepare the films, toluene, dichlorometane, tetrahydrofuran and acetone.

Fig. 1 XRD diffraction pattern of B, OB, and PMMA /5%OB

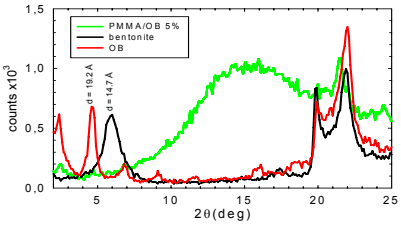

Fig. 2. TEM micrograph of PMMA/2%OB

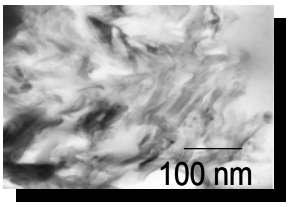

In Figure 1, XRD diffraction patterns (using Cu Kalfa radiation), reports the spacing between ordered layers of clay via the presence of the d_{100} or basal spacing. The original B exhibits a peak associated with a spacing of 14.7 A, whereas the expanded OB shows a value of 19,2 A. The absence of this basal peak suggests a high dispersion of clay platelets (exfoliation) in the PMMA/OB with 5% OB. The broad peak at around $15^{o}=2\theta$ is due to the amorphous hallow of the atactic PMMA nanocomposite. The efficiency of the intercalation can be also check by TEM microphotographs. Figure 2 clearly shows that the OB layers are mainly exfoliated in the PMMA/OB with 2% OB.

Fig. 3 FTIR curves of PMMA/OB PCNs and PMMA/B

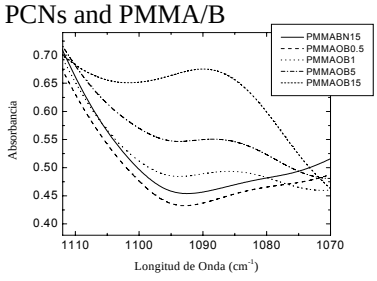

The FTIR spectra of the Si-O stretching region are shown in Figure 3 for PMMA/OB with varying % OB concentration, and PMMA with 15% of natural B. The graph shows the presence of a peak with increasing intensity and slight shift of its maximum towards higher λ^{-1} position as the OB content increases. The absence of this peak in the PMMA/B sample corroborates their previous assignation to Si-O groups [1] interacting with polymer molecules. The significant changes of this peak with the OB content obviously reflect the variation in the distribution of environments of the Si-O bonds, providing also an indication of the increasing overall degree of intercalation/exfoliation.

Figure 4 shows the dielectric spectra of the PMMA films prepared with the different solvents and the compressed molded sample. It displays a series of well established intrinsic relaxation signals [2], i.e., γ (methyl groups), γ' (adsorbed polar water molecules), β (carboxymethyl side groups flip), β' (postulated as a main chain rearrangement accompanying the side group flip,

characterized as a rotation around the local chain axis), and long-range conformational change of the polymer backbone. (A) displays the secondary relaxations whose intensity and profile vary with the selected solvent. The glass transition is shown at higher temperaturas (B) as a huge peak, with intensity and temperature position (Tg) variations among the different solvents. The whole spectra of the cast samples exhibit evident intensity attenuation as compared to the molded film. A lower value of Tg is also a common feature among the cast samples. Comparable Tg trends have been obtained by DSC technique. Traces of the different solvents are expected to reside in relatively strong binding sites [2], e.g., hydrogen bonded to C=O groups. The measured amount of the remanent acetone, dichlorometane, toluene, and tetrahidrofuran solvents, obtained by NMR, is 0.30, 0.40, 9.00, and 14.00% respectively. The samples with higher solvent contents exhibit lower Tg values. The retained solvent molecules, trapped inside the PMMA films, affect the dynamics of the segmental and the localized dielectric relaxations. This effect differs in function of the nature and the amount of the solvent, and it could be partly explained by acid-base interactions between PMMA and the solvents[3].

Fig. 4 Low temperatura (A), and High temperature (B) TSDC spectra of PMMA molded film and cast films from different solvents.

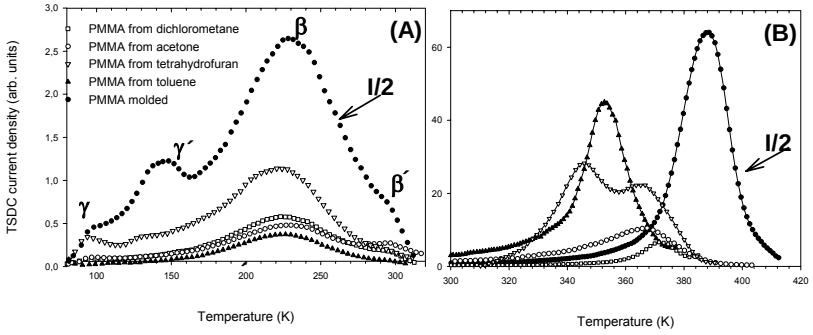

Fig. 5 Low temperatura (A), and High temperature (B) TSDC spectra of PMMA/OB PCNs.

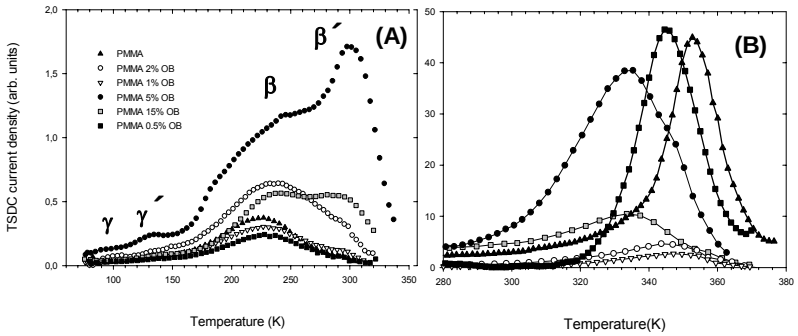

Figure 5 (A) shows that, on increasing the OB content the intensity of the low temperature relaxations decreases in the sample with 0.5% OB, increases up to 5% OB, and then drops again at 15% OB. A positive high-temperature shift of the low temperature spectra is observed in the samples with 2, 5, and 15% OB. This shift, related with the enhancement of the β´ process, could be explained by the increased exfoliation, as it increases the rotational mobility of the PMMA chains[4]. Figure 5 (B) shows that the temperature position of the dielectric manifestation of the glass transition is a decreasing function of the OB content. Similar Tg decreasing trend was obtained by DSC. This behavior is consistent with previous results[4-5] and have been rationalized assuming that the layered silicates reduce the intermolecular (cooperative) domain size, which increases with the exfoliation. However, as the layered silicate/polymer interactions could restrict segmental mobility, the outcome should be a "tug-of-war", where the influence of these opposite effects must be accounted for.

References:

[1] K. C. Cole, *Macromolecules*, **41(3)** (2008) 834-843.
[2] I. M. Kalogeras, E. R. Neagu, and A. Vassilikou-Dova; *Macromolecules* **37**, (2004)1042-1053.
[3] S. Bistac, J. Schultz, *Mat. Sci. & Eng.*, **31** (1997) 347-350.
[4] R. Davis, A. J. Bur, M. McBrearty, Y. Lee, J. W. Gilman, and P. R. Start; *Polymer* **45**, (2004) 6487-6493.
[5] J. Mijovic, H. Lee, J. Kenny, and J. Mays, *Macromolecules*, **39(6)**, 2006) 2172-2182.

THE DIFFERENT SPECIES OF TELLUROPENTAHIONATES AS PRECURSORS FOR FORMATION OF COPPER CHALCOGENIDES LAYERS ON THE SURFACE OF POLYAMIDE

Judita Sukyte, Skirma Žalenkienė, Remigijus Ivanauskas, Vitalijus Janickis
Department of Inorganic chemistry, Kaunas Technological University, Radvilenu pl. 19, LT – 50254 Kaunas, Lithuania, judita.sukyte@ktu.lt

Metal chalcogenides semi – conducting materials have found many applications in opto – electronic, solar cell and photovoltaic devices. There have been a wide variety of techniques for the formation thin layers of copper chalcogenides on various dielectrics, and on the polymers too. There is presently great interest in the development of low – cost and simple processing methods. Our approach follows the sorption – diffusion process described previously [1-2].

This method uses a single-source molecular precursor which are introduced into the simple reactor and undergo diffusion – sorption on a substrate surface followed by reaction with copper salts to give the copper chalcogenide along with desorption of any by-products. The different species of telluropentathionate as source for S and Te have been applied in our work. The salts of sodium or potassium telluropentathionate, $Na_2TeS_4O_6\ 2H_2O$, $K_2TeS_4O_6\ 2H_2O$, have been prepared according to published procedures [3] by means of the Norris and Fay reaction between tellurous acid and thiosulfate:

$$H_2TeO_3 + 4S_2O_3^{2-} + 4H^+ = S_4O_6^{2-} + TeS_4O_6^{2-} + 3H_2O$$

Monotelluropentathionic $H_2TeS_4O_6$ acid has been isolated from its barium salt $BaTeS_4O_6{\cdot}2H_2O$ in the raction with sulfuric acid [2].

Polyamide as semi-hydrophilic polymer due to multifunctional chelating groups, namely carboxylic and amido, sorbs telluropentathionate ions containing a mixed chain of three divalent chalcogen atoms $-O_3S-S-Te-S-SO_3-$ from their solutions [3]. The dimensions of unit cell of *trans* form of telluropentathionate ion are: a = 5.043, b = 10.434, c = 22.372 Å [4]. The interaction of Cu(II/I) salt with the sorbed telluropentathionate ions leads to the formation of mixed copper chalcogenides layers with various chemical, phase composition (Fig. 1), surface morphology (Fig. 2) and electrical resistance (Table).

The surface morphology and structure were observed by AFM [Fig. 2]. In dependence of the exposure in the precursor solution, the layers of chalcogenides with various thicknesses might be formed. CuTe and CuS interface appears graded with substantial interdiffusion between the layers. The islands observed due to surface roughness.

The resistances of the copper chalcogenides on PA formed using different species of telluropentathionates decreases from 1.80×10^3 to 1.2-2.9 kΩ/□ as the content of tellurium increases from 0.15 to 0.74 - 0.84 μmol/cm^2. The increase of Te content results in the increase of film thickness (from 250 nm for 0.14 μmol/cm^2 Te to 2.7 μm for 0.7-0.8 μmol/cm^2 Te). This factor partly counteracted the increase of conductivity caused by the increase of Te content.

The careful choice of the treatment methods using the different forms of telluropentathionates as precursors enable us to form electrically conductive or semiconductive copper sulfides – tellurides layers and establish the regularities of their formation.

References:

[1] V. J. Šukyte, R. Ivanauskas and V. Janickis, Polish J. Chem., **79** (2005) p. 759-771.
[2] S. Zalenkiene, J. Sukyte, R. Ivanauskas, V. Janickis, I. J. Photoenergy, **40**, (2007) p. 2660.
[3] O. Foss. Acta Chem. Scand., **3** (1949) p. 708–716
[4] Maroy K. 1975. Crystal structures of Penta-, Selenopenta-, Telluropenta-, and Hexathionates. Doctoral thesis, Bergen.

Table. The content of Te and the resistance of the copper chalcogenides layers on PA surface

Exposure, h	Te content (μmol/cm^2)in PA surface			Sheet resistance (kΩ/□) of PA exposed at 20° in 0.1mol·dm^{-3}		
	$Na_2TeS_4O_6$	$K_2TeS_4O_6$	$H_2TeS_4O_6$	$Na_2TeS_4O_6$	$K_2TeS_4O_6$	$H_2TeS_4O_6$
0.5	0.147	0.067		1.19×10^3	256.43	
1.0	0.160	0.189	0.147	360.4	41.444	1.80×10^3
2.0	0.154	0.268	0.247	623.9	9.85	4.34×10^3
3.0	0.359	0.364	0.324	5.30	9.89	243-893
12	0.450	0.775	0.828		1.57	1.19
24	0.764	0.826	0.742		2.92	1.43

Figures:

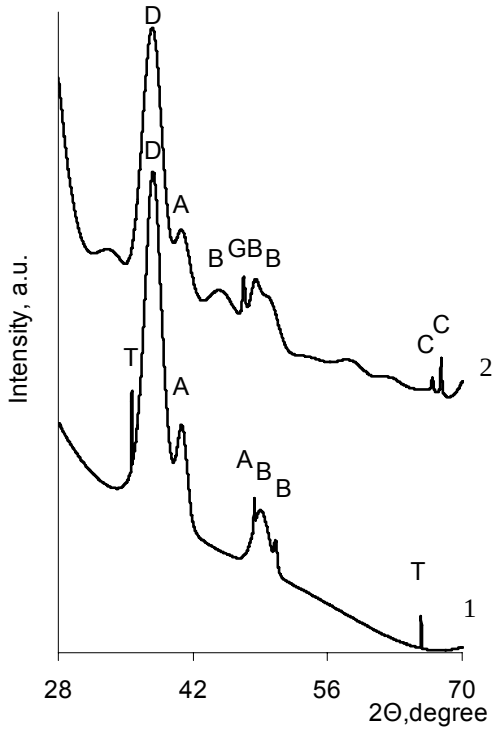

Fig. 1

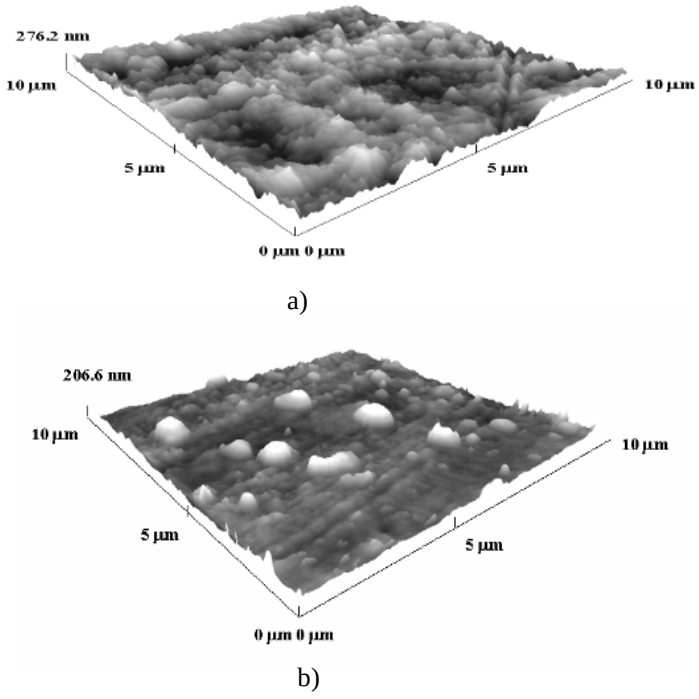

Fig. 2

Fig.1. X–ray diffraction patterns (A –anilite Cu_7S_4, D – djurleite $Cu_{1.9375S}$, S – digenite $Cu_{1.8}S$, C – hexagonal copper telluride Cu_2Te, T – tetragonal copper telluride $Cu_{3.18}Te_2$, B – vulcanite CuTe, E – copper telluride $Cu_{2.72}Te_2$) of chalcogenides layers on PA treated 3h at 20°C in 0.1 mol·dm^{-3} $H_2TeS_4O_6$ (1); 0.1 mol·dm^{-3} $Na_2TeS_4O_6$ solution in 0.2 mol×dm^{-3} HCl (2)

Fig. 2. AFM top view of copper chalcogenides layers on PA treated:
a) 3 h at 20 °C in 0.1 mol dm^{-3} $Na_2TeS_4O_6$ solution at 276.2 nm;
b) 24 h at 20 °C in 0.1 mol dm^{-3} $H_2TeS_4O_6$ at 206.6 nm

A DNA CHIP FOR SIMULTANEOUS DETECTION OF MICROORGANIMS IN WATER SAMPLES: COLIFORM BACTERIA, NON-MANDATORY BACTERIA, HEPATITIS A VIRUS AND NOROVIRUSES

Filipa Vale1, Ana Maria Silva1, Ana Teresa Silva1, Maria José Vale1,Cecília Calado1, Tito Silva1 and Helena Vieira2.
1 Faculdade de Engenharia, Universidade Católica Portuguesa, Rio de Mouro, Portugal.
2 BIOALVO SA, Edificio ICAT, Campus da FCUL, Lisbon, Portugal.
Contact: filipavale@fe.ucp.pt

The use of surveillance systems demonstrates that waterborne pathogens are responsible for several diseases associated either with either consuming of contaminated drinking water, or contacting polluted recreational waters. To assure water quality not only mandatory microorganisms should be screened for. Emergent pathogens that represent danger to public health should also be analysed. Culture methods used routinely in water microbiology (bacteriology) laboratories are long time consumable. Moreover some of the emergent pathogens are not represented by conventional indicator bacteria, which limit the screening power of the current methodology. The present study aims at developing a rapid method to simultaneously detect several microorganisms (bacteria, protozoa, and virus) in water samples by the use of a DNA chip (AQUACHIP©). Species specific DNA probes will be implemented on a chip, allowing detection of which sample is positive for which microorganism.

The first selected microorganisms were the Portuguese and European Community mandatory microbiological parameters and indicator parameters required to water intended for human consumption, delivered by public distribution systems, trucks or cistern-ships, or used in the alimentary industry. These are the coliform bacteria group, *Escherichia coli*, Enterococcus and *Clostridium perfringens* (including spores). For this microorganism we have developed 9 probes, 1 for total coliform, 5 for *E. coli*, 2 for Enterococcus, and 1 for *Clostridium perfringens* (figure 1A). All these probes have been amplified by PCR amplified from pure cultures and validated against artificial samples.

The group of non-mandatory selected microorganisms were selected according to their impact on public health. These are *Pseudomonas aeruginosa*, *Staphylococcus aureus*, *Legionella pneumophila*, *E. coli* O157, *Campylobacter coli* and *C. jejuni*, *Salmonella* spp. and *Shigella* spp., each with one selected probe (Figure 1B). All these probes have been amplified by PCR from pure cultures and will be validated against artificial samples.

The analysis of the viral genomes in study (we have started with hepatitis A virus and noroviruses genogroup 1) revealed highly conserved sequences, which were amplified by RT-PCR, using specific primers (one for each viral group), in order to obtain the probes for viral detection (Figure 1C). These probes were both cloned and hepatitis A virus probe was validated by dot blot using artificial samples. The hepatitis A virus probe and the Noroviruses (GI) probes which were cloned into pBS KS were further sequenced to confirmed their sequence. The BLAST results confirm that these probes are specific for their viral groups.

In the future, further tests are needed to evaluate the probes efficiency in water samples of the water supply network. These species specific DNA probes will be implemented on

a chip, and for that future work will include chip support (e.g. glass or silica) and an appropriate label detection method selection.

This work is founded by Fundação Calouste Gulbenkian, program Environment and Health 2005.

References:

1. Fong T.-T.and Lipp E. K. (2005). Enteric Viruses of Humans and Animals in Aquatic Environments: Health Risks, Detection and Potential Water Quality Assessment Tools. Microbiol. Mol. Biol. Rev. 69:357-371.
2. Lemarchand, K., L. Masson, and R. Brousseau. 2004. Molecular Biology and DNA Microarray Technology for microbial quality Monitoring of water. Crit. Rev. Microbiol. 30: 145-172.
3. Straub, T. M., D. P. Chandler. 2003. Towards a unified system for detecting waterborne pathogens. J. Microbiol. Meth. 53: 185-197.

A. Mandatory microorganisms

	E. coli				*E. faecalis*	*E. faecium*	Total coliform	*C. perfringens*
Probe number	4	5	7	8	2	3	1	6
pb	162	186	139	187	140	161	147	184
Ratio sequenced genomes detected	6/13	4/13	13/13	13/13	1/1	-/-	*Escherichia*, *Klebsiella* *Enterobacter* *Citrobacter* *Moellerella* *Morganella* *Salmonella* *Shigella* *Yersinia* *Hafnia* *Erwinia* *Proteus* *Serratia* *Among othres*	1/1

B. Non-mandatory microorganisms

	S. aureus	*L. pneumophila*	*E. coli* O157	*C. jejuni*	C. coli	*Shigella* spp.	*Faecal coliforms*	*Salmonella* spp.	*P. aeruginosa*
Probe number	9	10	11	12	13	15	16	17	18
pb	128	128	152	107	134	111	164	110	141
Ratio sequenced genomes detected	14/14	4/4	2/2	5/5	-/-	6/6	13/13	7/7	3/3

C. Virus

	HAV	**NV (GI)**
Probe number	19	20
pb	222	118

Figure 1. Identification of probes selected for each microorganism group. A. Mandatory microorganisms. B. Non-mandatory microorganisms. C. Virus.

LOW-DIMENSIONAL METALLIZED BIODEGRADABLE POLYMERS PREPARATION, STUDY AND APPLICATION

M. Vantsyan[1], G. Popova[1], T. Shukshina[2], E. Vasilieva[3]
[1]Mendeleyev University of Chemical Technology of Russia, Miusskaya sq. 9, Moscow, Russia
[2]Moscow Engineering-Physical Institute, Kashirskoe highway, 31, Moscow, Russia
[3]St. Petersburg State Polytechnic University, Polytechnicheskaya street, 29, St. Petersburg, Russia
galina@muctr.edu.ru

Last decade metallized polymers with unconventional properties are objects of significant research interest for environmental protection, bionanotechnology, radiophysics, etc. Biocompatible, biodegradable and bacteriostatic siloxane / carbonate copolymer (commercial product, MM 50 000) was applied as a support (thickness about 1 μm) for magnetronic (I) and ion-plasma (II) deposition. These methods were developed for preparation of Cu-containing hybrid (I) or Ni and Au-coating (II). X-ray, AFM, STM and other techniques were used for metallized polymers characterization. Surface structure, optical and mechanical properties were found to be dependent on deposition time, temperature, coating thickness. For gold coatings (thickness about 80 nm) the most favourable results on durability, were obtained, its defectless area is 43 nm. Electric, magnetic and acoustic properties are demonstrated for low-dimensional metallized copolymers, their potential application is discussed.

Acknowledgements
The authors are grateful for financial support to Russian Ministry of Education and Science Program “Scientific Potential Development for Higher Education”, Project 5118.

References:

[1] D. Kim, N. Yuzh, V.K.Kim, E.S.Vasilieva, E.A.Kaydash, O.V.Tolochko, Glass Physics and Chemistry (Rus.), **3** (2007) 304.
[2] M.B.Zheneva, V.M.Kopylov, V.A.Kovyazin, I.B.Sokolskaya, V.V.Kireev, I.M. Raigorodsky, VMS (Rus.), Ser. A, **7** (2004) 693.
[3] B. Yoon, P. Koshkinen, B. Huber, O. Kostki, B. von Issendorff, H. Hakkinen, M. Moseler, U. Landman, Chem. Phys. Chem., **8** (2007) 157.

MAGNETIZATION REVERSAL PROCESS IN SPIN SPRING MAGNETS. ELECTRONIC STRUCTURE CALCULATIONS

A. Vega[1], *V.M. Uzdin*[2]

1. Dep. de Física Teórica, Atómica y Óptica, University of Valladolid, 47005 Valladolid, SPAIN
2. St. Petersburg State University, Universitetskaya nab. 7/9, St. Petersburg, 199178 RUSSIA

vegat@phenix.fam.cie.uva.es

One of the nanostructures in which a non-collinear magnetic structure can be continuously and reversibly tuned by an external magnetic field is the spin spring permanent magnet which consists of exchange-coupled hard and soft magnetic bilayers or multilayers. Exchange spring media are of technological interest as permanent magnets but are also promising nanostructures for magnetic recording[1,2]. Various experimental methods have been used for the investigation of magnetic ordering in spring magnets[3,4], which in turn became a model system for benchmarking different methods to study non-collinear magnetism. Due to their complexity, the interpretation of experimental data has been made so far with the help of phenomenological models[3,4].

For the description of the magnetization reversal process in exchange spring magnets with Fe (and Fe capped by Cr or V) as the soft phase, we developed an atomic-scale quantum-mechanical theory for itinerant magnetism based on a realistic non-collinear Tight-Binding formulation of the Hamiltonian with universal parameters for each chemical element. Therefore, the behaviour of the soft magnetic films as a function of the intensity and orientation of an external magnetic field is described in the framework of fully self-consistent electronic structure calculations. Our results reproduce qualitatively all the main trends experimentally observed.

In Fig.1 we show the calculated spin-configuration for the 100ML thick Fe slab in an external magnetic field applied in the film plane. Fig. 2 illustrates the angle between the magnetic moment of the Fe layers and the easy axis of the hard magnet for different external fields applied opposite to this easy axis. In Fig. 3 we plot the reversible part of the hysteresis loop. The critical intensity of the external field required for the onset of the non-collinear spiral formation depends on both the thickness of the soft magnetic phase and on the orientation of the field, and the spin spiral structure undergoes a change of chirality in rotating fields. Our theoretical approach opens new prospects for investigating the response of other nanostructures to external magnetic fields, beyond the usual phenomenological models.

References:

[1] R.H. Victora and X. Shen, IEEE Trans. Mag. **41** (2005), 537.
[2] D. Suess, App. Phys. Lett. **89** (2006), 113105.
[3] E.E. Fullerton et al., Phys. Rev. B **58** (1998), 12193.
[4] R. Rhölsberger et al., Phys. Rev. Lett. **89** (2002), 237201.

Figures:

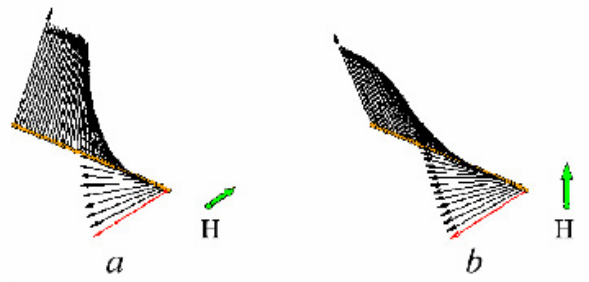

FIG. 1: Calculated spin configuration of the 100 ML thick Fe slab in an external magnetic field ($h = 3.0 \times 10^{-5}$), applied in the film plane opposite (a) and perpendicular (b) to the easy axis of the substrate (hard magnet). The direction of the lower (red) Fe moment is fixed along this easy axis. The arrows are proportional to the local magnetic moments. Only each second layer is shown. See also [21].

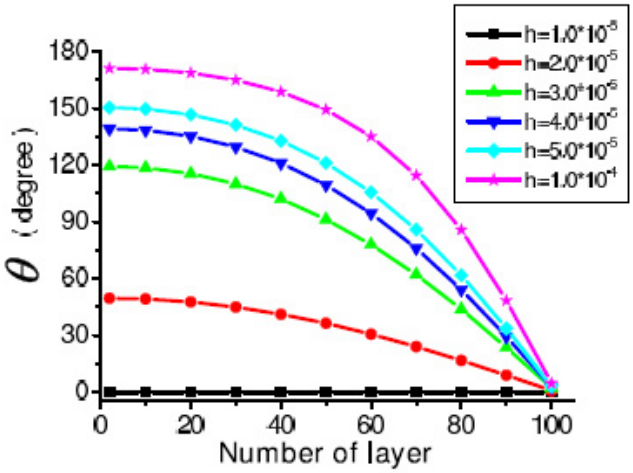

FIG. 2: Layer dependence of the angle θ_i between the magnetic moment and the easy axis of the hard magnet for different values of the external magnetic field applied opposite to the easy axis. The surface layer has number 1.

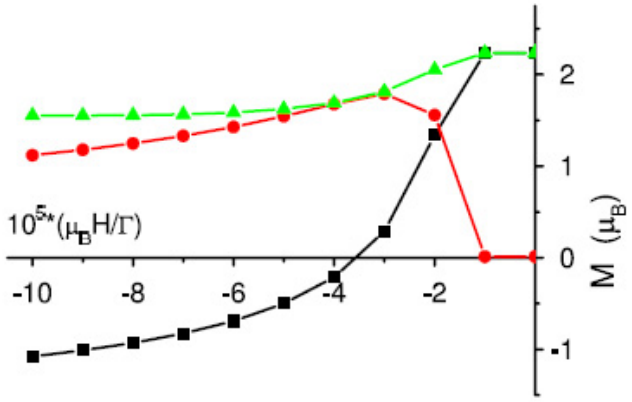

FIG. 3: Average modulus (triangles), longitudinal (squares) and transverse (circles) components of the magnetic moment (see text) as a function of the external magnetic field applied opposite to the easy axis of the hard magnet. See also [21].

Field emission properties of carbon nanotube arrays grown in porous anodic alumina

F. Odorici[5], R. Angelucci[1,5], I. Boscolo[2], S. Cialdi[2], A. Ciorba[3], M. Cuffiani[4,5], L. Malferrari[5], A. Montanari[5], R. Rizzoli[1,5], M. Rossi[3], V. Sessa[6], M. L. Terranova[6], G. P. Veronese[4,5]

1. CNR – IMM sezione di Bologna, via Gobetti 101, 40129 Bologna, Italy
2. INFN and Dipartimento di Fisica Università di Milano, via Celoria 16, 20133 Milano, Italy
3. Dipartimento di Energetica, Università di Roma "La Sapienza" via A. Scarpa 16, 00161 Roma, Italy
4. Dipartimento di Fisica Università di Bologna, V.le B. Pichat 6/2, 40127 Bologna, Italy
5. INFN, V.le B. Pichat 6/2, 40127 Bologna, Italy
6. Dipartimento di Scienze e Tecnologie Chimiche, MINASlab, Università di Roma "Tor Vergata"- INFN, via della Ricerca Scientifica, 00133 Roma, Italy

veronese@bo.imm.cnr.it

Carbon nanotubes (CNTs), with their excellent electronic properties and extremely high aspect ratio, represent an ideal material for building electron sources based on field emission [1]. The field emission phenomenon, especially from single or isolated tips, is quite successfully represented by the Fowler-Nordheim equation. However, such model often fails the attempt to describe the field emission from populations of CNTs and the comparison with experimental data is usually in disagreement with expectations. Such discrepancies arise when considering large numbers of CNTs, where collective effects are present and influence the measured I–V characteristics. In this case, questions concerning the enhancement factor dependence on the tips density or the space charge effect can be studied only if emitters have quite uniform height and density. In this work we study the emission properties of multi-wall CNTs grown within anodic alumina templates. For such materials the source can be modelled as an ordered and uniform array of emitters and theoretical predictions can be compared with experimental measurements in a direct way.

The alumina template was obtained by electrochemical anodization of an iperpure aluminum foil, in oxalic acid solution 0.3 M, at 40 V d.d.p. and 5 ^{o}C, obtaining a regular honeycomb-like structure with pores diameters and pitch of 60 and 100 nm respectively [2]. The growth of vertically aligned CNTs in the alumina template is obtained by catalyst-assisted CVD, after the electrochemical deposition of cobalt seeds in the bottom of the alumina pores. CVD was performed at atmospheric pressure in a quartz hot wall furnace, warmed up to 700 ^{o}C, where a 1 hour annealing in H_2 flow was followed by a 30 min deposition step, in a 15 % C_2H_2 gas mixture in N_2. Typical morphology of the obtained CNTs in porous alumina is shown in Fig. 1.

Field emission measurements were performed in a high vacuum chamber (10^{-7} mbar) equipped with micrometric translators to move the sample along the three axes [3]. The distance of the anode from the flat cathode (sample) and the position in the (x,y) plane are PC-controlled with a minimum incremental step of 0.1 μm in the x-y plane and 1 μm in the z-direction. The effective anode-cathode distance is determined via the measurement of the anode-cathode capacitance and the current is measured with rms noise of about 1 pA. Typical field emission current density curves as a function of the applied electrical field are shown in Fig. 2. Experimental results prove that CNT matrices can produce quite high and stable current densities.

Simulation of the emitters array, by mean of the COMSOL Multiphysics software, was used to calculate the electric field dependence on different CNTs geometries (height, interspacing, apex shapes, etc.) and to predict the corresponding field enhancement factors. Comparison between the experimentally measured field enhancement factors and the expected values are discussed.

References

[1] N. S. Xu, S. Ejaz Huq, “Novel cold cathode materials and applications”, Materials Science and Engineering, R **48** (2005) 47-189.
[2] R. Angelucci et al., “A novel position detector based on nanotechnologies: the NanoChanT project” Nucl. Phys. B **150** (2006) 140–143.
[3] I. Boscolo et al., “Capacitive and analytical approaches for the analysis of field emission from carbon nanotubes in a sphere to plane diode”, J. Vac. Sci. Technology B **25** (2007), 1253.

Figures:

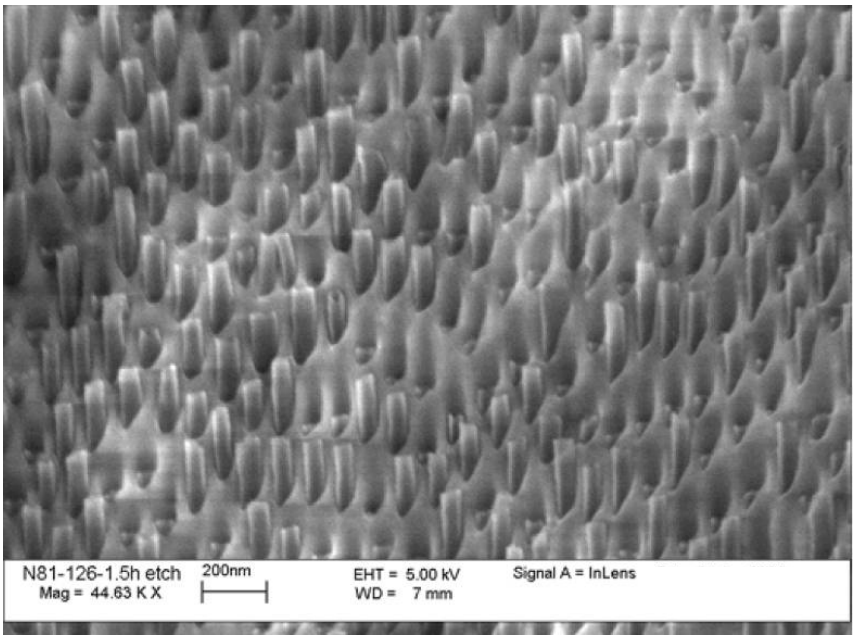

Fig.1 Matrix of multi-wall CNTs within alumina template

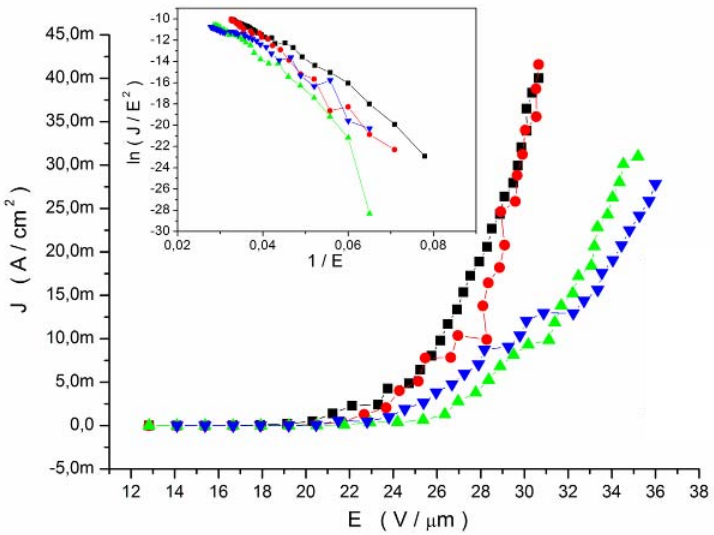

Fig. 2 Current density vs. the external electric field.
The inset shows the representation in the Fowler-Nordheim plane.